Dipl.-Ing. Peter Wilhelm Zach, BSc.

New Phosphorescent Benzoporphyrin Complexes with Remarkable Photophysical Properties - From Synthesis to Applications

DISSERTATION

zur Erlangung des akademischen Grades

Doktor der technischen Wissenschaften

eingereicht an der

Technischen Universität Graz

Betreuer

Assoc. Prof. kand. Sergey Borisov

Institut für Analytische Chemie und Lebensmittelchemie
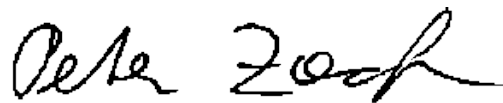Technische Universität Graz

Univ.-Prof. Dipl.-Chem. Dr.rer.nat. Ingo Klimant

Graz, April 2018

II

EIDESSTATTLICHE ERKLÄRUNG

Ich erkläre an Eides statt, dass ich die vorliegende Arbeit selbstständig verfasst, andere als die angegebenen Quellen/Hilfsmittel nicht benutzt, und die den benutzten Quellen wörtlich und inhaltlich entnommenen Stellen als solche kenntlich gemacht habe. Das in TUGRAZonline hochgeladene Textdokument ist mit der vorliegenden Dissertation identisch.

08.03.2018
Datum

Unterschrift

IV

NO RAGRETS

NOT EVEN AN A FOR AN E

Danksagung

Abstract

This thesis describes the preparation of two new classes of benzoporphyrin derivatives, accessible with only little synthetic effort compared to known alternatives. Platinum(II) and palladium(II) complexes of the first class were synthesized within four steps via template method and show enhanced solubility and photostability as well as a bathochromic shift (higher wavelengths) of the absorption spectra. Besides their increased phosphorescence brightness in the NIR, these compounds display a decreased energy gap between the excited singlet and triplet state, resulting in unexpected thermally-activated delayed fluorescence (TADF) in the red part of the electromagnetic spectrum.

The second class of benzoporphyrin derivatives is prepared within a one-step π-extension of known compounds (e.g. Pt-TPTBP) with help of the Scholl reaction, leading to intramolecularly bridged species. Moreover, substitution of the benzoporphyrins core with several moieties such as fluorene, carbazole, benzoyl, etc. was performed via Friedel-Crafts acylation or Suzuki as well as Sonogashira coupling reactions. While the resulting modified complexes feature higher quantum yields compared to parent benzoporphyrins, the bridged species, shows remarkable bathochromic shifts of absorption (approximately 680 nm) as well as emission spectra up to 880 nm.

The drastically altered photophysical properties of these new benzoporphyrins enables applications beyond the usage as indicators for optical oxygen sensing. The unique dually emissive character of the palladium(II) analogues of the first class of dyes, was used to design a dual sensor for simultaneous determination of oxygen and temperature, based on a single indicator dye and operating in a self-referenced manner. The outstanding bathochromic shift of absorption and emission spectra of the bridged platinum(II) complex was further utilized to design an oxygen transducer used in a new concept of optical glucose sensing. This makes use of a single optode for oxygen-compensated determination of glucose. Additionally, application of all compounds as efficient sensitizers for triplet-triplet-annihilation (TTA) upconversion was demonstrated.

Kurzfassung

In dieser Arbeit wird die Herstellung zweier neuer Klassen von Benzoporphyrin Derivaten beschrieben, welche verglichen zu bereits bekannten Farbstoffen nur einen geringen synthetischen Aufwand erfordern. Platin(II) und Palladium(II) Komplexe der ersten Klasse wurden mittels der Template Methode in vier Schritten synthetisiert und weisen sowohl erhöhte Löslichkeit und Photostabilität als auch eine bathochrome Verschiebung (zu höheren Wellenlängen) des Absorptionsspektrums auf. Neben der größeren Leuchtdichte und Emission von Phosphoreszenz im NIR, besitzen diese Verbindungen auch einen geringeren Energieunterschied zwischen dem angeregten Singulett und Triplet Zustand, was zu einer unerwarteten thermisch-aktivierten verzögerten Fluoreszenz (TADF) im roten Bereich des elektromagnetischen Spektrums führt.

Die zweite Klasse der Benzoporphyrin Derivate lässt sich durch eine Erweiterung des π-Systems in einer einstufigen Reaktion aus bereits bekannten Verbindungen (z.B. Pt-TPTBP) herstellen; wie zum Beispiel mit Hilfe der Scholl Reaktion, die zu einer intramolekular verbrückten Spezies führt. Des Weitern wurden auch Substitutionen mit Fluoren-, Carbazol- sowie Benzoyl-gruppen etc. am Benzoporphyrinring über Friedel-Crafts Acyclierung sowie Suzuki und Sonogashira Kupplungsreaktionen untersucht. Während die daraus entstandenen modifizierten Komplexe eine höhere Quantenausbeute, verglichen mit bereits existierenden Benzoporphyrinen besitzen, weist die verbrückte Spezies eine beachtliche bathochrome Verschiebung der Absorption (ca. 680 nm) als auch der Emission mit bis zu 880 nm auf.

Die deutliche Veränderung der photophysikalischen Eigenschaften der neuen Benzoporphyrine ermöglicht Anwendungen, die weit über die konventionelle optische Messung von Sauerstoff hinausgehen. Die einzigartige Fähigkeit der zweifachen Emission (verzögerte Fluoreszenz und Phosphoreszenz) der Palladium(II) Analoga der ersten Klasse wurde verwendet um zum ersten Mal einen Dual-Sensor für die simultane Bestimmung von Sauerstoff und Temperatur (beide selbstreferenziert) mittels einer einzigen Messsonde zu designen. Die spektakuläre bathochrome Verschiebung der Absorption und Emission des verbrückten Platin(II) Komplexes ermöglicht dessen Anwendung als Sauerstoff Sensor in einem komplett neuen Konzept der optischen Glukose Messung, unter erstmaliger Verwendung einer einzelnen Optode für die Sauerstoff referenzierte Bestimmung an einer einzigen Stelle. Zusätzlich erweisen sich alle Verbindungen als effiziente Sensibilisatoren für die Triplet-Triplet-Annihilation (TTA) basierende Upconversion.

1 Table of Contents

Part 1: Introduction

Part 2: Results

Part 3: Appendix

Part I
Introduction

2 Scope of the Thesis

Oxygen, is not only an essential source of life on earth but also one of the most important and therefore best investigated chemical species. Determination of its concentration is from great importance in various fields of research as well as industry, such as environmental and marine analysis, chemistry, medicine, industrial production monitoring et cetera. [1] The fact, that not only quantification of oxygen but in most cases continuous monitoring of its concentration is desirable, induce the great success of optical sensor technology in this field. Another reason are the numerous advantages of optical oxygen sensors, compared to chemical (Winkler titration) as well as electrochemical measurement principles. [1] After decades of intensive research it comes therefore as no real surprise, that the determination of oxygen by optical means (based on luminescence quenching) is possible the most established and viable alternative to other detection systems on the market, such as electrochemical methods.

Contingent on the great interest towards optical oxygen sensing, an enormous amount of different oxygen indicators has been prepared and investigated over time. Herein, metalloporphyrins with platinum(II) and palladium(II) as central atom and especially benzoporphyrins have raised huge attention, due to their outstanding photophysical properties as wells as their straightforward synthetic strategy. Despite their success as indicators for optical sensing and in several other fields of application, some properties still display room for improvement in the future. Besides modification of their solubility and photostability, an even more pronounced bathochromic shift (higher wavelengths) of the absorption as well the emission spectra of benzoporphyrins is highly desirable, enabling not only drastic improvements within existing applications but would also possibly lead to a number of new ones. Aim of the thesis was therefore the enhancement of the previously described properties and primarily the application of these modified new benzoporphyrin derivatives in optical oxygen sensing. However, as a result of the drastically altered photophysical properties of these indicator dyes, several other potential applications aroused.

This thesis is written in a cumulative manner, consisting of a theoretical background, three manuscripts (first author) published or prepared for submission in peer-reviewed journals, followed by a chapter of experiments on related topics and finally a conclusion of the whole work done within the thesis.

The theoretical background provides information on fundamentals of luminescence processes, the determination of important photophysical parameters as well as possible mechanisms for luminescence quenching. Moreover, this part contains the description of chemical sensors in general, with particular focus on optical sensors used for the determination of oxygen, temperature and glucose. Finally, an overview of existing red light excitable, NIR emitting indicators for optical oxygen sensing and other applications, focusing on benzoporphyrins is given. This knowledge is important for further basic understanding of topics dealt within the thesis.

Chapter 5 deals with the synthesis of highly soluble and photostable benzoporphyrin derivatives with drastically enhanced photophysical properties and significant bathochromic shift of absorption and emission spectra. These electron-deficient platinum(II) and palladium(II) complexes feature dual phosphorescence and unusually efficient thermally activated delayed fluorescence (TADF), enabling not only application as optical oxygen sensor, but also as sensitizer in triplet-triplet-annihilation (TTA) based upconversion and especially as dual sensor for oxygen and temperature sensing, the first time with a single emitter.

Chapter 6 introduces a new synthetic strategy for one step π-extension of the benzoporphyrins core via intramolecular bridging using the Scholl reaction. The resulting bridged platinum(II) compounds, with outstanding bathochromic shift of the absorption as well as the emission spectra, are then applied within a new concept for optical glucose sensing based on a single optode, initially enabling oxygen referenced quantification of glucose in one single spot.

Chapter 7 presents further possibilities of π-extension for existing benzoporphyrin complexes within one step by Suzuki or Sonogashira coupling reactions as well as Friedel-Crafts acylation. The resulting platinum(II) complexes show significant bathochromic shifts of the absorption spectra and increased quantum yields in the NIR region compared to standard benzoporphyrins. Their sensitivity to oxygen makes them promising indicators for in vivo applications; moreover they are perfectly suitable as sensitizer for TTA based upconversion allowing more efficient harvesting of red light.

Chapter 5
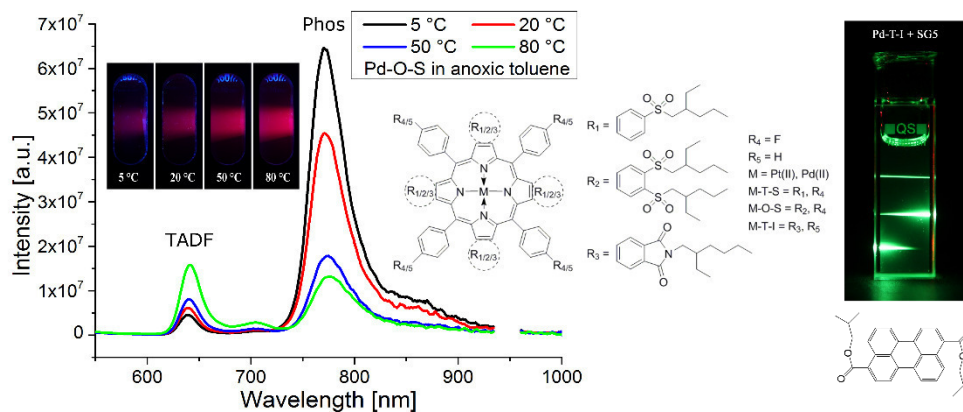
Chapter 6
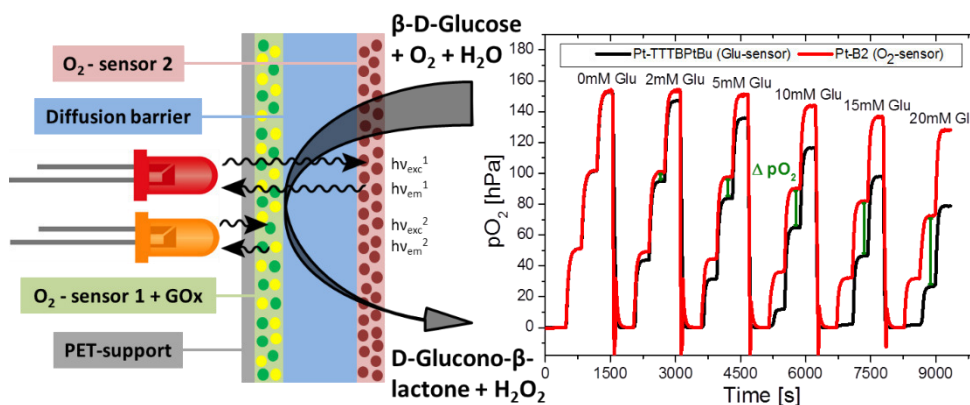
Chapter 7
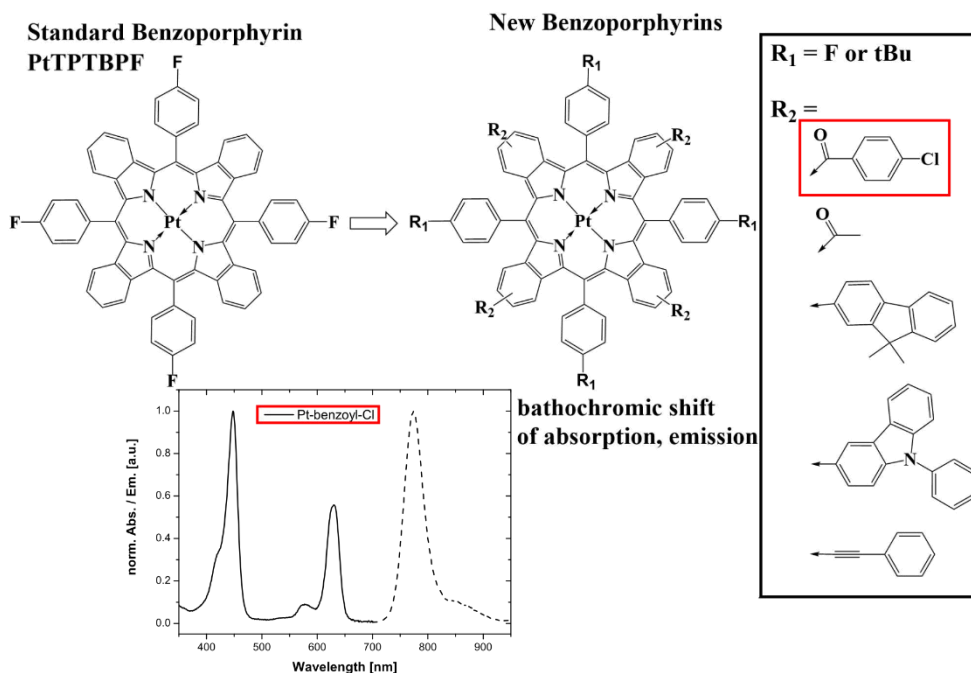
3 Theoretical Background

3.1 Fundamentals of Luminescence

This chapter as well as the following sub-chapters are based on references [1]–[4], others will be cited separately.

To understand the fundamentals of luminescence, it is important to know a little bit more about photons first. Photons are particles without mass or charge traveling with constant maximum relativistic speed, namely the speed of light, which is approximately $3*10^8$ m/s in vacuum. Due to this, their energy is not defined by mass times velocity but in fact by their frequency. And this frequency can now be transformed into energy and wavelength by using the following equation (1):

$$E = h * v = \frac{h*c}{\lambda} \qquad (1)$$

Here, E is the energy of the photon, h the Planck's constant, and v the wave frequency of the photons energy, which can be fragmented into c, the speed of light, and the wavelength λ. Thus, photons can be generated in various ways. One of the most common possibilities hereby, is the transition of an electron from a higher to a lower energetic level, whereby a photon is emitted. The term describing this de-excitation process or relaxation of electronically excited states of any organic/ inorganic substance to the lower lying ground state following the rules of the MO-theory, is called luminescence. A luminophore can therefore be defined as an atom or a group of several, acting as one unit during the emission process of light. The excitation of such an electron can be a result of various environmental influences, wherefore several types of luminescence have to be distinguished. In photoluminescence the molecule undergoes the transition from the ground state to the electronically excited state by absorption of light (photons of a certain wavelength).

3.1.1 Absorption

The absorption of photons (absorbance A) through matter is defined by the Lambert-Beer's law (equation (2)), which is described by the decadic logarithm of the ratio of the incident light intensity (I_0) to the intensity of the transmitted light (I) at a specific wavelength. The molar absorption coefficient ε, which is specific for a substance at a given wavelength, is independent on the optical path length (d) through the sample as well as on the concentration (c) of the absorbing species in the solution.

$$A = \log \frac{I_0}{I} = \varepsilon * c * d \qquad (2)$$

Since Lambert-Beer's law doesn't take the possibility of other influences like scattering effects in the media, re-emission of light or various molecular interactions into account, it can only be applied for highly diluted samples with only marginal turbidity.

The process, in which an electron of a molecule is raised from the most stable ground state, with the lowest energy, to an energetically higher excited state, by absorption of a photon, is extremely

fast and takes place in about 10^{-15} s. Due to the fast movements of the electrons compared with the heavy nuclei, the atoms can be regarded stationary, according to the Born-Oppenheimer approximation. Moreover, the Frank-Condon principle assumes that electronic transitions take place without any change in the position of the nuclei of the atoms, which means that the distance in the ground as well as in the excited state is virtually the same.

In absorption and fluorescence spectroscopy, transitions between two types of orbitals are from great importance and these are the LUMO (lowest occupied molecular orbital) and the HOMO (highest occupied molecular orbital), in respect to the ground state, due to the fact that here the transition energy is the smallest. Therefore, the absorption of a photon typically leads to electronic excitation from the vibrational ground state (in the electronic ground state) to a transition in the excited vibrational state of the excited electronic state. An electron or a molecule in this state has a great variety of potential relaxation pathways; returning radiative or non-radiative to the ground state or being transformed into another species. All of the possible transitions can be well explained with a Perrin-Jablonski diagram (figure 3.1).

3.1.2 The Perrin-Jablonski Diagram
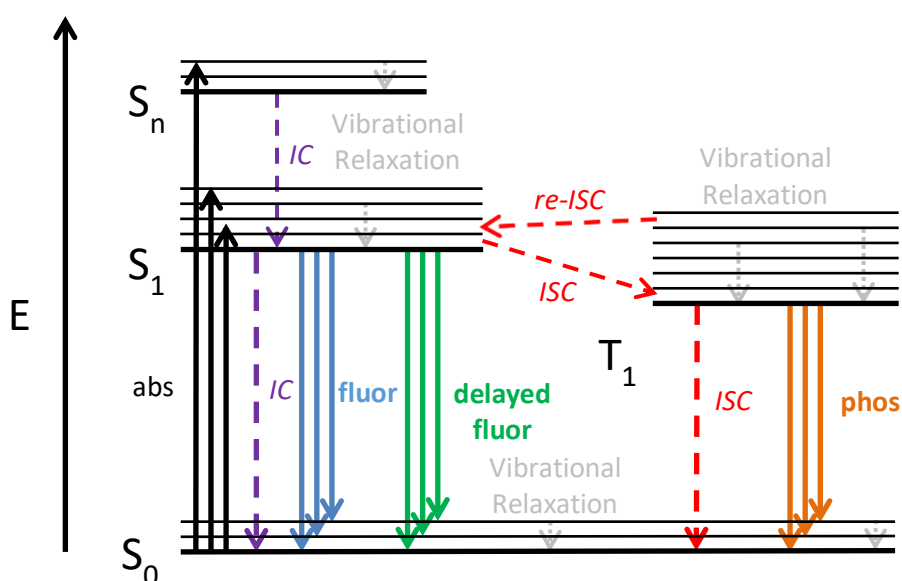
Figure 3.1 The Perrin-Jablonski diagram illustrating possible processes of a luminophore between excitation & emission of light

In the Perrin-Jablonski diagram (figure 3.1) the solid horizontal lines illustrate possible energy states (thick lines) and the vibrational states (thin lines) of an electron or molecule, while dotted arrows show non-radiative and straight arrows radiative processes. Here S_0 is the ground state, whereas S_1, S_n and T_1 represent the excited singlet and triplet states, respectively. According to Hund's rule the triplet state is energetically lower than the singlet state. Note that usually both excitation and emission always start at the vibrational base level of its state, either ground or excited state. Reason therefore is the fact that changes between vibrational levels are much faster than transitions between states.

Electronic transitions can generally just occur when the spin multiplicity during the excitation does not change. Accordingly, only singlet-singlet and triplet-triplet transitions are quantum-mechanically allowed, while singlet-triplet transitions are forbidden due to the changing spin. However, this phenomenon is still observed due to spin-orbit-coupling, which describes the interaction of magnetic fields resulting from the electron's orbit and its spin. Spin-forbidden transitions are favored in presence of heavy atoms (with a large atomic number), at low temperatures (where collisions with solvent molecules are prevented) and when the molecule is embedded in solid or rigid matrices (e.g. polymers).

3.1.3   Non-Radiative De-Excitation Processes

Internal Conversion (IC)

Internal conversion is a non-radiative transition between two states with the same energy, without a change in spin multiplicity. IC usually takes around 10^{-11} to 10^{-9} s and is mostly ensued by vibrational relaxation (thermal dissipation or collision with other molecules) to its vibrational ground state. Depending on the energy gap between the two involved electronic states, IC can be efficient from S_2 to S_1, but due to the larger energy gap is less efficient between S_1 to S_0, wherefore it can compete with fluorescence, inter system crossing and even phosphorescence.

Intersystem Crossing (ISC)

ISC is a non-radiative transition between two iso-energetic vibrational levels of different spin multiplicity, namely S_1 and T_1. This transition has a time scale of 10^{-7} to 10^{-9} s, is commonly an intermediate step on the de-excitation pathway and followed by vibrational relaxation to the ground state of T_1. Even though ISC is principally forbidden, its probability can be increased via spin-orbit-coupling in the presence of heavy atoms, as mentioned above.

3.1.4   Radiative De-Excitation Processes

Fluorescence

The emission of photons, as a result of the transition between two singlet energy states, from S_1 to S_0 (with some exceptions) is defined as fluorescence and its characteristics are therefore independent of the excitation wavelength. Although fluorescence happens actually within a time scale of 10^{-15} s (as fast as absorption of a photon), the molecule remains for a certain time in the excited singlet state (typically 10^{-10} to 10^{-7} s), before relaxing to a less vibrationally excited state of the singlet electronic ground state. Due to this effect, the energy gap between the initial and the final state of the transition is reduced and a bathochromic shift (shift to longer wavelengths) between the absorbed and emitted photons is observable, which is generally known as the Stokes

shift. However, the opposite effect is also possible, due to the energy distribution according to Boltzmann, resulting in a hypsochromic shift of the fluorescence. Since both processes, absorption and fluorescence, show a similar spacing of the vibrational levels (in excited and ground state), following the Frank-Condon principle, fluorescence appears like a mirror image of the absorption peak.

Phosphorescence

Phosphorescence describes the relaxation from the excited triplet state, accompanied by emission of photons, into a state with changed spin multiplicity, typically a transition from T_1 to S_0. These emitted photons show even higher bathochromic shift, due to fact that the excited triplet state is energetically even lower than the excited singlet state. The transition is again spin forbidden, but can be rendered possible due to spin-orbit-coupling. However, in solution or higher temperatures phosphorescence competes with reverse- and intersystem crossing and subsequent vibrational relaxation. At low temperatures or if the molecule is embedded in a rigid matrix, the probability for phosphorescence can be significantly increased. Due to the long-lived and stable triplet energy state, the lifetimes of phosphorescence are in the time scale of 10^{-6} up to several seconds and sometimes even minutes.

Reverse-Intersystem Crossing and Delayed Fluorescence

As can be seen in the Perrin-Jablonski diagram (figure 3.1), the transition of a molecule from the excited triplet state T_1 to the excited singlet state S_1, called a re-ISC is generally possible via thermal activation, followed by all possibilities for further transitions such as fluorescence or IC. Re-ISC can be achieved as long as the provided thermal energy for this transition is sufficient (highly temperature dependent), the energy gap between the singlet and triplet states is appropriate and the lifetime of the excited triplet state is long enough. The resulting fluorescence is called E-type (first discovered with eosin) or thermally activated delayed fluorescence (TADF) and demonstrates characteristic spectral properties like fluorescence, but shows a prolonged lifetime and as mentioned high temperature dependency.

Another type of delayed fluorescence is the P-type (first discovered with pyrene). This phenomenon is not subsequent to re-ISC but refers to a process called triplet-triplet-annihilation (TTA), which originates from a bimolecular process (collision of two molecules) in the excited triplet state T_1, occurring in concentrated solutions. While one of those collided molecules returns via non-radiative transition to the ground state S_0, the other has sufficient energy to return to the excited singlet state S_1, from where on emission of photons takes place. TTA is strongly dependent on the excited triplet state concentration as well as lifetime and is characterized by a quadratic dependence of the excitation light intensity and a halved decay time constant compared to delayed fluorescence without TTA.

Triplet-Triplet-Annihilation based upconversion

A system for TTA based upconversion is composed of two main components, a sensitizer and an annihilator molecule, both (metal) organic dyes, with matching energy levels of the excited triplet state (energetically lower triplet state of the annihilator; figure 3.2).
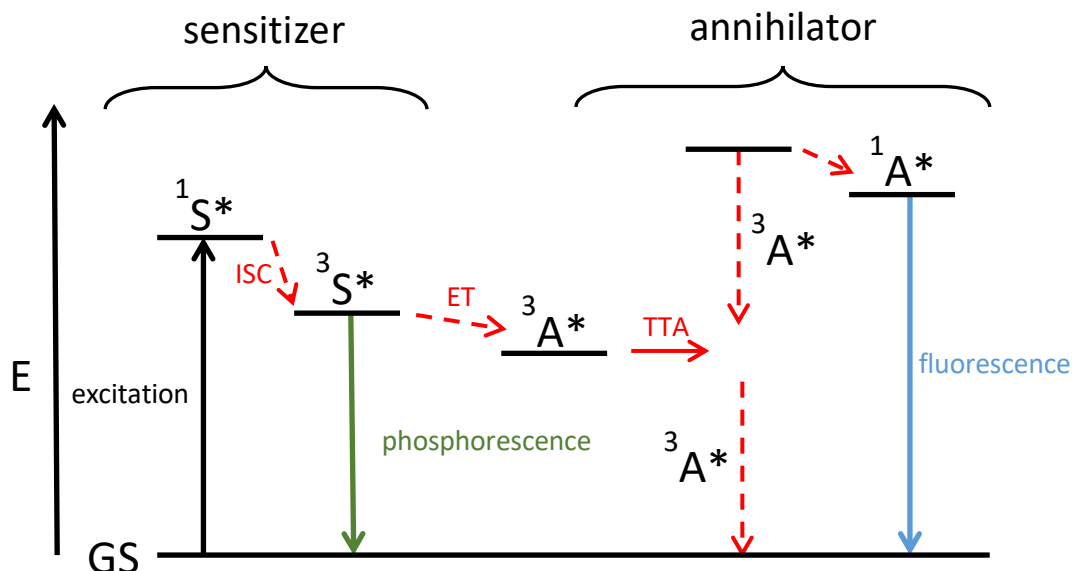
Figure 3.2 Schematic Jablonski diagram illustrating the process of TTA based upconversion

First, the sensitizer has to be excited (absorption of low energetic light), resulting in the population of the singlet excited state, followed by subsequent ISC, which is facilitated in the presence of heavy atoms, to the excited triplet state. Due to the high concentration of the dyes and the long lifetime of the sensitizer molecule, the energy from the latter is transferred to the annihilator, within an energy transfer reaction (ET; usually a Dexter process), requiring contact of the two components. As a result from the ET the excited triplet state of the annihilator molecules is populated. Subsequent collision of those, leads to the promotion of one annihilator in the excited singlet state, followed by emission of (upconverted) fluorescence (higher energy as excitation light), while the other undergoes non-radiative transition to the ground state (following the spin statistic law; figure 3.2). Contingent on the fact, that oxygen effectively quenches triplet states, it should be removed from the system. Important photophysical parameters, concerning sensitizer and annihilator molecules, enabling efficient TTA based upconversion are described in more detail in 3.3.2.

3.1.5 Quantum Yields

The quantum yield describes the efficiency of the radiative processes (fluorescence or phosphorescence) after excitation of an electron or molecule and its return back to the ground state. It is defined as the ratio of emitted photons to absorbed photons and can be close to unity if the radiative pathway, mostly fluorescence, is dominating over the non-radiative processes such as IC or ISC. The correlation of all these processes can be seen in equation 3 to 5:

$$\Phi_F = \frac{k_r^S}{k_r^S + k_{nr}^S} = k_r^S * \tau_S \qquad (3)$$

$$\Phi_{ISC} = \frac{k_{ISC}}{k_r^S + k_{nr}^S} = k_{ISC} * \tau_S \qquad (4)$$

$$\Phi_P = \frac{k_r^T}{k_r^T + k_{nr}^T} * \Phi_{ISC} \qquad (5)$$

Here, k_r is the rate constant for the radiative processes of the respective energy state, while k_{nr} represents the overall non-radiative rate constant and τ the lifetime of the respective energy state. Quantum yields are very easily affected by interaction with other molecules (collision with various quenchers) or generation of ground state complexes. Furthermore, other parameters like pH, polarity but also viscosity can have a serious impact too. However, quantum yields and lifetime are by far most effected by the higher efficiency of non-radiative processes in relation to thermal agitation (collisions with solvent molecules as well as intermolecular vibrations and rotations) at higher temperatures.

The determination of quantum yields can be performed experimentally on two different ways; relatively to a compound with known quantum yields or absolutely by using the integrating sphere. In case of the relative approach, the emission spectrum (maximum at similar wavelengths) of the known compound has to be obtained first, followed by the measurement of the target compound with exactly the same settings. The quantum yield can then be calculated from equation 6 [5]:

$$\Phi_f^i = \Phi_f^S * \frac{1 - 10^{-A_S(\lambda_{ex})}}{1 - 10^{-A_i(\lambda_{ex})}} * \frac{\int_{\lambda_{em}} F^i(\lambda_{em})}{\int_{\lambda_{em}} F^S(\lambda_{em})} * \frac{n_i^2}{n_S^2} \qquad (6)$$

Where, Φ_f^i is the quantum yield of the sample and Φ_f^S the quantum yield of the known standard. While A_x is the absorption at the respective wavelength λ_{ex}, $F^x(\lambda_{em})$ represents the integral fluorescence and n_x resembles the refractive indices of the used solvents for the sample and the standard.

Absolute determination of the quantum yields is performed with an integrating sphere, also called Ulbricht's sphere. The walls of this spherical cavity are coated with diffuse, highly reflective material generating numerous diffuse scattering processes with the incident light, destroying any spatial information while still preserving its intensity. Overall four measurements have to be acquired; intensity spectra of the absorption as well as the emission with and without the sample (using a blank instead). Finally, the absolute quantum yields can be calculated from equation 7 by integrating and subtracting the received data:

$$\Phi = \frac{E_c - E_a}{L_a - L_c} \qquad (7)$$

Where L_a and L_c are the terms of the integrated excitation profile from the integrating sphere with the blank and the sample, E_a and E_c are the integrated luminescence from the blank and the sample from the integrating sphere.

While accurate determination of fluorescence quantum yields doesn't pose a problem, quantification of phosphorescence quantum yields in the NIR region is quite challenging, as evidenced in literature. The reported values of several compounds demonstrate variations by a factor of 3-4 or more, even when established under similar conditions. [6] Besides an incorrect

calibration of the detectors (inadequate correction of the spectral sensitivity of the photomultipliers), the usage of various reference materials and the poor availability of suitable NIR luminescent standards plays an important role. Moreover, the sensitivity of most photomultipliers in the NIR region is known to be rather low. [7] Contingent on the long lifetime of those compounds, an anoxic atmosphere has to be ensured over the whole course of the experiment, due to the high probability of quenching by molecular oxygen. As a result, quantum yields of respective compounds can obviously be regarded as standard values but nevertheless have to be challenged.

3.1.6 Lifetime

When a molecule reaches the excited energy state, after excitation by a short pulse of light, it has several possible radiative but also non-radiative pathways for de-excitation, which can both be described by first order kinetics (equation 8). In the case of radiative transitions (fluorescence or phosphorescence), relaxation doesn't happen immediately but after a certain time span, which is known as the excited state lifetime. Since these are statistical values and refer to the average time of the molecules in the respective excited state before emitting a photon, a large number of molecules is needed to determine the lifetimes confidentially.

$$-\frac{d[A^*]}{dt} = k * [A^*] \qquad (8)$$

While [A*] is the concentration of species A in the excited state, k is the sum of all possible de-activation rates (radiative and non-radiative). Subsequent integration of this equation 8 using the following definition for the excited state lifetime τ (equation 9):

$$k = \frac{1}{k_r + k_{nr}} = \tau * t \qquad (9)$$

Results in equation 10:

$$[A^*]_t = [A^*]_0 * e^{-t/\tau} \qquad (10)$$

Regarding equation 10, the intensity of fluorescence decreases, if species A is no longer excited. In short, luminescence lifetime is defined as the time span in which 63% of the excited electrons relax back to the ground state S_0. Depending on the decay time of the molecule, different dynamic phenomena like collisional quenching are possible.

Determination of the excited state lifetimes of luminophores can be done with different methods either in frequency domain via phase-fluorimetry or in time domain via single-photon-counting (SPC; figure 3.3). In phase-fluorimetry the molecule is excited by sinusoidally modulated light of a certain frequency. This excitation leads to harmonic response (partially demodulated in respect to the excitation) of the molecule, which is again sinusoidally modulated at the same frequency but delayed in phase. Determination of the phase shift (ϕ), which is related to the lifetime of the luminophore according to equation 11 and 12, allows the calculation of the lifetime τ, over the angular frequency ω and frequency f respectively (figure 3.3).

$$tan(\phi) = \omega * \tau_{\phi} \qquad (11)$$

$$\omega = 2 * \pi * f \qquad (12)$$

However, it has to be noted that the above defined equation 11 is only valid for mono exponential decay behavior and should therefore in case of doubt be compared with the results of a lifetime measurement in time domain (figure 3.3).

As observable in figure 3.3, within a measurement in time domain the molecules are excited by a pulse or steady irradiation. The decay curve is recorded in real time when the excitation source is switched off. The resulting decay curve can then be subsequently fitted to obtain the lifetime of the molecule. While measurements in the time domain are truly not affected by excitation light changes and enable simple detection of multi-exponential behavior, determination of the lifetime in frequency domain (via phase-fluorimetry) is affected at high excitation intensities [8] but nevertheless much easier to perform, regarding the effort concerning the utilized devices.
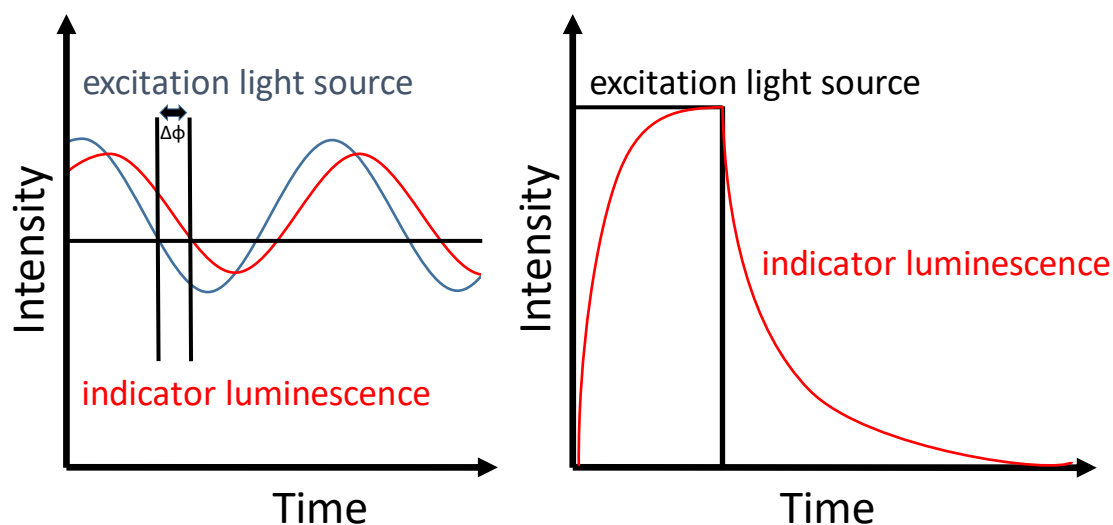
Figure 3.3 Schemes of lifetime measurements in frequency domain (left) and time domain (right)

3.1.7   Luminescence Quenching

The term of luminescence quenching describes a process in which the intensity (and sometimes even the lifetime) of a luminophore is reduced, due to various intermolecular photophysical events such as collisions, electron or energy transfer, excimer formation et cetera. During these interactions the luminophore is not destroyed or chemically altered, as e.g. in photobleaching, but just follows a new reversible non-radiative de-excitation pathway. While in the case of static quenching the transition of the luminophore to its excited state is prevented, dynamic quenching leads to a non-radiative relaxation from the excited to the ground state (figure 3.4).
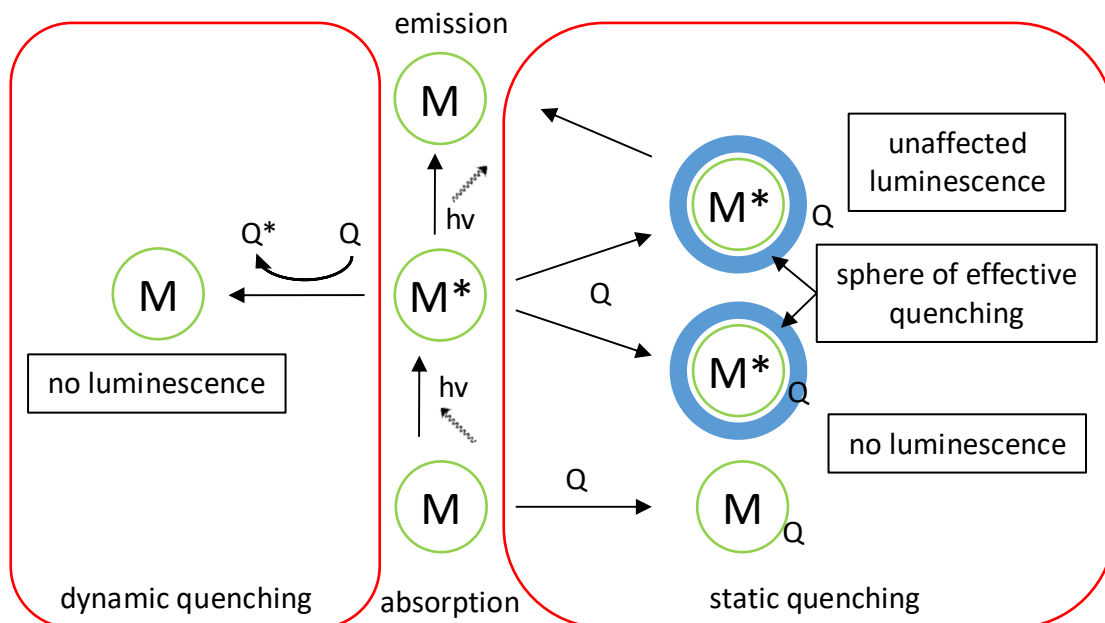
Figure 3.4 Illustration of the processes for static and dynamic quenching

Static Quenching

Generally static quenching (figure 3.4), which can be distinguished in two different mechanisms, occurs if the quencher is present in very high concentration and due to the close proximity, has a high probability to react with the luminophore. This can lead either to the formation of ground state non-fluorescent complexes, or to quenching, caused by a sphere of effective quenching according to Perrin (figure 3.4). Here the luminescence of the luminophore is quenched, but only if the quencher is inside a certain sphere of the excited molecule. In both cases static quenching leads to a decrease in concentration of the free luminophores, reducing the luminescence intensity, but not the excited state lifetime, since molecules in its excited state are not affected by the quencher.

Dynamic Quenching

In dynamic or also called collisional quenching (figure 3.4), the luminophores and the quencher collide with each other, leading to an energy transfer from the excited luminophore to the quencher and subsequent non-radiative decay of the luminophore. Since this type of quenching is diffusion limited (and also time dependent), it requires sufficient long lifetimes of the luminophore, as well as surrounding media with sufficiently low viscosity, to enable unrestricted movement of the quencher. This type of quenching affects not only the luminescence intensity of the luminophores but also proportionally their lifetime, cause all molecules are likely to collide with the quencher during their excited state lifetime. The phenomenon of dynamic quenching with oxygen constitutes the basis of an optical oxygen sensor, as will be explained later in 3.2.2.

Stern-Volmer-Equation

The Stern-Volmer equation 13 can be used to illustrate both quenching phenomena (figure 3.4), simply describing the change of the luminescence intensity (I) and the lifetime (τ) in presence of quencher $[Q]$ to the intensity / lifetime without the quencher I_0, τ_0.

$$\frac{I_0}{I} = \frac{\tau_0}{\tau} = 1 + K_{SV} * [Q] = 1 + k_q * \tau_0 * [Q] \qquad (13)$$

The Stern-Volmer constant K_{SV}, is the combination of k_q and τ_0, which depends on the environment of the luminophore, the temperature as well as sterical factors and directly defines the sensitivity of a luminophore to a specific quencher.

It is noteworthy to mention that the Stern-Volmer relation describes an ideal system and should result in a linear relation with K_{SV} as the slope, when plotting experimental data of $\frac{I_0}{I}$ versus [Q]. However, a real calibration can deviate from this theoretical behavior for many reasons, such as e.g. a bi-exponential decay instead of the expected mono exponential decay. While addition of static quenching would lead to an upward curvature of the line, luminescence quenching in an inhomogeneous system (with multiple K_{SV} values) would show a downward curvature. The latter effect can be often observed, when a luminophore is embedded in a polymeric matrix, resulting in possible microheterogeneities, that no longer demonstrate a mono exponential decay behavior. Therefore a variation of the Stern-Volmer equation, the two site-model, [9] was developed.

The two-site-model (equation 14) assumes location of the luminophore in two microenvironments, with different quenching properties, instead of one homogenous environment.

$$\frac{I}{I_0} = \frac{f}{1+K_{SV1}*[Q]} + \frac{1-f}{1+K_{SV2}*[Q]} \qquad (14)$$

Here, K_{SV1} and K_{SV2} are the Stern-Volmer constants for the two microenvironments (f = factor for the distribution of the luminophore). Although this model involves some simplifications, it is in most cases well suitable for fitting experimental data of luminophores embedded in various polymers. [9]

3.2 Chemical Sensors

This chapter and the following sub-chapters are based on references [1], [10]–[15], others are cited independently.

"Chemical sensors are miniaturized devices that can deliver real time and on-line information on the presence of specific compounds or ions in even complex samples." (Cambridge Definition [13]) According to this definition, the task of a chemical sensor is the transformation of chemical information into an analytically interpretable signal. The two essential parts within such a device are the receptor and the transducer. While the receptor reacts to changes of the analyte, or even interacts with the analyte within the measurement system, the transducer converts the received data (chemical information) into a further processable signal. Chemical sensors can be based on various operating principles, such as electrochemical, thermometric, mass sensitive or optical etc. Independent on their measurement principle, some of the most important criteria that should be

fulfilled by a chemical sensor are a fast and reversible response to concentration changes of the analyte as well as high selectivity and sensitivity towards the respective species. Ideally a sensor should be a small low-cost device, that is user friendly and nevertheless demonstrate good stability regarding operational and shelf life. In recent time, more and more effort was put in the development of new chemical sensors resulting in a large variety of sensors with a wide range of measurement principles for almost all conceivable analytes. This thesis concentrates on optical sensors, which are based on the phenomenon of luminescence, with a special focus on optical oxygen sensors and the associated versatile applications.

3.2.1 Optical Sensors

The main components of an optical sensor are obviously, the same as in a chemical sensor, namely the receptor and the transducer. The signal transduction in an optical sensor is based on the change of optical properties like absorption, luminescence (fluorescence and/or phosphorescence), optothermal effect, light scattering, refractive index, Raman spectroscopy and many more.

In the case of a luminescence based optical sensor setup (figure 3.5), the sensor is typically build up by the following components. One important components in such a sensor system is the excitation source, which generally enables the luminescence phenomenon. The light source of choice is in most cases a LED, due to its low costs and great variability concerning the selection of the excitation wavelength. Since light is used to transport the information, optical fibers are also part of the setup. Another component, is the sensing material (receptor), which is in direct contact with the analyte and reacts to its changes. For quantification of the received signal a (photo-) detector (transducer), mostly a photodiode, is needed. Additional optical elements like filters, which are often placed between the receptor and the transducer, to cut off interfering signals and to enable better wavelength selection, or lenses, to focus the guided light for an increase of the obtained signal, can be also part of the optical setup.
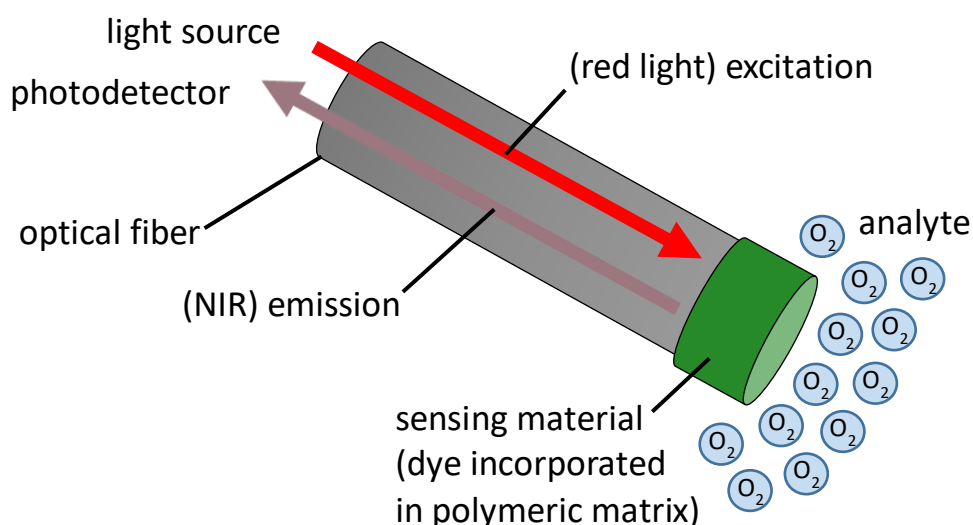

Figure 3.5 Scheme of a luminescence based optical sensor setup (e.g. for oxygen)

The setup of an optical sensor combined with its luminescence based measurement principle gives rise to several advantages over other sensor systems, such as electrical or electrochemical sensors, which often require a reference electrode. This circumstance makes optical sensors not only robust against electromagnetic impacts, but enables also miniaturization, decrease of production costs and increase of user friendliness. Another big advantage is, that in optical sensors the information is transmitted by light, allowing complete separation of the sensing and the read out device (almost / non-invasive remote and contactless sensing). The fact that receptor and the rest of the optical sensor can be physically separated, simplifies not only requirements for the buildup of the remaining components but also enables measurements under sterile or even harsh conditions such as high temperatures and pressures, toxic, corrosive or in chemically aggressive environments. Besides all these advantages optical sensors have to fulfill similar demands as already described above in 3.2. High selectivity to the analyte, reversibility and stability, but especially the sensitivity plays an important role, due to its effect on the dynamic range, detection limit as well as resolution of the sensor. Depending on the application of the sensor, the response time (t_{90}) can also be from great importance, particularly when applied for real-time analysis.

3.2.2 Optical Oxygen Sensor

An optical oxygen sensor is generally build up as described in 3.2.1 and figure 3.5, with the supplement that the above mentioned sensing material, is sensitive to oxygen (quencher). The working principle of optical oxygen sensors based on the phenomenon of luminescence relies on dynamic quenching of the luminophore by oxygen, as depicted in 3.1.8. This type of quenching is dependent on collision of the luminophore and the quencher; it's therefore a diffusion limited process, decreasing both the luminescence intensity and lifetime. During the collision of the luminophore in its excited energy state and oxygen, in its ground state (triplet state), the energy is passed on to oxygen within an energy transfer reaction between these two molecules. As a result, the luminophore returns back to its ground state, in a non-radiative transition, while oxygen is excited to its first excited singlet state. Although oxygen in its excited singlet state can undergo the previously described processes, radiative or non-radiative de-excitation, it should be noted that singlet oxygen is an extremely reactive species, which easily reacts or oxidizes electron-rich organic compounds and therefore can also chemically de-activate within a reaction. [2]

Influences on Sensitivity

The before mentioned oxygen sensitive material usually consists of an oxygen sensitive dye (luminophore), which is incorporated in an oxygen-permeable polymeric matrix. The luminescent indicator can be either physically embedded or chemically attached (e.g. covalently bound) to the respective polymer. The task of the matrix is not only to prevent the dye from leaching out into the environment outside the polymer, but also to maintain the desired concentration of the dye as well

as a defined environment. Moreover, the matrix should prevent aggregation of the incorporated luminophores and also be a physical and chemical barrier to counteract penetration of unwanted compounds. Properties of the respective matrix can also help to gather emission light, prevent from biofouling and increase chemical but also oxidation stability. However, the key factor of the matrix and with it, its highest priority, is the permeability towards oxygen, since this is one of the two factors that directly affect the sensors sensitivity (equation 15 and 16). The second crucial parameter concerning the sensitivity towards oxygen is the excited state lifetime of the dye; the longer the lifetime, the higher the probability of quenching by oxygen, resulting in a higher sensibility of the sensor (equation 15).

$$K_{SV} = \tau_0 * k_q \qquad\qquad (15)$$

$$Sensitivity \propto \tau_0 * P \qquad\qquad (16)$$

Here, P is the permeability of the polymeric matrix and τ_0 is the lifetime of the embedded dye in absence of oxygen (quencher). According to the following equation 17, P is described by the diffusion coefficient D and the solubility S of the quencher (oxygen). [16]

$$P = D * S \qquad\qquad (17)$$

Although the solubility of oxygen in most polymeric matrices is similar, and thus has no strong impact on the sensitivity, this parameter should be considered as well. The diffusion in a polymeric matrix, however, has a great influence on the sensitivity since the quenching mechanism is diffusion controlled. Higher diffusion will directly lead to an increased quenching constant k_q resulting in an increased sensitivity of the dye towards oxygen. [17] While polystyrene is commonly used as model matrix for oxygen sensors, allowing comparison to already existing dyes, polymethylmethacrylate is also often a matrix of choice. For the design of trace oxygen sensors, not only dyes with long lifetimes are necessary, but also polymers with high permeability, such as polydimethylsiloxane, ormosils or various silicones.

Sensor Characteristics

Disregarding of how well-considered the selection of the dye and the polymeric matrix could possibly be, optical oxygen sensors tend to deviate from their ideal behavior in several ways (see below), which should be kept in mind. [18]

One of those problems concerns their stability; it is known that sensors can show degradation and chemical aging over longer periods of use. Another point is their sensitivity towards photobleaching (alteration of the dye due to illumination). Of special interest is here the environment of the dye (photobleaching in solution strongly depends on the used solvent) and of the energy state of the molecule (the excited state might be more prone to chemical reactions), especially when in contact with in situ generated singlet oxygen. A less significant factor concerning oxygen sensors, is the cross sensitivity to other quenchers, which could possible interfere the determination of oxygen. However, the most important deviation from its ideal behavior, that has to be considered, is definitely the temperature crosstalk, which affects virtually every optical sensor. This is due to some

photophysical properties concerning the sensor system itself, like varying oxygen diffusion speed as well as changing probabilities of non-radiative decay pathways at different temperatures. [18]

Sensing Methodologies

The influence of oxygen on the concentration of the dye molecules in the excited triplet state enables the determination of two read-out parameters; the luminescence intensity as well as the luminescence lifetime. Determination of the oxygen concentration directly by measuring the luminescence intensity is difficult, due to many influential factors such as varying dye concentration, photobleaching, scattering effects, intensity fluctuation of the excitation source et cetera. A ratiometric approach (usage of a second dye, excitable at the same wavelength with distinguishable emission characteristic, which is not quenchable by oxygen as reference in the same matrix) can eliminate some problems but cannot compensate for leaching or photobleaching of the oxygen sensitive dye and additionally introduces drift in case of leaching or photobleaching of the reference. Detection of the oxygen concentration via lifetime based measurements, however, enables elimination of all major drawbacks of intensity based oxygen determination. As already explained in 3.1.7, lifetime based measurements are either possible in time or in frequency domain, whereas the setup for the latter is easier to use and more compact for field trips and therefore more commonly applied.

In 3.3 a more detailed overview of metalloporphyrins applied as optical oxygen sensor is given.

3.2.3   Optical Temperature Sensors

Besides oxygen, temperature is possibly the most fundamental parameter in science history, where measurement by optical means plays also a very important role, emphasizing its big importance in sensor technology. Sensing temperature has an enormously wide field of applications ranging from aerodynamics, over biology and chemistry to medicine and military technology as wells as in the storage of food and other goods. Similarly huge is the number of different types of thermometers used for the various applications and also their different working principles, starting with liquid-filled glass thermometers on the basis of thermal expansion of different materials. Alternatives include manometric thermometers (investigating pressure as a function of temperature), resistance (of metal conductors) thermometers or thermoelectric thermometers based on the Seebeck-effect. [19] In recent years, the trend is fortunately away from liquid-filled thermometers, due to environmental and health issues, towards non-toxic and easy to use thermoelectric thermometers, which on the contrary demonstrate other drawbacks like the necessity of being linked to the sensor at the sampling site, vulnerable when applied in harsh, corrosive environments as well as interference from electromagnetic fields. Although all, so far mentioned, different types of thermometers have their pros and cons in variable ways for different applications, almost all share one, not unimportant drawback, and that's the inability of being easily miniaturized and therefore not suitable for

investigation of temperature with a spatial resolution of <10 µm (e.g. inside cells).

This demand can easily be accomplished by optical sensing, which furthermore offers the possibility of contactless measurement of temperature and large-scale imaging. Also here several optical methods, which can further be subdivided in active and passive optical imaging techniques, such as thermal reflection, absorption, Rayleigh and Raman scattering but also luminescence exist. The latter has attracted much attention in recent years and is almost solely based on the usage of luminescent molecular probes and nanoparticles, which can both be incorporated in the respective sample (also in cells) or deposited on its surface.

The group of molecular probes can be classified into organic compounds, metal-ligand complexes and lanthanide complexes. One prominent, long-known representative of organic compounds is the family of rhodamine and its derivatives. These fluorophores are characterized by high brightness, low costs and are excitable in the visible range. The luminescence of e.g. rhodamine B is highly temperature dependent [20] in the range from 273 to 373 K, making this fluorophore highly suitable for sensing temperature in microfluidic, [21] cells [22] as well as planar sensor films. [23] Besides fluorescence, also the phenomenon of (thermally activated) delayed fluorescence (TADF) has been used for optical thermometry successfully as shown by Fister et al. [24] Here, acridine yellow was incorporated in a rigid saccharide glass, investigating the TADF/phosphorescence intensity ratio, which features sensitivity to temperature in the range of 223 to 323 K. Moreover, temperature dependency of TADF from fullerene C_{70}, embedded in polymer films (in absence of oxygen) at temperatures higher 293 K was observed. [25] Recently, Steinegger et al. reported carbazole-substituted dicyanobenzenes and anthraquinone based intramolecular charge-transfer dyes with very high temperature dependency of the TADF decay times in the range of 278 – 323 K. [26] Contingent on the long lifetime of these TADF emitters, but also those of phosphorescent metal-ligand complexes, these dyes are prone to oxygen quenching. To overcome this cross-sensitivity, they need to be incorporated into polymers with low oxygen permeability when used as temperature probe. Appropriate polymers, hardly permeable to oxygen, would be poly(vinyl chloride), poly(vinyl alcohol), poly(styrene acrylonitrile), but particularly polyacrylonitrile (PAN), due to its low water uptake and therefore shielding ability towards changes in pH. [27]

The class of metal-ligand complexes demonstrates moderate brightness, absorption in the visible region of the spectrum, lifetimes in µs range and most importantly large Stokes shifts, enabling easy separation of scattered excitation light. Here, the group of polypyridyl complexes, mostly with ruthenium or iridium as central atom, embedded in PAN or poly(vinyledene chloride-co-acrylonitrile) are one of the most typically used probes for measuring temperature. Ir(ppy)$_2$(carbac) dissolved in PAN for instance, displays especially high sensitivity to temperature, low cross-sensitivity to oxygen and linear dependency of intensity and lifetime over a wide range (274 – 323 K), but unfortunately low molar absorption coefficients. [28] Additionally, cyclometallated platinum complexes as well as platinum porphyrins, which are more closely examined in 3.3, since these complexes are well-known and commonly used as oxygen indicators, were investigated as temperature sensing probes. Other members of this group, which show thermochromic shifts of the luminescence,

include polynucleic metal complexes of mostly Cu(I) but also Ag, Au and Pt. [29], [30] Luminescent lanthanide containing chelate complexes (mostly β-diketonate ligands), particularly with europium(III) [31] and terbium (III) as central atom, are another often used group of molecular probes for determination of temperature. These compounds display even longer lifetimes up to 2 ms, larger Stokes shifts, sharp emission bands but only moderate brightness. Their thermosensing performance can further be improved by introduction of lanthanide ions into coordination polymer frameworks. [32] Besides molecular probes, diverse nanomaterials, divided in quantum dots, metal clusters, nanoparticles and nanogels, as well as bulk materials based on phosphor, lanthanide-doped or upconversion bulk materials have demonstrated high sensitivity to temperature, contributing to the big success of optical probes in this field.

Sensor Characteristics

Generally one has to admit, that actually almost all luminophores demonstrate temperature dependent characteristics of emission properties, which is due to the Boltzmann distribution. [3], [33] Nevertheless far from all possess the desirable photophysical properties (explained later on) to be suitable as optical temperature sensor. Reason for this temperature dependence, is the higher efficiency of non-radiative de-excitation pathways as well as the increased thermal agitation leading to collisions of/with surrounding molecules providing further energy for transitions at elevated temperatures. The rate of the non-radiative transitions (k_{nr}) can be put in relation to the temperature via the Arrhenius equation 18:

$$k_{nr} \sim e^{-\Delta E/kT} \qquad (18)$$

where ΔE represents the energy difference of the base level of the excited state and the overlap point of a potential non-radiative decay state and k the Boltzmann constant. Since k_{nr} is also part of equation 3-5 and 9, concerning the quantum yields and the excited state lifetime, these parameters are evidently affected as well. Moreover, the sensing methodologies of temperature sensors are accordingly the same to those of oxygen sensors described in 3.2.2, with the supplement of anisotropy based measurements as an additional method of read-out.
Finally, the desirable photophysical properties for an optical temperature sensors include high sensitivity and brightness (high molar absorption coefficient and quantum yields), increased photostability and a bathochromic shift of absorption and emission wavelength (lower background of fluorescence in samples).

Dual Sensors for Oxygen and Temperature

As described in chapter 3.2.2 the response of optical oxygen sensors, similar to other chemosensors, is temperature-dependent and therefore needs to be compensated for. This can be done by different means. One possibility is the utilization of an external probe, such as for example a resistance thermometer. [14], [34] Unfortunately, this method suffers from poor spatial

resolution and is simply not suitable for a number of applications where oxygen and temperature have to be determined simultaneously, remotely and non-invasively, such as in food packaging and storage. [35] Alternatively, temperature compensation can also be obtained by using an optical temperature probe, which can be ideally even combined with the oxygen sensitive species to a dual sensor. [36]–[38] Applications for such dual sensors besides food industry include the area of microbiology (e.g. growth monitoring of various organisms) [39] as well as the reaction monitoring in chemical processes. [31]

While determination of oxygen as well as temperature by optical means (based on the phenomenon of luminescence) is well-established, simultaneous detection of these two parameters is not such an easy task. However, due to the increasing number of applications where simultaneous detection of oxygen and temperature is highly demanded, much effort was put in the development and design of dual sensors for these parameters. Such sensors generally consist of one luminescent probe for temperature sensing and a second luminescent complex for the quantification of oxygen. [40] While in earlier sensors, both probes featured excitation using a single wavelength, [31], [40]–[43] more recent systems display excitation of the two sensing indicators at two different wavelengths. [44], [45] In most dual sensing systems the two probes are dispersed in a single matrix [31], [44], [46], even though also concepts based dyes embedded in separate polymer layers exist. [42] The majority of existing concepts for dual sensors is based on measuring the lifetime of the luminescence signal, due to the various advantages (described in 3.2.2) compared to direct intensity based measurement. Read-out of the lifetimes is usually performed in frequency domain, even though approaches based on time domain exist as well. [42] Although numerous different systems of dual sensors exist, quantum dots, phosphors, europium(III) and ruthenium(II) complexes, are the commonly used temperature probes, while most oxygen sensitive probes are based on either ruthenium(II) complexes or various platinum(II) and palladium(II) porphyrins. [40], [47]

Independent of the used probes, all so far existing concepts of dual sensors suffer from some drawbacks, such as cross-sensitivity with respect to the analyte as well as optical and spectral cross-talk. Moreover, cross-leaching of the components and long response times in case of dual layer sensors can occur, whereas two indicators within one layer may display increased photodecomposition and signal drifts due to chemical interferences of the two probes. All these factors have a huge impact on the systems complexity and therefore often seriously hinder its performance. [48]–[50]

However, most if not all of the mentioned drawbacks could be overcome by utilizing one single probe, sensitive to both parameters, incorporated in a suitable matrix. In order to achieve exactly this, we took advantage of the unique dually emissive character (TADF and phosphorescence; figure 3.6) of our new dyes, to obtain the first time a sensing material enabling simultaneous and self-referenced sensing of oxygen and temperature with one single probe, which is subject of chapter 5. [7]
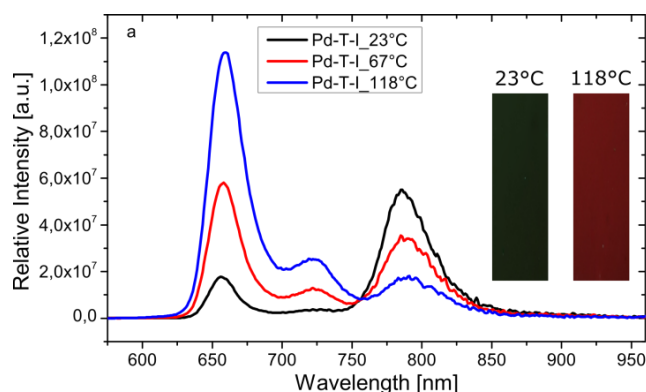
Figure 3.6 Temperature dependency of the emission spectra of Pd-T-I in polystyrene and photographic images at 23 and 118 °C upon excitation with UV-Lamp at 365 nm under anoxic conditions [7]

3.2.4   Optical Glucose Sensors

The quantification of glucose is without any doubt one of the most crucial analytical tasks of modern times and has therefore also attracted much attention in science community. Determination of this parameter is from great importance in various fields of research including biotechnology, biochemistry as well as in the food technology, but especially, and more than ever, in medicine, for the investigation of the glucose level in blood. Reason for this development is the ageing society, the world's growing population and the alarmingly increasing number of people with diabetes mellitus. Already in 2014, 8.5% of adults aged 18 years and older (422 million people) suffered from this disease. [51] Diabetes mellitus (inherited or acquired) is either characterized by the inability of insulin production of the pancreas, or by the inefficiency to use the produced insulin. Both types lead to a drastically increased concentration of glucose in blood and result in damage of nerves and blood vessels. [51]

Therefore, investigation of glucose in blood in general and particular focus on continuous glucose monitoring techniques (which when combined with an insulin pump act as artificial pancreas) has been and will be a topic of great importance in the future. Even though electrochemical methods are the most established ones nowadays concerning the glucose quantification,[52] optical sensing technology can still be an interesting alternative. Optical sensors display several advantages such as low production costs, simple design and handling and enable miniaturization. They are free of electromagnetic interferences, due to the use of photons instead of electrons, which is particularly interesting for patients with heart pace makers and in the field of cancer therapy. Moreover, optical sensors do not require a reference electrode and enable sterile remote sensing through the skin as well as simultaneous multiparametric measurement of various other analytes such as pO_2, pH, Na^+ and K^+.

Sensor Characteristics

Over the years several different optical schemes of sensing glucose have emerged, whereby the methods of surface plasmon resonance (SPR) and fluorescence accomplished the biggest success. In the following, the most important types for recognition of glucose are presented, with a special focus on enzymatic glucose sensors relying on the enzyme glucose oxidase. However,

selective recognition is the most crucial requirement for selective detection of glucose and this can be obtained by various means. While some use the recognition ability of particular enzymes, others utilize the capability of natural receptors such as apoenzymes or glucose-binding proteins or the affinity of glucose to lectins (concanavalin A).[53], [54] Another group is based on organic boronic acids [55] acting as molecular receptor for saccharides. However, the most widely used and commercially available approach is the recognition of glucose based on monitoring of the consumption (quenching) of oxygen during the enzymatic oxidation catalyzed by glucose oxidase (GOx) according to equation 19: [12], [56], [57]

$$\beta\text{-D-glucose} + O_2 \xrightarrow{GOx} \text{D-glucono-1,5-lactone} + H_2O_2 \qquad (19)$$

Alternatively, the formation of hydrogen peroxide could be of course measured as well. The usage of enzymes in general and with it the conversion of glucose into more easily detectable products, resulted in sensors demonstrating a very high selectivity for glucose over other saccharides.[56]

Oxygen sensors used as transducers in such enzymatic biosensors are well established and can be easily read out as described in 3.2.2, whereby mostly phase-fluorimetry is the method of choice. Unfortunately, the response of these type of sensors is affected by oxygen fluctuations in the sample (blood), resulting in a further, obligatory detection of the oxygen partial pressure. [58] In order to guarantee precise compensation of oxygen heterogeneities (e.g. in tissue), a close proximity of the glucose and the reference oxygen sensor is essential. [59] Despite, the slightly increased complexity of the composite glucose sensor, enzymatic glucose sensors based on oxygen optodes remain the most promising alternative to electrochemical sensors, due to the high versatility and robustness of these transducers.[34] Typical probes for usage as oxygen sensors as well as desirable photophysical properties are discussed in 3.3.2.

However, the proof of this concept was already demonstrated by Pasic et al. in 2007, [60] in which two fiber-optic oxygen sensors (one optode with immobilized GOx) were combined to a rather bulky hybrid sensor setup. Nacht et al. [61] presented a modified system in 2015 using NIR indicator dyes and a novel miniaturized phase-fluorimeter (called BiLuMOS) with integrated infusion catheter connected to an insulin pump. Despite all these improvements, complete separation of the emission signals from the indicators was not possible due to a certain overlapping of their absorption spectra. Moreover, the two sensors (glucose and oxygen reference sensor) were situated at different parts on the catheter, hampering accurate compensation of oxygen. To minimize the optical cross-talk we prepared a bridged platinum(II) benzoporphyrin derivative with a higher bathochromic shift (figure 3.7). We also realized a new sensing concept, in which both oxygen indicators are located in different layers of one sensing element (optode), only separated by the enzymatic layer and a diffusion barrier, enabling quantification of glucose by determination of ΔpO_2 in one single spot (figure 3.7). This topic is fully covered within the second publication in chapter 6. [62]
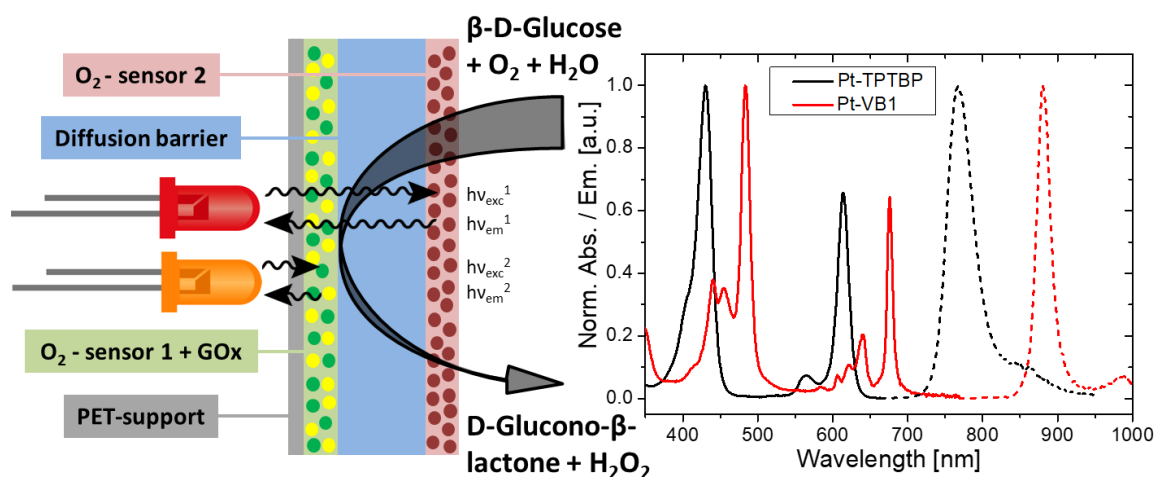
Figure 3.7 New concept of glucose quantification based on the use of a single optode (left) and absorption/emission spectra of Pt-TPTBP and the bridged platinum(II) benzoporphyrin derivative in anoxic toluene (right) [62]

3.3 Indicators for Optical Oxygen Sensing

This chapter and following sub-chapters are based on reference [1], others will be quoted independently.

Contingent on the great interest for oxygen and the enormous success of the optical sensor technology in this field, as described in the introduction, decades of intensive research led to a huge number of oxygen indicators, suitable for various different applications. These indicators can be classified in two main groups; absorption (reversible or irreversible) and luminescence based indicators, whereby the latter ones are the most common, commercially available types and therefore described in more detail. As mentioned in 3.2.1 they rely on dynamic quenching of the luminescence by molecular oxygen and can be read out via phase-fluorimetry. Besides polycyclic aromatic hydrocarbons, polypyridyl and cyclometallated complexes and many others, metalloporphyrins with platinum(II) and palladium(II) as central atom are definitely the most popular luminophores, wherefore the next chapters will be focused on their development, synthetic strategies, photophysical properties but also on their applications in different fields of research.

3.3.1   Metalloporhyrins as commonly used UV/Vis Indicators

Porphyrins (figure 3.8) play a very important role in many biological processes essential to life and are probably one of the most important as well as functional pigments found in nature. Their chemical structure matches a square, planar 18 π-electron aromatic macrocycle assembled of four pyrroles and four methine carbons. [63]
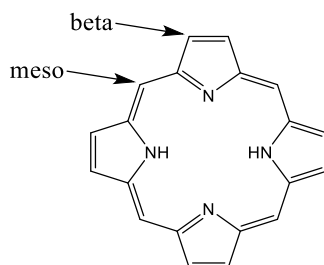
Figure 3.8 Chemical structure of an unsubstituted porphyrin

Porphyrins are characterized by structural robustness, chemical stability, desirable absorption and emission properties, pronounced aromaticity and the ability of versatile metal coordination. [63] Moreover, the electronic ground structure of the porphyrin demonstrates a high potential for various modifications and substitutions, enabling not only extension of the porphyrins π-system by fusion of different aromatic fragments [64] but allows also manipulations at its planarity [65], resulting in tuneability of optoelectronic as well as photophysical properties. [66] Basic knowledge about the connection between their structure and (photophysical) properties is crucial for the development of new porphyrin compounds for a specific purpose of application. [67]

Introduction of platinum(II) or palladium(II) into the porphyrins core enhances their photophysical properties further, rendering these compounds conclusively the most important and commonly used indicators for optical oxygen sensing. Pt(II) and Pd(II) porphyrins demonstrate strong room temperature phosphorescence, with excited state lifetimes, depended on the central atom, ranging from microseconds up to milliseconds and sufficiently high quantum yields. Moreover, they enable excitation in the blue as well as in the green region of the electromagnetic spectrum with moderate to high molar absorption coefficients displaying large Stokes' shifts. While the palladium(II) complexes show longer lifetimes, contingent on the smaller spin-orbit coupling of the lighter metal [68], platinum(II) compounds possess shorter decay times and higher quantum yields (by factor 2 to 3), resulting in an overall increased brightness of the dye.

Pt(II) and Pd(II) complexes of ocytaethylporphyrin (OEP) were one the first indicators of this dye class, which have been immobilized in several oxygen permeable polymeric matrices, such as polystyrene, sol-gels, ethyl cellulose et cetera and were widely used as optical oxygen sensor. [69] Besides good solubility in solvents and polymers, due to the ethyl moieties, these indicators suffered from rather low photostability, wherefore they were mostly replaced by tetrakis(pentafluorophenyl)porphyrin (TFPP). Platinum(II) and palladium(II) complexes of these compounds show drastically increased photostability, which can be explained by the introduction of perfluorophenyl substituents in the meso-position of the porphyrin core and the resulting electron-withdrawing character of this group. [70] This effect leads to a reduction of the electron density on the porphyrins ring system and subsequently decreases the probability of potential oxidation by reactive singlet oxygen, which is one of the assumed main reasons for photobleaching. Furthermore, this compound displays a bathochromic shift of absorption and emission, similar lifetimes but slightly lower quantum yields. The introduction of fluorine atoms, however, enables not only incorporation in various polymeric matrices, but makes polymerization and crosslinking

and even covalent coupling via nucleophilic substitution of the para-fluorine atom to different polymers possible, resulting in highly photostable and biocompatible sensing films. [71]

Although, absorption and emission of TFPP are already bathochromically shifted compared to OEP, both and several other similar porphyrin derivatives, can only be excited in the blue (Soret band) and the green part (Q band) of the electromagnetic spectrum, followed by emission from 650 to 740 nm. This circumstance hampers and sometimes even limits utilization of these dyes for oxygen measurement in biological samples, scattering media, marine sediments, tissue or blood et cetera. Reason therefore is the high level of autofluorescence, upon excitation in the UV/Vis region, due to the presence of various natural compounds (nucleotides FAD and NAD), which are also fluorescent. Red light excitable indicator dyes with accordingly bathochromically shifted NIR emission would not only overcome the mentioned drawbacks but also result in better compatibility with optical components. The advantages of lower energetic excitation (longer wavelengths), the consequent development of the respective dyes and their benefits, challenges as well as possible applications are content of the next chapter.

3.3.2 NIR Indicators based on Benzoporphyrins

Excitation with red light (approximately 610 - 700 nm) is, as mentioned above very beneficial for many applications due to a significantly lower light scattering by the tissue, absorption of natural compounds and resulting autofluorescence in biological tissues. Moreover, lower energetic light exhibits higher penetration depths compared to Vis light (basic concept of multiphoton microscopy), and enables usage of cheaper optical components, such as red laser diodes as well as cheap and compact Si photodiodes, whose sensitivity increases with wavelengths higher than 600 nm (maximum from 850 to 900 nm). [72]

These photodiodes are therefore perfectly suitable to detect emission in the adjacent part of the electromagnetic spectrum, which is called the infrared (IR) region (700 nm to 1 mm), which can be subdivided in three regions (near-, mid-, far-infrared). The most relevant part of the IR light is the near-infrared part (from 700 to 2500 nm). [73] Here, especially the region from 700 to 900 nm is well-known as the optical window, due to several therapeutic applications, including measurements in blood, tissues and cells as well as real time *in vivo* imaging of biological samples. [73] The NIR region is also from great interest for many industrial applications, particularly in the sector of organic solar cells and photovoltaics, contingent on the fact that almost 50% of the sun's energy hitting the earth is NIR radiation. [73]

Development and Characteristics of NIR Indicators

Bathochromic shift of the porphyrin's absorption and emission band can be realized following various synthetic strategies, wherefore only the most relevant ones are mentioned here. Although, modification via reduction and oxidation of the porphyrin's macrocycle (producing chlorins [74] or porphyrin lactones [75] and ketones [69], respectively) have led to compounds, which were successfully applied as optical oxygen sensors, the success of the extension of the porphyrin's π-system obtained by fusion of diverse external aromatic fragments is incomparable. [76] Depending on the aromatic moiety fused at the β-pyrrole position of the porphyrins core, tetrabenzo- [65], [66], [77] tetranaphtha- [78]–[81] or even tetraanthroporphyrins [73], [82] were prepared, whereby the former undeniably achieved the biggest success in various applications (more details later). Platinum(II) complexes of these porphyrinoids enable excitation ranging from 614 up to 762 nm and display emission from 770 to 1020 nm. [73] However, all of these π-extended complexes show a strong tendency to π-π-stacking and aggregation, [83] caused by their planar structure, resulting into decreased solubility as well as photostability the higher the degree of π-extension is. [73], [84] The low solubility of these compounds can be either enhanced by introduction of bulky groups (e.g. tert-butyl groups or long alkyl-chains) in β- or meso-position, or by substitution with phenyl groups in the meso-position, both leading to decreased planarity of the π-system, as well as a small bathrochromic shifts. [80], [85], [86] Hereby, it could also been shown that extension of the π-system in meso-position does not have a huge impact on the photophysical properties, due to the out-of-plane position to the porphyrins core. [73]

As can be assumed from their chemical structure, metalloporphyrins are generally hydrophobic compounds, regardless of previously mentioned substitutions and as a consequence insoluble in water or other physiological fluids. In order to be suitable for various biological or medical applications, their solubility has to be modified differently. The most commonly applied methods for this purpose, are entrapment (covalently or not) of the dye in polymeric nanoparticles, [87] the formation of dye conjugates or even dendrimers [88], [89], but that's a completely different matter altogether.

However, as already noted previously, photostability of the dyes can be enhanced by substitution with fluorine atoms (or other electron withdrawing moieties), which furthermore also slightly increases solubility and is accompanied by a small shift to higher wavelengths. [72], [85]

The key factor for the design of new NIR emitters, demonstrating bathochromic shift of absorption and emission, is therefore, the reduction of the energy gap between the HOMO and LUMO of the respective compound, since this disparity strongly affects the optical and the electronic properties of each organic molecule. [90] A significantly smaller, but still visible impact on the photophysical properties is attributed to the substituents of the respective ligands (or meso-position substituents), as explained previously. While electron-withdrawing groups, result in stabilization of the HOMO, due to the reduction of electron density from the metal in the porphyrins core, and hypsochromic shift of the emission signal, electron donating species display an inverted effect. [73], [91]

Classical Benzoporphyrins

While the first synthesis and mention of this type of porphyrin compound dates back in the 1940s by Helberger et al. [92] and in the 1950s by Linstead et al. [93], benzoporphyrins have in the meantime attracted remarkable attention over the world, not only in research, but also in a wide field of applications. The kind of nowadays standard benzoporphyrin is either platinum(II) or palladium(II) benzoporphyrin with 4 substituted phenyl rings in meso-position, called tetraphenyl-tetrabenzoporphyrin (TPTBP; figure 3.9), which are hereafter described in more detail in place of the diversity of all developed benzoporphyrin derivatives. [77], [94] Introduction of phenyl groups, resulting in non-planar structures with drastically enhanced solubility, was necessary to generally increase their further functional applicability, as described above. Photostability of these compounds is moderate when compared to TFPP, but nevertheless sufficient for its application purposes and could be further enhanced easily by substitution of hydrogen by fluorine atoms in the phenyl rings in meso-position. [72]

M = platinum(II) or palladium(II)
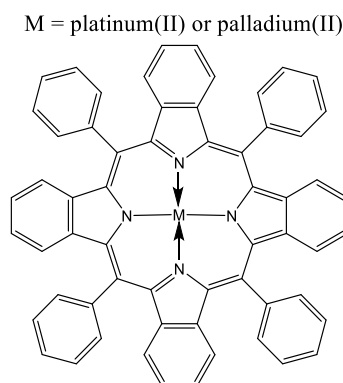
Figure 3.9 Chemical structure of platinum(II) and palladium(II) tetraphenyltetrabenzoporphyrin (TPTBP)

Pt-TPTBP, for instance, possesses an absorption spectrum similar to platinum(II) porphyrins such as TFPP or OEP but the absorption is significantly bathochromically shifted. The spectrum is characterized by one Soret band (from approximately 375 to 450 nm) with a maximum peak around 430 nm and two Q bands, whereby the more intense one is located between 580 to 640 nm, with a maximum at approximately 614 nm. Moreover, this dye demonstrates high brightness, achieved by molar absorption coefficients of roughly 200.000 M^{-1} cm^{-1} in the blue and 135.000 M^{-1} cm^{-1} in the red part of the spectrum as well as high quantum yields for phosphorescence ($> 20\%$ at room temperature) in the NIR at 770 nm. The excited state lifetime of about 47 µs (in toluene) and the possibility of incorporation in polymeric matrices (e.g. polystyrene) retaining similar decay times, enables the preparation of an optical oxygen sensor suitable from 0 to 100% oxygen saturation. [77]

The palladium(II) analogue exhibits similar absorption characteristics, which are further bathochromically shifted (due to the heavy atom effect of the metal) by 14 nm in both bands, but with significantly higher molar absorption coefficients of 415.000 and 175.000 M^{-1} cm^{-1}. Pd-TPTBP also displays good (decreased by factor 2 compared to the Pt(II) analogue) quantum yields of phosphorescence (at room temperature), with emission around 800 nm but significantly longer lifetime of around 286 µs in solution. Contingent on the higher lifetime and the increased sensitivity

to oxygen (with restriction of the matrix), this compound is perfectly qualified for usage in oxygen trace measurements by optical means. [77]

Synthetic Strategies to Benzoporphyrin Derivatives

Besides desirable photophysical properties of the dyes, the synthetic strategy for preparation of those compounds is also an important factor influencing the potential applicability later on. The two most important synthetic pathways, concerning benzoporphyrins, are the Lindsey condensation method [95], [96] and the template method. [97], [98] The first method represents a more elaborate strategy, mostly involving several synthetic steps for the preparation of the precursor pyrrole, [85] in which the porphyrin complex is first generated under standard Lindsey conditions, until finally the metalated benzoporphyrin is obtained via oxidative aromatization. The latter comprises three synthetic steps; formation of the Zn(II) complex within a modified template condensation, [99] demetalation of this compound in acidic media and finally metalation of the metal-free benzoporphyrin. While this synthetic pathway is quite straightforward and time saving, using inexpensive and readily available starting materials, the compounds have to tolerate high temperatures (280 °C) and the yields for the first step are relatively low (6 to 8 %). This circumstance enables nevertheless preparation of the dye in multigram-scale but compared to the Lindsey method limits the variety of suitable precursors and therefore restricts preparation of versatile benzoporphyrin compounds with several, not highly temperature stable, functional groups. [7] However, both methods are interesting for the synthesis of π-extended porphyrins caused by their different advantages (simplicity of the template method and greater variety of suitable precursors for the condensation under Lindsey conditions).

Field of Applications for Benzoporphyrins

Extension of the π-conjugated system of a porphyrin, leading to platinum(II) and palladium(II) TPTBP and numerous other benzoporphyrin derivatives, featuring excitation by red light, NIR emission, high brightness, excellent thermal and chemical stability as well as sufficiently good solubility and photostability enables applications in a wide range of many different fields. Besides optical oxygen sensing [100] for *in vivo* imaging of tissue oxygenation in biomedicine [101] as well as two-photon imaging of oxygenation of biological samples [6] or as potential dual sensor for oxygen and temperature, [7] these include medical and therapeutic applications (for generation of singlet oxygen in photodynamic therapy, [102], [103] enzymatic biosensors for optical glucose sensing, [60], [61], [104] et cetera). Moreover, benzoporphyrins are also used in photonic applications ranging from NIR organic light emitting diodes (OLEDs) technology [105] to photocatalysis and photovoltaics as potential sensitizers in TTA-based upconversion systems, [7], [106] which is discussed in more detail below.

Sensitizers for Triplet-Triplet-Annihilation based Upconversion

In the last decade, a new upconversion concept based on triplet-triplet-annihilation (TTA) has attracted much attention, not only in science community but also in industry. Since red light excitable dyes displaying phosphorescence (at room temperature) in the NIR are particularly suitable as sensitizers for TTA based upconversion, various platinum(II) as well as palladium(II) benzoporphyrin complexes have found a new application. [107] Moreover, the sensitizers should efficiently absorb light (high molar absorption coefficient), show high efficiency of ISC and feature long triplet lifetimes, which almost perfectly fits the characteristics of a benzoporphyrin. The annihilator (e.g. different perylenes) on the other side is intended to demonstrate very high fluorescence quantum yields as well as high solubility and photostability. [108] The triplet energy level of the annihilator must be lower than the one of the sensitizer to maximize the energy transfer within the TTA process. TTA based upconversion can thus be simply described as conversion of low energetic light (high wavelength) to higher energetic light (lower wavelength), based on an energy transfer from the sensitizer to the annihilator molecule. The exact process of TTA based upcoversion is described in detail in 3.1.5. Even though this process is commonly observed in concentrated, anoxic solutions (due to quenchability of this process by oxygen) of the two dye molecules, TTA based upconversion could already be detected in diluted polymer solutions (with incorporated sensitizer and annihilator molecules) as well as in traces in solid polymer films. [106], [109] One of the most important advantages of TTA based upconversion, compared to other techniques, is the compatibility with low excitation power density, which is typical for solar light as well as the tuneability of the system concerning variation of excitation and emission wavelength by exchanging either the sensitizer or the annihilator. [108] TTA upconversion, using benzoporphyrins (figure 3.10), is therefore a very promising candidate for application in photocatalysis, optics but especially for photovoltaics and optical oxygen sensing (e.g. nanoparticles featuring TTA as potential new generation of imaging agents for in vivo measurements). This phenomenon is more closely examined in chapter 5 [7] and chapter 7.
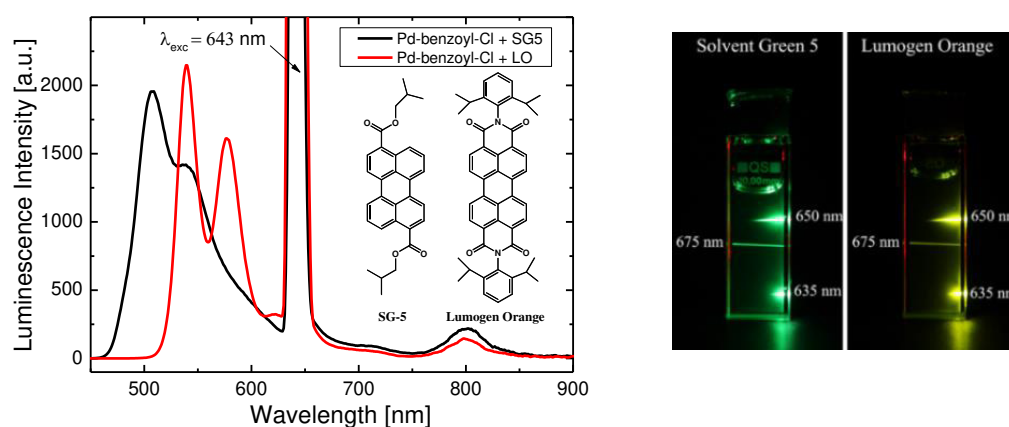
Figure 3.10 Emission spectra (λ_{exc} 643 nm) of the TTA system based on of Pd-benzoyl-Cl as sensitizer and two different perylene annihilators (Solvent Green 5 (SG5) and Lumogen Orange (LO)) in anoxic toluene (left) and photographic images of the upconverted fluorescence for the same TTA upconversion system (right)

Alternative Indicators to Benzoporphyrins

Needless to say that benzoporphyrins are not the only class of metalloporphyrins that enable excitation using red light followed by emission in the NIR region. In the following the most interesting and known alternatives of NIR emitting porphyrinoids with their photophysical properties are presented (figure 3.11).

M = platinum(II) or palladium(II)

Benzo-aza Hybridporphyrin

Naphthaporphyrin   Benzo-naphtha Hybridporphyrin

Anthroporphrin
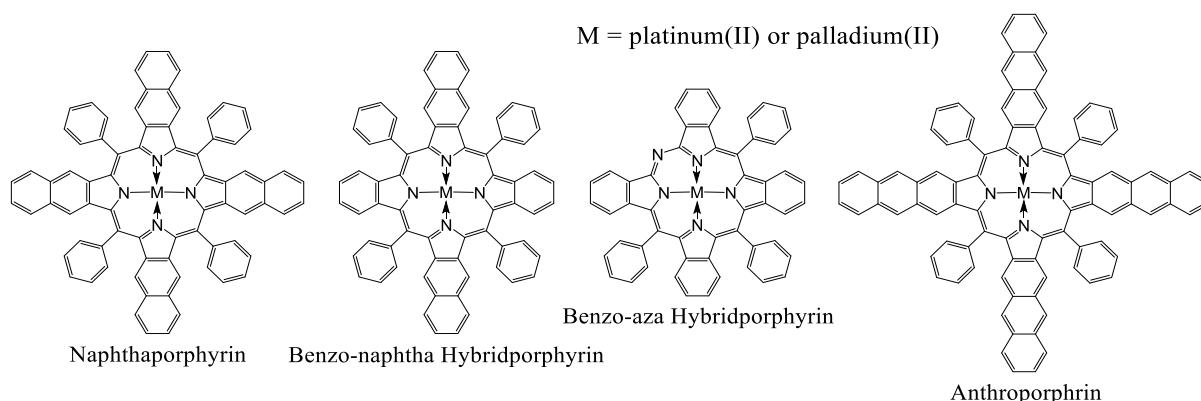
Figure 3.11 Chemical structure of known NIR emitting porphyrins beside benzoporphyrins

One quite known alternative are naphthoporphyrins (figure 3.11), which are prepared by fusion of naphtha moieties in β-pyrrole position of the porphyrin core. Herein, each naphtha moiety results in a bathochromic shift of 20 nm in the Q band, leading to a possible overall shift of 80 nm when tetra-substituted and to a narrow absorption maximum at approximately 680 nm for a platinum(II) complex. [78]–[80] Unfortunately, this huge bathochromic shift is accompanied by drastically lowered solubility (tendency towards aggregation) and photostability as well as reduced quantum yields, correlating well to the extent of fused naphtha moieties to the porphyrin. Even though enhancement of solubility and photostability is possible, as described above, the sophisticated multistep synthesis to achieve those dyes, combined with the mentioned drawbacks, seriously limits their field of potential applications.

Another class of porphyrins is achieved by hybridization of benzoporphyrins with either naphtha- or azaporphyrins (figure 3.11). [110], [111] Aim of this method is the preparation of a new luminophores in which the desirable photophysical and chemical properties of two different species are combined. Although in both cases the absorption (approximately 630 to 690 nm) as well as the emission properties (810 to 880 nm) are bathochromically shifted (less pronounced in azabenzoporphyrins) and well tunable by stepwise substitution, the luminescence quantum yield and partly the lifetime are shortened. While hybrids with naphtha moieties results again in compounds with reduced solubility and photostability, [110] azabenzoporphyrins demonstrate sufficient solubility and even enhanced photostability; higher than the ones of TPTBP, which can be attributed to the excellent chemical, thermal and photostability of phthalocyanines. [111]

A further species, which is obtained via fusion of anthracene moieties to the porphyrin's core in β-position are so called anthroporphyrins (figure 3.11). [82] Platinum(II) complexes of these compounds even feature a bathochromically shifted absorption with a maximum at 762 nm and

emission at 1020 nm. However, as could be assumed, due to the increased extension of the π-system, quantum yields are extremely decreased, as well as solubility and photostability of these derivatives. [73]

Additional ways of π-extension of the porphyrin's core, resulting in so called rigid porphyrins with significant shift of absorption and emission characteristics to higher wavelengths, include attaching of other aromatic units via triple bonds [112] or fusion of porphyrins with other porphyrins leading to dimers or even oligomers also called tapes.[113]–[115] Unfortunately, all these compounds suffer from the same drawbacks as mentioned previously. Analyzing several π-extended compounds an energy gap law correlation is observable, indicating a limited potential for the extension of absorption and emission to longer wavelengths, which is caused by the substantial increase of the non-radiative decay rate with the decreasing T_1 - S_0 energy gap. [73] As a consequence most NIR absorbing porphyrinoids are non-emissive. [63], [86], [113], [116] For practical applications, it is therefore necessary to find a compromise between the bathochromic shift of absorption and the phosphorescence quantum yield.

Contingent on the great demand for NIR indicators for various applications and the circumstance that so far existing porphyrinoids don't accomplish the desired photophysical properties yet, several synthetic approaches modifying existing benzoporphyrins were investigated.

The Scholl reaction, a condensation of aromatic compounds applying Lewis acids (e.g. $AlCl_3$), [116]–[118] was used to intramolecularly bridge benzoporphyrin derivatives, leading to a significant bathochromic shift of absorption as well as emission characteristics, is subject of the second publication presented in chapter 6. [62]

Moreover, modification of platinum(II) benzoporphyrins via Suzuki and Sonogashira coupling reaction as well as Friedel-Crafts acylation with various compounds was performed, resulting in dyes with enhanced photophysical properties and an adequate shift to higher wavelengths, covered in the third publication in chapter 7.

Aim of this thesis was the preparation of benzoporphyrin derivatives with enhanced solubility and photostability as well as bathochromic shift of absorption and emission properties, while still retaining their outstanding brightness, fulfilling the great demands of NIR indicators for optical oxygen sensing and various other fields of applications.

4 References

[1] M. Quaranta, S. M. Borisov, and I. Klimant, "Indicators for optical oxygen sensors," *Bioanal. Rev.*, vol. 4, no. 2–4, pp. 115–157, Dec. 2012.

[2] Bernard Valeur, *Molecular Fluorescence: Principles and Applications*. Weinheim; New York: Wiley-VCH Verlag GmbH, 2001.

[3] J. R. Lakowicz, *Principles of fluorescence spectroscopy*. New York: Springer, 2006.

[4] P. W. Atkins, *Physikalische Chemie*. Wiley-VCH Verlag GmbH, 2008.

[5] K. Rurack and M. Spieles, "Fluorescence Quantum Yields of a Series of Red and Near-Infrared Dyes Emitting at 600−1000 nm," *Anal. Chem.*, vol. 83, no. 4, pp. 1232–1242, Feb. 2011.

[6] T. V. Esipova, H. J. Rivera-Jacquez, B. Weber, A. E. Masunov, and S. A. Vinogradov, "Two-Photon Absorbing Phosphorescent Metalloporphyrins: Effects of π-Extension and Peripheral Substitution," *J. Am. Chem. Soc.*, vol. 138, no. 48, pp. 15648–15662, Dec. 2016.

[7] P. W. Zach, S. A. Freunberger, I. Klimant, and S. M. Borisov, "Electron-Deficient Near-Infrared Pt(II) and Pd(II) Benzoporphyrins with Dual Phosphorescence and Unusually Efficient Thermally Activated Delayed Fluorescence: First Demonstration of Simultaneous Oxygen and Temperature Sensing with a Single Emitter," *ACS Appl. Mater. Interfaces*, vol. 9, no. 43, pp. 38008–38023, Nov. 2017.

[8] C. Larndorfer, S. M. Borisov, P. Lehner, and I. Klimant, "The effect of high light intensities on luminescence lifetime based oxygen sensing," *Analyst*, vol. 139, no. 24, pp. 6569–6579, Nov. 2014.

[9] E. R. Carraway, J. N. Demas, B. A. DeGraff, and J. R. Bacon, "Photophysics and photochemistry of oxygen sensors based on luminescent transition-metal complexes," *Anal. Chem.*, vol. 63, no. 4, pp. 337–342, Feb. 1991.

[10] P. Gründler, *Chemische Sensoren: Eine Einführung für Naturwissenschaftler und Ingenieure*. Berlin: Springer, 2004.

[11] C. McDonagh, C. S. Burke, and B. D. MacCraith, "Optical Chemical Sensors," *Chem. Rev.*, vol. 108, no. 2, pp. 400–422, Feb. 2008.

[12] S. M. Borisov and O. S. Wolfbeis, "Optical Biosensors," *Chem. Rev.*, vol. 108, no. 2, pp. 423–461, Feb. 2008.

[13] O. S. Wolfbeis, "Fiber-Optic Chemical Sensors and Biosensors," *Anal. Chem.*, vol. 78, no. 12, pp. 3859–3874, Jun. 2006.

[14] X. Wang, O. S. Wolfbeis, and R. J. Meier, "Luminescent probes and sensors for temperature," *Chem. Soc. Rev.*, vol. 42, no. 19, pp. 7834–7869, Sep. 2013.

[15] M.-S. Steiner, A. Duerkop, and O. S. Wolfbeis, "Optical methods for sensing glucose," *Chem. Soc. Rev.*, vol. 40, no. 9, pp. 4805–4839, Aug. 2011.

[16] P. Neogi, *Diffusion in Polymers*. New York: CRC Press, 1996.

[17] A. Mills, "Controlling the sensitivity of optical oxygen sensors," *Sens. Actuators B Chem.*, vol. 51, no. 1, pp. 60–68, Aug. 1998.

[18] O. S. Wolfbeis, "Editorial: Probes, Sensors, and Labels: Why is Real Progress Slow?," *Angew. Chem. Int. Ed.*, vol. 52, no. 38, pp. 9864–9865, Sep. 2013.

[19] *Temperature Measurement*. Chichester: Wiley-VCH, 2001.

[20] J. Ferguson and A. W. H. Mau, "Spontaneous and stimulated emission from dyes. Spectroscopy of the neutral molecules of acridine orange, proflavine, and rhodamine B," *Aust. J. Chem.*, vol. 26, no. 8, pp. 1617–1624, 1973.

[21] D. Ross, M. Gaitan, and L. E. Locascio, "Temperature Measurement in Microfluidic Systems Using a Temperature-Dependent Fluorescent Dye," *Anal. Chem.*, vol. 73, no. 17, pp. 4117–4123, Sep. 2001.

[22] F. Ye, C. Wu, Y. Jin, Y.-H. Chan, X. Zhang, and D. T. Chiu, "Ratiometric Temperature Sensing with Semiconducting Polymer Dots," *J. Am. Chem. Soc.*, vol. 133, no. 21, pp. 8146–8149, Jun. 2011.

[23] H. D. Duong and J. I. Rhee, "Exploitation of thermo-effect of rhodamine B entrapped in sol–gel matrix and silica gel for temperature detection," *Sens. Actuators B Chem.*, vol. 124, no. 1, pp. 18–23, Jun. 2007.

[24] J. C. Fister, D. Rank, and J. M. Harris, "Delayed Fluorescence Optical Thermometry," *Anal. Chem.*, vol. 67, no. 23, pp. 4269–4275, Dec. 1995.

[25] C. Baleizão, S. Nagl, S. M. Borisov, M. Schäferling, O. S. Wolfbeis, and M. N. Berberan-Santos, "An Optical Thermometer Based on the Delayed Fluorescence of C70," *Chem. – Eur. J.*, vol. 13, no. 13, pp. 3643–3651, Apr. 2007.

[26] A. Steinegger, I. Klimant, and S. M. Borisov, "Purely Organic Dyes with Thermally Activated Delayed Fluorescence—A Versatile Class of Indicators for Optical Temperature Sensing," *Adv. Opt. Mater.*, vol. 5, no. 18, p. n/a-n/a, Sep. 2017.

[27] J. Brandrup, E. H. Immergut, and E. A. Grulke, *Polymer Handbook*, 4th Edition., vol. 2. Wiley.

[28] L. H. Fischer, S. M. Borisov, M. Schaeferling, I. Klimant, and O. S. Wolfbeis, "Dual sensing of pO2 and temperature using a water-based and sprayable fluorescent paint," *Analyst*, vol. 135, no. 6, pp. 1224–1229, May 2010.

[29] V. W.-W. Yam and K. K.-W. Lo, "Luminescent polynuclear d 10 metal complexes," *Chem. Soc. Rev.*, vol. 28, no. 5, pp. 323–334, 1999.

[30] P. C. Ford, E. Cariati, and J. Bourassa, "Photoluminescence Properties of Multinuclear Copper(I) Compounds," *Chem. Rev.*, vol. 99, no. 12, pp. 3625–3648, Dec. 1999.

[31] S. M. Borisov and O. S. Wolfbeis, "Temperature-Sensitive Europium(III) Probes and Their Use for Simultaneous Luminescent Sensing of Temperature and Oxygen," *Anal. Chem.*, vol. 78, no. 14, pp. 5094–

5101, Jul. 2006.

[32] K. Miyata *et al.*, "Chameleon Luminophore for Sensing Temperatures: Control of Metal-to-Metal and Energy Back Transfer in Lanthanide Coordination Polymers," *Angew. Chem. Int. Ed.*, vol. 52, no. 25, pp. 6413–6416, Jun. 2013.

[33] Z. Y. Zhang and L. S. Grattan, *Fiber Optic Fluorescence Thermometry*. Springer, 1994.

[34] X. Wang and O. S. Wolfbeis, "Optical methods for sensing and imaging oxygen: materials, spectroscopies and applications," *Chem. Soc. Rev.*, vol. 43, no. 10, pp. 3666–3761, Apr. 2014.

[35] A. Mills, "Oxygen indicators and intelligent inks for packaging food," *Chem. Soc. Rev.*, vol. 34, no. 12, pp. 1003–1011, Dec. 2005.

[36] S. M. Borisov, R. Seifner, and I. Klimant, "A novel planar optical sensor for simultaneous monitoring of oxygen, carbon dioxide, pH and temperature," *Anal. Bioanal. Chem.*, vol. 400, no. 8, pp. 2463–2474, Jun. 2011.

[37] C.-S. Chu and T.-H. Lin, "A new portable optical sensor for dual sensing of temperature and oxygen," *Sens. Actuators B Chem.*, vol. 202, pp. 508–515, Oct. 2014.

[38] M. E. Köse, A. Omar, C. A. Virgin, B. F. Carroll, and K. S. Schanze, "Principal Component Analysis Calibration Method for Dual-Luminophore Oxygen and Temperature Sensor Films: Application to Luminescence Imaging," *Langmuir*, vol. 21, no. 20, pp. 9110–9120, Sep. 2005.

[39] S. M. Borisov, C. Krause, S. Arain, and O. S. Wolfbeis, "Composite Material for Simultaneous and Contactless Luminescent Sensing and Imaging of Oxygen and Carbon Dioxide," *Adv. Mater.*, vol. 18, no. 12, pp. 1511–1516, Jun. 2006.

[40] T.-W. Sung and Y.-L. Lo, "Dual sensing of temperature and oxygen using PtTFPP-doped CdSe/SiO2 core–shell nanoparticles," *Sens. Actuators B Chem.*, vol. 173, pp. 406–413, Oct. 2012.

[41] H. Lam, G. Rao, J. Loureiro, and L. Tolosa, "Dual Optical Sensor for Oxygen and Temperature Based on the Combination of Time Domain and Frequency Domain Techniques," *Talanta*, vol. 84, no. 1, pp. 65–70, Mar. 2011.

[42] C. Baleizão, S. Nagl, M. Schäferling, M. N. Berberan-Santos, and O. S. Wolfbeis, "Dual Fluorescence Sensor for Trace Oxygen and Temperature with Unmatched Range and Sensitivity," *Anal. Chem.*, vol. 80, no. 16, pp. 6449–6457, Aug. 2008.

[43] C. S. Chu and Y. L. Lo, "A Plastic Optical Fiber Sensor for the Dual Sensing of Temperature and Oxygen," *IEEE Photonics Technol. Lett.*, vol. 20, no. 1, pp. 63–65, Jan. 2008.

[44] S. M. Borisov, A. S. Vasylevska, C. Krause, and O. S. Wolfbeis, "Composite Luminescent Material for Dual Sensing of Oxygen and Temperature," *Adv. Funct. Mater.*, vol. 16, no. 12, pp. 1536–1542, Aug. 2006.

[45] A. S. Kocincova, S. M. Borisov, C. Krause, and O. S. Wolfbeis, "Fiber-Optic Microsensors for Simultaneous Sensing of Oxygen and pH, and of Oxygen and Temperature," *Anal. Chem.*, vol. 79, no. 22, pp. 8486–8493, Nov. 2007.

[46] M. I. J. Stich, S. Nagl, O. S. Wolfbeis, U. Henne, and M. Schaeferling, "A Dual Luminescent Sensor Material for Simultaneous Imaging of Pressure and Temperature on Surfaces," *Adv. Funct. Mater.*, vol. 18, no. 9, pp. 1399–1406, May 2008.

[47] C.-S. Chu and C.-A. Lin, "Optical fiber sensor for dual sensing of temperature and oxygen based on PtTFPP/CF embedded in sol–gel matrix," *Sens. Actuators B Chem.*, vol. 195, pp. 259–265, May 2014.

[48] S. Nagl and O. S. Wolfbeis, "Optical multiple chemical sensing: status and current challenges," *Analyst*, vol. 132, no. 6, pp. 507–511, May 2007.

[49] M. Gouterman *et al.*, "Dual luminophor pressure-sensitive paint: III. Application to automotive model testing," *Meas. Sci. Technol.*, vol. 15, no. 10, p. 1986, 2004.

[50] P. A. S. Jorge, C. Maule, A. J. Silva, R. Benrashid, J. L. Santos, and F. Farahi, "Dual sensing of oxygen and temperature using quantum dots and a ruthenium complex," *Anal. Chim. Acta*, vol. 606, no. 2, pp. 223–229, Jan. 2008.

[51] "WHO | Diabetes," *WHO*. [Online]. Available: http://www.who.int/mediacentre/factsheets/fs312/en/. [Accessed: 07-Nov-2017].

[52] A. Heller and B. Feldman, "Electrochemical Glucose Sensors and Their Applications in Diabetes Management," *Chem. Rev.*, vol. 108, no. 7, pp. 2482–2505, Jul. 2008.

[53] B. M. Cummins, J. T. Garza, and G. L. Coté, "Optimization of a Concanavalin A-Based Glucose Sensor Using Fluorescence Anisotropy," *Anal. Chem.*, vol. 85, no. 11, pp. 5397–5404, Jun. 2013.

[54] P. W. Barone and M. S. Strano, "The use of Single-Walled Carbon Nanotubes for Optical Glucose Detection," in *In Vivo Glucose Sensing*, John Wiley & Sons, Inc., 2009, pp. 317–329.

[55] H. S. Mader and O. S. Wolfbeis, "Boronic acid based probes for microdetermination of saccharides and glycosylated biomolecules," *Microchim. Acta*, vol. 162, no. 1–2, pp. 1–34, Jul. 2008.

[56] A. Pasic, H. Koehler, L. Schaupp, T. R. Pieber, and I. Klimant, "Fiber-optic flow-through sensor for online monitoring of glucose," *Anal. Bioanal. Chem.*, vol. 386, no. 5, pp. 1293–1302, Nov. 2006.

[57] M. Marazuela and M. Moreno-Bondi, "Fiber-optic biosensors – an overview," *Anal. Bioanal. Chem.*, vol. 372, no. 5–6, pp. 664–682, Mar. 2002.

[58] L. Li and D. R. Walt, "Dual-Analyte Fiber-Optic Sensor for the Simultaneous and Continuous Measurement of Glucose and Oxygen," *Anal. Chem.*, vol. 67, no. 20, pp. 3746–3752, Oct. 1995.

[59] M. Rumpler, M. Hajnsek, P. Baumann, T. R. Pieber, and I. Klimant, "Monitoring tissue oxygen heterogeneities and their influence on optical glucose measurements in an animal model," *J. Clin. Monit. Comput.*, pp. 1–4, Jun. 2017.

[60] A. Pasic, H. Koehler, I. Klimant, and L. Schaupp, "Miniaturized fiber-optic hybrid sensor for continuous glucose monitoring in subcutaneous tissue," *Sens. Actuators B Chem.*, vol. 122, no. 1, pp. 60–68, Mar. 2007.

[61] B. Nacht *et al.*, "Integrated catheter system for continuous glucose measurement and simultaneous insulin infusion," *Biosens. Bioelectron.*, vol. 64, pp. 102–110, Feb. 2015.

[62] P. W. Zach, O. T. Hofmann, I. Klimant, and S. M. Borisov, "NIR phosphorescent intramolecularly bridged benzoporphyrins and their application in an oxygen-compensated glucose optode," *Anal. Chem.*, Jan. 2018.

[63] T. Tanaka and A. Osuka, "Conjugated porphyrin arrays: synthesis, properties and applications for functional materials," *Chem. Soc. Rev.*, vol. 44, no. 4, pp. 943–969, Feb. 2015.

[64] A. Mills and A. Lepre, "Controlling the Response Characteristics of Luminescent Porphyrin Plastic Film Sensors for Oxygen," *Anal. Chem.*, vol. 69, no. 22, pp. 4653–4659, Nov. 1997.

[65] O. S. Finikova, A. V. Cheprakov, I. P. Beletskaya, P. J. Carroll, and S. A. Vinogradov, "Novel versatile synthesis of substituted tetrabenzoporphyrins," *J. Org. Chem.*, vol. 69, no. 2, pp. 522–535, Jan. 2004.

[66] C. M. B. Carvalho, T. J. Brocksom, and K. T. de Oliveira, "Tetrabenzoporphyrins: synthetic developments and applications," *Chem. Soc. Rev.*, vol. 42, no. 8, pp. 3302–3317, Mar. 2013.

[67] J. E. Rogers *et al.*, "Observation and Interpretation of Annulated Porphyrins: Studies on the Photophysical Properties of meso-Tetraphenylmetalloporphyrins," *J. Phys. Chem. A*, vol. 107, no. 51, pp. 11331–11339, Dec. 2003.

[68] D. Eastwood and M. Gouterman, "Porphyrins: XVIII. Luminescence of (Co), (Ni), Pd, Pt complexes," *J. Mol. Spectrosc.*, vol. 35, no. 3, pp. 359–375, Sep. 1970.

[69] D. B. Papkovsky, "New oxygen sensors and their application to biosensing," *Sens. Actuators B Chem.*, vol. 29, no. 1–3, pp. 213–218, Oct. 1995.

[70] S.-K. Lee and I. Okura, "Photostable Optical Oxygen Sensing Material: PlatinumTetrakis(pentafluorophenyl)porphyrin Immobilized in Polystyrene," *Anal. Commun.*, vol. 34, no. 6, pp. 185–188, Jan. 1997.

[71] Y. Tian, B. R. Shumway, and D. R. Meldrum, "A New Crosslinkable Oxygen Sensor Covalently Bonded into Poly(2-hydroxyethyl methacrylate)-CO-Polyacrylamide Thin Film for Dissolved Oxygen Sensing," *Chem. Mater. Publ. Am. Chem. Soc.*, vol. 22, no. 6, pp. 2069–2078, Mar. 2010.

[72] G. N. S. M. Borisov, "New NIR-emitting complexes of platinum(II) and palladium(II) with fluorinated benzoporphyrins," *J. Photochem. Photobiol. -Chem. - J PHOTOCHEM PHOTOBIOL -CHEM*, vol. 201, no. 2, pp. 128–135, 2009.

[73] H. Xiang, J. Cheng, X. Ma, X. Zhou, and J. J. Chruma, "Near-infrared phosphorescence: materials and applications," *Chem. Soc. Rev.*, vol. 42, no. 14, pp. 6128–6185, Jun. 2013.

[74] F.-P. Montforts, B. Gerlach, and F. Hoeper, "Discovery and Synthesis of Less Common Natural Hydroporphyrins," *Chem. Rev.*, vol. 94, no. 2, pp. 327–347, Mar. 1994.

[75] G. Khalil *et al.*, "Synthesis and spectroscopic characterization of Ni, Zn, Pd and Pt tetra(pentafluorophenyl)porpholactone with comparisons to Mg, Zn, Y, Pd and Pt metal complexes of tetra(pentafluorophenyl)porphine," *J. Porphyr. Phthalocyanines*, vol. 06, no. 02, pp. 135–145, Feb. 2002.

[76] T. D. Lash, "Modification of the porphyrin chromophore by ring fusion: identifying trends due to annelation of the porphyrin nucleus," *J. Porphyr. Phthalocyanines*, vol. 5, no. 3, pp. 267–288, Mar. 2001.

[77] S. M. Borisov, G. Nuss, and I. Klimant, "Red light-excitable oxygen sensing materials based on platinum(II) and palladium(II) benzoporphyrins," *Anal. Chem.*, vol. 80, no. 24, pp. 9435–9442, Dec. 2008.

[78] O. S. Finikova, A. V. Cheprakov, P. J. Carroll, and S. A. Vinogradov, "Novel route to functionalized tetraaryltetra[2,3]naphthaloporphyrins via oxidative aromatization," *J. Org. Chem.*, vol. 68, no. 19, pp. 7517–7520, Sep. 2003.

[79] V. V. Rozhkov, M. Khajehpour, and S. A. Vinogradov, "Luminescent Zn and Pd tetranaphthaloporphyrins," *Inorg. Chem.*, vol. 42, no. 14, pp. 4253–4255, Jul. 2003.

[80] O. S. Finikova, S. E. Aleshchenkov, R. P. Briñas, A. V. Cheprakov, P. J. Carroll, and S. A. Vinogradov, "Synthesis of Symmetrical Tetraaryltetranaphtho[2,3]porphyrins," *J. Org. Chem.*, vol. 70, no. 12, pp. 4617–4628, May 2005.

[81] A. V. C. Mikhail A. Filatov, "The synthesis of new tetrabenzo- and tetranaphthoporphyrins via the addition reactions of 4,7-dihydroisoindole," *Tetrahedron*, vol. 67, no. 19, pp. 3559–3566, 2011.

[82] H. Yamada *et al.*, "Synthesis and Characterization of Tetraanthroporphyrins," *Org. Lett.*, vol. 10, no. 14, pp. 2947–2950, Jul. 2008.

[83] T. Ishizuka, Y. Saegusa, Y. Shiota, K. Ohtake, K. Yoshizawa, and T. Kojima, "Multiply-fused porphyrins--effects of extended π-conjugation on the optical and electrochemical properties," *Chem. Commun. Camb. Engl.*, vol. 49, no. 53, pp. 5939–5941, Jul. 2013.

[84] C. Borek *et al.*, "Highly Efficient, Near-Infrared Electrophosphorescence from a Pt–Metalloporphyrin Complex," *Angew. Chem. Int. Ed.*, vol. 46, no. 7, pp. 1109–1112, Feb. 2007.

[85] Y. Zems, A. G. Moiseev, and D. F. Perepichka, "Convenient synthesis of a highly soluble and stable phosphorescent platinum porphyrin dye," *Org. Lett.*, vol. 15, no. 20, pp. 5330–5333, Oct. 2013.

[86] J. D. Spence and T. D. Lash, "Porphyrins with Exocyclic Rings. 14.1 Synthesis of Tetraacenaphthoporphyrins, a New Family of Highly Conjugated Porphyrins with Record-Breaking Long-Wavelength Electronic Absorptions," *J. Org. Chem.*, vol. 65, no. 5, pp. 1530–1539, Feb. 2000.

[87] Y. Cao, Y.-E. Lee Koo, and R. Kopelman, "Poly(decyl methacrylate)-based fluorescent PEBBLE swarm nanosensors for measuring dissolved oxygen in biosamples," *The Analyst*, vol. 129, no. 8, p. 745, 2004.

[88] I. Dunphy, S. A. Vinogradov, and D. F. Wilson, "Oxyphor R2 and G2: phosphors for measuring oxygen by oxygen-dependent quenching of phosphorescence," *Anal. Biochem.*, vol. 310, no. 2, pp. 191–198, Nov. 2002.

[89] A. Y. Lebedev, A. V. Cheprakov, S. Sakadzić, D. A. Boas, D. F. Wilson, and S. A. Vinogradov, "Dendritic phosphorescent probes for oxygen imaging in biological systems," *ACS Appl. Mater. Interfaces*, vol. 1, no. 6, pp. 1292–1304, Jun. 2009.

[90] G. Qian and Z. Y. Wang, "Near-Infrared Organic Compounds and Emerging Applications," *Chem. – Asian J.*, vol. 5, no. 5, pp. 1006–1029, May 2010.

[91] K. Dedeian, P. I. Djurovich, F. O. Garces, G. Carlson, and R. J. Watts, "A new synthetic route to the preparation

of a series of strong photoreducing agents: fac-tris-ortho-metalated complexes of iridium(III) with substituted 2-phenylpyridines," *Inorg. Chem.*, vol. 30, no. 8, pp. 1685–1687, Apr. 1991.

[92]   J. H. Helberger, A. von Rebay, and D. B. Hevér., "Über die Einwirkung von Metallen auf o-Cyanacetophenon sowie auf 3-Methylphtalimidin; Synthese des Tetrabenzoporphins. III. Mitteilung zur Kenntnis der Benzoporphine," *Justus Liebigs Ann. Chem.*, vol. 533, no. 1, pp. 197–215, Jan. 1938.

[93]   P. A. Barrett, R. P. Linstead, F. G. Rundall, and G. a. P. Tuey, "197. Phthalocyanines and related compounds. Part XIX. Tetrabenzporphin, tetrabenzmonazaporphin and their metallic derivatives," *J. Chem. Soc. Resumed*, no. 0, pp. 1079–1092, Jan. 1940.

[94]   D. B. P. S. M. Borisov, "Photophysical properties of the new phosphorescent platinum(II) and palladium(II) complexes of benzoporphyrins and chlorins," *J. Photochem. Photobiol. -Chem. - J PHOTOCHEM PHOTOBIOL -CHEM*, vol. 206, no. 1, pp. 87–92, 2009.

[95]   J. S. Lindsey, H. C. Hsu, and I. C. Schreiman, "Synthesis of tetraphenylporphyrins under very mild conditions," *Tetrahedron Lett.*, vol. 27, no. 41, pp. 4969–4970, 1986.

[96]   J. S. Lindsey, I. C. Schreiman, H. C. Hsu, P. C. Kearney, and A. M. Marguerettaz, "Rothemund and Adler-Longo reactions revisited: synthesis of tetraphenylporphyrins under equilibrium conditions," *J. Org. Chem.*, vol. 52, no. 5, pp. 827–836, Mar. 1987.

[97]   K. Ichimura *et al.*, "Formation of tetrabenzoporphine skeleton by the reactions of phthalimide with zinc carbonates," *Inorganica Chim. Acta*, vol. 186, no. 1, pp. 95–101, Aug. 1991.

[98]   S. M. Borisov and I. Klimant, "Efficient metallation in diphenylether – A convenient route to luminescent platinum(II) complexes," *Dyes Pigments*, vol. 83, no. 3, pp. 312–316, Dec. 2009.

[99]   L. H. Hutter, B. J. Müller, K. Koren, S. M. Borisov, and I. Klimant, "Robust optical oxygen sensors based on polymer-bound NIR-emitting platinum(II)–benzoporphyrins," *J. Mater. Chem. C*, vol. 2, no. 36, pp. 7589–7598, Aug. 2014.

[100]   C. Staudinger and S. M. Borisov, "Long-wavelength analyte-sensitive luminescent probes and optical (bio)sensors," *Methods Appl. Fluoresc.*, vol. 3, no. 4, p. 042005, 2015.

[101]   I. B. Rietveld, E. Kim, and S. A. Vinogradov, "Dendrimers with tetrabenzoporphyrin cores: near infrared phosphors for in vivo oxygen imaging," *Tetrahedron*, vol. 59, no. 22, pp. 3821–3831, May 2003.

[102]   S. Pervaiz and M. Olivo, "Art and science of photodynamic therapy," *Clin. Exp. Pharmacol. Physiol.*, vol. 33, no. 5–6, pp. 551–556, Jun. 2006.

[103]   R.-M. Szeimies, "Geschichte der Photodynamischen Therapie," *Aktuelle Dermatol.*, vol. 31, no. 5, pp. 193–197, May 2005.

[104]   M. Rumpler *et al.*, "First application of a transcutaneous optical single-port glucose monitoring device in patients with type 1 diabetes mellitus," *Biosens. Bioelectron.*, vol. 88, no. Supplement C, pp. 240–248, Feb. 2017.

[105]   K. R. Graham *et al.*, "Extended Conjugation Platinum(II) Porphyrins for use in Near-Infrared Emitting Organic Light Emitting Diodes," *Chem. Mater.*, vol. 23, no. 24, pp. 5305–5312, Dec. 2011.

[106]   M. Hollauf *et al.*, "Dye functionalized-ROMP based terpolymers for the use as a light up-converting material via triplet–triplet annihilation," *J. Mater. Chem. C*, vol. 5, no. 30, pp. 7535–7545, Aug. 2017.

[107]   T. N. Singh-Rachford and F. N. Castellano, "Triplet Sensitized Red-to-Blue Photon Upconversion," *J. Phys. Chem. Lett.*, vol. 1, no. 1, pp. 195–200, Jan. 2010.

[108]   J. Zhao, S. Ji, and H. Guo, "Triplet–triplet annihilation based upconversion: from triplet sensitizers and triplet acceptors to upconversion quantum yields," *RSC Adv.*, vol. 1, no. 6, pp. 937–950, Oct. 2011.

[109]   S. M. Borisov, R. Saf, R. Fischer, and I. Klimant, "Synthesis and properties of new phosphorescent red light-excitable platinum(II) and palladium(II) complexes with Schiff bases for oxygen sensing and triplet-triplet annihilation-based upconversion," *Inorg. Chem.*, vol. 52, no. 3, pp. 1206–1216, Feb. 2013.

[110]   F. Niedermair *et al.*, "Tunable Phosphorescent NIR Oxygen Indicators Based on Mixed Benzo- and Naphthoporphyrin Complexes," *Inorg. Chem.*, vol. 49, no. 20, pp. 9333–9342, Sep. 2010.

[111]   S. M. Borisov, G. Zenkl, and I. Klimant, "Phosphorescent Platinum(II) and Palladium(II) Complexes with Azatetrabenzoporphyrins--New Red Laser Diode-Compatible Indicators for Optical Oxygen Sensing," *ACS Appl. Mater. Interfaces*, vol. 2, no. 2, pp. 366–374, Feb. 2010.

[112]   S. M. LeCours, H.-W. Guan, S. G. DiMagno, C. H. Wang, and M. J. Therien, "Push−Pull Arylethynyl Porphyrins: New Chromophores That Exhibit Large Molecular First-Order Hyperpolarizabilities," *J. Am. Chem. Soc.*, vol. 118, no. 6, pp. 1497–1503, Jan. 1996.

[113]   J. P. Lewtak and D. T. Gryko, "Synthesis of π-extended porphyrins via intramolecular oxidative coupling," *Chem. Commun.*, vol. 48, no. 81, pp. 10069–10086, Sep. 2012.

[114]   P. N. Taylor *et al.*, "Conjugated porphyrin oligomers from monomer to hexamer," *Chem. Commun.*, no. 8, pp. 909–910, Jan. 1998.

[115]   T. K. Ahn *et al.*, "Relationship between Two-Photon Absorption and the π-Conjugation Pathway in Porphyrin Arrays through Dihedral Angle Control," *J. Am. Chem. Soc.*, vol. 128, no. 5, pp. 1700–1704, Feb. 2006.

[116]   V. V. Diev *et al.*, "Porphyrins Fused with Unactivated Polycyclic Aromatic Hydrocarbons," *J. Org. Chem.*, vol. 77, no. 1, pp. 143–159, Nov. 2011.

[117]   P. Rempala, J. Kroulík, and B. T. King, "Investigation of the Mechanism of the Intramolecular Scholl Reaction of Contiguous Phenylbenzenes," *J. Org. Chem.*, vol. 71, no. 14, pp. 5067–5081, Jun. 2006.

[118]   Y. Lu and J. S. Moore, "Semi-fused hexaphenyl hexa-peri-hexabenzocoronene: a novel fluorophore from an intramolecular Scholl reaction," *Tetrahedron Lett.*, vol. 50, no. 28, pp. 4071–4077, Jul. 2009.

Part II
Results

Chapter 5

Electron-Deficient Near-Infrared Pt(II) and Pd(II) Benzoporphyrins with Dual Phosphorescence and Unusually Efficient Thermally Activated Delayed Fluorescence – First Demonstration of Simultaneous Oxygen and Temperature Sensing with a Single Emitter

5 Electron-Deficient Near-Infrared Pt(II) and Pd(II) Benzoporphyrins with Dual Phosphorescence and Unusually Efficient Thermally Activated Delayed Fluorescence – First Demonstration of Simultaneous Oxygen and Temperature Sensing with a Single Emitter

Authors: Peter W. Zach,[a] Stefan A. Freunberger, [b] Ingo Klimant, [a] Sergey M. Borisov [a]*

(a) Institute of Analytical Chemistry and Food Chemistry, Graz University of Technology, Stremayrgase 9, 8010, Graz, Austria.
(b) Institute for Chemistry and Technology of Materials, Graz University of Technology, Stremayrgase 9, 8010, Graz, Austria.
*E-Mail: sergey.borisov@tugraz.at

5.1 Abstract

We report a family of Pt and Pd benzoporphyrin dyes with versatile photophysical properties and easy access from cheap and abundant chemicals. Attaching 4 or 8 alkylsulfone groups onto a meso-tetraphenyltetrabenzoporphyrin (TPTBP) macrocylcle renders the dyes highly soluble in organic solvents, photostable and electron-deficient with the redox potential raised up to 0.65 V versus the parent porphyrin. The new dyes intensively absorb in the blue (Soret band, 440-480 nm) and in the red (Q band, 620-650 nm) parts of the electromagnetic spectrum and show bright phosphorescence at room-temperature in the NIR with quantum yields up to 30% in solution. The small singlet–triplet energy gap yields unusually efficient thermally activated delayed fluorescence (TADF) at elevated temperatures in solution and in polymeric matrices with quantum yields as high as 27% at 120 °C, which is remarkable for benzoporphyrins. Apart from oxygen sensing these properties enable unprecedented simultaneous, self-referenced oxygen and temperature sensing with a single indicator dye: whereas oxygen can be determined either via the decay time of

phosphorescence or TADF, the temperature is accessed via the ratio of the two emissions. Moreover, the dyes are efficient sensitizers for triplet-triplet annihilation (TTA)-based upconversion making possible longer sensitization wavelength than the conventional benzoporphyrin complexes. The Pt-octa-sulfone dye also features interesting semi-reversible transformation in basic media, which generates new NIR absorbing species.

5.2 Introduction

Porphyrins play a central role in many biological processes pivotal to life and are probably the most important functional pigments found in nature.[1] They are square, planar 18 π-electron aromatic macrocycles comprising four pyrroles and four methine carbons. A rich variety of substituents in the macrocycle and of the central transition metal cation endows them with diverse functionality in nature and in human-designed applications. Platinum(II) and palladium(II) porphyrins are very popular luminophores due to their strong room temperature phosphorescence and large Stokes shifts.[2] Efficient quenching of phosphorescence by molecular oxygen enables optical oxygen sensors.[3] Phosphorescent dyes absorbing in the red part of electromagnetic spectrum and emitting in the so called near-infrared (NIR) optical window (700-950 nm) are particularly promising for various medical and therapeutic applications due to high tissue transparency and low autofluorescence.[4] For instance, they proved to be excellent tools for microscopic *in vivo* imaging of tissue oxygenation, e.g., of tumors, blood vessels, brain slices etc. [5] Recently, NIR phosphorescent dyes were applied as indicators in a system combining continuous subcutaneous glucose monitoring and insulin infusion. [6]

Similarly to other chemosensors, the response of optical oxygen sensors is temperature-dependent and has to be compensated for. This can be done via an external probe (e.g. a resistance thermometer) or with an optical temperature probe,[7] which can be combined with the oxygen probe in a dual sensor.[8]–[10] Whereas the first method lacks spatial resolution, dual sensors are complex in design and often suffer from undesirable effects including optical cross-talk and chemical interferences between oxygen and temperature probes. Although numerous systems for simultaneous sensing of oxygen and temperature have been reported, to the best of our knowledge there are no systems based on a single probe.

Phosphorescent dyes are also particularly useful as sensitizers for upconversion systems based on triplet-triplet annihilation (TTA).[11],[12] TTA upconversion overcomes the drawbacks of other upconversion techniques such as lanthanide upconversion and multi-photon excitation. It is observed at low excitation power densities (typical for e.g., solar light) [13] and enables variation of the excitation and emission wavelength by tuning triplet sensitizer and triplet acceptor. Recent research was focused on developing highly photostable and soluble triplet sensitizers for the red region of the spectrum.[14]–[17] Sensitizers with a small singlet-triplet energy gap are advantageous since they enable longer sensitization wavelengths and are compatible with annihilators with relatively high triplet state energy.

The most promising way to achieve a bathochromic shift of the absorption and the emission bands of porphyrinoids is the extension of the π-conjugated system of the porphyrin core through fusion of various aromatic moieties at the β-pyrrole positions [18], [19] leading, for example, to tetrabenzoporphyrins (TBP)[20] or tetranaphthaloporphyrins (TNP).[21] These complexes have only moderate solubility due to strong tendency to π-π-stacking,[22] but the solubility can be improved by introducing phenyl rings at the meso-position of the porphyrin core and other bulky substituents such as tert-butyl groups.[6] Photostability is another parameter which may need improvement; it is, for instance, particularly poor for naphthoporphyrins bearing no electron-withdrawing substituents.[23] Zems et al. have recently reported the multi-step synthesis (10 steps) of a highly soluble platinum(II) porphyrin with excellent solubility and very high photostability.[24]

Herein we present electron-deficient highly soluble and photostable platinum(II) and palladium(II) benzoporphyrins bearing alkylsulfone groups that are accessible via a convenient and simple synthetic strategy with only four steps from cheap and abundant precursors. All new dyes feature a smaller singlet-triplet energy gap compared to state-of-the-art benzoporphyrins. This gives rise to unusually efficient thermally activated delayed fluorescence (TADF) at elevated temperatures. We will demonstrate their applicability for simultaneous measurement of oxygen and temperature with a single probe, which is so far unique in literature. We also show that the new dyes are very promising for TTA-based upconversion since they can harvest more energy in the red part of the spectrum and transfer it to a variety of annihilators.

5.3 Experimental Section

5.3.1 Materials

(3aR,7aS)-3a,4,7,7a-tetrahydroisobenzofuran-1,3-dione, 2-ethylhexane-1-thiol, potassium t-butoxide, 2-ethylhexylamine, N-chlorosuccinimide, thiophenol, potassium carbonate, tetraoctylammonium hydroxide solution (20% in methanol), trifluoroacetic acid, chlorotrimethylsilane and water-free dichloromethane (DCM) were purchased from Sigma Aldrich. Meta-chloroperoxybenzoic acid (m-CPBA), 1,2,4-trimethylbenzene (TMB), aluminum oxide (neutral, 50-200 µm; Al_2O_3), Poly(styrene-co-acrylontrile) (PSAN; 25 wt% acrylonitrile; Mw = 165,000 g·mol^{-1}) and polystyrene (PS; Mw = 260,000 g·mol^{-1}) were obtained from Acros Organics. 1,8-diaza-7-bicyclo[5.4.0]undecene (DBU), perylene and dimethylacetamide (DMA) were from Fluka. Ethyl 2-isocyanoacetate, 2-(4-fluorophenyl)acetic acid and Solvent Green 5 (diisobutyl 3,9-perylenedicarboxylate) were purchased from ABCR. Dry dimethylformamide (DMF), dry hexane silica gel 60 and zinc oxide were obtained from Merck. Zinc-4-fluorophenylacetate was obtained as a white precipitate in an exchange reaction between zinc acetate and 2-(4-fluorophenyl)acetic acid. Sodium hydrogen carbonate, sodium sulfate, sodium chloride and sodium carbonate were from VWR. 4,5-dichlorophthalonitrile and boron trifluoride etherate, were purchased from TCI. Ultrafine TiO_2 P170 was obtained from Kemira. Silicone E4 was purchased from Wacker chemicals (Munich, Germany). N,N′-bis-(2,6-diisopropylphenyl)-perylene-3,4,9,10-tetracarboxylic acid diimide

(Lumogen F Orange) and N,N′-bis-(2,6-diisopropylphenyl)-1,6,7,12-tetraphenoxyperylene-3,4:9,10- tetracarboxylic acid diimide "Lumogen red" were obtained from Kremer Pigmente GmbH and Co. KG (Aichstetten, Germany). Cyclohexane (CH), ethyl acetate (EE), n-hexane, dry tetrahydrofuran (THF) as well as toluene and chloroform in HPLC-grade were obtained from Roth. Methanol (MeOH) was from Baker (Munich, Germany), whereas ethanol (EtOH) was from Australco (Spillern, Austria). Toluene and dichloromethane (DCM) were obtained from Fisher Chemicals. Nitrogen, argon (both 99.999% purity) was purchased from Air Liquide (Graz, Austria), oxygen (99.999% purity) and oxygen (2%) in nitrogen (test gas) from Linde Gas (Graz, Austria). Poly(ethylene terephthalate) (PET) support Melinex 505 was purchased from Pütz (Taunusstein, Germany).

Platinum chloride and palladium chloride for the synthesis of the respective precursor were obtained from ChemPur. The precursors Pt(C$_6$H$_5$CN)$_2$Cl$_2$ as well as the Pd(C$_6$H$_5$CN)$_2$Cl$_2$ were obtained by stirring PtCl$_2$ or PdCl$_2$ in boiling benzonitrile for one hour and precipitating the resulted product with hexane. The formed yellow product was filtered, washed with hexane, and dried at 60 °C in the vacuum oven. The reference compounds platinum(II) and palladium(II) complexes of meso-tetraphenyltetrabenzoporpyhrin (Pt-TPTBP and Pd-TPTBP, respectively)[25] and BF$_2$ chelate of [5-(4-buthoxyphenyl)-3-phenyl-1H-pyrrol-2-yl][5-(4-buthoxyphenyl)-3-phenylpyrrol-2-ylidene]amine ("dibutoxy-aza-BODIPY") were prepared according to a literature procedure.[26]

5.3.2 Synthesis

4,5-bis((2-ethylhexyl)thio)phthalonitrile

The reaction was conducted according to the literature procedure.[27] 4,5-dichlorophthalonitrile (9.00 g, 45.68 mmol, 1.00 eq) was first dissolved in 100 mL dimethylacetamide (DMA) in a 2-neck round bottom flask and the solution was degassed in argon counterflow for 10 minutes. Then ground, dry K$_2$CO$_3$ (18.00 g, 130.2 mmol, 2.85 eq) was added and the solution was again degassed for further 10 minutes. 2-ethylhexane-1-thiol (14.71 g, 100.6 mmol, 2.20 eq, ρ=0.8430 g/mL) was added and the resulting reaction mixture was heated to 90 °C for 8 hours (vigorous stirring). Afterwards, the reaction mixture was poured onto dest. H$_2$O and extracted with DCM (3 times). The organic fraction was washed with dest. H$_2$O (6 × 100 mL) to remove dimethylacetamide, dried over Na$_2$SO$_4$, before the solvent was finally evaporated in vacuo to afford the product as yellow oil. Yield: 14.85 g, 78 %.

^{1}H NMR (300 MHz, Chloroform-*d*) δ 7.41 (s, 2H), 2.97 (d, *J* = 6.2 Hz, 4H), 1.71 (p, *J* = 6.2 Hz, 2H), 1.58-1.40 (m, 8H), 1.36-1.26 (m, 8H), 0.94-0.84 (m, 12H).

*Zinc(II) meso-tetra(4-fluorophenyl)-tetra(4,5-bis(2-ethylhexylthio))benzoporphyrin (**Zn-O-T**)*
4,5-bis((2-ethylhexyl)thio)phthalonitrile (12.94 g, 31.05 mmol, 4.00 eq), 2-(4-fluorophenyl)acetic acid (11.96 g, 77.59 mmol, 10.00 eq), zinc-4-fluorophenylacetate (2.90 g, 7.76 mmol, 1.00 eq) were mixed together and homogenized with a ceramic pestle in a mortar. Approximately 700 mg of the mixture were weighed in 4 mL glass vials equipped with a stirring bar. The vials were sealed with a metal cap and put on a 160 °C heating block and then heated up to 280 °C. After reaching 280 °C the stirrer was started and the reaction mixture was kept at this temperature for 40 minutes. Then the vials were removed from the heating source and cooled down. Afterwards the vials were smashed with a hammer and the reaction products were dissolved in 800 mL acetone in an ultrasonic bath. The pieces of glass were separated via filtration and the solvent was removed under reduced pressure. The residue was re-dissolved in 800 mL cyclohexane/n-hexane (2:1) and washed with methanol (6 × 300 mL). The impurities were removed via column chromatography (silica-gel, CH:DCM, 2:1) and the product dried in the vacuum oven at 60 °C. Yield: 0.92 g, 6%. This intermediate was used in further step without further purification.
UV-Vis: $\lambda_{max}/\varepsilon$ (nm, $M^{-1}cm^{-1}$) in toluene: 478/ 347.000, 625/ 19.000, 678/ 115.000
MALDI: m/z: [M^+]; $C_{124}H_{160}F_4N_4S_8Zn$, calc.: 2103.966; found: 2103.964

*Meso-tetra(4-fluorophenyl)-tetra(4,5-bis(2-ethylhexylthio))benzoporphyrin (**H₂-O-T**)*
Zn-O-T (430 mg, 204.3 µmol) was dissolved in 200 mL DCM and 50 mL of 4 M HCl were added. The resulting protonated ligand could be determined via absorption spectra (λ_{max} (nm)/relative intensity) in toluene: 423/ 0.090, 524/ 1.00, 662/ 0.076, 721/ 0.087). The organic phase was washed twice with and then with saturated $NaHCO_3$-solution until only neutral ligand was observed in the absorption spectra. Finally the organic layer was once more washed with dest. H_2O, dried over Na_2SO_4 and the solvent was removed under reduced pressure. Yield: 380 mg, 91%. The product was introduced in the next step without further purification due to its high tendency to oxidation.
UV-Vis: $\lambda_{max}/\varepsilon$ (nm, $M^{-1}cm^{-1}$) in toluene: 475/ 155.000, 490/ 154.000, 614/ 12.000, 668/ 50.000, 717/ 17.000
MALDI: m/z: [M^+]; $C_{124}H_{162}F_4N_4S_8$, calc.: 2040.053; found: 2040.038

*Meso-tetra(4-fluorophenyl)-tetra(4,5-bis(2-ethylhexylsulfoneyl))benzoporphyrin (**H₂-O-S**)*
H₂-O-T (245 mg, 120 µmol, 1.00 eq) was dissolved in 30 mL DCM in a round bottom flask and m-CPBA (518 mg, 3 mmol, 25.00 eq) was added slowly to the stirring solution using a plastic spatula. The solution was shielded from light and the reaction progress monitored via absorption spectra and TLC. After complete conversion, the reaction mixture was quenched with saturated $NaHCO_3$-solution, extracted with DCM (3 × 60 mL) and dried over Na_2SO_4. The solvent was removed under reduced pressure. Finally, the crude product was purified via column chromatography (silica-gel, CH:EE, 9:1) to yield **H₂-O-S** as dark green solid. Yield: 165 mg, 60 %.
UV-Vis. λ_{max}(nm)/relative intensity in toluene: 488/ 1.00, 599/ 0.061, 638/ 0.088, 709/ 0.011
^{1}H NMR (300 MHz, Methylene Chloride-d_2) δ 8.48 – 8.20 (m, 16H), 7.89 – 7.68 (m, 8H), 3.69 –

3.43 (m, 16H), 1.95 (dq, J = 12.0, 6.5 Hz, 8H), 1.55 – 1.36 (m, 33H), 1.33 – 1.14 (m, 35H), 0.88 – 0.78 (m, 50H).

^{13}C NMR (76 MHz, CD$_2$Cl$_2$) δ 167.12, 163.77, 138.14, 135.91, 135.79, 135.76, 118.40, 117.87, 117.59, 60.59, 35.03, 32.96, 28.50, 26.32, 14.17, 10.39.

MALDI: m/z: [M$^+$]; C$_{124}$H$_{162}$F$_4$N$_4$O$_{16}$S$_8$, calc.: 2296.973; found: 2296.988

*Pt(II) meso-tetra(4-fluorophenyl)-tetra(4,5-bis(2-ethylhexylsulfoneyl))benzoporphyrin (**Pt-O-S**)*

H$_2$-O-S (50 mg, 22.77 µmol, 1.00 eq) was dissolved in TMB (15 mL) in a 2-neck-round bottom flask and heated to 175 °C while bubbling N$_2$ through the reaction mixture. Then Pt(C$_6$H$_5$CN)$_2$Cl$_2$ (103 mg, 217.7 µmol, 10 eq) was added slowly in small portions (5 × 2 eq pre-dissolved in hot TMB) from a pre-heated addition funnel (100 °C) over a period of 3 hours. The reaction progress was monitored via absorption spectra. After completion the reaction mixture was cooled down to room temperature, the by-products were removed via filtration over a short pad of silica-gel. The solvent was removed under reduced pressure at 80 °C. The crude product was further purified via column chromatography (silica-gel, CH:EE, 9:1). The product containing fractions were determined via absorption spectrum and the solvent was removed under reduced pressure. Yield: 165 mg, 60 %.

UV-Vis: λ$_{max}$/ε (nm, M^{-1}cm^{-1}) in toluene: 455/ 370.000, 572/ 25.000, 621/ 229.000

^{1}H NMR (500 MHz, CD$_2$Cl$_2$) δ 8.22 (s, 16H), 7.76 (dq, J = 8.4, 2.8 Hz, 8H), 3.62 – 3.49 (m, 16H), 1.95 (dq, J = 11.6, 5.8 Hz, 8H), 1.49 (q, J = 7.1 Hz, 16H), 1.45 – 1.34 (m, 20H), 1.33 – 1.17 (m, 36H), 0.92 – 0.78 (m, 47H)

^{13}C NMR (126 MHz, CD$_2$Cl$_2$) δ 166.07, 164.05, 139.24, 137.33, 136.67, 134.55, 134.49, 129.97, 120.74, 117.81, 117.63, 60.21, 34.61, 32.56, 28.09, 25.93, 22.69, 13.73, 9.97.

MALDI: m/z: [M$^+$]; C$_{124}$H$_{160}$F$_4$N$_4$O$_{16}$S$_8$Pt, calc.: 2489.9211; found: 2489.9229

*Pd(II) meso-tetra(4-fluorophenyl)-tetra(4,5-bis(2-ethylhexylsulfoneyl))benzoporphyrin (**Pd-O-S**)*

H$_2$-O-S (45 mg, 19.59 µmol, 1.00 eq) was dissolved in toluene (10 mL) in a 2-neck-round bottom flask and heated to 110 °C, while bubbling N$_2$ through the reaction mixture. Then Pd(C$_6$H$_5$CN)$_2$Cl$_2$ (9 mg, 23.51 µmol, 1.2 eq) was added slowly in small portions (4 × 0.3 eq pre-dissolved in hot toluene) from a pre-heated addition funnel (100 °C) over a period of 2 hours. The reaction progress was monitored via absorption spectra. After completion the reaction mixture was cooled down to room temperature, the by-products were removed via filtration over a short pad of silica-gel. The solvent was removed under reduced pressure at 60 °C. The crude product was further purified via column chromatography (silica-gel, CH:EE, 4:1). The product containing fractions were determined via absorption spectrum and the solvent was removed under reduced pressure. Yield: 36 mg, 77%.

UV-Vis. λ$_{max}$/ε (nm, M^{-1}cm^{-1}) in toluene: 422/ 36.000, 438/ 58.000, 469/ 446.000, 588/ 23.000 636/ 195.000

^{1}H NMR (300 MHz, CD$_2$Cl$_2$) δ 8.29 – 8.16 (m, 16H), 7.75 (t, J = 8.4 Hz, 8H), 3.69 – 3.37 (m, 15H), 2.03 – 1.85 (m, 8H), 1.51 – 1.44 (m, 16H), 1.43 – 1.33 (m, 24H), 1.32 – 1.12 (m, 34H), 0.93 – 0.74 (m, 47H).

^{13}C NMR (76 MHz, CD_2Cl_2) δ 167.11, 163.76, 139.93, 139.05, 137.53, 135.36, 135.32, 135.23, 135.13, 130.32, 120.62, 118.12, 117.83, 60.59, 35.00, 32.95, 28.49, 26.31, 23.12, 14.15, 10.38.

MALDI: m/z: [M+]; $C_{124}H_{160}F_4N_4O_{16}S_8Pd$, calc.: 2400.8601; found: 2400.6062

4-((2-ethylhexylthio)phthalonitrile

4-nitrophthalonitrile (8.50 g, 49.10 mmol, 1.00 eq) was first dissolved in 110 mL dimethylacetamide (DMA) in a 2-neck round bottom flask and the solution was degassed in argon-counterflow for 10 minutes. Then ground, dry K_2CO_3 (19.34 g, 139.92 mmol, 2.85 eq) was added and the solution was degassed again for further 10 minutes. Then 2-ethylhexane-1-thiol (10.77 g, 73.64 mmol, 1.5 eq, ρ=0.8430 g/mL) was added and the resulting reaction mixture heated to 90 °C for 15 hours (vigorous stirring). Afterwards the reaction mixture was poured onto dest. H_2O and extracted with DCM (6 times). The organic fraction was washed with dest. H_2O (6 x 100 mL) to remove DMA, then dried over Na_2SO_4 before the solvent was finally evaporated under reduced pressure. Finally, the crude product was purified via column chromatography on silica gel to afford the product as yellow oil. Yield: 12.82 g, 96 %.

^{1}H NMR (300 MHz, $CDCl_3$) δ 7.63 (d, J = 8.3 Hz, 1H), 7.55 (d, J = 1.9 Hz, 1H), 7.49 (dd, J = 8.4, 2.0 Hz, 1H), 2.97 (d, J = 6.2 Hz, 2H), 1.66 (p, J = 6.2 Hz, 1H), 1.55- 1.37 (m, 4H), 1.31 (dh, J = 7.3, 3.7 Hz, 4H), 0.99-0.84 (m, 6H).

*Zinc(II) meso-tetra(4-fluorophenyl)-tetra(4-(2-ethylhexylthio))benzoporphyrin (**Zn-T-T**)*

The synthesis and purification were performed analogously to **Zn-O-T** but 18.00 g (66.08 mmol, 4.00 eq) of 4-((2-ethylhexyl)thio)phthalonitrile, 25.46 g (165.19 mmol, 10.00 eq) of 2-(4-fluorophenyl)acetic acid and 6.14 (16.52 mmol, 1.00 eq) of zinc 4-fluorophenylacetate were used instead. This intermediate was used in further step without further purification. Yield: 0.98 g, 4%.

UV-Vis. λ_{max}(nm)/relative intensity in toluene: 470/ 1.00, 615/ 0.058, 666/ 0.312

MALDI: m/z: [M+]; $C_{92}H_{96}F_4N_4S_4Zn$, calc.: 1526.5754; found: 1526.6571

*Meso-tetra(4-fluorophenyl)-tetra(4-(2-ethylhexylthio))benzoporphyrin (**H₂-T-T**)*

The demetalation was performed analogously to **H₂-O-T** but with 512 mg (335.21 µmol, 1.00 eq) of **Zn-T-T**. The product was introduced in the next step without further purification due to its high tendency to oxidation. Yield: 485 mg, 97%

λ_{max}(nm)/relative intensity in toluene: 474/ 1.00, 599/ 0.202, 649/ 0.173, 707/ 0.059

MALDI: m/z: [M+]; $C_{92}H_{98}F_4N_4S_4$, calc.: 1463.6642; found: 1463.9174

*Meso-tetra(4-fluorophenyl)-tetra(4-(2-ethylhexyl)sulfoneyl))benzoporphyrin (**H$_2$-T-S**)*

The synthesis and purification were performed analogously to **H$_2$-O-S** but 450 mg (307.36 µmol, 1.00 eq) of **H$_2$-T-T** was dissolved in 30 mL DCM in a round bottom flask and m-CPBA (663 mg, 3.84 mmol, 12.50 eq) were used instead. Yield: 230 mg, 47 %.

UV-Vis. λ_{max}(nm)/relative intensity in toluene: 475/ 1.00, 593/ 0.054, 631/ 0.109

^{1}H NMR (300 MHz, Methylene Chloride-d$_2$) δ 8.48 – 8.20 (m, J = 7.8, 6.7 Hz, 8H), 7.87 – 7.54 (m, 29H), 3.13 – 2.91 (m, 10H), 1.93 – 1.81 (m, 4H), 1.52 – 1.31 (m, 24H), 1.33 – 1.10 (m, 28H), 0.94 – 0.72 (m, 40H).

^{13}C NMR (76 MHz, CD$_2$Cl$_2$) δ 166.40, 163.08, 137.17, 136.40, 136.32, 125.31, 117.29, 117.01, 60.14, 34.86, 34.62, 32.87, 32.72, 28.53, 26.25, 26.08, 23.09, 14.18, 10.36.

MALDI: m/z: [M$^+$]; C$_{92}$H$_{98}$F$_4$N$_4$O$_8$S$_4$, calc.: 1591.6235; found: 1591.6461

*Pt(II) meso-tetra(4-fluorophenyl)-tetra(4-(2-ethylhexyl)sulfoneyl))benzoporphyrin (**Pt-T-S**)*

The synthesis and purification were performed analogously to **Pt-O-S** but 55 mg (34.55 µmol, 1.00 eq) of **H$_2$-T-S** and 20 mg (41.46 µmol, 1.2 eq) of Pt(C$_6$H$_5$CN)$_2$Cl$_2$ (4 x 0.3 eq) were used instead. Yield: 40 mg, 65 %.

UV-Vis. $\lambda_{max}/\varepsilon$ (nm, M^{-1}cm^{-1}) in toluene: 441/ 255.000, 570/ 18.000, 619/ 145.000

^{1}H NMR (500 MHz, CD$_2$Cl$_2$) δ 8.31 – 8.19 (m, 8H), 7.88 – 7.78 (m, 4H), 7.78 – 7.66 (m, 10H), 7.63 (dd, J = 4.3, 1.6 Hz, 2H), 7.41 (dd, J = 8.6, 3.3 Hz, 2H), 7.30 (dd, J = 8.6, 3.4 Hz, 2H), 3.02 (q, J = 5.6 Hz, 8H), 1.88 (dh, J = 12.6, 6.2 Hz, 4H), 1.48 (p, J = 6.4, 5.9 Hz, 8H), 1.44 – 1.33 (m, 8H), 1.29 – 1.14 (m, 17H), 0.88 – 0.80 (m, 24H).

^{13}C NMR (76 MHz, CD$_2$Cl$_2$) δ 166.44, 163.11, 140.72, 140.60, 138.11, 137.41, 136.64, 136.59, 135.53, 135.42, 125.13, 117.70, 117.42, 60.14, 34.86, 32.86, 28.53, 26.25, 23.09, 14.17, 10.37.

MALDI: m/z: [M$^+$]; C$_{92}$H$_{96}$F$_4$N$_4$O$_8$S$_4$Pt, calc.: 1784.8007; found: 1784.6431

*Pd(II) meso-tetra(4-fluorophenyl)-tetra(4-(2-ethylhexyl)sulfoneyl))benzoporphyrin (**Pd-T-S**)*

The synthesis and purification were performed analogously to **Pd-O-S** but 60 mg (37.7 µmol, 1.00 eq) of **H$_2$-T-S** and 17 mg (45.2 µmol, 1.2 eq) of Pd(C$_6$H$_5$CN)$_2$Cl$_2$ were used instead. Yield: 41 mg, 64 %.

UV-Vis. $\lambda_{max}/\varepsilon$ (nm, M^{-1}cm^{-1}) in toluene: 426/ 53.000, 454/ 328.000, 585/ 17.000, 633/ 125.000

^{1}H NMR (300 MHz, CD$_2$Cl$_2$) δ 8.37 – 8.15 (m, 8H), 7.89 – 7.61 (m, 16H), 7.43 (dd, J = 8.6, 2.0 Hz, 2H), 7.32 (dd, J = 8.7, 2.0 Hz, 2H), 3.10 – 2.93 (m, 8H), 1.87 (p, J = 5.3 Hz, 4H), 1.51 – 1.35 (m, 13H), 1.30 – 1.12 (m, 20H), 0.93 – 0.76 (m, 26H).

^{13}C NMR (76 MHz, CD$_2$Cl$_2$) δ 166.42, 163.09, 141.02, 140.88, 139.25, 138.47, 138.03, 137.79, 136.94, 136.89, 135.75, 135.64, 125.18, 125.01, 124.73, 117.57, 117.29, 60.16, 34.86, 32.86, 28.53, 26.26, 23.09, 14.17, 10.37.

MALDI: m/z: [M$^+$]; C$_{92}$H$_{96}$F$_4$N$_4$O$_8$S$_4$Pd, calc.: 1694.3896 ; found: 1694.5107

*Pt(II) meso-tetraphenyl-tetra(2-(2-ethylhexyl)hexahydro-1H-isoindole-1,3(2H)-dione)porphyrin (**Pt-TPThIIP**)*

The synthesis and purification were performed analogously to **Pt-O-S** but 100 mg (64.26 µmol, 1.00 eq) of **H$_2$-TPThIIP** (obtained according to a modified literature procedure, see supporting information) and 303 mg (642.6 µmol, 10 eq) of Pt(C$_6$H$_5$CN)$_2$Cl$_2$ 5 × 2 eq) were used instead. Yield: 56 mg, 50 %.

UV-Vis. λ_{max}(nm)/relative intensity in toluene: 416/ 1.00, 525/ 0.106, 555/ 0.053

*Pt(II) meso-tetraphenyl-tetrabenzo-1-(2-ethylhexyl)pyrrolidine-2,5-dione-porphyrin (**Pt-T-I**)*

Pt-TPThIIP (56 mg, 32.02 µmol, 1.00 eq) was dissolved in toluene (8 ml) in a Schlenk flask under a flow of argon and heated to 110 °C. Then DDQ (109 mg, 480.2 µmol, 15 eq) was added in argon counterflow and the reaction mixture was stirred for 4 hours. The reaction was shielded from light and the reaction progress monitored via absorption spectra and TLC. After complete conversion, the reaction mixture was quenched with Na$_2$SO$_3$-solution(10%), extracted with DCM (3 × 25 mL) and dried over Na$_2$SO$_4$. The solvent was removed under reduced pressure. Finally, the crude product was purified via column chromatography (silica gel, CH:EE, 8:1) The product containing fractions were determined via absorption spectrum and dried in the vacuum oven at 60 °C. Yield: 18 mg, 32 %.

UV-Vis. λ_{max}/ε (nm, M^{-1}cm^{-1}) in toluene: 463/ 283.000, 582/ 21.000, 633/ 184.000

^{1}H NMR (300 MHz, CD$_2$Cl$_2$) δ 8.29 (d, J = 7.1 Hz, 8H), 8.21 (t, J = 7.5 Hz, 4H), 8.06 (t, J = 7.5 Hz, 8H), 7.43 (s, 8H), 3.52 (d, J = 7.1 Hz, 8H), 1.85 – 1.70 (m, 4H), 1.37 – 1.20 (m, 41H), 0.92 – 0.81 (m, 28H).

^{13}C NMR (76 MHz, CD$_2$Cl$_2$) δ 168.62, 141.39, 140.45, 137.62, 134.06, 131.20, 130.70, 129.49, 121.57, 120.01, 54.00, 42.54, 39.05, 31.19, 29.22, 24.48, 23.54, 14.40, 10.79.

MALDI: m/z: [M$^+$]; C$_{100}$H$_{96}$N$_8$O$_8$Pt, calc.: 1732.7025; found: 1732.6790

*Pd(II) tetraphenyl-tetra(2-(2-ethylhexyl)hexahydro-1H-isoindole-1,3(2H)-dione)porphyrin (**Pd-TPThIIP**)*

The synthesis and purification were performed analogously to **Pd-O-S** but 95 mg (61.05 µmol, 1.00 eq) of **H$_2$-TPThIIP** and 94 mg (244.2 µmol, 4 eq) of Pd(C$_6$H$_5$CN)$_2$Cl$_2$ (4 x 1 eq) were used instead. Yield: 60 mg, 59 %.

λ_{max}(nm)/relative intensity in toluene: 431/ 1.00, 539/ 0.090, 572/ 0.005

*Pd(II) meso-tetraphenyltetrabenzo-1-(2-ethylhexyl)pyrrolidine-2,5-dione-porphyrin (**Pd-T-I**)*

The synthesis and purification were performed analogously to **Pt-T-I** but 60 mg (36.13 µmol, 1.00 eq) of **Pd-TPThIIP** and 123 mg (542.0 µmol, 15 eq) of DDQ were used instead. Yield: 24 mg, 40 %.

UV-Vis. λ_{max}/ε (nm, M^{-1}cm^{-1}) in toluene: 478/ 390.000, 597/ 22.000, 648/ 179.000

^{1}H NMR (300 MHz, CD_2Cl_2) δ 8.29 (d, 8H), 8.21 (t, J = 7.5 Hz, 4H), 8.06 (t, J = 7.5 Hz, 8H), 3.52 (d, J = 7.1 Hz, 8H), 1.85 – 1.71 (m, 4H), 1.39 – 1.16 (m, 38H), 0.97 – 0.78 (m, 27H).

^{13}C NMR (76 MHz, CD_2Cl_2) δ 167.27, 140.05, 139.10, 136.27, 132.71, 129.85, 129.35, 128.15, 120.23, 118.67, 41.20, 37.70, 29.84, 27.87, 23.14, 22.20, 13.05, 9.45.

MALDI: m/z: [M$^+$]; $C_{100}H_{96}N_8O_8Pd$, calc.: 1642.6415; found: 1642.7184

5.3.3 Preparation of Sensor Films

Sensor films of various thicknesses (wet film thickness of 25 or 75 µm) were prepared by coating the dye "cocktails" on a dust-free PET support using a 25 mm-wide Gardner coating knife (Pompano Beach, United States). The polystyrene (as well as PSAN)-based "cocktails" typically contained 1 - 2.5 wt% dye (in respect of the polymer) and 8-10 wt% of polymer dissolved in chloroform (HPLC-grade). After the coating, the sensor films were dried for 24 hours at 60 °C to ensure complete removal of solvent.

For the TADF measurements the polystyrene or PSAN-based dye "cocktails" in $CHCl_3$ ($1.12 \cdot 10^{-6}$ M of the dye) were knife coated on a glass slide (thickness of the wet film: 12.5 µm) which was silanised with chlorotrimethylsilane prior to use. The sensors were dried in the oven at 60 °C for 12 hours.

5.3.4 Measurements

NMR and Mass Spectra

^{1}H and ^{13}C NMR were recorded on a 300 MHz instrument (Bruker AVANCE III) or 500 MHz from Varian. In all ^{1}H and ^{13}C spectra, the residual signal of the deuterated solvent was used as an internal standard to reference the chemical shifts δ. Data analysis was done with the MestraNova NMR software. High resolution mass spectra were recorded using a Micromass TofSpec 2E as positive reflector on a Bruker Ultraflex Extreme MALDI-TOF/TOF spectrometer. The mass spectra were analyzed with the FlexAnalysis 3.0 software (Bruker Daltonics).

Absorption and Luminescence Spectra, Quantum Yield and Decay time measurements

The absorption spectra were recorded on a CARY 50 UV-Vis spectrophotometer from Varian (Palo Alto, United States). Molar absorption coefficients were determined in toluene (HPLC-grade) as an average of three independent measurements. Photophysical studies in solutions were performed for the dye concentrations of between 2 and $4 \cdot 10^{-6}$ mol·l^{-1}. Luminescence spectra were recorded on a FluoroLog® 3 spectrofluorometer from Horiba Scientific equipped with a NIR-sensitive R2658 photomultiplier from Hamamatsu (300-1050 nm). Relative quantum yields in toluene were determined according to Crosby and Demas [28] using solution of dibutoxy-aza-BODIPY in chloroform as a reference (Φ = 36%). All dye solutions were deoxygenated in a screw-cap cuvette (Hellma; Müllheim, Germany) by bubbling argon through the solution for 10 minutes. For the TADF

studies in solution the temperature of the cuvette was adjusted with a Peltier-element cuvette adaptor from Varian. Absolute quantum yields of the dyes embedded in polystyrene were measured using a Quanta-ϕ integrating sphere from Horiba. To ensure deoxygenated conditions within the experiment, the stamped out pieces of dye-coated PET support were placed in a 5% Na_2SO_3 solution containing traces of $CoCl_2$ as a catalyst. Phosphorescence decay times in solution were determined in the frequency domain with a Firesting oxygen meter from Pyro Science (Aachen, Germany) (modulation frequencies of 4 kHz and 500 Hz for Pt(II) and Pd(II) complexes, respectively).

TADF Measurements of Immobilized Dyes

The glass slides were placed in a home-made flow-through cell through which the gas was passed with a pressure of 1 bar. The gas was heated to the respective temperature in a home-made oven. The exact temperature in the chamber of the flow-through cell was determined using a Pt-100 temperature sensor connected to a Firesting oxygen meter from Pyro Science. Excitation was either performed with the 450 W xenon lamp (steady state measurements) or with SpectraLED 460 nm (decay time measurements) from Horiba.

Photostability Tests

Dye solutions in toluene (HPLC-grade) were placed in a screw-cap cuvette (Hellma; Müllheim, Germany) and illuminated with a high-power LED (λ_{max} 617 nm, LT-2033, www.LED-TECH.de) at the 28 V and 550 mA. The light of the LED-array was focused onto the glass cuvette using a lens from Edmund optics. The photon flux was 18.000 µmol s^{-1} m^{-2} µA (irradiance 350 mW·cm^{-2}) as determined with a Li-250A light meter from Li-COR (Nebraska, USA). For measurements at air saturation the cuvette was unsealed and shaken after each irradiation interval to ensure air saturation in the sample. For measurements at anoxic conditions the dye solution in the cuvette was bubbled through with argon for ten minutes prior to the experiment. The cuvette was unsealed after each irradiation interval, and the solvent was refilled to compensate its loss caused by the argon bubbling. Before starting the next irradiation/measurement cycle the dye solution was again deoxygenated by argon bubbling for 3 minutes.

Cyclic voltammetry measurements

Cyclic voltammetry measurements were performed with 1 mM dye concentration and 0.05 M tetrabutylammonium perchlorate in dry dichloromethane as the supporting electrolyte at a 1.6 mm diameter Au disk electrode (BAS Inc.) at a scan rate of 0.1 V·s^{-1}. The working electrode was polished with 0.05 □m Alumina, rinsed with dry ethanol, and dried under vacuum. Pt and Ag wires served as the counter and pseudo reference electrode, respectively. The reference potential was calibrated versus the ferrocene/ferrocenium (Fc/Fc^+) couple. The measurement cell and electrolyte

were purged with argon prior to the measurements. All measurements were done inside an Ar filled glove box (MBraun) in the dark using a Biologic SP-300 electrochemical work station.

Oxygen response of the polystyrene sensors

Calibration of all sensors was carried out using a Firesting oxygen meter form Pyro Science. The modulation frequency for all the Pt(II)-dyes was 4 kHz, whereas the modulation frequency for all the Pd(II)-dyes was 500 Hz. The composition of the gas was adjusted using a custom-build gas-mixing device based on mass-flow controllers from MKS (Munich, Germany) and Voegtlin (Hamburg, Germany) by mixing compressed air, nitrogen and oxygen. Temperatures were controlled and kept constant by a cryostat ThermoHaake DC50.

Upconversion experiments

Upconversion measurements were performed on FluoroLog® 3 spectrofluorometer from Horiba. Besides excitation of the sensitizer-annihilator solutions in toluene with a 450 W xenon lamp (standard), a laser diode (635 nm, from Roithner-Laser.com) was used. Due to the high concentration of the sensitizer-annihilator solutions all spectra were recorded in the front-face mode. All solutions were deoxygenated in a screw-cap cuvette (Hellma) by bubbling argon through the solution for 10 minutes. For the kinetic measurements the following transmission filters (50%, 25%, 10%, 5%) were used. The quantum yields of the upconverted fluorescence were roughly estimated by comparing the emission of the annihilator and the emission of the sensitizer without the annihilator as well as the emission of an 5,5-difluoro-1,3,7,9-tetraphenyl-5H-4l4,5l4-dipyrrolo[1,2-c:2',1'-f][1,3,5,2]triazaborinine [29] used as a reference. The photographic images of the upconverted fluorescence were acquired using 635, 650 and 675 laser diodes (Roithner) with Canon 5D camera.

5.4 Results and Discussion

5.4.1 Synthesis

The platinum(II) and palladium(II) complexes of the octa- and tetra-sulfone dyes (Pt(II)-O-S, Pt(II)-T-S) were conveniently prepared in only four steps following the template method (Figure 5.1). Generally, template condensation starting from very cheap and readily available chemicals such as phthalimide and phenylacetic acid represents an alternative way to the more elaborate synthetic pathway used by Zems et al. (Figure 5.2), in which the porphyrin is prepared under standard Lindsey conditions[30] and converted into benzoporpyhrin via oxidative aromatization. On the other hand, the template method was often reported to produce a number of side products (benzyl-substituted porphyrins), which are extremely challenging to remove.[31], [32] Moreover, not all compounds are suitable for the use in template condensation, since they must tolerate very high temperatures (340-360 °C). Recently, Hutter et al.[33] reported a modified version of the template method yielding analytically pure benzoporphyrins in which phthalonitrile was used instead of

phthalimide with the condensation performed at only 280 °C. This modified method was adapted for the synthesis of Pt(II)-O-S and Pt(II)-T-S dyes using 4,5-bis(2-ethylhexylthio)phthalonitrile or 4-(2-ethylhexylthio)phthalonitrile, respectively, as starting compounds (Figure 5.1). The phthalonitriles were reacted with 4-fluorophenylacetic acid in presence of zinc phenylacetate to give the thio-substituted zinc porphyrins in 6% and 4% yield for 4,5-bis(2-ethylhexylthio)phthalonitrile or 4-(2-ethylhexylthio)phthalonitrile, respectively. Although such yields may appear low at the first glance, they allow preparation of the benzoporphyrins on a multi-gram scale, considering availability of the starting compounds and extreme simplicity of the procedure. Importantly, attempts to use the 4,5-bis(2-ethylhexylsulfonyl)phthalonitrile as starting compound were not successful due to formation of phthalocyanine instead of the benzoporphyrin.

Metal-free thio-substituted porphyrins were obtained by demetalation of the zinc complexes in acidic media (4M HCl). They were oxidized by excess of 3-chloroperoxybenzoic acid to the respective sulfone-substituted porphyrins in about 50% yield and finally converted to the metal complexes using Pt(II) and Pd(II) dichlorodibenzonitrile complexes as precursors.[31], [33] NMR and mass spectrometry (Fig. S 5.38-76, SI) confirmed the identity and purity of the compounds and showed that no other products (such as benzyl-substituted side products or partly oxidized porphyrins) were formed. Note that thio-substituted zinc complexes and the metal-free porphyrins are prone to oxidation (particularly in presence of light), requiring particular care during purification and storage.
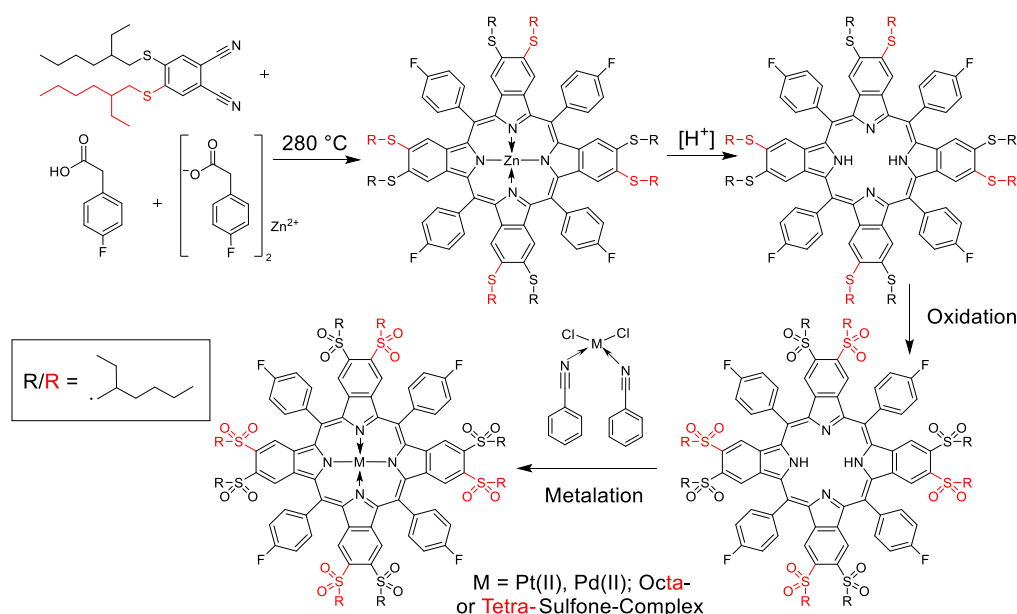
Figure 5.1 Synthesis of the Pt(II)/Pd(II) tetra-sulfone (T-S) and octa-sulfone (O-S) benzoporphyrins.
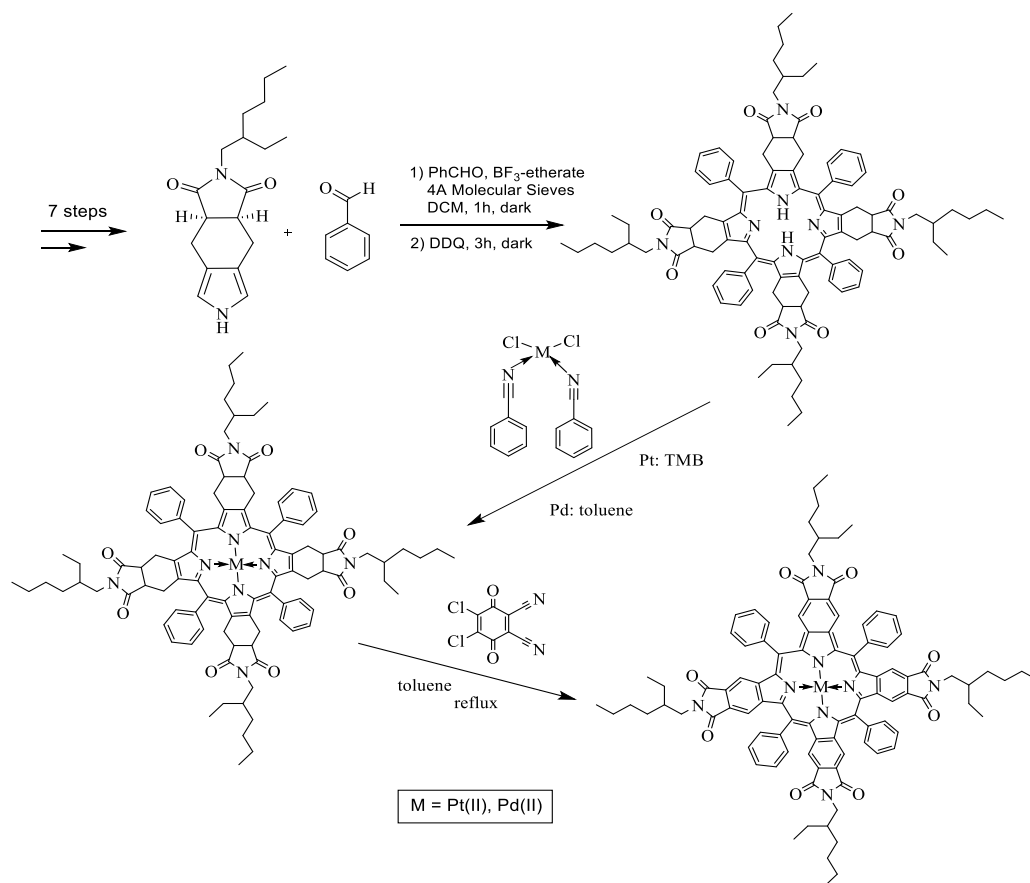
Figure 5.2 Synthesis of the Pt(II)/ Pd(II)-T-I dyes.

Additionally, we prepared imide-modified Pt(II) benzoporphyrin following a procedure of Zems et al.[24] with several modifications (Figure 5.2), which required 10 synthetic steps (SI). The Pd(II) analog was also synthesized. Evidently, both methods are equally interesting for the synthesis of π-extended porphyrins due to different advantages (simplicity of the template method and greater variety of suitable precursors for the condensation under Lindsey conditions).

5.4.2 Electrochemical properties

Table 5.1 provides an overview of half-wave potentials obtained for the new complexes as well as for Pt(II) and Pd(II) complexes with TPTBP used as references (the cyclic voltammograms can be found in the SI, Fig. S 5.1-8). The half-wave potentials $E_{\frac{1}{2}}$ increase with increasing electron-withdrawing effect of the substituents in the order TPTBP < T-S < T-I < O-S. The same trend was observed in case of fluorinated (benzo)porphyrins.[25], [34] The positive shift for all the synthesized dyes indicates a significantly lowered HOMO, resulting in improved oxidation stability due to the lowered electron density at the metalloporhyrin core. In all cases at least two reversible one-electron reductions and two reversible one-electron oxidations were observed. The obtained half-wave potentials for the Pt-T-I dyes correlate well with the data of Zems et al.[24] Pt-O-S, which oxidation potential is again 0.2 V more positive compared to Pt-T-I, appears to be the most electron-deficient benzoporphyrin reported to date and has its potential increased by nearly 0.7 V compared to Pt-TPTBP.

Table 5.1 Half-wave potentials (V vs. Fc/Fc⁺) of benzoporphyrin complexes in DCM containing 0.05 M TBAClO₄ at a scan rate of 0.1 V·s⁻¹.

Dye	$E_{½\,red.\,3}$ [V]	$E_{½\,red.\,2}$ [V]	$E_{½\,red.\,1}$ [V]	$E_{½\,ox.\,1}$ [V]	$E_{½\,ox.\,2}$ [V]	$E_{½\,ox.\,3}$ [V]
Pt-O-S	-2.03	-1.65	***-1.17***	***0.89***	1.18	-
Pd-O-S	-2.09	-1.70	***-1.24***	***0.79***	1.01	-
Pt-T-S	-	-1.98	***-1.57***	***0.60***	1.02	-
Pd-T-S	-	-1.87	***-1.50***	***0.57***	0.89	1.26
Pt-T-I	-1.99	-1.69	***-1.39***	***0.69***	1.05	-
Pd-T-I	-2.00	-1.67	***-1.40***	***0.64***	0.89	-
Pt-TPTBP	-	-	***-1.84***	***0.21***	0.83	1.43
Pd-TPTBP	-	-2.23	***-1.84***	***0.16***	0.66	-

5.4.3 Photophysical Properties

As expected, all the complexes show very good solubility in organic solvents including solvents as apolar as cyclohexane. In contrast, the dyes are poorly soluble in methanol and other polar solvents and are insoluble in water. Figure 5.3 shows the spectral properties of the new Pt(II) and Pd(II) benzoporphyrin complexes. The dyes efficiently absorb in the blue (Soret band) and the red part of the spectrum (Q bands) and possess exceptionally high molar absorption coefficients (Table 5.2). The absorption bands for the Pd(II) complexes are bathochromically shifted by about 15 nm compared to their Pt(II) analogs. The absorption bands shift bathochromically in the order T-S < O-S < T-I. For comparison, the absorption bands of the non-substituted Pd(II)-TPTBP and Pt(II)-TPTBP complexes[25] are located at shorter wavelengths than those of the tetra-sulfone complexes (Table 5.2). Thus, the new dyes offer significant improvement over TPTBP complexes: (i) The absorption of the Pt(II) complexes becomes compatible to the emission of 455 and 465 nm LEDs, which are amongst the brightest LEDs available. Upon excitation with blue light the new dyes can be viewed as ultra-bright mega-Stokes emitters. (ii) The Q-band of the Pt-O-S complex and particularly of the T-I complex show excellent compatibility with the light of He-Ne lasers (632.8 nm) and of red laser diodes (635 nm), thus enabling a variety of potential applications (e.g., in *vivo* imaging). (iii) The Pd-T-I complex having the longest absorption wavelength is a promising alternative to naphthoporphyrin complexes.
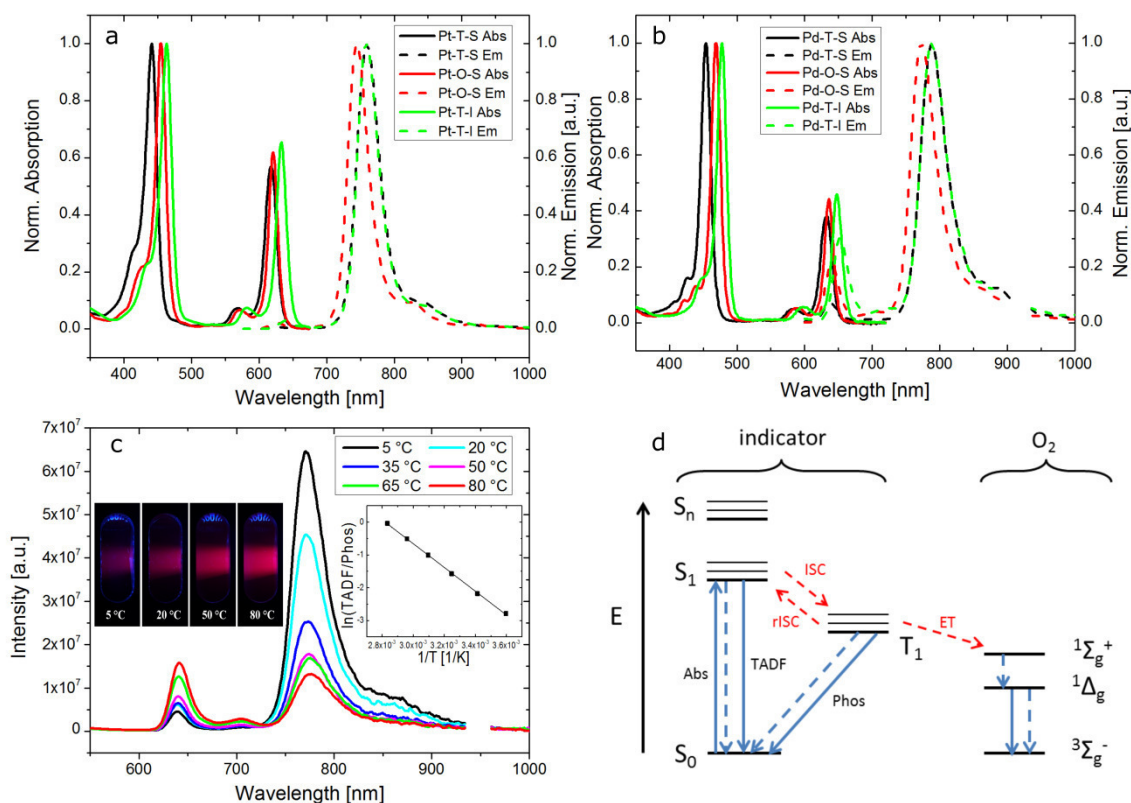
Figure 5.3 (a) and (b) Absorption (solid lines) and emission (dashed lines) spectra of Pt(II) and Pd(II) complexes in toluene, respectively. T = 25 °C; anoxic conditions for emission measurements; c) Temperature dependency of the emission spectra of Pd-O-S in anoxic toluene; the inserts show the photographic images of the solution under excitation with 465 nm LED and the Arrhenius dependence for the ratio of TADF and phosphorescence; d) scheme of photoluminescence processes: TADF, phosphorescence and quenching by O₂.

Table 5.2 Photophysical properties of the Pt(II) and Pd(II) complexes in toluene solution at 25 °C.

Dye	Abs. λ_{max} (ε) [nm (l·mol⁻¹·cm⁻¹)]	Em. λ_{max} TADF [nm]	Em. λ_{max} phos [nm]	$\Delta E(S_1-T_1)$ [cm⁻¹]ᵃ	Φ_{TADF}	Φ_{Phos}	τ_0 Phos [µs]
Pt-TPTBP	430 (205.000); 614 (136.000)	620	770	3142	0.001	0.21	47
Pt-T-S	441 (255.000); 619 (145.000)	624	756	2798	0.002	0.30	41
Pt-O-S	455 (370.000); 621 (229.000)	625	742	2523	0.004	0.30	33
Pt-T-I	463 (283.000); 633 (184.000)	639	755	2404	0.002	0.080	12
Pd-TPTBP	443 (416.000); 628 (173.000)	635	800	3248	0.003	0.083	286
Pd-T-S	454 (328.000); 633 (125.000)	639	786	2927	0.003	0.082	157
Pd-O-S	469 (446.000); 636 (195.000)	640	772	2672	0.010	0.095	161
Pd-T-I	478 (390.000); 648 (179.000)	652	786	2615	0.004	0.028	53

a – calculated from the difference of λ_{max} for TADF and phosphorescence bands

Interestingly, the Pt-O-S dye in dimethylformamide (DMF) solution shows an unexpected semi-reversible transformation upon addition of the basic tetra-octyl ammonium (TOA) hydroxide solution (20% in MeOH). A strong bathochromic shift of the absorption spectra (91 nm for the Soret-band and 193 nm for the Q-band) is accompanied by a color change of the dye solution from green to pink (Fig. S 5.10). This effect is most likely caused by the highly electron deficient properties of the dye, since similar behavior was also detected for the Pd-O-S and Pt-T-S dye, but not Pt-TPTBP. A similar behavior was observed in other solvents such as THF or pyridine and with other bases such as tetra-butyl ammonium (TBA) hydroxide (pK$_a$ of H$_2$O = 15.75)[35] and tetra-butyl ammonium fluoride (pK$_a$ of HF = 3.2).[35] This reaction is semi-reversible and adding traces of an acid (CF$_3$COOH or HCl) regenerates the original absorption spectra (Fig. S 5.11). The semi-reversible nature of this reaction suggests nucleophilc substitution by the anion (OH$^-$ or F$^-$) as the possible mechanism. The original aromatic NMR signals (7.75 – 8.5 ppm) including two signals in the aliphatic region (CH$_2$-group close to the sulfur at 3.6 ppm and the neighboring CH-group at 1.8 ppm) are lost (Fig. S 5.12-19, SI) upon stepwise addition of TOA-OH and regenerated upon addition of acid. Even though the bathochromically shifted species are in solution stable for several weeks, the reaction product could not isolated so far, limiting further investigations of this highly interesting reaction.

The new benzoporphyrin complexes show strong room-temperature phosphorescence in deoxygenated organic solvents such as toluene (Fig. 5.3). Remarkably, despite longer wavelength of absorption of the Q-bands compared to that of the TPTBP complexes, the emission maxima of the new dyes are shifted bathochromically (Table 5.2). Accurate determination of quantum yields in the NIR is challenging as evidenced in a wide literature. For Pt-TPTBP, for instance, reported quantum yields range from 35% or 51% in toluene (the short τ_0 of 30 μs in the former case may indicate quenching by oxygen) [36][25] to 67% in polyethylene glycol[37] and 70% in 2-Me-THF.[18] Very large errors are possible due to choice of poorly suitable luminescence standards and/or inadequate correction of the emission spectra for the spectral sensitivity of the photomultiplier as recently discussed by Vinogradov and co-workers.[38] The sensitivity of PMTs is known to be notoriously poor in the NIR part of the spectrum even in case of the most sensitive PMT models. In contrast to fluorescent dyes, commonly used as luminescent standards for quantum yield measurements, phosphorescent benzoporphyrins feature much larger Stokes´ shifts. Therefore, it is very challenging to find a suitable candidate which, on one hand, will emit in the same spectral range as the benzoporphyrins (700-800 nm) and, on the other hand, will possess pronounced and easily measurable absorption at the excitation wavelengths of these dyes (600-650 nm). Among the dyes reported in literature,[39] BF$_2$ chelate of [5-(4-methoxyphenyl)-3-phenyl-1H-pyrrol-2-yl][5-(4-methoxyphenyl)-3-phenylpyrrol-2-ylidene]amine ("dimethoxy-aza-BODIPY")[26][40] appears to fulfil these properties. Notably, extremely similar dibutoxy-aza-BODIPY[26] features identical spectral properties as the dimethoxy-aza-BODIPY.[26][40] First, we calculated the quantum yields for this compound relative to that of the "Lumogen red" dye (Φ = 96% in CHCl$_3$)[41] using the excitation in the blue part of the spectrum (λ = 460 nm) where both dyes

have a secondary absorption maxima. The obtained quantum yield for the dibutoxy-aza-BODIPY in CHCl$_3$ was identical to the one reported for dimethoxy-aza-BODIPY (36%) in the same conditions.[40] In the next step, the QYs of the benzoporphyrins in toluene were determined relative to that of the dibutoxy-aza-BODIPY. As can be seen (Table 5.2), the quantum yield for the Pt-TPTBP was found to be 21% and equals the absolute value obtained with an integrating sphere from Horiba. However, this value is significantly lower than the reported ones including the one measured in our group (51%)[25] which appear to be strongly overestimated. Analysis of the obtained quantum yields (Table 5.2) leads to conclusion that the substitution with sulfon groups has beneficial effect on the quantum yields, which is particularly pronounced in case of the Pt(II) dyes (1.5-fold improvement for T-S and O-S compared to Pt-TPTBP).

The most striking feature of the new dyes, however, is thermally activated delayed fluorescence, which is particularly strong for the Pd(II) complexes (Fig. 5.3b, 5.3d, Table 5.2) and can already at room temperature clearly be observed by naked eye (Fig. 5.3c, insert). Comparably strong TADF is very rare for Pt(II) and Pd(II) (benzo)porphyrin complexes. During preparation of the revised manuscript, Esipova et al. published structurally similar tetraimide-substituted Pt(II)- and Pd(II)-benzoporphyrins also featuring TADF (~1% quantum yield).[42] Only few porphyrins including metal-free dye and Zn(II) complexes,[43]–[47] Lu(III) tetrabenzoporphyrin[48] and Pt(II) and Pd(II) porphyrins[49] were reported to show TADF of unknown brightness. The quantum yield of TADF of Sn(IV) porphyrin was reported to be 0.6% at 23 °C and 2% at 117 °C.[50] Although the quantum yields of TADF for the solutions of the new Pd(II) dyes are similar to that of the Sn(IV) porphyrin, much higher values are obtained in rigid matrices at elevated temperatures (see below). Note that despite a large number of recently reported dyes show efficient TADF in view of their potential applications in OLED technology,[51]–[56] those emitting in the red and NIR remain extremely rare.[57], [58]

The observed emission can be unambiguously assigned to TADF on the basis of the temperature dependence (Fig. 5.3c, insert), identical decay times of TADF and phosphorescence, and the linear relation between TADF intensity and excitation intensity with a slope of 1 (SI, Fig. S 5.9), proofing that no other radiative process like triplet-triplet annihilation based delayed fluorescence are involved. Interestingly, we could also record weak yet measurable TADF for Pt(II)- and Pd(II)-TPTBP complexes, which has been overseen in the previous studies involving these compounds. The Pt(II) complexes show significantly less efficient delayed fluorescence than the Pd(II) analogs, which correlates well with the much shorter luminescence lifetime of the former and faster deactivation of the T$_1$ state via phosphorescence.

Highly efficient TADF of the new metalloporphyrins can be explained by their fairly small singlet-triplet energy gap ΔE_{S1-T1} of 2400-2700 cm^{-1} (Fig. 5.3d, Table 5.2), which enables reverse inter-system crossing. These values are similar to that of eosin (ΔE_{S1-T1} 2984 cm^{-1})[59] and are within the boundaries for the state-of-the-art TADF emitters (80-4000 cm^{-1}).[59], [60] ΔE_{S1-T1} decreases in the order TPTBP > T-S > O-S > T-I, which correlates well with the TADF-to-phosphorescence ratio (Table 5.2). This ratio is the highest for the T-I complexes (i.e., those with the lowest energy

gap) despite their emission quantum yields being much lower than those of the O-S complexes. In absolute terms, the Pd-O-S complex shows the highest TADF quantum yield with TADF clearly visible with a naked eye even at 5 °C.

Fig. 5.3c (insert) shows Arrhenius dependence for the TADF-to-phosphorescence ratio. It allows estimating the activation energy ΔE according to the equation of Parker and Hatchard [61]:

$$\frac{\Phi_{TADF}}{\Phi_{Phos}} = \tau_0 \cdot \Phi_F \cdot A \cdot e^{-\frac{\Delta E}{kT}}$$

(1)

where τ_0 is the natural radiative lifetime of the triplet state, A is a frequency factor and k is the Boltzmann constant. Since the quantum yield of the prompt fluorescence was too small to be measured, only ΔE is meaningful. The plots of $\ln(\Phi_{TADF}/\Phi_{Phos})$ against $1/T$ are linear as predicted (correlation coefficient 0.9994). ΔE was obtained to be 30.1 kJ·mol^{-1} or 2520 cm^{-1}, which is very close to the values of the triplet-singlet energy gap obtained from the emission spectra (ΔE_{S1-T1} = 2672, Table 5.2).

Interestingly, the T-I complexes have significantly lower luminescence quantum yields in solutions compared to the other metalloporphyrins (Table 5.2). Zems et al. [24] reported 45% for the Pt(II) tetra-imide complex, which appears to be strongly overestimated (only 8% in our measurement) and is in good correlation with QYs recently obtained by Vinogradov and co-workers for a very similar compound. [42] The non-radiative constants ($k_{nr} = (1-\Phi)/\tau$) for the T-I complexes are thus much higher than for the TPTBP, T-S and O-S complexes (Table S 5.1, SI).The phosphorescence decay times of the new Pt(II) and Pd(II) complexes are shorter than those of Pt-TPTBP and Pd-TPTBP, respectively, (Table 5.2) which together with the quantum yields indicates higher values of the radiative constant ($k_r = \Phi/\tau$). (Table S 5.1, SI).

5.4.4 Photostability

This property is of particular interest for practical applications, where high light intensities are applied for long time such as in upconversion. The benzoporphyrin derivatives may become unstable against oxidation and reduction by the destabilization of the third LUMO and the first HOMO of the porphyrin due to π-ring expansion.[62] Photostability of naphthoporphyrins and their molecular hybrids with benzoporphyrins is particularly low.

Preliminary experiments revealed very poor photostability of the thio-substituted Zn-complex (Zn-O-T) in air-saturated solution, which might be due to oxidation of the macrocycle by photosensitized singlet oxygen promoted by the electron-donating character of the thio-groups. Indeed, the zinc complex was almost completely destroyed within 7 minutes irradiation with a blue LED array (λ_{max}=458 nm; 10.79 V, 0.689 A, 7.4 W) (Fig. S 5.20, SI). Interestingly, photostability of the complex in anoxic toluene is similarly poor (Fig. S 5.21, SI), suggesting that intramolecular redox processes are the main degradation route of the excited dye. High photostability of the T-S and O-S benzoporphyrins was expected due to the strong electron-withdrawing effect of these substituents. Similarly, excellent photostability was shown for the Pt(II)-tetra-imide complex.[24] Indeed, all the

dyes proved to be highly photostable and only marginal changes (within the measurement inaccuracy) are observed upon prolonged illumination with high light intensity in air-saturated solutions (Fig. 5.4). The photobleaching rates are similar for all the dyes and also to that of Pt-TPTBP, which does not agree with the results reported by Zems et al. (about 5 times faster bleaching of Pt-TPTBP compared to Pt-T-I) who, however, used much harsher conditions (irradiation with 500 W halogen lamp at 90 °C). Furthermore, Pt-T-S and Pt-O-S show equally hardly any change in the absorption over 6 hours irradiation in anoxic toluene (Fig. S 5.22, SI). The nature of the solvent plays a crucial role with for the photobleaching rates. For example, Pt-O-S and Pt-TPTBP were almost completely destroyed after 15 min irradiation in dimethylformamide (Fig. S 5.23, SI), where photoreduction may be a predominant photodegradation mechanism. Therefore, the choice of suitable solvents or matrices is extremely important to achieve the best performance in the respective application.
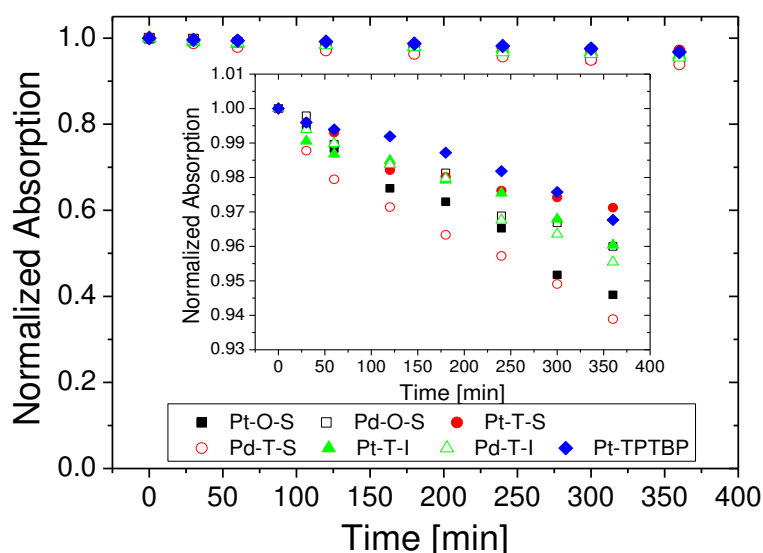
Figure 5.4 Photodegradation profiles for the metalloporphyrins in air-saturated toluene solution at 25 °C upon irradiation with a high power 617 nm LED (28 V, 550 mA, photon flux: 18.000 µmol s^{-1} m^{-2}; irradiance 350 mW·cm^{-2}).

5.4.5 TADF of the polymer-immobilized dyes

Immobilizing the dyes in polymers is essential for the design of optical oxygen sensors. Although the new dyes can be embedded in a variety of polymers, polystyrene was chosen as a model substrate due to its good optical properties, adequate chemical stability and moderate oxygen permeability, which makes it widely used in the sensor community. Moreover, many nanoparticle-based materials are available on basis of polystyrene and its co-polymers, which is very useful for designing optical nanoprobes. Fig. 5.5 confirms similar photophysical properties of the polystyrene-immobilized and dissolved dyes. Although NIR phosphorescence dominates the emission at room temperature, TADF is clearly visible for the Pd(II) complexes (Fig. 5.5b). With Pd-O-S and Pd-T-I the phosphorescence is almost entirely converted to TADF at temperatures around 120 °C (Fig.

5.5c, video SI). At this temperature it reaches impressive 27% for both dyes. Compared to the properties in the solution, the quantum yields improve significantly (Table 5.3) particularly in case of the T-I complexes. Brightness enhancement is likely to be due to rigidization of the matrix diminishing the radiativeless deactivation. In fact, the phosphorescence decay times are also significantly higher in polystyrene compared to the toluene solution (Table 5.4).

Interestingly, even Pd-TPTBP shows fairly strong TADF under these conditions, confirming that the observed phenomenon is general for all presented porphyrin complexes. In full agreement with the values of the singlet-triplet energy gap and the solution measurements, the TADF-to-phosphorescence ratio is the highest for Pd-T-I, followed by Pd-O-S, Pd-T-S and finally Pd-TPTBP (Table 5.3). This ratio increases for all complexes about 20-fold from 23-26 °C to 116-130 °C (Table 5.3).
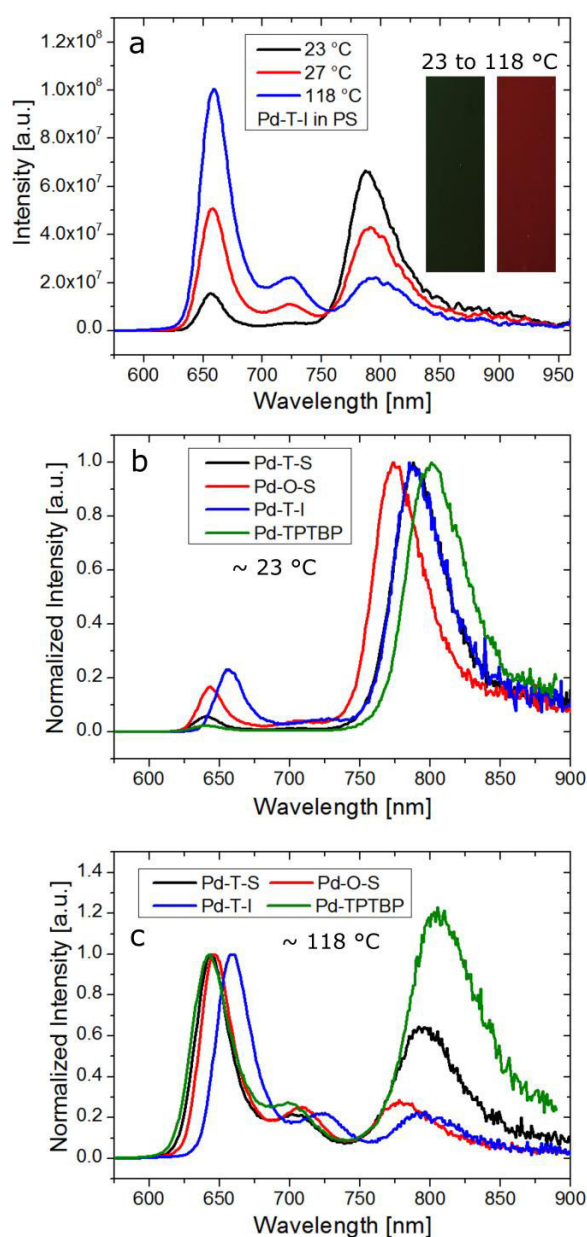
Figure 5.5 (a) Temperature dependency of the emission spectra of Pd-T-I in polystyrene and photographic images of the same material at 23 and 118 °C excited with an UV-Lamp at 365 nm (all under N$_2$ atmosphere); (b) Normalized emission spectra of Pd-T-S, Pd-O-S, Pd-T-I and Pd-TPTBP at 23 - 25 °C and (c) at 116 - 130 °C in polystyrene under N$_2$ atmosphere.

Table 5.3 Quantum yields of thermally activated delayed fluorescence (TADF) and phosphorescence of selected dyes in polystyrene matrix.

dye	Temp. [°C]	Φ_{TADF}	Φ_{Phos}	$\Phi_{TADF/Phos}$
Pd-T-S	23	0.010	0.16	0.065
	116	0.11	0.069	1.598
Pd-O-S	23	0.031	0.19	0.161
	120	0.27	0.084	3.225
Pd-T-I	23	0.038	0.15	0.258
	118	0.27	0.060	4.558
Pd-TPTBP	26	0.005	0.14	0.037
	120	0.072	0.069	1.051
Pt-O-S	26	0.011	0.47	0.023
	130	0.092	0.25	0.362
Pt-TPTBP	27	0.002	0.33	0.005
	133	0.020	0.15	0.138

5.4.6 Optical Oxygen Sensors

Optical oxygen sensing is undoubtedly one of the most important applications of porphyrin complexes. Since phosphorescence is a predominant process at ambient temperature, only phosphorescence quenching was investigated. Fig. 5.6 shows the Stern-Volmer plots for polystyrene-immobilized dyes. The non-linear plots can be described by a "two-site model"[63] which assumes localization of an oxygen-sensitive chromophore in two microenvironments (resulting from micro-inhomogeneities in the polymer) possessing different gas permeabilities:

$$\frac{I}{I_0} = \frac{\tau}{\tau_0} = \frac{f}{1+K_{SV1}*[O_2]} + \frac{1-f}{1+(K_{SV1}*m)*[O_2]} \qquad (2)$$

f is the fraction of the total emission of the first environment; K_{SV1} and $K_{SV2}=(K_{SV1} \cdot m)$ are the Stern-Volmer constants for the two environments. The obtained fit parameters are summarized in Table 5.4. As expected from the τ_0 values, the sensitivity of the Pd(II) complexes is significantly higher than that of the Pt(II) complexes. While the polystyrene optodes based on the Pt(II) dyes are best suitable for measurements from 1 to 1000 hPa O_2, the Pd(II) porpyhrin-based sensors make much lower oxygen partial pressures accessible. The sensing behavior of the octa- and tetra-sulfone complexes is very similar (Fig. 5.6, Table 5.4). The Stern-Volmer plots for the T-I dyes are significantly more linear, which indicates higher homogeneity of the environment. Notably, the sensitivity can be further greatly increased by immobilizing the complexes into matrixes with higher oxygen permeability. Excellent solubility in apolar media may be very helpful, for instance, in case of silicone rubbers which are materials of choice for designing trace oxygen sensors. [64]
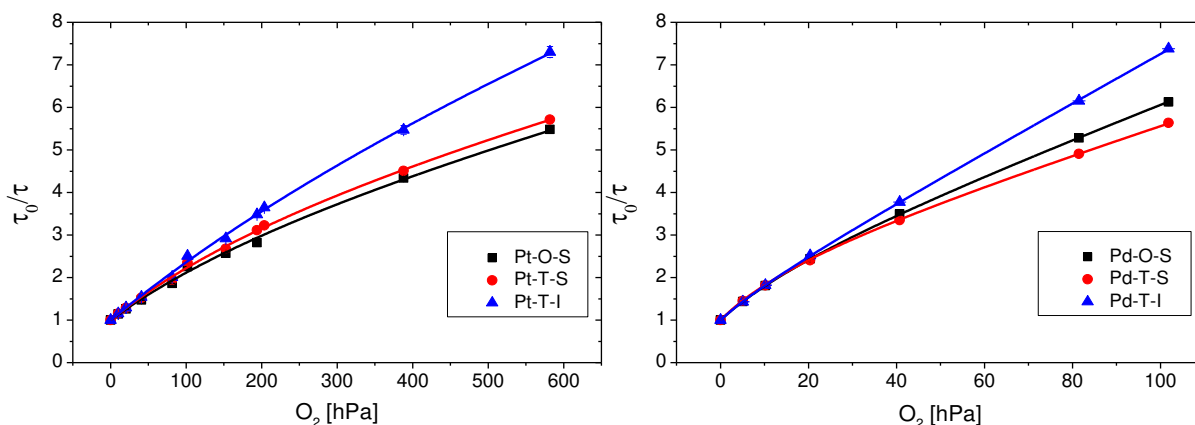
Figure 5.6 Stern-Volmer plots (phosphorescence) for the Pt(II) and Pd(II) complexes embedded in polystyrene (at 25 °C).

Despite our expectations that the highly soluble dyes can be embedded into polymers in a very high concentration without aggregation, we found pronounced decrease in the phosphorescence decay times under these conditions (Fig. S 5.24, SI). In fact, increasing the concentration of the Pt(II) complexes from 2 to 5 wt.% resulted in a decrease of the lifetime by 7% for Pt-O-S, 10% for Pt-T-S and 15% for Pt-T-I. Less soluble Pt-TPTBP showed much smaller decrease in the τ_0 in the same conditions (2%) despite its higher molar concentration. The same trend was observed at 20% wt., where a decrease of 41% for Pt-O-S and Pt-T-S, 53% for Pt-T-I, but only 17% for Pt-TPTBP was measured. It is likely that smaller molecules such as Pt-TPTBP are more easily dissolved in polystyrene and show less tendency to aggregation in this matrix, whereas more sterically demanding dyes tend to aggregate due to formation of apolar microdroplets and separation of the phases. The results are likely to be different in apolar matrixes such as silicones showing much better compatibility with the new dyes rather than TPTBP complexes. Nevertheless, the lower concentration range where the aggregation effects in polystyrene are negligible, is fully adequate for manufacturing of oxygen sensors.

Table 5.4 Photophysical and oxygen sensing properties of Pt(II) and Pd(II) benzoporphyrin complexes in polystyrene.

Dye	absolute Φ [%][b]	f	m	K_{SV} [hPa⁻¹]			τ_0 [µs]			temp. coeff. at 25 °C [%τ_0/K]
				10 °C	25 °C	40 °C	10 °C	25 °C	40 °C	
Pt-O-S	47	0.860	0.054	0.012	0.015	0.019	46.5	45.9	45.1	0.102
Pd-O-S	19	0.767	0.101	0.099	0.119	0.142	350	328	308	0.421
Pt-T-S	34	0.868	0.043	0.014	0.017	0.020	50.1	49.5	48.7	0.097
Pd-T-S	16	0.738	0.075	0.115	0.130	0.144	379	360	338	0.376
Pt-T-I	33	0.945	0.031	0.013	0.015	0.018	41.9	40.8	39.5	0.204
Pd-T-I	15	0.659	0.213	0.115	0.130	0.144	287	265	244	0.537

b – Phosphorescence quantum yields.

Accelerated photostability tests of the polystyrene sensors were performed by positioning sensor spots (5 mm diameter) onto a distal end of a plastic fiber connected to the read-out device from Pyro Science (624 nm LED, 100% LED intensity, 100 ms integration time). Under anoxic conditions, the luminescence intensity decreased by maximum of 0.502% per 2500 measurement points for Pt-O-S and 0.349% per 2500 measurement points for Pd-O-S, whereas at air saturation the decrease of Pt-O-S was in average 1.31% per 2500 measurement points in the first 500 minutes and slowed down with time to 0.18% per 2500 measurement points from 500 to 1000 minutes. Note that an integration time of 10 ms and 10% LED intensity (100-fold lower light dose than used in accelerated tests) are sufficient to acquire a measurement point, which indicates suitability of the sensors for very long measurements. Further improvement may be possible via optimization of the polymer matrix, since the decrease in luminescence intensity and decay time are more likely to be caused by formation of quenching groups in the proximity of the dye (caused by reaction of the photosensitized singlet oxygen with the polymer) rather than by bleaching of the dye itself.

5.4.7 Application as dual sensor for determination of oxygen and temperature

As was mentioned above, simultaneous determination of oxygen and temperature is of high importance for practical applications and in fact is essential for precise oxygen quantification. So far, a temperature probe had to be used in parallel with the oxygen probe either fully independently or combined in a dually-sensing material. The unique dually emissive character of the new dyes makes them potentially suitable for simultaneous sensing of the two parameters with a single probe. In order to demonstrate the feasibility of the approach we selected Pd-O-S complex due to its strongest TADF. Since oxygen permeability of polystyrene is too high for measurements in the most relevant concentration range (0-210 hPa) it was substituted by commercially available copolymer of styrene and acrylonitrile (25 wt% acrylonitrile) featuring lower oxygen permeability (P = 3.5·10^{-14} cm^2·Pa·s^{-1} compared to 1.9·10^{-13} cm^2·Pa·s^{-1} in case of polystyrene).[65]

Fig. 5.7 shows that simultaneous sensing of both parameters is indeed possible. As can be observed (Fig. 5.7a and 5.7b), the NIR phosphorescence is gradually converted into TADF as the temperature increases. This effect is very similar for both extremes: anoxic conditions (Fig. 5.7a) and air-saturated conditions (Fig. 5.7b). Interestingly, in the second case the intensity of TADF at 125.4 °C is lower than that at 113.4 °C which might be due to change in the oxygen quenching efficiency above the T$_g$ of the polymer (which is in the range of 104-127 °C).[66], [67] Fig. 5.7c shows that the ratio of TADF to phosphorescence is virtually independent on pO$_2$ and thus serves as a self-referenced analytical parameter for temperature measurement. The decay time profiles (Fig. 5.7d) are mono-exponential in the absence of oxygen but become bi-exponential in its presence which is not uncommon for optical oxygen sensors. Therefore, average lifetimes were calculated via $\tau_{av} = \frac{\sum_{i=1}^{n} B_i T_i^2}{\sum_{i=1}^{n} B_i T_i}$ where the B$_i$ is the pre-exponential factor and T$_i$ - the individual lifetimes. Importantly, the decay time traces are identical for phosphorescence and TADF. This allows determining the second parameter (pO$_2$) in the lifetime mode. Depending on the temperature

and therefore on the intensity of the respective luminescence component either phosphorescence (lower temperatures) or TADF (higher temperatures) can be analyzed to maintain the best S/N ratio. The decay times decrease with temperature at all oxygen concentrations (Fig. 5.7e). The Stern-Volmer plots (Fig. 5.7f) are typical for oxygen sensors with higher quenching efficiency at elevated temperatures despite comparably strong shortening of τ_0 in these conditions. As expected, the oxygen sensitivity is lower than in polystyrene (Fig. 5.7f). In summary, combination of the decay time and ratiometric read-out makes it possible to access information about both oxygen and temperature with a single indicator dye. Importantly, both measurements are self-referenced. Further improvements can include substitution of PSAN with a copolymer with higher content of acrylonitrile which would reduce the quenching by oxygen to more optimal factor (τ_0/τ ~3-4 at air saturation). Of course, modification of the indicator which would result in even higher proportion of TADF already at RT is highly welcomed since it would enable reliable dual sensing at temperatures below 20 °C. For the current system, the signals of TADF at temperatures below 20 °C and air saturation might be too low to be reliably quantified with compact devices based on photodiodes although, as demonstrated above, the decay times can be reliably measured with a much more sensitive photomultiplier-based set-up.
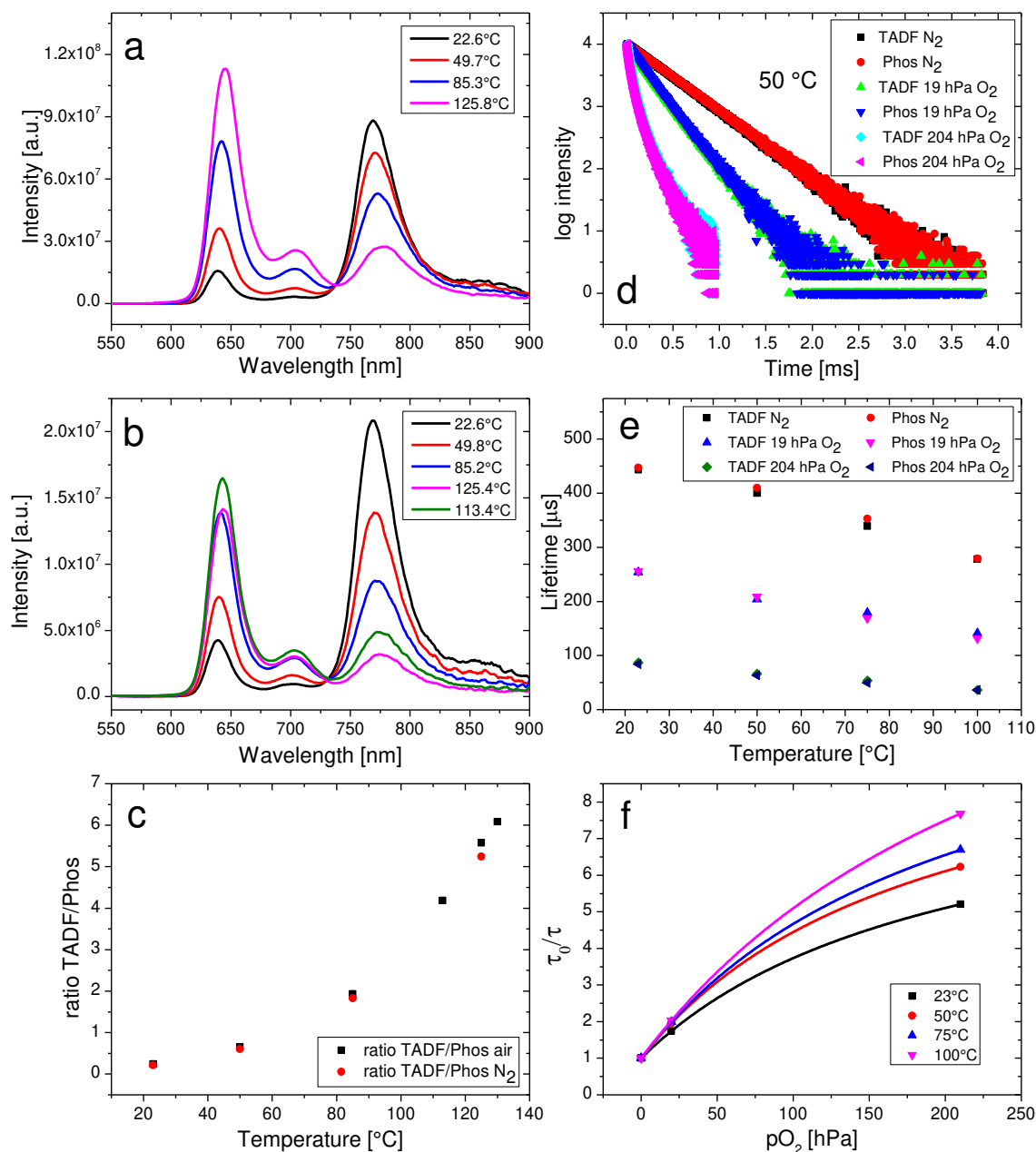
Figure 5.7 (a) and (b): temperature dependency of the emission spectra of Pd-O-S in PSAN under anoxic conditions air saturation, respectively. Note that slits of fluorometer were different for both conditions; (c): calculated ratio of TADF and phosphorescence at different temperatures for the same conditions; (d): examples of the decay curves of TADF and phosphorescence at 50 °C; (e): temperature and oxygen dependency of the lifetimes of TADF and phosphorescence; (f): Stern-Volmer plots at different temperatures.

5.4.8 Dyes as sensitizers in triplet-triplet-annihilation-based upconversion systems

Triplet-triplet annihilation-based upconversion (TTA) has recently attracted much attention in the scientific community since it may enable exploiting low-energy long wavelength radiation in photovoltaics. TTA (TTA-upconversion scheme in SI S 5.1) relies on a sensitizer (S), which should efficiently absorb light at a given wavelength and transfer its energy to an annihilator (A), generating higher energy fluorescence *via* triplet-triplet annihilation.[13] The sensitizer is required to have a high molar absorption coefficient, high efficiency of intersystem crossing,[13] and the long triplet lifetime necessary for efficient triplet-triplet energy transfer. Particularly, excitation with red to NIR light is highly interesting because of the considerable solar power and low photovoltaics efficiency in this region.[16], [17], [68], [69] Additionally, good solubility in organic solvents and polymers and high photostability are essential. The new benzoporphyrin derivatives fulfill these requirements almost perfectly. Their sensitizing capabilities were investigated in anoxic toluene solutions containing $1 \cdot 10^{-4}$ M sensitizer (perylene dyes, structures Fig. S 5.37 SI) and $5 \cdot 10^{-4}$ M annihilator. Figure 5.8a Table S 5.2, and Fig. S 5.25-36 (SI) show that all new dyes perform as efficient sensitizers for the upconverted fluorescence. Quadratic dependence of fluorescence on excitation intensity (xenon lamp) was observed for all dyes (Fig. S 5.25-30, SI) (slope of the logarithmic plot approximately 2) as is typical for nonlinear processes like TTA based upconversion.[16], [70]–[72] In contrast, measurements conducted with the 635 nm laser diode reveal a linear region with a slope of unity indicating saturation conditions (Fig. S 5.31-36, SI).[73]
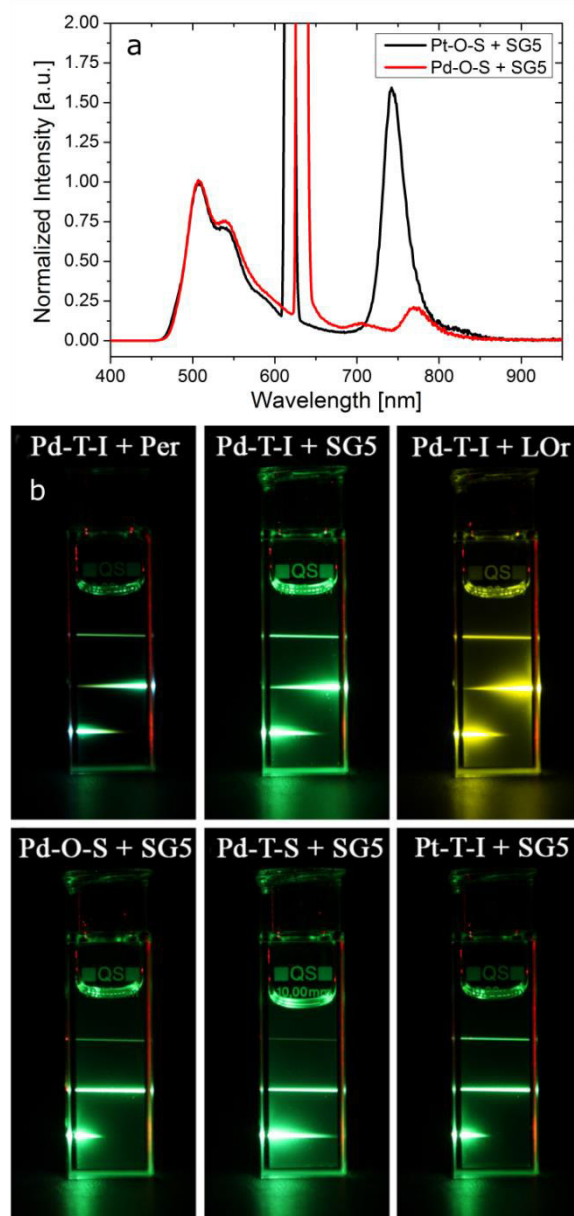
Figure 5.8 (a) Emission spectra of 1·10⁻⁴ M Pt/Pd-O-S in toluene in presence of 5·10⁻⁴ M Solvent Green 5 (SG5) as annihilator when excited with a 450 W xenon-lamp. (b) Photographic images of 5·10⁻⁵ M deoxygenated toluene solutions of various sensitizers and different annihilators (C = 2.5·10⁻⁴ M; Per=perylene, SG5=solvent green 5 & LOr=Lumogen orange) upon excitation with several laser diodes (675 nm, 650 nm and 635 nm, top to bottom).

The sensitizing efficiency of the new dyes is similar or better to that of the TPTBP derivatives used in many studies so far. A notable advantage of the T-I and O-S dyes is that they enable sensitizing the upconverted fluorescence at significantly longer wavelengths than the TPTBPs (Fig. 5.8b). As suggested by the absorption spectra, Pd-T-I can efficiently sensitize upconverted fluorescence even at 675 nm excitation. For comparison, a Pd(II) complex with mono-naphtho-tribenzo-tetraphenyl-porphyrin,[23] found to be very useful in upconversion applications,[74] absorbs at similar wavelengths (λ_{max} =654 nm), albeit with significantly lower molar absorption coefficients, bathochromically shifted emission (λ_{max} = 849 nm), and the limitation of moderate photostability.[23] A small singlet-triplet energy gap also enables sensitizing for annihilators with at rather long emission wavelengths such as Lumogen orange (Fig. 5.8b).

5.4.9 Conclusions

Highly electron-deficient platinum(II) and palladium(II) benzoporphyrin complexes bearing alkylsulfone groups have been conveniently prepared in a four step synthetic route (template method), starting from cheap and readily available materials. The new platinum(II) and palladium(II) complexes can be efficiently excited in blue and in red parts of the electromagnetic spectrum and are compatible with many popular excitation sources (ultrabright blue and red LEDs, He-Ne laser and red laser diodes). Additionally, the new porphyrins are highly soluble in various organic solvents and polymers including cyclohexane and polystyrene and show very good photostability. The dyes show thermally activated delayed fluorescence (TADF) and strong phosphorescence in the NIR region at room temperature, which qualifies them for optical oxygen sensors. Particularly the Pd(II) complexes have already at room temperature fairly efficient TADF, which dramatically increases with temperature to reach as much as 27% for the Pd-O-S and Pd-T-I complexes at 120 °C. TADF of the new dyes is much stronger than that of state-of-the-art porphyrin complexes, which is explained by the unusually small singlet-triplet energy gap of the former.

The temperature dependence of the emission has ratiometric character and enables thus dual oxygen and temperature sensing based on a single emitter which is unprecedented in the literature. In the dual sensor the temperature information is obtained from the TADF-to-phosphorescence ratio while oxygen concentration is determined from the phosphorescence or TADF decay times, which are identical.

Finally, the platinum(II) and palladium(II) complexes were both found to efficiently sensitize triplet-triplet annihilation based upconversion. Bathochromically shifted absorption of particularly the tetra-imide dyes enables longer sensitization wavelengths compared to state-of-the-art benzoporphyrin sensitizers. Additionally, the most electron-deficient compound semi-reversibly forms NIR absorbing species in basic media, which calls for a more detailed investigation. Overall, it can be concluded that outstanding photophysical properties of the new porphyrins make them particularly interesting for a broad variety of photonic applications ranging from OLED technology and photovoltaics, to 2-photon imaging of oxygenation of biological samples. Particularly for the last application, TADF will be of special benefit since the spectral overlap between the required NIR excitation and the emission can be avoided in contrast to state-of-the-art phosphorescent probes, which emission in the NIR overlaps with excitation.

Associated Content

Supporting Information

The Supporting Information is available free of charge on the ACS Publications website at DOI:
Experimental section; synthesis, electrochemical and photophysical properties, data on reversible transformation of Pt-O-S, photostability, optical oxygen sensors, TTA upconversion, ^{1}H and ^{13}C NMR, mass spectrometry (PDF) and video clip of Pd-O-S and Pd-T-I as temperature sensor.

Acknowledgements

5.4.10 References

[1] T. Tanaka and A. Osuka, "Conjugated porphyrin arrays: synthesis, properties and applications for functional materials," *Chem. Soc. Rev.*, Jan. 2014.

[2] M. Quaranta, S. M. Borisov, and I. Klimant, "Indicators for optical oxygen sensors," *Bioanal. Rev.*, vol. 4, no. 2–4, pp. 115–157, Dec. 2012.

[3] X. Wang and O. S. Wolfbeis, "Optical methods for sensing and imaging oxygen: materials, spectroscopies and applications," *Chem. Soc. Rev.*, vol. 43, no. 10, pp. 3666–3761, Apr. 2014.

[4] C. Staudinger and S. M. Borisov, "Long-wavelength analyte-sensitive luminescent probes and optical (bio)sensors," *Methods Appl. Fluoresc.*, vol. 3, no. 4, p. 042005, 2015.

[5] J. Lecoq *et al.*, "Simultaneous two-photon imaging of oxygen and blood flow in deep cerebral vessels," *Nat. Med.*, vol. 17, no. 7, pp. 893–898, Jul. 2011.

[6] B. Nacht *et al.*, "Integrated catheter system for continuous glucose measurement and simultaneous insulin infusion," *Biosens. Bioelectron.*, vol. 64, pp. 102–110, Feb. 2015.

[7] X. Wang, O. S. Wolfbeis, and R. J. Meier, "Luminescent probes and sensors for temperature," *Chem. Soc. Rev.*, vol. 42, no. 19, pp. 7834–7869, Sep. 2013.

[8] X. Zhou, F. Su, Y. Tian, R. H. Johnson, and D. R. Meldrum, "Platinum (II) porphyrin-containing thermoresponsive poly(N-isopropylacrylamide) copolymer as fluorescence dual oxygen and temperature sensor," *Sens. Actuators B Chem.*, vol. 159, no. 1, pp. 135–141, Nov. 2011.

[9] L. H. Fischer, S. M. Borisov, M. Schaeferling, I. Klimant, and O. S. Wolfbeis, "Dual sensing of pO2 and temperature using a water-based and sprayable fluorescent paint," *Analyst*, vol. 135, no. 6, pp. 1224–1229, May 2010.

[10] M. I. J. Stich, L. H. Fischer, and O. S. Wolfbeis, "Multiple fluorescent chemical sensing and imaging," *Chem. Soc. Rev.*, vol. 39, no. 8, pp. 3102–3114, Jul. 2010.

[11] A. Monguzzi, J. Mezyk, F. Scotognella, R. Tubino, and F. Meinardi, "Upconversion-induced fluorescence in multicomponent systems: Steady-state excitation power threshold," *Phys. Rev. B*, vol. 78, no. 19, p. 195112, Nov. 2008.

[12] T. N. Singh-Rachford and F. N. Castellano, "Triplet Sensitized Red-to-Blue Photon Upconversion," *J. Phys. Chem. Lett.*, vol. 1, no. 1, pp. 195–200, Jan. 2010.

[13] J. Zhao, S. Ji, and H. Guo, "Triplet–triplet annihilation based upconversion: from triplet sensitizers and triplet acceptors to upconversion quantum yields," *RSC Adv.*, vol. 1, no. 6, pp. 937–950, Oct. 2011.

[14] J.-H. Kim, F. Deng, F. N. Castellano, and J.-H. Kim, "High Efficiency Low-Power Upconverting Soft Materials," *Chem. Mater.*, vol. 24, no. 12, pp. 2250–2252, Jun. 2012.

[15] K. Xu, J. Zhao, X. Cui, and J. Ma, "Photoswitching of triplet–triplet annihilation upconversion showing large emission shifts using a photochromic fluorescent dithienylethene-Bodipy triad as a triplet acceptor/emitter," *Chem. Commun.*, vol. 51, no. 10, pp. 1803–1806, Jan. 2015.

[16] T. N. Singh-Rachford, A. Haefele, R. Ziessel, and F. N. Castellano, "Boron dipyrromethene chromophores: next generation triplet acceptors/annihilators for low power upconversion schemes," *J. Am. Chem. Soc.*, vol. 130, no. 48, pp. 16164–16165, Dec. 2008.

[17] A. Monguzzi *et al.*, "Efficient Broadband Triplet–Triplet Annihilation-Assisted Photon Upconversion at Subsolar Irradiance in Fully Organic Systems," *Adv. Funct. Mater.*, vol. 25, no. 35, pp. 5617–5624, Sep. 2015.

[18] C. Borek *et al.*, "Highly Efficient, Near-Infrared Electrophosphorescence from a Pt–Metalloporphyrin Complex," *Angew. Chem. Int. Ed.*, vol. 46, no. 7, pp. 1109–1112, Feb. 2007.

[19] V. V. Rozhkov, M. Khajehpour, and S. A. Vinogradov, "Luminescent Zn and Pd tetranaphthaloporphyrins," *Inorg. Chem.*, vol. 42, no. 14, pp. 4253–4255, Jul. 2003.

[20] C. M. B. Carvalho, T. J. Brocksom, and K. T. de Oliveira, "Tetrabenzoporphyrins: synthetic developments and applications," *Chem. Soc. Rev.*, vol. 42, no. 8, pp. 3302–3317, Mar. 2013.

[21] O. S. Finikova, A. V. Cheprakov, and S. A. Vinogradov, "Synthesis and luminescence of soluble meso-

unsubstituted tetrabenzo- and tetranaphtho[2,3]porphyrins," *J. Org. Chem.*, vol. 70, no. 23, pp. 9562–9572, Nov. 2005.

[22] T. Ishizuka, Y. Saegusa, Y. Shiota, K. Ohtake, K. Yoshizawa, and T. Kojima, "Multiply-fused porphyrins--effects of extended π-conjugation on the optical and electrochemical properties," *Chem. Commun. Camb. Engl.*, vol. 49, no. 53, pp. 5939–5941, Jul. 2013.

[23] F. Niedermair *et al.*, "Tunable Phosphorescent NIR Oxygen Indicators Based on Mixed Benzo- and Naphthoporphyrin Complexes," *Inorg. Chem.*, vol. 49, no. 20, pp. 9333–9342, Oct. 2010.

[24] Y. Zems, A. G. Moiseev, and D. F. Perepichka, "Convenient synthesis of a highly soluble and stable phosphorescent platinum porphyrin dye," *Org. Lett.*, vol. 15, no. 20, pp. 5330–5333, Oct. 2013.

[25] S. M. Borisov, G. Nuss, W. Haas, R. Saf, M. Schmuck, and I. Klimant, "New NIR-emitting complexes of platinum(II) and palladium(II) with fluorinated benzoporphyrins," *J. Photochem. Photobiol. -Chem. - J PHOTOCHEM PHOTOBIOL -CHEM*, vol. 201, no. 2, pp. 128–135, 2009.

[26] S. Schutting, T. Jokic, M. Strobl, S. M. Borisov, D. de Beer, and I. Klimant, "NIR optical carbon dioxide sensors based on highly photostable dihydroxy-aza-BODIPY dyes," *J. Mater. Chem. C*, vol. 3, no. 21, pp. 5474–5483, May 2015.

[27] M. G. Walter, A. B. Rudine, and C. C. Wamser, "Porphyrins and phthalocyanines in solar photovoltaic cells," *J. Porphyr. Phthalocyanines*, vol. 14, no. 09, pp. 759–792, Sep. 2010.

[28] G. A. Crosby and J. N. Demas, "Measurement of photoluminescence quantum yields. Review," *J. Phys. Chem.*, vol. 75, no. 8, pp. 991–1024, Apr. 1971.

[29] A. Loudet, R. Bandichhor, L. Wu, and K. Burgess, "Functionalized BF2 Chelated Azadipyrromethene Dyes," *Tetrahedron*, vol. 64, no. 17, pp. 3642–3654, Apr. 2008.

[30] J. S. Lindsey, H. C. Hsu, and I. C. Schreiman, "Synthesis of tetraphenylporphyrins under very mild conditions," *Tetrahedron Lett.*, vol. 27, no. 41, pp. 4969–4970, 1986.

[31] S. M. Borisov and I. Klimant, "Efficient metallation in diphenylether – A convenient route to luminescent platinum(II) complexes," *Dyes Pigments*, vol. 83, no. 3, pp. 312–316, Dec. 2009.

[32] K. Ichimura *et al.*, "Formation of tetrabenzoporphine skeleton by the reactions of phthalimide with zinc carbonates," *Inorganica Chim. Acta*, vol. 186, no. 1, pp. 95–101, Aug. 1991.

[33] L. H. Hutter, B. J. Müller, K. Koren, S. M. Borisov, and I. Klimant, "Robust optical oxygen sensors based on polymer-bound NIR-emitting platinum(II)–benzoporphyrins," *J. Mater. Chem. C*, vol. 2, no. 36, pp. 7589–7598, Aug. 2014.

[34] K. M. Kadish *et al.*, "Influence of Electronic and Structural Effects on the Oxidative Behavior of Nickel Porphyrins," *Inorg. Chem.*, vol. 41, no. 25, pp. 6673–6687, Dec. 2002.

[35] F. G. Bordwell, "Equilibrium acidities in dimethyl sulfoxide solution," *Acc. Chem. Res.*, vol. 21, no. 12, pp. 456–463, Dec. 1988.

[36] K. R. Graham *et al.*, "Extended Conjugation Platinum(II) Porphyrins for use in Near-Infrared Emitting Organic Light Emitting Diodes," *Chem. Mater.*, vol. 23, no. 24, pp. 5305–5312, Dec. 2011.

[37] C. Mongin, J. H. Golden, and F. N. Castellano, "Liquid PEG Polymers Containing Antioxidants: A Versatile Platform for Studying Oxygen-Sensitive Photochemical Processes," *ACS Appl. Mater. Interfaces*, vol. 8, no. 36, pp. 24038–24048, Sep. 2016.

[38] T. V. Esipova, H. J. Rivera-Jacquez, B. Weber, A. E. Masunov, and S. A. Vinogradov, "Two-Photon Absorbing Phosphorescent Metalloporphyrins: Effects of π-Extension and Peripheral Substitution," *J. Am. Chem. Soc.*, vol. 138, no. 48, pp. 15648–15662, Dec. 2016.

[39] A. M. Brouwer, "Standards for photoluminescence quantum yield measurements in solution (IUPAC Technical Report)," *Pure Appl. Chem.*, vol. 83, no. 12, pp. 2213–2228, Aug. 2011.

[40] A. Gorman, J. Killoran, C. O'Shea, T. Kenna, W. M. Gallagher, and D. F. O'Shea, "In Vitro Demonstration of the Heavy-Atom Effect for Photodynamic Therapy," *J. Am. Chem. Soc.*, vol. 126, no. 34, pp. 10619–10631, Sep. 2004.

[41] G. Seybold and G. Wagenblast, "New perylene and violanthrone dyestuffs for fluorescent collectors," *Dyes Pigments*, vol. 11, no. 4, pp. 303–317, 1989.

[42] T. V. Esipova, H. J. Rivera-Jacquez, B. Weber, A. E. Masunov, and S. A. Vinogradov, "Stabilizing g-States in Centrosymmetric Tetrapyrroles: Two-Photon-Absorbing Porphyrins with Bright Phosphorescence," *J. Phys. Chem. A*, vol. 121, no. 33, pp. 6243–6255, Aug. 2017.

[43] M. Kořínek, P. Klinger, R. Dědic, J. Pšenčík, A. Svoboda, and J. Hála, "Delayed fluorescence of meso-tetraphenylporphyrin in acetone and in dimethylsulphoxide," *J. Lumin.*, vol. 122, pp. 247–249, Jan. 2007.

[44] D. Wróbel, I. Hanyż, R. Bartkowiak, and R. M. Ion, "Fluorescence and Time-Resolved Delayed Luminescence of Porphyrins in Organic Solvents and Polymer Matrices," *J. Fluoresc.*, vol. 8, no. 3, pp. 191–198, Sep. 1998.

[45] J. Feitelson and D. Mauzerall, "Reactions of triplet states of a porphyrin measured by delayed fluorescence," *J. Phys. Chem.*, vol. 86, no. 9, pp. 1623–1628, Apr. 1982.

[46] Y. Onoue, K. Hiraki, and Y. Nishikawa, "Studies on Room Temperature Phosphorometric and Delayed Fluorometric Analysis. I. Delayed Fluorometric Analysis of Porphyrin Derivatives," *Bull. Chem. Soc. Jpn.*, vol. 54, no. 9, pp. 2633–2635, Sep. 1981.

[47] I. Lukomsky, V. Gottfried, and S. Kimel, "Delayed fluorescence of porphyrins in different media," *J. Fluoresc.*, vol. 4, no. 1, pp. 49–51, Mar. 1994.

[48] S. A. Vinogradov and D. F. Wilson, "Metallotetrabenzoporphyrins. New phosphorescent probes for oxygen measurements," *J. Chem. Soc. Perkin Trans. 2*, no. 1, p. 103, 1995.

[49] J. B. Callis, M. Gouterman, Y. M. Jones, and B. H. Henderson, "Porphyrins XXII: Fast fluorescence, delayed fluorescence, and quasiline structure in palladium and platinum complexes," *J. Mol. Spectrosc.*, vol. 39, no. 3, pp. 410–420, Sep. 1971.

[50] A. Endo, M. Ogasawara, A. Takahashi, D. Yokoyama, Y. Kato, and C. Adachi, "Thermally Activated Delayed

Fluorescence from Sn4+–Porphyrin Complexes and Their Application to Organic Light Emitting Diodes — A Novel Mechanism for Electroluminescence," *Adv. Mater.*, vol. 21, no. 47, pp. 4802–4806, Dec. 2009.

[51] X. Cai, B. Gao, X.-L. Li, Y. Cao, and S.-J. Su, "Singlet–Triplet Splitting Energy Management via Acceptor Substitution: Complanation Molecular Design for Deep-Blue Thermally Activated Delayed Fluorescence Emitters and Organic Light-Emitting Diodes Application," *Adv. Funct. Mater.*, vol. 26, no. 44, pp. 8042–8052, Nov. 2016.

[52] X.-L. Chen *et al.*, "Highly efficient cuprous complexes with thermally activated delayed fluorescence and simplified solution process OLEDs using the ligand as host," *J. Mater. Chem. C*, vol. 3, no. 6, pp. 1187–1195, Jan. 2015.

[53] Y. J. Cho, S. K. Jeon, B. D. Chin, E. Yu, and J. Y. Lee, "The Design of Dual Emitting Cores for Green Thermally Activated Delayed Fluorescent Materials," *Angew. Chem. Int. Ed.*, vol. 54, no. 17, pp. 5201–5204, Apr. 2015.

[54] J. Lee, K. Shizu, H. Tanaka, H. Nomura, T. Yasuda, and C. Adachi, "Oxadiazole- and triazole-based highly-efficient thermally activated delayed fluorescence emitters for organic light-emitting diodes," *J. Mater. Chem. C*, vol. 1, no. 30, pp. 4599–4604, Jul. 2013.

[55] S. Y. Lee, C. Adachi, and T. Yasuda, "High-Efficiency Blue Organic Light-Emitting Diodes Based on Thermally Activated Delayed Fluorescence from Phenoxaphosphine and Phenoxathiin Derivatives," *Adv. Mater.*, vol. 28, no. 23, pp. 4626–4631, Jun. 2016.

[56] H. Uoyama, K. Goushi, K. Shizu, H. Nomura, and C. Adachi, "Highly efficient organic light-emitting diodes from delayed fluorescence," *Nature*, vol. 492, no. 7428, pp. 234–238, Dec. 2012.

[57] J. Lee *et al.*, "Controlled emission colors and singlet–triplet energy gaps of dihydrophenazine-based thermally activated delayed fluorescence emitters," *J. Mater. Chem. C*, vol. 3, no. 10, pp. 2175–2181, Feb. 2015.

[58] S. Wang, X. Yan, Z. Cheng, H. Zhang, Y. Liu, and Y. Wang, "Highly Efficient Near-Infrared Delayed Fluorescence Organic Light Emitting Diodes Using a Phenanthrene-Based Charge-Transfer Compound," *Angew. Chem. Int. Ed.*, vol. 54, no. 44, pp. 13068–13072, Oct. 2015.

[59] Z. Yang *et al.*, "Recent advances in organic thermally activated delayed fluorescence materials," *Chem. Soc. Rev.*, vol. 46, no. 3, pp. 915–1016, Feb. 2017.

[60] Y. Tao *et al.*, "Thermally Activated Delayed Fluorescence Materials Towards the Breakthrough of Organoelectronics," *Adv. Mater.*, vol. 26, no. 47, pp. 7931–7958, Dec. 2014.

[61] C. A. Parker and C. G. Hatchard, "Triplet-singlet emission in fluid solutions. Phosphorescence of eosin," *Trans. Faraday Soc.*, vol. 57, no. 0, pp. 1894–1904, Jan. 1961.

[62] J. Mack, Y. Asano, N. Kobayashi, and M. J. Stillman, "Application of MCD spectroscopy and TD-DFT to a highly non-planar porphyrinoid ring system. New insights on red-shifted porphyrinoid spectral bands," *J. Am. Chem. Soc.*, vol. 127, no. 50, pp. 17697–17711, Dec. 2005.

[63] E. R. Carraway, J. N. Demas, B. A. DeGraff, and J. R. Bacon, "Photophysics and photochemistry of oxygen sensors based on luminescent transition-metal complexes," *Anal. Chem.*, vol. 63, no. 4, pp. 337–342, Feb. 1991.

[64] B. J. Müller, T. Burger, S. M. Borisov, and I. Klimant, "High performance optical trace oxygen sensors based on NIR-emitting benzoporphyrins covalently coupled to silicone matrixes," *Sens. Actuators B Chem.*, vol. 216, pp. 527–534, Sep. 2015.

[65] J. Brandrup, E. H. Immergut, and E. A. Grulke, *Polymer Handbook*, 4th Edition., vol. 2. Wiley.

[66] A. M. A. El Wafa, S. Okada, and H. Nakanishi, "Poling and its relaxation studies of polycarbonate and poly(styrene-co-acrylonitrile) doped by a nonlinear optical chromophore," *Dyes Pigments*, vol. 69, no. 3, pp. 239–244, Jan. 2006.

[67] B. Ellis and R. Smith, *Polymers: A Property Database, Second Edition*. CRC Press, 2008.

[68] J.-H. Kim, F. Deng, F. N. Castellano, and J.-H. Kim, "High Efficiency Low-Power Upconverting Soft Materials," *Chem Mater*, 2012.

[69] K. Xu, J. Zhao, X. Cui, and J. Ma, "Photoswitching of triplet–triplet annihilation upconversion showing large emission shifts using a photochromic fluorescent dithienylethene-Bodipy triad as a triplet acceptor/emitter," *Chem Commun*, Dezember 2014.

[70] R. R. Islangulov, J. Lott, C. Weder, and F. N. Castellano, "Noncoherent low-power upconversion in solid polymer films," *J. Am. Chem. Soc.*, vol. 129, no. 42, pp. 12652–12653, Oct. 2007.

[71] T. N. Singh-Rachford, J. Lott, C. Weder, and F. N. Castellano, "Influence of temperature on low-power upconversion in rubbery polymer blends," *J. Am. Chem. Soc.*, vol. 131, no. 33, pp. 12007–12014, Aug. 2009.

[72] S. M. Borisov, R. Saf, R. Fischer, and I. Klimant, "Synthesis and properties of new phosphorescent red light-excitable platinum(II) and palladium(II) complexes with Schiff bases for oxygen sensing and triplet-triplet annihilation-based upconversion," *Inorg. Chem.*, vol. 52, no. 3, pp. 1206–1216, Feb. 2013.

[73] Y. Y. Cheng *et al.*, "On the efficiency limit of triplet–triplet annihilation for photochemical upconversion," *Phys. Chem. Chem. Phys.*, vol. 12, no. 1, pp. 66–71, Dec. 2009.

[74] A. J. Svagan, D. Busko, Y. Avlasevich, G. Glasser, S. Baluschev, and K. Landfester, "Photon Energy Upconverting Nanopaper: A Bioinspired Oxygen Protection Strategy," *ACS Nano*, vol. 8, no. 8, pp. 8198–8207, 2014.

5.5 Supporting Information

5.5.1 Synthesis

(3aR,7aS)-2-(2-ethylhexyl)-3a,4,7,7a-tetrahydro-1H-isoindole-1,3(2H)-dione
The reaction was conducted according to literature [4]. (3aR,7aS)-3a,4,7,7a-tetrahydroisobenzofuran-1,3-dione (35.00 g, 230.0 mmol, 1.00 eq) and 4 Å molecular sieves (50.00 g) were dissolved in 100 mL dry DMF, filled in a 2-neck-flask under argon counterflow followed by addition of 2-ethylhexylamine (32.70 g, 253.0 mmol, 1.10 eq), yielding a cloudy white solution. The reaction mixture was deoxygenated by bubbling N2 through the solution for 10 minutes under vigorous stirring. The flask was closed and the reaction was refluxed for 24 hours under inert atmosphere. Reaction progress was controlled via TLC (CH:EE, 3:1). Finally DMF was removed using a rotary evaporator and the obtained product was distilled under reduced pressure (0.60 mbar, 180°C) to finally receive (3aR,7aS)-2-(2-ethylhexyl)-3a,4,7,7a-tetrahydro-1H-isoindole-1,3(2H)-dione as a yellow oil. Yield: 43.22 g, 71%

^{1}H NMR (300 MHz, Chloroform-d) δ 5.97 – 5.79 (m, 2H), 3.34 (d, J = 7.3 Hz, 2H), 3.12 – 2.97 (m, 2H), 2.60 (ddt, J = 14.0, 4.2, 2.2 Hz, 2H), 2.31 – 2.09 (m, 2H), 1.68 (hept, J = 6.5 Hz, 1H), 1.21 (ddt, J = 19.2, 11.0, 4.8 Hz, 8H), 0.85 (td, J = 7.1, 4.8 Hz, 6H).

(3aS,7aR)-5-chloro-2-(2-ethylhexyl)-6-(phenylthio)hexahydro-1H-isoindole- 1,3(2H)-dione
The reaction was conducted according to literature [4]. N-chlorosuccinimide (12.08 g, 90.5 mmol), 1.08 eq) was first completely dissolved (ultrasonic bath) in dry DCM (400 mL) under argon atmosphere in a 2-neck-flask. The flask was then immersed in an EtOH/liquid-N2 bath at 0°C while N2 was bubbled through the reaction mixture in argon counterflow for 30 minutes. Followed by dropwise addition (exothermic reaction) of thiophenol (9.969 g, 90.5 mmol, 1.08 eq, ρ=1.08 g/mL) dissolved in 12 mL dry DCM over 40 minutes, which gave rise to a color change from yellow to orange. The content was allowed to stir for 10 minutes at room temperature. Then the flask was cooled to -41°C with an EtOH/liquid-N2-bath followed by slow addition (over 35 minutes) of (3aR,7aS)-2-(2-ethylhexyl)-3a,4,7,7a-tetrahydro-1H-isoindole-1,3(2H)-dione (22.00 g, 83.5 mmol, 1.00 eq) as a solution in 60 mL of dry DCM which was before deoxygenated by bubbling N2 trough the solution for 10 minutes. The mixture was then brought to room temperature, by vigorous stirring for one hour before the by-product of succinimide was quickly filtered off. The solvent was removed under reduced pressure and the resulting orange oil was finally purified via column chromatography. The reaction progress was controlled via TLC (CH:EE, 4:1). Yield: 25.75 g, 76 %

^{1}H NMR (300 MHz, Chloroform-d) δ 7.48 – 7.40 (m, 2H), 7.39 – 7.28 (m, 3H), 4.27 – 4.17 (m, 1H), 3.58 (q, J = 4.2 Hz, 1H), 3.47 – 3.35 (m, 2H), 3.22 – 3.04 (m, 1H), 2.91 (td, J = 8.1, 4.1 Hz, 1H), 2.70 – 2.41 (m, 2H), 2.41 – 2.27 (m, 1H), 2.25 – 2.11 (m, 1H), 1.84 – 1.71 (m, 1H), 1.35 – 1.19 (m, 8H), 0.95 – 0.83 (m, 6H).

(3aS,7aR)-5-chloro-2-(2-ethylhexyl)-6-(phenylsulfonyl)hexahydro-1H-isoindole-   1,3(2H)-dione

The reaction was conducted according to literature [4]. (3aS,7aR)-5-chloro-2-(2-ethylhexyl)-6-(phenylthio)hexahydro-1H-isoindole-1,3(2H)-dione (43.00 g, 105.4 mmol, 1.00 eq) was dissolved in 600 mL of dry DCM - while bubbling N_2 through the solution - in a 1 L round bottom flask. Then it was immersed into an EtOH/liquid-N_2 bath (0°C) and the solution was stirred vigorously for 30 minutes. The purified m-CPBA (47.61 g, 275.9 mmol, 2.62 eq) was added continuously every 15 seconds in small portions (exothermic reaction) with plastic spatulas over 30 minutes, resulting in a milky white hard to stir solution at the end of the addition. The reaction mixture was then brought to room temperature. After one hour vigorous stirring the by-product of m-chlorobenzoic acid was removed under vaccum filtration. The filtrate was washed with DCM (3 x 70 mL), whereas the combined organic solutions were concentrated under reduced pressure to an approximate volume of 450 mL and then washed with a 10% sodium carbonate solution (3 x 60 mL), followed by drying over Na_2SO_4 and the removal of the solvent under reduced pressure. The received yellow oil was directly used in the next reaction step without any further purification step. The reaction progress was controlled via TLC (CH:EE, 3:1). Yield: 45.38 g, 98 %

^{1}H NMR (300 MHz, Chloroform-*d*) δ 7.98 – 7.87 (m, 2H), 7.78 – 7.68 (m, 1H), 7.68 – 7.55 (m, 2H), 4.71 – 4.62 (m, 1H), 3.53 – 3.45 (m, 1H), 3.44 – 3.30 (m, 3H), 3.09 – 2.97 (m, 1H), 2.67 – 2.53 (m, 1H), 2.52 – 2.28 (m, 2H), 2.25 – 2.12 (m, 1H), 1.80 – 1.68 (m, 1H), 1.34 – 1.12 (m, 8H), 0.94 – 0.78 (m, 6H).

(3aR,7aS)-2-(2-ethylhexyl)-5-(phenylsulfonyl)-3a,4,7,7a-tetrahydro-1H-isoindole-   1,3(2H)-dione

The reaction was conducted according to literature [4]. (3aS,7aR)-5-chloro-2-(2-ethylhexyl)-6-(phenylsulfonyl)hexahydro-1H-isoindole-1,3(2H)-dione (27.40 g, 62.3 mmol, 1.00eq) was dissolved in 250 mL of dry DCM in a 2-neck round bottom flask (yellow solution) and cooled down to -78°C in an EtOH/N_2 bath for 30 minutes while bubbling N_2 through the solution in argon counterflow. 1,8-Diaza-7-bicyclo[5.4.0]undecene (11.55 g, 75.9 mmol, 1.22 eq) was then added rapidly, after degassing the solution for 1 minute, via an addition funnel, which led to a dark brown-green solution. The flask was then immersed into an EtOH/liquid-N_2 bath (0°C), where the reaction mixture was allowed to stir for 10 minutes. Finally the mixture was washed with 5% HCl (3 x 60 mL) and dried over Na_2SO_4. The solvent was removed under reduced pressure to obtain a yellow oil. Yield: 22.93 g, 91 %

^{1}H NMR (300 MHz, Chloroform-*d*) δ 7.80 (dd, *J* = 7.3, 1.8 Hz, 2H), 7.67 – 7.59 (m, 1H), 7.57 – 7.49 (m, 2H), 7.15 (dt, *J* = 6.3, 3.1 Hz, 1H), 3.25 – 2.96 (m, 4H), 2.92 – 2.76 (m, 2H), 2.53 – 2.39 (m, 2H), 1.59 – 1.45 (m, 1H), 1.33 – 1.01 (m, 12H), 0.91 – 0.76 (m, 9H).

tert-butyl-6-(2-ethylhexyl)5,7-dioxo-2,4,4a,5,6,7,7a,8-octahydropyrrolo[3,4-f]isoindole-1-carboxylate

The reaction was conducted according to literature [4]. Potassium t-butoxide (1.44 g, 12.81mmol, 1.88 eq) was first dissolved in dry THF (100mL) in a 2-neck round bottom flask (vigorous stirring) under inert atmosphere. The solution was deoxygenated for ten minutes, producing a yellow solution. Afterwards the flask was subsequently immersed in an EtOH/liquid-N_2 bath (0°C) for 30 minutes and tert-butyl-isocyanoacetate (1.91 g, 13.56mmol, 1.99 eq, ρ=0.97 g/mL) was added rapidly, yielding a bright brown/red transparent solution, which was furthermore stirred for 45 minutes at 0°C. (3aR,7aS)-2-(2-ethylhexyl)-5-(phenylsulfonyl)-3a,4,7,7a-tetrahydro-1H-isoindole-1,3(2H)-dione (2.75 g, 6.81mmol, 1.00 eq) was dissolved in 35 mL dry THF and added dropwise over 40 minutes to the previous solution with the aid of an addition funnel. Then the reaction mixture was brought to room temperature and allowed to stir for one hour while the reaction progress was monitored via TLC. Finally the solvent was removed under reduced pressure. The residue was re-dissolved in DCM (120 mL), subsequently washed with brine (3 x 50 mL) and the combined organic fractions were dried over sodium sulfate. The solvent was removed under reduced pressure to afford orange oil, which was further purified via flash chromatography. Yield: 2.27 g, 83 %

^{1}H NMR (300 MHz, Chloroform-*d*) δ 8.77 (s, 1H), 6.69 – 6.62 (m, 1H), 3.76 (ddd, *J* = 15.3, 4.0, 1.8 Hz, 1H), 3.31 – 3.10 (m, 5H), 2.83 – 2.60 (m, 2H), 1.57 (s, 9H), 1.52 – 1.39 (m, 1H), 1.30 – 1.03 (m, 4H), 0.94 – 0.60 (m, 10H).

6-(2-ethylhexyl)5,7-dioxo-2,4,4a,5,6,7,7a,8-octahydropyrrolo[3,4-f]isoindole-1-carboxylic acid

The reaction was conducted according to literature [4]. tert-butyl 6-(2-ethylhexyl)5,7-dioxo-2,4,4a,5,6,7,7a,8-octahydropyrrolo[3,4-f]isoindole-1-carboxylate (1.20 g, 2.98 mmol, 1.00 eq) was transferred in a 2-neck round bottom flask purged with nitrogen for 5 minutes and shielded from light by covering with aluminum foil. Then 33% hydrobromic acid in acetic acid (40 mL, excess) was added to the flask, while vigorous stirring, dissolving the white solid leading to a bright orange solution. After 45 minutes the content was subsequently poured into a cold (0°C) KH_2PO_4 solution (10%, 100 mL). The aqueous phase was extracted three times with ethyl acetate, before the combined organic phases were dried over Na_2SO_4. The solvent was removed under reduced pressure to afford orange oil. The product, which is a mixture of carboxylic acid / pyrrole (9:1), was used in the next step without further purification. Yield: 1.01 g, 98 %

^{1}H NMR (300 MHz, Chloroform-*d*) δ 8.94 (s, 1H), 6.76 (s, 1H), 3.81 (d, *J* = 15.6 Hz, 1H), 3.30 – 3.15 (m, 5H), 2.86 – 2.75 (m, 1H), 2.75 – 2.64 (m, 1H), 2.05 (s, 1H), 1.20 – 1.08 (m, 6H), 0.92 – 0.78 (m, 8H), 0.75 – 0.66 (m, 4H).

2-(2-ethylhexyl)3a,4,8,8a-tetrahydropyrrolo[3,4-f]isoindole-1,3(2H,6H)-dione

6-(2-ethylhexyl)5,7-dioxo-2,4,4a,5,6,7,7a,8-octahydropyrrolo[3,4-f]isoindole-1-carboxylic acid(500 mg, 1.44 mmol, 1.00 eq) were dissolved in a 2-neck round bottom flask in pyridine (20 mL) and purged with nitrogen for 5 minutes. Then the content was heated to 115 °C, while still passing nitrogen through the reaction mixture leading to the evaporation of pyridine, which was in the following condensed, gathered and then again added to the mixture. This procedure was repeated 4 times, the content (with traces of pyridine) was neutralized by washing with 0.5 M HCl (10 mL) and then purified via filtration over a pad of silica (eluent CH:EE, 2:1). The solvent was removed under reduced pressure to afford a yellow solid. The product was covered with aluminum foil (light-sensitive) and dried in the vacuum oven at 60°C. Yield: 306 mg, 70 %

^{1}H NMR (300 MHz, Chloroform-*d*) δ 7.86 (s, 1H), 6.52 (d, *J* = 2.6 Hz, 2H), 3.31 – 3.07 (m, 6H), 2.80 – 2.65 (m, 2H), 1.53 – 1.39 (m, 1H), 1.29 – 0.94 (m, 5H), 0.94 – 0.76 (m, 6H), 0.75 – 0.65 (m, 3H).

Meso-tetraphenyltetra2-(2-ethylhexyl)hexahydro-1H-isoindole-1,3(2H)-dione-porphyrin (H2-TPThIIP)

Freshly distilled benzaldehyde(140 mg, 1.32mmol, 4.00 eq) was dissolved in dry DCM (120 mL; dried over 4Å molecular sieves for 1 week) in a 2-neck round bottom flask. After4 Å molecular sieves (1.3 g) were added to the solution, the content was purged with argon gas for 1 hour while stirring. 2-(2-ethylhexyl)3a,4,8,8a-tetrahydropyrrolo[3,4-f]isoindole-1,3(2H,6H)-dione (400 mg, 1.32mmol, 4.00 eq) dissolved in dry, deoxygenated DCM (2 mL) was added in argon countercurrent to the solution, the flask shielded from light (covered with aluminum foil) and the content stirred for 20 minutes. Boron trifluorideetherate(46 mg, 324.1μmol, 1.00 eq) was added dropwise in argon countercurrent with the aid of an addition funnel accompanied by a color change of the solution from yellow to red-brown. After 90 minutes stirring (in the dark) DDQ (361 mg, 1.59mmol, 4.80eq) was added rapidly leading to a green solution, which was then again stirred for 4 hours in the dark. Reaction progress is monitored through UV-Vis spectroscopy by the growth of the Soret band at 462 nm (in toluene). Afterwards the molecular sieves were filtered off and washed with DCM (3x25 mL) and the solvent was removed under reduced pressure. The greenish solids were re-dissolved in DCM/THF and passed through a short pad of silica, washed with Na₂CO₃ (50mL, 10%), brine and then dried over sodium sulfate. After removal of the solvent mixture under reduced pressure, the product was dried in the vacuum oven at 60°C yielding a green-brown solid, which was used as crude mixture in the next step. Yield: 201 mg, 39 %

λ$_{max}$(nm)/relative intensity in toluene: 356/ 0.173, 407/ 0.192, 462/ 1.00, 620/ 0.040, 674/ 0.117

5.5.2 Electrochemical properties
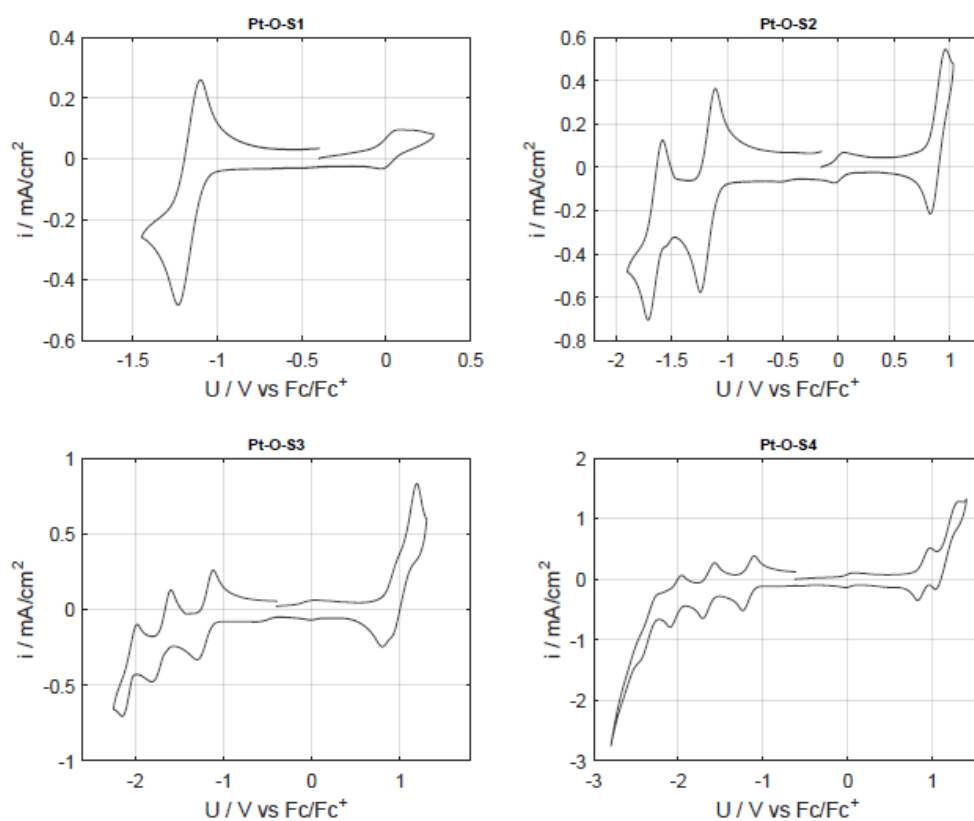
Figure S 5.1 Cyclic voltammetry of Pt-O-S in DCM containing 0.1 M TBAPClO₄ at a scan rate of 0.1 V s⁻¹
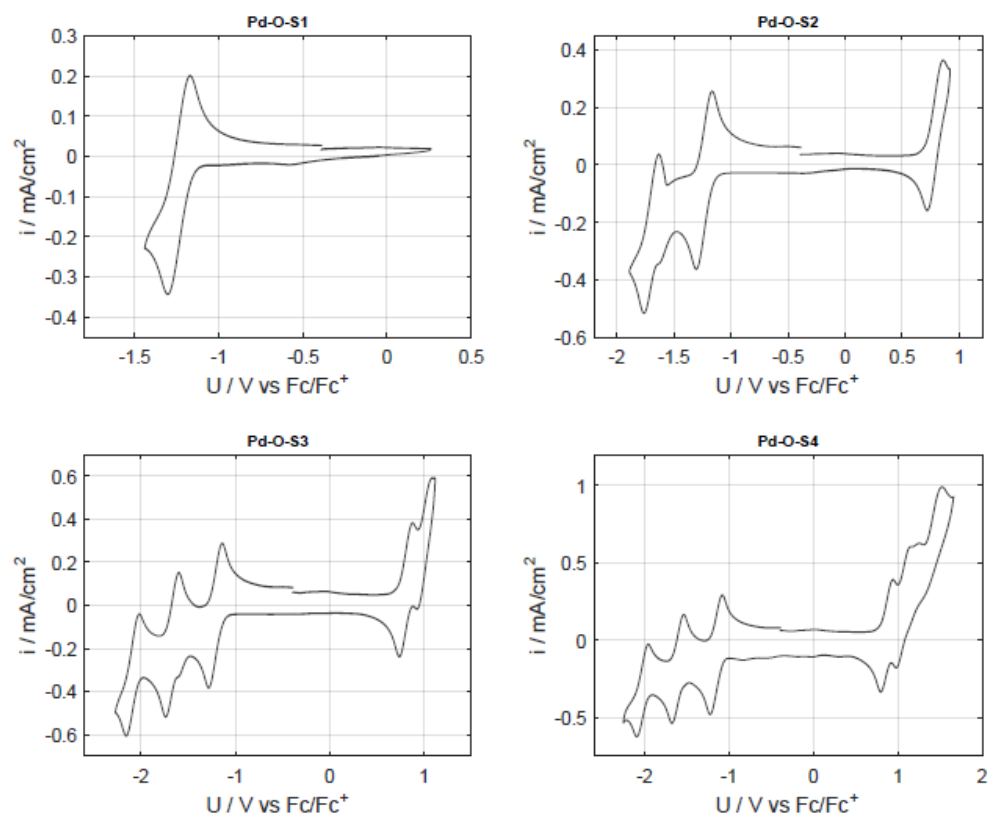
Figure S 5.2 Cyclic voltammetry of Pd-O-S in DCM containing 0.1 M TBAPClO₄ at a scan rate of 0.1 V s⁻¹
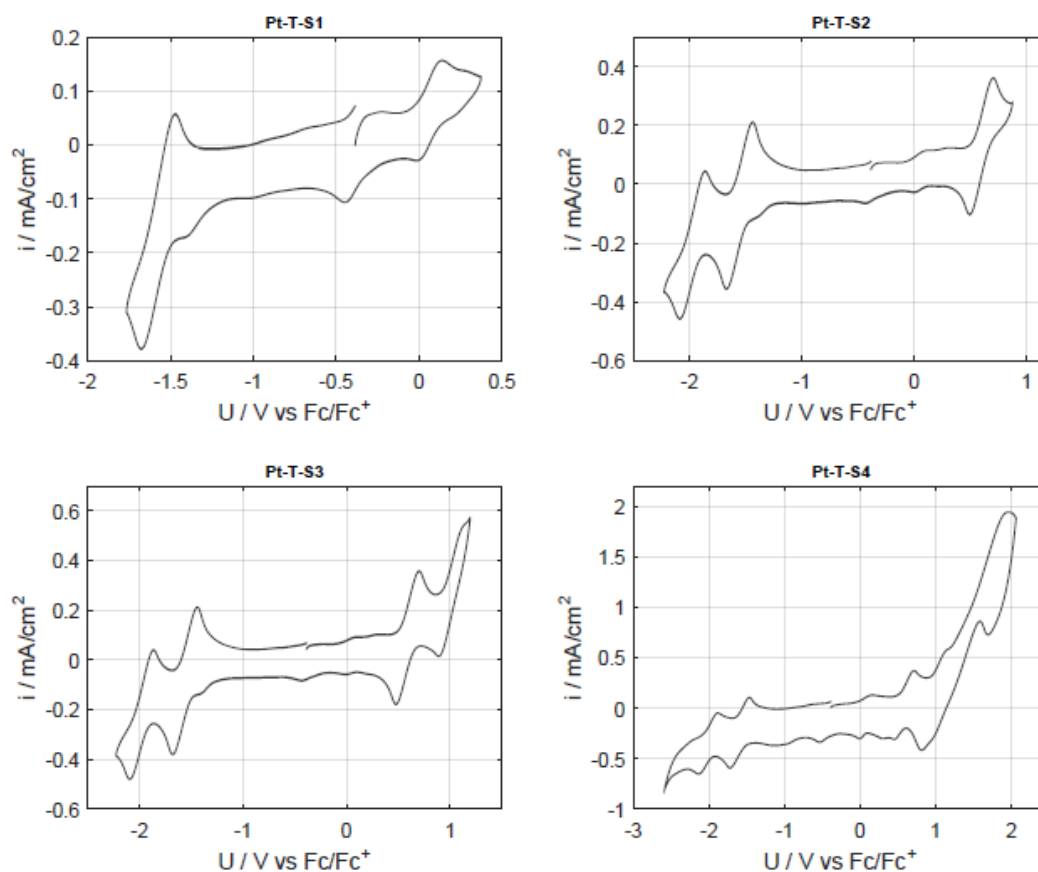
Figure S 5.3 Cyclic voltammetry of Pt-T-S in DCM containing 0.1 M TBAPClO₄ at a scan rate of 0.1 V s⁻¹
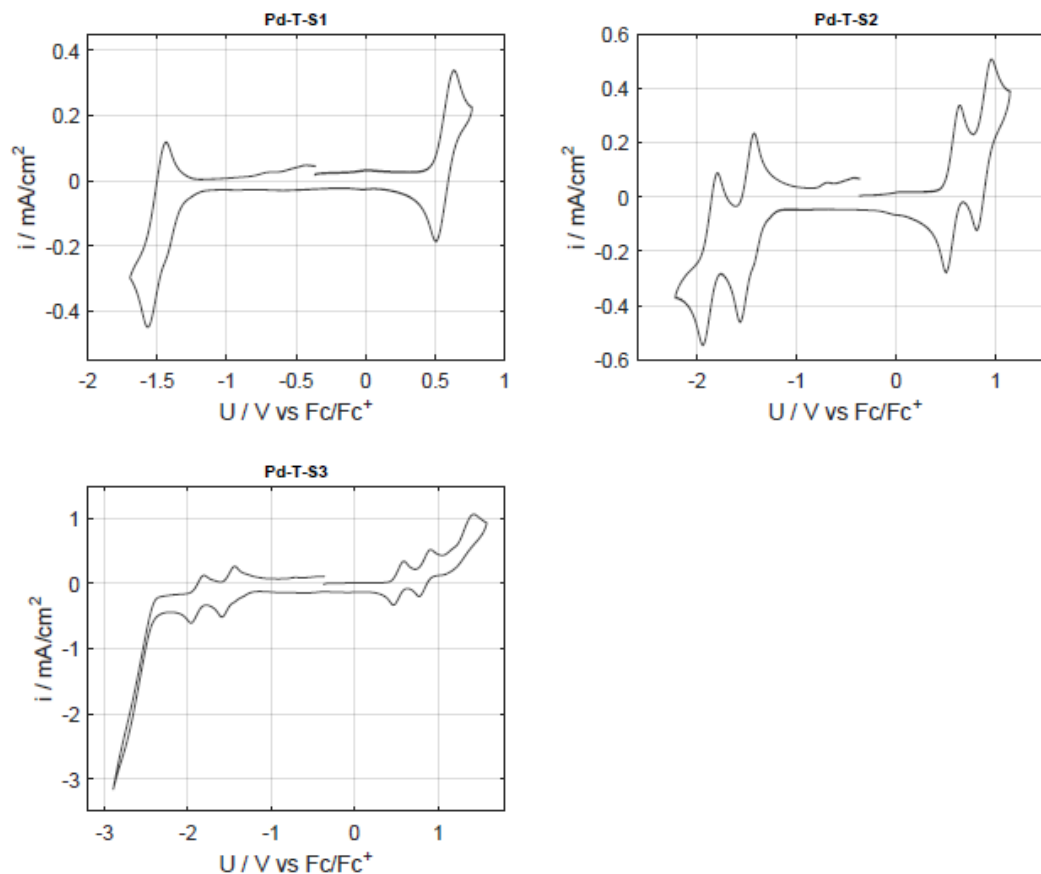
Figure S 5.4 Cyclic voltammetry of Pd-T-S in DCM containing 0.1 M TBAPClO₄ at a scan rate of 0.1 V s⁻¹
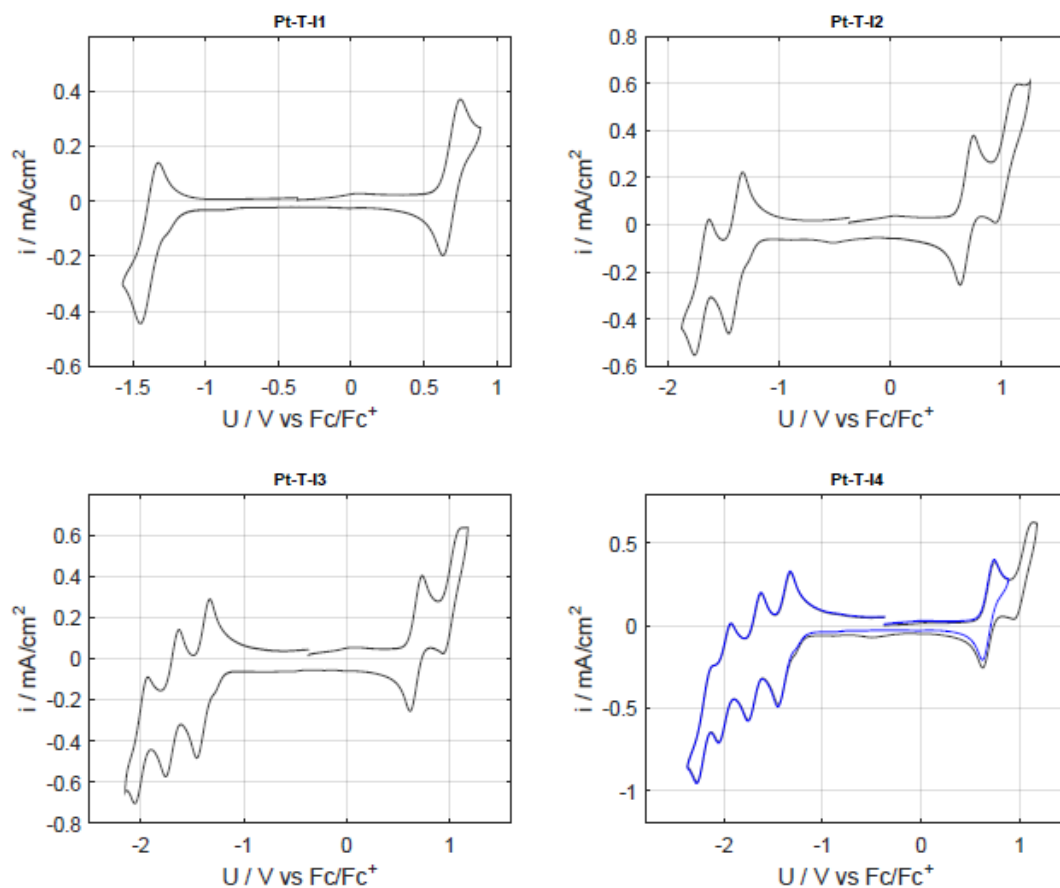
Figure S 5.5 Cyclic voltammetry of Pt-T-I in DCM containing 0.1 M TBAPClO₄ at a scan rate of 0.1 V s⁻¹
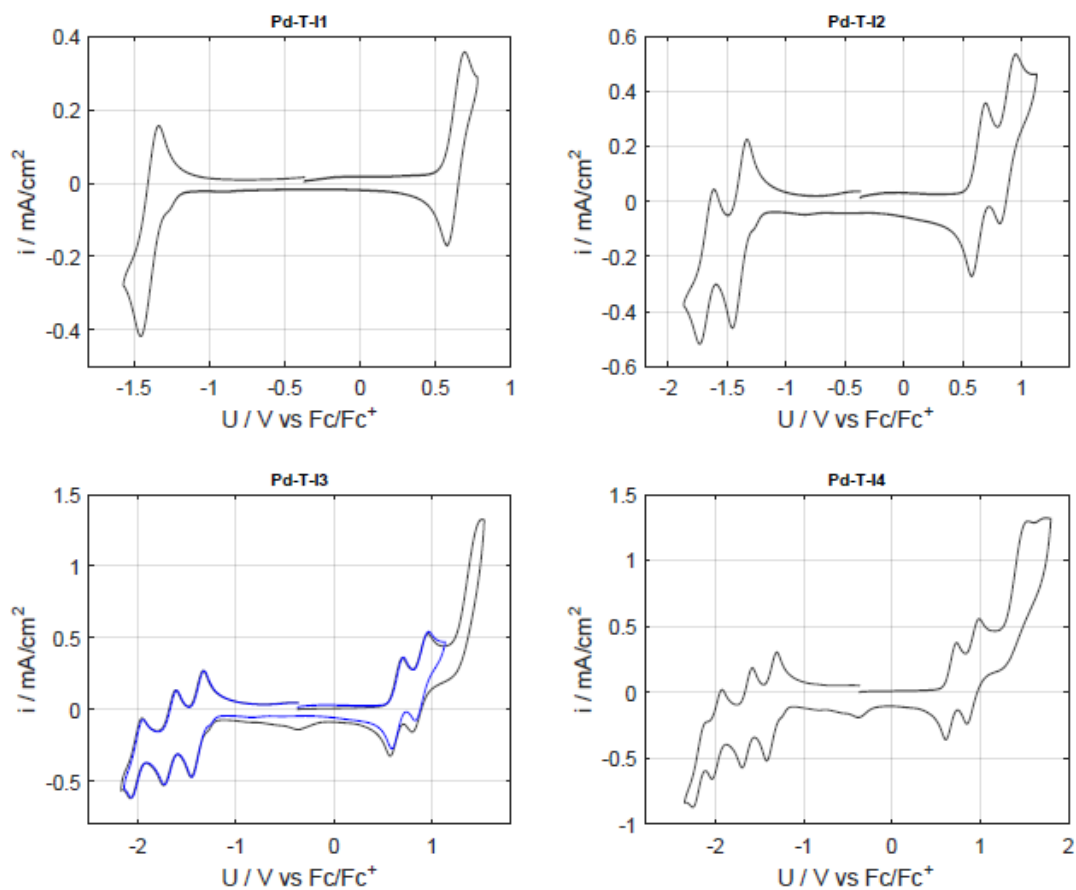
Figure S 5.6 Cyclic voltammetry of Pd-T-I in DCM containing 0.1 M TBAPClO₄ at a scan rate of 0.1 V s⁻¹
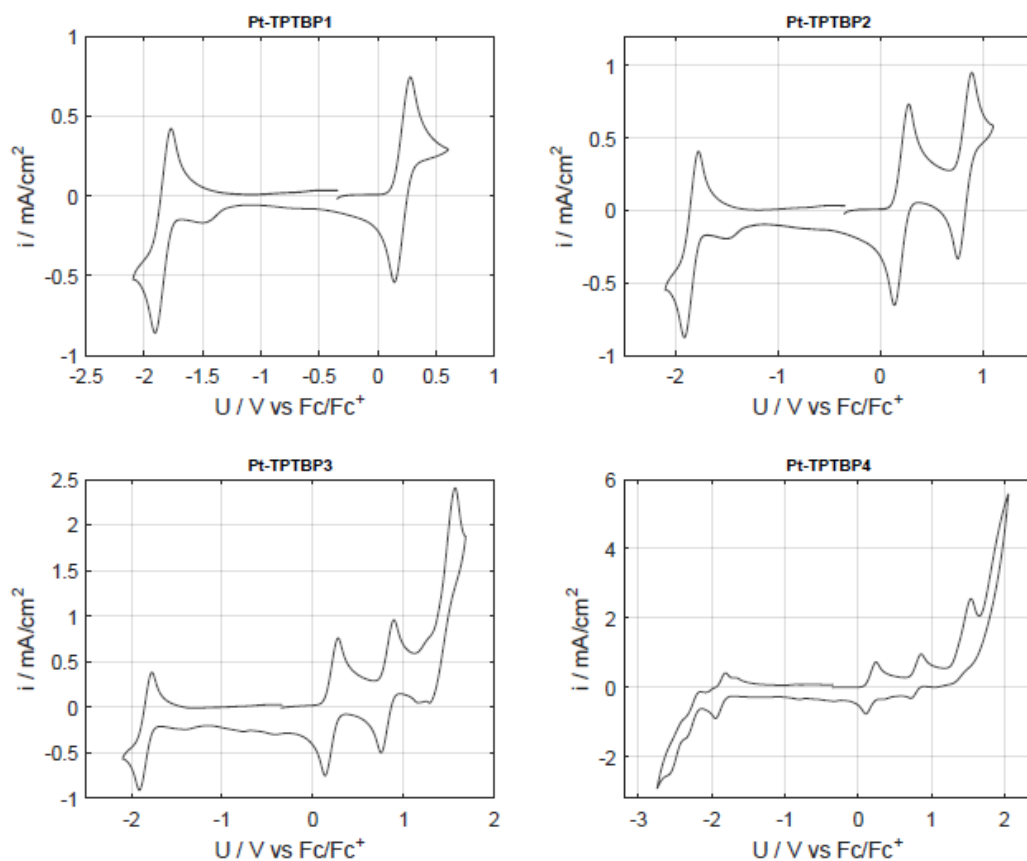
Figure S 5.7 Cyclic voltammetry of Pt-TPTBP in DCM containing 0.1 M TBAPClO₄ at a scan rate of 0.1 V s⁻¹
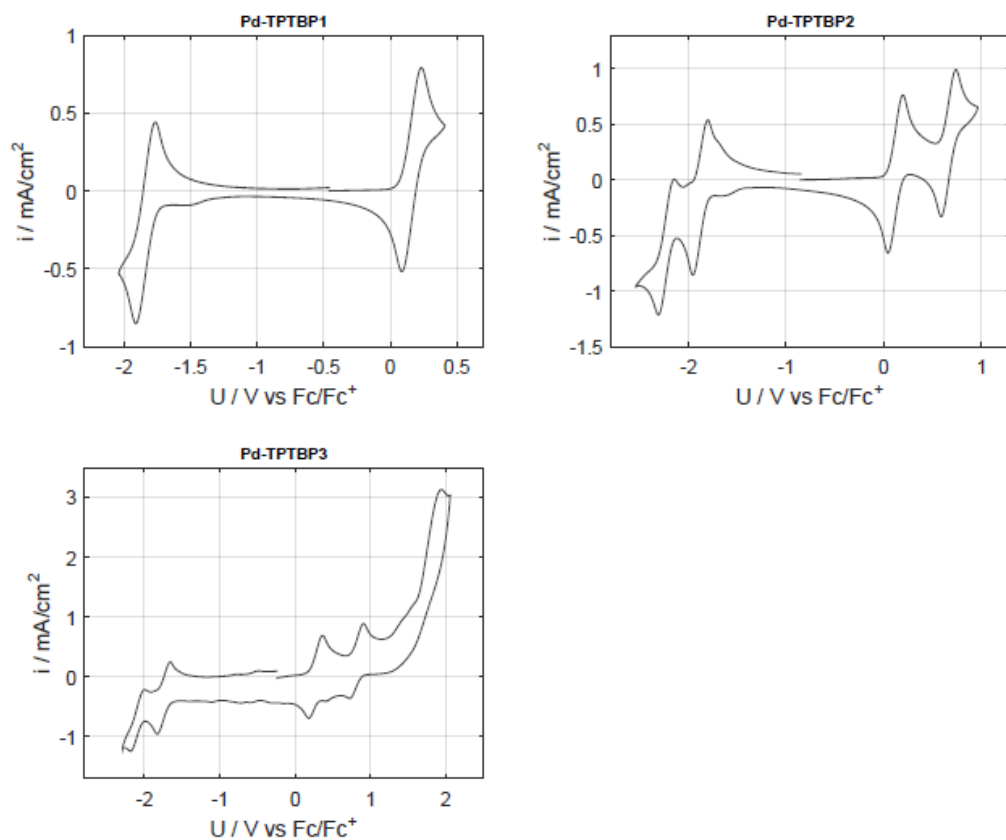
Figure S 5.8 Cyclic voltammetry of Pd-TPTBP in DCM containing 0.1 M TBAPClO₄ at a scan rate of 0.1 V s⁻¹

5.5.3 Photophysical properties
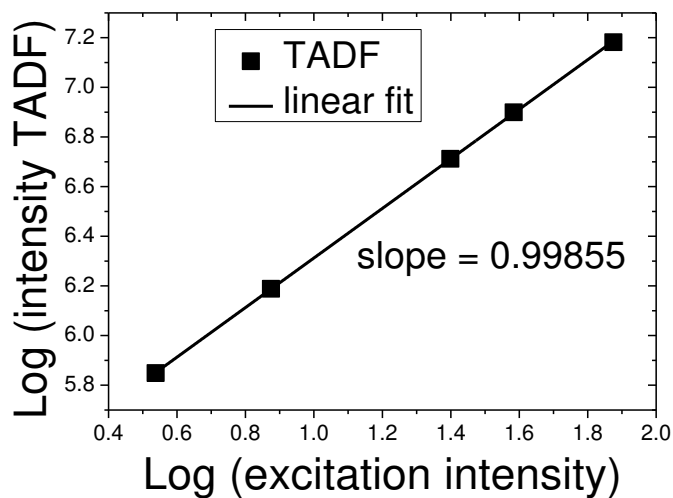
Figure S 5.9 Linear dependency of the intensity of TADF on the intensity of the excitation light

Table S 5.1 Radiative and non-radiative constants for the Pt(II) and Pd(II) complexes in toluene solution at 25 °C

Dye	Overall Φ	τ_0 Phos [µs]	$k_r \cdot 10^{-3}$ [s^{-1}][a]	$k_{nr} \cdot 10^{-3}$ [s^{-1}][b]
Pt-TPTBP	0.21	47	4.5	16.8
Pt-T-S	0.30	41	7.3	17.0
Pt-O-S	0.30	33	9.1	21.1
Pt-T-I	0.082	12	6.8	76.5
Pd-TPTBP	0.086	286	0.30	3.2
Pd-T-S	0.085	157	0.54	5.8
Pd-O-S	0.11	161	0.68	5.5
Pd-T-I	0.032	53	0.60	18.2

(a) – radiative rate constant $k_r = \Phi/\tau$

(b) – non radiative rate constant $k_{nr} = (1-\Phi)/\tau$

5.5.4 Reversible transformation of the Pt-Octa-Sulfone complex in basic media
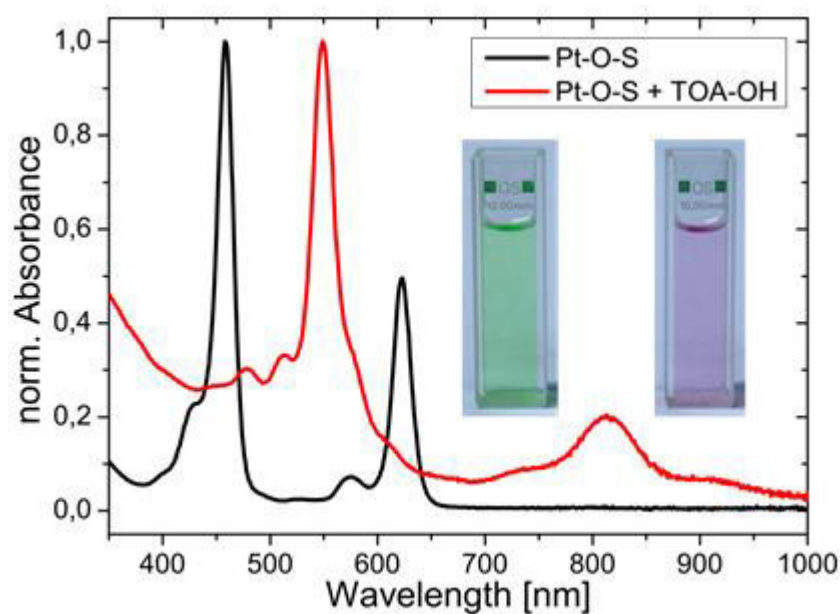
Figure S 5.10 Spectral properties of Pt-O-S (black line, left photographic image) and the product of the semi-reversible transformation (red line, right image) in presence of tetra-octyl ammonium hydroxide in DMF
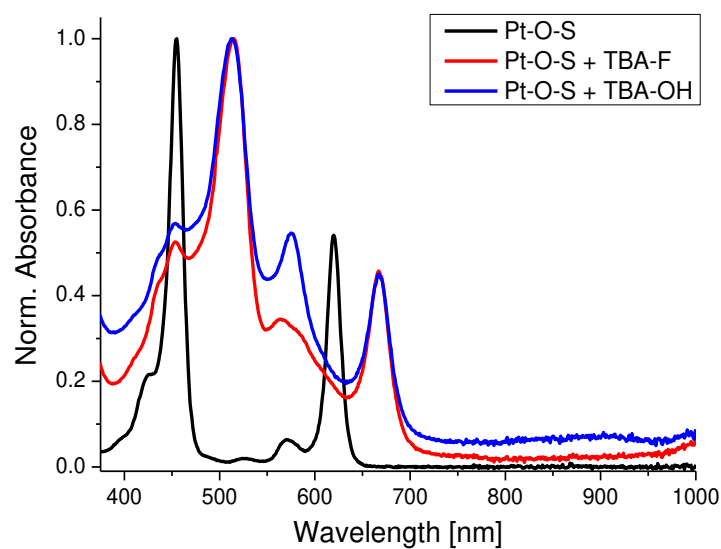
Figure S 5.11 Semi-reversible transformation of Pt-O-S in presence of tetra-butyl ammonium hydroxide/fluoride (TBA-OH/F) in THF
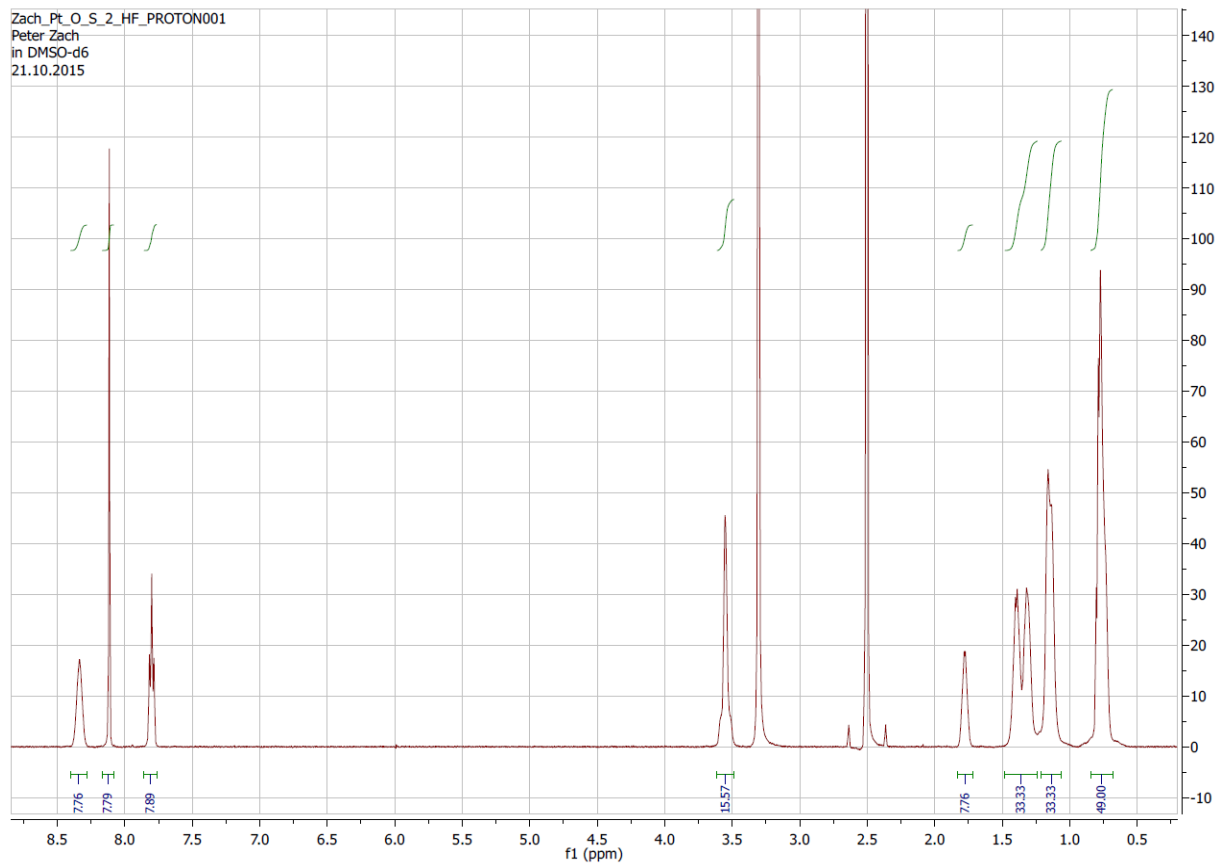
Figure S 5.12 NMR-Spectra (^{1}H) of Pt-O-S in deuterated DMSO
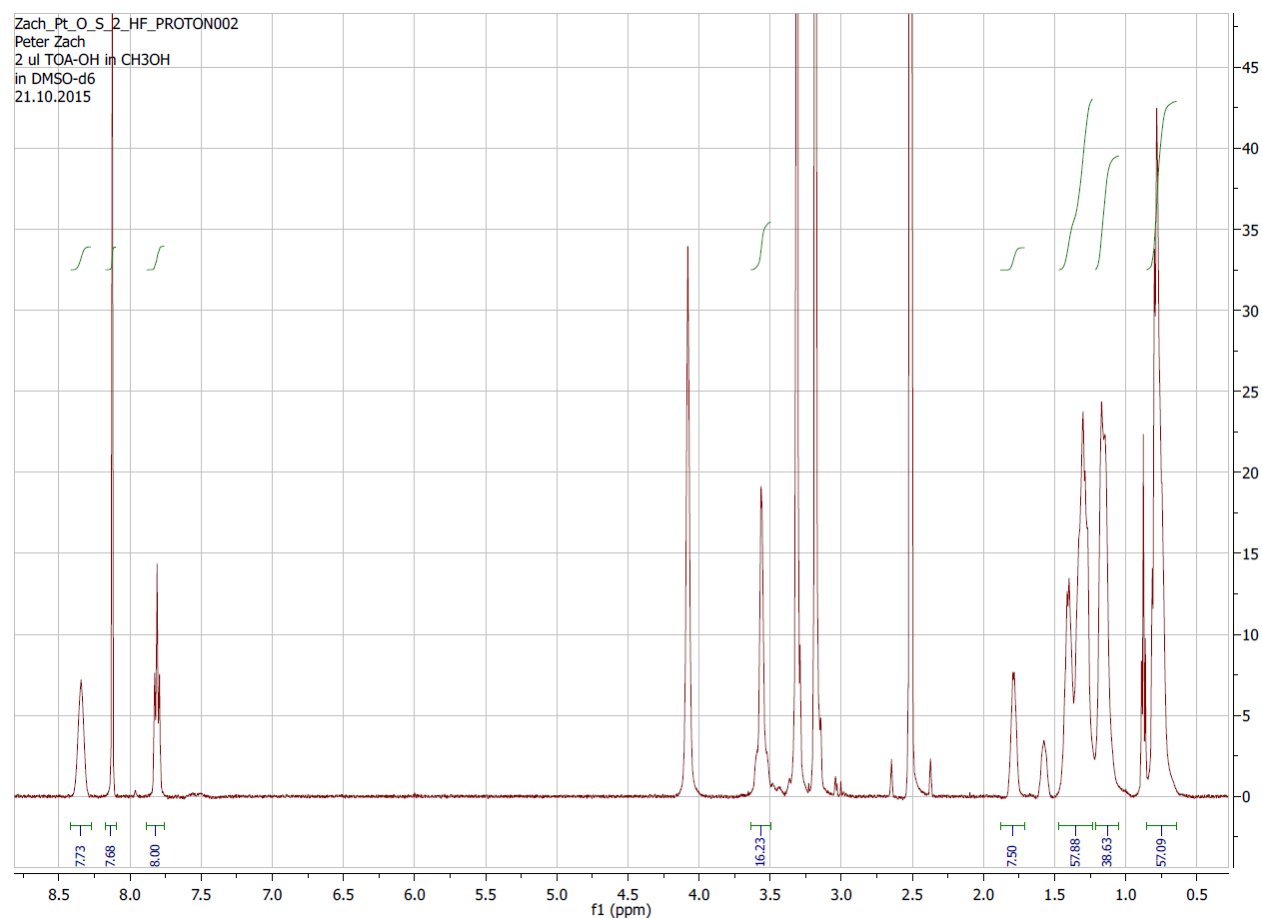
Figure S 5.13 NMR-Spectra (^{1}H) of Pt-O-S in deuterated DMSO and 2 µl of TOA-OH solution (20% in MeOH)
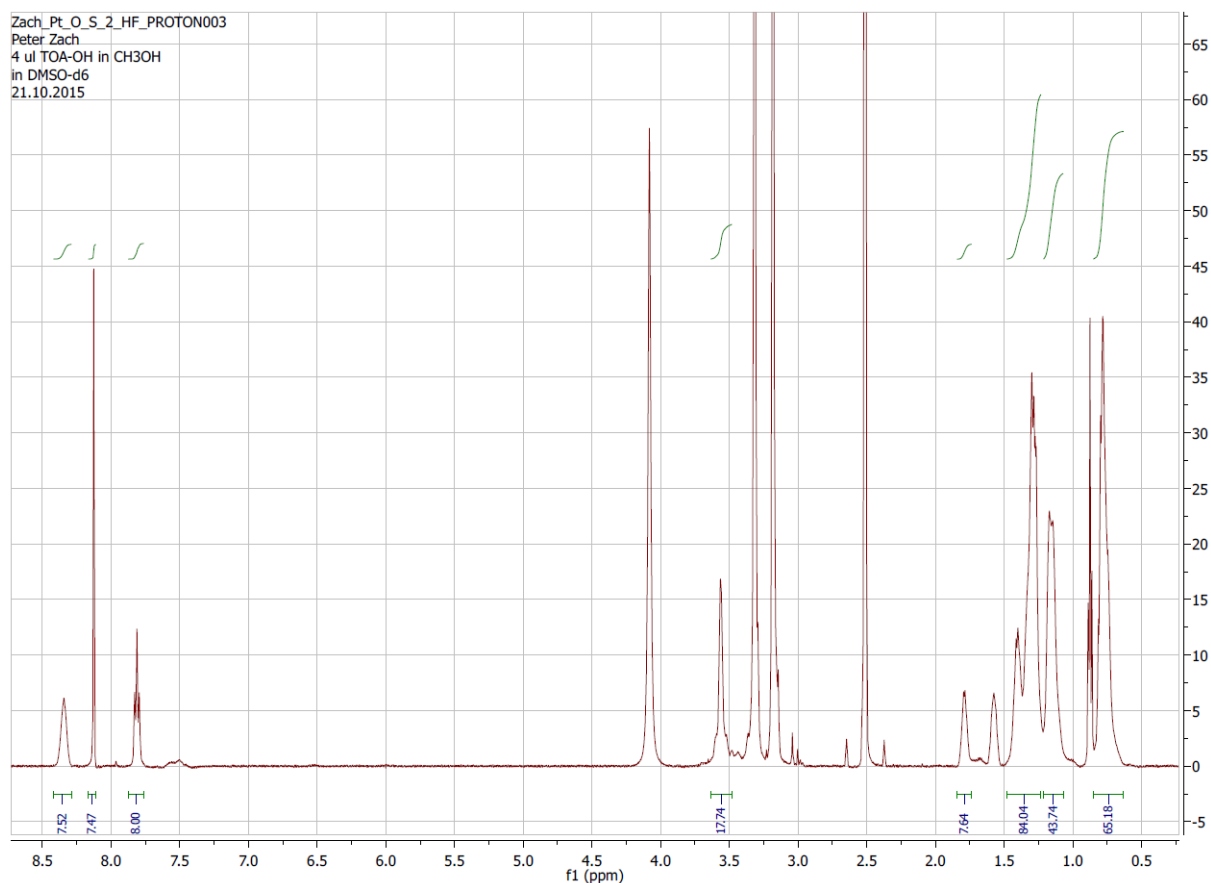
Figure S 5.14 NMR-Spectra (¹H) of Pt-O-S in deuterated DMSO and 4 µl of TOA-OH solution (20% in MeOH)
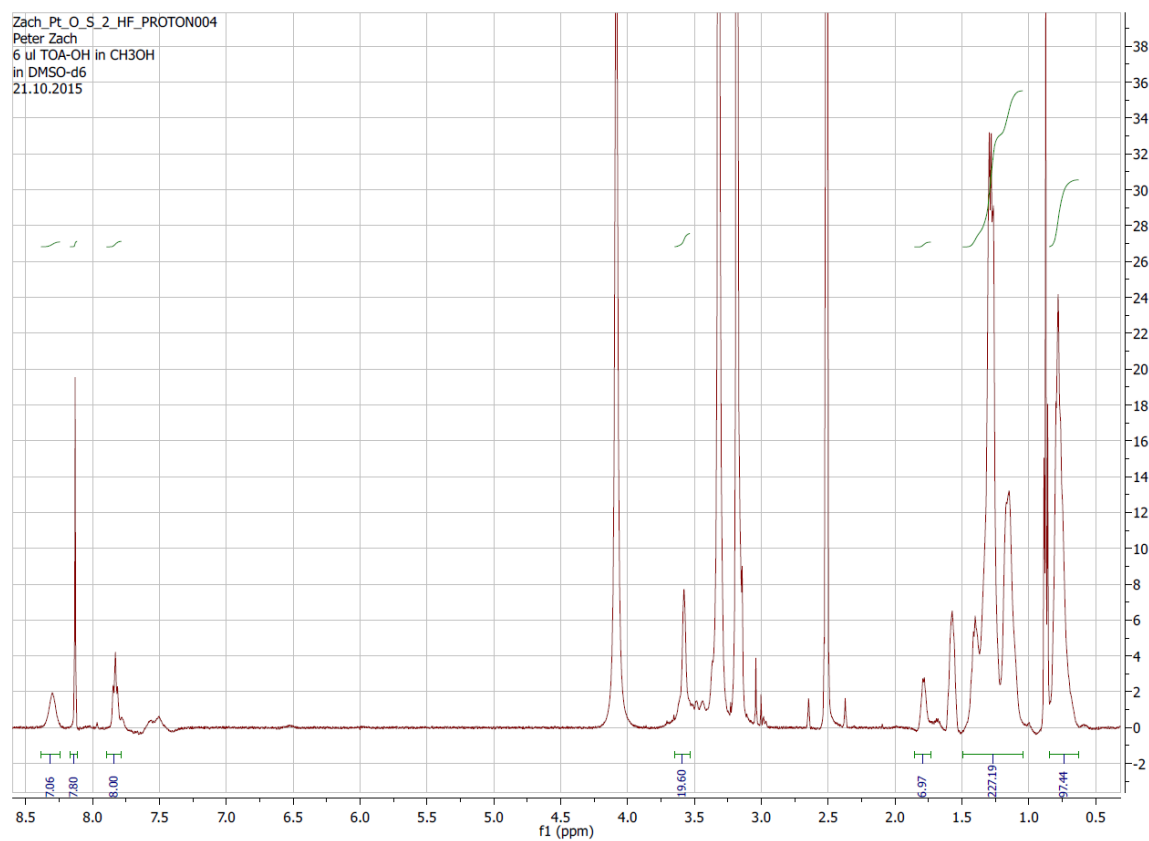
Figure S 5.15 NMR-Spectra (¹H) of Pt-O-S in deuterated DMSO and 6 µl of TOA-OH solution (20% in MeOH)
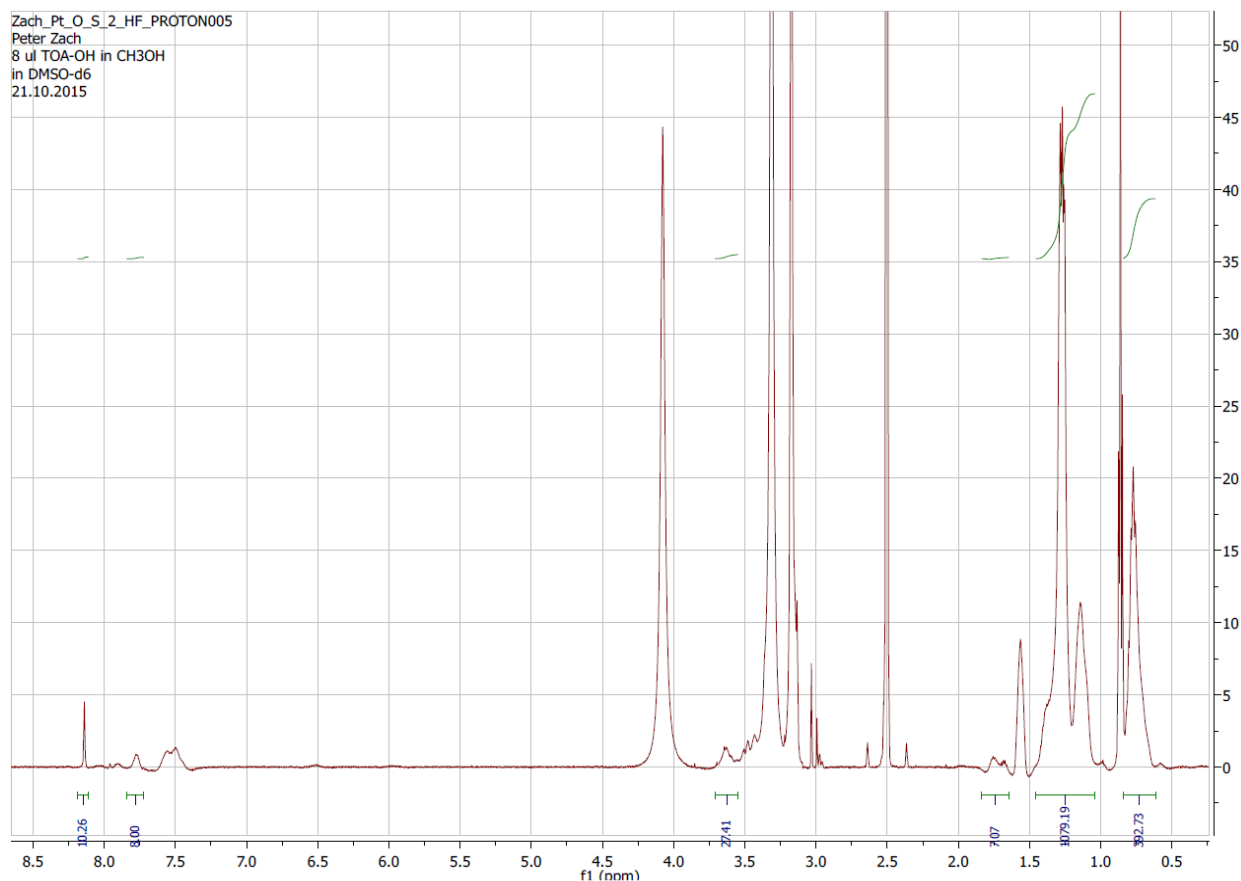
Figure S 5.16 NMR-Spectra (^{1}H) of Pt-O-S in deuterated DMSO and 8 µl of TOA-OH solution (20% in MeOH)
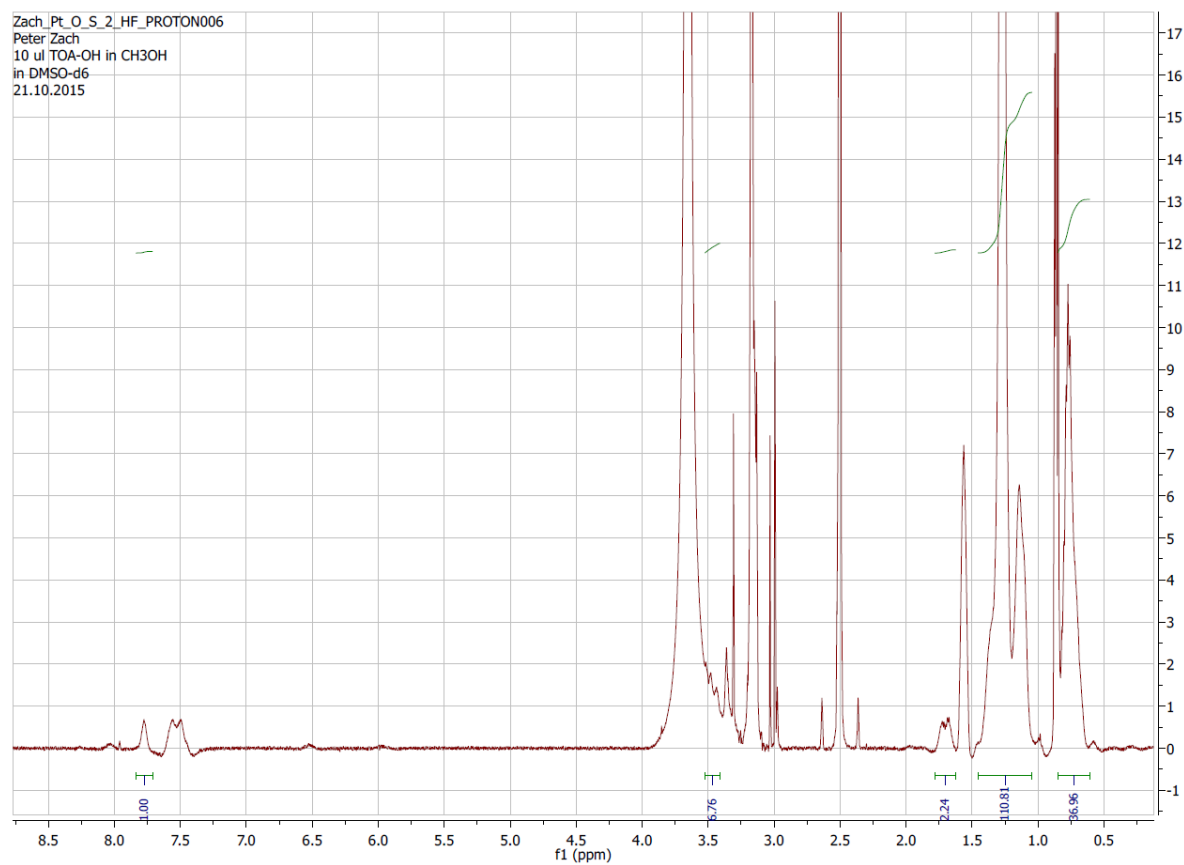
Figure S 5.17 NMR-Spectra (^{1}H) of Pt-O-S in deuterated DMSO and 10 µl of TOA-OH solution (20% in MeOH)
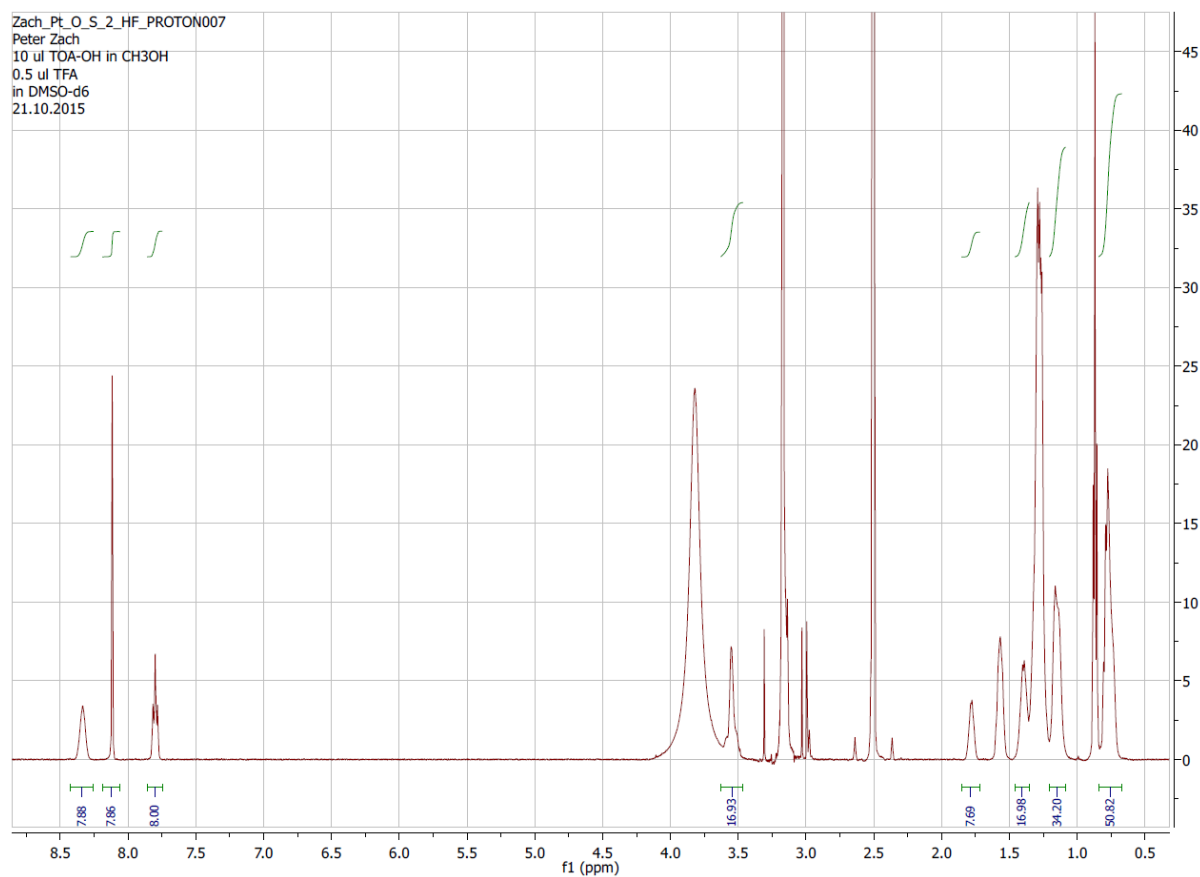
Figure S 5.18 NMR-Spectra (¹H) of Pt-O-S in deuterated DMSO and 10 µl of TOA-OH solution (20 % in MeOH) and 0.5 µl TFA
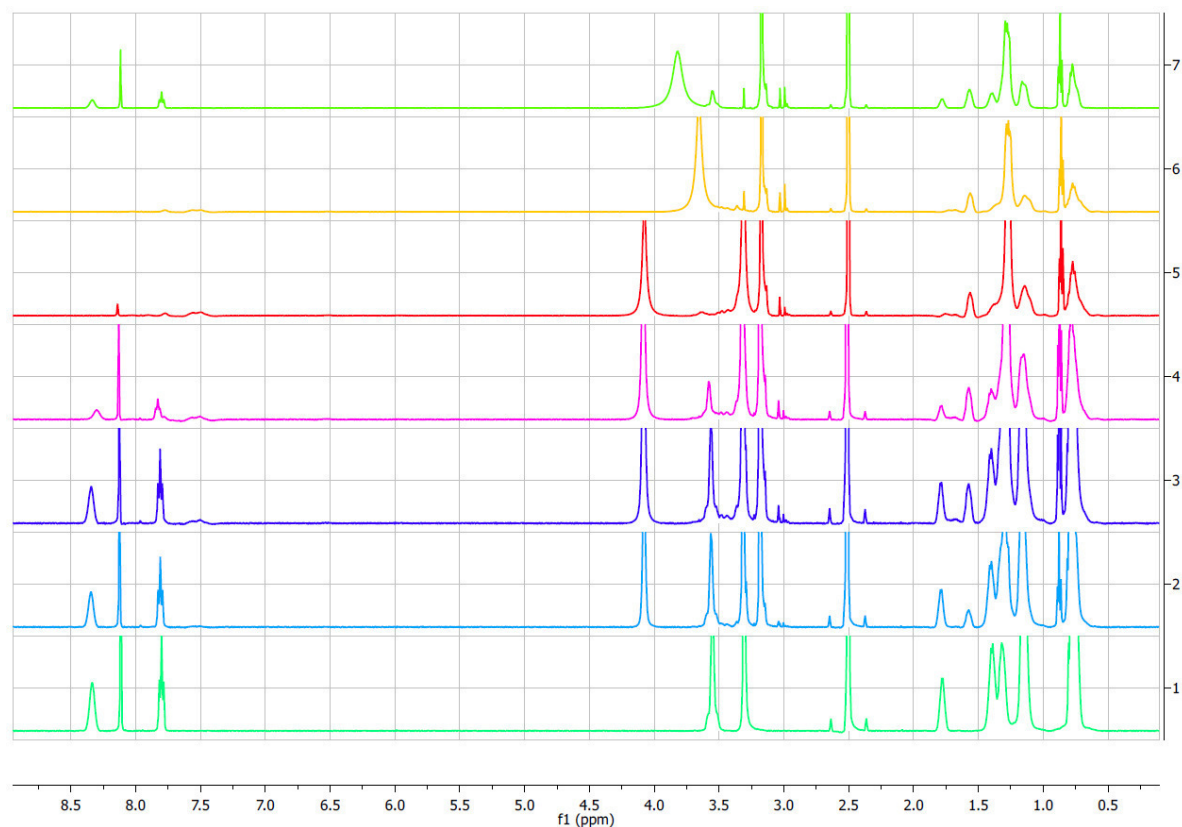
Figure S 5.19 ¹H NMR-spectra of Pt-O-S (1) in deuterated DMSO after addition of 2 µl TOA-OH each time (2,3,4,5,6), overall 10 µl and 0.5 µl TFA (7)

5.5.5 Photostability
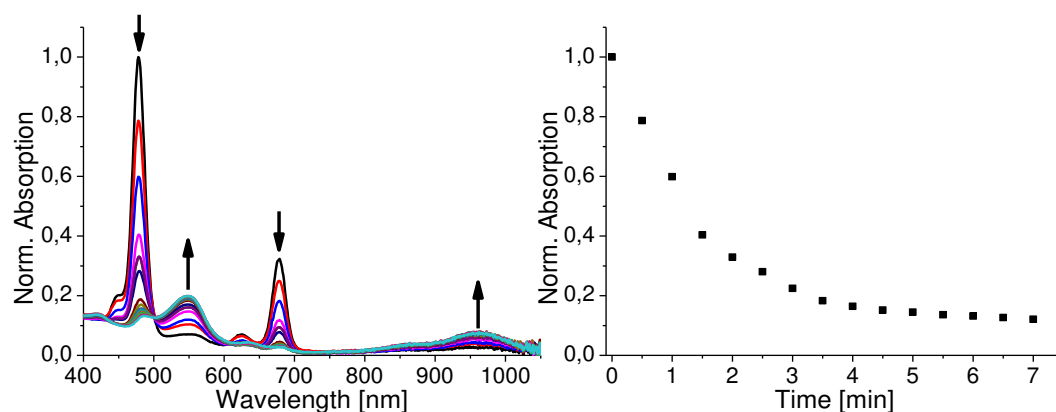
Figure S 5.20 Photodegradation curves for Zn-O-T complex in air saturated toluene solution at room temperature. Irradiation is performed with a blue LED array (λmax=458 nm; 10.79 V, 0.689 A, 7.4 W)
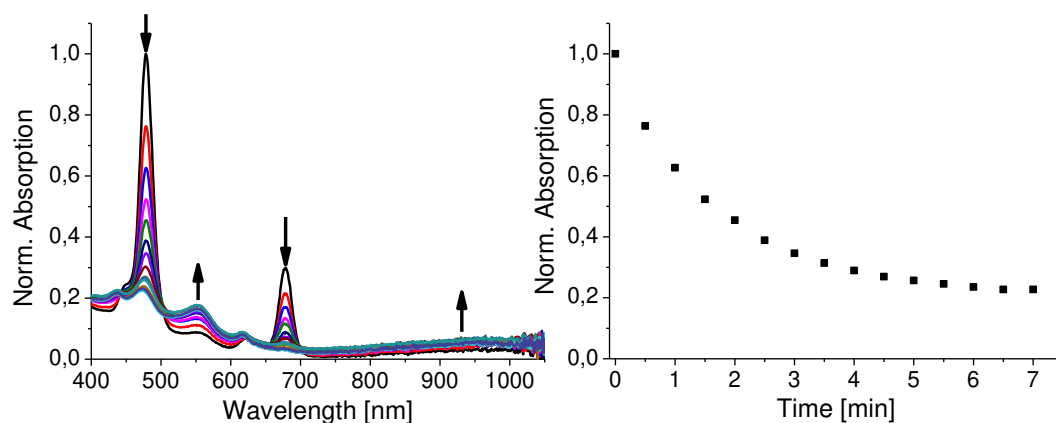
Figure S 5.21 Photodegradation curves for Zn-O-T complex in deoxygenated toluene solution at room temperature. Irradiation is performed with a blue LED array (λmax=458 nm; 10.79 V, 0.689 A, 7.4 W)
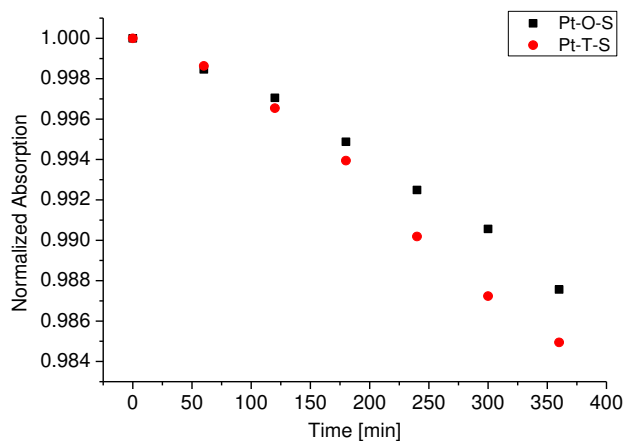
Figure S 5.22 Photo-degradation profiles for the platinum(II) tetra- and octa-sulfone in anoxic toluene at 25 °C upon irradiation with a high power 617 nm LED (28V, 550 mA, irradiance 350 mW cm^{-2})
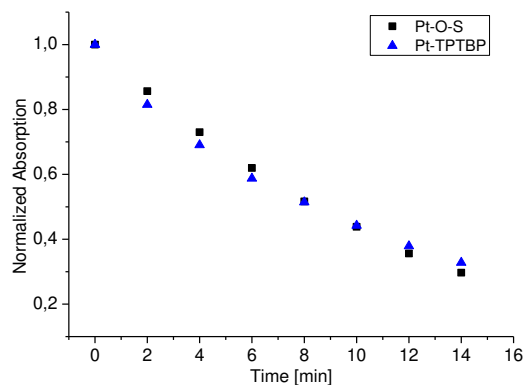
Figure S 5.23 Photo-degradation profiles for the Pt-O-S, Pt-TPBP in anoxic DMF at 25 °C upon irradiation with a high power 617 nm LED (28V, 550 mA, irradiance 350 mW cm⁻²)

5.5.6 Optical oxygen sensors
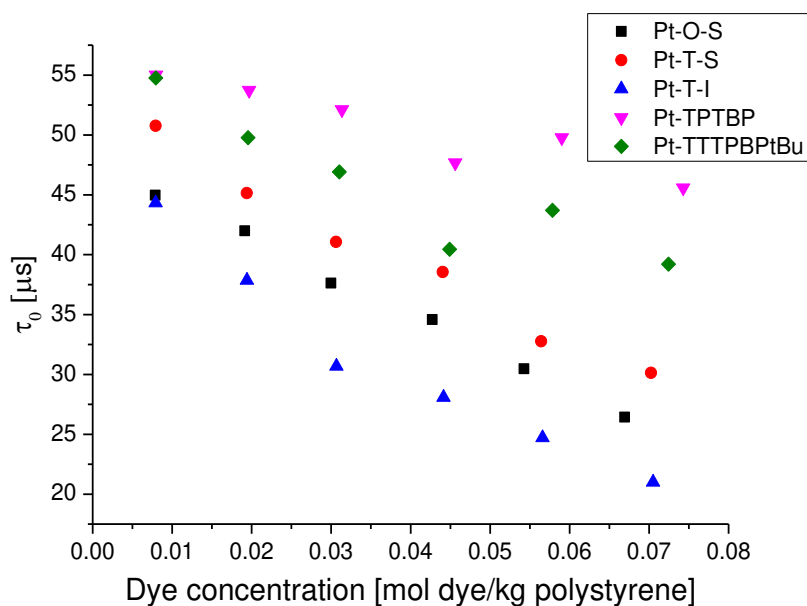
Figure S 5.24 Dependency of the lifetime of selected dyes to different concentrations in polystyrene under anoxic conditions (5 w% Na₂SO₃ solution with traces of CoCl₂), average decay times acquired with a phase fluorometer from PyroScience (624 nm LED, 20 % LED intensity, 10 ms integration time)

5.5.7 Application in Triplet-Triplet-Annihilation-Based Upconversion Systems
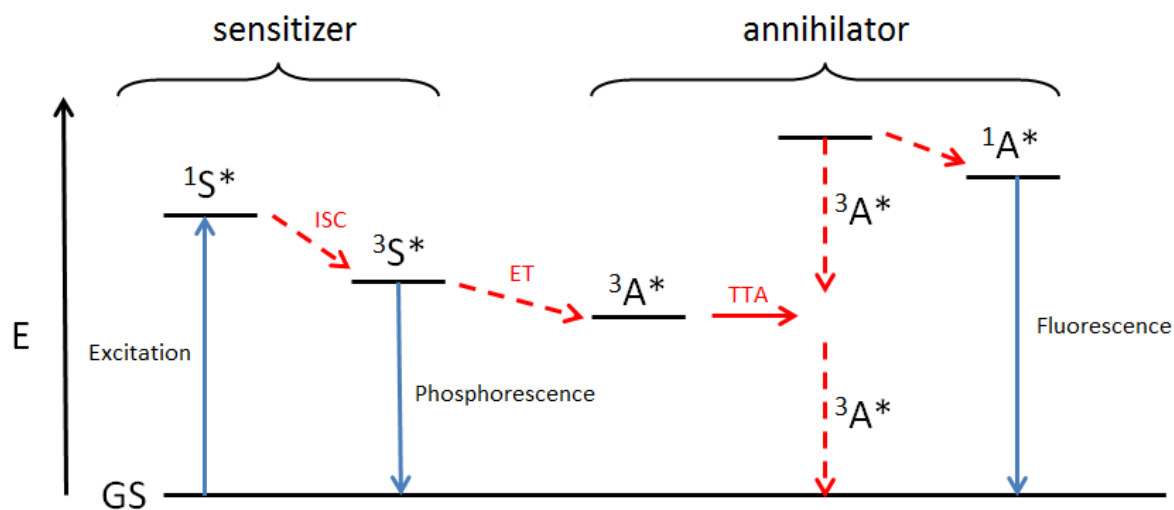
Scheme S.5.1 Triplet-Triplet-Annihilation based upconversion
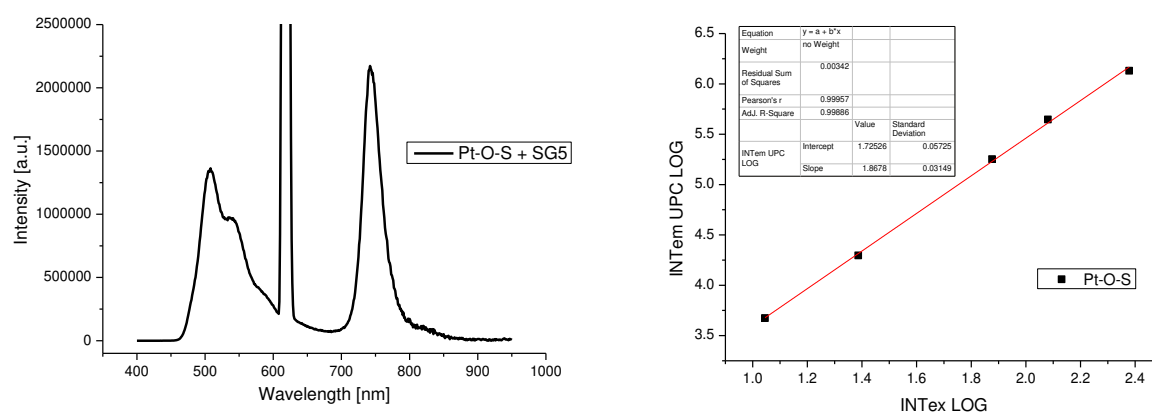
Figure S 5.25 Emission spectra of toluene solution of Pt-O-S (C = 1*10⁻⁴ M) with Solvent Green 5 (SG5) as annihilator (C = 5*10⁻⁴ M) excited with 450 W xenon-lamp at 621 nm and RT (left) and quadratic dependence of the light intensity (right)
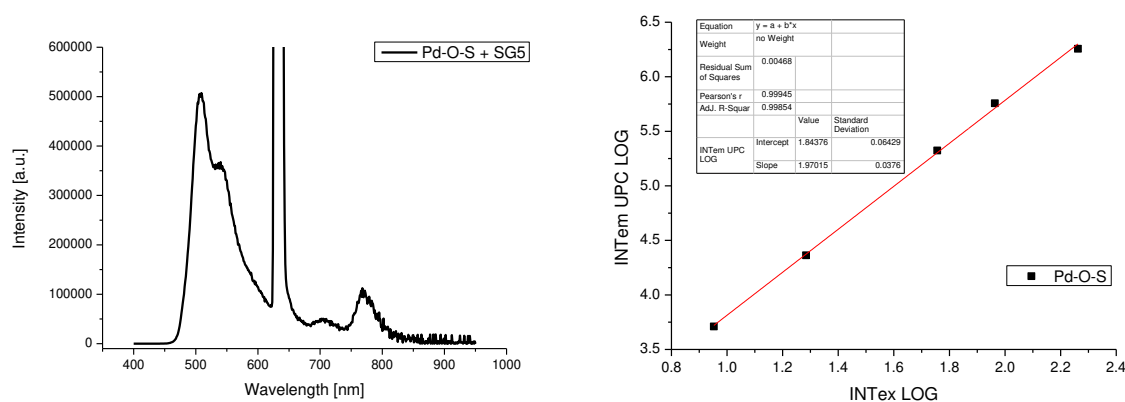
Figure S 5.26 Emission spectra of toluene solution of Pd-O-S (C = 1*10⁻⁴ M) with Solvent Green 5 (SG5) as annihilator (C = 5*10⁻⁴ M) excited with 450 W xenon-lamp at 636 nm and RT (left) and quadratic dependence of the light intensity (right)
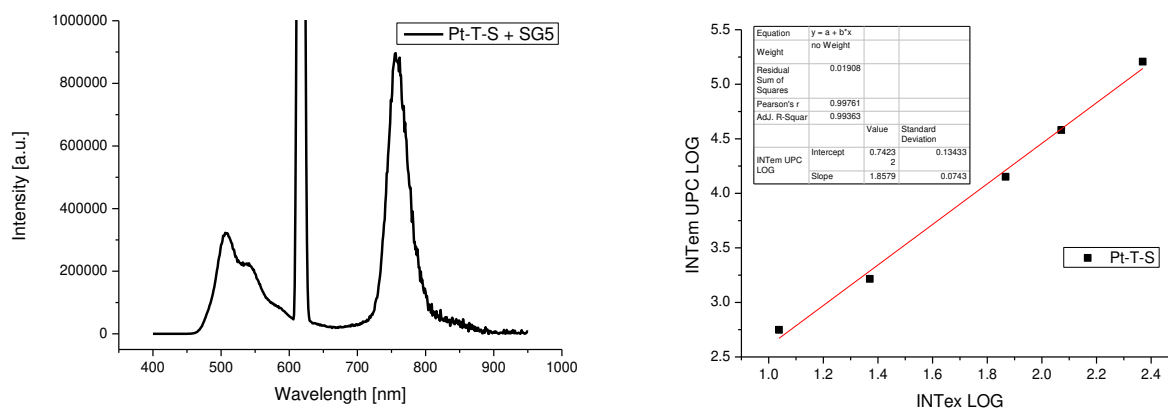
Figure S 5.27 Emission spectra of toluene solution of Pt-T-S (C = 1*10⁻⁴ M) with Solvent Green 5 (SG5) as annihilator (C = 5*10⁻⁴ M) excited with 450 W xenon-lamp at 619 nm and RT (left) and quadratic dependence of the light intensity (right)
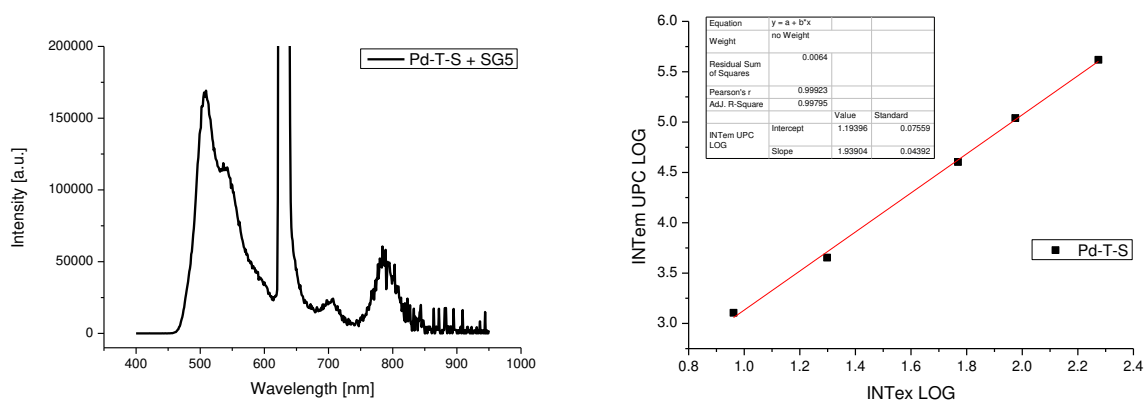
Figure S 5.28 Emission spectra of toluene solution of Pd-T-S (C = 1*10⁻⁴ M) with Solvent Green 5 (SG5) as annihilator (C = 5*10⁻⁴ M) excited with 450 W xenon-lamp at 633 nm and RT (left) and quadratic dependence of the light intensity (right)
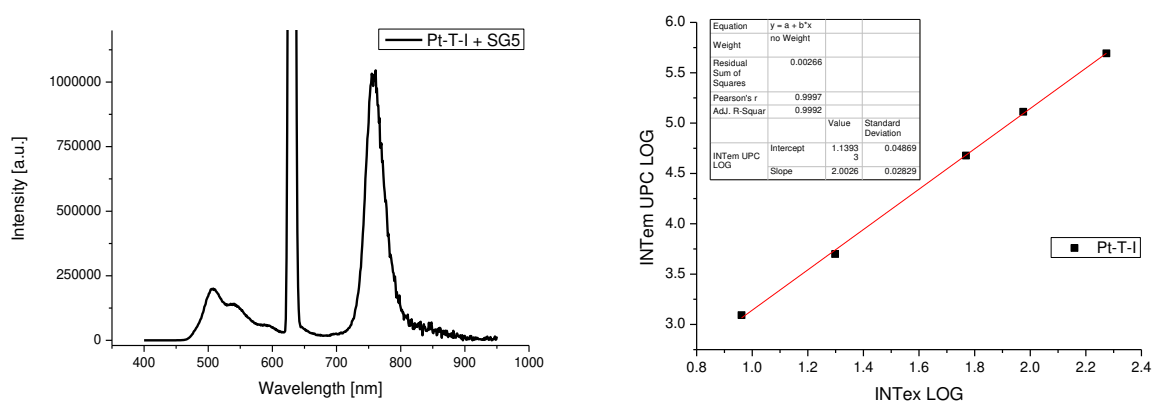
Figure S 5.29 Emission spectra of toluene solution of Pt-T-I (C = 1*10⁻⁴ M) with Solvent Green 5 (SG5) as annihilator (C = 5*10⁻⁴ M) excited with 450 W xenon-lamp at 633 nm and RT (left) and quadratic dependence of the light intensity (right)
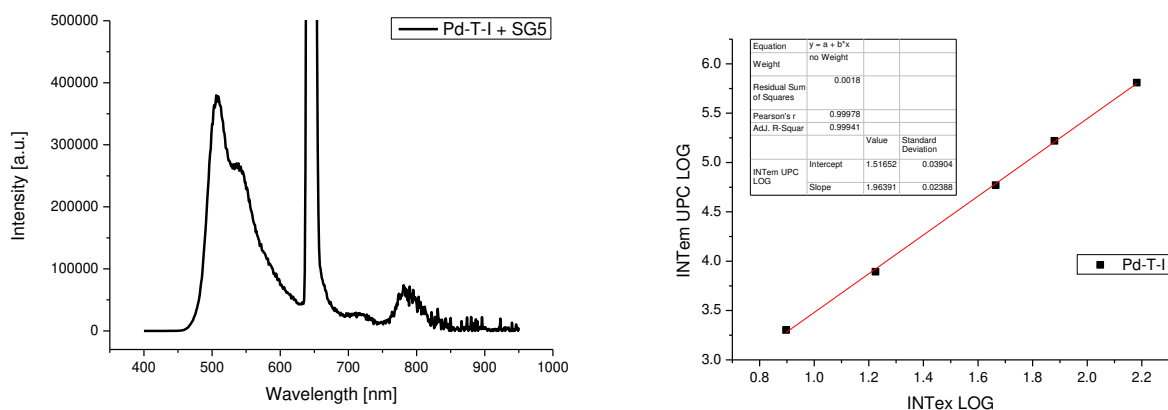
Figure S 5.30 Emission spectra of toluene solution of Pd-T-I (C = 1*10^{-4} M) with Solvent Green 5 (SG5) as annihilator (C = 5*10^{-4} M) excited with 450 W xenon-lamp at 648 nm and RT (left) and quadratic dependence of the light intensity (right)
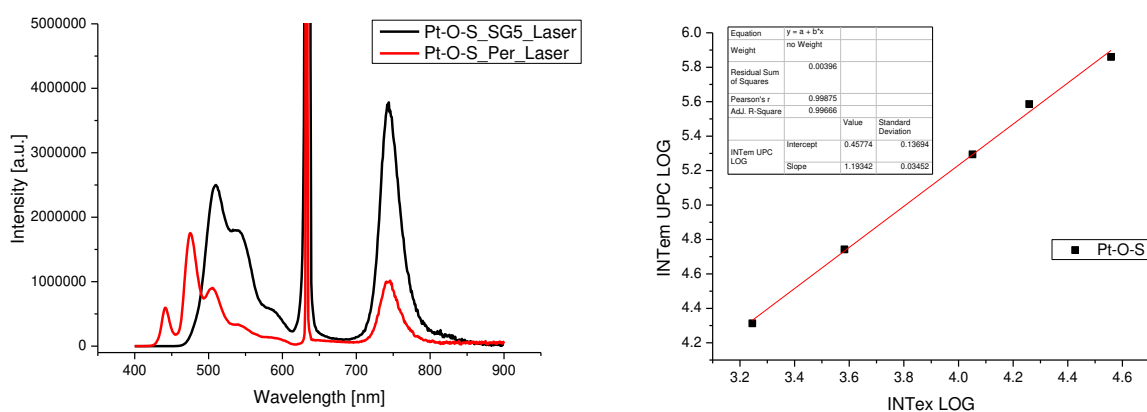
Figure S 5.31 Emission spectra of toluene solution of Pt-O-S (C = 5*10^{-5} M) with Solvent Green 5 (SG5) and Perylene (Per) as annihilators (C = 2.5*10^{-4} M) excited with 635 nm laser diode and RT (left) and linear dependence of the light intensity (right)
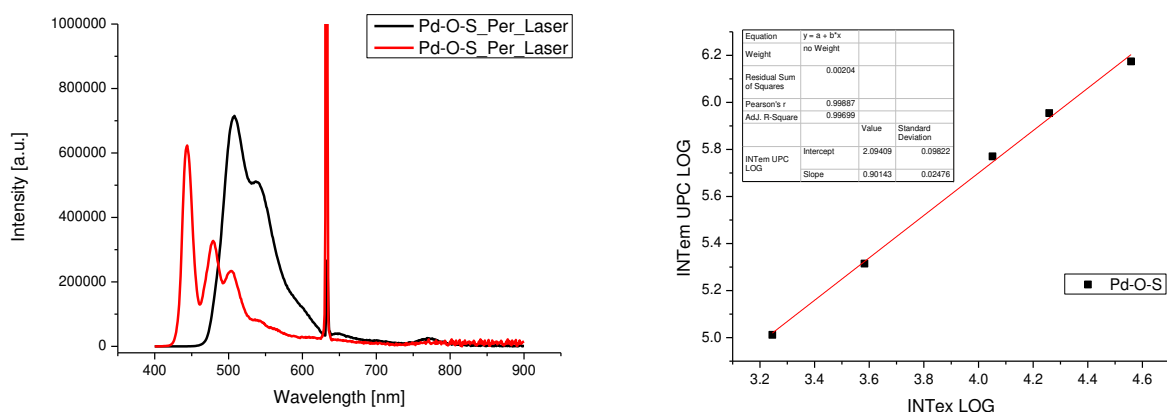
Figure S 5.32 Emission spectra of toluene solution of Pd-O-S (C = 5*10^{-5} M) with Solvent Green 5 (SG5) and Perylene (Per) as annihilators (C = 2.5*10^{-4} M) excited with 635 nm laser diode and RT (left) and linear dependence of the light intensity (right)
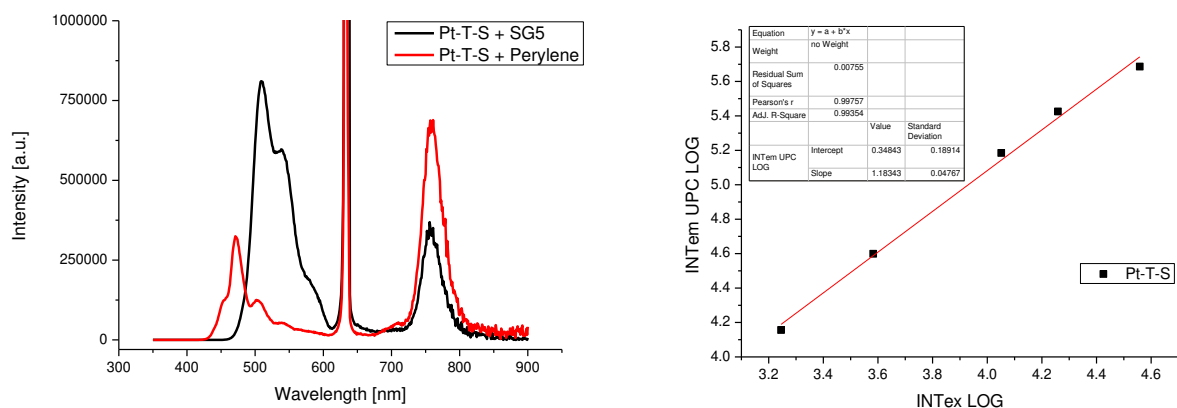
Figure S 5.33 Emission spectra of toluene solution of Pt-T-S (C = 5*10⁻⁵ M) with Solvent Green 5 (SG5) and Perylene (Per) as annihilators (C = 2.5*10⁻⁴ M) excited with 635 nm laser diode and RT (left) and linear dependence of the light intensity (right)
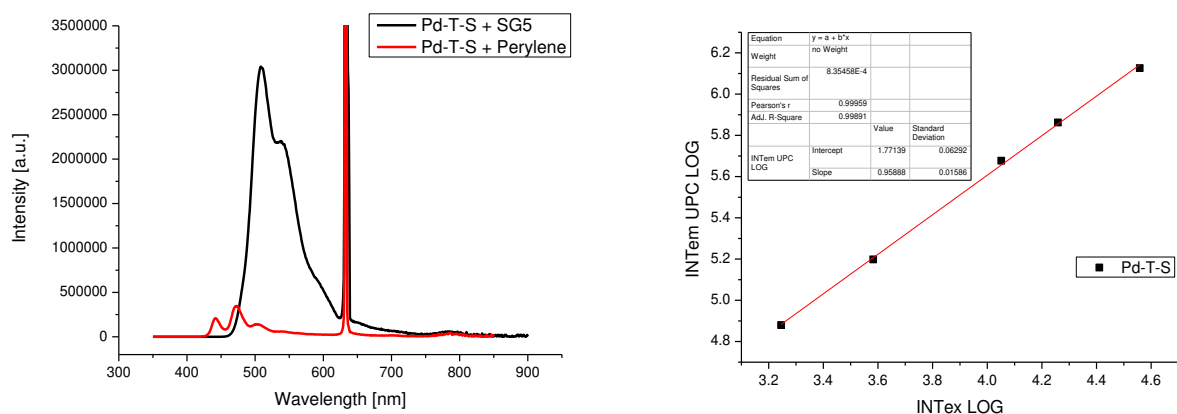
Figure S 5.34 Emission spectra of toluene solution of Pd-T-S (C = 5*10⁻⁵ M) with Solvent Green 5 (SG5) and Perylene (Per) as annihilators (C = 2.5*10⁻⁴ M) excited with 635 nm laser diode and RT (left) and linear dependence of the light intensity (right)
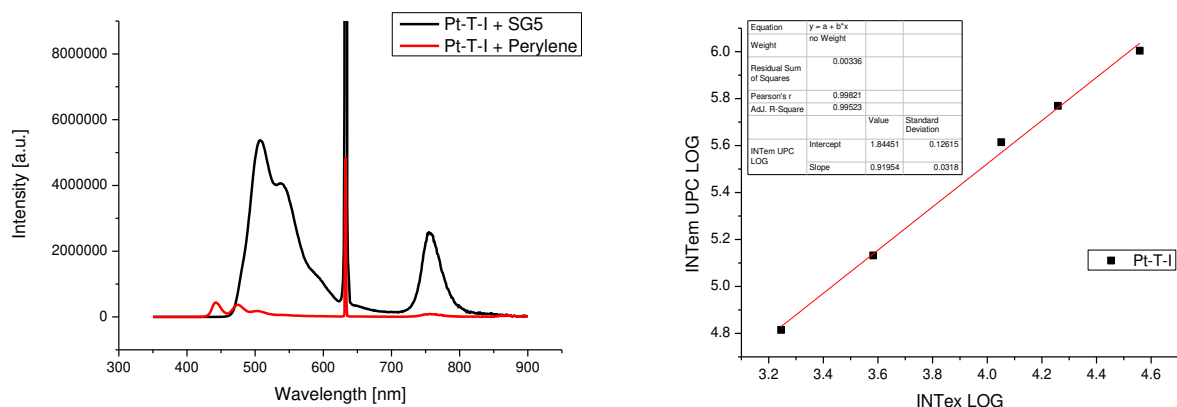
Figure S 5.35 Emission spectra of toluene solution of Pt-T-I (C = 5*10⁻⁵ M) with Solvent Green 5 (SG5) and Perylene (Per) as annihilators (C = 2.5*10⁻⁴ M) excited with 635 nm laser diode and RT (left) and linear dependence of the light intensity (right)
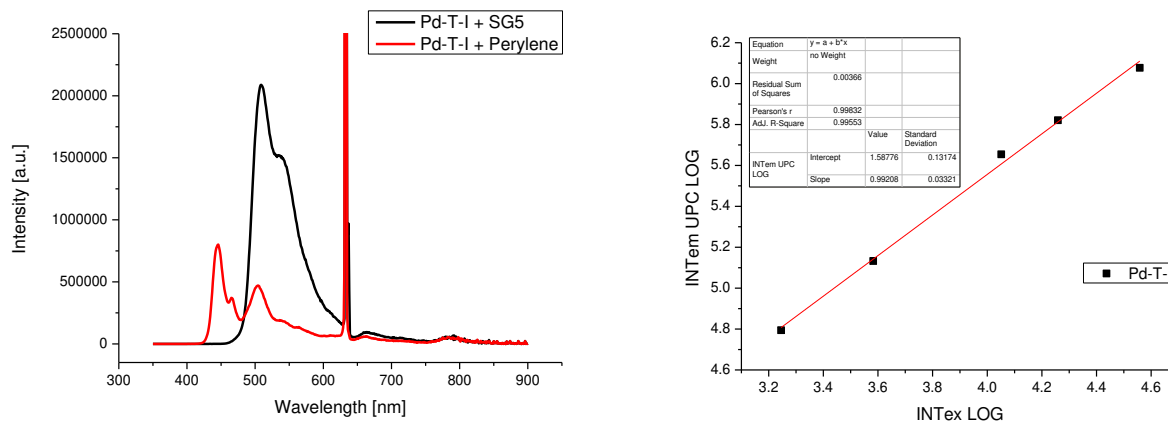
Figure S 5.36 Emission spectra of toluene solution of Pd-T-I (C = 5*10^{-5} M) with Solvent Green 5 (SG5) and Perylene (Per) as annihilators (C = 2.5*10^{-4} M) excited with 635 nm laser diode and RT (left) and linear dependence of the light intensity (right)

Table S 5.2 Upconversion quantum yields (Φ_{UPC}) of platinum(II) and palladium(II) benzoporpyhyrin sensitizers with SG5 as the annihilator in anoxic toluene solutions excited by a xenon lamp (450 W) and 635 nm laser-diode the relative light intensity of the excitation source at different wavelengths.

dye	λ_{Exc} [nm]	light intensity [mW*cm^{-2}]	relative light intensity	Φ_{UPC} at resp. λ_{Exc} [nm]	normalized Φ	QY laser
Pt-O-S	621	4.60	0.95	0.023	0.026	0.060
Pd-O-S	636	3.44	0.73	0.010	0.012	0.20
Pt-T-S	619	4.52	0.93	0.007	0.0083	0.098
Pd-T-S	633	3.55	0.75	0.005	0.0097	0.14
Pt-T-I	633	3.55	0.75	0.003	0.0057	0.098
Pd-T-I	648	2.81	0.60	0.008	0.023	0.095
PtTPTBP	614	4.19	1.00	0.017	0.018	0.091
PdTPTBP	628	4.06	0.85	0.016	0.022	0.071

* slope = 1 (saturation values, light density 682.73 mW/cm^2

Note that in case of the xenon lamp (450 W), the intensity of the excitation source reduces in the red part of the spectrum and is not identical for different sensitizers. Therefore, we normalized the Φ to the intensity of the xenon lamp at 614 nm assuming the quadratic dependence of the upconverted fluorescence on the intensity of the excitation light.

Perylene (Per)   Solvent Green 5 (SG5)   Lumogen Orange (LOr)
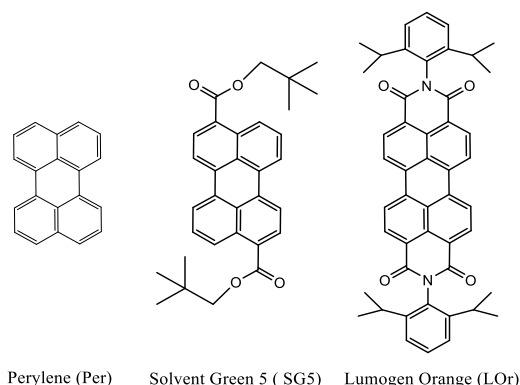
Figure S 5.37 Different annihilators used for TTA-upconverison

91

5.5.8 ^{1}H NMR and ^{13}C NMR Characterization

^{1}H NMR (300 MHz, Chloroform-d) δ 5.88 (t, 2H), 3.34 (d, J = 7.3 Hz, 2H), 3.05 (t, 2H), 2.70 − 2.49 (m, 2H), 2.31 − 2.09 (m, 2H), 1.75 − 1.58 (m, 1H), 1.36 − 1.02 (m, 8H), 0.93 − 0.76 (m, 6H).
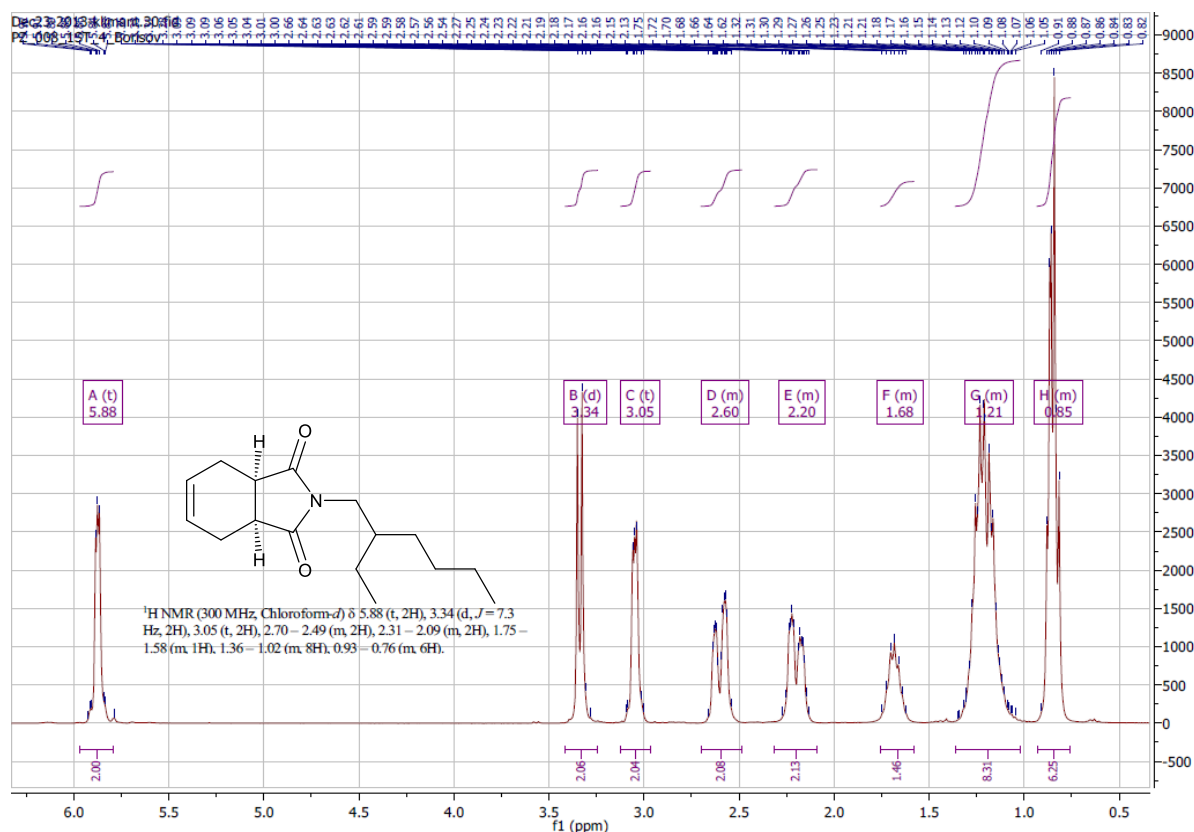
Figure S 5.38 NMR-Spectra (^{1}H) of (3aR,7aS)-2-(2-ethylhexyl)-3a,4,7,7a-tetrahydro-1H-isoindole-1,3(2H)-dione

^{1}H NMR (300 MHz, Chloroform-d) δ 7.48 − 7.40 (m, 2H), 7.39 − 7.28 (m, 3H), 4.27 − 4.17 (m, 1H), 3.58 (q, J = 4.2 Hz, 1H), 3.47 − 3.35 (m, 2H), 3.22 − 3.04 (m, 1H), 2.91 (td, J = 8.1, 4.1 Hz, 1H), 2.70 − 2.41 (m, 2H), 2.41 − 2.27 (m, 1H), 2.25 − 2.11 (m, 1H), 1.84 − 1.71 (m, 1H), 1.35 − 1.19 (m, 8H), 0.95 − 0.83 (m, 6H).
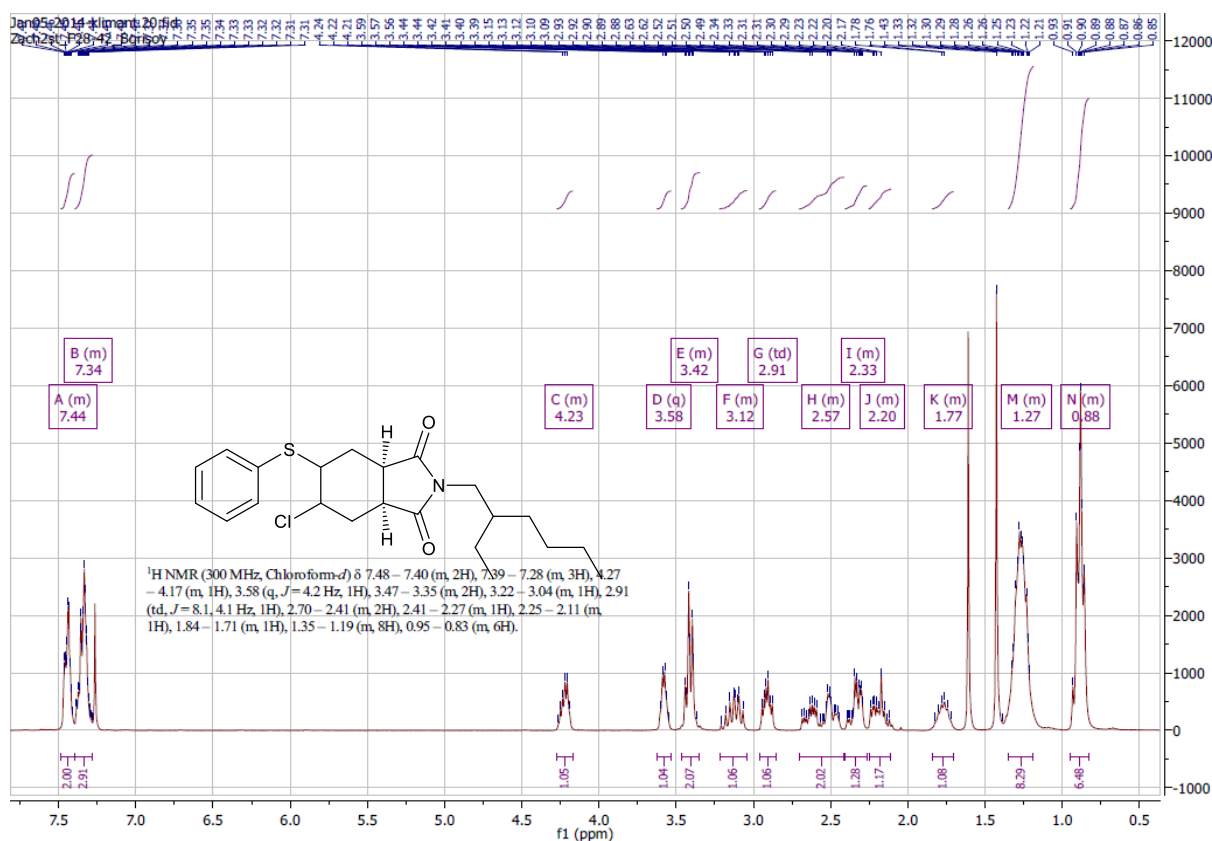
Figure S 5.39 NMR-Spectra (^{1}H) of (3aS,7aR)-5-chloro-2-(2-ethylhexyl)-6-(phenylthio)hexahydro-1H-isoindole- 1,3(2H)-dione
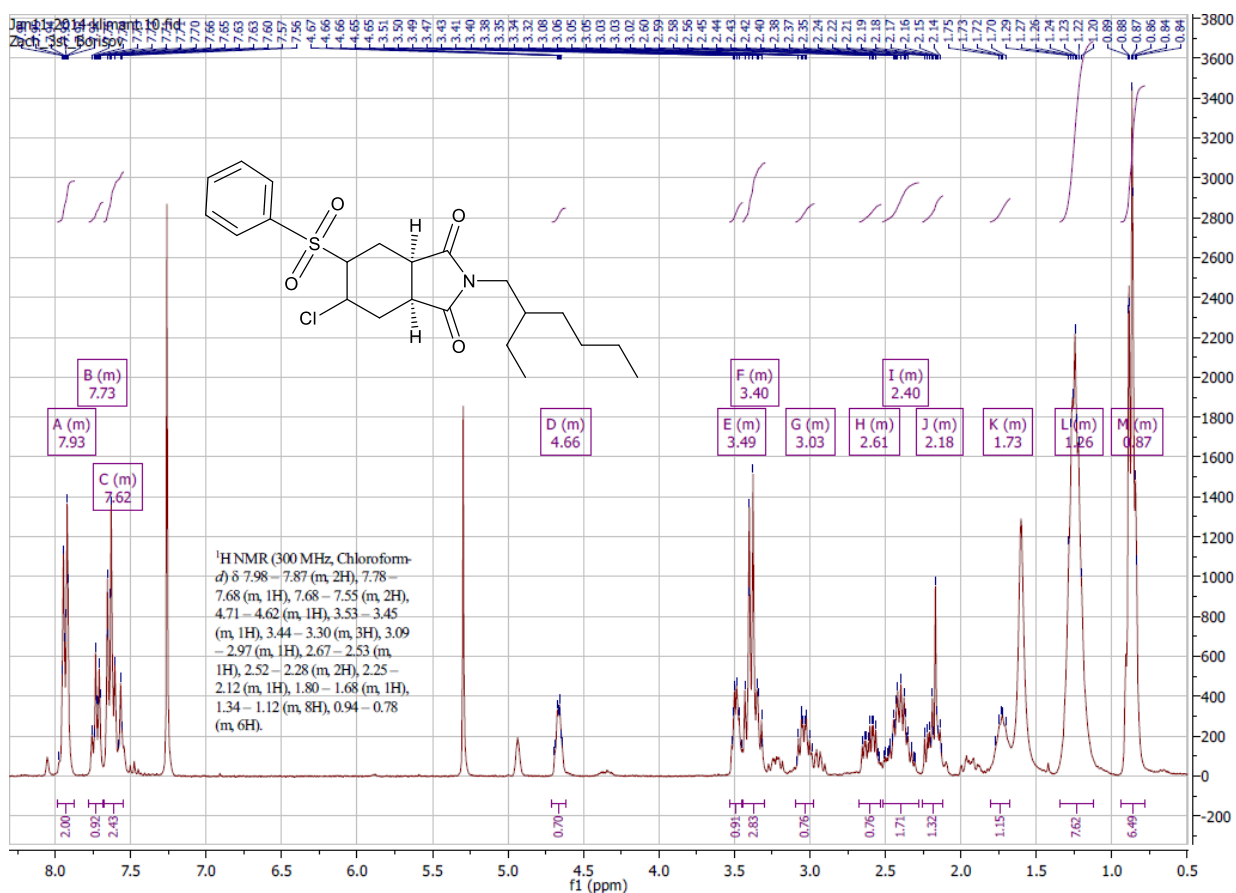
Figure S 5.40 NMR-Spectra (¹H) of (3aS,7aR)-5-chloro-2-(2-ethylhexyl)-6-(phenylsulfonyl)hexahydro-1H-isoindole- 1,3(2H)-dione
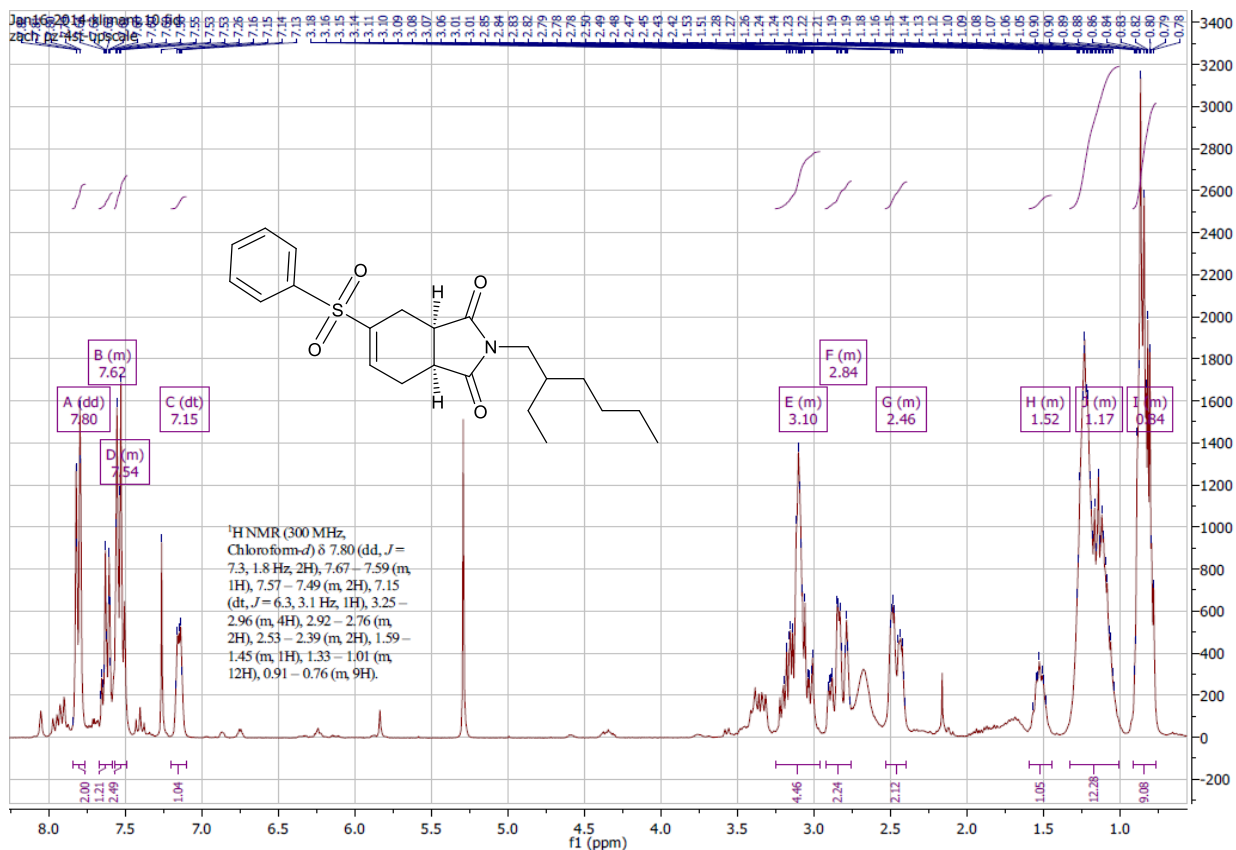
Figure S 5.41 NMR-Spectra (¹H) of (3aR,7aS)-2-(2-ethylhexyl)-5-(phenylsulfonyl)-3a,4,7,7a-tetrahydro-1H-isoindole- 1,3(2H)-dione
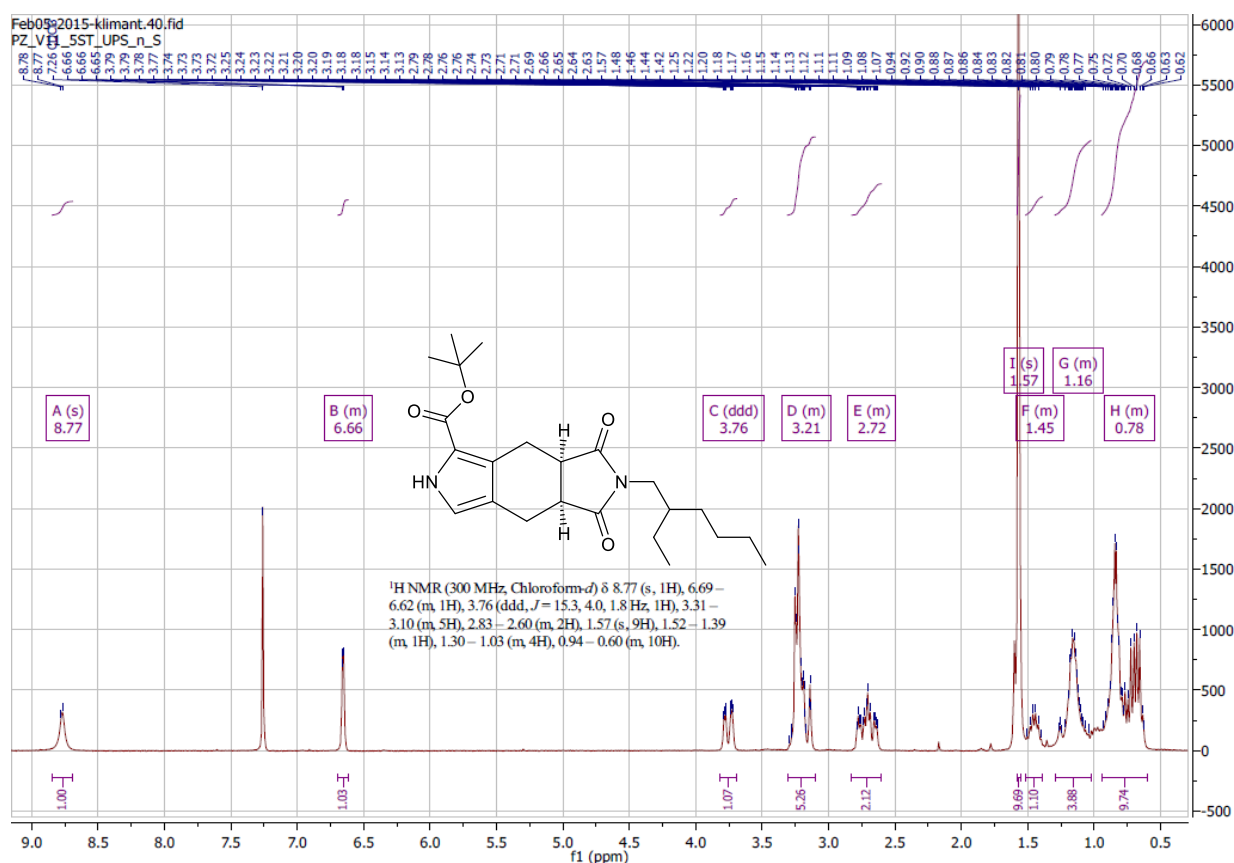
Figure S 5.42 NMR-Spectra (¹H) of tert-butyl 6-(2-ethylhexyl)5,7-dioxo-2,4,4a,5,6,7,7a,8-octahydropyrrolo[3,4-f]isoindole-1-carboxylate
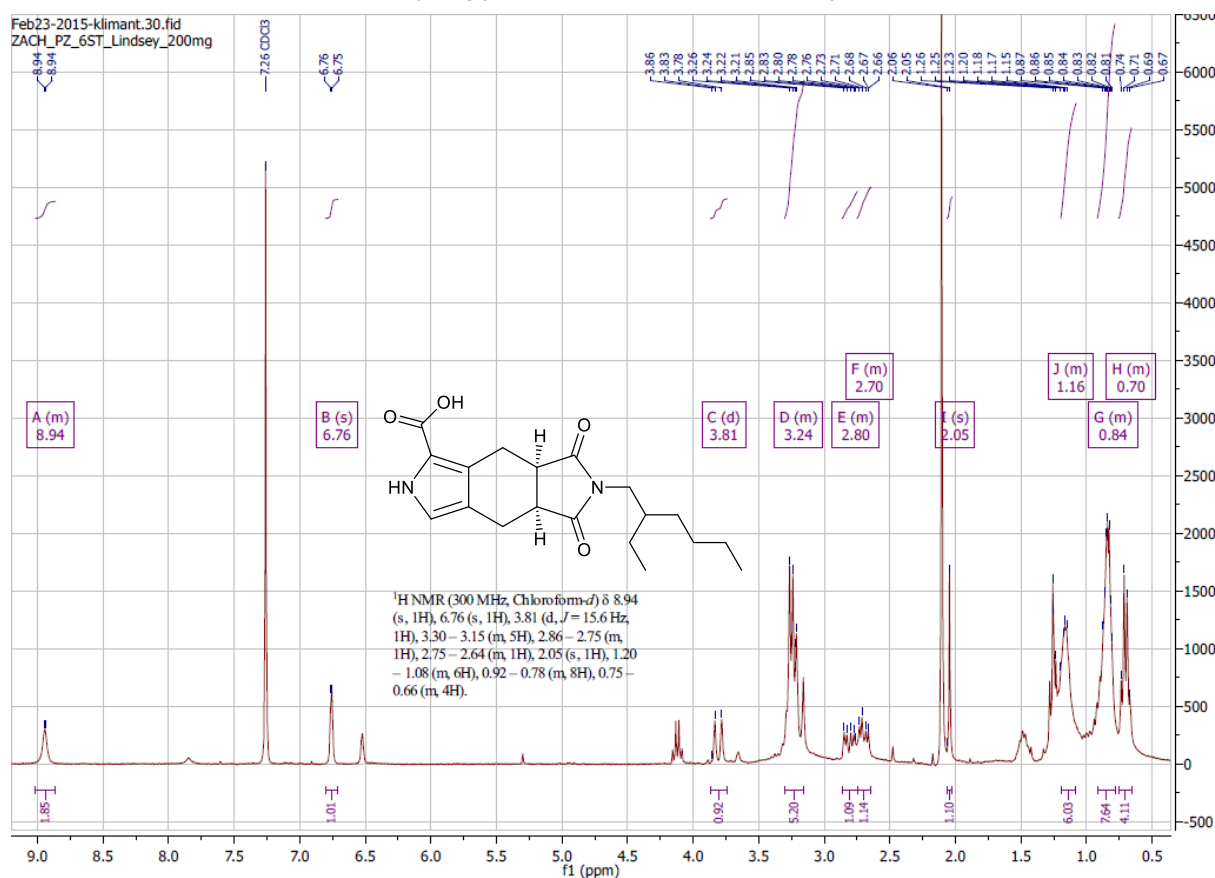
Figure S 5.43 NMR-Spectra (¹H) of 6-(2-ethylhexyl)5,7-dioxo-2,4,4a,5,6,7,7a,8-octahydropyrrolo[3,4-f]isoindole-1-carboxylic acid
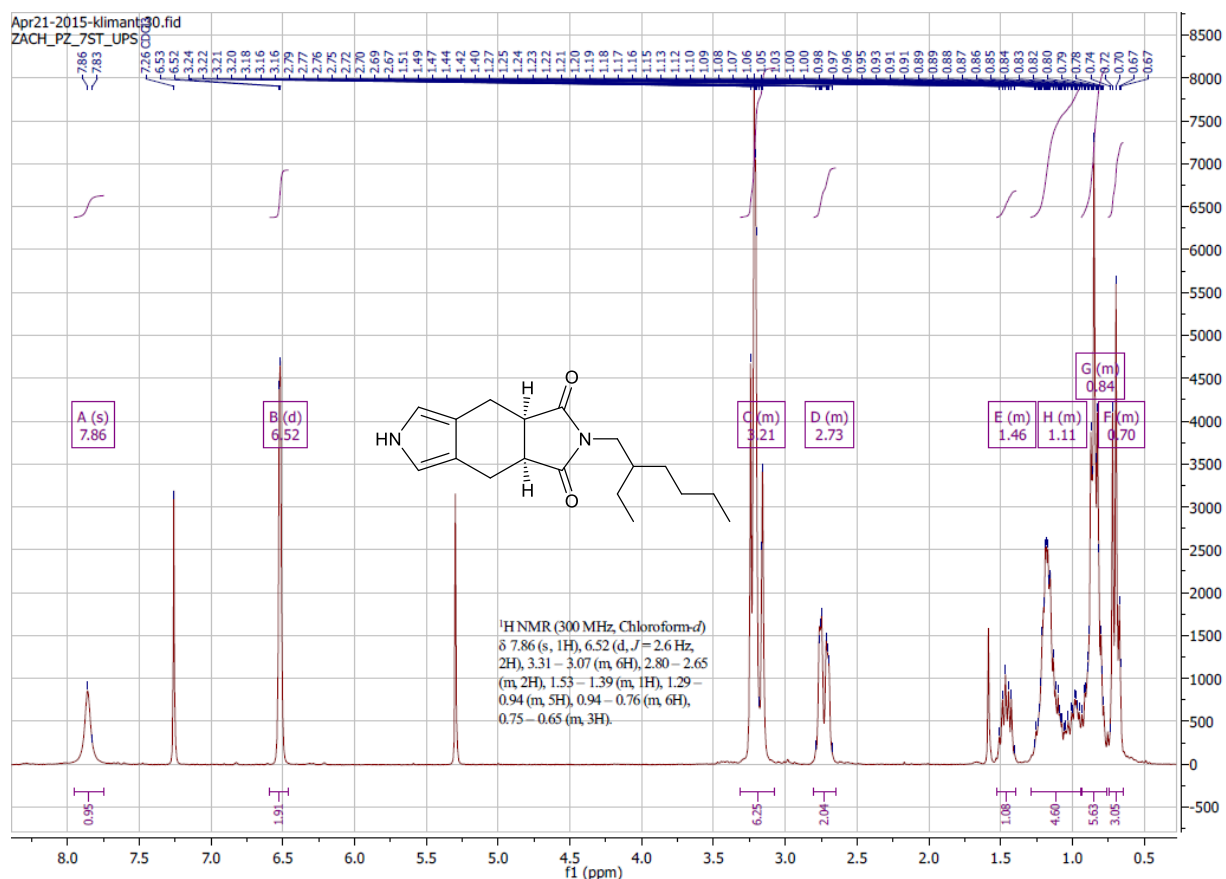
Figure S 5.44 NMR-Spectra (^{1}H) of 2-(2-ethylhexyl)3a,4,8,8a-tetrahydropyrrolo[3,4-f]isoindole-1,3(2H,6H)-dione
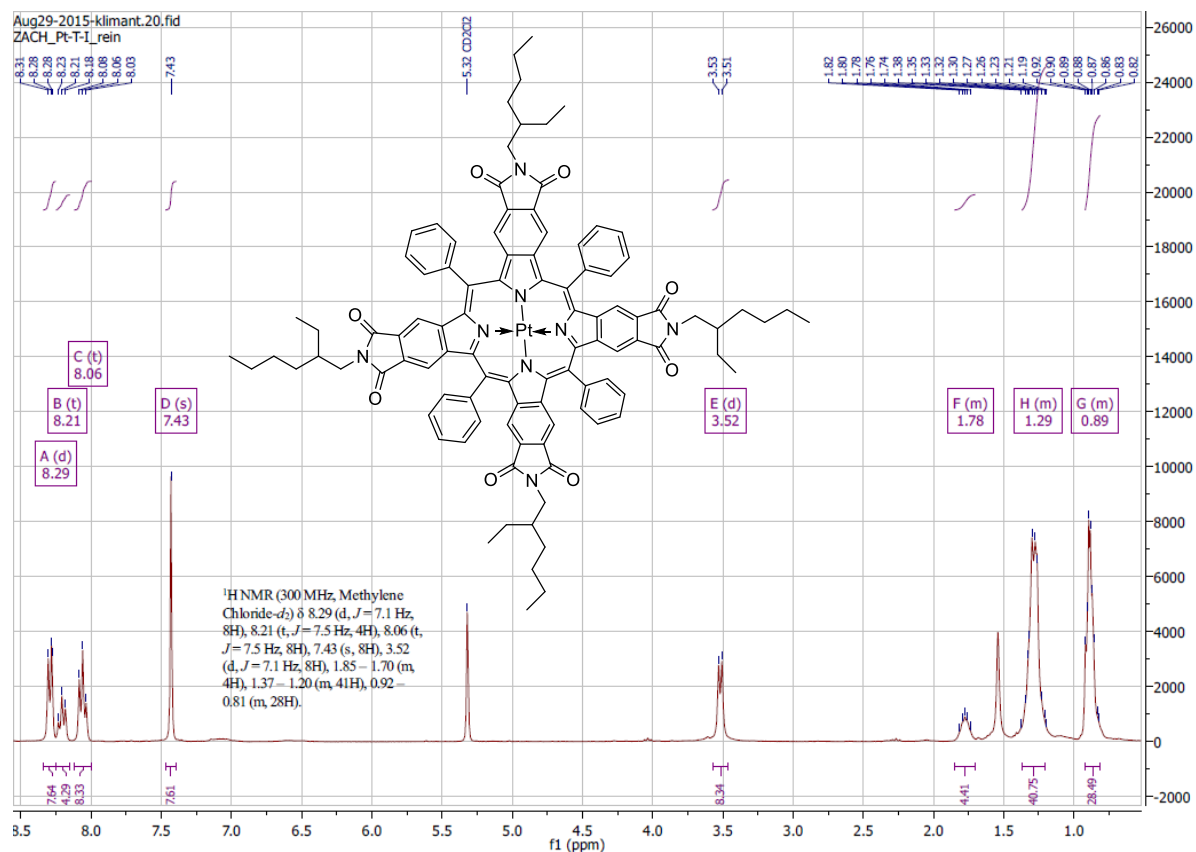
Figure S 5.45 NMR-Spectra (^{1}H) of Pt(II) meso-tetraphenyltetrabenzo-1-(2-ethylhexyl)pyrrolidine-2,5-dione-porphyrin (Pt-T-I)
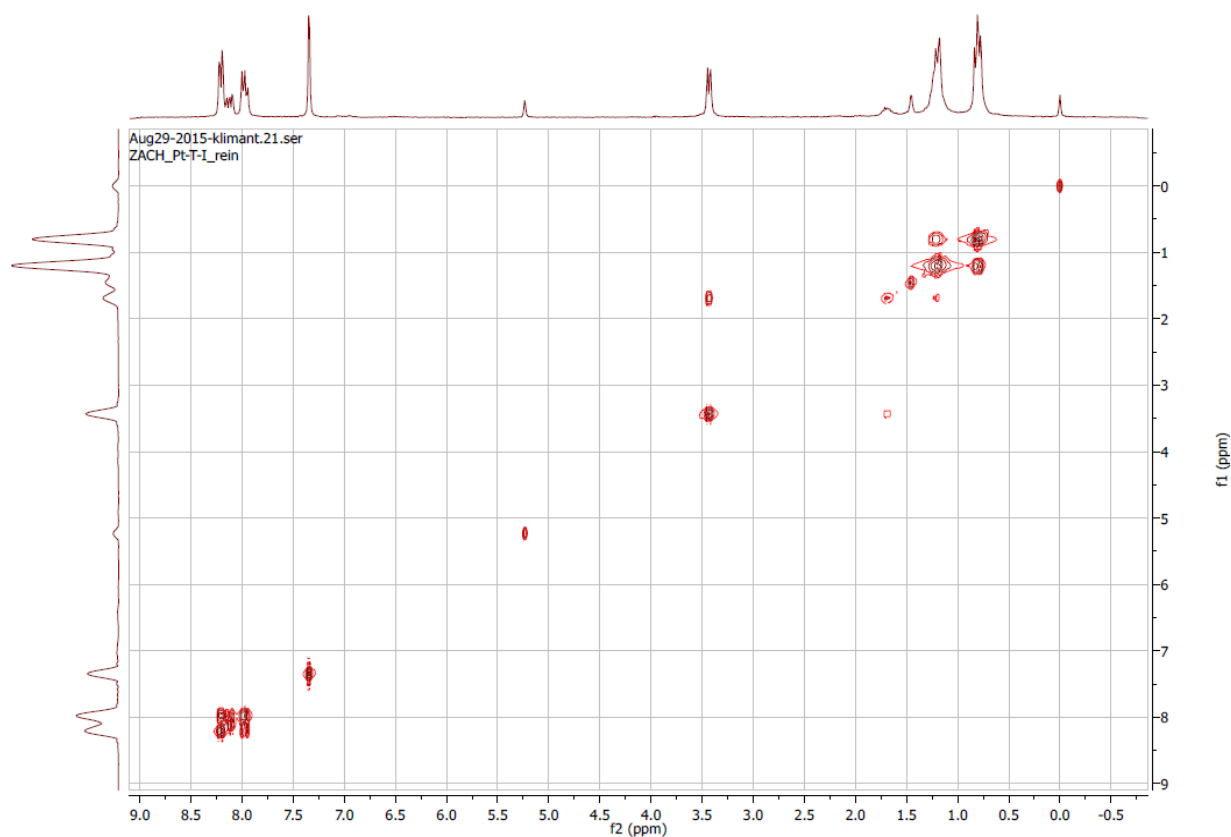
Figure S 5.46 NMR-Spectra (H-H-COSY) of Pt(II) meso-tetraphenyltetrabenzo-1-(2-ethylhexyl)pyrrolidine-2,5-dione-porphyrin (Pt-T-I)

^{13}C NMR (76 MHz, CD₂Cl2) δ 168.62, 141.39, 140.45, 137.62, 134.06, 131.20, 130.70, 129.49, 121.57, 120.01, 54.00, 42.54, 39.05, 31.19, 29.22, 24.48, 23.54, 14.40, 10.79.
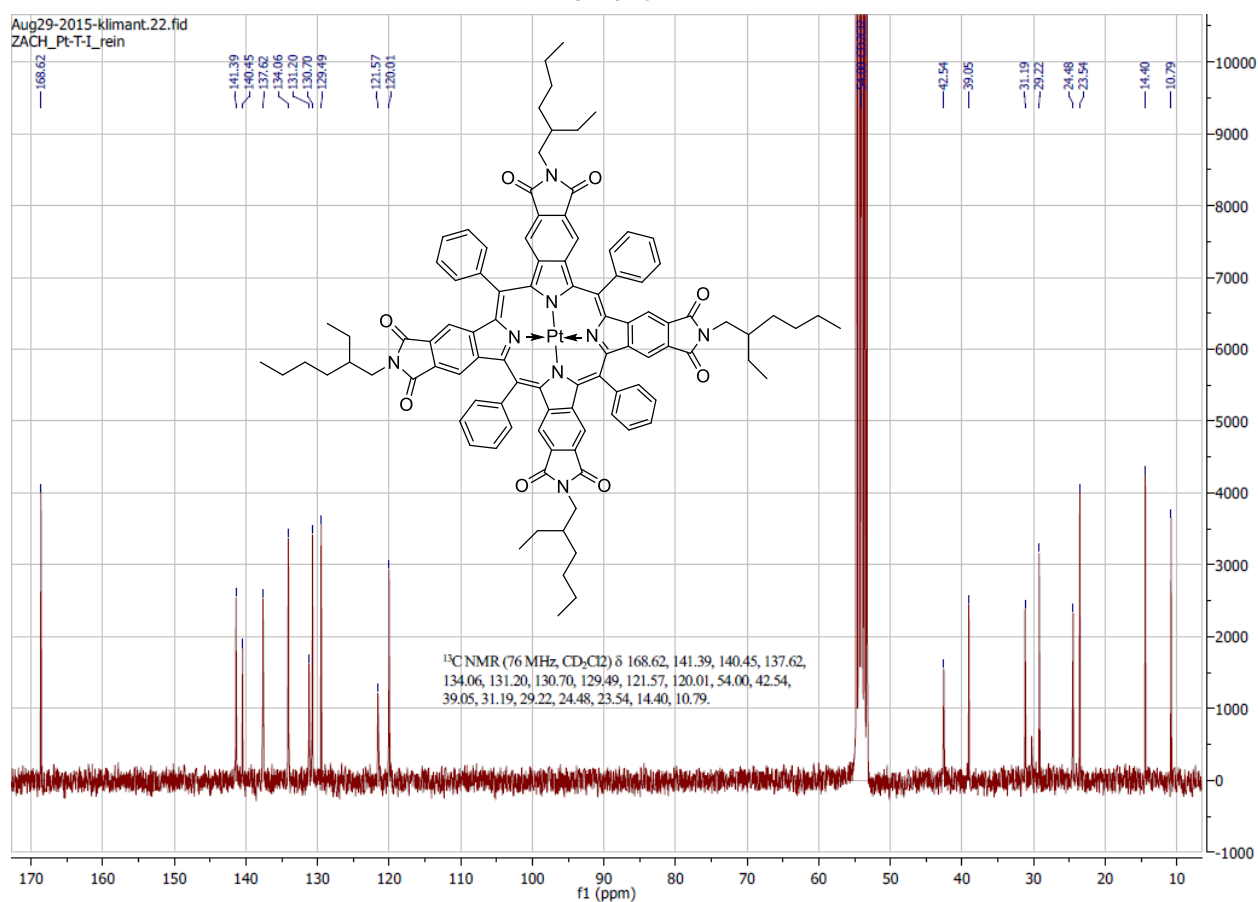
Figure S 5.47 NMR-Spectra (^{13}C) of Pt(II) meso-tetraphenyltetrabenzo-1-(2-ethylhexyl)pyrrolidine-2,5-dione-porphyrin (Pt-T-I)
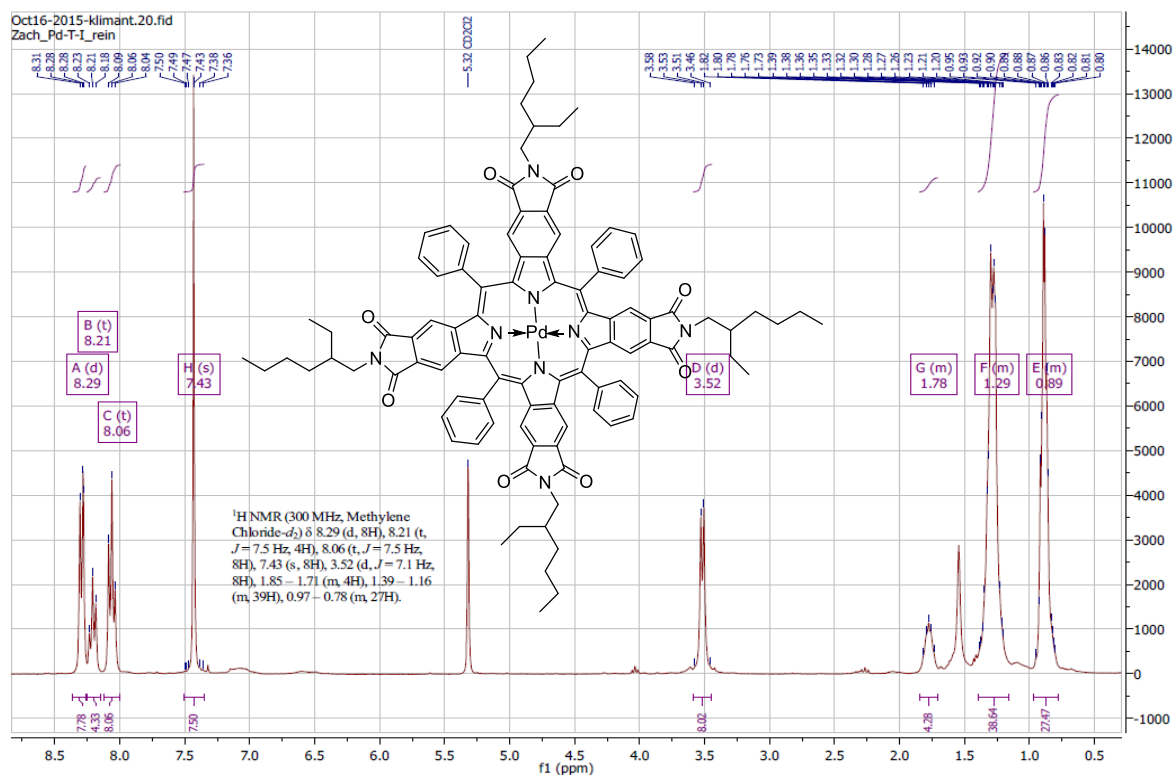
Figure S 5.48 NMR-Spectra (¹H) of Pd(II) meso-tetraphenyltetrabenzo-1-(2-ethylhexyl)pyrrolidine-2,5-dione-porphyrin (Pd-T-I)
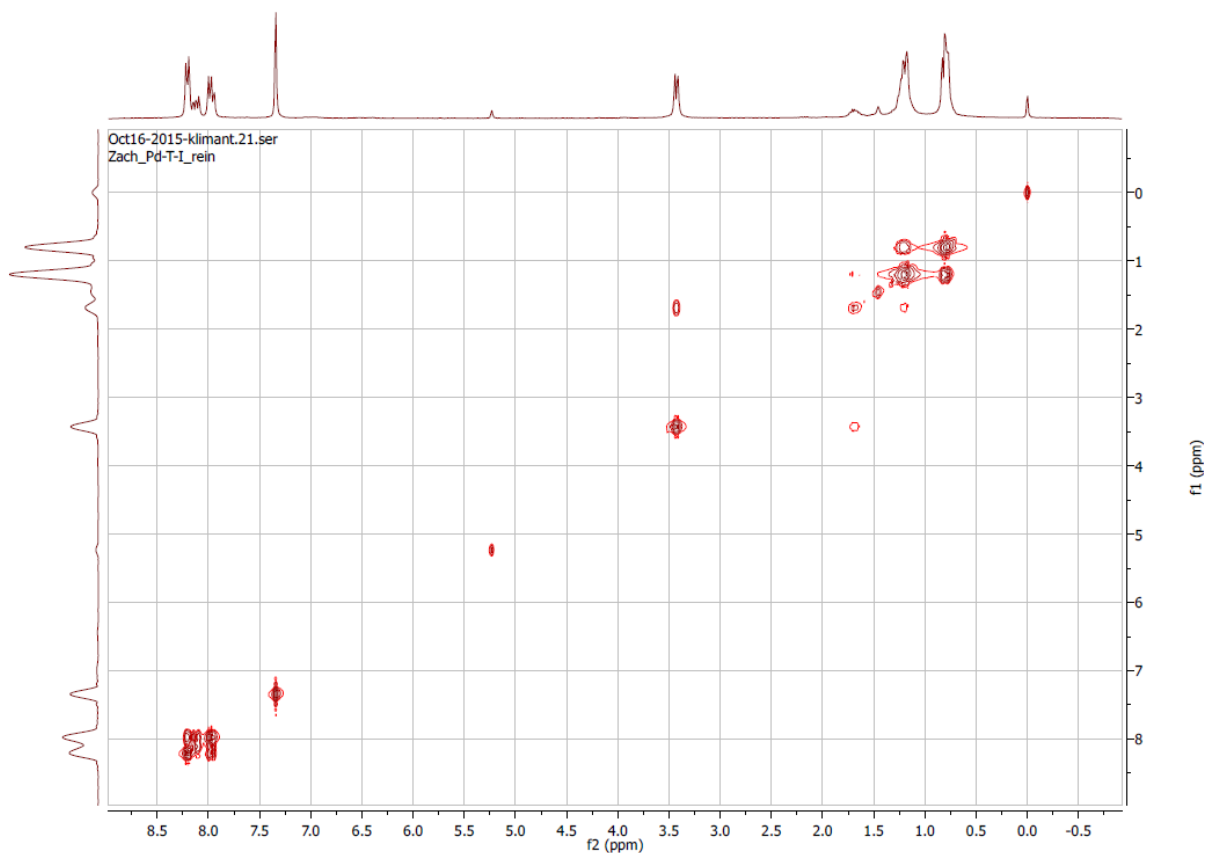
Figure S 5.49 NMR-Spectra (H-H-COSY) of Pd(II) meso-tetraphenyltetrabenzo-1-(2-ethylhexyl)pyrrolidine-2,5-dione-porphyrin (Pd-T-I)
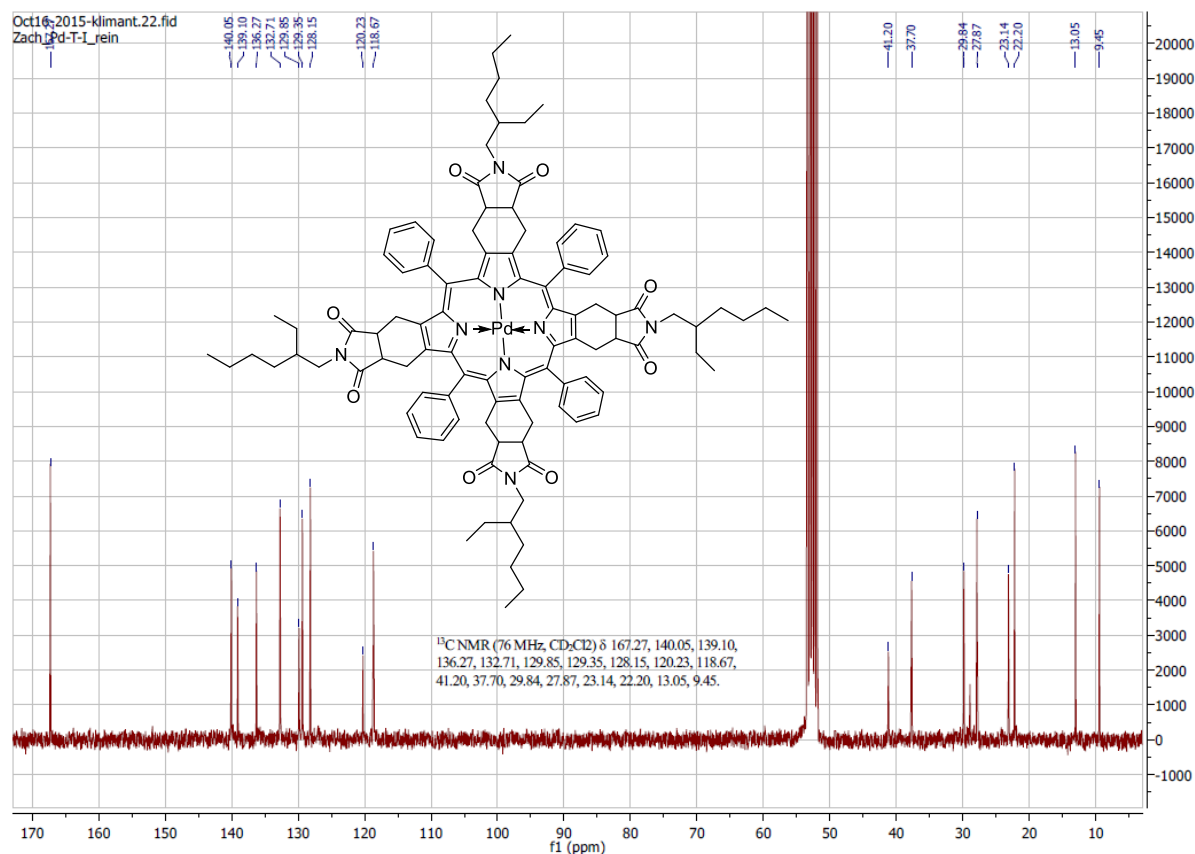
Figure S 5.50 NMR-Spectra (¹³C) of Pd(II) meso-tetraphenyltetrabenzo-1-(2-ethylhexyl)pyrrolidine-2,5-dione-porphyrin (Pd-T-I)
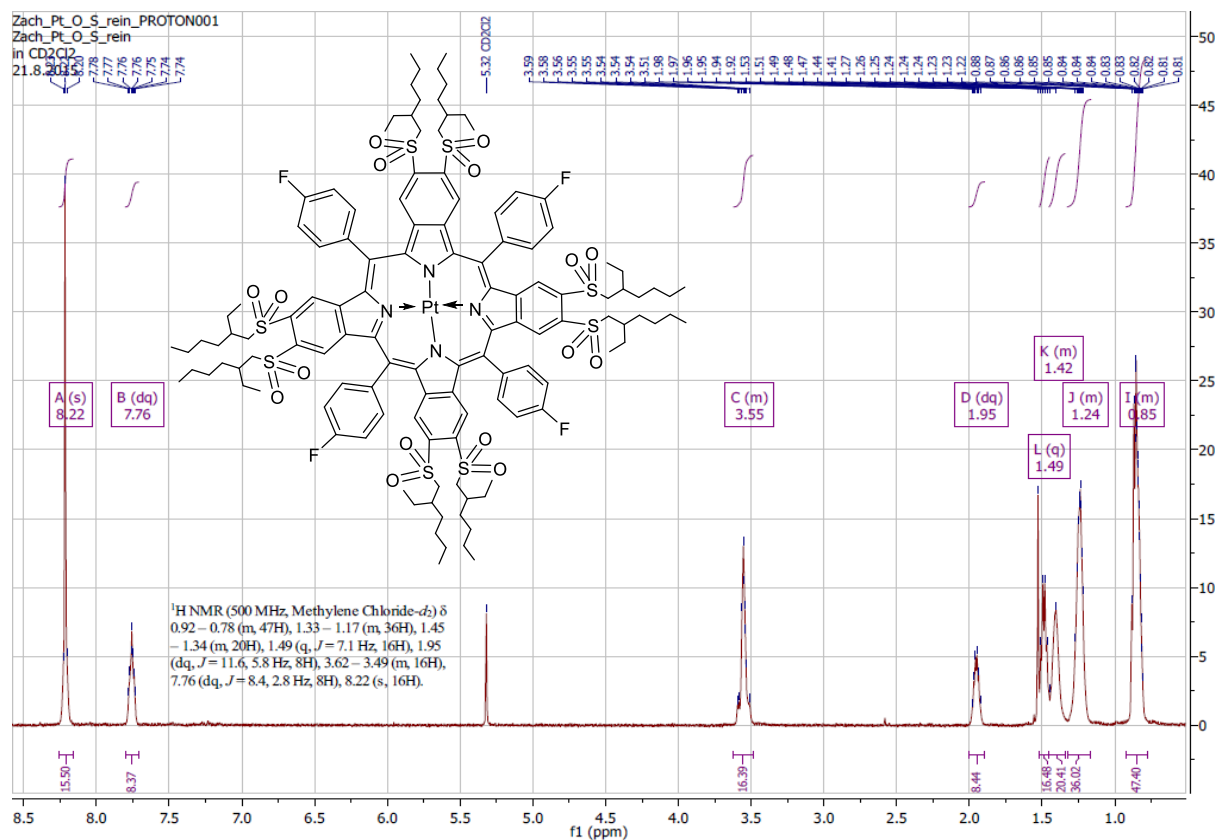
Figure S 5.51 NMR-Spectra (¹H) of Pt(II) meso-tetra(4-fluorophenyl)tetra(4,5-bis((2-ethylhexyl)sulfonyl)benzo-porphyrin (Pt-O-S)
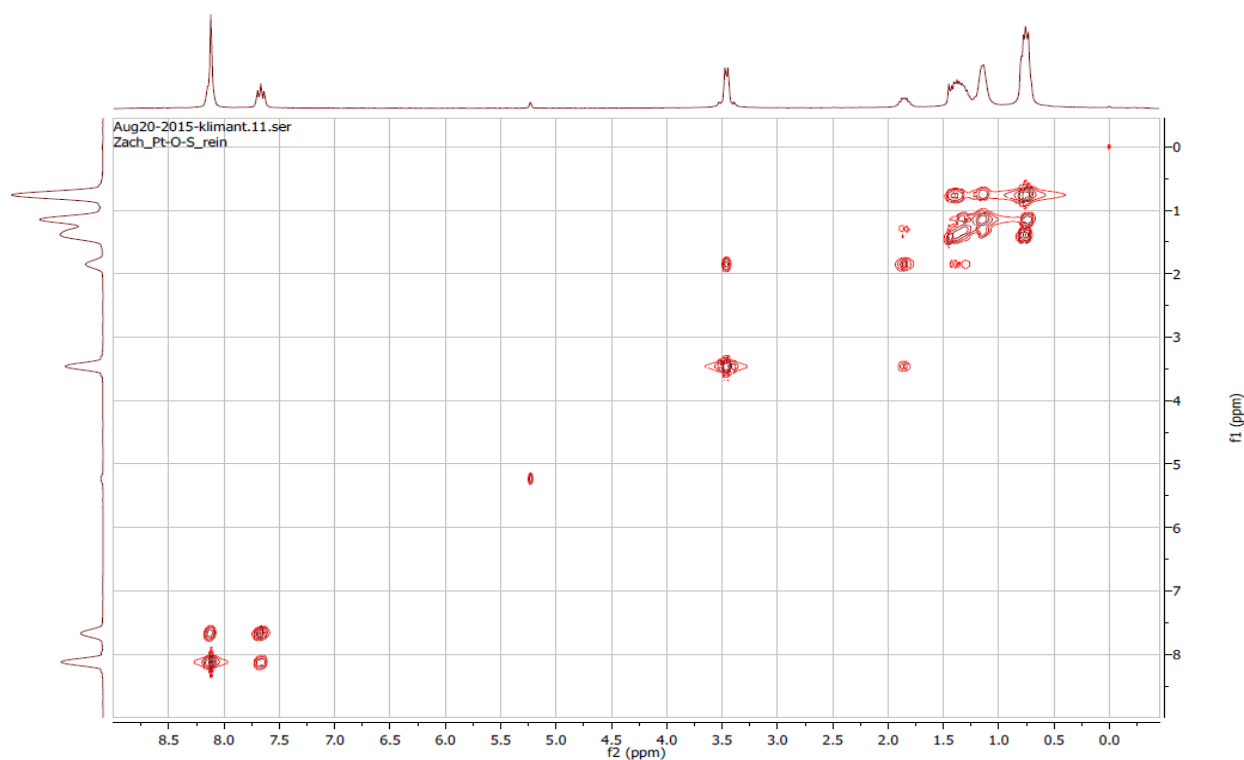
Figure S 5.52 NMR-Spectra (H-H-COSY) of Pt(II) meso-tetra(4-fluorophenyl)tetra(4,5-bis((2-ethylhexyl)sulfonyl)benzo-porphyrin (Pt-O-S)
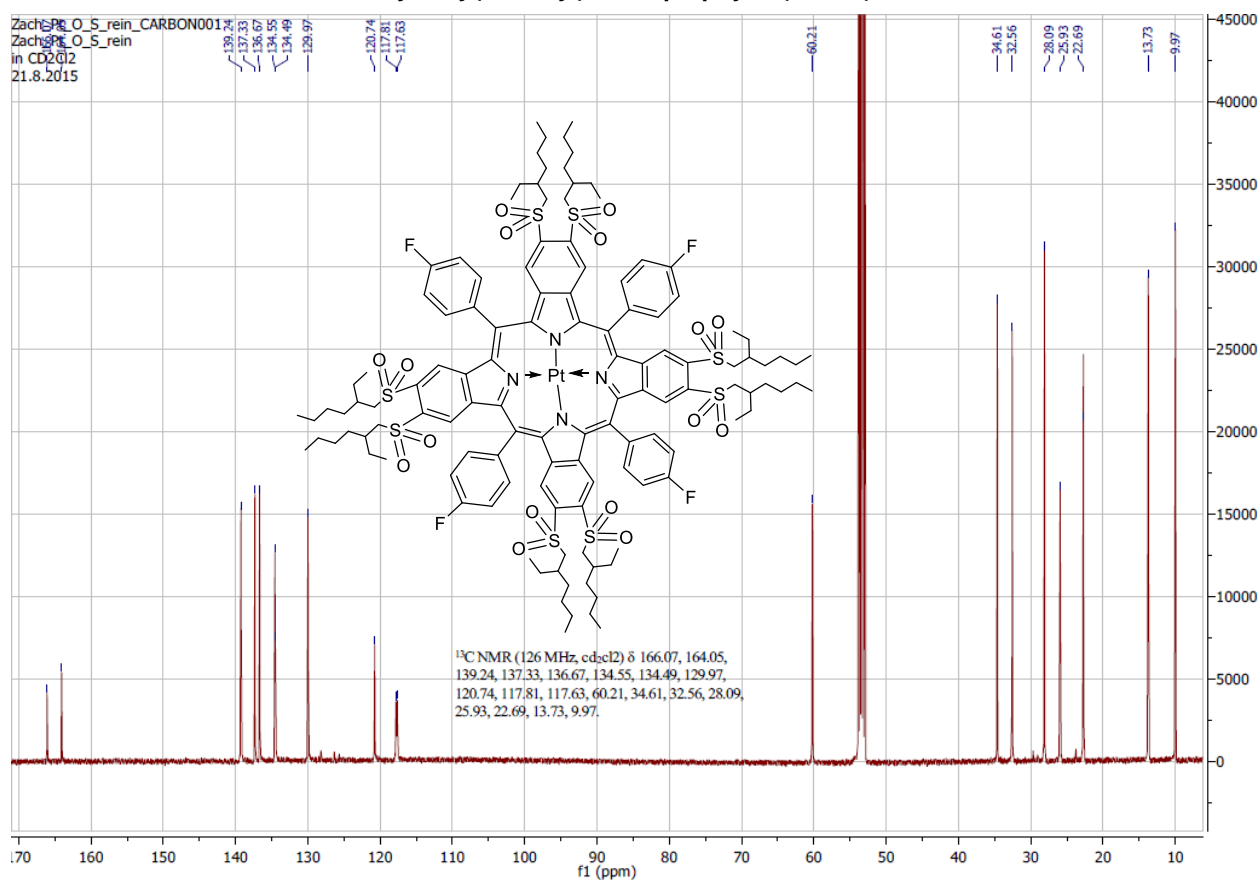
Figure S 5.53 NMR-Spectra (^{13}C) of Pt(II) meso-tetra(4-fluorophenyl)tetra(4,5-bis((2-ethylhexyl)sulfonyl)benzo-porphyrin (Pt-O-S)

^{13}C NMR (76 MHz, CD₂Cl2) δ 167.14, 163.78, 139.65, 137.69, 137.07, 134.88, 130.39, 121.15, 118.26, 117.99, 60.58, 35.01, 32.95, 28.49, 26.30, 23.13, 14.15, 10.38.
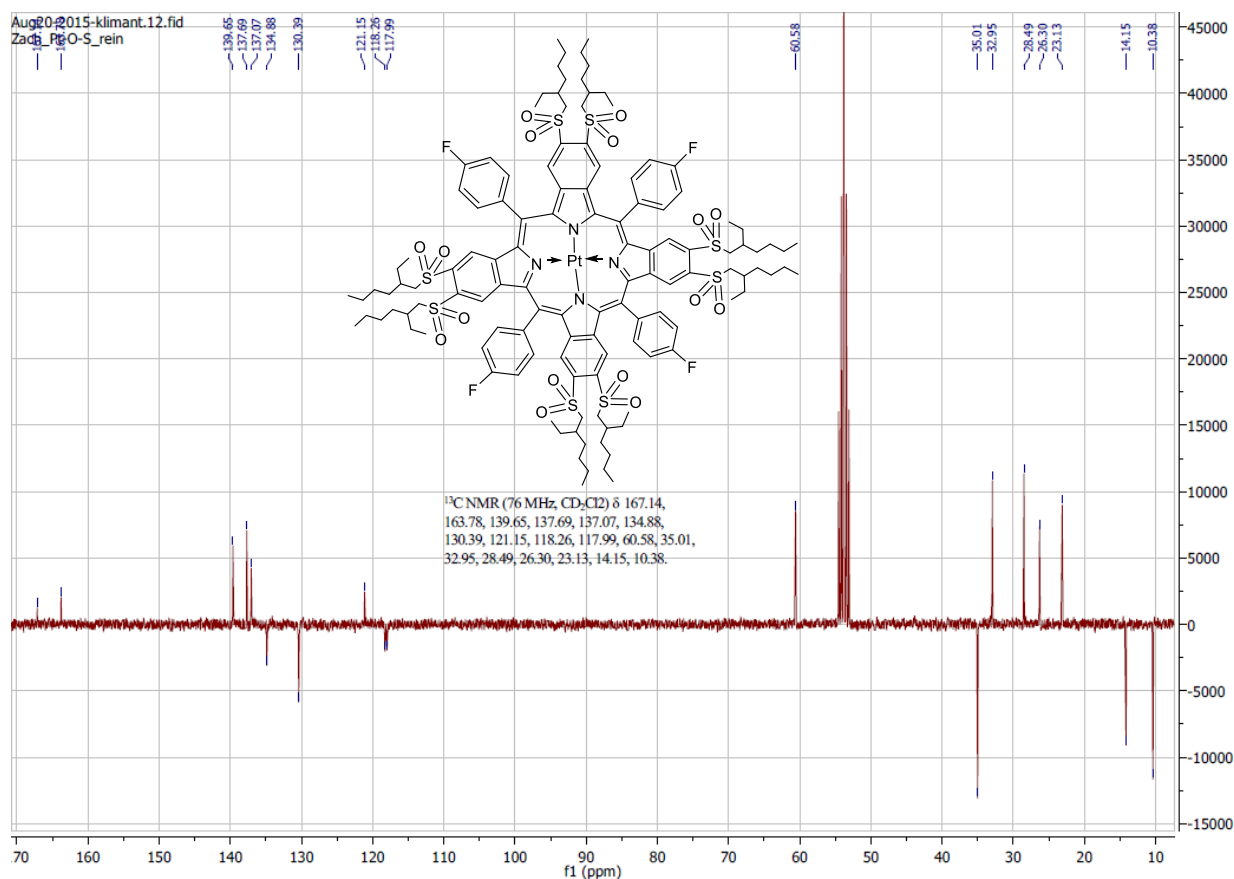
Figure S 5.54 NMR-Spectra (^{13}C-APT) of Pt(II) meso-tetra(4-fluorophenyl)tetra(4,5-bis((2-ethylhexyl)sulfonyl)benzo-porphyrin (Pt-O-S)

^{1}H NMR (300 MHz, Methylene Chloride-d_2) δ 8.29 – 8.16 (m, 16H), 7.75 (t, J = 8.4 Hz, 8H), 3.69 – 3.37 (m, 15H), 2.03 – 1.85 (m, 8H), 1.51 – 1.44 (m, 16H), 1.43 – 1.33 (m, 24H), 1.32 – 1.12 (m, 34H), 0.93 – 0.74 (m, 47H).
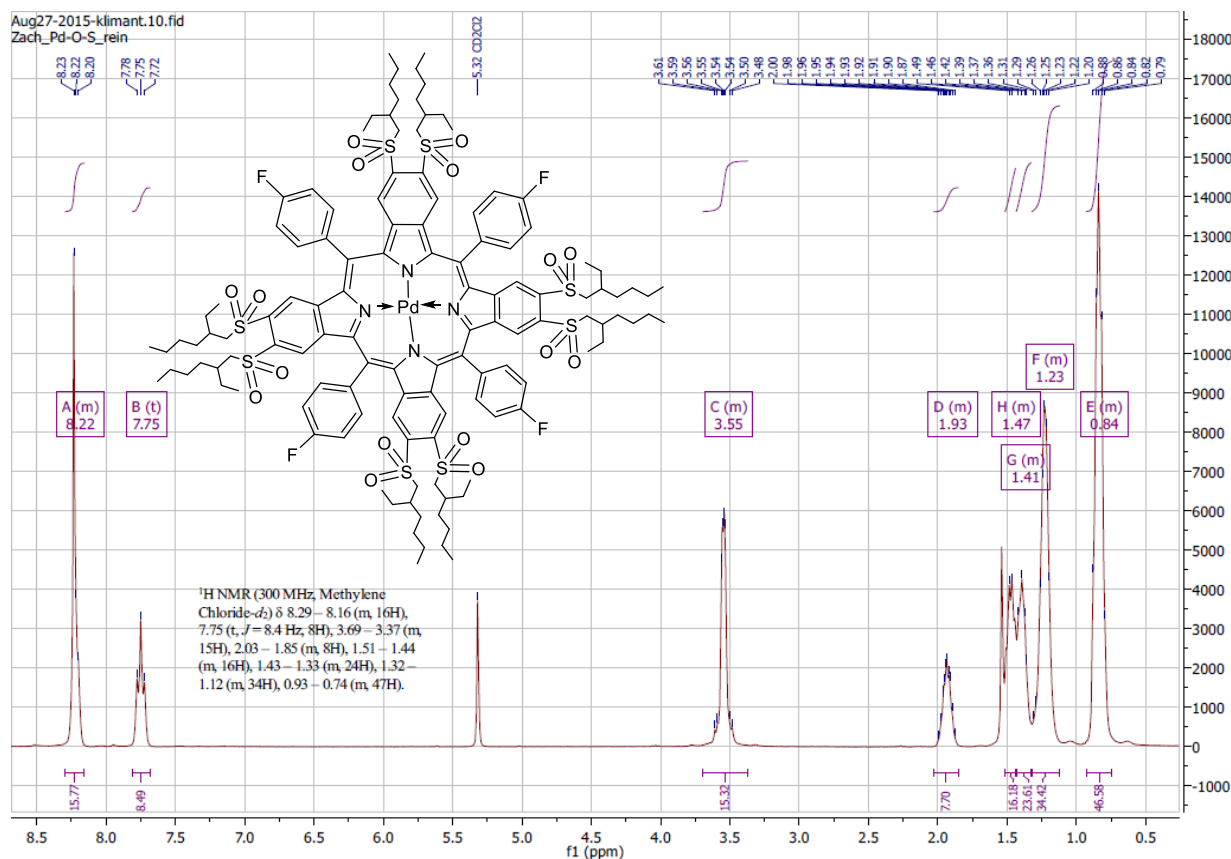
Figure S 5.55 NMR-Spectra (^{1}H) of Pd(II) meso-tetra(4-fluorophenyl)tetra(4,5-bis((2-ethylhexyl)sulfonyl)benzo-porphyrin (Pd-O-S)
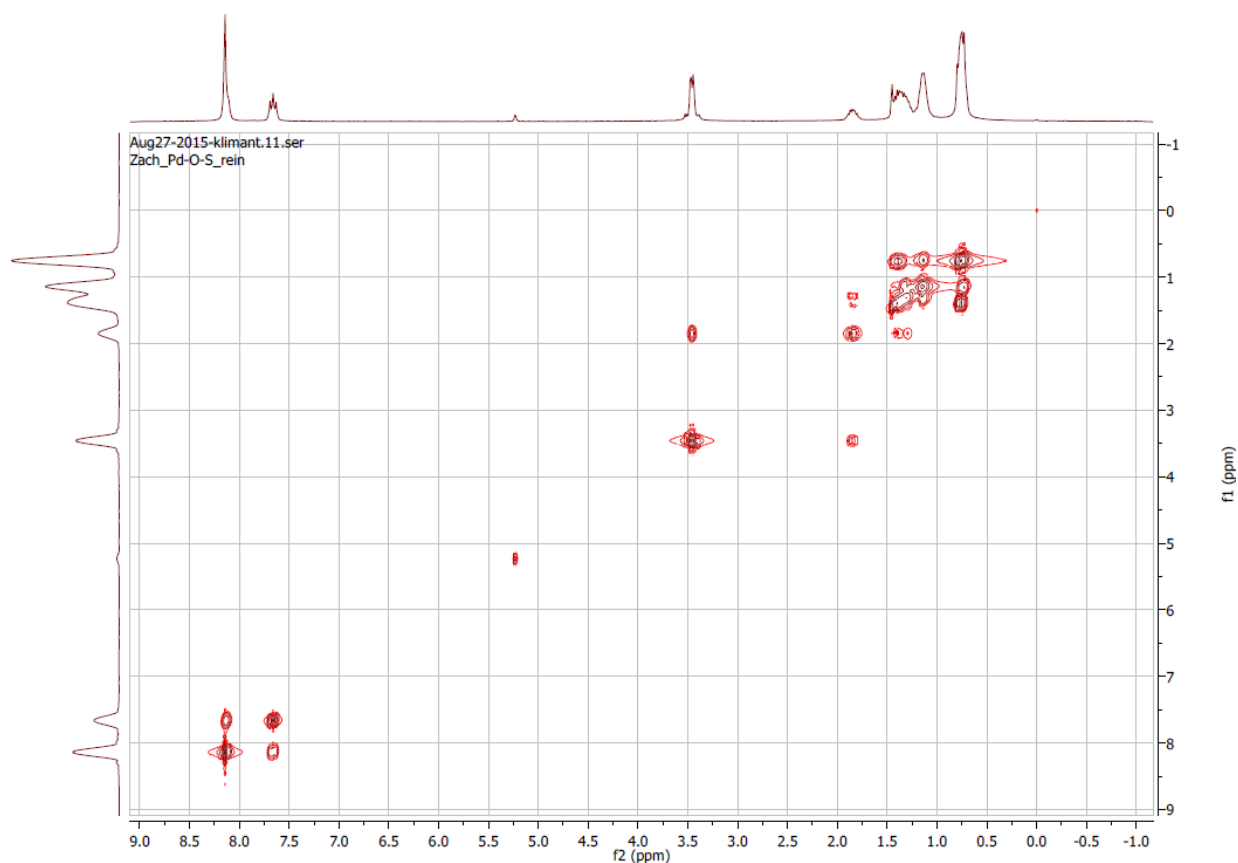
Figure S 5.56 NMR-Spectra (H-H-COSY) of Pd(II) meso-tetra(4-fluorophenyl)tetra(4,5-bis((2-ethylhexyl)sulfonyl)benzo-porphyrin (Pd-O-S)

^{13}C NMR (76 MHz, CD$_2$Cl$_2$) δ 167.11, 163.76, 139.93, 139.05, 137.53, 135.36, 135.32, 135.23, 135.13, 130.32, 120.62, 118.12, 117.83, 60.59, 35.00, 32.95, 28.49, 26.31, 23.12, 14.15, 10.38.
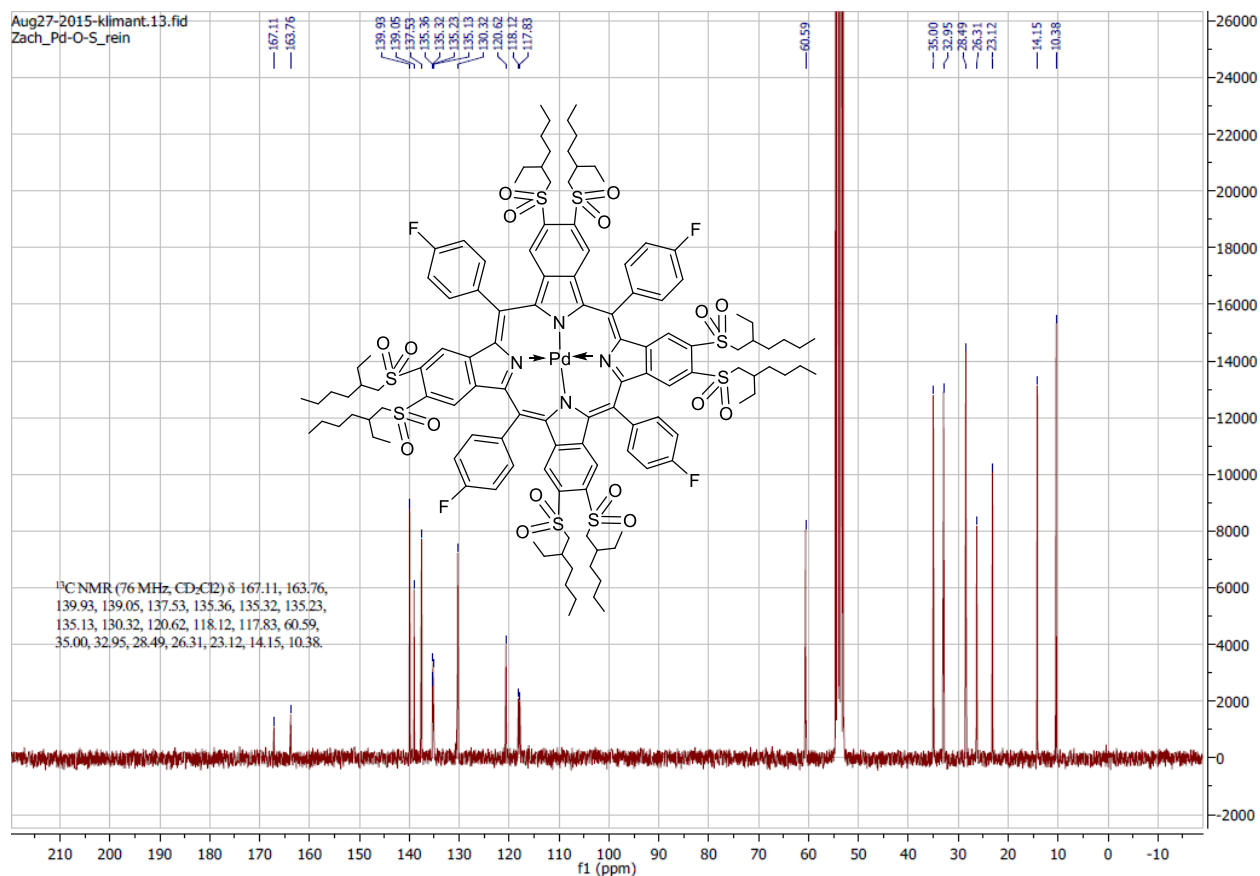
Figure S 5.57 NMR-Spectra (^{13}C) of Pd(II) meso-tetra(4-fluorophenyl)tetra(4,5-bis((2-ethylhexyl)sulfonyl)benzo-porphyrin (Pd-O-S)

Aug27-2015eklimant.12.fid
Zach_Pd₂O-S_rein

¹³C NMR (76 MHz, CD₂Cl2) δ 167.11, 163.76, 139.93, 139.05, 137.53, 135.36, 135.32, 135.24, 135.13, 130.32, 120.62, 118.12, 117.83, 60.59, 35.00, 32.95, 28.49, 26.31, 23.12, 14.15, 10.38.
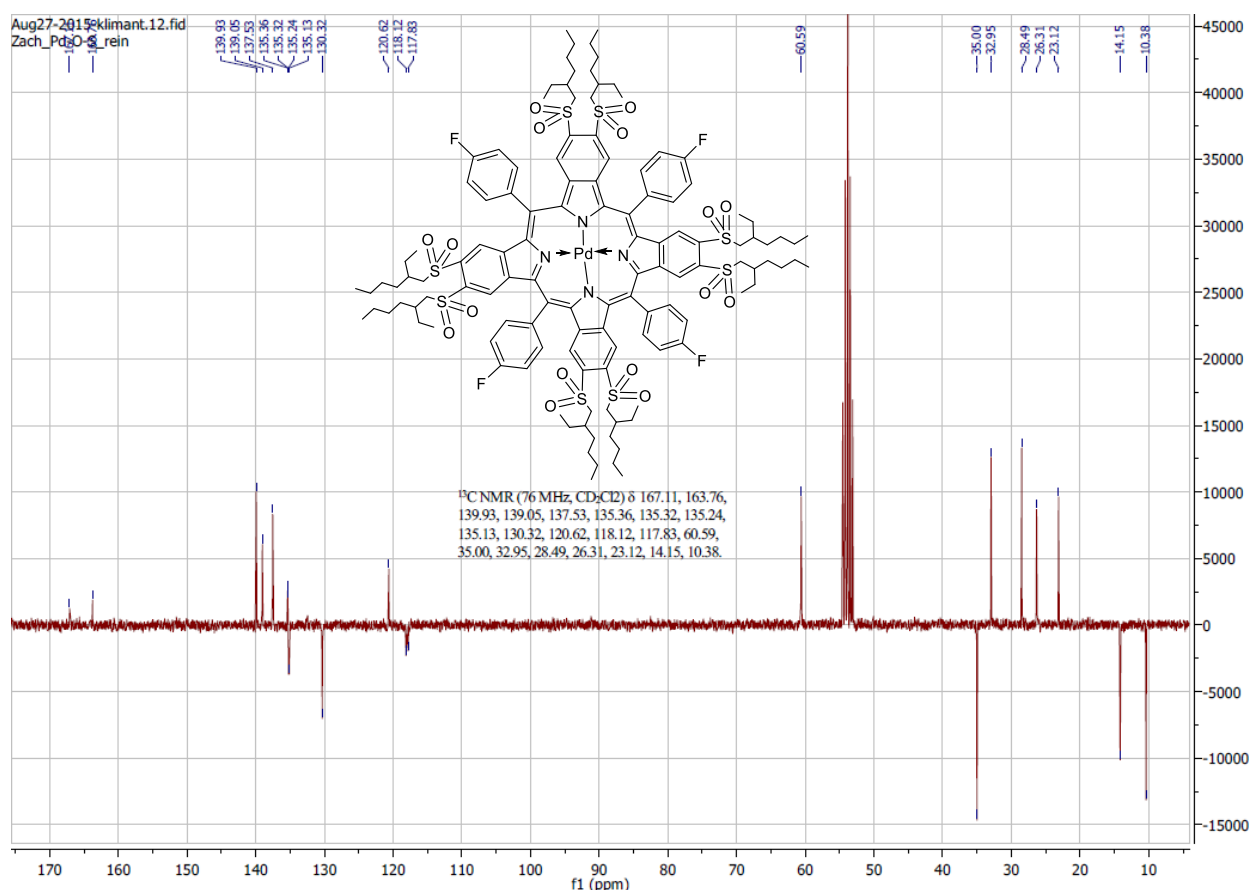
Figure S 5.58 NMR-Spectra (¹³C-APT) of Pd(II) meso-tetra(4-fluorophenyl)tetra(4,5-bis((2-ethylhexyl)sulfonyl)benzo-porphyrin (Pd-O-S)

Zach_Pt_T_S_rein_PROTON001
Peter Zach
Zach_Pt_T_S_rein in CD2Cl2

¹H NMR (500 MHz, Methylene Chloride-d₂) δ 8.31 − 8.19 (m, 8H), 7.88 − 7.78 (m, 4H), 7.78 − 7.66 (m, 10H), 7.63 (dd, J = 4.3, 1.6 Hz, 2H), 7.41 (dd, J = 8.6, 3.3 Hz, 2H), 7.30 (dd, J = 8.6, 3.4 Hz, 2H), 3.02 (q, J = 5.6 Hz, 8H), 1.88 (dh, J = 12.6, 6.2 Hz, 4H), 1.48 (p, J = 6.4, 5.9 Hz, 8H), 1.44 − 1.33 (m, 8H), 1.29 − 1.14 (m, 17H), 0.88 − 0.80 (m, 24H).
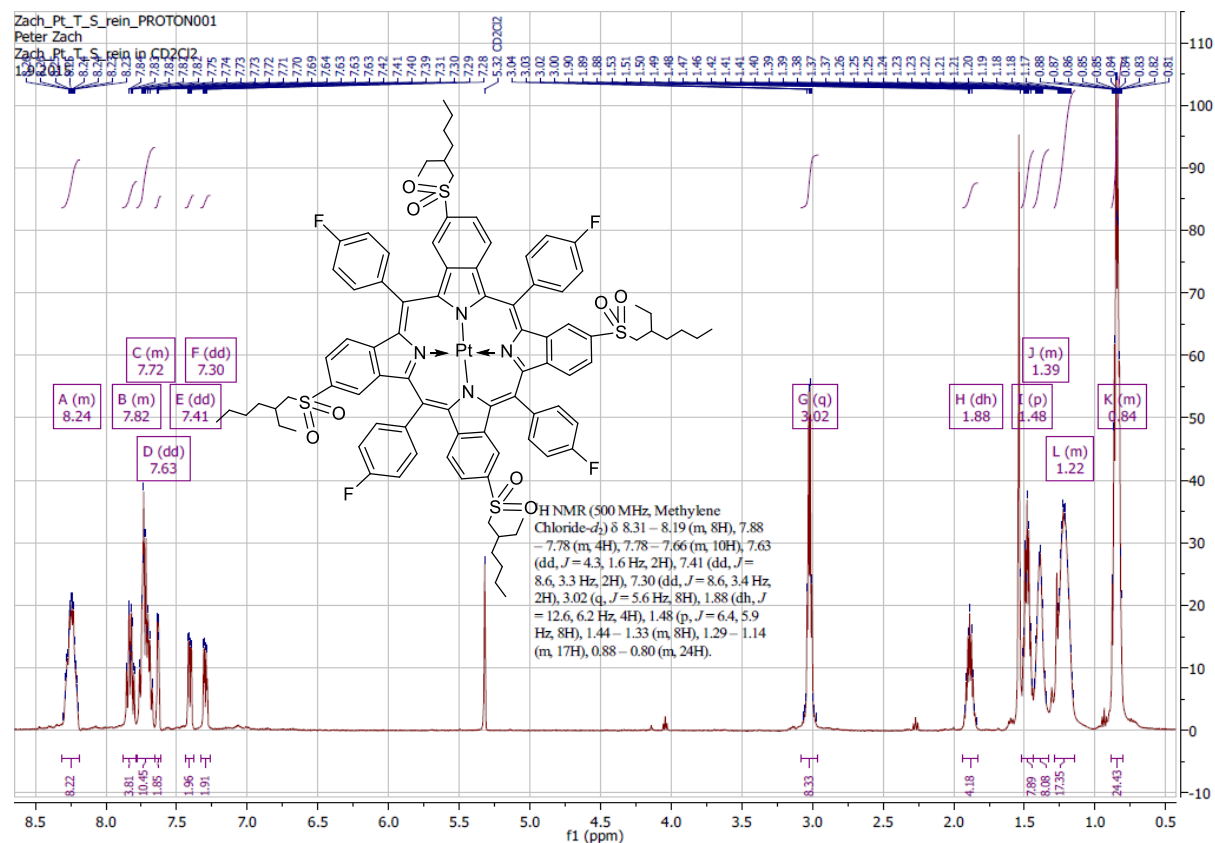
Figure S 5.59 NMR-Spectra (¹H) of Pt(II) -meso-tetra(4-fluorophenyl)tetra(4-((2-ethylhexyl)sulfonyl)benzo-porphyrin (Pt-T-S)
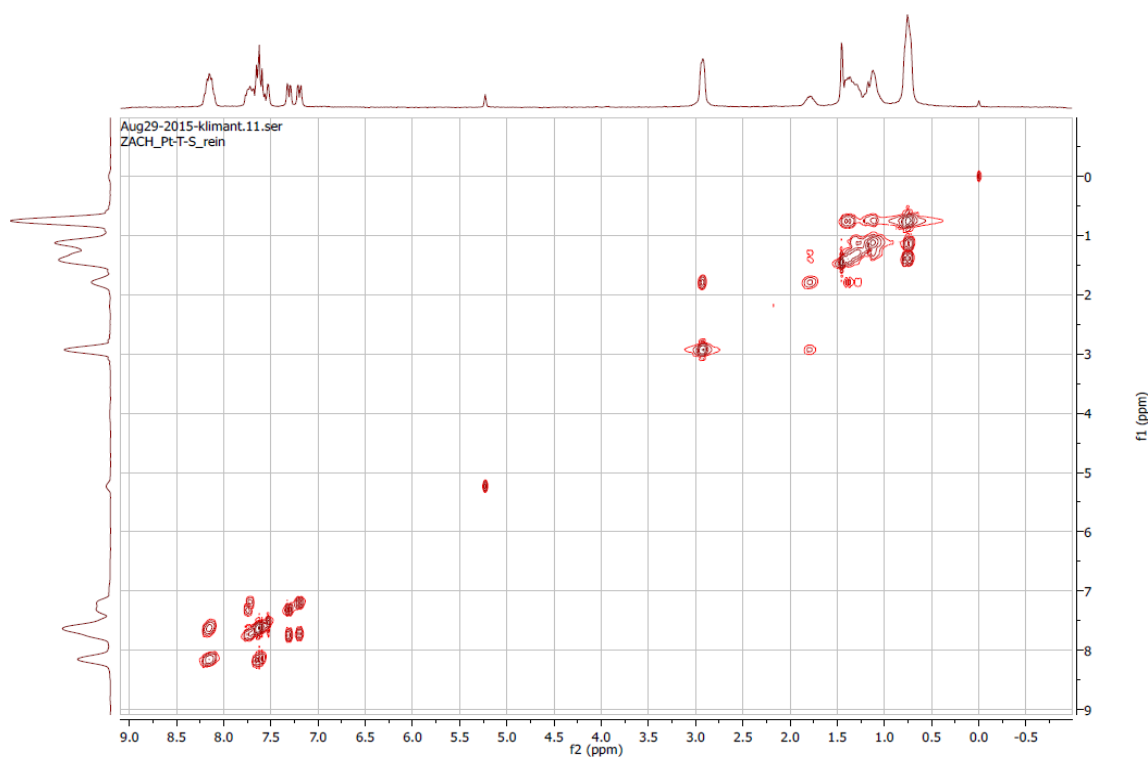
Figure S 5.60 NMR-Spectra (H-H-COSY) of Pt(II) -meso-tetra(4-fluorophenyl)tetra(4-((2-ethylhexyl)sulfonyl)benzo-porphyrin (Pt-T-S)

^{13}C NMR (76 MHz, CD$_2$Cl2) δ 166.44, 163.11, 140.72, 140.60, 138.11, 137.41, 136.64, 136.59, 135.53, 135.42, 125.13, 117.70, 117.42, 60.14, 34.86, 32.86, 28.53, 26.25, 23.09, 14.17, 10.37.
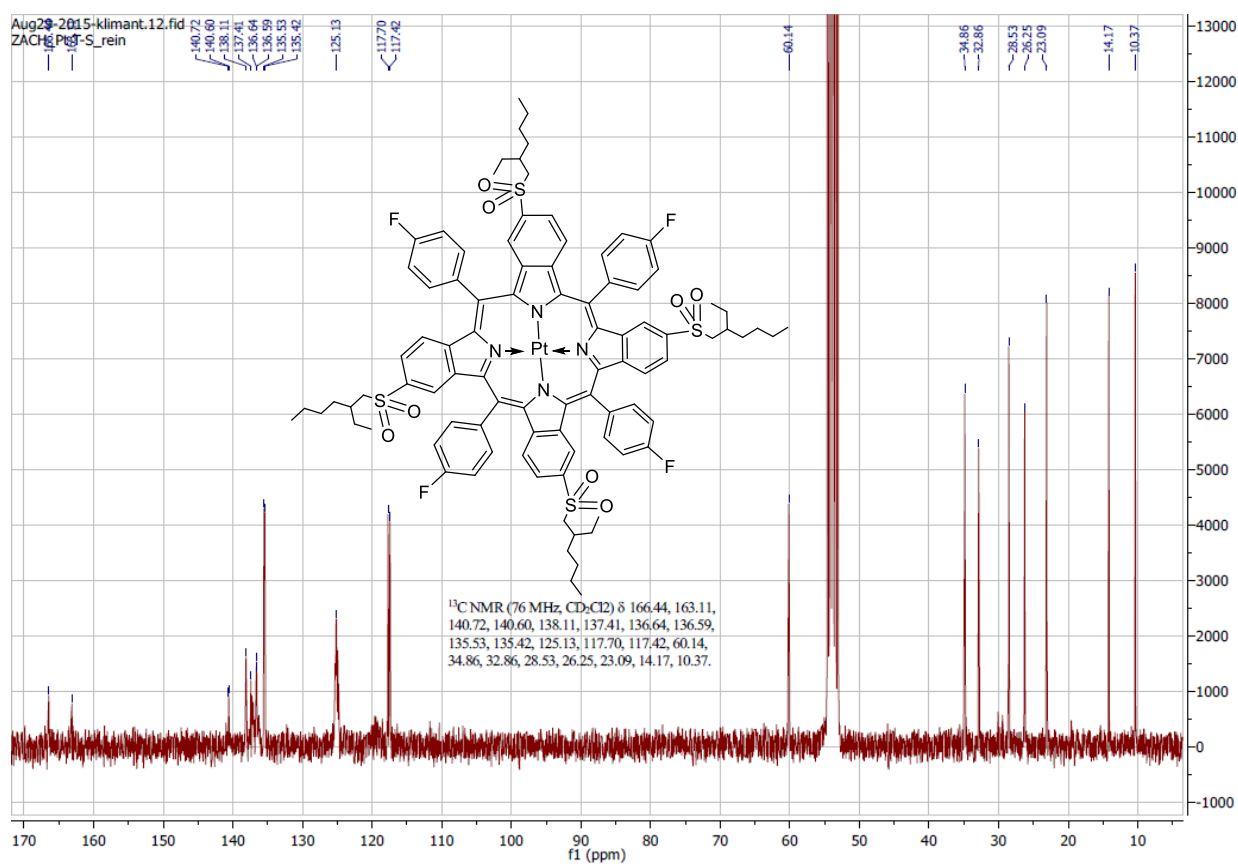
Figure S 5.61 NMR-Spectra (^{13}C) of Pt(II) -meso-tetra(4-fluorophenyl)tetra(4-((2-ethylhexyl)sulfonyl)benzo-porphyrin (Pt-T-S)
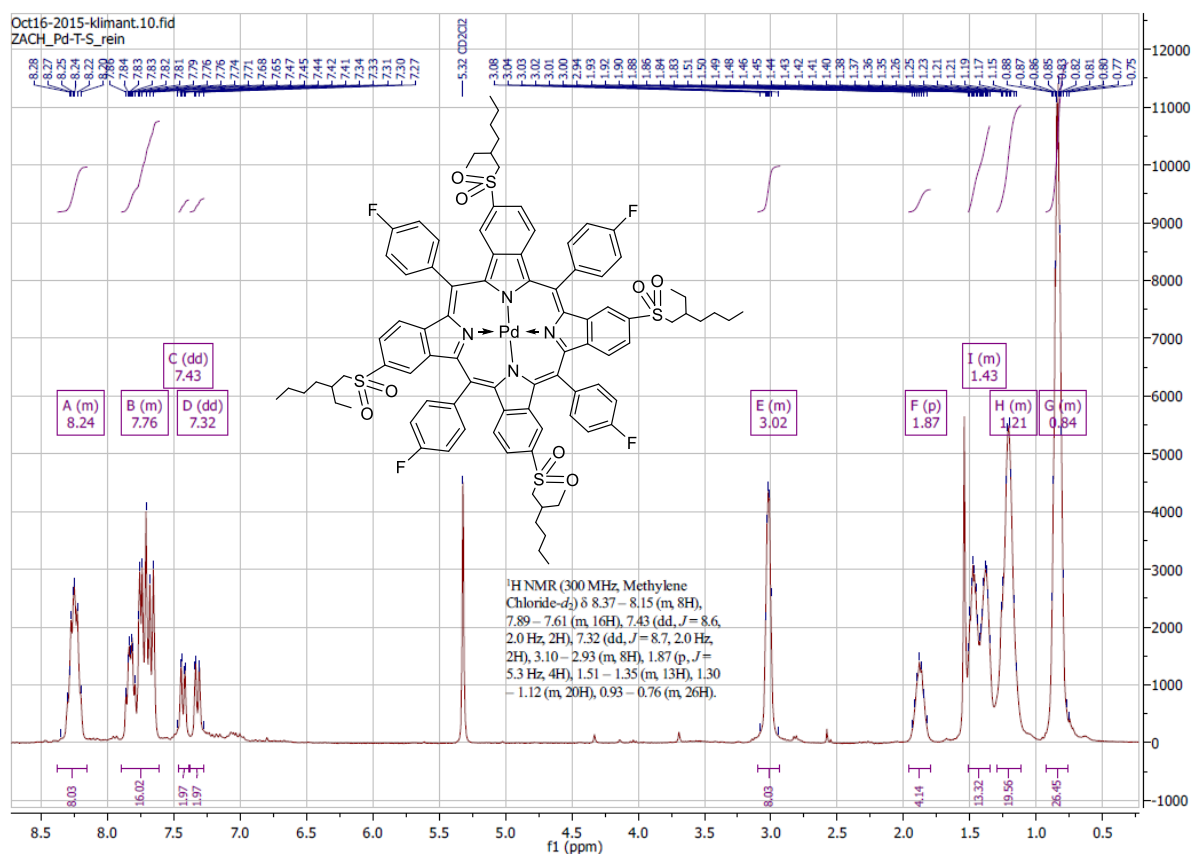
Figure S 5.62 NMR-Spectra (¹H) of Pd(II) -meso-tetra(4-fluorophenyl)tetra(4-((2-ethylhexyl)sulfonyl)benzo-porphyrin (Pd-T-S)
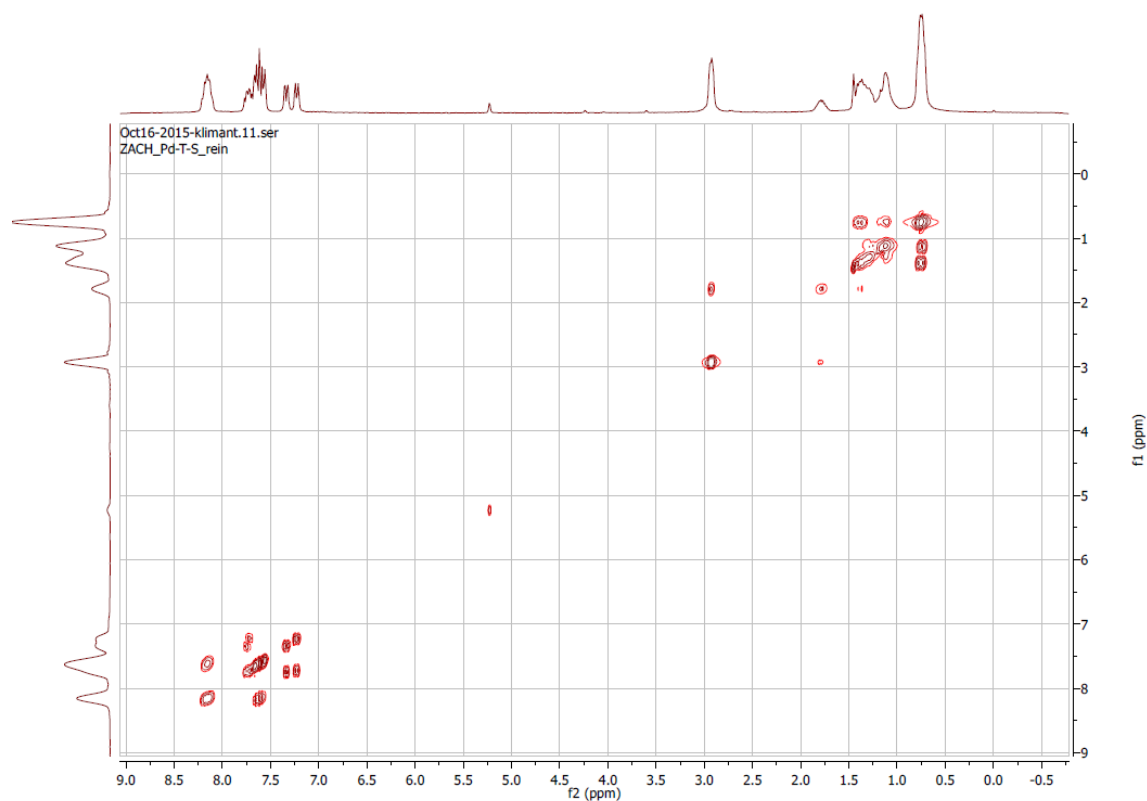
Figure S 5.63 NMR-Spectra (H-H-COSY) of Pd(II) -meso-tetra(4-fluorophenyl)tetra(4-((2-ethylhexyl)sulfonyl)benzo-porphyrin (Pd-T-S)
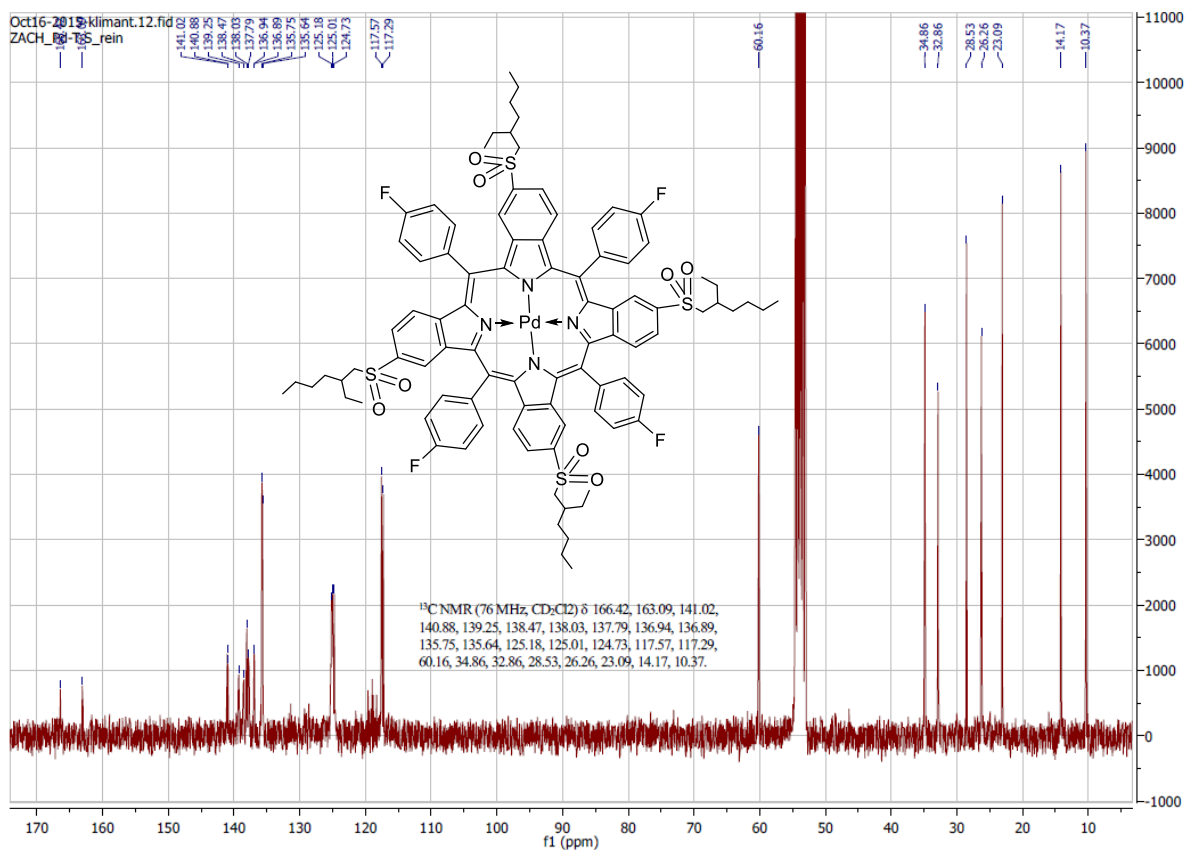
Figure S 5.64 NMR-Spectra (^{13}C) of Pd(II) -meso-tetra(4-fluorophenyl)tetra(4-((2-ethylhexyl)sulfonyl)benzo-porphyrin (Pd-T-S)

5.5.9 Mass Spectrometry: Ionization (MALDI / DCTB)
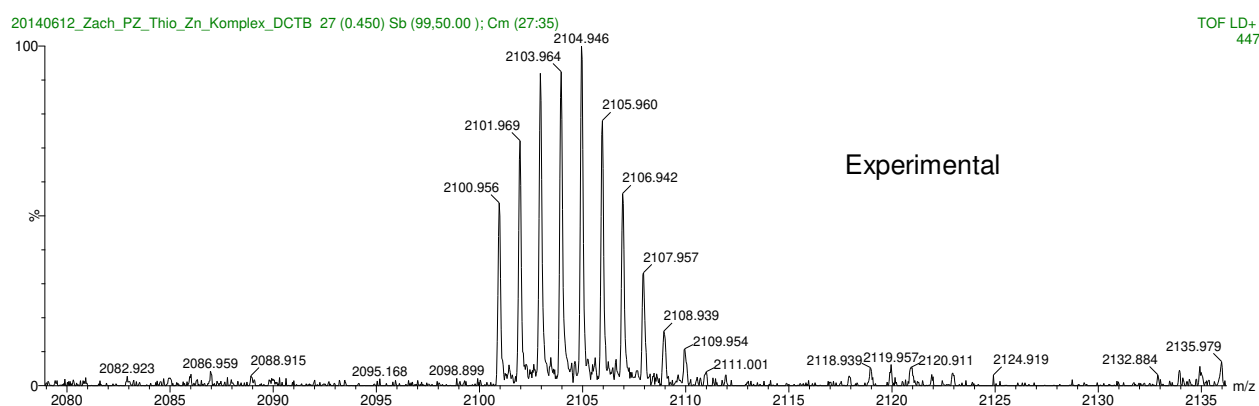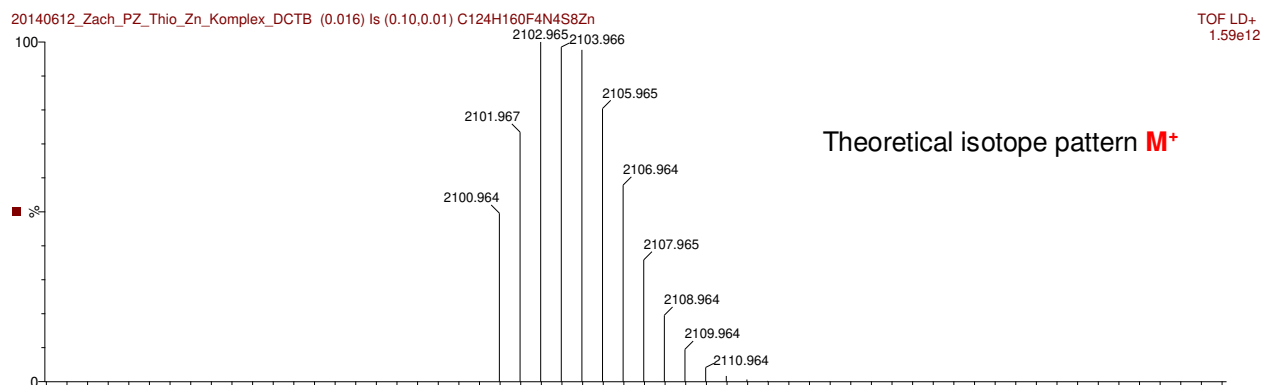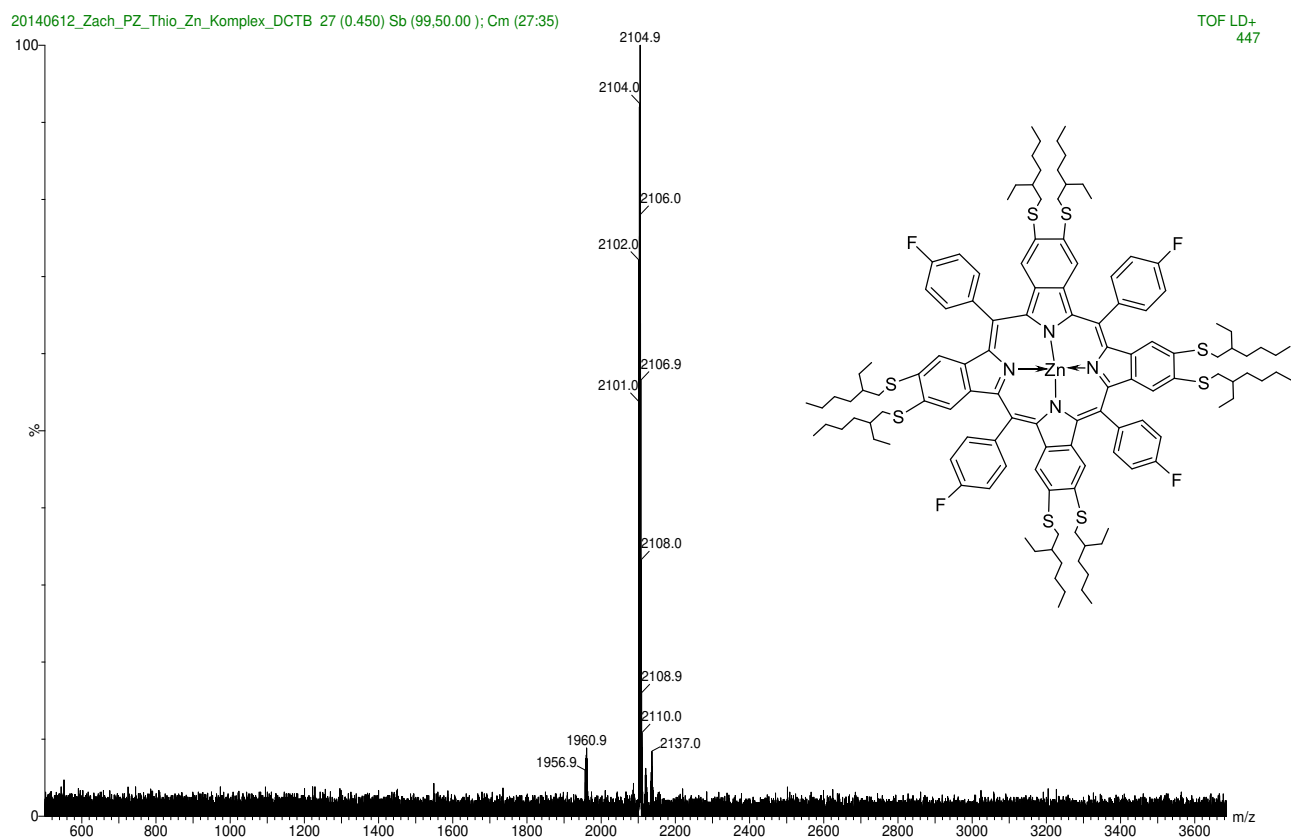
Figure S 5.65 Mass-Spectra of Zinc(II) meso-tetra(4-fluorophenyl)tetra(4,5-bis((2-ethylhexyl)thio)benzo-porphyrin (Zn-O-T)
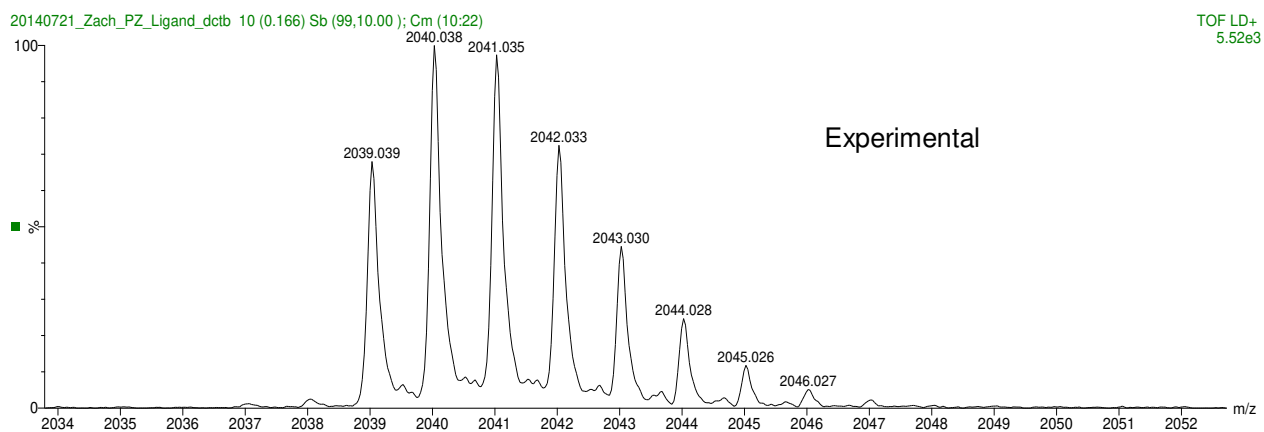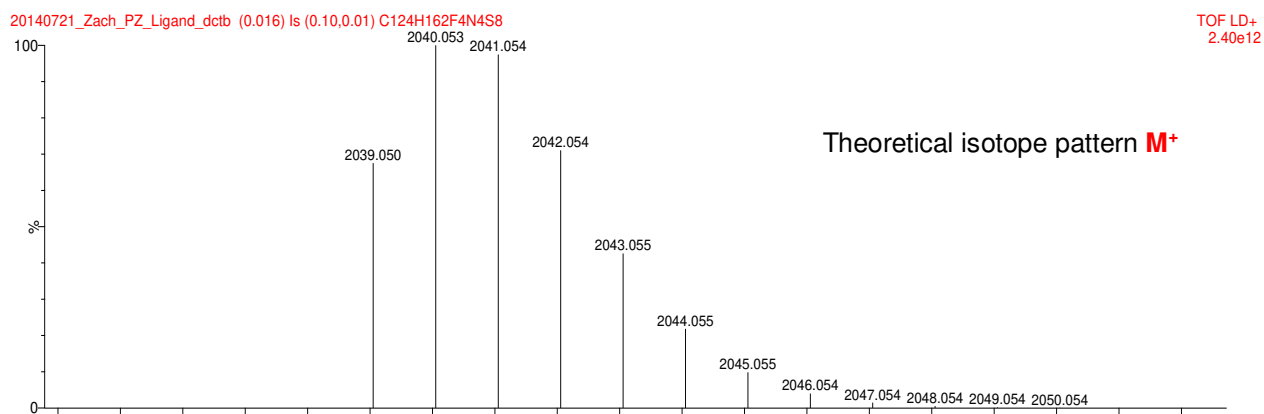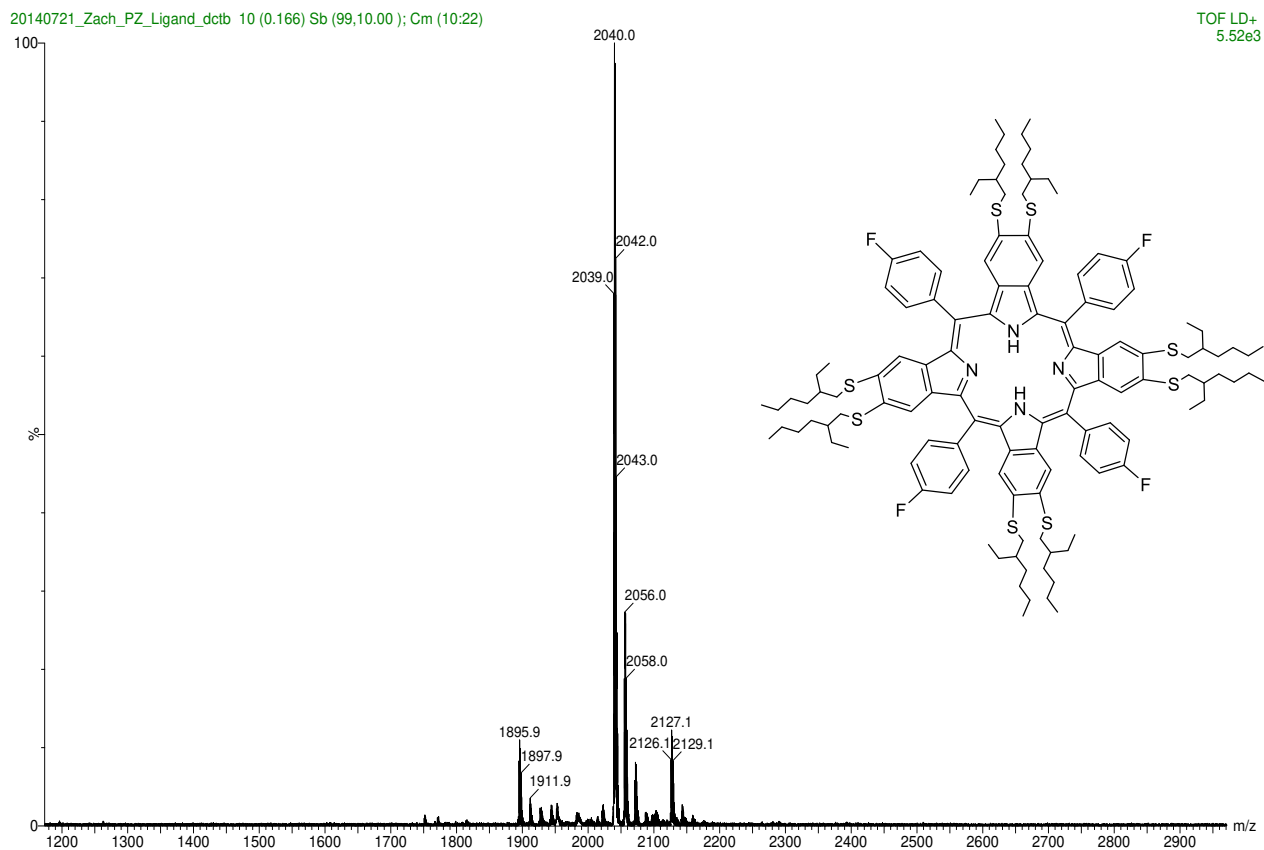
Figure S 5.66 Mass-Spectra of Meso-tetra(4-fluorophenyl)tetra(4,5-bis((2-ethylhexyl)thio)benzoporphyrin (H₂-O-T)
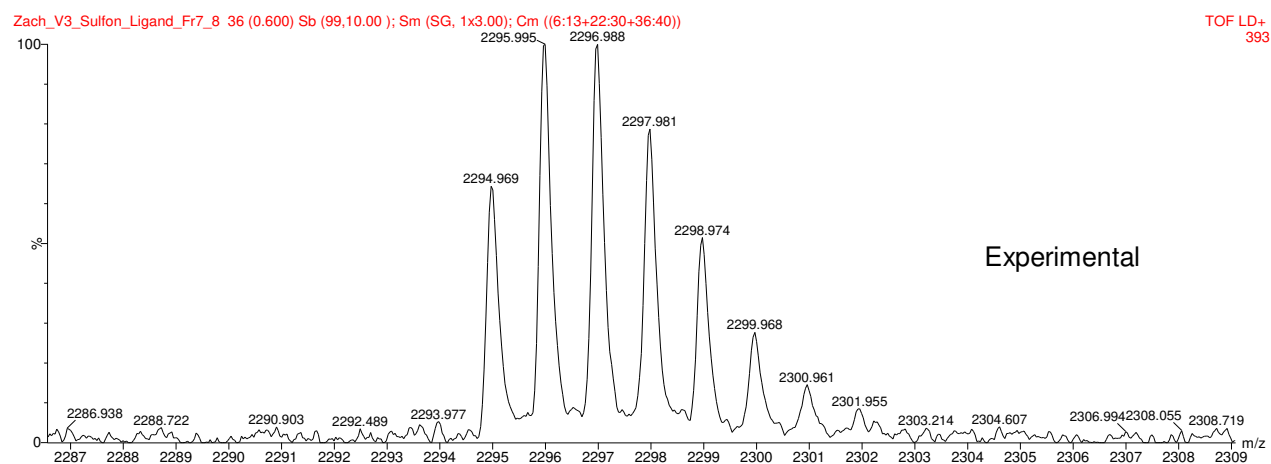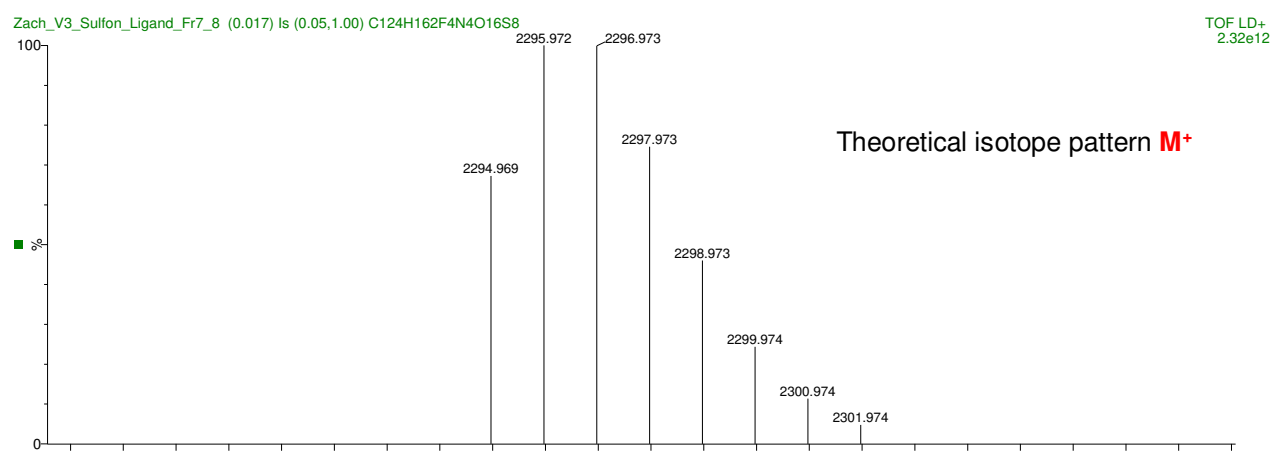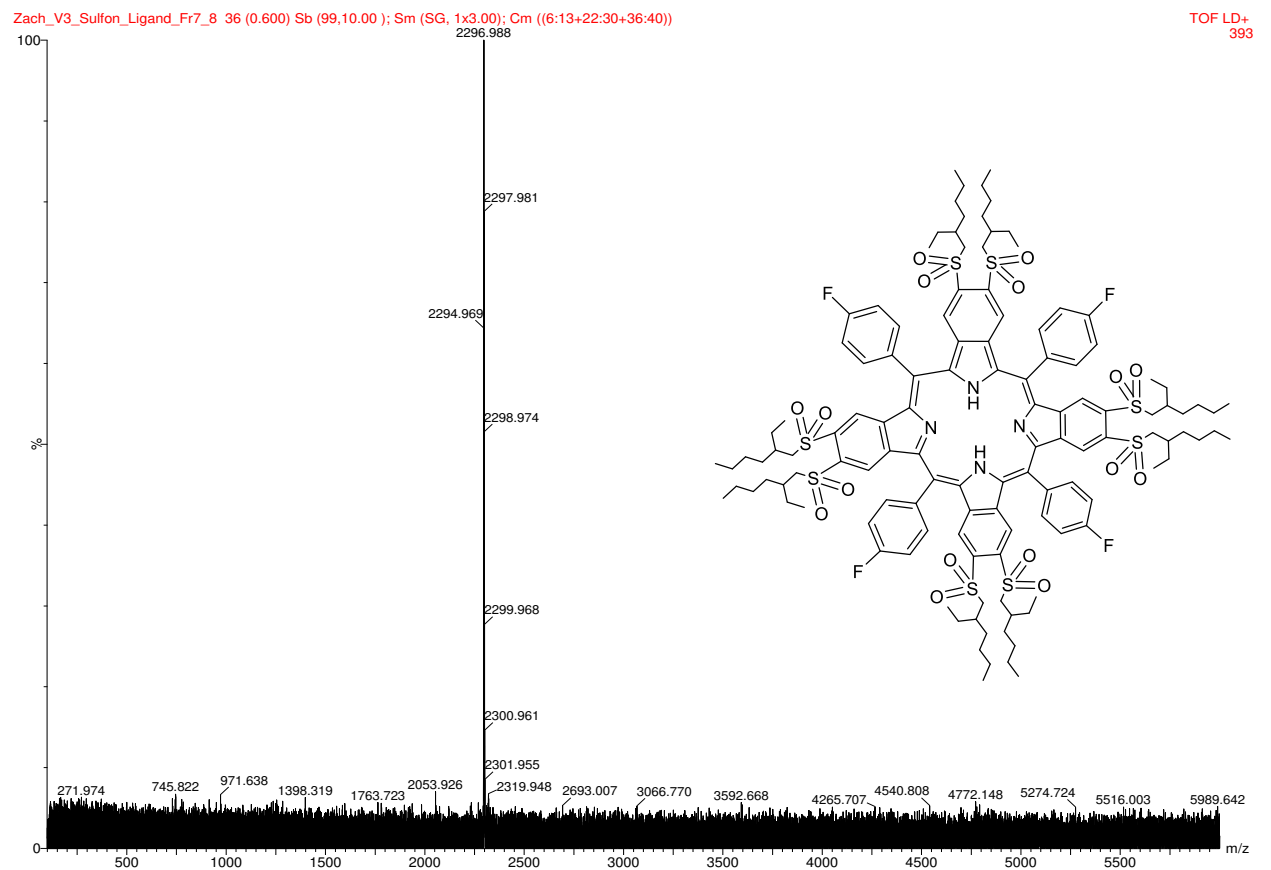
Figure S 5.67 Mass-Spectra of Meso-tetra(4-fluorophenyl)tetra(4,5-bis((2-ethylhexyl)sulfonyl)benzoporphyrin (H₂-O-S)
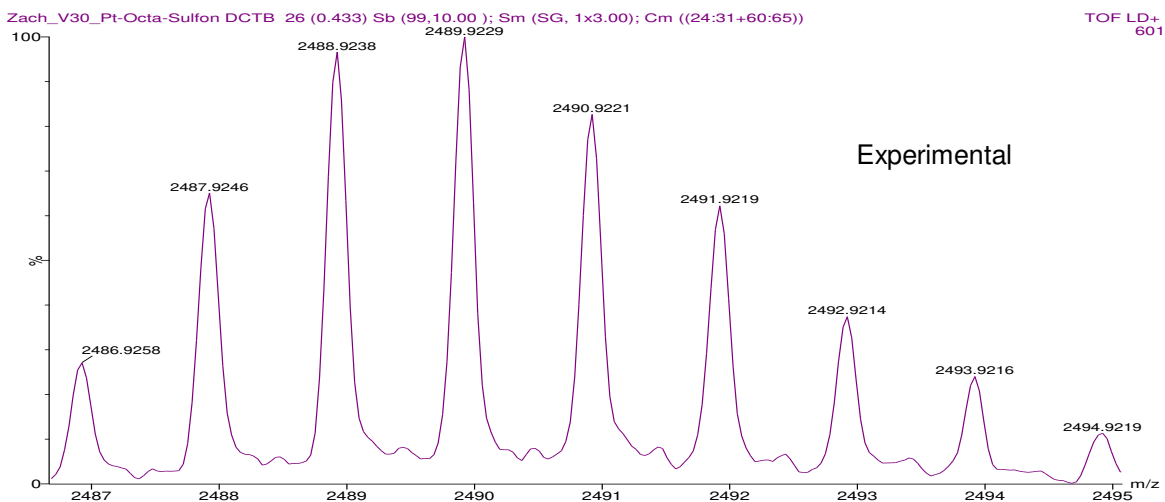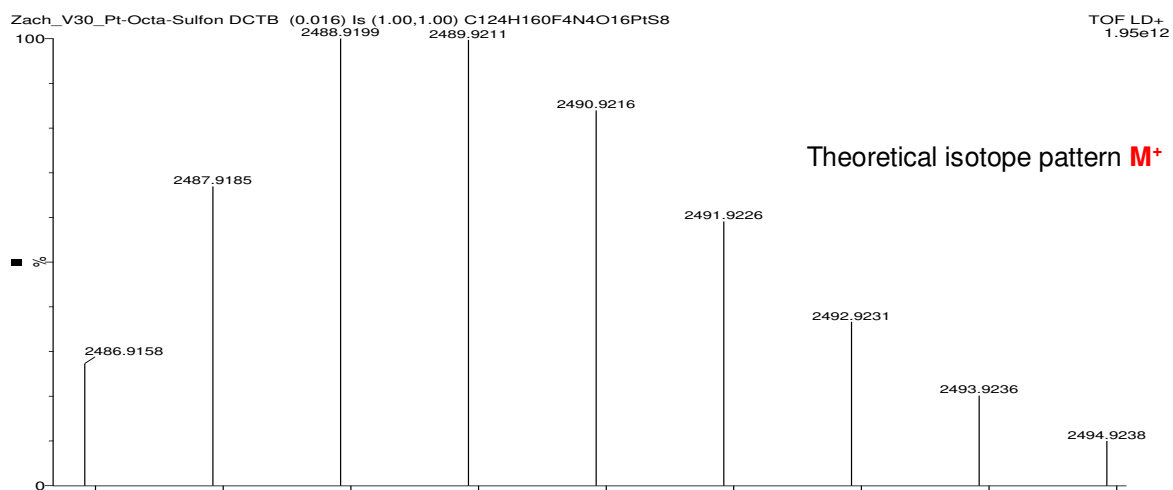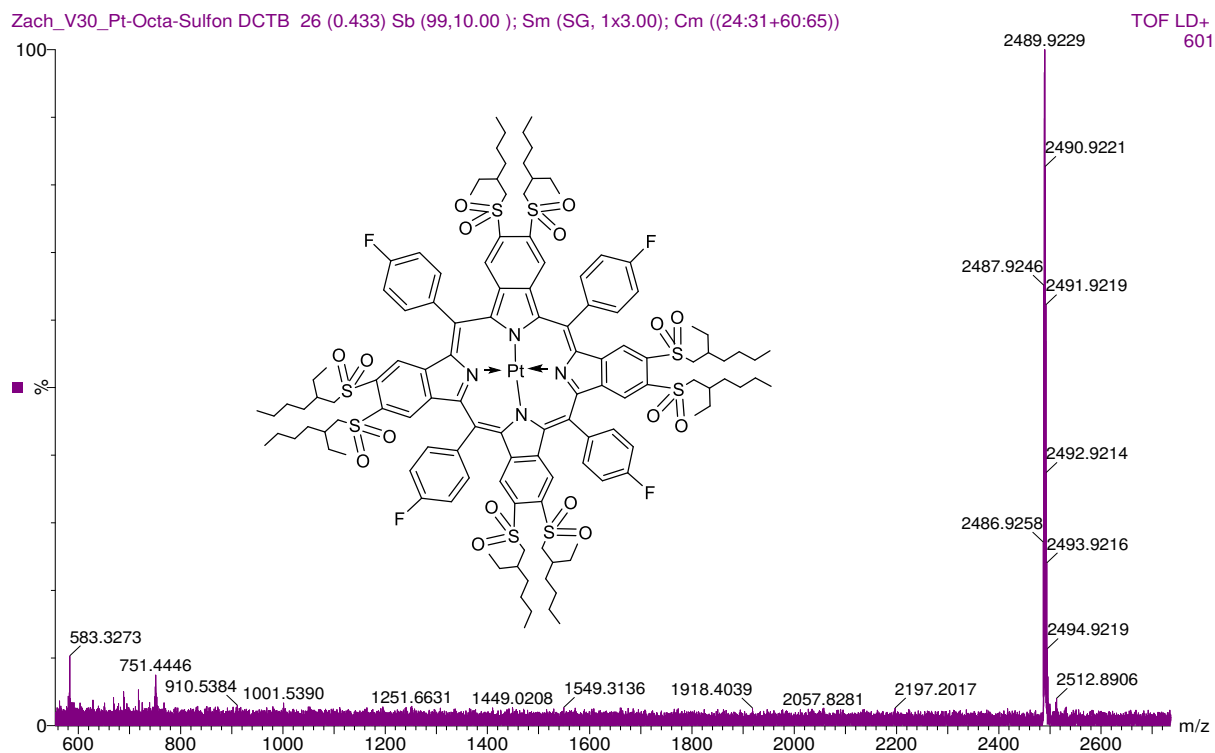
Figure S 5.68 Mass-Spectra of Pt(II) meso-tetra(4-fluorophenyl)tetra(4,5-bis((2-ethylhexyl)sulfonyl)benzo-porphyrin (Pt-O-S)

Zach_V33_Pd-Octa-Sulfon-HF1_DCTB 19 (0.317) Sb (99,10.00); Sm (SG, 1x3.00); Cm ((18:24+46:49)) TOF LD+ 312

Zach_V33_Pd-Octa-Sulfon-HF1_DCTB (0.017) Is (1.00,1.00) C124H160F4N4O16PdS8 TOF LD+ 1.55e12

Theoretical isotope pattern **M⁺**

Zach_V33_Pd-Octa-Sulfon-HF1_DCTB 19 (0.317) Sb (99,10.00); Sm (SG, 1x3.00); Cm ((18:24+46:49)) TOF LD+ 312

Experimental

Figure S 5.69 Mass-Spectra of Pd(II) meso-tetra(4-fluorophenyl)tetra(4,5-bis((2-ethylhexyl)sulfonyl)benzo-porphyrin (Pd-O-S)
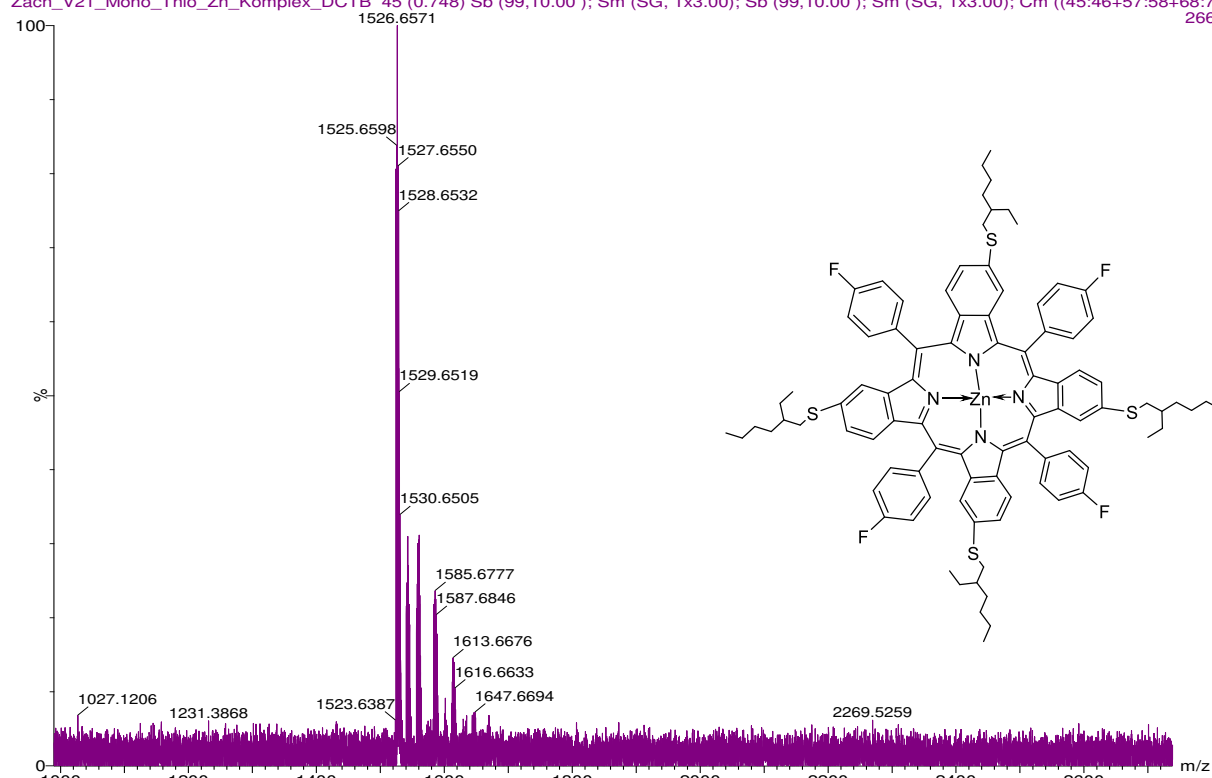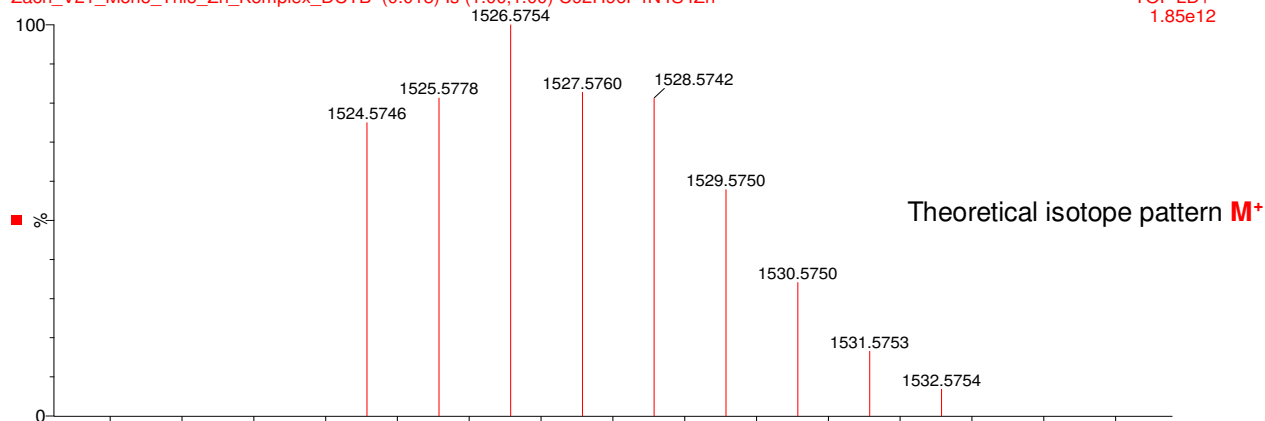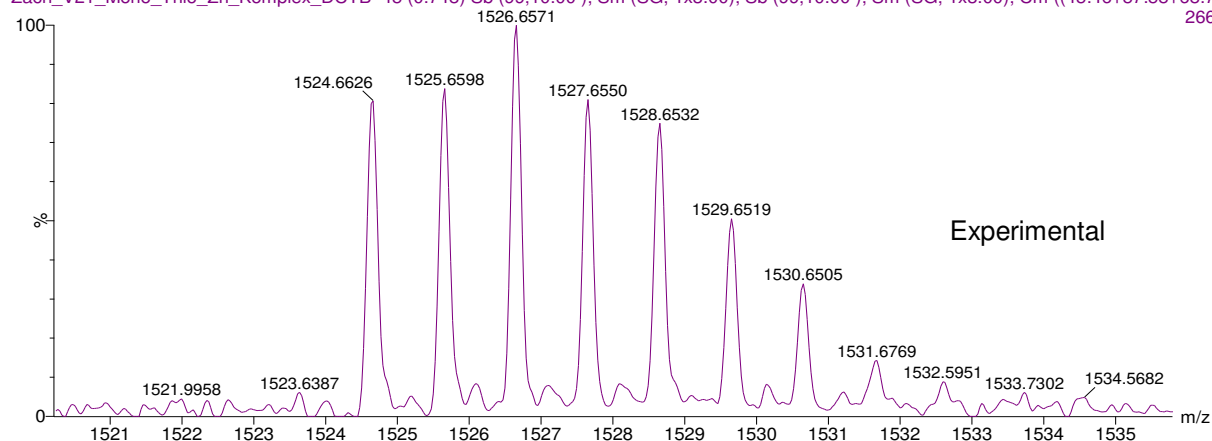
Figure S 5.70 Mass-Spectra of Zinc(II) meso-tetra(4-fluorophenyl)tetra(4- ((2-ethylhexyl)thio)benzo-porphyrin (Zn-T-T)

Figure S 5.71 Mass-Spectra of Meso-tetra(4-fluorophenyl)tetra(4-((2-ethylhexyl)thio)benzoporphyrin (H₂-T-T)

Figure S 5.72 Mass-Spectra of Meso-tetra(4-fluorophenyl)tetra(4-((2-ethylhexyl)sulfonyl)benzoporphyrin (H$_2$-T-S)
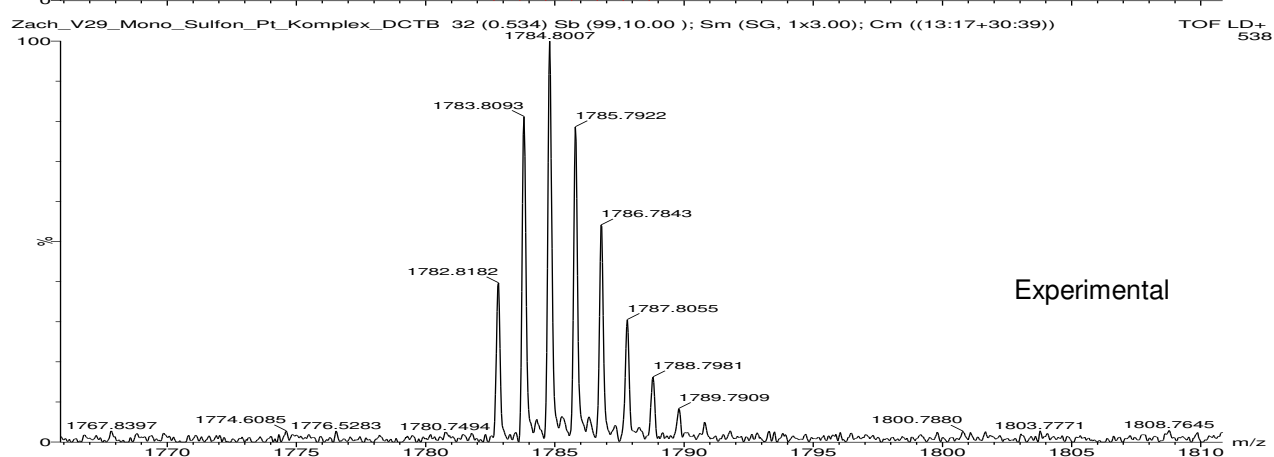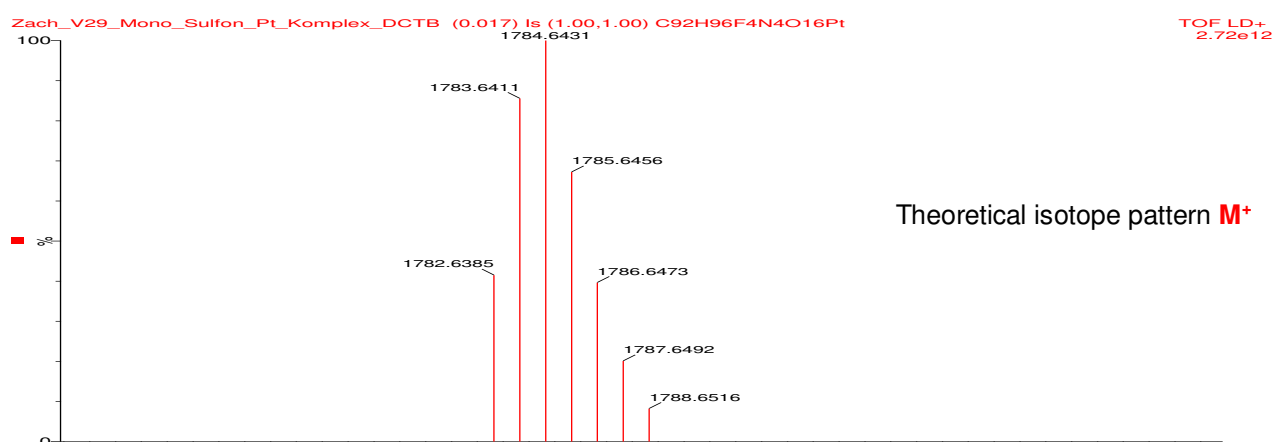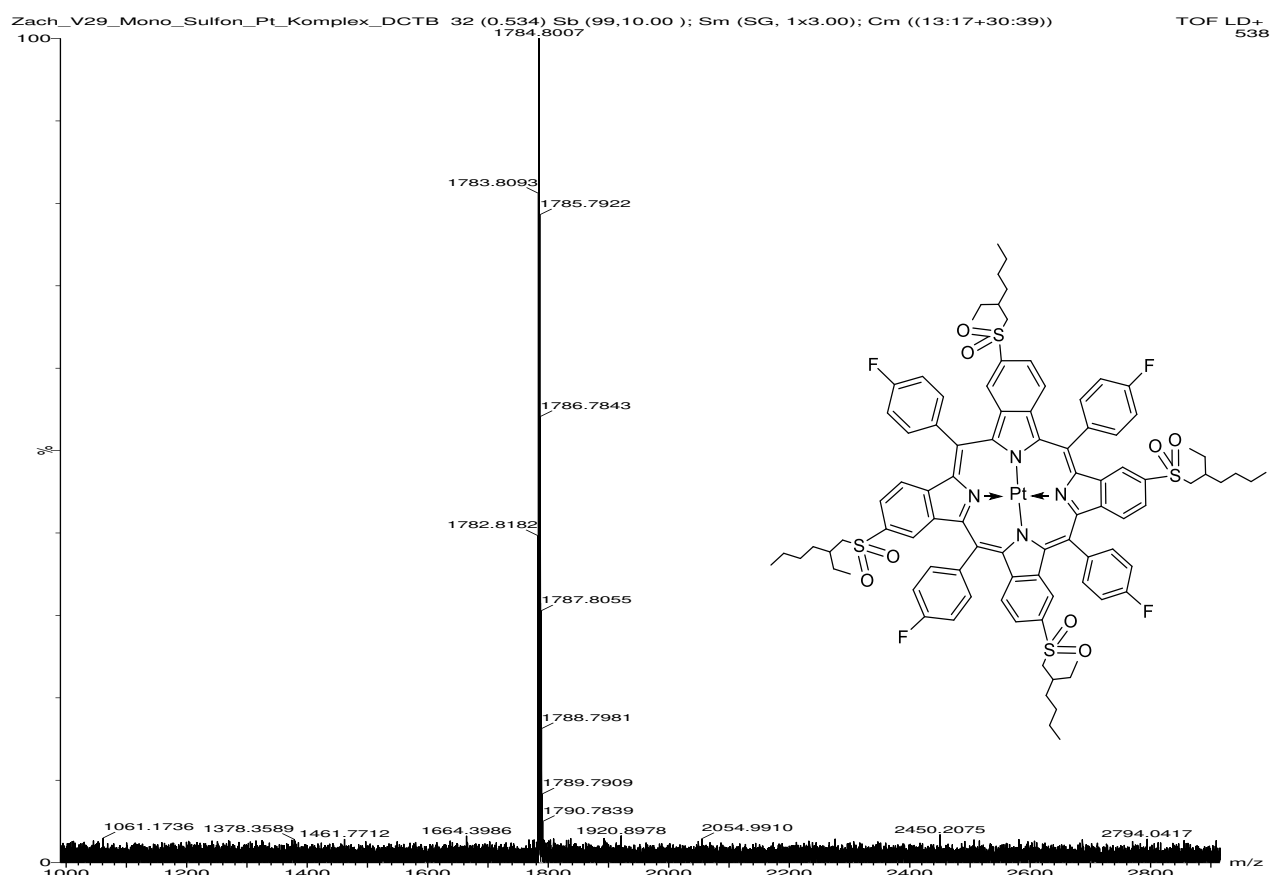
Figure S 5.73 Mass-Spectra of Pt(II) -meso-tetra(4-fluorophenyl)tetra(4-((2-ethylhexyl)sulfonyl)benzo-porphyrin (Pt-T-S)
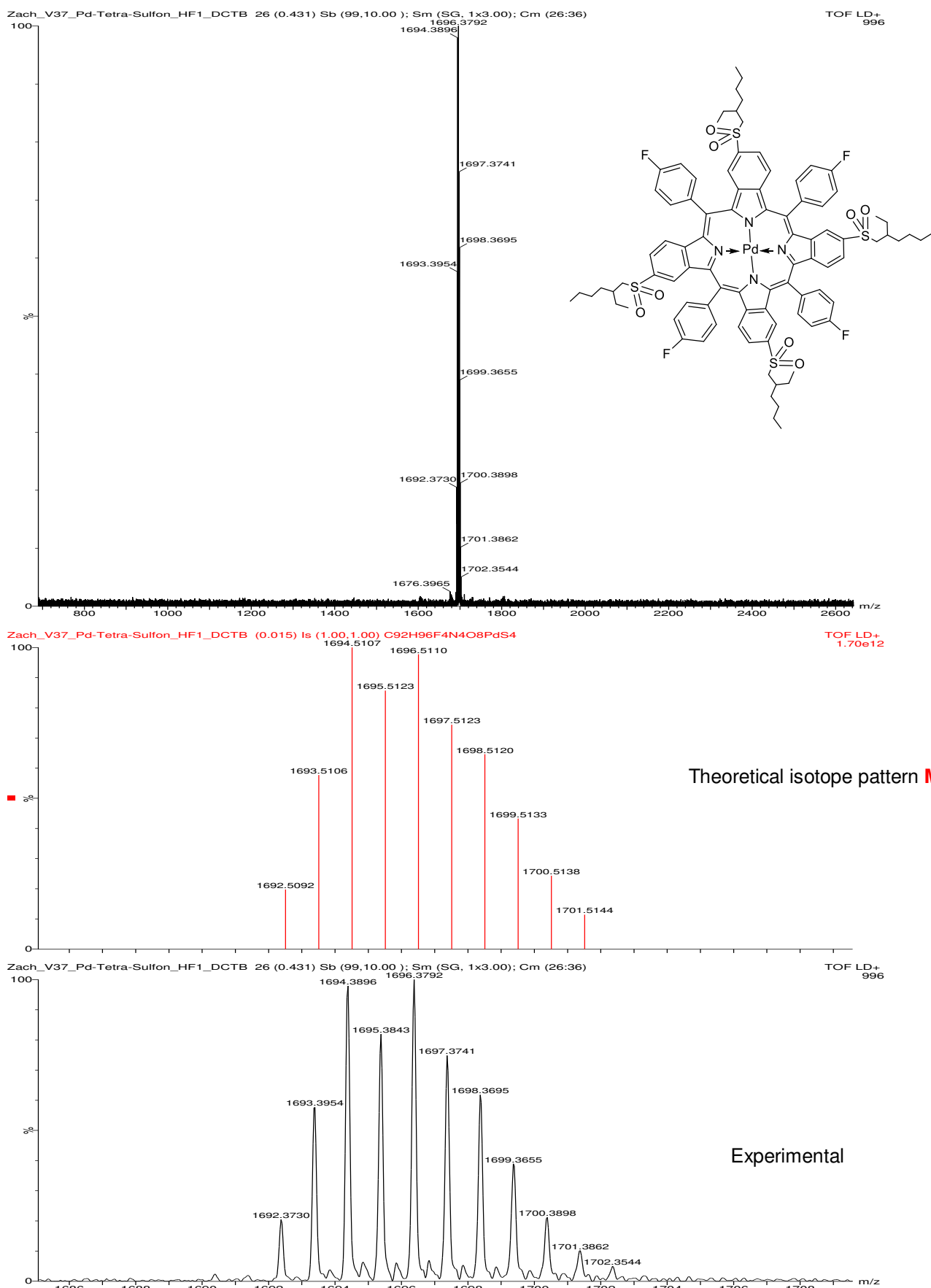
Figure S 5.74 Mass-Spectra of Pd(II) meso-tetra(4-fluorophenyl)tetra(4-((2-ethylhexyl)sulfonyl)benzo-porphyrin (Pd-T-S)
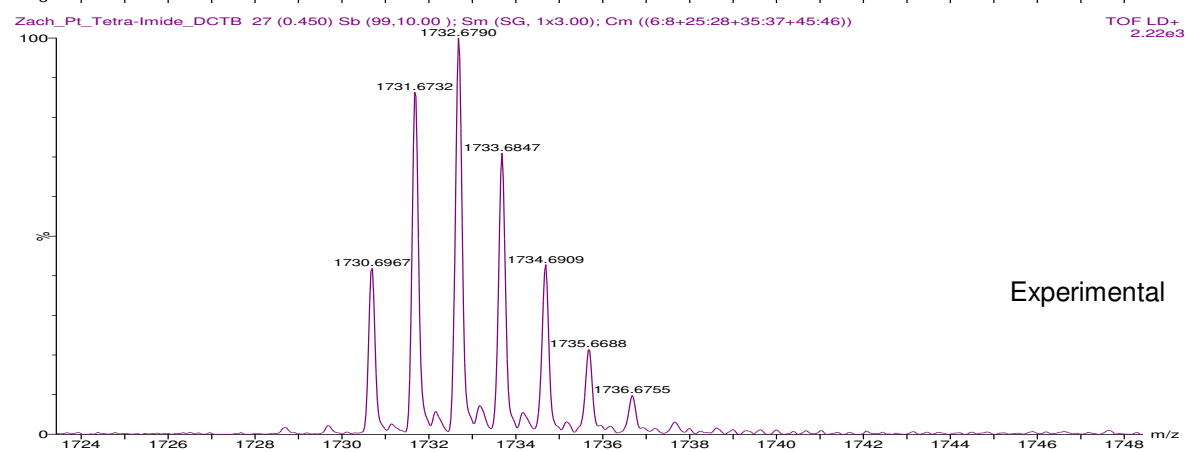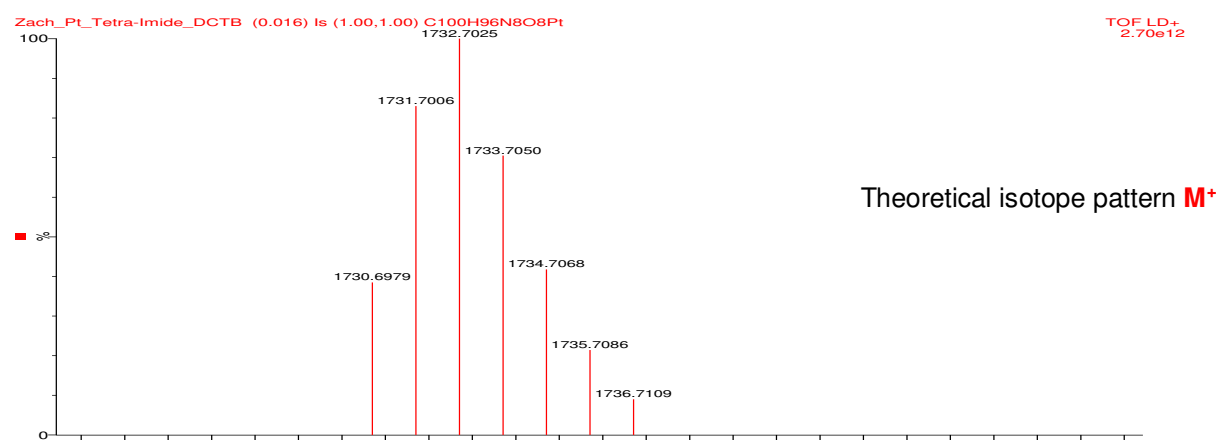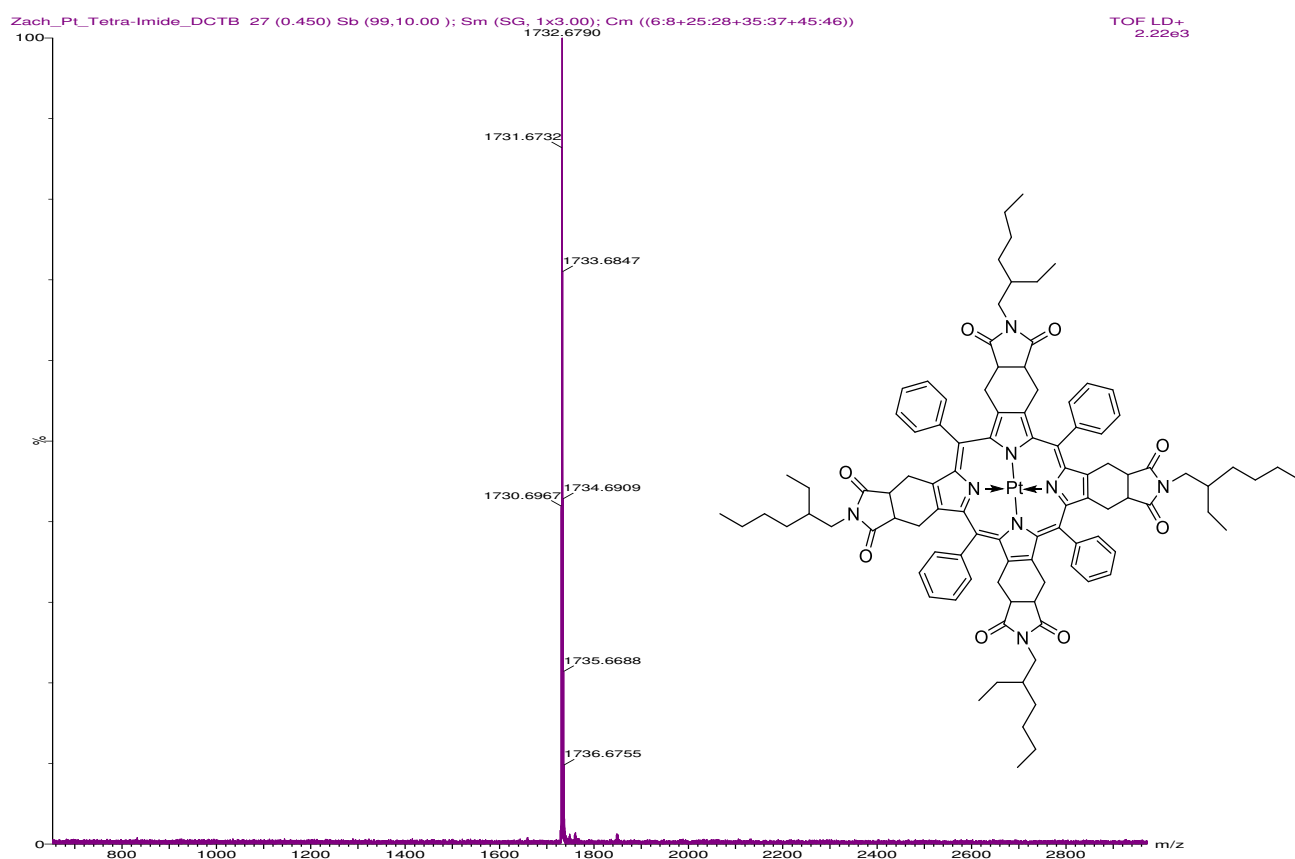
Figure S 5.75 Mass-Spectra of Pt(II) meso-tetraphenyltetrabenzo-1-(2-ethylhexyl)pyrrolidine-2,5-dione-porphyrin (Pt-T-I)
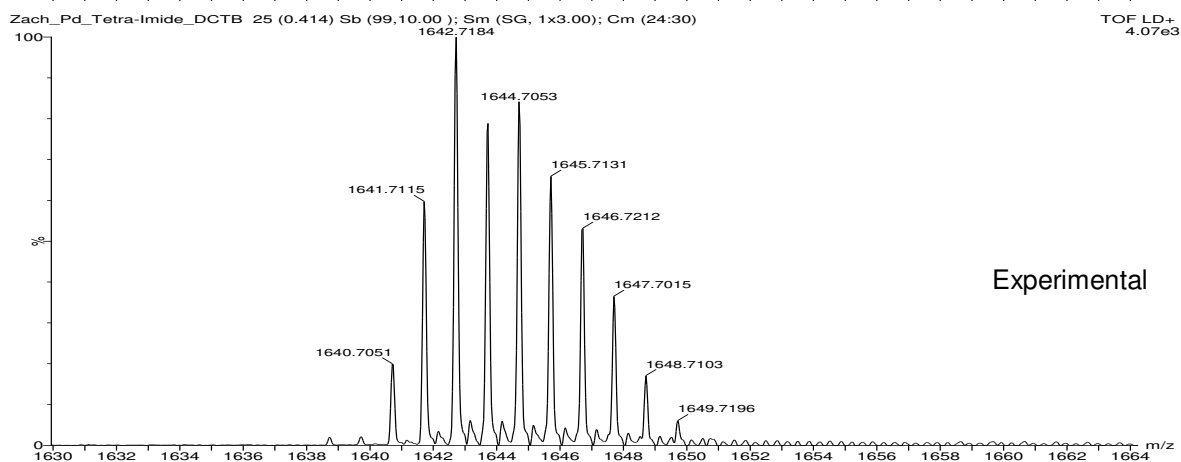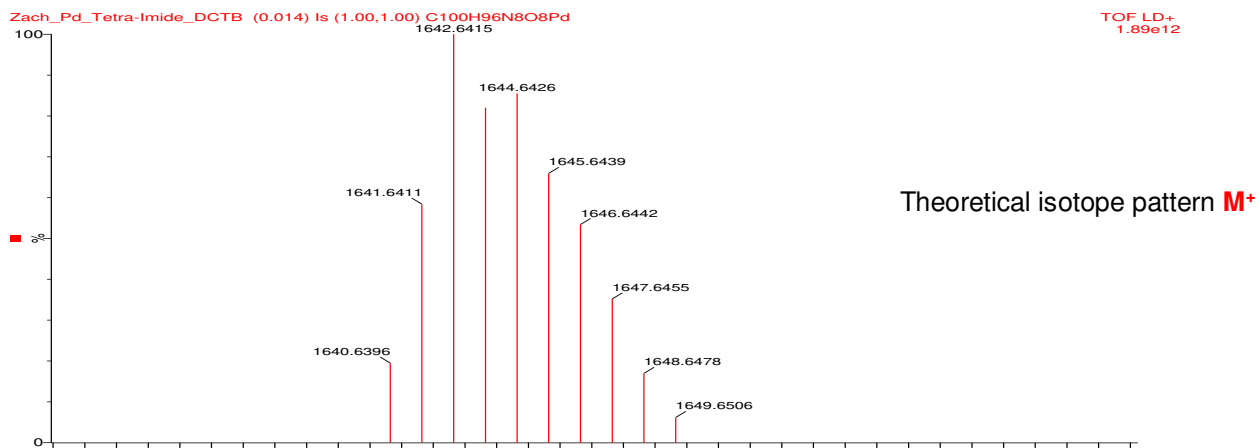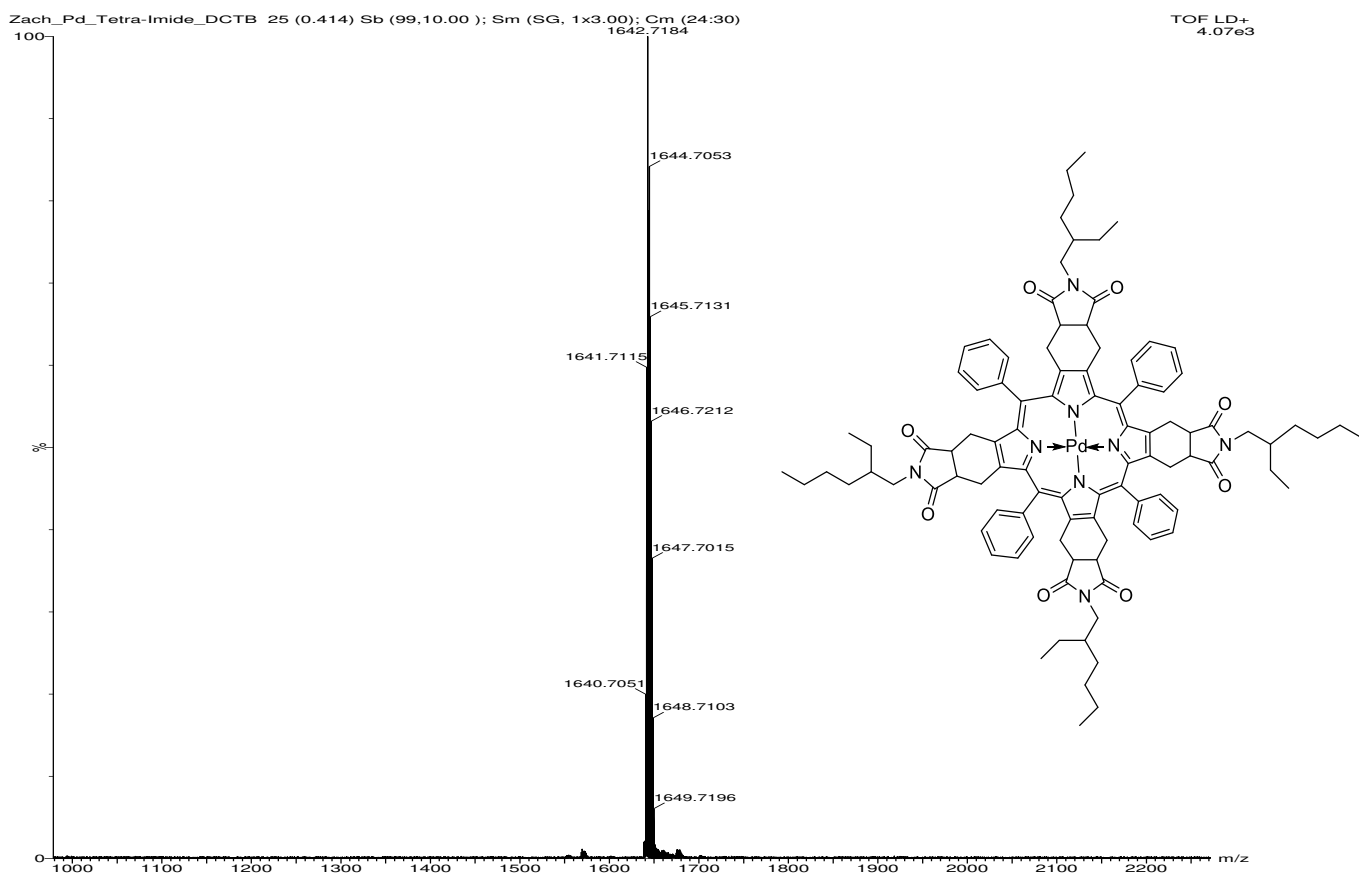
Figure S 5.76 Mass-Spectra of Pd(II) meso-tetraphenyltetrabenzo-1-(2-ethylhexyl)pyrrolidine-2,5-dione-porphyrin (Pd-T-I)

Chapter 6

NIR Phosphorescent Intramolecularly Bridged Benzo-porphyrins and Their Application in Oxygen-Compensated Glucose Optode
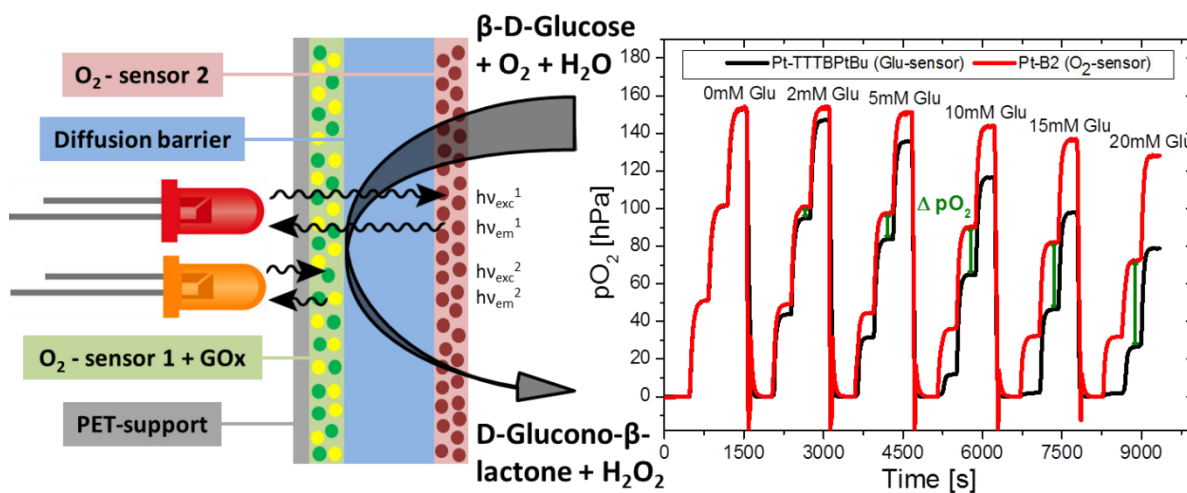
6 NIR Phosphorescent Intramolecularly Bridged Benzo-porphyrins and Their Application in Oxygen-Compensated Glucose Optode

Authors: Peter W. Zach,[a] Oliver T. Hofmann,[b] Ingo Klimant,[a] and Sergey M. Borisov[a*]

[a] Institute of Analytical Chemistry and Food Chemistry, Graz University of Technology, Stremayrgasse 9, 8010, Graz, Austria. E-mail: sergey.borisov@tugraz.at

[b] Institute of Solid State Physics, Graz University of Technology, Petersgasse 16, 8010, Graz, Austria.

6.1 Abstract

A glucose optode measuring the internal oxygen gradient is presented. The multilayer biosensor is composed of: (i) analyte-impermeable transparent support, (ii) first oxygen-sensing layer combined with an enzymatic layer, (iii) diffusion barrier, and (iv) second oxygen-sensing layer. To make this design suitable for measurement in subcutaneous tissue, a pair of NIR phosphorescent indicators with very different spectral properties is chosen. Combination of a conventional Pt(II) tetrabenzoporphyrin dye (absorption and emission maxima at 617 and 772 nm, respectively) used in the first layer and a new intramolecularly bridged Pt(II) complex (absorption and emission maxima at 673 and 872 nm, respectively) in the second layer enables efficient separation of both emission signals. This specially designed dye class is accessible via Scholl-reaction from tetraphenyltetrabenzoporphyrin complexes. For the first time, the new optode allows simultaneous glucose and oxygen measurement in a single spot and therefore accurate compensation of oxygen heterogeneities resulting from fluctuations in the tissue. The presented material covers the dynamic ranges from 0 to 150 hPa O_2 and from 0 to 360 mg/dL (20 mM) glucose (at 37 °C).

6.2 Introduction

Quantification of glucose is undoubtedly one of the most important analytical tasks today. Glucose is an important analyte in biotechnology, biology, and food industry, but sensing glucose in blood is definitely of highest interest.[1] Already in 2014, 8.5% of adults aged 18 years and older (422 million people) suffered from diabetes mellitus.[2] This chronic disease (inherited or acquired) is characterized by deficiency of the insulin production by the pancreas, or by the inefficiency of use of the produced insulin, resulting in a very high concentration of glucose in blood damaging especially the nerves and blood vessels.[2] Therefore, research on glucose measurement in blood in general and particularly on continuous glucose monitoring techniques (which in combination with an insulin pump makes artificial pancreas possible) has been a topic of great importance. Although electrochemical methods of glucose quantification are the most established ones,[3] optical sensing technology can provide an interesting alternative.[1] Optical sensors are cost-effective, enable simple design and handling, are easy to miniaturize and are free of electromagnetic interferences.[1] Several concepts of optical glucose monitoring make use of different types of recognition and utilize either natural receptors such as apoenzymes and lectins (concanavalin A)[4],[5] or synthetic ones like boronic acids.[6] Another large group of sensors is based on monitoring of the formation or consumption of metabolites during enzymatic oxidation of glucose catalysed by glucose oxidase (GOx).[7]–[9] These sensors benefit from very high selectivity for glucose over other saccharides.[7] Enzymatic glucose sensors based on oxygen optodes remain the most promising ones due high versatility and robustness of these transducers.[10] However, the signal of these sensors is affected by oxygen fluctuations in the sample, resulting in necessity of an additional detection of the oxygen partial pressure.[11] This, for instance, can be realized with help of an array of fiber-optic oxygen and glucose sensors.[11]–[13] Such solution, however, neither enables subcutaneous glucose monitoring through skin nor compensates for microheterogeneities in oxygen distribution in tissues.[14], [15]

Evidently, conventional UV-Vis indicators are not suitable for subcutaneous measurement due to strong light scattering by the tissue, efficient light absorption by skin pigments and haemoglobin as well as strong autofluorescence. Oxygen indicators operating in the so-called NIR optical window[16] overcome the above limitations.[17]–[19] Nacht et al.[20] reported a catheter-based array for continuous measurement of glucose and oxygen in subcutaneous tissue. Unfortunately, the overlapping absorption of the chosen indicator dyes (Pt(II) tetraphenylterabenzoporphyrin and aza-triphenyl-tetrabenzoporphyrin complexes) did not enable complete separation of the luminescence signals from the indicators. Additionally to the optical cross-talk, the glucose and the reference oxygen sensors were located at different parts of the infusion catheter, so that accurate compensation of the glucose measurement for oxygen variations was not possible.

Furthermore, such configuration results in much lower signal for the sensor positioned closer to the end of the catheter due to its deeper position in the tissue.

In respect to minimisation of the optical cross-talk, potential improvements are limited by availability of NIR oxygen indicators with acceptable photophysical properties. Particularly, despite large Stokes shift exceeding 200 nm, Pt(II) and Pd(II) aza-triphenyltetrabenzoporphyrins show only minor bathochromic shift of absorption compared to the parent tetraphenyltetrabenzoporphyrins.[21] On the other hand, the absorption maxima of the complexes of naphthoporphyrins[22] and their molecular hybrids with benzoporphyrins[23] can be extended up to 689 nm (Pt(II) tetraphenyltetranaphthoporphyrin),[24], [25] but these dyes suffer from poor solubility and photostability[23] and synthetic routes to analogues with improved properties are challenging.[26]

In this contribution we report a new class of NIR phosphorescent emitters which are accessible via one-step modification of Pt(II) tetraphenyltetrabenzoporphyrin (TPTBP) in an intramolecular rigidization via Scholl reaction. Remarkable photophysical properties of the new dyes enable subcutaneous sensing of glucose and oxygen in combination with Pt(II) tetraphenyltetrabenzoporphyrin derivatives. Moreover, in order to ensure an even more accurate compensation of the glucose sensors we realized a new sensing concept in which both oxygen indicators are located in different layers of a single material separated by the enzymatic layer and a diffusion barrier.

6.3 Experimental Section

6.3.1 Materials and Methods

1,2-dichlorobenzene, poly(styrene-co-divinylbenzene)-microspheres (PS-DVB, 8 µm particle size), 1,4-diazabicyclo[2.2.2octane] (DABCO), 1,4-butandiol, poly(tetrahydrofuran) (poly(THF), average Mn ~1000 g mol^{-1}), and glucose oxidase (EC 1.1.3.2 from Aspergillus niger, 200 U/mg) were ordered from Sigma-Aldrich and aluminum trichloride from Fluka. Molybdenum pentachloride, and di-n-butyldilauryltin were purchased from ABCR and Silica-gel 60 from Merck. Polystyrene (PS; Mw = 260000 g mol^{-1}) was obtained from Acros Organics. Hydrogels Hydromed D4 and D7 were obtained from AdvanSource (www.advbiomaterials.com). Sodium sulfate, sodium dihydrogen phosphate, and sodium chloride were from VWR. Dicyclohexylmethane-4,4'-diisocyanate was purchased from TCI. All the solvents and triethylamine (TEA) were from Roth; anhydrous ethanol was from Fisher Scientific. Nitrogen (99.999 % purity) was purchased from Air Liquide and oxygen (99.999 % purity) from Linde Gas GmbH. Poly(ethyleneterephthalate) (PET) support Melinex 505 was purchased from Pütz (Taunusstein, Germany). Pt(II) tetraphenyltetrabenzoporphyrin (Pt-TPTBP) and Pt(II) tetratolyl-tetra-(t-butyl)tetrabenzoporphyrin (Pt-TTTBPtBu) were synthesized analogously to the literature procedure,[27] with details provided in the supporting information.

Synthesis

Synthesis of Pt-B1

Pt-TPTBP (48.00 mg, 47.6 μmol, 1.00 equiv) was dissolved in 12 mL of 1,2-dichlorobenzene in a closed 25 mL round-bottom flask. Then aluminum trichloride (825.4 mg, 6.190 mmol, 130 equiv) was added and the solution was ultrasonicated for 10 minutes, resulting in a color change from dark-green to a brownish-red. The reaction mixture was quickly heated to 155 °C in an oil bath accompanied by bubbling of oxygen through the solution. The reaction progress was monitored via absorption spectra; the samples (10 μL) were neutralized with 30 μL of TEA and diluted with dichloromethane (DCM). After completion, the reaction mixture was allowed to cool to room temperature under continuous O_2-bubbling through the solution. The reaction mixture was neutralized with a DCM/TEA solution (40:1 v/v) and the obtained precipitate was removed via centrifugation. The solution was shaken with H_2O (3 x 100 mL) to remove the excess of TEA and dried over Na_2SO_4. The solvent was removed under reduced pressure. The product was purified via column chromatography (silica-gel) and subsequently washed with cyclohexane (3 x 15 mL), yielding a green solid. Yield: 4.3 mg, 9%.

UV-Vis absorption spectra: $\lambda_{max}/\varepsilon$ (nm/$M^{-1}cm^{-1}$) in toluene: 440/40.000; 455/45.000; 483/100.000; 606/7.000; 622/10.000; 641/20.000; 676/56.000.

MALDI: m/z: [M^+] $C_{60}H_{28}N_4Pt$: calcd, 999.1967; found, 999.1927.

Synthesis of Pt-B2

Synthesis and purification of Pt-B2 was performed analogously to modification of Pt-TPTBP (1), but Pt-TTTBPtBu (48.00 mg, 35.5 μmol, 1.00 equiv) was used instead. A total of 48 mL 1,2-dichlorobenzene and 614.8 mg (4.6 mmol, 130 equiv) of aluminum trichloride were used. Yield: Pt-B2 4.0 mg, 11%. Pt-B3 and Pt-B4 were isolated as by-products with yields of 3.1 mg (8%) and 1.2 mg (3%), respectively (supporting information).

UV-Vis absorption spectra: $\lambda_{max}/\varepsilon$ (nm/$M^{-1}cm^{-1}$) in toluene: 443/42.000, 457/47.000, 485/110.000, 619/12.000, 640/23.000, 673/58.000.

Synthesis of hydrophobic polyurethane (PU-THF)

Poly(THF) (1.00 g, 1.00 mmol, 1.00 equiv) and 1,4-butanediol (180 mg, 2.00 mmol, 2.00 equiv) were dissolved in 30 mL of dry THF in a Schlenk flask under argon atmosphere. The mixture was stirred for 10 minutes. Then dicyclohexylmethane-4,4'-diisocyanate (0.89 g, 3.4 mmol, 3.4 equiv), 1,4-diazabicyclo[2.2.2octane] (DABCO) (5 mg, 0.045 mmol), and di-n-butyldilauryltin (22 mg, 0.035 mmol) were added under argon atmosphere. The reaction mixture was heated to 60 °C and stirred for 16 h. After completion the reaction mixture was cooled down to room temperature and the polymer precipitated in 300 mL of a mixture of EtOH/H_2O (1:1 v/v), centrifuged, and then dried in the vacuum oven at 75 °C for 24 h. Yield: 1.4 g.

GPC Analysis: $M_n = 1.43*10^4$ g mol^{-1}; $M_w = 2.36*10^4$ g mol^{-1}; $M_w/M_n = 1.65$; $M_z = 3.38*10^4$ g mol^{-1}, $M_z/M_w = 1.43$

Immobilization of Pt-B2 and Pt-TTTBPtBu into PS-DVB beads

A solution of 2 mg Pt-B2 in 1 mL of chloroform ($CHCl_3$) was slowly added to a 20% (w/v) dispersion of PS-DVB microspheres in $CHCl_3$. The mixture was stirred for 10 min. Then, 3 mL of a mixture of ethanol (EtOH)/ H_2O (1:1 v/v) were slowly added, followed by 10 min of stirring. The solvent was removed under reduced pressure, the residue re-dissolved in a mixture of EtOH/H_2O (4:1 v/v), then centrifuged twice and dried in the vacuum oven at 75 °C for 24 h.

A solution of 5 mg Pt-TTTBPtBu in 1.5 mL of tetrahydrofuran (THF) was slowly added to a 20% (w/v) dispersion of PS-DVB beads in THF. The mixture was stirred for 10 min. Then 3 mL of H_2O were slowly added, followed by 10 min of stirring. The mixture was then poured into 40 mL H_2O, filtered, washed 5 times with a mixture of EtOH/H_2O (4:1 v/v) and dried in the vacuum oven at 75 °C for 24 h.

Preparation of the oxygen sensor

The sensor was prepared by knife-coating the "cocktail" containing 0.05 wt% Pt-B2 dye and 10 wt% of polystyrene in chloroform (HPLC-grade). After the coating, the sensor films were dried for 24 h at 60 °C to ensure complete removal of solvent.

Preparation of the glucose sensor

A total of 25 mg of Pt-TTTBPtBu-PS-DVB microspheres and 50 mg of D7 hydrogel were dispersed/dissolved in a mixture of 300 mg EtOH/H_2O (9:1 v/v) to obtain "cocktail 1". Meanwhile, 500 μL of EtOH were slowly added to the solution of 7.5 mg GOx in 150 μL H_2O, which immediately turned cloudy. The GOx precipitate was centrifuged twice, dispersed in 100 μL of EtOH/ H_2O (4:1 v/v) and mixed with the "cocktail 1" for 30 minutes. The mixture was knife coated on PET support (25 μm wet layer) that, prior to coating, was plasma-etched in an oxygen atmosphere using a Femto low-pressure plasma system form Diener electronic (Ebhausen, Germany). The solvents were allowed to evaporate at room temperature for 2 h. A total of 100 mg of PU-THF and 25 mg of D7 hydrogel were dissolved in 550 mg of EtOH/H_2O mixture (9:1 v/v) with the help of an ultrasonic finger (INULA; Vienna, Austria) using the following setting (duration overall: 3 min; amplitude: 15%; pulse on: 2 s; pulse off: 8 s), resulting in an opaque, colorless solution. This "cocktail" was then knife coated on the layer containing Pt-TTTBPtBu-PS-DVB and GOx (165 μm wet layer thickness). The foil was dried at RT for 3h and a "cocktail" containing 10 mg of Pt-B2-PS-DVB microspheres, 15 mg of D7 hydrogel, and 85 mg EtOH/H_2O (9:1 v/v) was coated to produce the last layer. After evaporation of the solvents at RT, the foil was stored in the

fridge at 5 °C in the darkness. The thickness of the knife-coated layers was determined using a Millimess 2000 Inductive Digital Comparator from Mahr (Göttingen, Germany).

6.3.2 Measurements

The absorption spectra were recorded on a CARY 50 UV-Vis spectrophotometer from Varian. Luminescence spectra were recorded on a FluoroLog® 3 spectrofluorometer from Horiba Scientific equipped with a NIR-sensitive R2658 photomultiplier from Hamamatsu. Determination of relative quantum yields was done according to Crosby and Demas using thesolution of BF_2 chelate of [5-(4-buthoxyphenyl)-3-phenyl-1H-pyrrol-2-yl][5-(4-buthoxyphenyl)-3-phenylpyrrol-2-ylidene]amine in chloroform as a reference (Φ = 36%).[28] All dye solutions were deoxygenated in a screw-cap cuvette (Hellma; Müllheim, Germany) by bubbling argon through the solution for 10 min. Photophysical studies in solutions were performed for the dye concentrations between 2 and $4 \cdot 10^{-6}$ mol·l^{-1}.

The phosphorescence decay times were acquired in frequency domain using a Firesting oxygen meter from PyroScience (Aachen, Germany) with a modulation frequency of 4 kHz. For characterization of the oxygen sensor, the composition of the gas was adjusted with a custom-build gas-mixing device based on mass-flow controllers from Voegtlin (Hamburg, Germany; www.red-y.com) by mixing compressed air, nitrogen, and oxygen. Temperatures were kept constant by a cryostat ThermoHaake DC50 (www.thermoscientific.de/home).

Characterization of the glucose sensor

All measurements were conducted in a climate cabinet (Memmert; Schwabach, Germany) at 37 °C. A round sensor spot with a diameter of 1 cm was punched out with a stamp (BGS technic; Wermelskirchen, Germany) and glued onto the inner wall of a 100 mL Schott bottle (2 cm above the bottle base) using vacuum fat. Optical read-out module BiLuMOS (described in detail by Nacht et al.[20] and modified here by replacing the 635 nm LED by a 670 nm LED) was positioned on the outer wall of the flask. The bottle was filled with 100 mL of a 150 mM NaCl solution, equipped with a magnetic stirring bar and sealed with a screw-cap containing a septum. A gas bubbler connected to a tube was positioned approximately 1 cm over the stirring bar, and an external thermometer (TFA Dostmann; Wertheim-Reicholzheim, Germany) and a cannula (for pressure compensation) were inserted through the septum. The solution was stirred at 500 rpm using a magnetic stirrer. The composition of the gas (0, 50, 100, and 150 hPa pO$_2$) was adjusted as described above for the oxygen sensor. The addition of the respective amount of glucose was done with a syringe and a cannula through the septum without opening the Schott bottle by using a glucose stock solution of 400 mg·mL^{-1}. Measurements were performed at 0, 2.4, 5.2, 10.5, 15 and 20 mM glucose.

6.4 Results and Discussion

6.4.1 Synthesis of the new NIR dyes

The precursors for the modification, Pt(II) complexes of tetraphenyltetrabenzoporphyrin (TPTBP) and its derivative bearing alkyl groups (Figure 6.1) are conveniently prepared in only three steps: formation of the Zn(II) complex in a modified template condensation,[27] demetalation in acidic media, and subsequent metalation of the metal-free porphyrin. Although the yields of Zn(II) porphyrins in template condensation are generally not high (5-10 %), the method allows preparation of the dyes on multi-gram scale due to simplicity of the procedure and low cost of starting compounds. In TPTBPs, the meso-positioned aryl substituents are out of plane and therefore they only very minor affect the spectral properties of the dyes (bathochromic shift of the absorption of the Q-band by about 5 nm for each aryl substituent). We perceived that intramolecular bridging will prevent the rotation of these substituents and result in significant extension of the conjugation. Scholl reaction (oxidative coupling of aromatic moieties in presence of Lewis acids such as $FeCl_3$, $AlCl_3$, $CuCl_2$)[29] was an evident choice to perform the intramolecular bridging of the benzoporphyrins. Although Scholl reaction is not common for fusion of different aromatic fragments in metal complexes, it is quite popular for modification of organic compounds.[30]–[32] Readily available Pt-TPTBP was chosen for the proof of concept experiments. The reaction was conducted in an oxidative atmosphere (bubbling O_2 through the solution) in 1,2-dichlorobenzene (bp 180.5 °C) in presence of $AlCl_3$ as Lewis acid. The resulted bridged product was isolated with the help of column chromatography. Mass spectra (Figure S 6.51, supporting information (ESI) revealed that the product Pt-B1 (Figure 6.1) was a mixture of four-fold bridged compounds resulting from the loss of 8 protons, namely the expected reaction product (MW of PtTPTBP - 8) and side products, which showed the substitution with chlorine and/or chlorobenzene originating from the solvent. Unfortunately, chromatographic separation of these products was not successful. The attempts to use alternative Lewis acids ($MoCl_5$, $FeCl_3$) as well as solvents (chloroform, nitromethane, 1,2-dichloroethane, trimethylbenzene, diphenylsulfone) to avoid the undesired side reactions were not successful. In order to elucidate the bridging pattern of the modified Pt-TPTBP compound, time-dependent density functional theory (TD-DFT) calculations were carried out for the precursor (Pt-TPTBP) and all the possible structures (Figure S 6.16, ESI). The calculations indicate (Figure S 6.17, ESI) that the structure presented in Figure 6.1 is the most likely from the 4-bridged species which can potentially form.
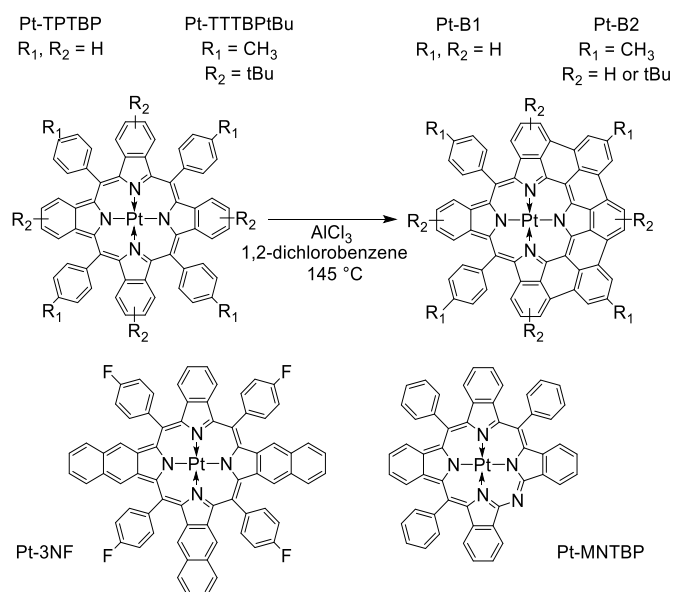
Figure 6.1 Chemical structures of precursors and bridged products Pt-B1 and Pt-B2 (according to DFT calculations), as well as reported Pt-3NF[23] and Pt-NTBP[21] NIR phosphorescent dyes.

The bridged product Pt-B1 has significantly lower solubility than the precursor, because the increased planarity of the macrocycle favours aggregation via π-π-stacking. This is an evident disadvantage for practical applications; thus we tried to overcome this limitation by introducing alkyl groups in different positions of the benzoporphyrin macrocycle. Surprisingly, only traces of the bridged product were observed upon reaction of the Pt(II) complex bearing 8 methyl groups in β-positions (Pt-TPTBPdM4; Figure S 6.3, ESI) as indicated by the absorption spectra (Figure S 6.20, ESI). Low reactivity of the octamethyl-complexes is likely to be due to sterical effects preventing formation of a stable intermediate with aluminum chloride. Another reason might be a good stabilization of the obtained cation by the two methyl-groups preventing the formation of the C-C bond. Scholl reaction of the Pt(II) meso-tetratolyltetrabenzoporphyrin complex bearing only four CH3 groups in the β-positions (Figure S 6.6, ESI) indicated the formation of 4-fold bridged species, but no sufficient conversion could be achieved due to rapid decomposition of the intermediates or the product (Figure S 6.22, SI). The attempts to perform 4-fold bridging with the corresponding Zn(II) complex (Zn-TTTBPmM4; Figure S 6.7, ESI) were not successful since only the mono-bridged complex was observed (Figures S 6.21 and S 6.48, ESI). In contrast to Scholl reaction with the more stable Pt(II) complex, the Zn(II) complex is demetalated in the presence of AlCl3 resulting in protonated metal-free porphyrin. Since the di-cation is less electron-rich compared to the metalated complex, the formation of further C-C bonds is prevented.

Finally, Scholl reaction with Pt(II) meso-tetra-tolyl-tetra-tert-butylbenzoporphyrin (Pt-TTTBPtBu) resulted in formation of the desired 4-bridged product (Pt-B2, Figure 6.1) along with two other differently bridged compounds (Pt-B3 and Pt-B4; (Figures S 6.14, S 6.53, S 6.54 and Table S 6.1, ESI), which were separated via column chromatography. The MS spectrum for bridged compound Pt-B2 (Figure S 6.52, ESI) indicates formation of 4-fold

bridged species, accompanied by the loss of 1-4 tBu groups due to Friedel-Crafts dealkylation and addition of chlorine atoms. The methyl groups in the meso-position of the porphyrin macrocycle are retained, which positively affects the solubility of the resulting products making immobilization of the dye into polymers possible. Due to acceptable solubility, the new Pt-B2 dye was chosen for further application in oxygen and glucose sensors.

6.4.2 Photophysical Properties

Intramolecular bridging of benzoporphyrin derivatives via Scholl reaction leads to a remarkable bathochromic shift of the Soret band and the Q-band (Figure 6.2, Table 6.1). In fact, for Pt-B1 shifts of about 50 and 60 nm are observed for the Soret and the Q-band, respectively. Absorption and emission properties of the 4-fold bridged products obtained from Pt-TPTBP (Pt-B1) and Pt-TTTBPtBu (Pt-B2) as well as emission quantum yield Φ and lifetime τ (Table 6.1 and S1, Figure S 6.14, ESI) are virtually identical, indicating that peripheral substitution with the alkyl groups neither affects the bridging pattern nor the spectral properties. Interestingly, the Soret and the most intense Q-band for the 4-fold substituted products Pt-B1 and Pt-B2 (Figures 6.2 and S 6.14, Table 6.1 and Table S 6.1, ESI) are much narrower than for the respective parent complexes (FWHM 185 and 480 cm^{-1} for Pt-B1 and Pt-TPTBP, respectively).
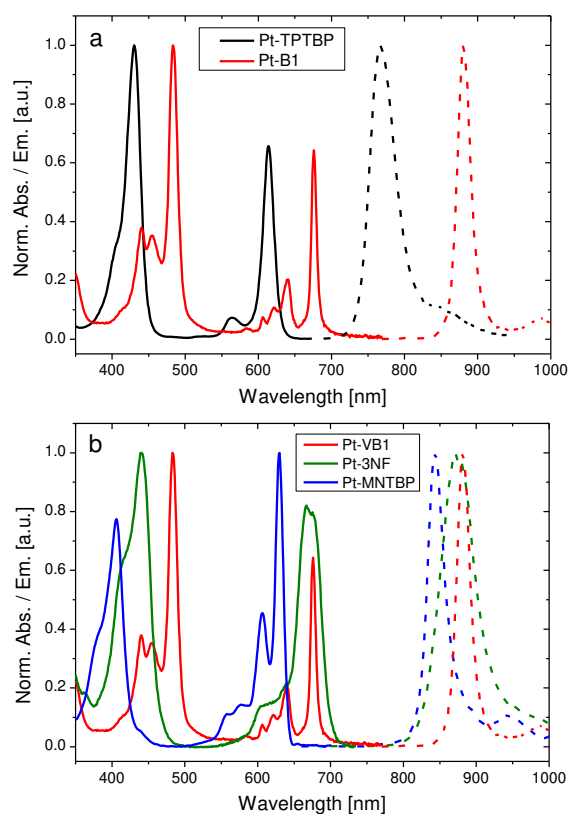
Figure 6.2 (a) Absorption (solid lines) and emission (dashed lines) spectra of Pt-TPTBP and bridged compound Pt-B1 in toluene. (b) Comparison of the spectral properties of Pt-B1 and reported NIR phosphorescent dyes with similar spectral properties.

127

The bridged compounds are phosphorescent at room temperature (Figure 6.2, Table 6.1). Similarly to the absorption, the phosphorescence band is bathochromically shifted compared to the parent compound and is narrower. The S_1-T_1 energy gap is almost not affected by the bridging (ΔE = 3300 and 3430 cm^{-1} for Pt-TPTBP and Pt-B1, respectively). Lower energy of the triplet state is responsible for decrease of the phosphorescence quantum yields, which are nevertheless sufficiently high (Table 6.1). The phosphorescence decay times are only slightly smaller than for Pt-TPTBP.

Table 6.1 Photophysical properties of Pt-B1 and the reported NIR metalloporphyrins in anoxic toluene.

Dye	Abs λ_{max} [nm], (ε(10^{-3} cm^{-1} M^{-1})	FWHM, Q band [cm^{-1}]*	Em λ_{max} [nm]	Stokes shift [cm^{-1}]	Φ [%]	τ [µs]
Pt-TPTBP	430 (205), 564 (16), 614 (136)	480	770	3300	20	47
Pt-B1	440 (40), 455 (45), 483 (100), 641 (20), 676 (56)	185	880	3430	7	39
Pt-3NF	441 (108), 618 (17.2), 635 (21.9), 667 (83.5), 678 (78.9)	775	870	3255	8	21
Pt-MNTBP	406 (106), 606 (61), 630 (137)	320	844	4025	9	40

*For the Q-band with the lowest energy

Overall, the new dyes show rather similar photophysical properties to those of Pt(II) meso-tetraphenyltrinaphthoporphyrin Pt-3NF (Figure 6.1) in respect to position of the Q-band and the phosphorescence peak, and the emission quantum yields (Table 6.1). However, the absorption and emission bands of the new dyes are significantly narrower, which is favourable for efficient spectral separation in the multi-parameter sensors. Both Pt-B1 and Pt-3NF show significantly longer absorption and emission maxima than the aza-triphenyltetrabenzoporphyrin Pt-MNTBP. Photostability of the new dye class with that of the naphthoporphyrins was also compared. Since the Soret band of Pt-3NF showed poor compatibility with the emission of the high power blue LED array, the analogous Pd(II) complex was used (λ_{max} = 456 nm). As can be observed (Figure 6.3) the photostability of these two classes of oxygen indicators is dramatically different. In fact, irradiation of air-saturated toluene solutions of both dyes by a high power 468 nm LED resulted in no visible degradation of Pt-B2 even after 90 min of continuous irradiation (Figure 6.3). In the same conditions, 32% of Pd-3NF was destroyed.
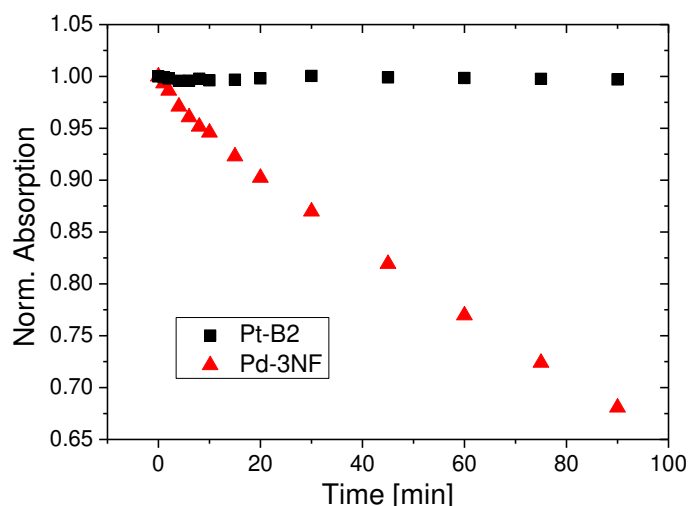
Figure 6.3 Photodegradation profiles for air-saturated toluene solutions of Pt-B2 and Pd-3NF (25 °C) upon irradia-tion with a high power blue LED array (λmax = 468 nm; 10.79 V, 0.689 A, 7.4 W, photon flux: 5000 μmol s^{-1} m^{-2})

Interestingly, intramolecular bridging of Pt-TTTBPtBu also results in formation of other species (Pt-B3 and Pt-B4, ESI) as by-products of Pt-B2. These phosphorescent dyes feature even longer absorption (> 710 nm) and emission maxima (> 950 nm) but significantly lower phosphorescence brightness (QYs ~ 1%). Although the structure of these compounds could not be elucidated so far, optimization of the synthetic procedure and variation of used precursors may possibly provide important insights in future.

6.4.3 Optical Oxygen Sensor

NIR phosphorescent properties of the new bridged dye enable preparation of a new generation of optical oxygen sensors. Pt-B2 was embedded into polystyrene as a model matrix (0.5 wt. % indicator). The phosphorescence is efficiently quenched by oxygen (Figure 6.4). Non-linear Stern-Volmer plots are typical for most oxygen sensors and can be explained by heterogeneity of the indicator environment.[33] "Two site model"[33] assumes localization of an oxygen-sensitive chromophore in two different microenvironments and adequately describes the non-linear Stern-Volmer plots even for the luminescence decay time:

$$\frac{\tau_0}{\tau} = \frac{1}{\frac{f}{1+K_{SV1}*pO2}+\frac{1-f}{1+(K_{SV1}*m)*pO_2}} \quad (1)$$

where τ_0 and τ are the lifetimes of the indicator in the absence and presence of oxygen, K_{SV1} and $K_{SV1} \cdot m$ are the Stern-Volmer constants for the first and the second site, respectively, and f is the fraction of the total emission for the first site.

The value of the Stern-Volmer constant K_{SV1} = 0.0145 hPa^{-1} is consistent with the oxygen permeability of polystyrene and the decay time of the indicator. Such sensitivity is optimal for measurement in physiologically relevant conditions. To obtain more sensitive sensors, matrixes with higher oxygen permeability (e.g. ethylcellulose, Ormosils, etc.) can be used.

Favorable spectral properties make the new oxygen sensor particularly promising for in vivo oxygen monitoring due to low attenuation of the red and NIR light in tissues. Moreover, the new material may become a valuable tool for pO_2 monitoring in photosynthetic systems since its long-wavelength emission, in contrast to that of the precursor, does not overlap with that of chlorophylls and bacteriochlorophylls (Figure S 6.15, ESI).
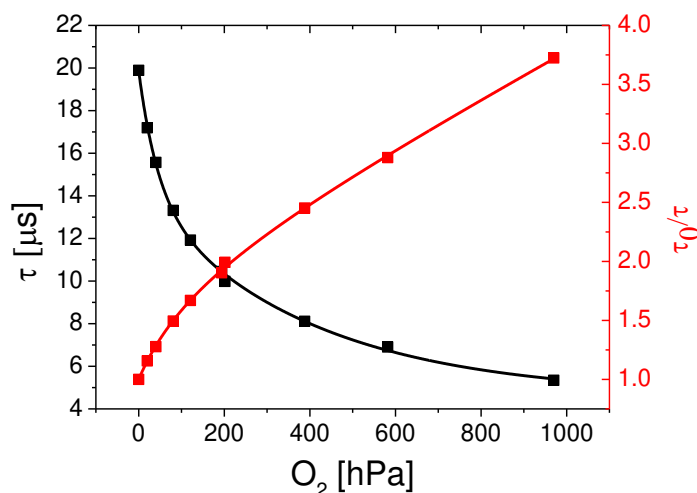
Figure 6.4 Lifetime and Stern-Volmer plot of Pt-B2 dissolved in polystyrene (25 °C).

6.4.4 Oxygen Flux Optode for Glucose Sensing

In contrast to the previous concepts[12], [15], [20] representing sensor arrays, the new glucose sensor consists of only one sensor element including three different layers (Figure 6.5). The general design follows the concept of the oxygen flux optode[34]–[37] with enzyme glucose oxidase (GOx) as an additional component. The ground layer is composed of the oxygen-sensitive microspheres (poly(styrene-co-divinylbenzene) doped with Pt(II) tetraphenyltetra(t-butyl)tetrabenzo-porphyrin, Pt-TTTBPtBu-PS-DVB) and microparticles of GOx dispersed in polyurethane hydrogel D7 and coated on a poly(ethylene terephthalate) (PET) support. Comparably large amount of GOx (9% wt) ensures stable performance of the material despite decrease of enzyme activity with time. In presence of glucose, oxygen is consumed:

$$\beta\text{-D-Glucose} + O_2 + H_2O \xrightarrow{\text{GOx}} \text{D-Glucono-}\beta\text{-lactone} + H_2O_2 \quad (2)$$
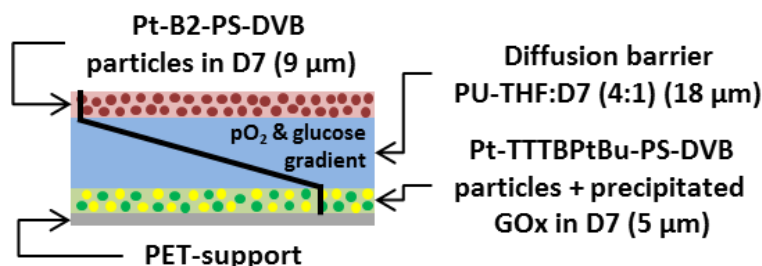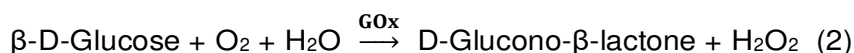
Figure 6.5 Cross-section of the oxygen flux optode. The thickness of the individual layers is an estimation since some intermixing occurs during the coating process.

The function of the second layer is to provide the diffusion barrier for glucose and oxygen in order to ensure that (i) response of the sensor is determined by mass transfer rather than by the reaction catalyzed by the enzyme i.e. all glucose molecules reaching the first layer will be converted to the products, and (ii) a gradient of oxygen is established as a result of this conversion. Overall, the layer allows to adjust the dynamic range of the sensor to physiologically relevant conditions. Unfortunately, none of the investigated commercially available materials was able to fulfill the required properties showing either too high or too low permeability for the reactants. For instance, polyurethane hydrogel D7 was found to be an adequate diffusion barrier only at 25 °C but failed at 37 °C due to higher degree of water uptake (35 and 46 % water uptake, respectively) and therefore higher permeability for glucose. To address this challenge, we prepared significantly more hydrophobic polyurethane (abbreviated as PU-THF) by polycondensation of 1,4-butandiol and polytetrahydrofuran with dicyclohexylmethane-4,4'-diisocyanate. The new polymer does not show a measurable water uptake and is therefore impermeable for glucose. Whereas it is not suitable as a diffusion barrier on its own, blending with hydrogel D7 allows for adjustment of the permeability in desired range.

The top layer consists of the second type of oxygen sensitive microspheres (Pt-B2 embedded into PS-DVB) dispersed in D7 hydrogel and is necessary for compensation of the O_2 cross-talk of the glucose biosensor. The obtained signal of the sensor corresponding to the glucose levels is the difference between the oxygen levels (ΔpO_2) measured by the two oxygen sensing elements. This difference originates from the oxygen gradient (Figure 6.5) in the diffusion barrier established due to oxygen depletion in the enzymatic reaction in the first layer.

6.4.5 Optical Setup for the Read-out of the Flux Sensor

Ideally, any optical cross-talk between the two indicators used in the flux optode should be avoided, but this condition was not fully met in the previously reported systems.[15], [20] Combination of the new NIR indicator with Pt-TTTBPtBu dye makes it possible to overcome this limitation. Interrogation of the optode is possible with previously reported compact phase fluorometer BiLuMOS equipped with two LEDs for excitation and two emission channels. Although the main components of the device are the same as described previously,[20] the excitation sources were adapted for the new set of indicators. In the optical setup (Figure 6.6), the Pt-B2-based material is excited with a 670 nm LED. Importantly, Pt-TTTBPtBu does not absorb at all at this wavelength. On the other hand, Pt-TTTBPtBu is efficiently excited with a 615 nm LED. Despite that Pt-B2 shows some absorption at this wavelength, the resulting minor cross-talk can be eliminated by using a band-pass filter in the Pt-TTTBPtBu detection channel (Figure 6.6). A simple long-pass filter (RG830; Schott, Austria) in combination with plastic filter ("Medium-Blue", Lee, USA) is

sufficient to isolate the emission of Pt-B2. In order to compensate for the lower brightness of Pt-B2 and achieve comparable signals, the concentration of the Pt-B2-PS-DVB microspheres was higher than Pt-TTTBPtBu-PS-DVB microbeads.
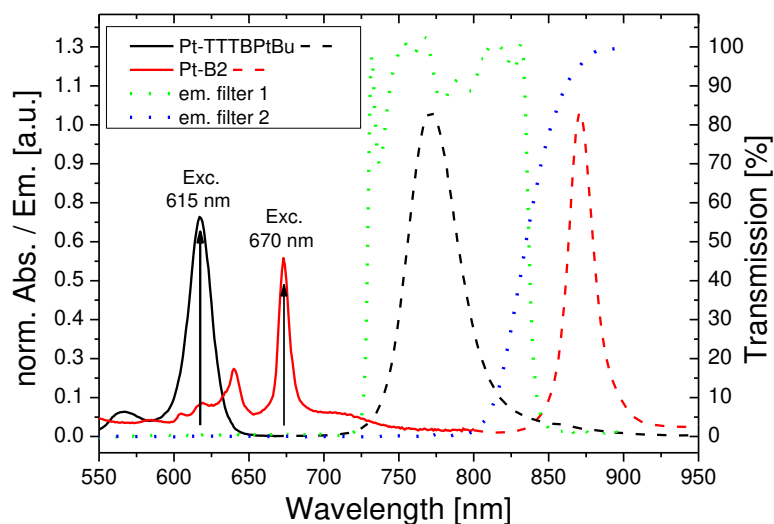
Figure 6.6 Spectral properties of the oxygen indicators used in the flux sensor and the optical components of the read-out device. Absorption spectra (solid lines) of Pt-TTTBPtBu and Pt-B2 and the peak excitation of the LEDs. Emission spectra (dashed lines) of the indicators and transmission spectra (dotted lines) of the respective optical filters.

6.4.6 Sensor Response

Figure 6.7a shows the response of the flux optode to glucose. Evidently, oxygen sensors in both layers show identical reading in the absence of glucose. As expected, pO_2 measured by the particles in the first layer decreases as the glucose concentration increases. On the other hand, the pO_2 readings in the upper layer are also minor affected by glucose. Nevertheless, even in the current design the difference between the two oxygen levels (ΔpO_2) measured by both bead types shows excellent correlation to glucose levels (Figure 6.7b) at pO_2 values from 50 to 150 hPa. Notably, the plots of ΔpO_2 versus C(glucose) are almost linear between 100 and 150 hPa pO_2. According to Simonsen et al., the mean intercellular subcutaneous pO_2 is 74.8 ± 5.2 hPa, with potential fluctuations up to ± 21 hPa,[38] which is within the range covered by the new optode. In respect to glucose concentrations, the new sensor covers the physiologically relevant range from hypoglycemia (<40 mg/dL; 2.4 mM) to hyperglycemia (>140 mg/dL; 7.8 mM).

The new sensor operates fully reversibly with ΔpO_2 returning to original values as the glucose is removed. Homogeneity of the multi-layered sensor as well as the stability of the components proved to be sufficient for practical applications. In fact, the mean values in the calibration plots presented in Figure 6.7b were acquired for three different sensor spots originating from the same foil over a period of three weeks (foil was stored in a fridge at 5 °C in darkness). Moreover, the long-term stability of the glucose sensor in solution at 37 °C was investigated over a period of 18 days

 (Figures S 6.29 and S 6.30, ESI). The sensor remains fully operable during this period, which indicates that no significant degradation in enzyme activity or leaching of the enzyme occurs. Interestingly, the calibration curve slightly changes in the first 5 days, which is likely to be due to rearrangement of the components in the diffusion barrier affecting its permeability for glucose and oxygen. After this initial period of time the sensor performance is remarkably stable over the next two weeks, suggesting that measurement for even longer periods will also be possible. Although the enzymatic activity is known to be pH-dependent, the response of the sensor is not affected by pH (Figure S 6.26, ESI). Evidently, the sensor can tolerate some change in enzyme activity caused by pH changes, enzyme degradation and other factors due to the fact that the enzyme is present in a large excess compared to the amount needed for conversion of the glucose molecules reaching the enzymatic layer.

Temperature affects the response of all chemo- and biosensors, and the new flux optode is no exception. The origin of the temperature crosstalk is rather complex, affecting not only the diffusion rate of glucose and oxygen, but also the rate of the enzyme-catalysed reaction as well as the sensitivity of the oxygen transducer.[20] Both oxygen sensing components show typical minor response to temperature which affects the τ_0 (decreases with temperature) and the K_{SV} (more efficient quenching at higher temperatures, Table S 6.2 and Figure S 6.23, ESI). These effects are known and can be compensated for. As mentioned above, effect of temperature on the enzymatic activity is likely not to affect the sensor response. We observed a slightly increase of (pO$_2$ values at 32 °C compared to 37 and 42 °C (Figure S 6.28, ESI) attributed to lower oxygen permeability of the diffusion barrier at lower temperatures. In fact, when the glucose sensor (no upper oxygen-sensing layer) was exposed to the rapid changes in the pO$_2$ (0 - 200 hPa, no added glucose) the dynamic response times t_{90} decreased with temperature (15.2, 11.9, and 10.7 s for 32, 37 and 42 °C, respectively). Although the dynamic range of the sensor can be further adjusted by variation of the thickness of the diffusion barrier (higher dynamics in ΔpO$_2$ for thicker layers, Figure S 6.24, ESI), or its composition, the presented design already demonstrates suitability of the new sensing concept for oxygen-compensated glucose sensing in physiologically relevant range.
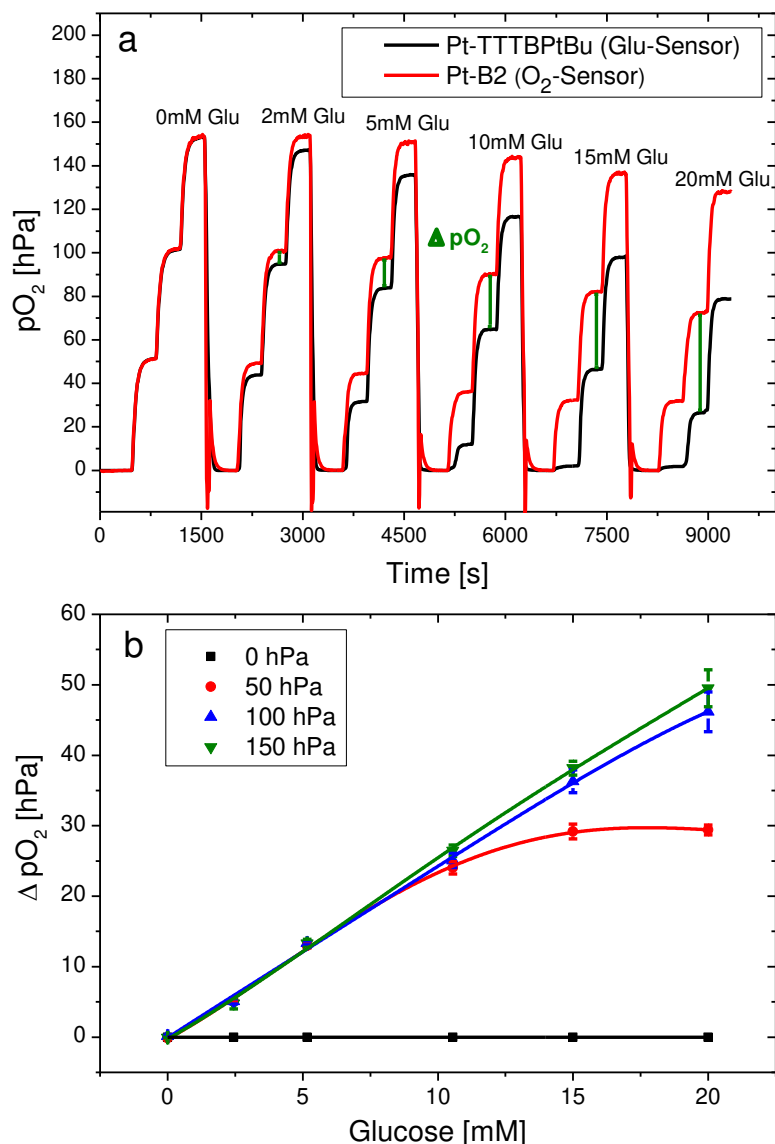
Figure 6.7 (a) Dynamic response of the sensor element to glucose from 0 to 20 mM in a continuous-flow measurement at different pO₂ from 0 to 150 hPa pO₂ at 37 °C. (b) Calculated mean ΔpO₂ values for 3 independent measurements (3 different sensor spots over a period of 3 weeks).

6.4.7 Conclusions

We presented a new concept of glucose quantification which is based on the use of a single optode composed of two optical oxygen sensing layers. In course of the enzymatic reaction, oxygen in the lowest layer located in proximity of the support and the enzyme is depleted, giving rise to the difference of the pO_2 values measured by the two sensing components. To make the concept suitable for subcutaneous sensing of glucose, a pair of NIR phosphorescent indicators is selected to achieve complete spectral separation of the luminescence signals. Whereas the first indicator is a conventional Pt(II) benzoporphyrin dye, the second dye belongs to a new group of phosphorescent emitters. A photostable bridged benzoporphyrin obtained via intramolecular Scholl reaction features absorption and

NIR phosphorescence which are bathochromically shifted by about 60 nm and 110 nm, respectively, compared to the parent benzoporphyrin dye. By careful selection of the indicator chemistry and the composition of the diffusion barrier based on new polyurethane PU-THF, we were able to demonstrate oxygen-compensated glucose sensing under physiological conditions in the dynamic range of interest, covering potential hypo- and hyperglycemic events. Therefore, the new approach is expected to be of high potential for development of new generation of glucose optodes for diabetic patients. It is also likely to be of interest for design of other types of enzymatic sensors based on oxygen transducers, such as oxygen-compensated lactate sensors.

Associated Content

The Supporting Information is available free of charge on the ACS Publications website at DOI: 10.1021/acs.analchem.7b04760

Synthesis, photophysical properties, DFT calculations, temperature dependency of dyes and sensor, stability tests, ^{1}H and ^{13}C NMR and mass spectra (PDF).

Acknowledgements

6.4.8 References

[1] M.-S. Steiner, A. Duerkop, and O. S. Wolfbeis, "Optical methods for sensing glucose," *Chem. Soc. Rev.*, vol. 40, no. 9, pp. 4805–4839, Aug. 2011.
[2] "WHO | Diabetes," *WHO*. [Online]. Available: http://www.who.int/mediacentre/factsheets/fs312/en/. [Accessed: 07-Nov-2017].
[3] A. Heller and B. Feldman, "Electrochemical Glucose Sensors and Their Applications in Diabetes Management," *Chem. Rev.*, vol. 108, no. 7, pp. 2482–2505, Jul. 2008.
[4] B. M. Cummins, J. T. Garza, and G. L. Coté, "Optimization of a Concanavalin A-Based Glucose Sensor Using Fluorescence Anisotropy," *Anal. Chem.*, vol. 85, no. 11, pp. 5397–5404, Jun. 2013.
[5] P. W. Barone and M. S. Strano, "The use of Single-Walled Carbon Nanotubes for Optical Glucose Detection," in *In Vivo Glucose Sensing*, John Wiley & Sons, Inc., 2009, pp. 317–329.
[6] H. S. Mader and O. S. Wolfbeis, "Boronic acid based probes for microdetermination of saccharides and glycosylated biomolecules," *Microchim. Acta*, vol. 162, no. 1–2, pp. 1–34, Jul. 2008.
[7] A. Pasic, H. Koehler, L. Schaupp, T. R. Pieber, and I. Klimant, "Fiber-optic flow-through sensor for online monitoring of glucose," *Anal. Bioanal. Chem.*, vol. 386, no. 5, pp. 1293–1302, Nov. 2006.
[8] M. Marazuela and M. Moreno-Bondi, "Fiber-optic biosensors – an overview," *Anal. Bioanal. Chem.*, vol. 372, no. 5–6, pp. 664–682, Mar. 2002.
[9] S. M. Borisov and O. S. Wolfbeis, "Optical Biosensors," *Chem. Rev.*, vol. 108, no. 2, pp. 423–461, Feb. 2008.
[10] X. Wang and O. S. Wolfbeis, "Optical methods for sensing and imaging oxygen: materials, spectroscopies and applications," *Chem. Soc. Rev.*, vol. 43, no. 10, pp. 3666–3761, Apr. 2014.
[11] L. Li and D. R. Walt, "Dual-Analyte Fiber-Optic Sensor for the Simultaneous and Continuous Measurement of Glucose and Oxygen," *Anal. Chem.*, vol. 67, no. 20, pp. 3746–3752, Oct. 1995.

[12] A. Pasic, H. Koehler, I. Klimant, and L. Schaupp, "Miniaturized fiber-optic hybrid sensor for continuous glucose monitoring in subcutaneous tissue," *Sens. Actuators B Chem.*, vol. 122, no. 1, pp. 60–68, Mar. 2007.

[13] O. S. Wolfbeis, I. Oehme, N. Papkovskaya, and I. Klimant, "Sol-gel based glucose biosensors employing optical oxygen transducers, and a method for compensating for variable oxygen background," *Biosens. Bioelectron.*, vol. 15, no. 1–2, pp. 69–76, Mar. 2000.

[14] M. Rumpler, M. Hajnsek, P. Baumann, T. R. Pieber, and I. Klimant, "Monitoring tissue oxygen heterogeneities and their influence on optical glucose measurements in an animal model," *J. Clin. Monit. Comput.*, pp. 1–4, Jun. 2017.

[15] M. Rumpler *et al.*, "First application of a transcutaneous optical single-port glucose monitoring device in patients with type 1 diabetes mellitus," *Biosens. Bioelectron.*, vol. 88, no. Supplement C, pp. 240–248, Feb. 2017.

[16] R. Weissleder, "A clearer vision for *in vivo* imaging," *Nat. Biotechnol.*, vol. 19, no. 4, p. nbt0401_316, Apr. 2001.

[17] S. A. Vinogradov and D. F. Wilson, "Metallotetrabenzoporphyrins. New phosphorescent probes for oxygen measurements," *J. Chem. Soc. Perkin Trans. 2*, no. 1, p. 103, 1995.

[18] J. Napp *et al.*, "Targeted Luminescent Near-Infrared Polymer-Nanoprobes for In Vivo Imaging of Tumor Hypoxia," *Anal. Chem.*, vol. 83, no. 23, pp. 9039–9046, Dec. 2011.

[19] Y.-E. Koo Lee *et al.*, "Near Infrared Luminescent Oxygen Nanosensors with Nanoparticle Matrix Tailored Sensitivity," *Anal. Chem.*, vol. 82, no. 20, pp. 8446–8455, Oct. 2010.

[20] B. Nacht *et al.*, "Integrated catheter system for continuous glucose measurement and simultaneous insulin infusion," *Biosens. Bioelectron.*, vol. 64, pp. 102–110, Feb. 2015.

[21] S. M. Borisov, G. Zenkl, and I. Klimant, "Phosphorescent Platinum(II) and Palladium(II) Complexes with Azatetrabenzoporphyrins--New Red Laser Diode-Compatible Indicators for Optical Oxygen Sensing," *ACS Appl. Mater. Interfaces*, vol. 2, no. 2, pp. 366–374, Feb. 2010.

[22] O. S. Finikova, S. E. Aleshchenkov, R. P. Briñas, A. V. Cheprakov, P. J. Carroll, and S. A. Vinogradov, "Synthesis of Symmetrical Tetraaryltetranaphtho[2,3]porphyrins," *J. Org. Chem.*, vol. 70, no. 12, pp. 4617–4628, May 2005.

[23] F. Niedermair *et al.*, "Tunable Phosphorescent NIR Oxygen Indicators Based on Mixed Benzo- and Naphthoporphyrin Complexes," *Inorg. Chem.*, vol. 49, no. 20, pp. 9333–9342, Sep. 2010.

[24] J. R. Sommer *et al.*, "Efficient near-infrared polymer and organic light-emitting diodes based on electrophosphorescence from (tetraphenyltetranaphtho[2,3]porphyrin)platinum(II)," *ACS Appl. Mater. Interfaces*, vol. 1, no. 2, pp. 274–278, Feb. 2009.

[25] R. Kumar *et al.*, "Near-Infrared Phosphorescent Polymeric Nanomicelles: Efficient Optical Probes for Tumor Imaging and Detection," *ACS Appl. Mater. Interfaces*, vol. 1, no. 7, pp. 1474–1481, Jul. 2009.

[26] A. V. Cheprakov and M. A. Filatov, "The dihydroisoindole approach to linearly annelated π-extended porphyrins," *J. Porphyr. Phthalocyanines*, vol. 13, no. 03, pp. 291–303, Mar. 2009.

[27] L. H. Hutter, B. J. Müller, K. Koren, S. M. Borisov, and I. Klimant, "Robust optical oxygen sensors based on polymer-bound NIR-emitting platinum(II)–benzoporphyrins," *J. Mater. Chem. C*, vol. 2, no. 36, pp. 7589–7598, Aug. 2014.

[28] P. W. Zach, S. A. Freunberger, I. Klimant, and S. M. Borisov, "Electron-Deficient Near-Infrared Pt(II) and Pd(II) Benzoporphyrins with Dual Phosphorescence and Unusually Efficient Thermally Activated Delayed Fluorescence: First Demonstration of Simultaneous Oxygen and Temperature Sensing with a Single Emitter," *ACS Appl. Mater. Interfaces*, vol. 9, no. 43, pp. 38008–38023, Nov. 2017.

[29] P. Rempala, J. Kroulík, and B. T. King, "Investigation of the Mechanism of the Intramolecular Scholl Reaction of Contiguous Phenylbenzenes," *J. Org. Chem.*, vol. 71, no. 14, pp. 5067–5081, Jun. 2006.

[30] P. Rempala, J. Kroulík, and B. T. King, "A Slippery Slope: Mechanistic Analysis of the Intramolecular Scholl Reaction of Hexaphenylbenzene," *J. Am. Chem. Soc.*, vol. 126, no. 46, pp. 15002–15003, Nov. 2004.

[31] S. R. Waldvogel and S. Trosien, "Oxidative transformation of aryls using molybdenum pentachloride," *Chem. Commun.*, vol. 48, no. 73, p. 9109, 2012.

[32] Y. Lu and J. S. Moore, "Semi-fused hexaphenyl hexa-peri-hexabenzocoronene: a novel fluorophore from an intramolecular Scholl reaction," *Tetrahedron Lett.*, vol. 50, no. 28, pp. 4071–4077, Jul. 2009.

[33] E. R. Carraway, J. N. Demas, B. A. DeGraff, and J. R. Bacon, "Photophysics and photochemistry of oxygen sensors based on luminescent transition-metal complexes," *Anal. Chem.*, vol. 63, no. 4, pp. 337–342, Feb. 1991.

[34] G. A. Holst, T. Köster, E. Voges, and D. W. Lübbers, "FLOX—an oxygen-flux-measuring system using a phase-modulation method to evaluate the oxygen-dependent fluorescence lifetime," *Sens. Actuators B Chem.*, vol. 29, no. 1, pp. 231–239, Oct. 1995.

[35] D. W. Lübbers, "Chemical in vivo monitoring by optical sensors in medicine," *Sens. Actuators B Chem.*, vol. 11, no. 1, pp. 253–262, Mar. 1993.

[36] M. Stücker *et al.*, "The Transepidermal Oxygen Flux from the Environment is in Balance with the Capillary Oxygen Supply," *J. Invest. Dermatol.*, vol. 114, no. 3, pp. 533–540, Mar. 2000.

[37] P. Hartmann, W. Ziegler, G. Holst, and D. W. Lübbers, "Oxygen flux fluorescence lifetime imaging," *Sens. Actuators B Chem.*, vol. 38, no. 1, pp. 110–115, Jan. 1997.

[38] L. Simonsen, J. Bülow, and J. Madsen, "Adipose tissue metabolism in humans determined by vein catheterization and microdialysis techniques," *Am. J. Physiol.*, vol. 266, no. 3 Pt 1, pp. E357-365, Mar. 1994.

6.5 Supporting Information

6.5.1 Synthesis

4,5-dimethylphthalonitrile

The reaction was conducted according to literature Ivanov et al. (*Russ. Chem. Bull.*, Bd. 57, Nr. 8, S. 1665–1670, Aug. 2008). A mixture of 1,2-dibromo-4,5-dimethylbenzene (0.50 g, 1.894 mmol, 1.00 eq), copper(I) cyanide (967.0 mg, 10.80 mmol, 5.70 eq) and copper(I) iodide (36.10 mg, 189.4 µmol, 0.10 eq) was dissolved in dry dimethylformamide (7 mL) in a Schlenk-flask, producing a milky green solution. The reaction mixture was then refluxed for 5 hours. After cooling down to room temperature, the dark-green reaction mixture was poured into a stirred iron(III) chloride solution (1.751 g, 10.80 mmol, 5.70 eq) in 100 mL water. The resulting precipitate was filtered of via vacuum filtration, washed with dest. H_2O (5 x 50 mL) and extracted with dichloromethane (150 mL). The combined organic phases were again washed with dest. H_2O (3 x 50 mL) to remove dimethylformamide, dried over Na_2SO_4 and finally the solvent was removed under reduced pressure, yielding a light yellow solid. The reaction progress was controlled via TLC cyclohexane:ethylacetate (5:1). Yield: Yellow solid, 248.5 mg, 84%

^{1}H NMR (300 MHz, Chloroform-*d*) δ 7.55 (s, 2H), 2.38 (s, 6H).

Zinc (II) meso-tetra-phenyl-tetra(di-methyl)benzoporphyrin (Zn-TPTBPdM₄)

4,5-dimethylphthalonitrile (1.110 g, 7.108 mmol, 4.00 eq), 2-phenylacetic acid (1.452 g, 10.66 mmol, 6.00 eq), zinc phenylacetate (600.0 mg, 1.777 mmol, 1.00 eq) were mixed together and homogenized with a ceramic pestle in a mortar and approximately 700 mg of the reaction mixture were weighed in each 3.5 mL glass vial equipped with a stirring bar. After sealing the vials with a metal cap they were placed on a heating block preheated at 250 °C. The mixture was heated to 280 °C and stirred for 40 min at this temperature. Afterwards the vials were cooled down to room temperature and then smashed with a hammer. The reaction
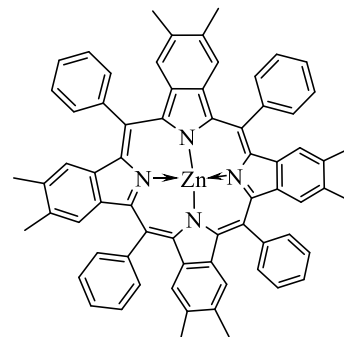
Figure S 6.1. Zn-TPTBPdM₄

mixture was dissolved in 200 mL acetone and put on the ultrasonic bath for ten minutes. The bits of glass were separated via vacuum filtration and the solution was concentrated under reduced pressure to an approximate volume of 60 mL. The concentrated reaction mixture was added dropwise to a 400 mL solution of ethanol:H_2O (1:1 + 10 mL saturated $NaHCO_3$ + 10 mL brine), producing a dark-green precipitate, which was then filtered off under vacuum. Afterwards the residue was washed with an ethanol:H_2O solution (1:2; 3 x 50 mL) and dried in the vaccum oven at 60 °C. The crude product was purified via column chromatography first on silica-gel (cyclohexane:ethylacetate 10:1) and then on aluminium oxide (cyclohexane:ethylacetate, 12:1) as stationary phase. The product containing fractions were determined via absorption spectra and the product was finally dried in the vacuum oven at 60°C. The obtained solid was washed with

cyclohexane on the ultrasonic bath for 10 minutes. This process was repeated three times. The dye was obtained after the removal of the light-green-brownish supernatant via centrifugation. Yield: dark green solid, 105.6 mg, 6%.

UV-VIS absorption spectra. $\lambda_{max}/\varepsilon$ (nm, $M^{-1}cm^{-1}$) in toluene: 457/ 219.400; 607/ 10.400; 654/ 71.400

^{1}H NMR (300 MHz, Benzene-d6) δ 8.41 – 8.28 (m, 8H), 7.78 – 7.59 (m, 12H), 7.31 (s, 8H), 2.27 (s, 24H).

MALDI: m/z: [M$^+$]; $C_{68}H_{52}N_4Zn$, calc. for 988.3483; found: 988.3426

Meso-tetra-phenyl-tetra(di-methyl)benzoporphyrin (H₂-TPTBPdM₄)

Zn-TPTBPdM$_4$ (50.00 mg, 50.48 μmol, 1.00 eq) was dissolved in 60 mL dichloromethane; 10 mL of 4 M HCl were slowly added. The resulting protonated ligand could be determined via absorption spectra in acetone (λ_{max} 499 nm). The acid was removed by shaking the organic phase with with dest. H$_2$O (2 x 30 mL) and then with saturated NaHCO$_3$-solution (2 x 30 mL) until only free ligand was observed in the absorption spectra. Finally the organic layer was once more washed with dest. H$_2$O (30 mL), dried over Na$_2$SO$_4$ and the solvent was removed under reduced pressure. Yield: dark green solid, 39.8 mg, 85%
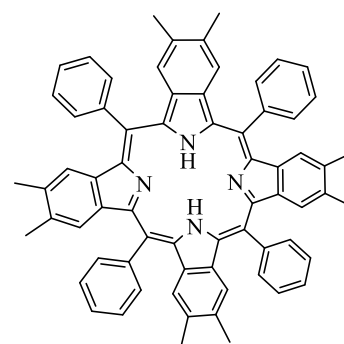
Figure S 6.2. H₂-TPTBPdM₄

UV-VIS absorption spectra. $\lambda_{max}/\varepsilon$ (nm, $M^{-1}cm^{-1}$) in toluene: 467/ 146.000; 593/ 8.100; 637/ 18.300; 699/ 7.100

Platinum (II) meso-tetra-phenyl-tetra(di-methyl)benzoporphyrin (Pt-TPTBPdM₄)

H$_2$-TPTBPdM$_4$ (20.0 mg, 21.57 μmol, 1.00 eq) was dissolved in 1,2,4-trimethylbenzene (30 mL) in a 2-neck-round bottom flask and heated to 145 °C, while bubbling N$_2$ through the reaction mixture. Then Pt(C$_6$H$_5$CN)$_2$Cl$_2$ (15.3 mg, 32.36 μmol, 1.50 eq) was added slowly in small portions (5 x 0.3 eq pre-dissolved in 1,2,4-trimethylbenzene) from a pre-heated addition funnel (100°C) over 3 hours. The reaction progress was monitored via absorption spectra (solvent: acetone). After complete conversion the reaction mixture was cooled down to room temperature, the metallic platinum

Figure S 6.3. Pt-TPTBPdM₄

removed via centrifugation and the solvent was removed under reduced pressure at 80 °C. The crude product was finally purified via column chromatography (silica-gel, cyclohexane:dichloromethane, 3:1). The product containing fractions were determined via absorption spectra, yielding a dark green solid. Yield: dark green solid, 13.5 mg, 56%

UV-VIS absorption spectra: λ_{max}/relative intensity (nm) in toluene: 428/1.00; 568/ 0.0843; 619/ 0.7079

MALDI: m/z: [M$^+$]; $C_{68}H_{52}N_4Pt$, calc. for 1120.3861; found: 1120.3761

Zinc (II) meso-tetra(4-tolyl)tetrabenzoporphyrin (Zn-TTolTBP)

The synthesis was performed analogously to (Zn-TPTBPdM₄) but phthalonitrile (9.11 g, 71.10 mmol, 4.00 eq), 2-(p-tolyl)acetic acid (13.35 g, 88.87 mmol, 5.00 eq) and zinc-4-tolylacetate (6.50 g, 17.77 mmol, 1.00 eq) were used instead. The crude product was purified via column chromatography, first on aluminium oxide (cyclohexane: ethylacetate, 4:1) and then on silica-gel (cyclohexane:ethylacetate, 6:1) as stationary phase. The product containing fractions were determined

Figure S 6.4. Zn-TolTTBP

via absorption spectra. The product was finally dried in the vacuum oven at 60 °C. The product washed with cyclohexane on the ultrasonic bath for 10 minutes. This process was repeated for three times. The insoluble dark-green sediment was obtained after the removal of the light-green-brownish supernatant via centrifugation. Yield: dark green solid, 1.30 g, 8%.

UV-VIS absorption spectra. $\lambda_{max}/\varepsilon$ (nm, M-1cm-1) in toluene: 463/ 185000; 653/ 44700

^{1}H NMR (300 MHz, Benzene-d6) δ 8.26 (d, J = 7.8 Hz, 8H), 7.68 (dt, J = 6.5, 3.3 Hz, 8H), 7.48 (d, J = 7.6 Hz, 8H), 7.30 (dt, J = 6.3, 3.6 Hz, 8H), 2.47 (s, 12H).

MALDI: m/z: [M⁺]; C₆₄H₄₄N₄Zn, calc. for 932.2858; found: 932.2932.
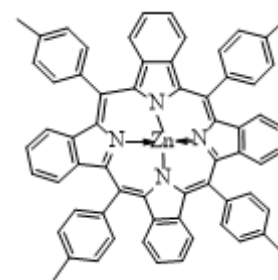
Meso-tetra(4-tolyl)tetrabenzoporphyrin (H₂-TTolTBP)

The synthesis was performed analogously to H₂-TPTBPdM₄ but 50 mg of Zn-TTTBP were used instead. Yield: dark green solid, 42.0 mg, 90%.

UV-VIS absorption spectra. $\lambda_{max}/\varepsilon$ (nm, M^{-1}cm^{-1}) in toluene: 468/ 115800
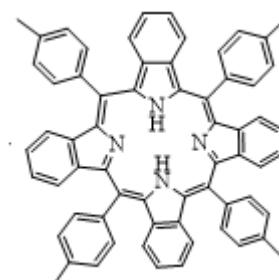
Figure S 6.5. H₂-TTolTBP

Platinum (II) meso-tetra(4-tolyl)tetrabenzoporphyrin (Pt-TTolTBP)

The synthesis was performed analogously to Pt-TPTBPdM₄ but 200 mg of H₂-TTolTBPmM₄ were used instead. The product was obtained as dark green solid. Yield: 26.7 mg, 63%.

UV-VIS absorption spectra. $\lambda_{max}/\varepsilon$ (nm, M^{-1}cm^{-1}) in toluene: 433/ 146800; 615/ 94900

^{1}H NMR (300 MHz, Chloroform-d) δ 8.11 (t, J = 6.7 Hz, 8H), 7.66 (d, J = 7.9 Hz, 8H), 7.21 (d, J = 3.4 Hz, 8H), 7.14 (dt, J = 6.4, 3.3 Hz, 7H), 2.79 (s, 12H).

MALDI: m/z: [M⁺]; C₆₄H₄₄N₄Pt, calc. for 1064.3235; found: 1064.3148
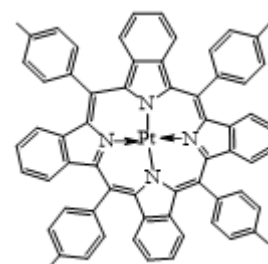
Figure S 6.6. Pt-TTolTBP

Zinc (II) meso-tetra-tolyl-tetra(mono-methyl)benzoporphyrin (Zn-TTTBPmM4)

The synthesis was performed analogously to (Zn-TPTBPdM4) but mono-methylphthalonitrile (6.722 g, 47.3 mmol, 4.00 eq), 2-(p-tolyl)acetic acid (15.98 g, 106.4 mmol, 9.00 eq) and zinc-4-tolylacetate (4.30 g, 11.82 mmol, 1.00 eq) were used instead. The crude product was purified via column chromatography, first on aluminium oxide (dichloromethane:ethylacetate, 10:1) and then on silica-gel (dichloromethane:ethyl acetate, 5:1) as stationary phase. The product containing fractions were determined via absorption spectra. The product was finally dried in the vacuum oven at 60 °C.

Figure S 6.7. Zn-TTTBPmM4

The product washed with cyclohexane on the ultrasonic bath for 10 minutes. This process was repeated for three times. The insoluble dark-green sediment was obtained after the removal of the light-green-brownish supernatant via centrifugation. Yield: dark green solid, 723.4 mg, 6%.

UV-VIS absorption spectra. $\lambda_{max}/\varepsilon$ (nm, $M^{-1}cm^{-1}$) in toluene: 462/ 212.000; 607/ 11.400; 654/ 58.000

^{1}H NMR (300 MHz, Chloroform-d) δ 8.21 – 8.07 (m, 8H), 7.66 (q, J = 7.2 Hz, 8H), 7.23 – 7.04 (m, 8H), 7.01 (s, 2H), 6.90 (s, 2H), 2.81 (t, J = 3.3 Hz, 12H), 2.38 – 2.29 (m, 12H).

MALDI: m/z: [M$^+$]; $C_{68}H_{52}N_4Zn$, calc. for 988.3483; found: 988.3405.
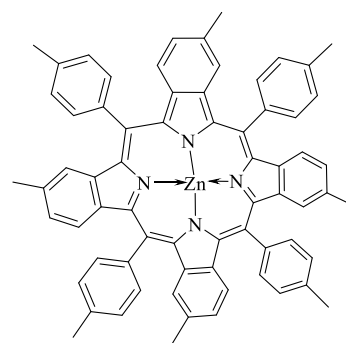
Bridged zinc (II) meso-tetra-tolyl-tetra(mono-methyl)benzoporphyrin (bridged Zn-TTTBPmM4)

Zn-TTolTBPmM4 (13.0 mg, 13.1 µmol, 1.00 eq) was dissolved in 13 mL dichlorobenzene for 5 minutes on the ultrasonic bath in a closed 25 mL round bottom flask. Then aluminum trichloride (437.5 mg, 3.281 mmol, 250 eq) was added to the solution and the reaction mixture was again put on the ultrasonic bath for 10 minutes, resulting in a color change from dark-green to a brownish-red. Afterwards the reaction mixture was

Figure S 6.8. Bridged Zn-TTTBPmM4

quickly heated to 155 °C, under moderate O$_2$-bubbling through the solution. The reaction progress was monitored via absorption spectra (solvent: dichloromethane), the samples taken from the reaction mixture were neutralized with 30 µL of triethylamine, visualized through a color change from dark-brown to light-brownish-green. After completion of the reaction the reaction mixture was allowed to cool down to room temperature under continuous O$_2$-bubbling through the solution. During the work-up the reaction mixture was neutralized with a dichloromethane: triethylamine solution (40:1) and the resulting precipitate was separated via centrifugation and washed with dichloromethane. The reaction mixture was washed with dest. H$_2$O (3 x 100 mL) and then dried over Na$_2$SO$_4$, before removal of solvent under reduced pressure. Finally the resulting green solid was purified via column chromatography (silica-gel, cond. cyclohexane, dichloromethane:tetrahydrofuran, 3:1), yielding a green solid. The solid was then re-dissolved in tetrahydrofuran (10 mL), heated to 40 °C and the produced complex re-metalized through the addition of zinc acetate (5.8 mg, 26.2 µmol, 2.00 eq) under continuous stirring for 10 minutes. The

solvent was removed under reduced pressure and the resulting green solid was again purified via column chromatography (aluminium oxide, dichloromethane: ethylacetate, 10:1) yielding a dark-green solid. The product containing fractions were determined via absorption spectra. Yield: green solid, 0.2 mg, 2%

UV-VIS absorption spectra. λ_{max}/relative intensity (nm): 492/ 1.00; 644/ 0.0849; 700/ 0.1632

MALDI: m/z: [M$^+$]; $C_{68}H_{50}N_4Zn$, calc. for 986.3327; found: 986.3288

Meso-tetra-tolyl-tetra(mono-methyl)benzoporphyrin (H$_2$-TTTBPmM$_4$)

The synthesis was performed analogously to H$_2$-TPTBPdM$_4$ but 50 mg of Zn-TTTBPmM$_4$ were used instead. Yield: dark green solid, 46.0 mg, 98%.

UV-VIS absorption spectra. λ_{max}/ε (nm, M^{-1}cm^{-1}) in toluene: 468/ 170.600; 594/ 9.700; 638/ 22.300; 699/ 8.700

Figure S 6.9. H₂-TTTBPmM₄

Platinum (II) meso-tetra-tolyl-tetra(mono-methyl)benzoporphyrin (Pt-TTTBPmM$_4$)

The synthesis was performed analogously to Pt-TPTBPdM$_4$ but 35 mg of H$_2$-TTolTBPmM$_4$ were used instead. The product was obtained as dark green solid. Yield: 26.7 mg, 63%.

UV-VIS absorption spectra. λ_{max}/ε (nm, M^{-1}cm^{-1}) in toluene: 432/ 157.300; 566/ 11.800; 617/ 106.500

MALDI: m/z: [M$^+$]; $C_{68}H_{52}N_4Pt$, calc. for 1120.3861; found: 1120.3890

Figure S 6.10. Pt-TTTBPmM₄

Zinc(II) meso-tetra-tolyl-tetra-tert-butylbenzoporphyrin (Zn-TTTBPtBu)

The synthesis was performed analogously to Zn-TPTBPdM$_4$ but 4-(tert-butyl)phthalonitrile (14.71 g, 79.85 mmol, 4.00 eq), 2-(p-tolyl)acetic acid (11.98 g, 79.78 mmol, 4.00 eq) and zinc 4-tolylacetate (7.29 g, 20.04 mmol, 1.00 eq) were used instead. Yield: 1.63 g, 7%.

UV-VIS absorption spectra. λ_{max}/relative intensity (nm): 456/ 1.00; 604/ 0.0518; 653/ 0.2607

^{1}H NMR (300 MHz, Chloroform-*d*) δ 8.30 – 8.10 (m, 8H), 7.75 – 7.63 (m, 9H), 7.60 – 7.23 (m, 12H), 2.79 (t, *J* = 11.7 Hz, 10H), 1.25 (s, 35H).

Figure S 6.11. Zn-TTTBPtBu

^{13}C NMR (76 MHz, CDCl₃) δ 147.72, 140.73, 138.93, 138.49, 136.79, 134.18, 133.99, 133.76, 129.90, 129.83, 129.71, 123.99, 123.37, 121.58, 35.11, 31.45, 21.81.
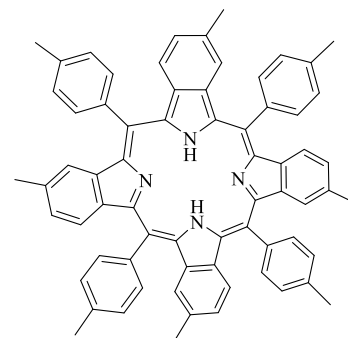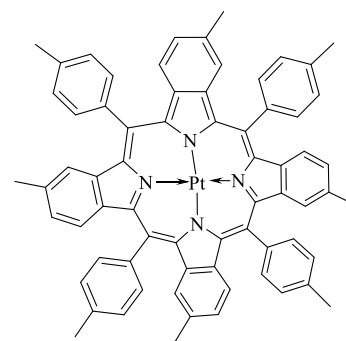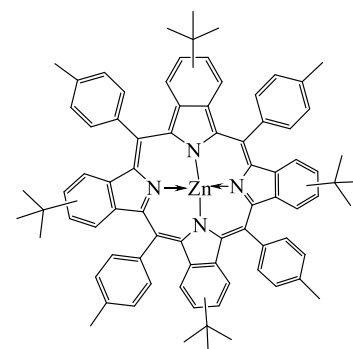
Meso-tetra-tolyl-tetra-tert-butylbenzoporphyrin (H2-TTTBPtBu)

The synthesis was performed analogously to H2-TPTBPdM4 but 1.51 g of Zn-TTTBPtBu were used instead.

Yield: 1.40 g, 98%.

UV-VIS absorption spectra. λ_{max}/relative intensity (nm): 461/ 1.00; 588/ 0.0447; 634/ 0.1230; 695/ 0.0421

^{1}H NMR (300 MHz, Chloroform-*d*) δ 8.24 – 8.06 (m, 8H), 7.64 – 7.55 (m, 9H), 7.51 – 7.11 (m, 16H), 1.24 – 1.04 (m, 39H), 2.69 (t, *J* = 11.1 Hz, 12H), 1.19 – 1.07 (m, 38H).
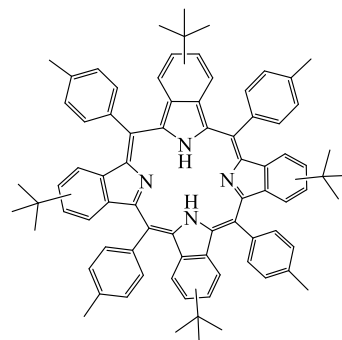
Figure S 6.12. H2-TTTBPtBu

Pt(II) meso-tetra-tolyl-tetra-tert-butylbenzoporphyrin (Pt-TTTBPtBu)

The synthesis was performed analogously to Pt-TPTBPdM4 but 1.1 g of H2-TTTBPtBu were used instead.

Yield: 802 mg, 62 %.

UV-VIS absorption spectra. UV-Vis: λ_{max}/ε (nm, $M^{-1}cm^{-1}$) in dichloromethane: 431/ 304.000; 568/ 23.000; 617/ 202.000

^{1}H NMR (300 MHz, Benzene-*d6*) δ 8.20 – 7.99 (m, 8H), 7.63 – 7.53 (m, 4H), 7.54 – 7.40 (m, 12H), 7.39 – 7.29 (m, 4H), 2.49 (d, *J* = 3.9 Hz, 12H), 1.23 (d, *J* = 1.6 Hz, 36H).

^{13}C NMR (76 MHz, C6D6) δ 147.76, 140.03, 138.66, 138.46, 136.30, 134.17, 134.10, 130.11, 124.32, 123.65, 121.67, 35.02, 31.43, 21.45.

MALDI: m/z: [M$^+$]; C80H46N4Pt, calc. for 1288.5742; found: 1288.5815
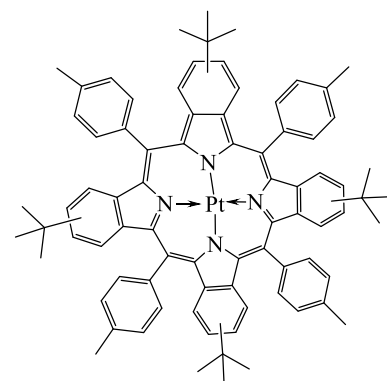
Figure S 6.13. Pt-TTTBPtBu

6.5.2 Photophysical properties
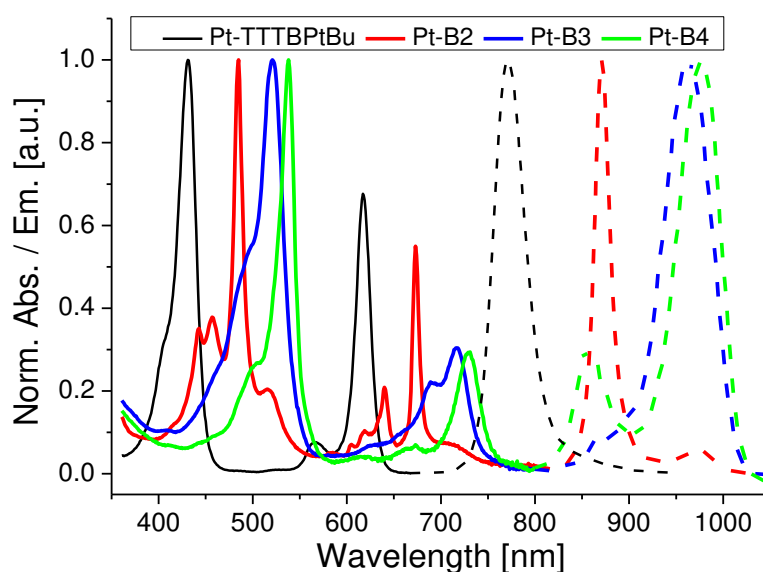
Figure S 6.14. Absorption (solid lines) & emission (dashed lines) spectra of Pt-TTTBPtBu and bridged products Pt-B2, Pt-B3 & Pt-B4 in anoxic toluene.

Table S 6.1 Photophysical properties of Pt-TTTBPtBu and Pt-B2, Pt-B3 and Pt-B4 in anoxic toluene

dye	Abs λ$_{max}$/ε (nm, M^{-1}cm^{-1}) λ$_{max}$/relative intensity	Em λ$_{max}$ [nm]	Φ [%]	lifetime τ [μs]
Pt-TTTBPtBu	431/ 1.00, 568/ 0.08, 617/ 0.68	772	28	57
Pt-B2	443/42.000, 457/47.000, 485/110.000, 619/12.000, 640/23.000, 673/58.000	872	6	36
Pt-B3	521/ 1.00, 689/ 0.2220, 717/ 0.3042	970	~1	10
Pt-B4	538/ 1.00, 731/ 0.2944	995	~1	14
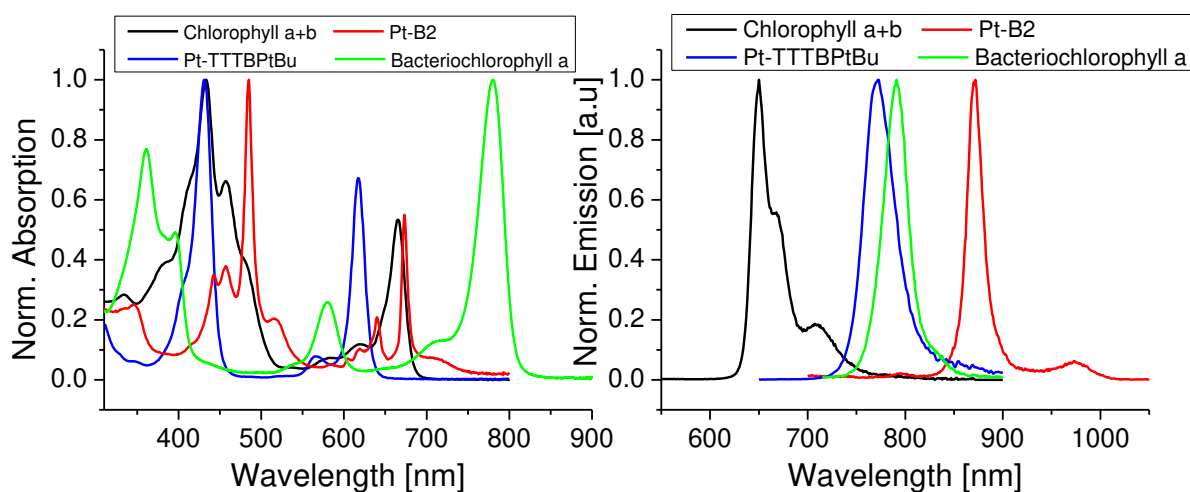
Figure S 6.15. Normalized absorption spectra (left) and emission spectra (right) of chlorophyll a and b mixture (extracted with CHCl₃ from spinache), bacteriochlorophyll a, Pt-TTTBPtBu and Pt-B2 in anoxic toluene at r.t.

6.5.3 DFT calculations

In order to elucidate the bridging pattern of in the modified Pt-TPTBP compound, time-dependent density functional theory (TD-DFT) calculations were carried out for the precursor (Pt-TPTBP) and all the possible structures (Fig. S13). The calculations indicate that Pt-B1 presented in Fig. S13 is the most likely from the 4-bridged species which can potentially form. Using the Gaussian09 package21 we employed the B3LYP hybrid functional together with the LANL2DZ basis set. We were mostly interested in the overall shape and relative spectral shifts of the absorption spectra, rather than accurately reproducing experimental peak position, and therefore neglected solvent effects and electron-vibration coupling in the present calculations. For the first 10 optical transitions, i.e. in the region above ca. 350 nm (below 3.5 eV), the TD-DFT calculations for the precursor (Pt-TPTBP) yield transitions with strong oscillator strengths at 565 nm (2.19 eV) and 402 nm (3.08 eV), i.e. the transition are shifted considerably to higher energies relative to the experiment. Both transitions are doubly degenerated, owing to the high symmetry of Pt-TPTBP. Identification of the synthesized compounds is possible on the basis of lifting of the symmetry and degree of peaks shift in the bridged products. Candidate compound 3 retains the four-fold symmetry. Consequently,

its calculated absorption spectrum (Fig. S16) also shows only two discernible (two-fold degenerated) transitions, which is clearly at variance with the experiment. In candidate compound 2 the four-fold symmetry is lifted, and while the calculated transitions at 620 nm and 471 nm compare very favourably to the experiment, the transition at 719 nm is at too small energies. Furthermore, we do not find an optical transition in the region between 400 nm and 500 nm. Combination of these two arguments renders also the assignment of the bridging product to candidate compound 2 (Fig. S15) unlikely. For Pt-B1 (Fig. S13 left), we find two transitions at 620 nm (2.00 eV) and 602 nm (2.06 eV), which are both blue-shifted compared to the experimental peaks. Furthermore, we find two quasi-degenerate transitions at 440 nm (2.81 eV), that can be associated to the experimental absorption at 483 nm. Importantly, also two transitions with significant oscillator strength are found at 431 nm (2.88 eV) and 423 nm (2.93 eV), which may explain the experimentally observed peaks in the high-energy region. We therefore conclude that Pt-B1 is most likely the structure that has been synthesized (Fig. S14).

bridged Pt-TPTBP (Pt-B1)   Candidate compound **2**   Candidate compound **3**
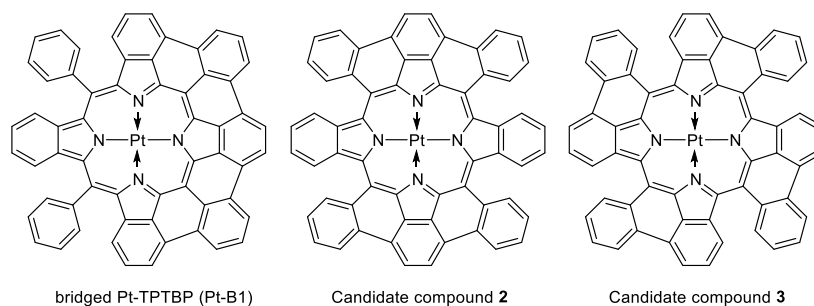
Figure S 6.16. Chemical Structures of candidate compounds for DFT calculations.
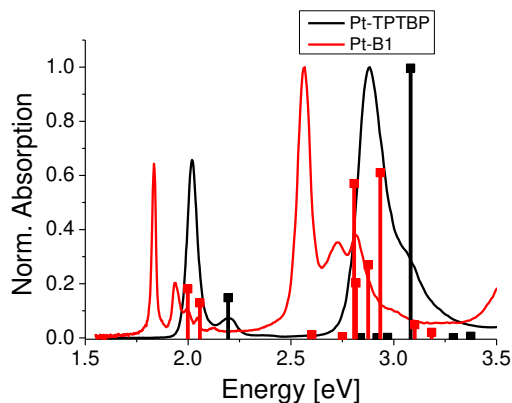
Figure S 6.17. Comparison of obtained absorption spectra of Pt-TPTBP and

Pt-B1 and the predictions of DFT-calculations.
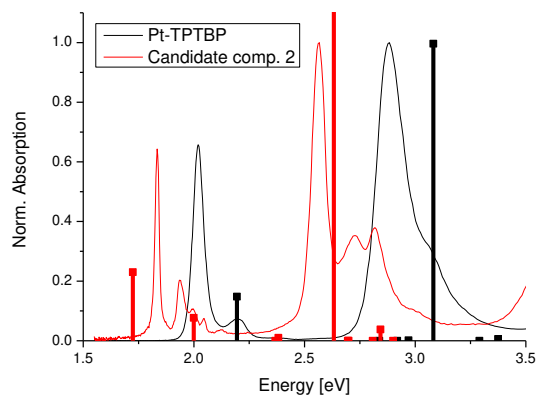
Figure S 6.18. Comparison of obtained absorption spectra of Pt-TPTBP and Candidate compound 2 and the predictions of DFT-calculations.
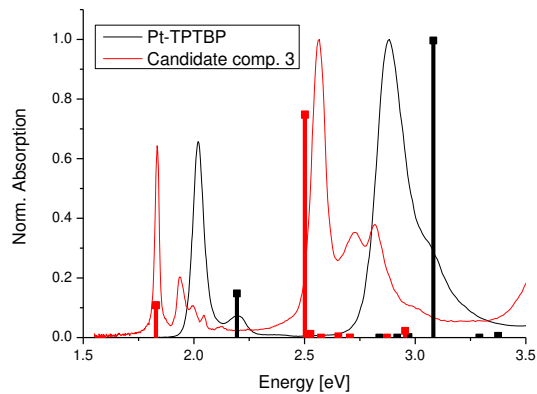
Figure S 6.19. Comparison of obtained absorption spectra of Pt-TPTBP and Candidate compound 3 and the predictions of DFT-calculations.
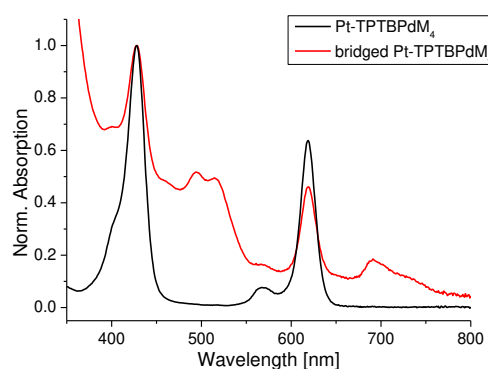
Figure S 6.20. Normalized absorption spectrum of Pt-TPTBPdM$_4$ (purified) and bridged product during Scholl reaction.
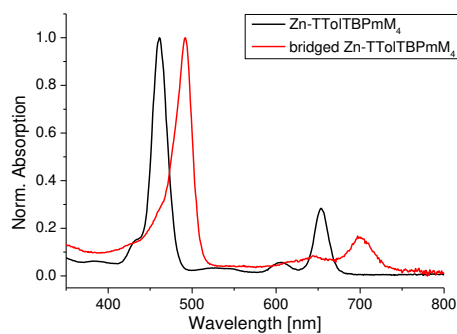
Figure S 6.21. Normalized absorption spectrum of bridged Zn-TPTBPmM$_4$ (purified).
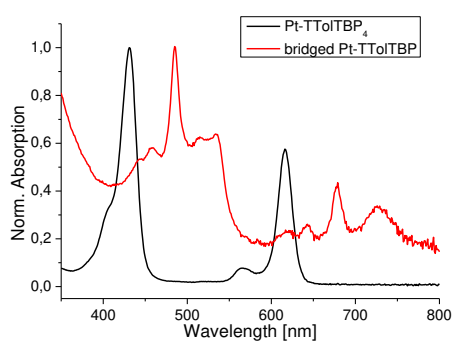
**Figure S 6.22. Normalized absorption spectrum of Pt-TTolTBP (purified)
and bridged product during Scholl reaction.**

6.5.4 Temperature dependency of Pt-TTTBPtBu and Pt-B2

Table S 6.2. Temperature dependency of the photophysical and oxygen-sensing properties of Pt-TTTBPtBu and Pt-B2 in PS-DVB beads

Dye	T, °C	τ_0, µs	$d\tau_0/dT$, %/K (at 37 °C)	K_{sv}, hPa^{-1}	dK_{sv}/dT, %/K (at 37 °C)
Pt-TTTBPtBu	32	50.04		0.0185	
	37	49.66	-0.13	0.0190	0.62
	42	49.40		0.0197	
Pt-B2	32	22.29		0.0096	
	37	21.90	-0.35	0.0099	0.55
	42	21.52		0.0102	

146
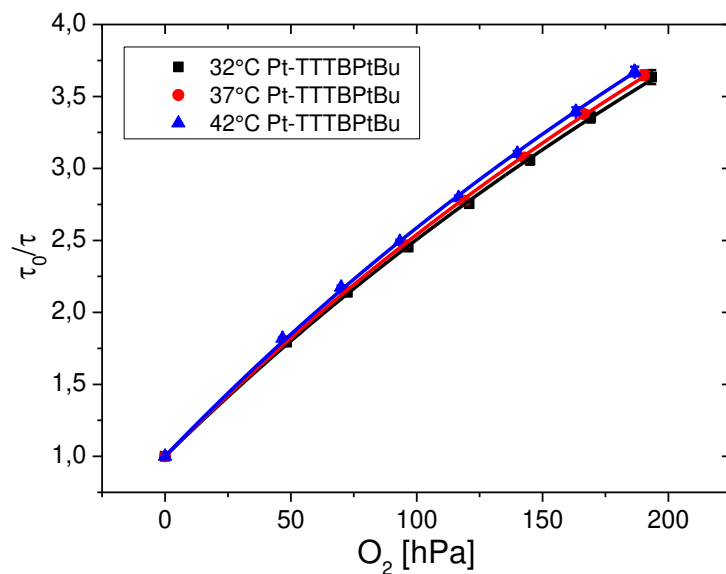
Figure S 6.23. Temperature dependency of Pt-TTTBPtBu/PS-DVB oxygen-sensing material

6.5.5 Influence of diffusion barrier thickness on dynamic range
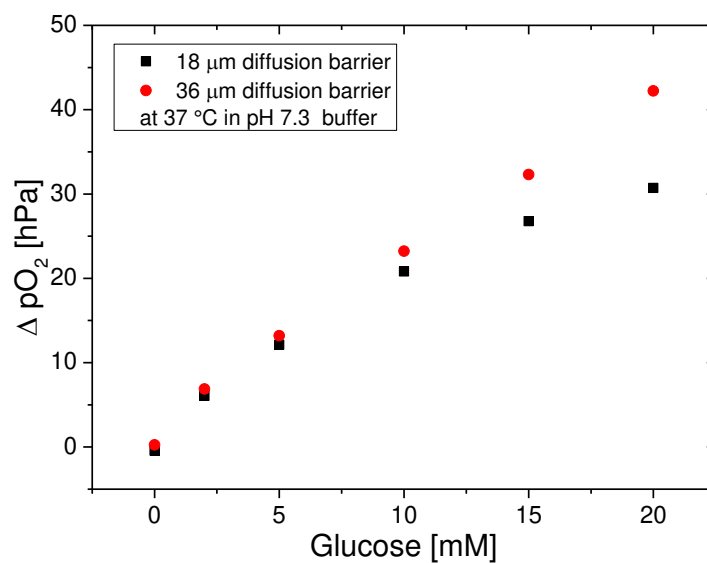
Figure S 6.24. Influence of diffusion barrier thickness on dynamic range of glucose sensor (37 °C, pH7.3 buffer, 150 mM NaCl) at 95 hPa oxygen.

6.5.6 Stability tests for the glucose sensor (without second O₂ sensing layer)
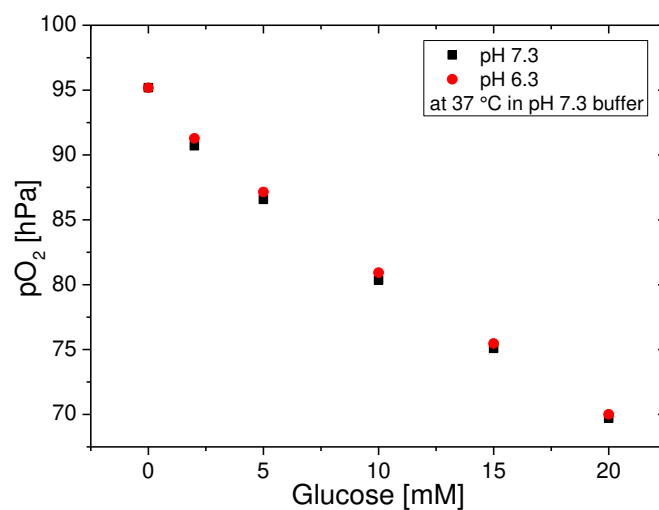
Figure S 6.25. Response of the glucose sensor at pH 7.3 and pH 6.3 buffer solutions with 150 mM NaCl
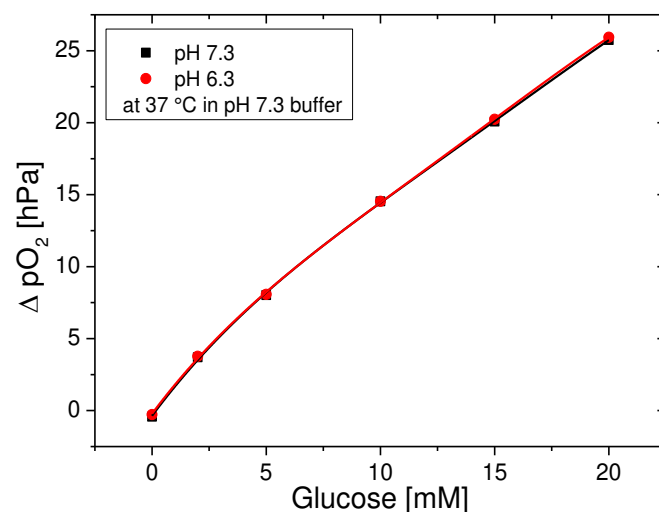
Figure S 6.26. Δ pO₂ response of the glucose sensor at pH 7.3 & pH 6.3 buffer solutions with 150 mM NaCl
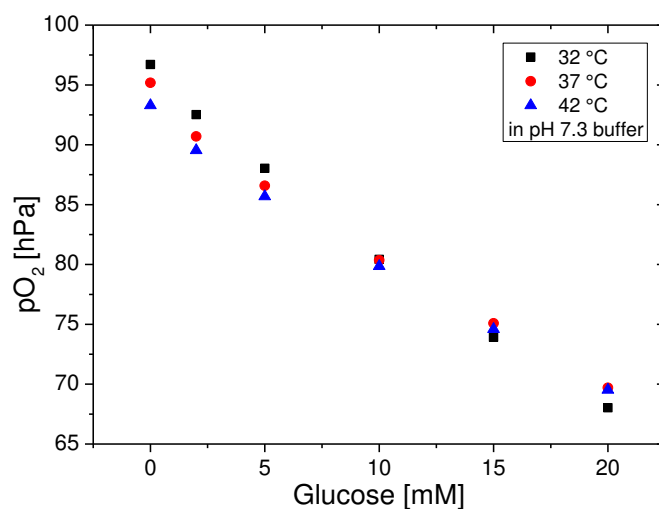
Figure S 6.27. Temperature dependency of the glucose sensor (pH 7.3, 150 mM NaCl). Note that pO₂ is also temperature dependent due to increase in the pH₂O at higher temperatures.
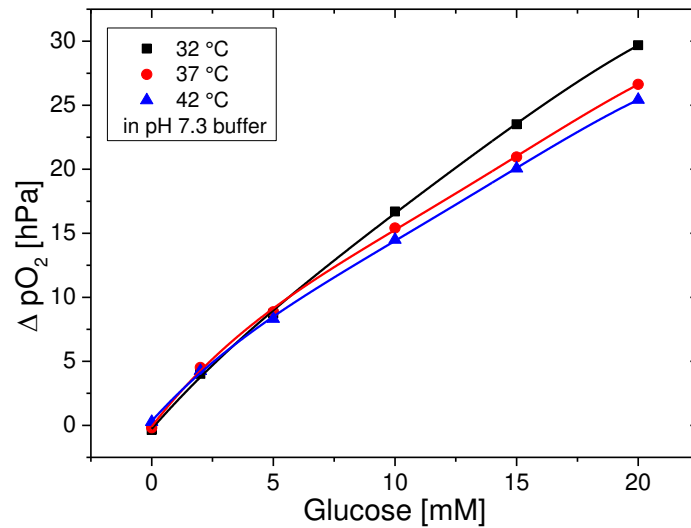
Figure S 6.28. ΔpO₂ response of the glucose sensor (pH 7.3, 150 mM NaCl) at different temperatures.
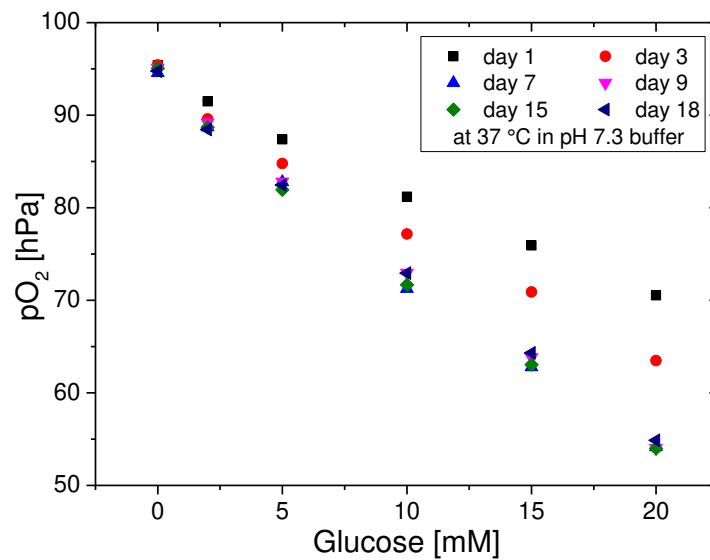
Figure S 6.29. Stability of the glucose sensor (37 °C, pH 7.3, 150 mM NaCl) over 18 days.
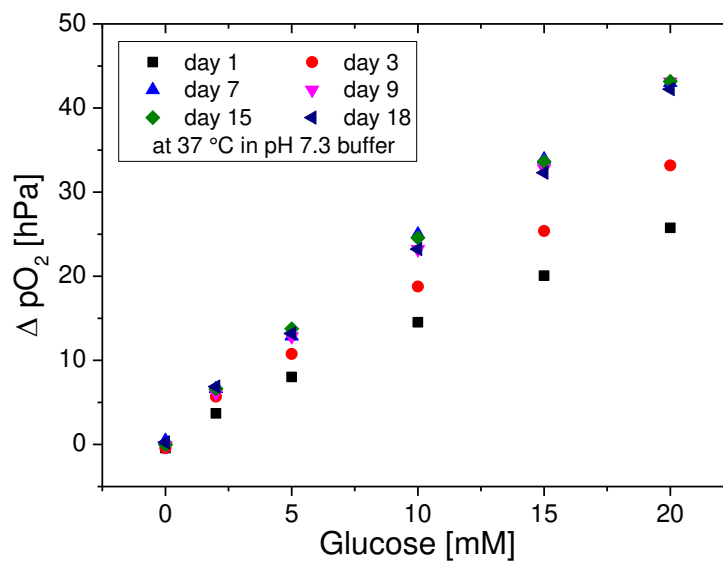
Figure S 6.30. Stability of the glucose sensor (37 °C, pH 7.3, 150 mM NaCl) over 18 days (ΔpO₂ plot).

6.5.7 NMR and Mass spectra

^{1}H and ^{13}C NMR were recorded on a 300 MHz instrument (Bruker AVANCE III) or 500 MHz from Varian. In all ^{1}H and ^{13}C spectra, the residual signal of the deuterated solvent was used as an internal standard to reference the chemical shifts δ. Data analysis was done with the MestraNova NMR software. High resolution mass spectra were recorded using a Micromass TofSpec 2E as positive reflector on a Bruker Ultraflex Extreme MALDI-TOF/TOF spectrometer. The mass spectra were analyzed with the FlexAnalysis 3.0 software (Bruker Daltonics).

^{1}H NMR (300 MHz, Benzene-d_6) δ 8.41 – 8.28 (m, 8H), 7.78 – 7.59 (m, 12H), 7.31 (s, 8H), 2.27 (s, 24H).

Figure S 6.31. ^{1}H NMR spectrum of Zn-TPTBPdM$_4$
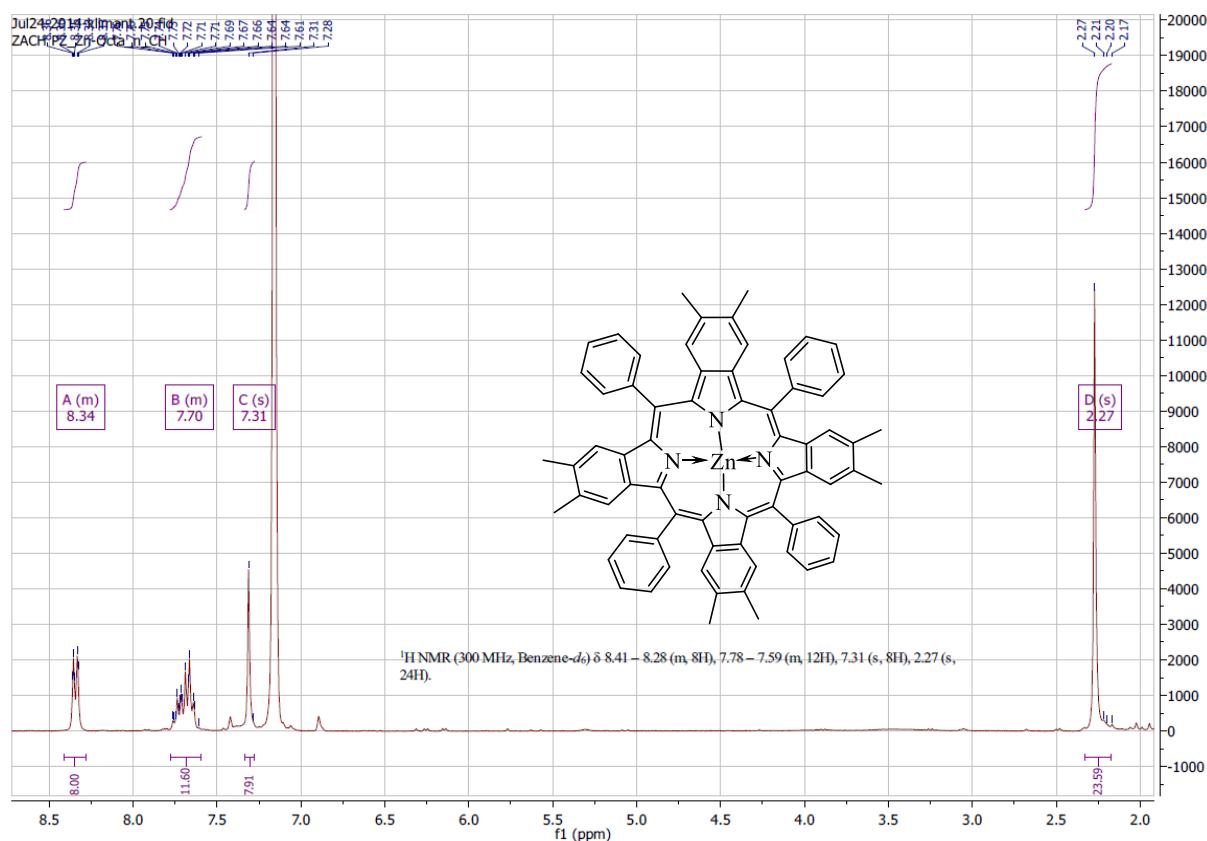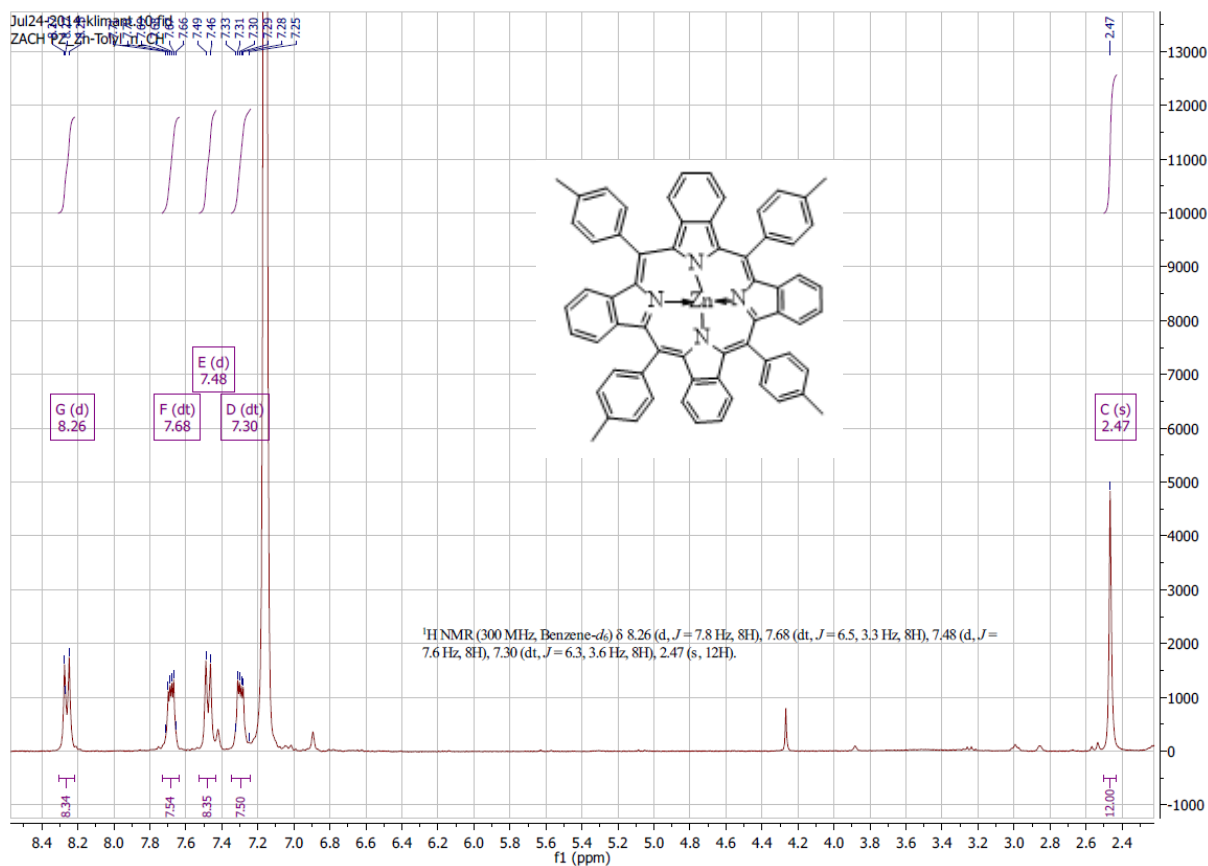
Figure S 6.32 ^{1}H NMR spectrum of Zn-TTolTBP

^{1}H NMR (300 MHz, Benzene-d_6) δ 8.26 (d, $J = 7.8$ Hz, 8H), 7.68 (dt, $J = 6.5$, 3.3 Hz, 8H), 7.48 (d, $J = 7.6$ Hz, 8H), 7.30 (dt, $J = 6.3$, 3.6 Hz, 8H), 2.47 (s, 12H).
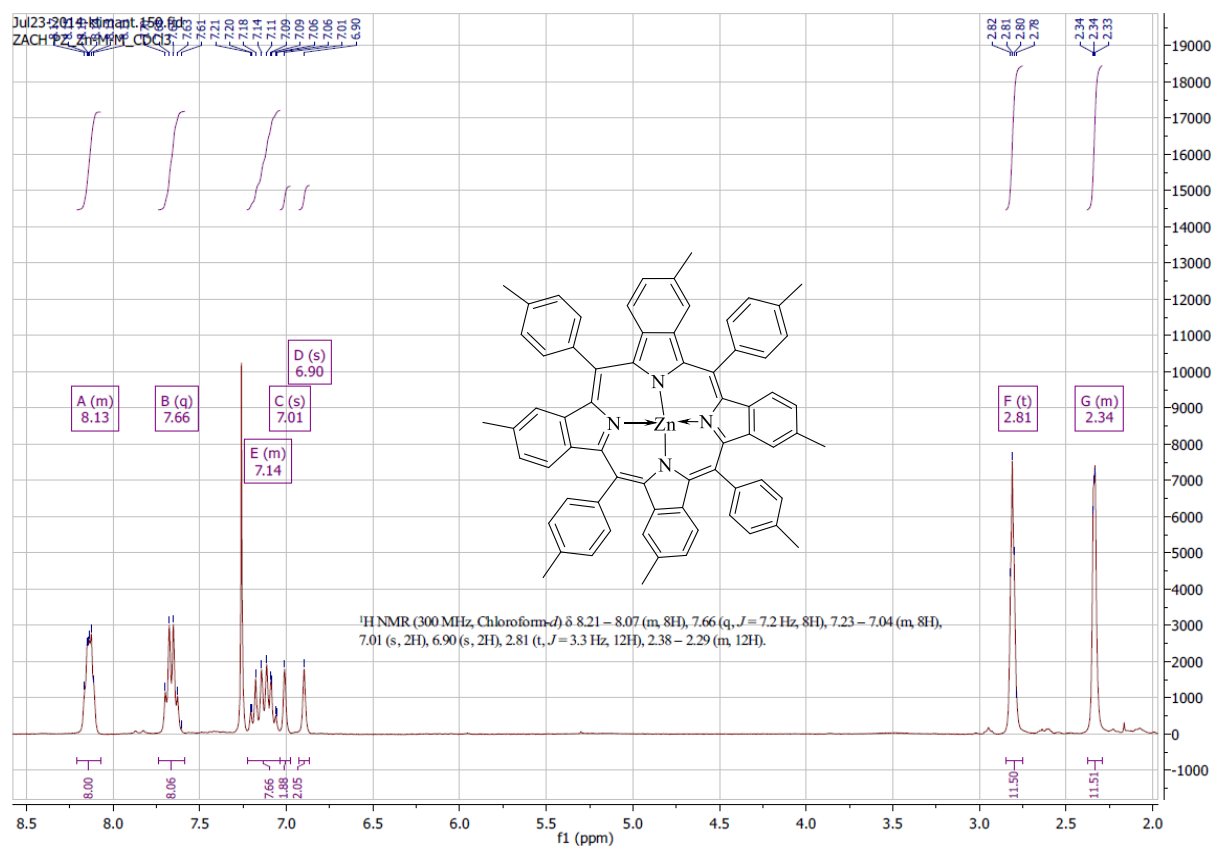
Figure S 6.33. ^{1}H NMR spectrum of Zn-TTTBPmM₄

^{1}H NMR (300 MHz, Chloroform-d) δ 8.21 – 8.07 (m, 8H), 7.66 (q, $J = 7.2$ Hz, 8H), 7.23 – 7.04 (m, 8H), 7.01 (s, 2H), 6.90 (s, 2H), 2.81 (t, $J = 3.3$ Hz, 12H), 2.38 – 2.29 (m, 12H).
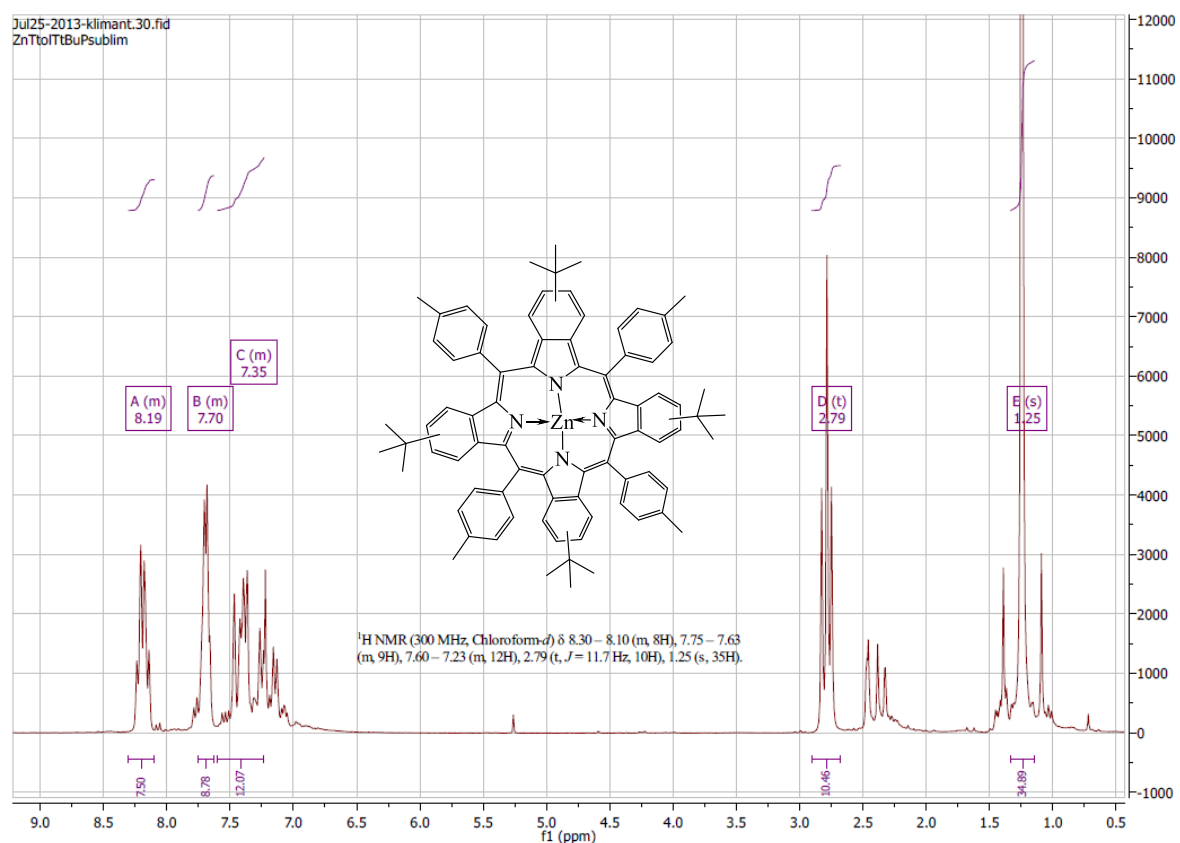
Figure S 6.34. ^{1}H NMR spectrum of Zn-TTTBPtBu
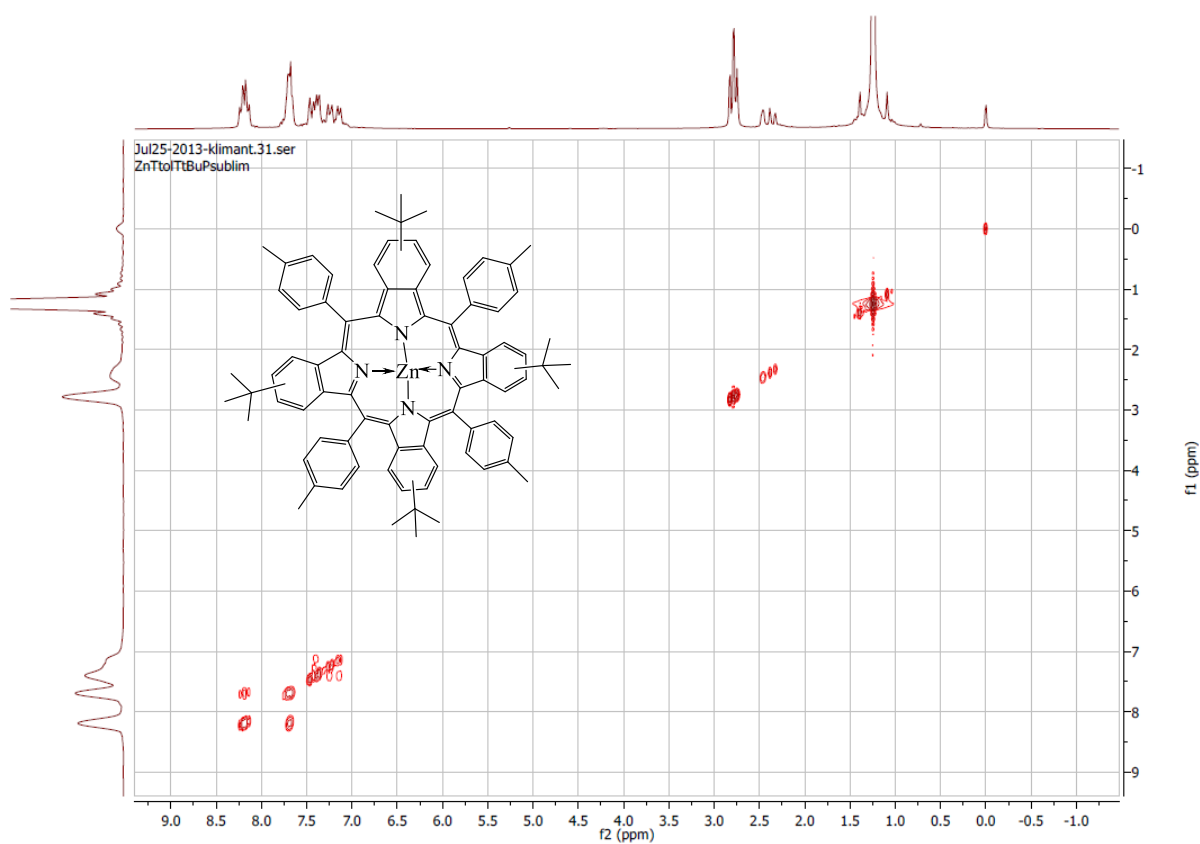
Figure S 6.35. H-H-Cosy NMR spectrum of Zn-TTTBPtBu
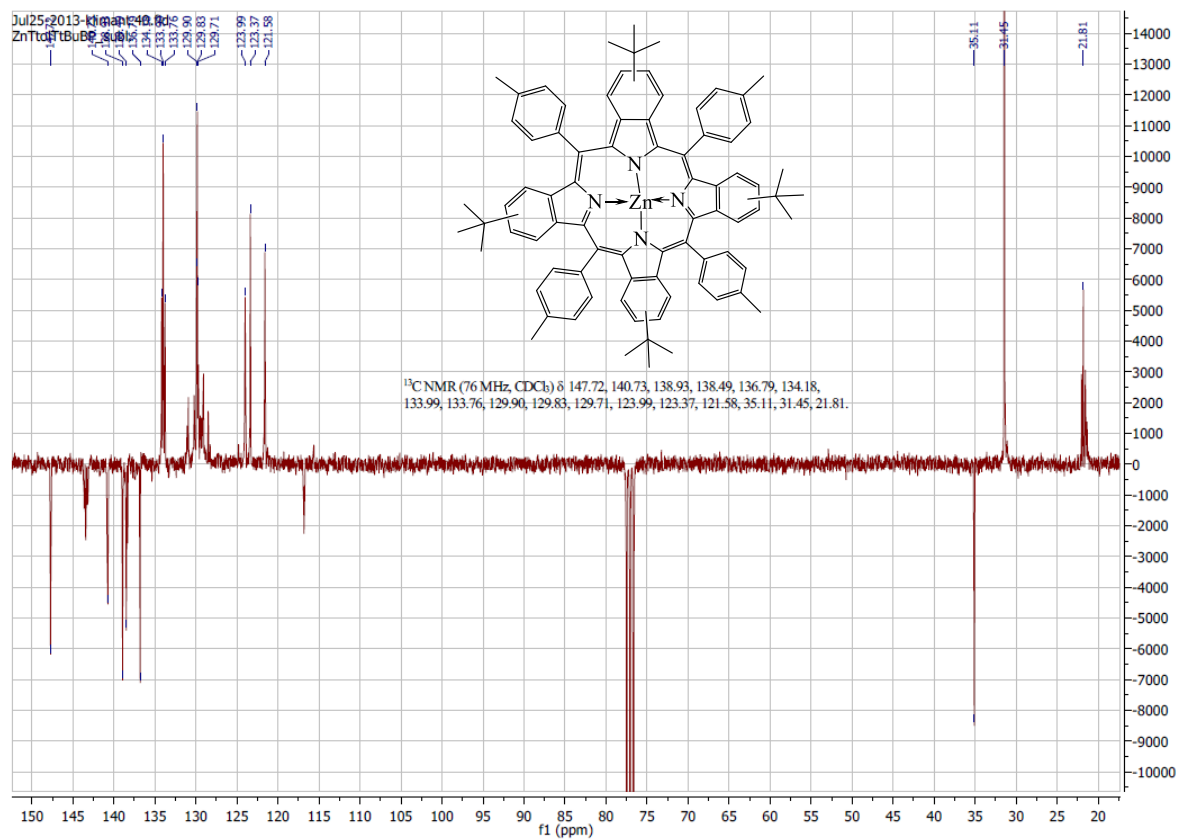
Figure S 6.36. ^{13}C-APT NMR spectrum of Zn-TTTBPtBu
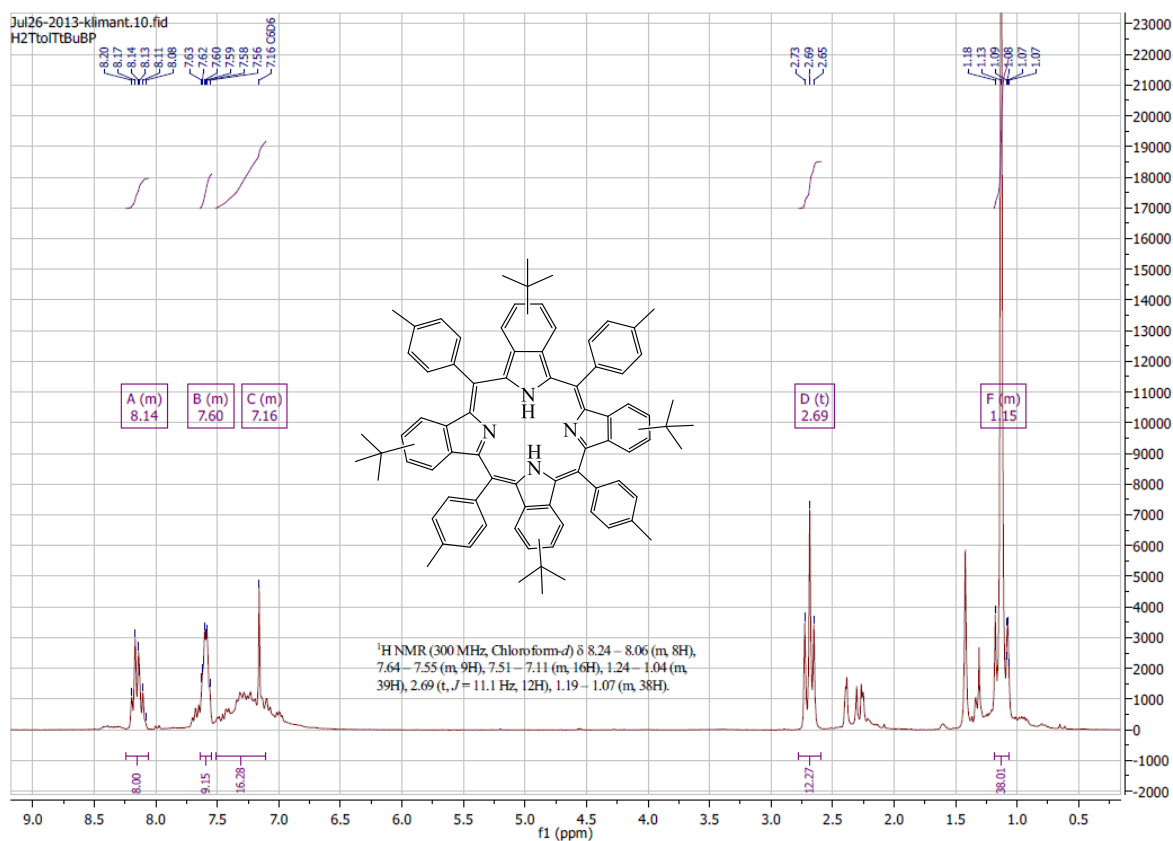
Figure S 6.37. ^{1}H NMR spectrum of H$_2$-TTTBPtBu
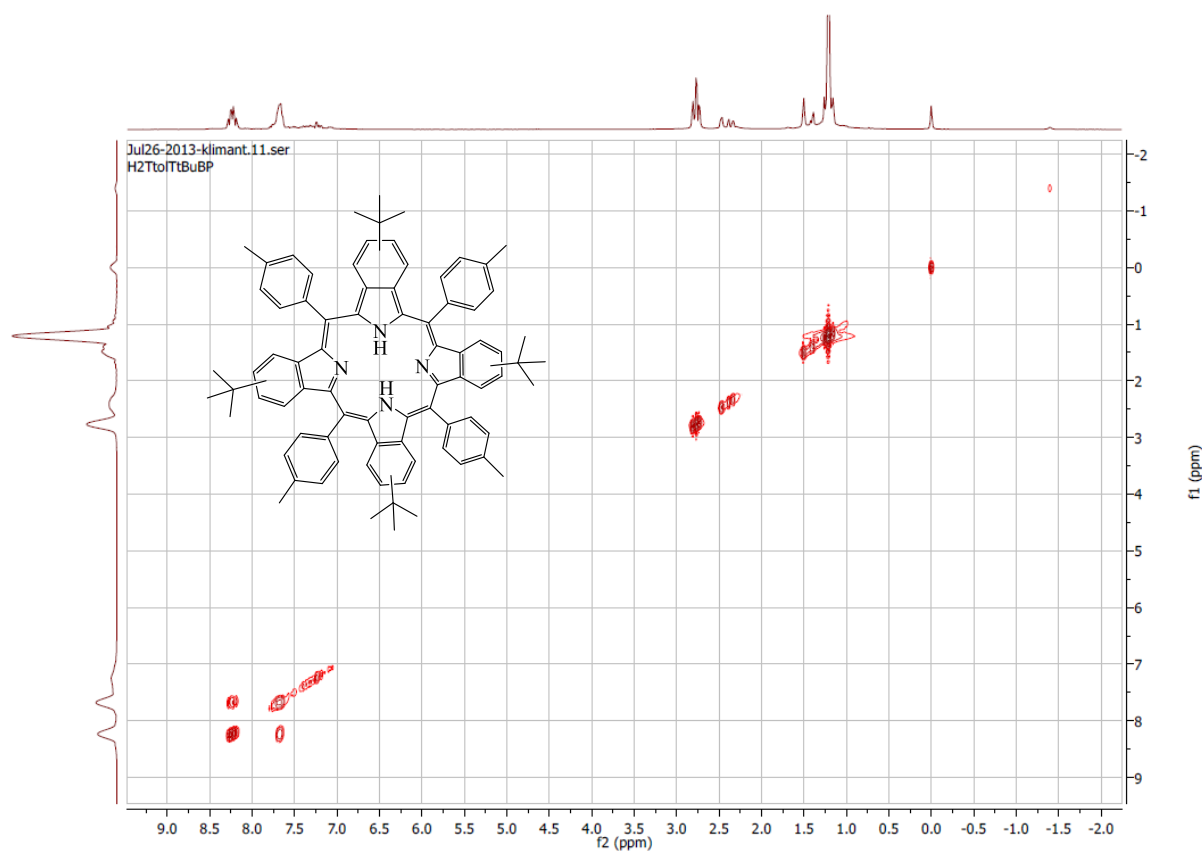
Figure S 6.38. H-H-Cosy NMR spectrum of H₂-TTTBPtBu

¹H NMR (300 MHz, Chloroform-*d*) δ 8.11 (t, *J* = 6.7 Hz, 8H), 7.66 (d, *J* = 7.9 Hz, 8H), 7.21 (d, *J* = 3.4 Hz, 9H), 7.14 (dt, *J* = 6.4, 3.3 Hz, 7H), 2.79 (s, 10H).
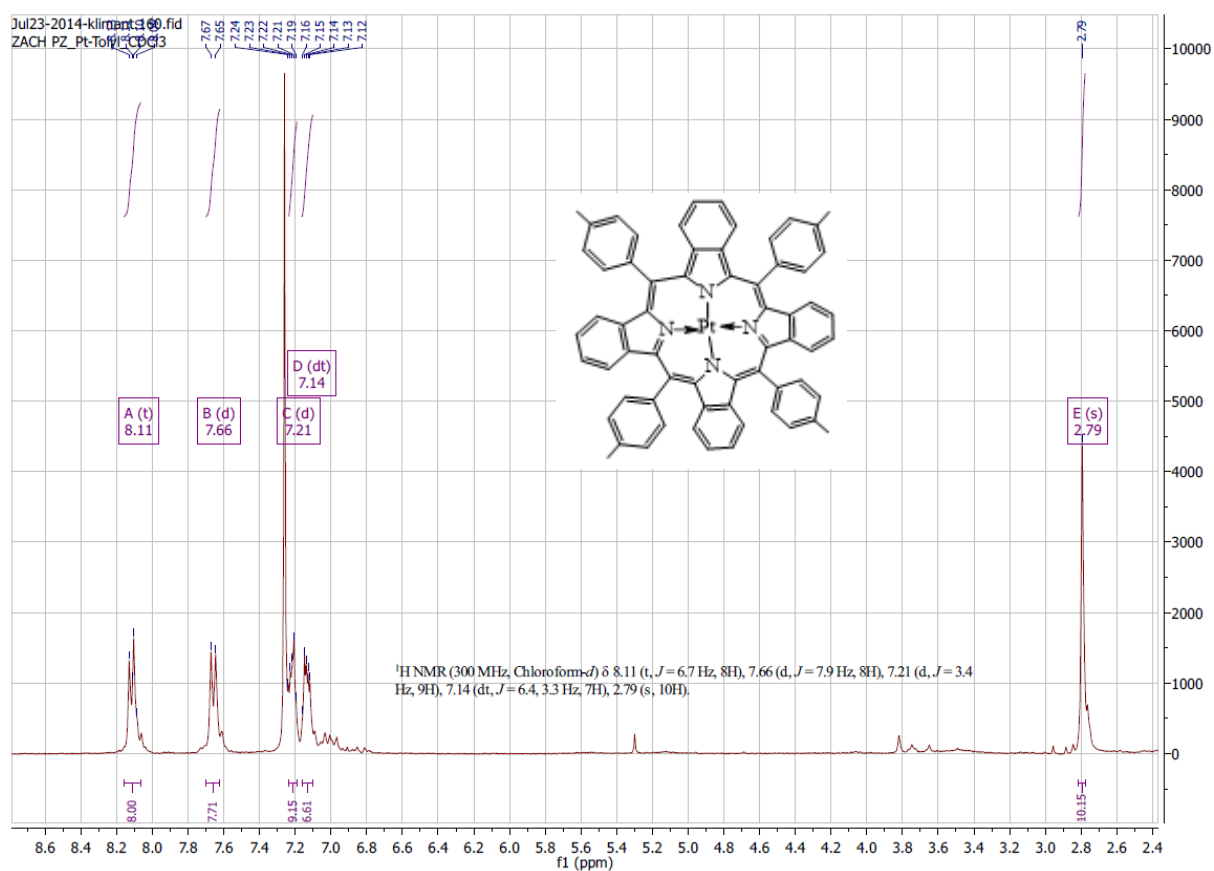
Figure S 6.39 ¹H NMR spectrum of Pt-TTolTBP
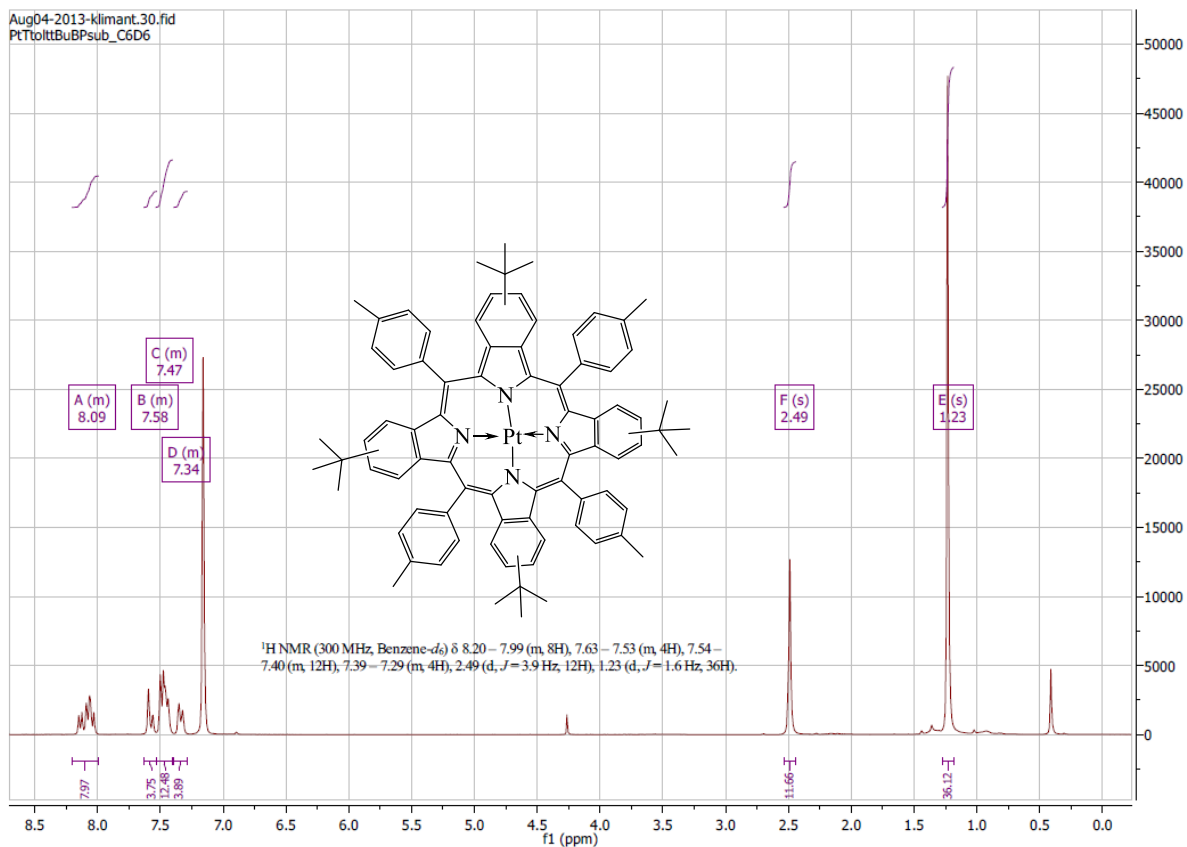
Figure S 6.40. ¹H NMR spectrum of Pt-TTTBPtBu

¹H NMR (300 MHz, Benzene-d_6) δ 8.20 − 7.99 (m, 8H), 7.63 − 7.53 (m, 4H), 7.54 − 7.40 (m, 12H), 7.39 − 7.29 (m, 4H), 2.49 (d, J = 3.9 Hz, 12H), 1.23 (d, J = 1.6 Hz, 36H).
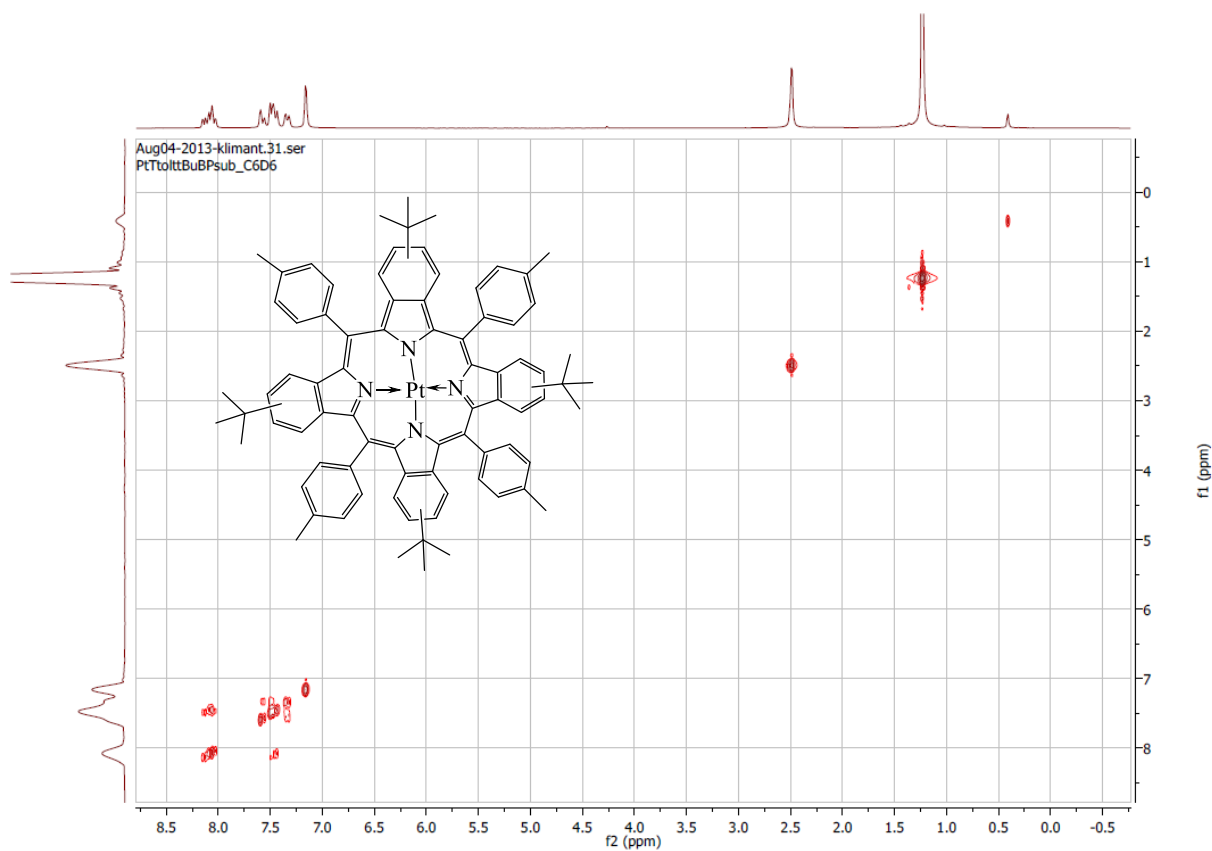
Figure S 6.41. H-H-Cosy NMR spectrum of Pt-TTTBPtBu

13C NMR (76 MHz, C₆D6) δ 147.76, 140.03, 138.66, 138.46, 136.30, 134.17, 134.10, 130.11, 124.32, 123.65, 121.67, 35.02, 31.43, 21.45.
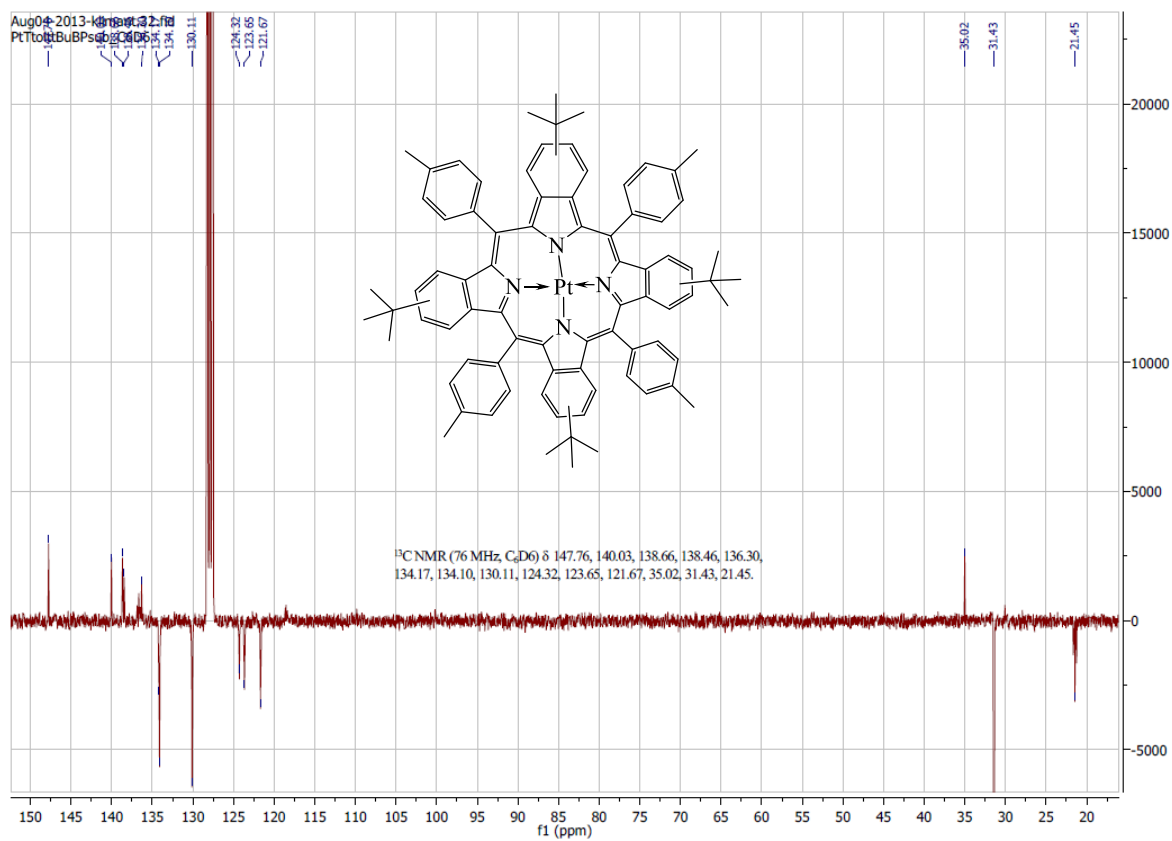
Figure S 6.42. ^{13}C-APT NMR spectrum of Pt-TTTBPtBu
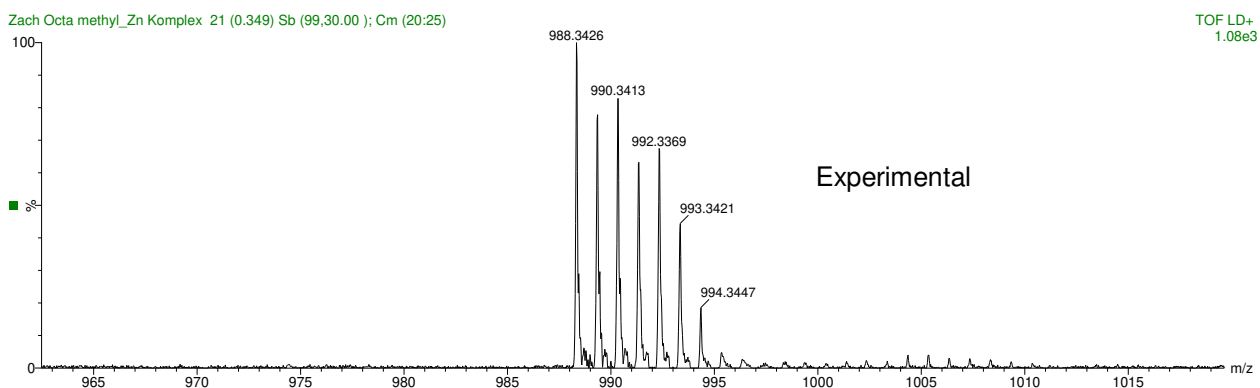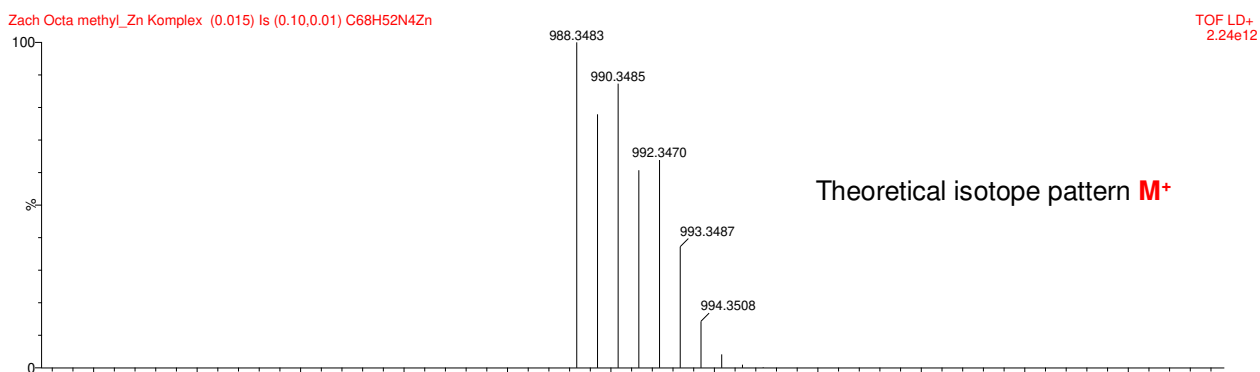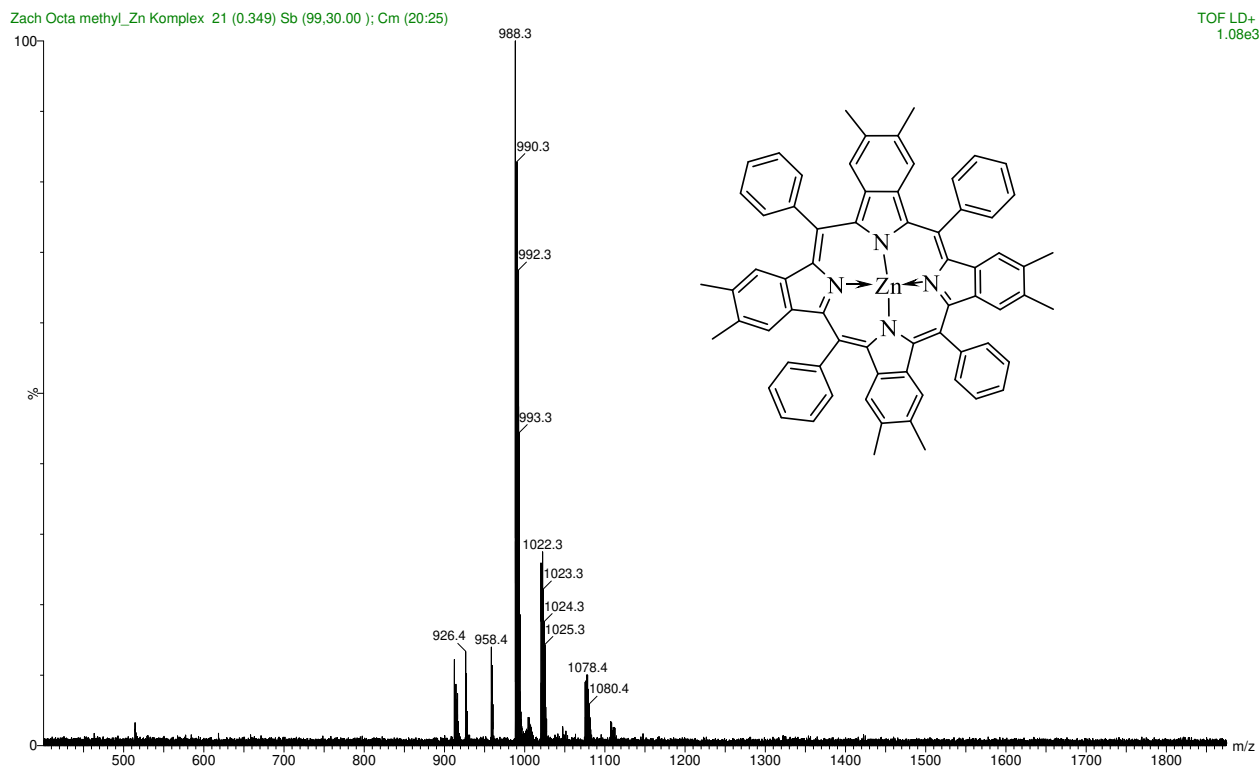
Figure S 6.43. Mass spectrum (MALDI-TOF) of Zn-TPTBPdM₄
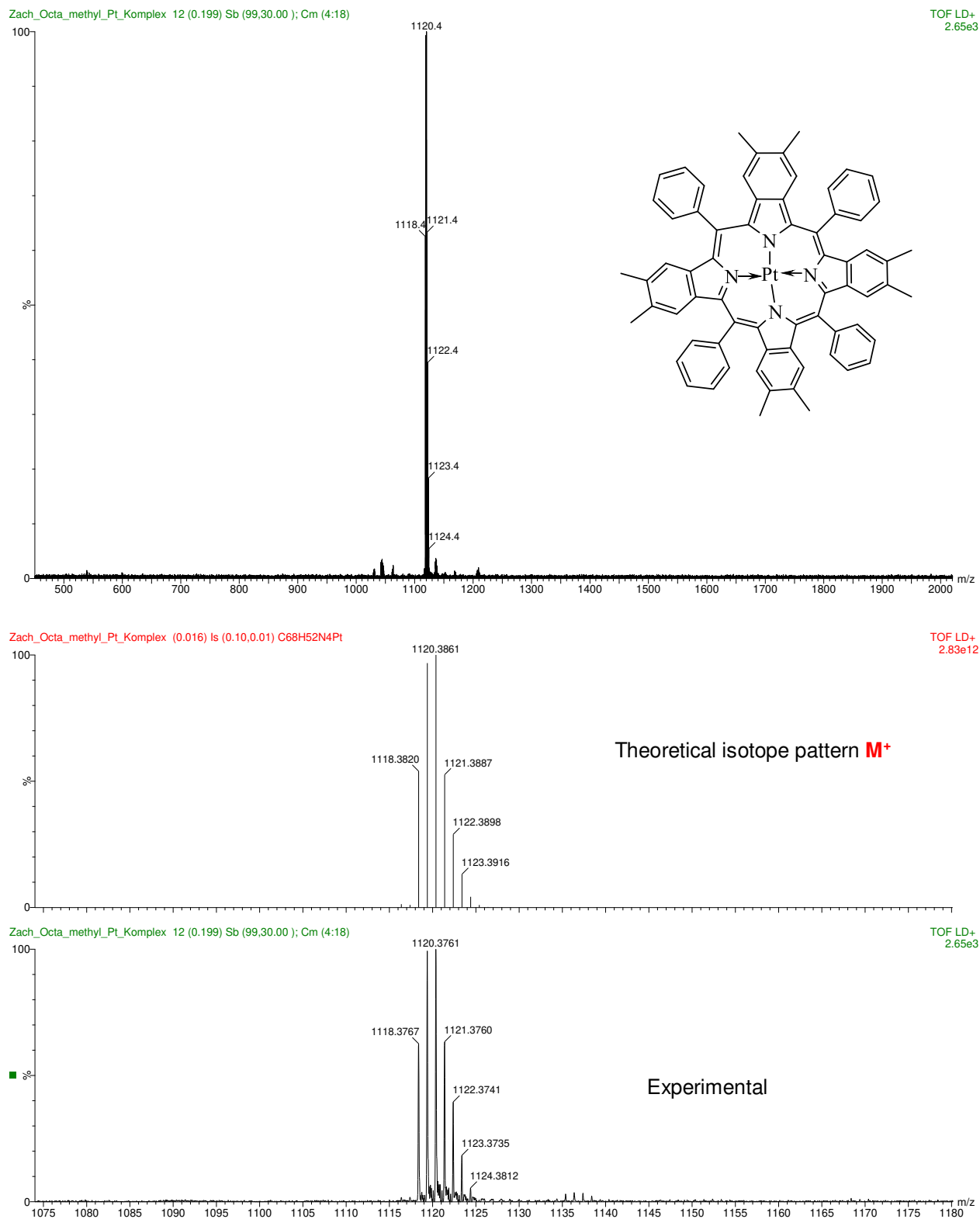
Figure S 6.44. Mass spectrum (MALDI-TOF) of Pt-TPTBPdM4
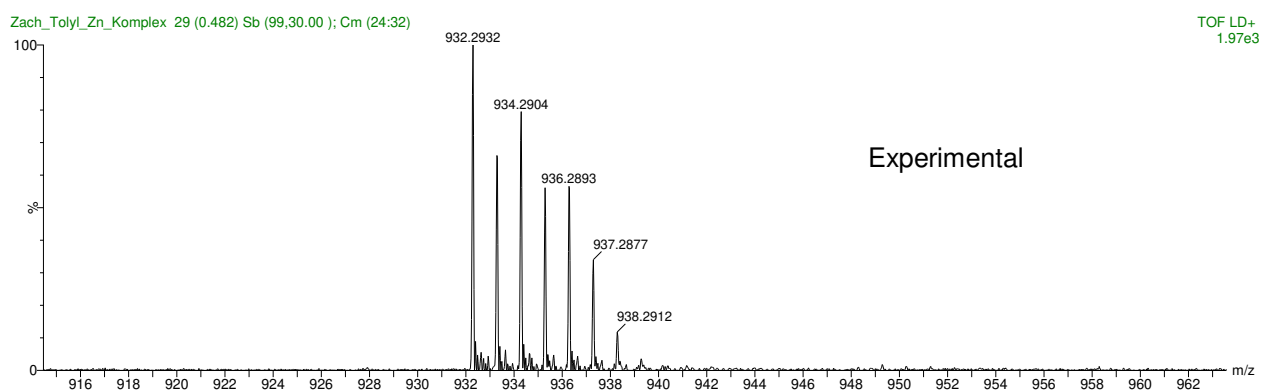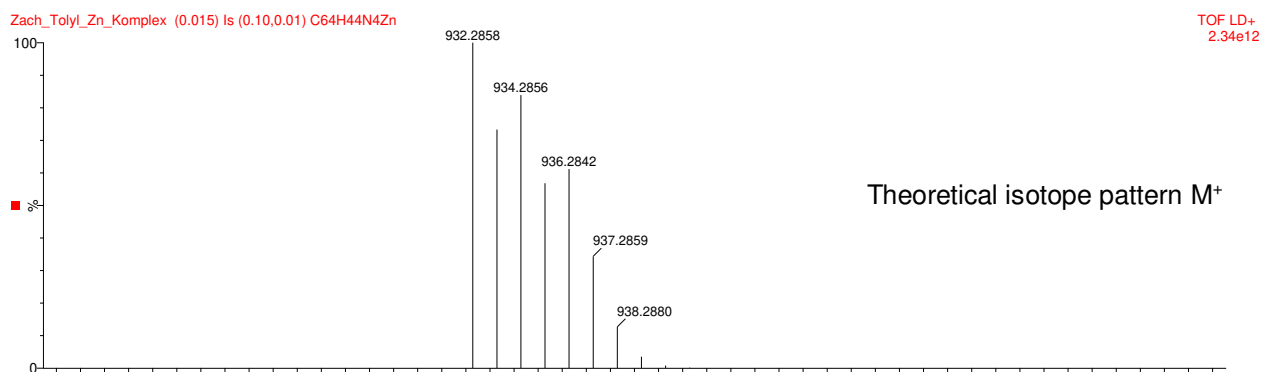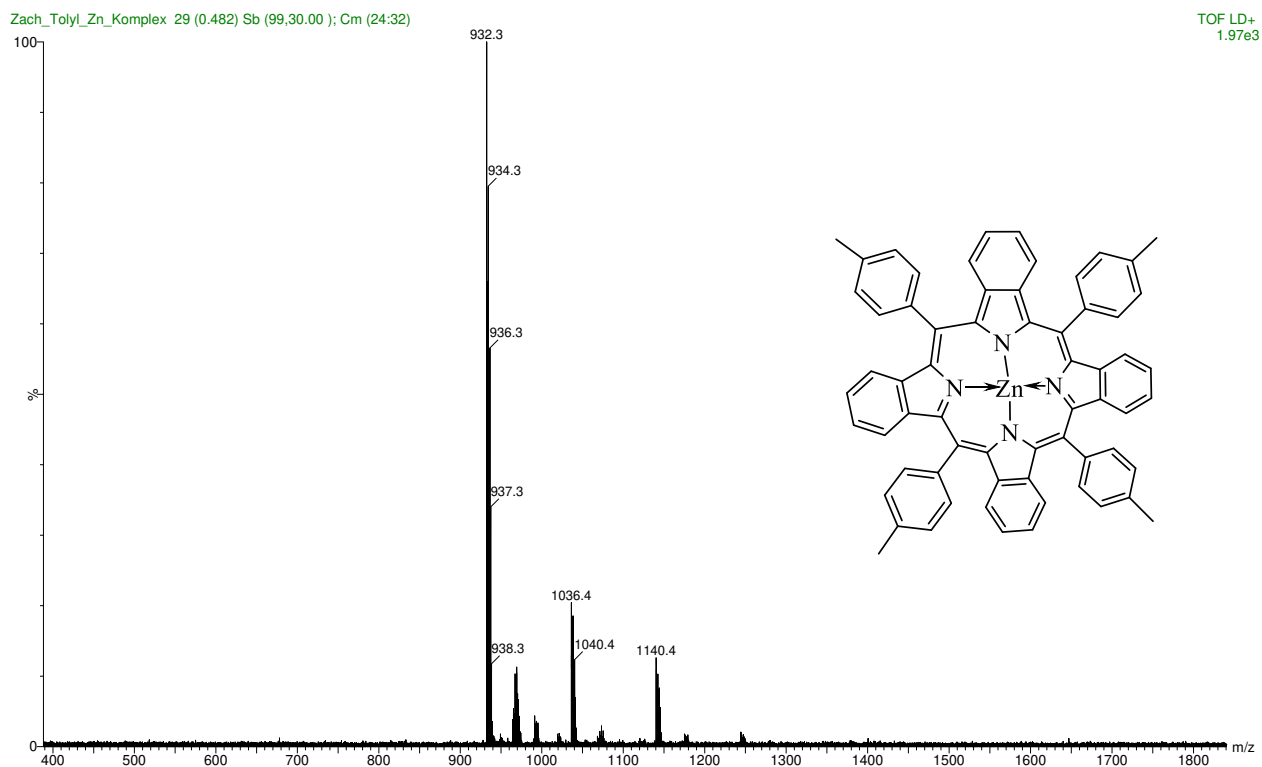
Figure S 6.45. Mass spectrum (MALDI-TOF) of Zn-TTolTBP
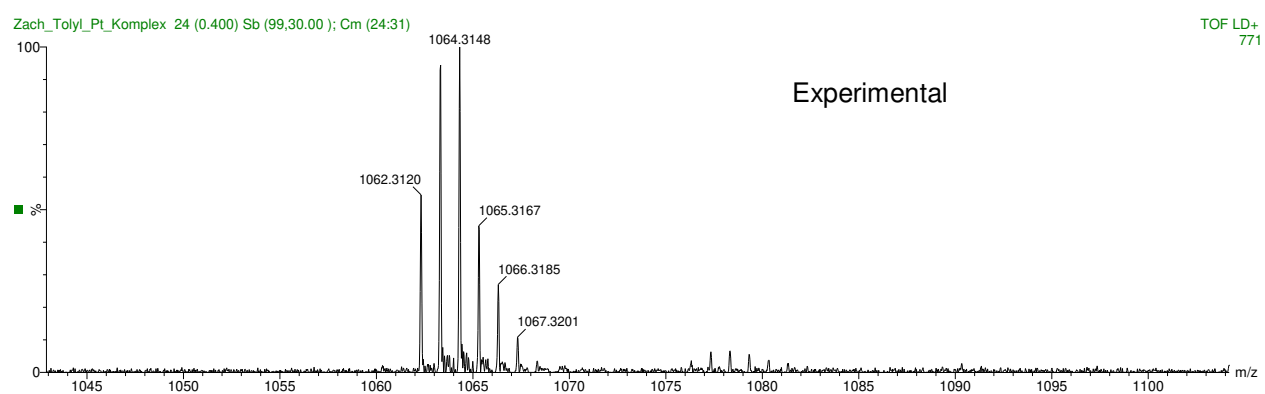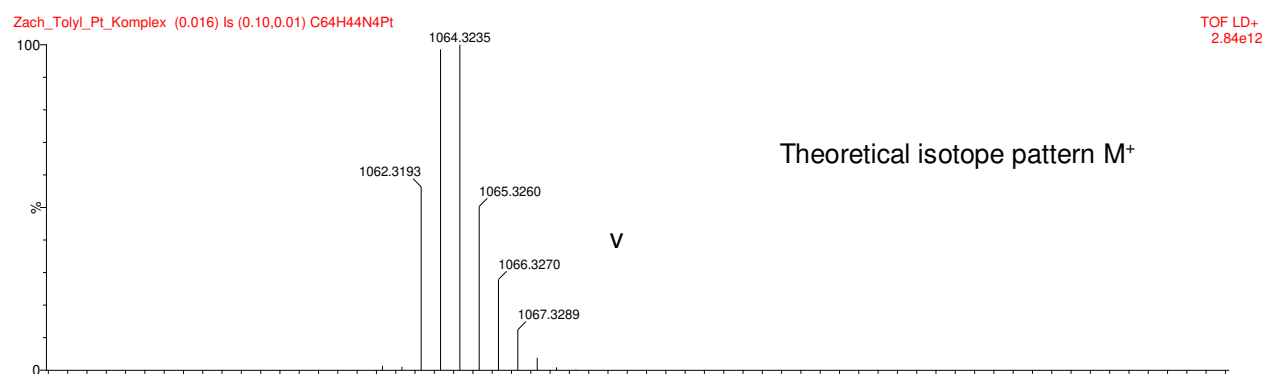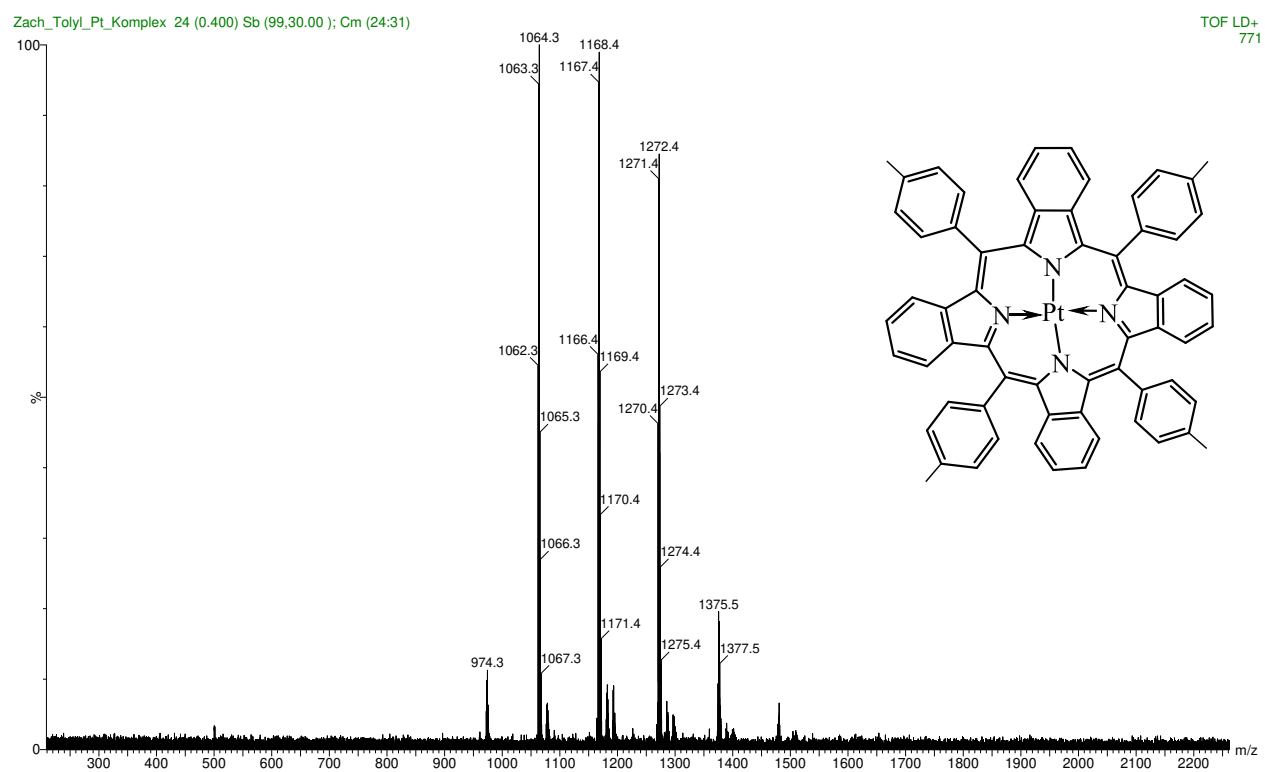
Figure S 6.46. Mass spectrum (MALDI-TOF) of Pt-TTolTBP
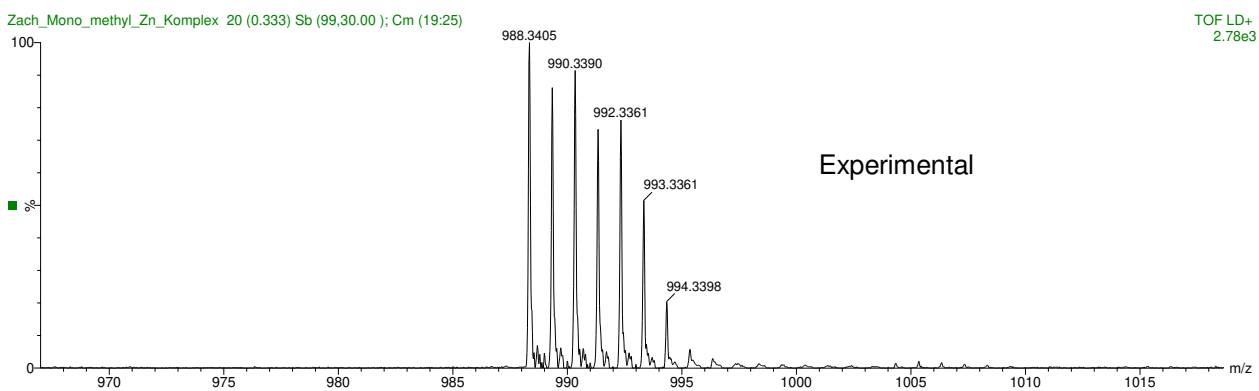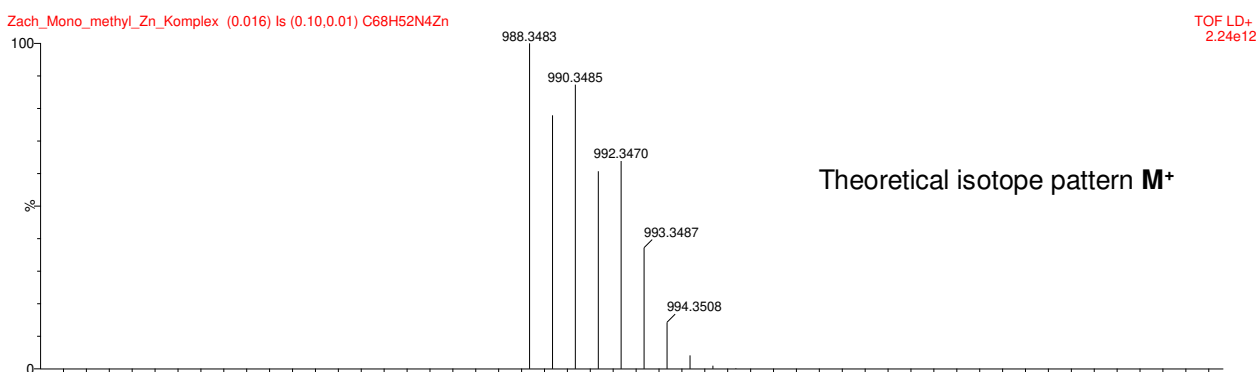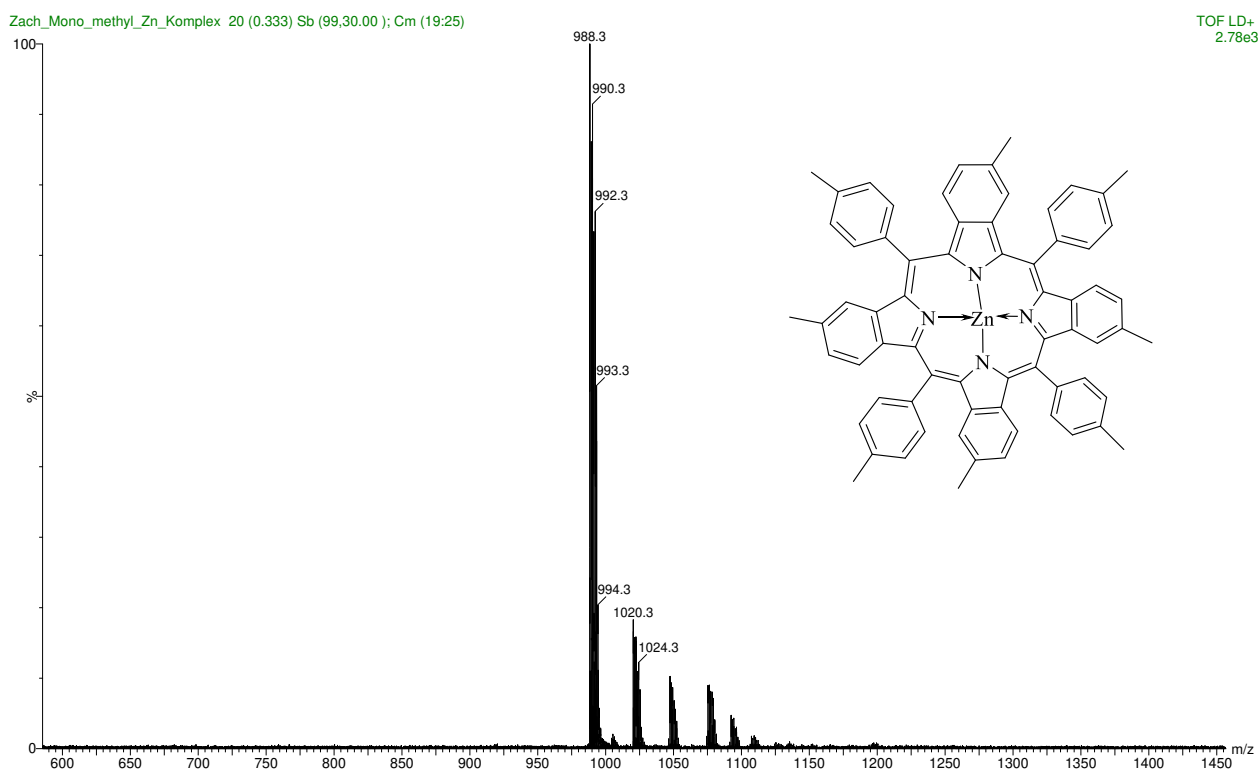
Figure S 6.47. Mass spectrum (MALDI-TOF) of Zn-TTTBPmM₄
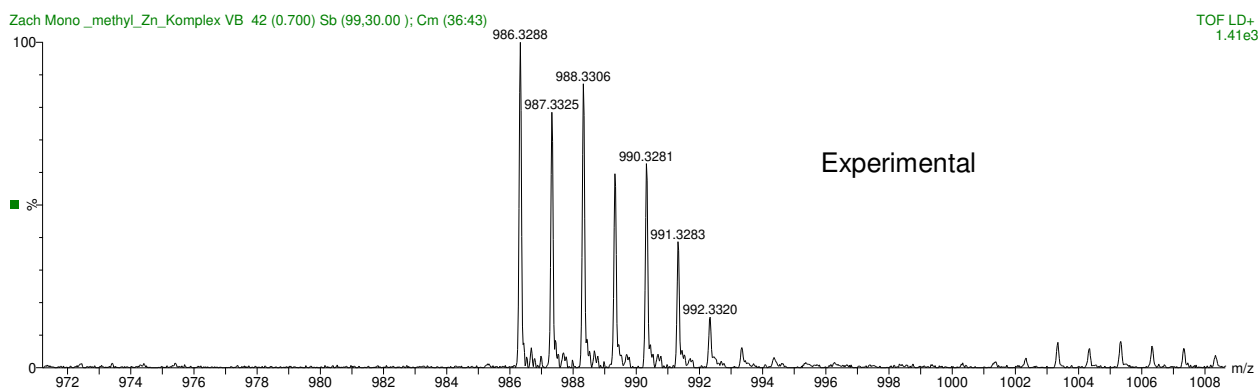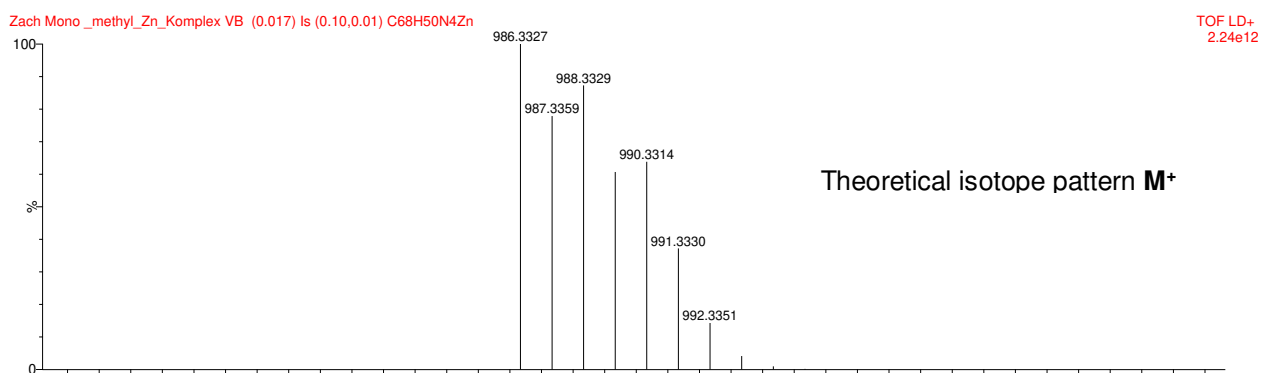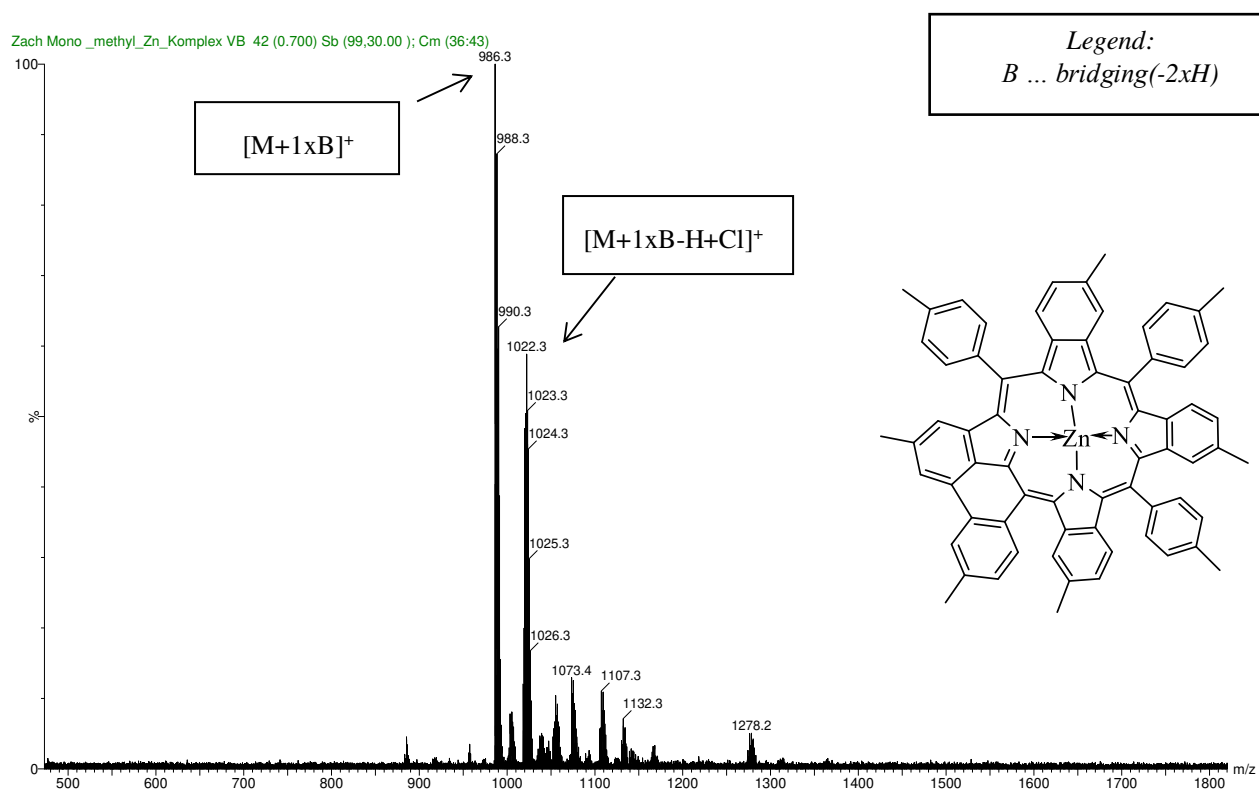
Figure S 6.48. Mass spectrum (MALDI-TOF) of bridged Zn-TTTBPmM₄
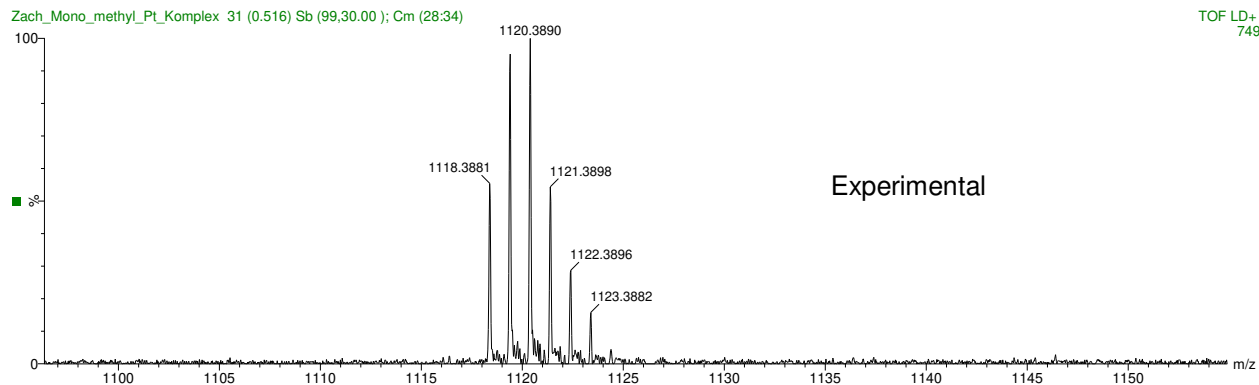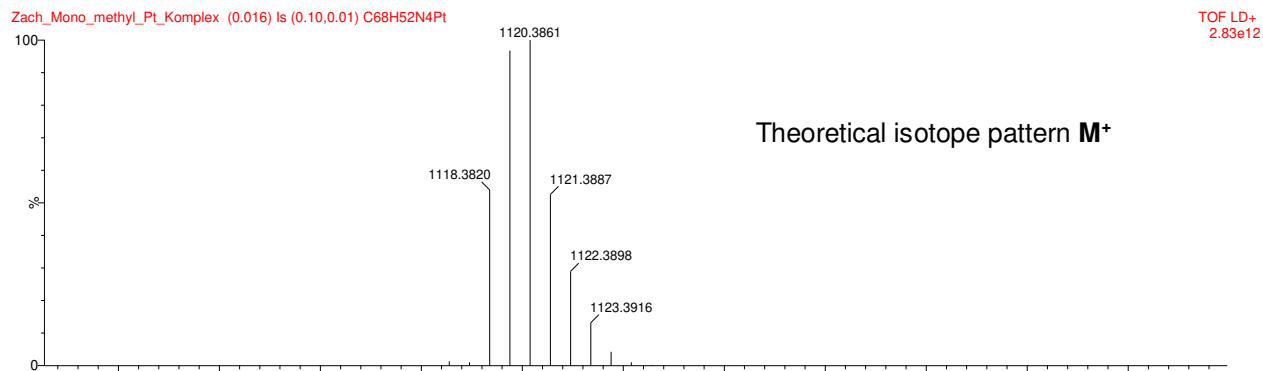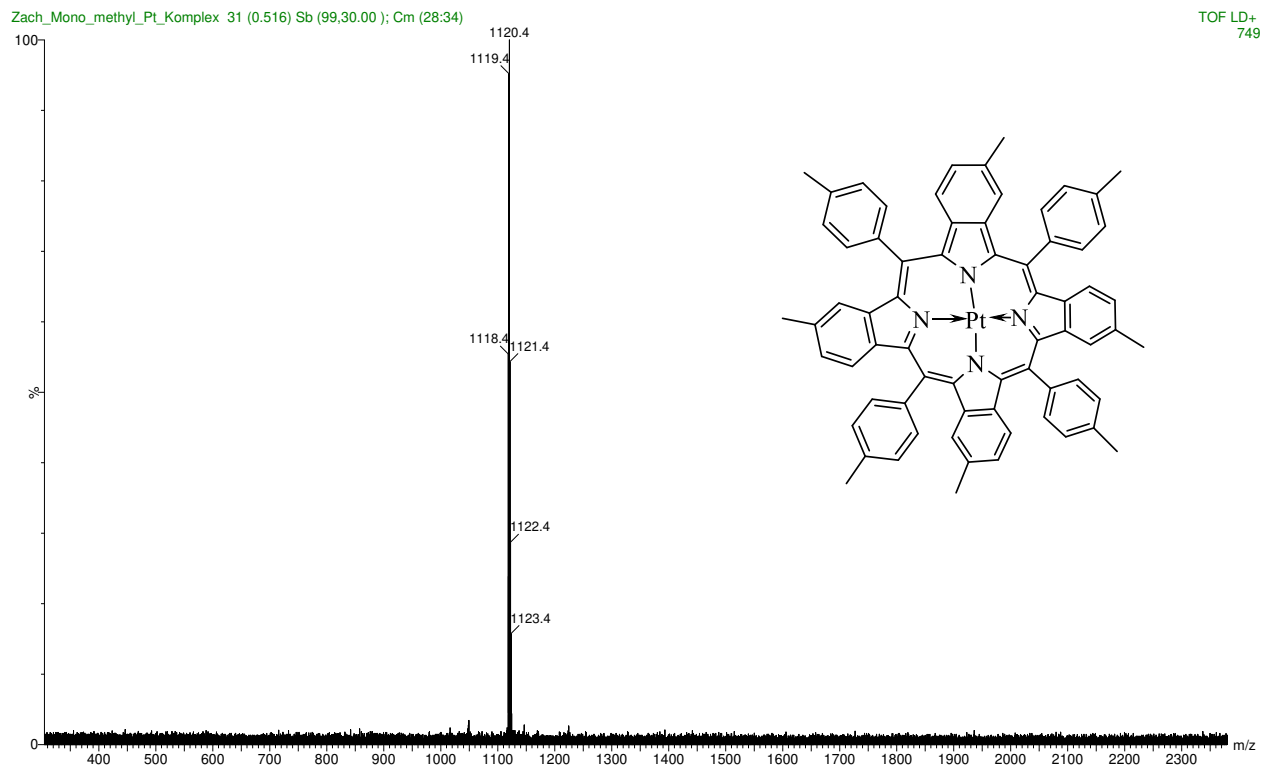
Figure S 6.49. Mass spectrum (MALDI-TOF) of Pt-TTTBPmM₄
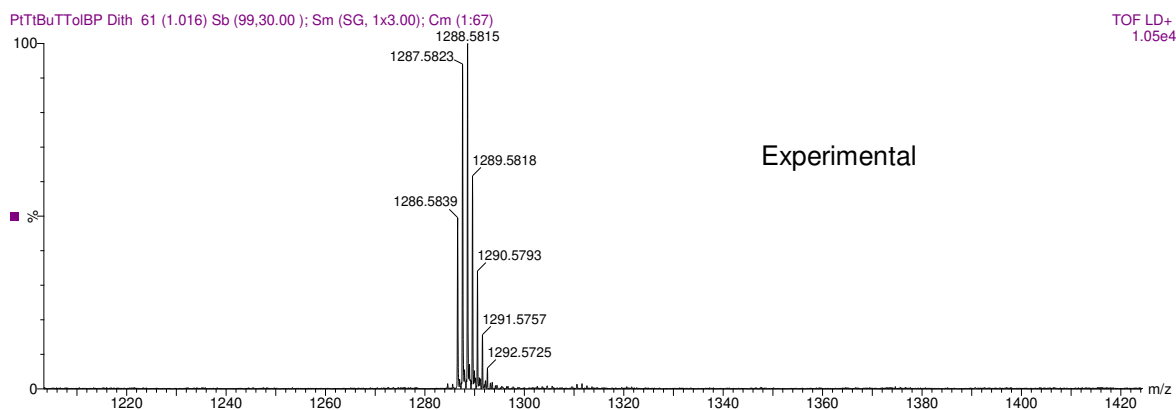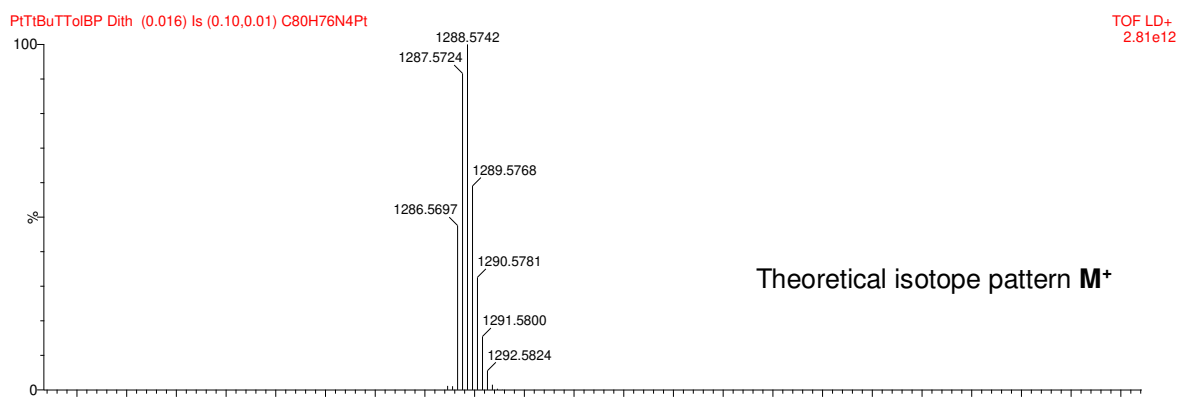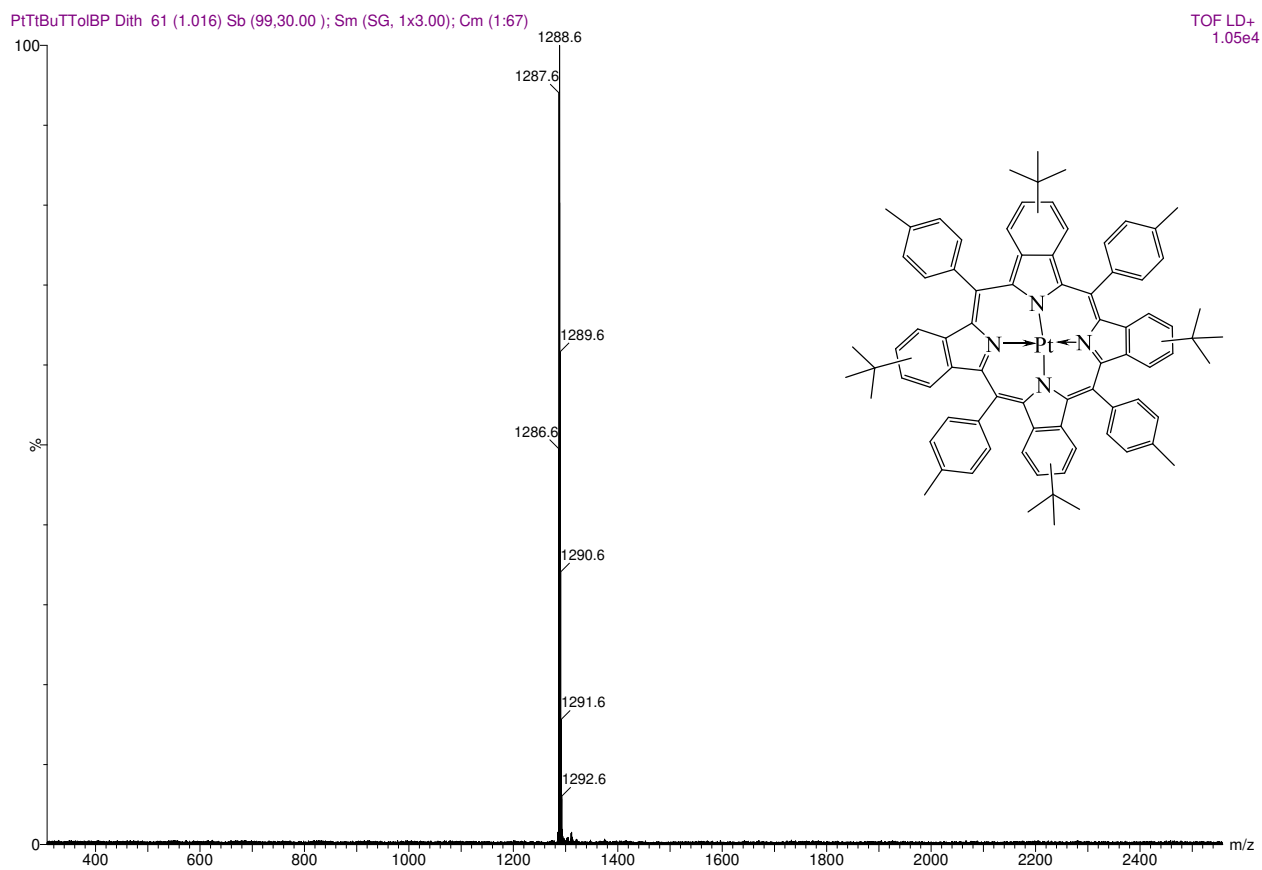
Figure S 6.50. Mass spectrum (MALDI-TOF) of Pt-TTTBPtBu
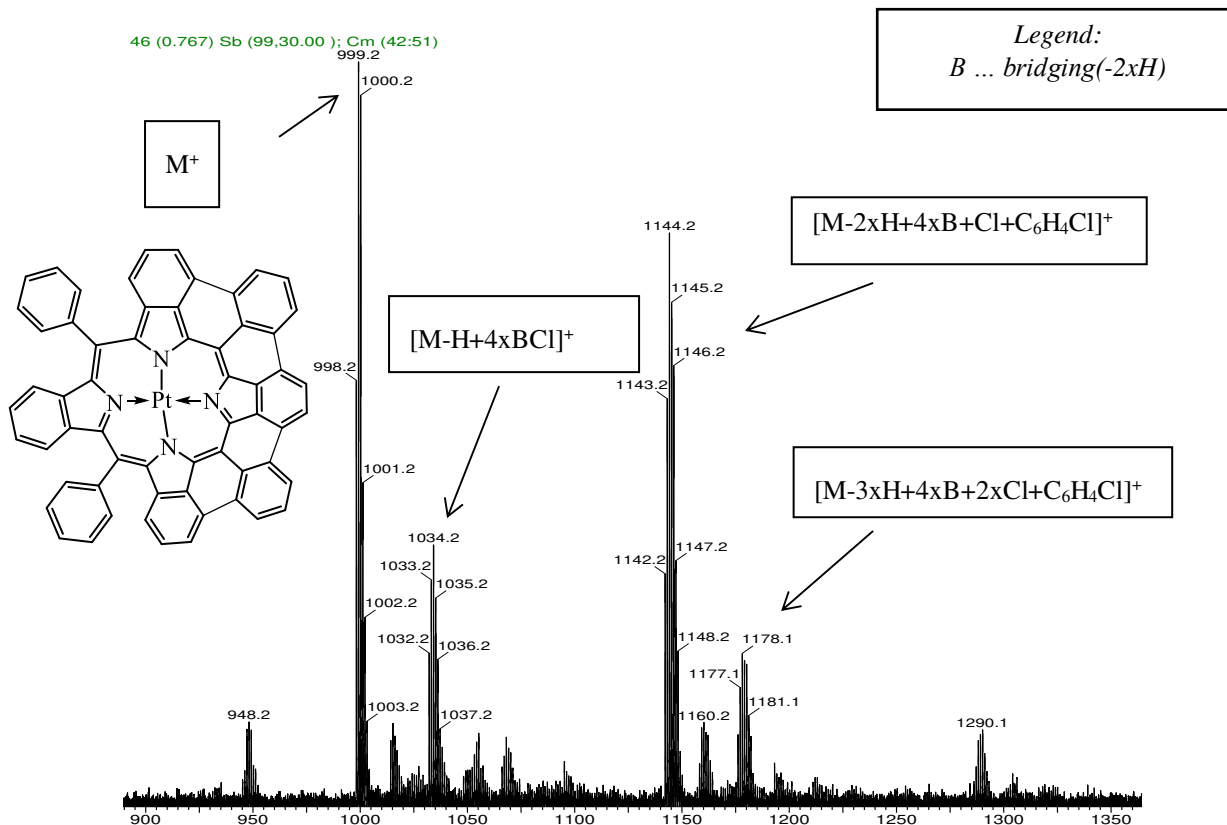
Figure S 6.51. Mass spectrum (MALDI-TOF) of bridged Pt-B1
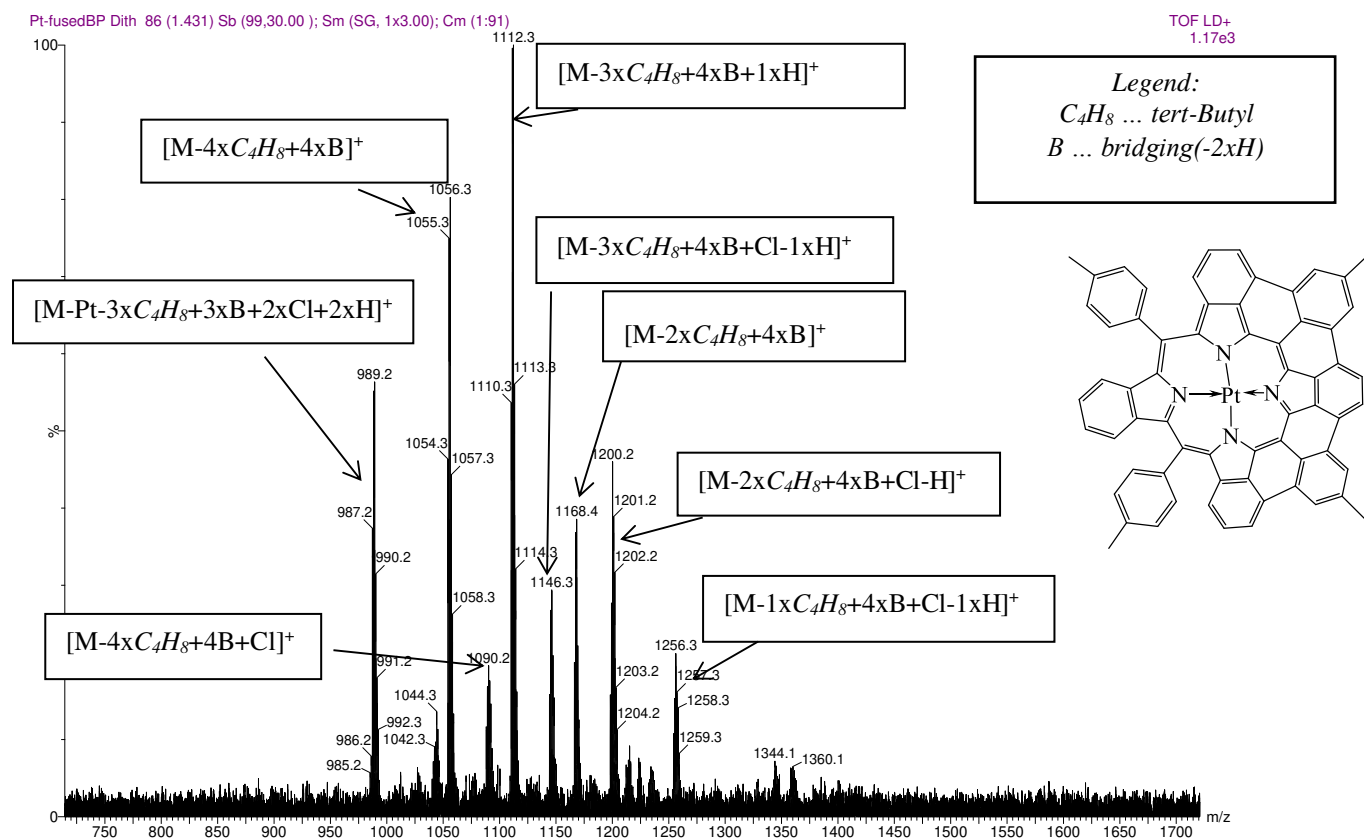
Figure S 6.52. Mass spectrum (MALDI-TOF) of bridged Pt-B2
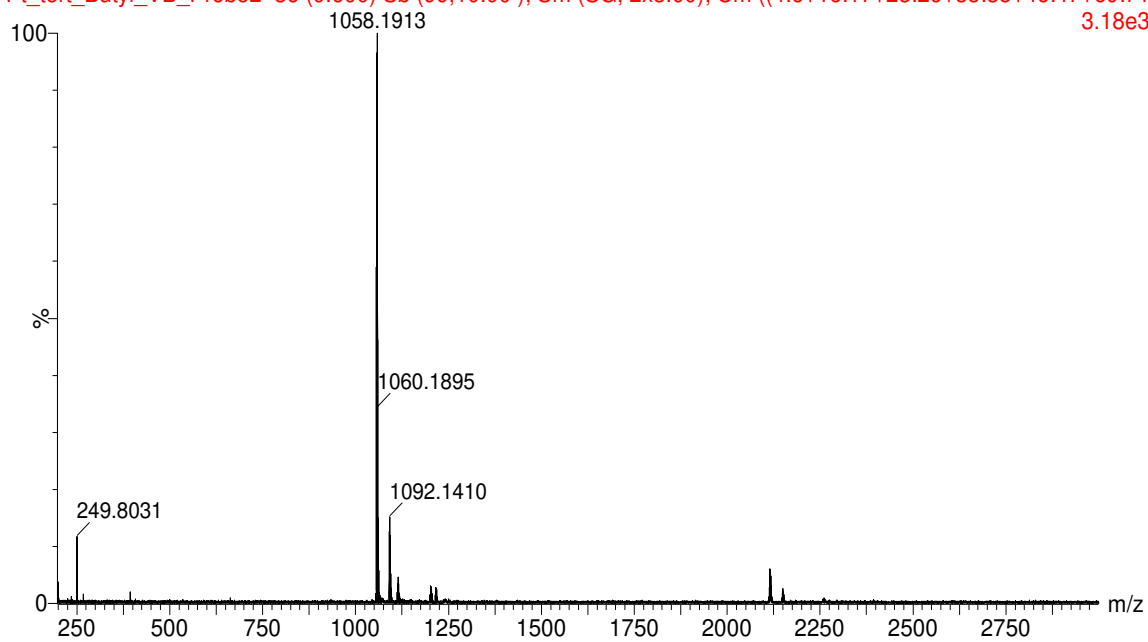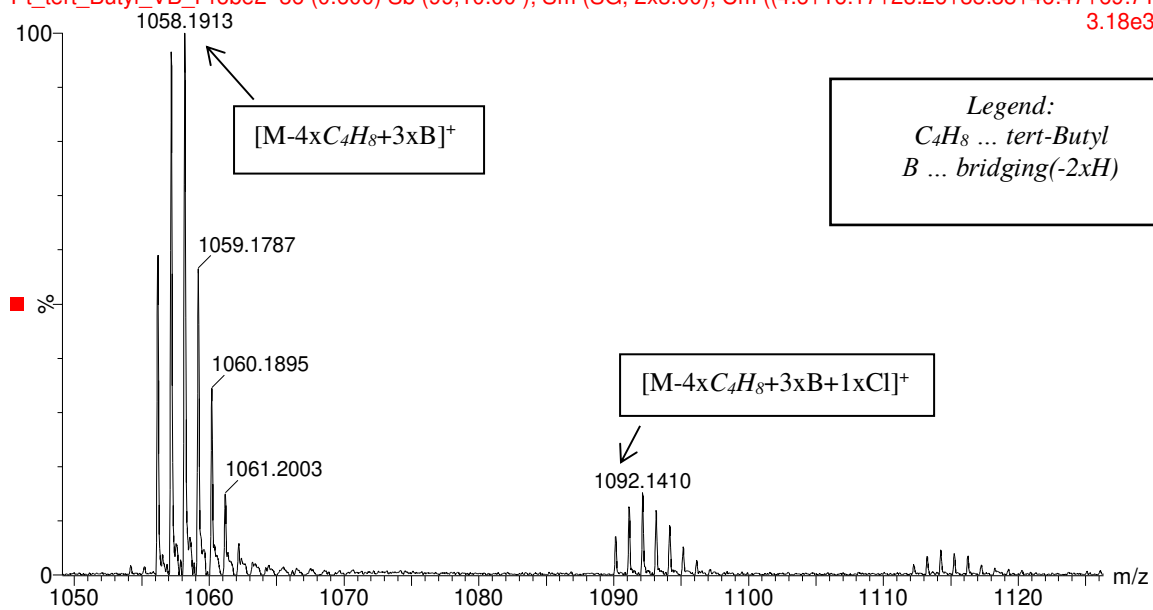
Figure S 6.53. Mass spectrum (MALDI-TOF) of bridged Pt-B3
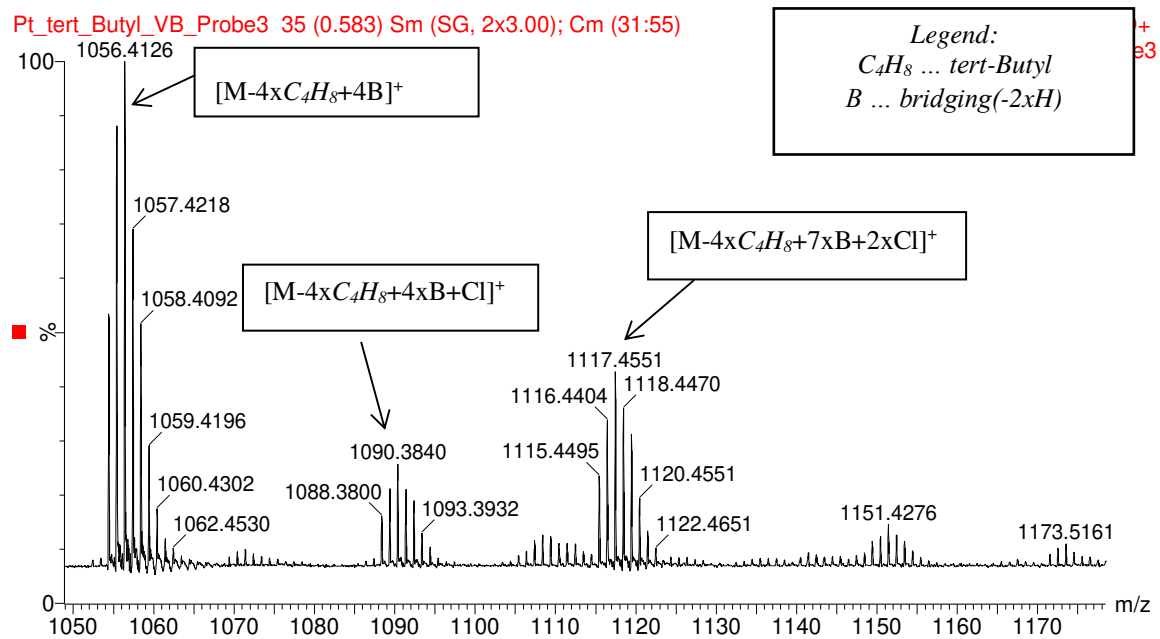
Figure S 6.54. Mass spectrum (MALDI-TOF) of bridged Pt-B4

Chapter 7

Tuning Photophysical Properties of Phosphorescent Benzo-porphyrin Complexes via 1-step π-Extension
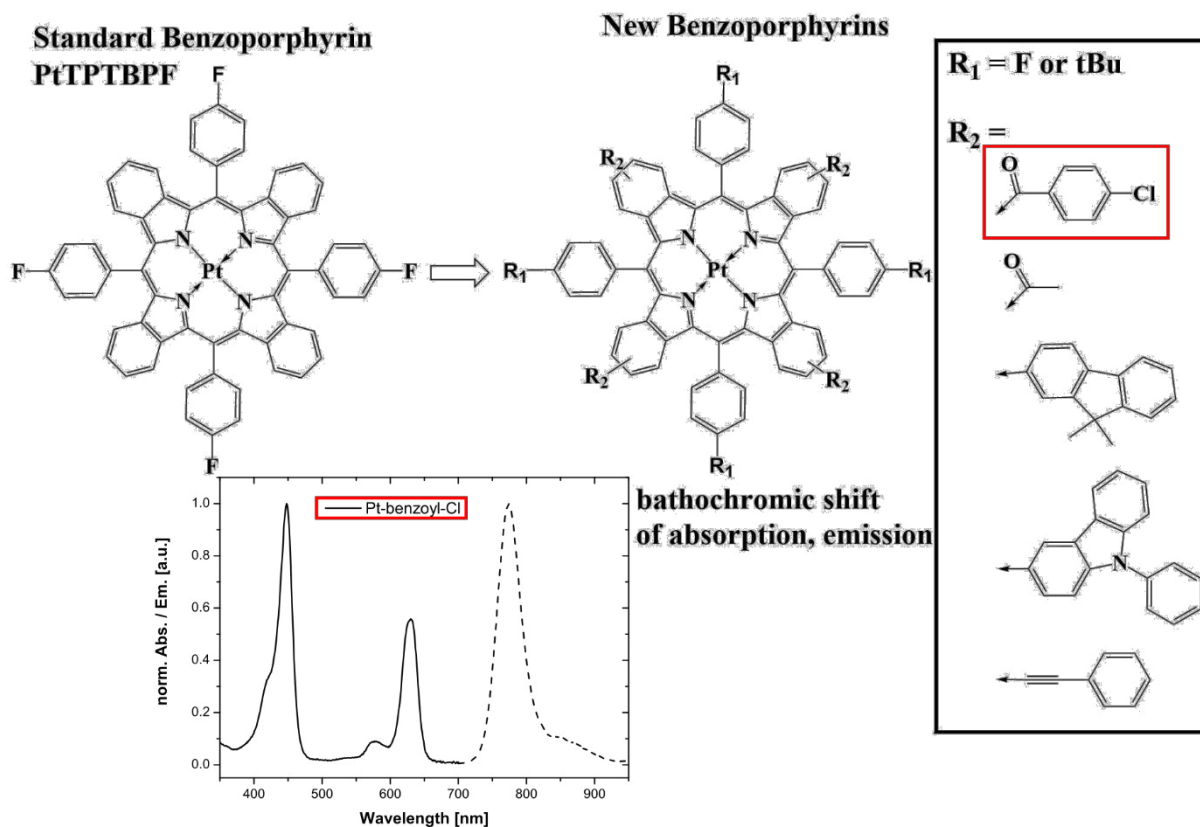
7 Tuning Photophysical Properties of Phosphorescent Benzo-porphyrin Complexes via 1-step π-Extension

This chapter will be submitted as Full Paper to

Dyes & Pigments

Peter W. Zach,[§] Maximilian Maierhofer,[§] Sabrina D. Püschmann, Ingo Klimant, and Sergey M. Borisov[*]

Institute of Analytical Chemistry and Food Chemistry, Graz University of Technology, Stremayrgasse 9, 8010, Graz, Austria. E-mail: sergey.borisov@tugraz.at

[§] these authors contributed equally

Keywords: π-extension, NIR, phosphorescence, platinum, oxygen, triplet-triplet-annihilation, upconversion

7.1 Abstract

Complexes of benzoporphyrins are highly promising for application in optical oxygen sensors, as triplet sensitizers for generation of singlet oxygen and upconverison based on triplet-triplet annihilation (TTA). Particularly, they benefit from efficient absorption in red part of the spectrum and strong NIR phosphorescence. In this contribution we investigate different stategies of tuning the photophysical properties of these readily available complexes via 1-step modification. The new π-extended derivates are obtained via Friedel-Crafts acylation of tetraphenyltetrabenzoporphyrin (TPTBP) complexes and by Suzuki or Sonogashira cross-coupling reaction of the tetrabromo-substituted benzoporphyrins. The Soret and Q absorption bands of the tetra-substituted dyes shift bathochromically by about 15 nm compared to the parent TPTBP compounds. The modifed dyes retain their NIR phosporescent properties and feature slight improvment of the quantum yield. Application in optical oxygen sensing materials and triplet-triplet annihilation-based upconverion systems is demonstrated.

7.2 Introduction

In the last couple of years, phosphorescent metal complexes excitable in the red part of the spectrum with efficient emission in the NIR-region received much attention due to their broad field of potential applications, for instance in organic light emitting diodes (OLEDs) [1], [2] and optical sensors [3]–[5]. Compared to UV-Vis dyes, these complexes are especially promising for sensing applications due to lower autofluorescence and light scattering, and, because of the compatibility to the NIR optical window (700 – 950 nm), enable measurements of oxygen (and glucose via an oxygen transducer) in tissues as well as in living organisms. [6]–[9] Due to efficient generation of singlet oxygen upon quenching, application of such systems in photodynamic therapy is also of high interest. [10]–[12] Such complexes were also intensively investigated as sensitizers in TTA-based upconversion systems for potential application in photovoltaics, [13], [14] bioimaging [15] and photocatalysis. [16] Red-light- and NIR-excitable sensitizers are especially attractive for the light conversion applications, since almost 50 % of the energy from the sun reaching the earth is NIR radiation [17] with a maximum flux of sunlight at approximately 680 nm. [18]

Bathochromic shift of the absorption and the emission bands of various porphyrinoids can be achieved in different ways. However, so far the most promising way was the extension of the π-conjugated system of the porphyrin core through fusion of various aromatic moieties at the β-pyrrole positions leading to tetrabenzoporphyrins (TBP) [19], [20] tetranaphthaloporphyrins (TNP) [2], [21]–[23] or even tetra-anthroporphyrins (TAP) [24]. Significant bathochromic shifts of absorption as well as emission were also achieved via modification of benzoporphyrins in an intramolecular Scholl reaction leading to bridged benzoporphyrin derivatives. [9] All these complexes possess phosphorescence ranging from 770 to 1020 nm but the non-radiative decay rate increases substantially with the decreasing T_1 - S_0 energy gap. [17] This indicates a limited potential for the extension of absorption and emission to longer wavelengths. In fact, most NIR absorbing porphyrinoids are non-emissive. [25]–[28] For many practical applications, it is therefore necessary to find a compromise between the bathochromic shift of absorption and the phosphorescence quantum yield (Φ). Another very important parameter is the photostability of the dyes which can be dramatically reduced by π-extension such as in case of naphthoporphyrins and their molecular hybrids with benzoporphyrins. [29] Although poor photostability and solubility of naphthoporphyrins can be improved, a sophisticated multistep synthesis is necessary. [21] Therefore, investigation of alternative possibilities for adjusting the spectral properties of the phosphorescent porphyrins via π-extension remains of much interest.

In this contribution we report the synthesis of new complexes prepared via one step modification of existing benzoporhyrins. Platinum(II)-meso-tetra-(4-t-butyl)phenyl-tetra-bromobenzo-porphyrin (Pt-TPTBPtBu$_4$Br$_4$) [30] was modified via Suzuki or Sonogashira coupling reaction and platinum(II)-meso-tetra(4-fluorophenyl)tetrabenzoporphyrin (Pt-TPTBPF) [31] with help of Friedel-Crafts acylation. The resulting platinum(II) benzoporphyrin

derivatives show a bathochromic shift of approximately 15 nm in the absorption and therefore become compatible with 632.8 nm line of He-Ne laser as well as 635 nm laser diodes. Furthermore, the new dyes possess similarly good photostability and solubility but higher phosphorescence quantum yields compared to the benzoporphyrin precursors (except Pt- Ph-acetylene).

7.3 Experimental Section

7.3.1 Materials

1,2-dichlorobenzene, copper(I) iodide, potassium carbonate, phenylacetylene and toluene were ordered from Sigma-Aldrich and acetyl chloride from Fluka. 4-Chlorobenzoyl chloride was purchased from ABCR and Silica-gel 60 and aluminum trichloride from Merck. Polystyrene (PS; Mw = 260000 g mol^{-1}) was obtained from Acros Organics. Sodium sulfate, potassium carbonate and sodium chloride were from VWR. Tetrakis(triphenylphosphine)palladium(0), 9-phenylcarbazole-3-boronic acid and 9,9-dimethylfluoren-2-boronic acid were purchased from TCI. All the solvents and triethylamine (TEA) were from and Roth. Nitrogen and oxygen (both of 99.999 % purity) were acquired from Air Liquide and Linde Gas GmbH, respectively. Poly(ethyleneterephthalate) (PET) support Melinex 505 was purchased from Pütz (Taunusstein, Germany). Platinum(II)-meso-tetra-(4-t-butyl)phenyl-tetra-bromobenzo-porphyrin (Pt-TPTBPtBu$_4$Br$_4$) and platinum(II)-meso-tetra(4-fluoro-phenyl)tetrabenzoporphyrin (Pt-TPTBPF) were synthesized analogously to the literature procedure. [30], [31] In all cases deionized water was used.

7.3.2 Synthesis

Pt-fluorene

Pt-TPTBPtBu$_4$Br$_4$ (20.0 mg, 12.9 µmol, 1.00 eq) was dissolved in toluene (6.5 mL) under argon atmosphere. 9,9-Dimethylfluorene-2-boronic acid (30.8 mg, 129 µmol, 10.0 eq) and K$_2$CO$_3$ as base (71.4 mg, 517 µmol, 40.0 eq) were added to the solution. The base was pre-dissolved in H$_2$O (1.5 mL). Catalyst Pd(PPh$_3$)$_4$ (0.89 mg, 0.77 µmol, 0.06 eq) was added and the reaction mixture was heated to 100 °C and stirred for 4 h. The reaction progress was monitored via absorption spectroscopy (solvent: toluene). The reaction mixture was cooled down to RT. After addition of DCM (dichloromethane), the organic layer was washed with H$_2$O and dried over Na$_2$SO$_4$ and the solvent was removed under reduced pressure. The crude product was purified via column chromatography (silica-gel, cond. cyclohexane (CH), CH:DCM), yielding a dark green solid. Yield: 5 mg, 17 %.

^{1}H NMR (300 MHz, CD$_2$Cl$_2$) δ 8.37 – 8.19 (m, 8H), 8.08 – 7.94 (m, 8H), 7.84 – 7.53 (m, 22H), 7.54 – 7.48 (m, 4H), 7.42 – 7.27 (m, 14H), 7.21 (d, J = 8.9 Hz, 2H), 7.10 (d, J = 8.6 Hz, 2H), 1.77 – 1.62 (m, 36H), 1.50 (s, 28H).

MALDI-TOF m/z [M$^+$] C$_{136}$H$_{116}$N$_4$Pt calcd: 2000.89, found: 2000.89

Pt-carbazole

Pt-carbazole was synthesized analogously to Pt-fluorene but using 25.0 mg (16.2 µmol, 1.00 eq) of Pt-TPTBPtBu$_4$Br$_4$ dissolved in toluene and tetrahydrofuran (THF) (6 +3 mL) and 9-phenylcarbazole-3-boronic acid (46.4 mg, 162 µmol, 10.0 eq) instead. The crude product was purified via column chromatography (silica-gel, cond. CH, CH:DCM, 3:1), yielding a dark green solid. Yield: 11 mg, 31 %.

^{1}H NMR (300 MHz, CD$_2$Cl$_2$) δ 8.39 – 8.09 (m, 16H), 7.97 (tt, J = 10.4, 4.1 Hz, 6H), 7.74 – 7.55 (m, 22H), 7.48 – 7.33 (m, 22H), 1.73 (t, J = 4.1 Hz, 9H), 1.64 – 1.53 (m, 17H), 1.45 – 1.31 (m, 8H).

MALDI-TOF: m/z [M$^+$] C$_{148}$H$_{112}$N$_8$Pt calcd: 2196.87, found: 2196.88

Pt-benzoyl-Cl

Pt-TPTBPF (20.0 mg, 18.5 µmol, 1.00 eq) was dissolved in 1,2-dichlorobenzene (8 mL) under argon atmosphere. 4-Chlorobenzoyl chloride (0.12 mL, 0.93 mmol, 50.0 eq) and AlCl$_3$ (40.0 mg, 0.30 mmol, 16.2 eq) were added to the solution. The reaction mixture was heated to 130 °C and stirred for 30 min. The reaction progress was monitored via absorption spectroscopy (solvent mixture of CHCl$_3$ and ethanol (EtOH) 10:1). After complete conversion the reaction mixture was cooled down to RT and treated with EtOH:H$_2$O (1:1 v/v, 40 mL) and stirred for 10 minutes to neutralize the excess of AlCl$_3$. After addition of DCM, the organic layer was washed with H$_2$O and dried over Na$_2$SO$_4$ and the solvent was removed under reduced pressure. The crude product was purified via column chromatography (silica-gel, cond. toluene, DCM:Tol, 7:1), yielding a dark green solid. Yield: 10 mg, 33%.

^{1}H NMR (300 MHz, CD$_2$Cl$_2$) 8.33 – 8.18 (m, 2H), 8.18 – 8.07 (m, 3H), 8.06 –7.92 (m, 2H), 7.80 (dt, J = 13.5, 7.5 Hz, 4H), 7.66 (d, J = 7.4 Hz, 2H), 7.53 (dd, J = 11.8, 5.4 Hz, 16H), 7.44 – 7.32 (m, 5H), 7.31 – 7.19 (m, 2H), 7.19 – 7.02 (m, 4H)

MALDI-TOF: m/z [M$^+$] C$_{88}$H$_{44}$Cl$_4$F$_4$N$_4$O$_4$Pt calcd: 1634.17, found: 1634.17

Pt-acetyl

This acylation was performed analogously to Pt-TPTBPF-benzoyl-Cl but with acetyl chloride (66 µL, 0.93 mmol, 50.0 eq) instead of 4-chlorobenzoyl chloride. The crude product was purified via flash column chromatography (silica-gel, cond. toluene, DCM:Tol, 8:1), yielding a dark green solid. Yield: 18.3 mg, 77%.

^{1}H NMR (300 MHz, CD$_2$Cl$_2$) δ 8.37 – 8.09 (m, 8H), 8.07 – 7.43 (m, 16H), 7.28 – 7.03 (m, 4H), 2.43 – 2.17 (m, 12H).

MALDI-TOF: m/z [M$^+$] C$_{68}$H$_{40}$F$_4$N$_4$O$_4$Pt calcd: 1248.26, found: 1248.22

Pt-Ph-acetylene

This synthesis was performed analogously to literature. [32], [33] Pt-TPTBPtBu$_4$Br$_4$ (50.0 mg, 32.3 µmol, 1.00 eq) and catalytic amount of CuI (1.23 mg, 6.50 µmol, 0.20 eq) was dissolved in 1.5 ml abs. THF and 0.7 ml abs. triethylamine (TEA) in a Schlenk flask under Ar atmosphere. Pd(PPh$_3$)$_4$ (3.73 mg, 3.23 µmol, 0.10 eq) and phenylacetylene (33.0 mg, 323 µmol, 10.00 eq) were added to the solution. The solution was stirred for 18 h at 75 °C. Conversion control of the reaction was performed via TLC (silica-gel, CH:DCM 3:1). The green solution was first washed 4 times with 10% CuSO$_4$ to remove the excess of TEA (clear solution). The product was extracted with DCM, the organic layer was dried over Na$_2$SO$_4$. The solvent was removed under reduced pressure. Further purification was conducted via flash column chromatography (silica-gel, cond. CH, CH:DCM 7:1) yielding fractions with different number of substituents. The product containing fractions were determined via absorption spectra. Yield: 2.0 mg, 4%.

^{1}H NMR (300 MHz, CD$_2$Cl$_2$) δ 8.16 (m, J = 14.8, 14.4, 9.0 Hz, 8H), 7.98 (td, J = 20.4, 5.7 Hz, 8H), 7.49 (m, J = 4.6 Hz, 5H), 7.37 (m, J = 5.1 Hz, 10H), 7.32 (s, 1H), 7.29 (d, J = 5.4 Hz, 2H), 7.25 (m, J = 14.6, 7.1 Hz, 5H), 7.22 – 7.19 (m, 1H), 7.16 (m, J = 13.1, 7.4 Hz, 7H), 7.10 – 7.03 (m, 2H), 1.68 (d, J = 8.1 Hz, 36H).

MALDI-TOF: m/z [M$^+$] C$_{108}$H$_{84}$N$_4$Pt calcd: 1632.63, found: 1632.67

7.3.3 Preparation of sensor films

The "cocktails" were prepared by dissolving the respective indicator (0.5 - 1 wt% in respect to the polymer) and polystyrene (10 wt% in respect to the solvent) in chloroform. Then the "cocktails" were knife-coated on a dust-free PET support using a 25 mm-wide Gardner coating knife (Pompano Beach, United States) with a wet thickness of 25 µm. Finally, the sensor films were dried for 24 hours at 60 °C to ensure complete removal of solvent.

7.3.4 Measurements

^{1}H and ^{13}C NMR were recorded on a 300 MHz instrument (Bruker AVANCE III). In all spectra, the residual signal of the deuterated solvent was used as an internal standard to reference the chemical shifts δ. Data analysis was performed with the MestreNova NMR software. High resolution mass spectra were recorded using a Micromass TofSpec 2E as positive reflector on a Bruker Ultraflex Extreme MALDI-TOF/TOF spectrometer. The mass spectra were analyzed with the FlexAnalysis 3.0 software (Bruker Daltonics).

The absorption spectra of the dyes were recorded on a CARY 50 conc UV-Vis spectrophotometer from Varian (Palo Alto, United States). Molar absorption coefficients were determined in three independent measurements. The luminescence spectra were recorded on a FluoroLog® 3 spectrofluorometer from Horiba Scientific equipped with a NIR-sensitive R2658 photomultiplier from Hamamatsu. Quantum yields were determined

according to Crosby and Demas [34] using a solution of dibutoxy-aza-BODIPY (BF_2 chelate of [5-(4-buthoxyphenyl)-3-phenyl-1Hpyrrol-2-yl][5-(4-buthoxyphenyl)-3-phenylpyrrol-2-ylid-ene]-amine) in chloroform as a reference (Φ = 36%). [35], [36] All dye solutions were deoxygenated in a screw-cap cuvette (Hellma; Müllheim, Germany) by bubbling argon through the solution for 10 min. Photophysical studies in solutions were performed for the dye concentrations of between 2 and $4*10^{-6}$ mol*L^{-1}. The phosphorescence decay times of the complexes in solution and in sensing foils were obtained in frequency domain using a Firesting oxygen meter from PyroScience (Aachen, Germany) at a modulation frequency of 4 kHz.

7.3.5 Photostability tests

The dye solutions in toluene (HPLC-grade) were filled in a screw-cap cuvette and illuminated with a high-power LED array ($λ_{max}$ 635 nm, www.LED-TECH.de) using a constant current LED driver from Dehner (Model: LED-350MA35W-IP67; Oestrich-Winkel, Germany) at the 35W and 350 mA. The light of the LED-array was focused onto the glass cuvette utilizing a lens from Edmund optics. The photon flux was > 20.000 µmol s^{-1} m^{-2} µA (irradiance 377 mW*cm^{-2}) as determined with a Li-250A light meter from Li-COR (Nebraska, USA). For measurements at air saturation the cuvette was unsealed and shaken after each irradiation interval to ensure air saturation in the sample.

7.3.6 Oxygen response of the polystyrene sensors

The composition of the gas was adjusted utilizing a custom-build gas-mixing device based on mass-flow controllers from MKS (Munich, Germany) and Voegtlin (Hamburg, Germany) by mixing compressed air, nitrogen and oxygen. The temperatures during the characterization were controlled and kept constant using a cryostat ThermoHaake DC50 (www.thermoscientific.de/home).

7.3.7 Upconversion experiments

The upconversion experiments were conducted on FluoroLog® 3 spectrofluorometer from Horiba. For excitation of the sensitizer-annihilator solutions in toluene a 450 W xenon lamp from the fluorometer or a laser diode (635 nm, from Roithner-Laser.com) were used. Due to the high concentration of the sensitizer-annihilator solutions all spectra were recorded in the front-face mode. The solutions were deoxygenated in a screw-cap cuvette by bubbling argon through the solution for 10 minutes. Neutral density filters (50%, 25%, 10%, 5% of

transmission) were used to modulate the intensity of the excitation light. The exact transmissions at the excitation wavelength were calculated from absorption spectra of the filters. The quantum yields of the upconverted fluorescence were roughly estimated by comparing the emission of the annihilator and the emission of the sensitizer without the annihilator. The photographic images of the upconverted fluorescence were acquired using 635, 650 and 675 nm laser diodes (Roithner) with Canon 5D camera.

7.4 Results and Discussions

7.4.1 Synthesis

The new complexes are prepared via one step modification of Pt(II)-meso-tetraaryltetrabenzoporphyrins conveniently accessible via a 3-step synthesis. The template condensation of either phthalimides or dicyanobenzenes with phenylacetic acid (Fig. 7.1) results in Zn(II) benzoporphyrins with moderate yields (5-10%) which however can be obtained on multi-gram scale from inexpensive chemicals. The Zn(II) complexes are demetalated in acidic conditions and the Pt(II) dyes are prepared via platination of the free-base porphyrin. It should be mentioned that only condensation using dicyanobenzenes results in analytically pure benzoporphyrins, whereas synthesis of the dyes in the "classical" template condensation is accompanied by formation of benzyl-fused adducts and other by-products (porphyrins without 1 Br atom) which are virtually impossible to separate. These by-products significantly diminish the yields of the aimed complexes in subsequent π-extension reactions. Since 4-bromodicyanobenzene is not commercially available and optimization of the yield was not the aim of the current study, we used the route starting from 4-bromophthalimide to obtain tetrabromo-substituted benzoporphyrins.
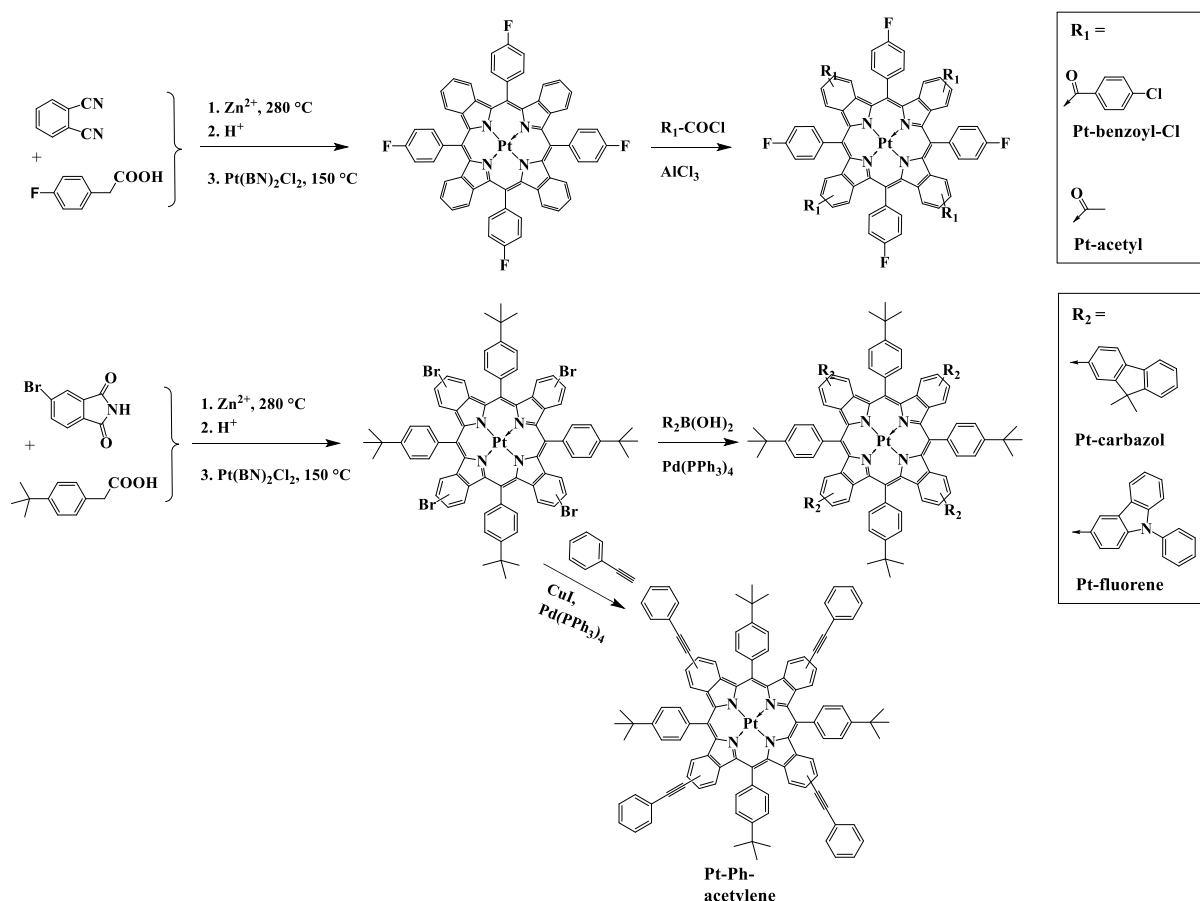
Figure 7.1 Synthesis of the new platinum(II) benzoporphyrin derivatives via one step modification of reported benzoporphyrin complexes available via template condensation.

Friedel-Crafts acylation of Pt-TPTBPF with either 4-chlorobenzoyl chloride or acetyl chloride in 1,2-dichlorobenzene in presence of AlCl₃ results in formation of Pt-benzoyl-Cl or Pt-acetyl, respectively, (ESI) in good yields (30-70%) obtained as a mixture of isomers (Figure 7.1).

Suzuki coupling reaction of Pt-TPTBPtBu₄Br₄ with the respective boronic acids (9,9-dimethylfluorene-2-boronic acid and 9-phenylcarbazole-3-boronic acid) led to formation of Pt-fluorene and Pt-carbazole derivatives, respectively (Figure 7.1). Sonogashira coupling of the same porphyrin with phenylacetylene resulted in the formation of Pt-Ph-acetylene (Figure 7.1). Due to above-mentioned impurities in Pt-TPTBPtBu₄Br₄ and incomplete substitution during the via Suzuki and Sonogashira reactions, the yields of the tetra-substituted products are very low and chromatographic purification is laborious.

7.4.2 Photophysical Properties

Fig. 7.2 shows absorption and emission spectra of the new platinum(II) benzoporphyrins in toluene in comparison with their respective benzoporphyrin precursors. Spectral properties of Pd-benzoyl-Cl are similar to those of Pt-acetyl and are presented in the supporting information. (Table S1 and Fig. S 7.2, ESI) π-extension via Suzuki and Sonogashira coupling

results in bathochromic shift of the Soret and Q bands by about 15 nm (Table 1). Interestingly, the π-extended complexes of fluorene, carbazole and Ph-acetylene have higher ratio of the molar absorption coefficients for the Q to Soret bands compared to the precursor.

Very similar bathochromic shift is observed upon introduction of acetyl and chlorobenzoyl groups in the same position. Interestingly, the Q-bands for these dyes are broader than for the Pt-TPTBPF precursor (FWHM of Pt-TPTBPF: 460 cm^{-1} at 615 nm; Pt-benzoyl-Cl: 666 cm^{-1} at 631 nm and Pt-acetyl: 634 cm^{-1} at 629 nm).
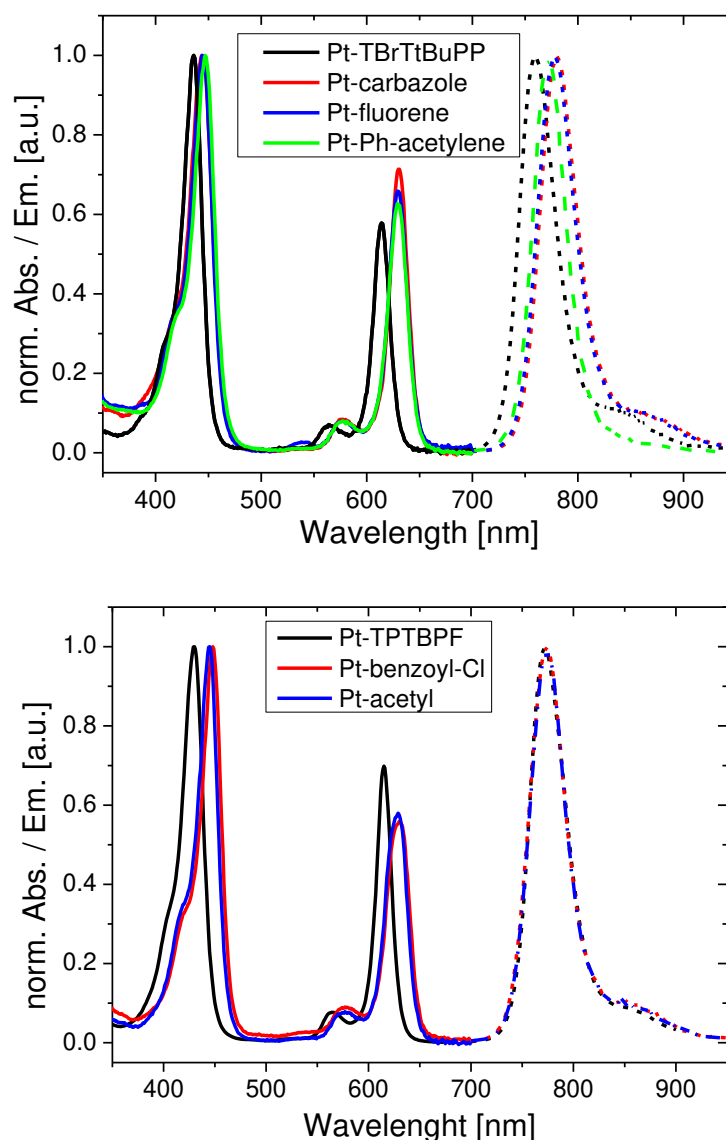
Figure 7.2. Absorption (solid lines) and emission (dashed lines) spectra of new Pt(II) complexes and precursors in toluene at 25 °C; anoxic conditions for emission measurements

These subtle effects, however, have pronounced impact on potential applications of the dyes in sensing and imaging. In fact, the new dyes are much better compatible with a number of light sources used in compact instruments and in microscopy such as bright blue 455-nm LED, 635-nm red laser diode, 455 nm line of the Ar laser and 632.8 nm line of the He-Ne laser. Importantly, all these sources almost perfectly fit the maxima of the Soret and

the Q-bands, which together with very high molar absorption coefficients (exceeding 210.000 and 110.000 $M^{-1}cm^{-1}$ for the Soret and the Q-band respectively) and high phosphorescence quantum yield (QY), Table 1, ensures unprecedented brightness. This can be of high interest if the dyes are used for imaging in cells and tissues. Notably, the position of the absorption bands of the new Pt(II) porphyrins is very similar to that of the Pd(II) complex with TPTBPF, which phosphorescence quantum yield is, however, significantly lower than for the Pt(II) complexes.

Table S 7.1. Photophysical properties of the new platinum(II) complexes and their precursors in anoxic toluene at 25 °C.

Complex	λ_{max} abs (ε), nm ($M^{-1}cm^{-1}$)	λ_{max} em, nm	Stokes shift, cm^{-1}	QY, Φ	τ, μs
Pt-TPTBPF	430 (212.000); 565 (16.300); 615 (146.000)	769	3260	0.24	50
Pt-fluorene	443 (274.000); 575 (22.000); 627 (171.000)	777	3080	0.28	45
Pt-carbazole	444 (240.000); 578 (21.400); 630 (171.700)	777	3000	0.29	44
Pt-benzoyl-Cl	448 (218.000); 579 (17.400); 631 (121.000)	773	2910	0.29	47
Pt-acetyl	445 (216.000); 577 (16.000); 629 (114.000)	773	2960	0.31	51
Pt-Ph-acetylene	446 (285.000), 577 (22.500) 630 (169.000)	772	2920	0.13	45

The new benzoporphyrin derivatives possess strong room-temperature phosphorescence in the NIR region in deoxygenated organic solvents such as toluene. The bathochromic shift of the emission spectra is smaller than the changes observed in the absorption spectrum, i.e. the new dyes possess smaller S_1-T_1 energy gap compared to the parent benzoporphyrins. This effect is particularly pronounced for the Pt-benzoyl-Cl and Pt-acetyl complexes, which show the behavior similar to that for the previously reported benzoporphyrins bearing highly electron-withdrawing sulfone groups in the same position [36]. Interestingly, all substitutions, except for the introduction of a triple bond in Pt-Ph-acetylene, favorably affect the phosphorescence quantum yields, which increase by about 25% compared to Pt-TPTBPF. This is again in good correlation to the properties of the sulfone-substituted complexes [36]. On the other hand, bulky phenylcarbazole and dimethylfluorene substituents may reduce radiativeless deactivation via molecular vibrations. Obviously, binding of phenyl-acetylene groups via triple bond, as it is the case for Pt-Ph-acetylene, results in similar absorption characteristics compared to the other Pt(II) complexes, but to a less pronounced bathochromic shift of the emission band and decreased quantum yields.

Apart from platinum(II) porphyrins, the respective palladium(II) analogs are also known for their fairly strong fluorescence. Compared to the Pt(II) porphyrins, the Pd(II) complexes generally feature bathochromically shifted absorption and emission, significantly longer phosphorescence decay times but lower quantum yields. Pd-benzoyl-Cl was obtained analogously to Pt-benzoyl-Cl from palladium(II) tetra(4-fluorophenyl)tetrabenzoporphyrin with good yields (Fig S 7.1, ESI). Its photophysical properties follow the above expectations with absorption maxima at 461, 595 and 645 nm (molar absorption coefficients 283.000, 16.000 and 108.000 $M^{-1}cm^{-1}$, respectively), emission maximum at 799 nm, phosphorescence decay time of 313 µs and quantum yield of 0.13 (all for anoxic toluene at 25 °C).

7.4.3   Photostability

This property is of great importance especially if the dye-based materials are exposed to high light densities or/and irradiated over a longer period of time, conditions which are typical for many applications such as upconversion or microscopy. Photodecomposition in air-saturated conditions might be particularly critical due to formation of singlet oxygen. Moreover, Pt-benzoyl-Cl possesses the benzophenone motive, which is a well-known photoinitiator. Photodegradation of the new platinum(II) complexes dissolved in air saturated toluene was tested upon continuous irradiation with a high power 635 nm LED array (35 W, 350 mA, photon flux: >20.000 µmol s^{-1} m^{-2}; irradiance 377 mW cm^{-2}). Fig. 7.3 shows that the photostability of the new porphyrins is rather similar to that of palladium(II) tetraphenyltetrabenzoporphyrin (Pd-TPTBP), which was chosen as a reference due to almost identical position of the Q-band corresponding to the excitation wavelength. Electron-withdrawing acetyl and chloro-benzoyl substituents improve the photostability whereas electron-donating phenylcarbazole and phenyl-acetylene slightly decrease it. Thus, photooxidation appears to be the most likely photodegradation mechanism. Despite faster photobleaching of Pt-carbazole and Pt-Ph-acetylene, even in this case the photostability is adequate for most applications. For instance, in sensing applications not only the intensities of the excitation light are much lower but also interrogation times of 10-20 ms are sufficient for acquisition of a measurement point.
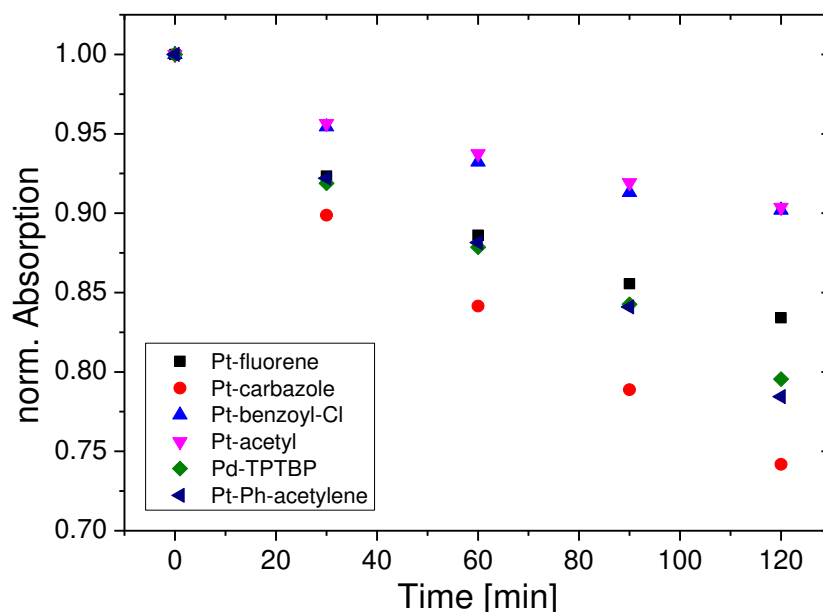
Figure 7.3. Photodegradation profiles for the new Pt(II) complexes and Pd-TPTBP as reference in air-saturated toluene solution at 25 °C upon irradiation with a high power 635 nm LED

7.4.4 Optical oxygen sensors

Because of the favorable photophysical properties the new dyes can be promising as indicators for application in optical oxygen sensors. In order to evaluate their sensing behavior, the dyes were embedded in polystyrene (0.5 % wt. of the indicator) serving as a model matrix. Not surprisingly, the phosphorescence of all dyes is efficiently quenched by oxygen (Fig. 7.4).
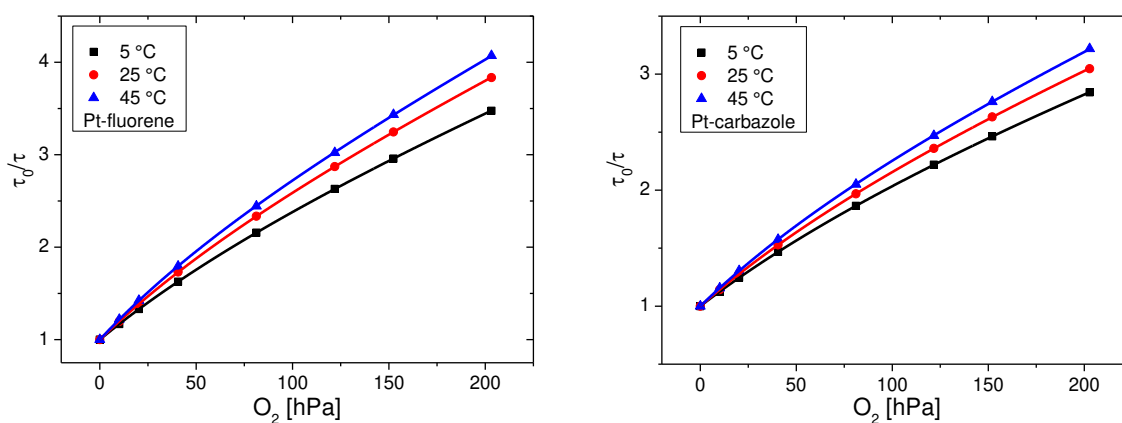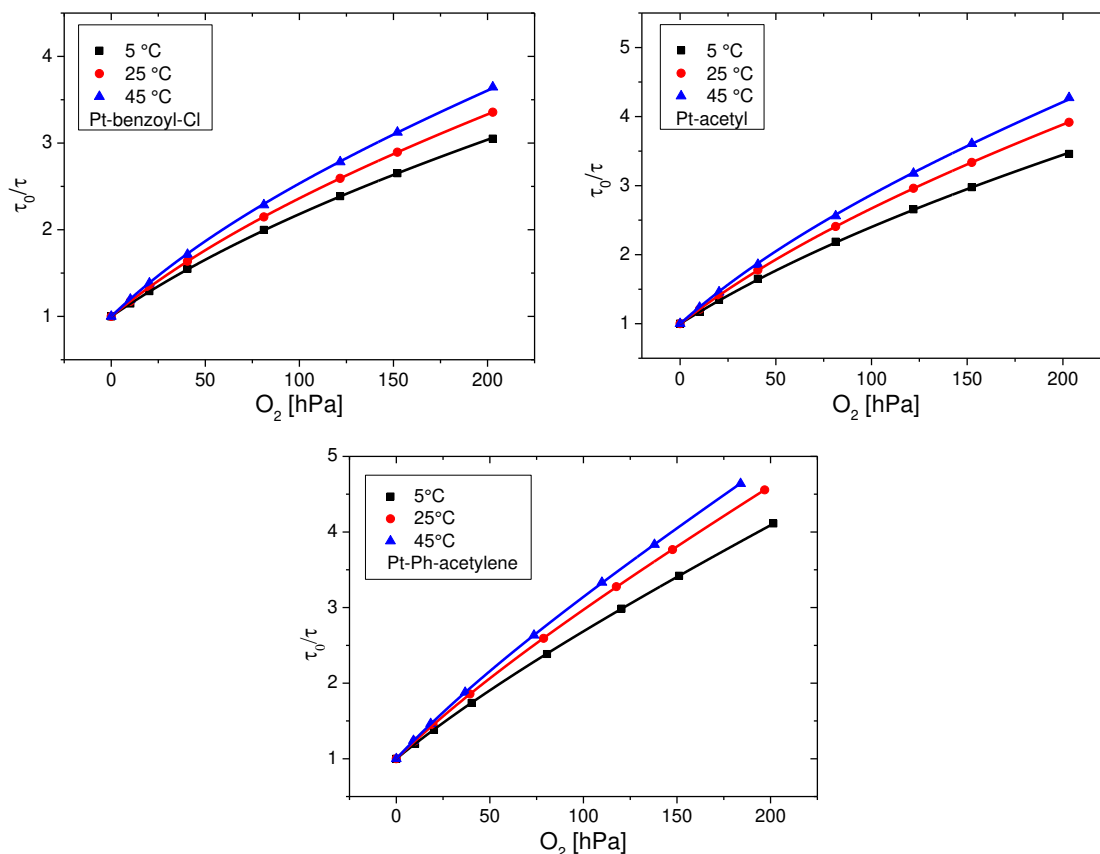
Figure 7.4. Stern-Volmer plots for the Pt(II) complexes embedded in polystyrene (at 25 °C).

The non-linear Stern-Volmer plots are typical for the oxygen sensors based on polystyrene-immobilized (benzo)porphyrins. The plots can be described by the so called "two-site model" [37] which assumes location of the indicator in two different microenvironments. The equation also adequately fits the decay time plots for the average decay times obtained in frequency domain:

$$\frac{\tau_0}{\tau} = \frac{1}{\frac{f}{1+K_{SV1}*p_{O2}}+\frac{1-f}{1+(K_{SV1}*m)*pO_2}} \quad (1)$$

where τ_0 and τ represent the lifetimes of the indicator under anoxic conditions and in presence of oxygen, while K_{SV1} and K_{SV1}*m are the Stern-Volmer constants for the two microenvironments, and f is the fraction of the overall emission for the first site. The fit parameters at different temperatures are summarized in Table 2.

It is evident that all the complexes have very similar behavior in respect to the quenching efficiency and the linearity of the Stern-Volmer plots. Interestingly, even the very bulky dimethylfluoreno and phenylcarbazole substituents have virtually no effect on quenching behavior. In respect to thermal quenching of phosphorescence (determined from the temperature dependency of the decay time under anoxic conditions) all the dyes are again rather similar with slightly higher temperature coefficients for Pt-benzoyl-Cl, Pt-acetyl and Pt-Ph-acetylene. Moreover, these properties match very well those of polystyrene-immobilized Pt-TPTBPF which was used as a reference material. Although the dynamic

range of the new sensors is from about 0.1 to 100 kPa, and thus is the same as for the parent compounds, it can be extended into significantly lower concentration range by using polymers with higher oxygen permeability (ethyl cellulose, Organically-modified silica etc.). Also, the sensitivity of the oxygen sensor based on Pd-benzoyl-Cl embedded in polystyrene (Table S2, Fig. S 7.3, ESI) is about 5-fold higher than for the sensor based on Pt-benzoyl-Cl (K_{sv1} at 25 °C is 1.03 and 0.22 kPa^{-1}, respectively) which is explained by significantly longer phosphorescence decay time of the Pd(II) complex (346 µs at 25 °C).

Table S 7.2. Fit parameters for the oxygen sensors based on the new benzoporphyrins embedded in polystyrene

Complex	f	m	τ_0/K_{SV1} at 5 °C, µs/kPa^{-1}	τ_0/K_{SV1} at 25 °C, µs/kPa^{-1}	τ_0/K_{SV1} at 45 °C, µs/kPa^{-1}	dτ/dt, %/K at 25 °C
Pt-TPTBPF [38]	0.85	0	-	52.6/0.218	-	0.07
Pt-fluorene	0.81	0.107	48.7/0.208	48.1/0.246	47.5/0.271	0.065
Pt-carbazole	0.78	0.103	47.0/0.160	46.4/0.182	45.6/0.201	0.074
Pt-benzoyl-Cl	0.80	0.075	51.3/0.184	50.6/0.220	49.5/0.255	0.089
Pt-acetyl	0.84	0.072	52.1/0.206	51.21/0.245	50.23/0.292	0.092
Pt-Ph-acetylene	0.83	0.147	45.9/0.235	45.0/0.281	44.0/0.309	0.105

7.4.5 Dyes as sensitizers in TTA-based upconversion systems

As mentioned above, benzoporphyrins have already been successfully used as synthesizers in triplet-triplet-annihilation (TTA) based upconversion systems. Briefly, after absorption of light by the sensitizer and inter-system crossing, an annihilator in triplet excited state is formed via triplet-triplet energy transfer from sensitizer to annihilator (Scheme S 7.1). Collision of two excited annihilator molecules results in formation of one of them in the singlet excited state following by fluorescence which is located at shorter wavelength compared to the excitation light. The annihilator should feature very high fluorescence quantum yields (close to unity), good solubility in organic solvents and outstanding photostability. [39], [40] In order to be useful for energy conversion applications, the sensitizer should efficiently absorb light in the red part of the electromagnetic spectrum due to the considerable solar power and low photovoltaics efficiency in this region [41]–[44] and transfer its energy to the annihilator. Not only benzoporphyrins [36] but also their molecular hybrids with naphthoporpyhrins proved to be viable sensitizers for TTA upconversion systems, [41], [42], [44], [45] but the photostability of the latter compounds is poor. [29] Since new synthesized benzoporphyrin derivatives benefit from higher quantum yields, bathochromically shifted absorption as well as emission and photostability similar to that of the parent benzoporphyrins, they are expected to be promising sensitizers for upconversion of red light. As a proof of concept, ability of the new dyes to act as sensitizers in TTA upconversion was investigated. As can be seen (Fig. 7.5, Fig. S 7.10-S13 ESI), bright upconversion from perylene dye Solvent Green 5 (2.5*10^{-4} M) is observed upon excitation of the new Pt(II) complexs (5*10^{-5} M) with a 635 laser diode. A quadratic dependence of

upconverted fluorescence on the intensity of excitation light was observed upon excitation of the dyes with a Xenon lamp (slope of the logarithmic plot approximately 2), Fig. S 7.4-S 7.9 ESI. On the contrary, excitation with the 635 nm laser diode revealed a linear region with a slope of unity demonstrating saturation conditions (Fig. S 7.10-15, ESI). [46] This phenomenon is typical for nonlinear processes like TTA based upconversion. [39]–[41], [47] Since the Q-bands of the Pd-benzoyl-Cl located at even longer wavelength compared to the corresponding Pt(II) complex, this dye may even be more promising sensitizer for the red part of the spectrum. Indeed (Fig. S 7.8, 7.9, 7.14 - 7.16, Table S3 ESI), bright upconversion was observed with two perylene dyes, Solvent Green 5 and Lumogen Orange even at comparably long excitation wavelengths.

Considering scientific progress in developing of nanoparticles featuring TTA, [15], [48, p. 633] the combination of the red-light-excitable sensitizers with different annihilators may result in a new generation of imaging agents for *in vivo* measurements which possess much higher brightness than the lanthanide nanoparticles. [49], [50]
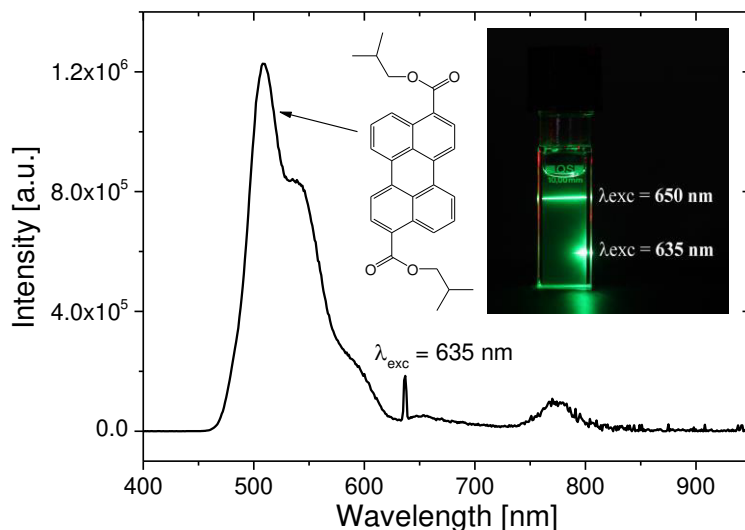
Figure 7.5. Left: Emission spectrum (λ_{exc} 635 nm) of the TTA system based on $5 \cdot 10^{-5}$ M of Pt-benzoyl-Cl and $2.5 \cdot 10^{-4}$ M of Solvent green 5 (structure shown) in anoxic toluene. The insert shows the photographic image of the upconverted fluorescence for the same system upon excitation of the solution with two laser diodes.

7.4.6 Conclusions

We have demonstrated several different strategies for modification of known benzoporphyrins complexes within one reaction step. Modification via Friedel-Crafts acylation is particularly efficient and can be performed with good yields both for Pt(II) and Pd(II) complexes. The new platinum(II) complexes show a bathochromic shift in the absorption spectra, now enabling efficient excitation with 635 nm laser diode/632.8 nm line of He-Ne laser (Q band) and with blue LEDs/455 nm line of the Ar laser (Q-band). Modification with the respective groups also results in increased quantum yields with the

exception of phenylacetylene-modified dye, whereas the decay time and photostability are similar to those of the parent compounds. The new dyes represent promising indicators for oxygen and glucose sensors, particularly in respect to *in vivo* applications, due to better light penetration and lower light scattering at longer wavelengths. The new complexes are also valuable sensitizers for TTA upconversion systems and allow more efficient harvesting of red light than the parent benzoporphyrin dyes. Even longer sensitization wavelengths can be achieved if the central atom is substituted to palladium(II).

Associated Content

Synthesis, photophysical properties, optical oxygen sensor, TTA upconversion,^{1}H and ^{13}C NMR and mass spectra (PDF).

Acknowledgements

7.4.7 References

[1] C. Borek *et al.*, "Highly Efficient, Near-Infrared Electrophosphorescence from a Pt–Metalloporphyrin Complex," *Angew. Chem. Int. Ed.*, vol. 46, no. 7, pp. 1109–1112, Feb. 2007.

[2] J. R. Sommer *et al.*, "Efficient Near-Infrared Polymer and Organic Light-Emitting Diodes Based on Electrophosphorescence from (Tetraphenyltetranaphtho[2,3]porphyrin)platinum(II)," *ACS Appl. Mater. Interfaces*, vol. 1, no. 2, pp. 274–278, Feb. 2009.

[3] X. Wang and O. S. Wolfbeis, "Optical methods for sensing and imaging oxygen: materials, spectroscopies and applications," *Chem. Soc. Rev.*, vol. 43, no. 10, pp. 3666–3761, Apr. 2014.

[4] C. Staudinger and S. M. Borisov, "Long-wavelength analyte-sensitive luminescent probes and optical (bio)sensors," *Methods Appl. Fluoresc.*, vol. 3, no. 4, p. 042005, 2015.

[5] J. Napp *et al.*, "Targeted Luminescent Near-Infrared Polymer-Nanoprobes for In Vivo Imaging of Tumor Hypoxia," *Anal. Chem.*, vol. 83, no. 23, pp. 9039–9046, Dec. 2011.

[6] A. Y. Lebedev, A. V. Cheprakov, S. Sakadzić, D. A. Boas, D. F. Wilson, and S. A. Vinogradov, "Dendritic phosphorescent probes for oxygen imaging in biological systems," *ACS Appl. Mater. Interfaces*, vol. 1, no. 6, pp. 1292–1304, Jun. 2009.

[7] M. A. Yaseen *et al.*, "Optical monitoring of oxygen tension in cortical microvessels with confocal microscopy," *Opt. Express*, vol. 17, no. 25, pp. 22341–22350, Dec. 2009.

[8] B. Nacht *et al.*, "Integrated catheter system for continuous glucose measurement and simultaneous insulin infusion," *Biosens. Bioelectron.*, vol. 64, pp. 102–110, Feb. 2015.

[9] P. W. Zach, O. T. Hofmann, I. Klimant, and S. M. Borisov, "NIR phosphorescent intramolecularly bridged benzoporphyrins and their application in an oxygen-compensated glucose optode," Anal. Chem., vol. 90, no. 4, pp. 2741–2748, Feb. 2018.

[10] S. Pervaiz and M. Olivo, "Art and science of photodynamic therapy," *Clin. Exp. Pharmacol. Physiol.*, vol. 33, no. 5–6, pp. 551–556, Jun. 2006.

[11] A. Yuan, J. Wu, X. Tang, L. Zhao, F. Xu, and Y. Hu, "Application of near-infrared dyes for tumor imaging, photothermal, and photodynamic therapies," *J. Pharm. Sci.*, vol. 102, no. 1, pp. 6–28, Jan. 2013.

[12] J. Qian, D. Wang, F. Cai, Q. Zhan, Y. Wang, and S. He, "Photosensitizer encapsulated organically modified silica nanoparticles for direct two-photon photodynamic therapy and In Vivo functional imaging," *Biomaterials*, vol. 33, no. 19, pp. 4851–4860, Jun. 2012.

[13] T. F. Schulze *et al.*, "Efficiency Enhancement of Organic and Thin-Film Silicon Solar Cells with Photochemical Upconversion," *J. Phys. Chem. C*, vol. 116, no. 43, pp. 22794–22801, Nov. 2012.

[14] J. S. Lissau, J. M. Gardner, and A. Morandeira, "Photon Upconversion on Dye-Sensitized Nanostructured ZrO2

Films," *J. Phys. Chem. C*, vol. 115, no. 46, pp. 23226–23232, Nov. 2011.

[15] Q. Liu, T. Yang, W. Feng, and F. Li, "Blue-Emissive Upconversion Nanoparticles for Low-Power-Excited Bioimaging in Vivo," *J. Am. Chem. Soc.*, vol. 134, no. 11, pp. 5390–5397, Mar. 2012.

[16] R. S. Khnayzer, J. Blumhoff, J. A. Harrington, A. Haefele, F. Deng, and F. N. Castellano, "Upconversion-powered photoelectrochemistry," *Chem. Commun.*, vol. 48, no. 2, pp. 209–211, Nov. 2011.

[17] H. Xiang, J. Cheng, X. Ma, X. Zhou, and J. J. Chruma, "Near-infrared phosphorescence: materials and applications," *Chem. Soc. Rev.*, vol. 42, no. 14, pp. 6128–6185, Jun. 2013.

[18] J. Hou *et al.*, "Bandgap and Molecular Energy Level Control of Conjugated Polymer Photovoltaic Materials Based on Benzo[1,2-b:4,5-b']dithiophene," *Macromolecules*, vol. 41, no. 16, pp. 6012–6018, Aug. 2008.

[19] L. H. Hutter, B. J. Müller, K. Koren, S. M. Borisov, and I. Klimant, "Robust optical oxygen sensors based on polymer-bound NIR-emitting platinum(II)–benzoporphyrins," *J. Mater. Chem. C*, vol. 2, no. 36, pp. 7589–7598, Aug. 2014.

[20] C. M. B. Carvalho, T. J. Brocksom, and K. T. de Oliveira, "Tetrabenzoporphyrins: synthetic developments and applications," *Chem. Soc. Rev.*, vol. 42, no. 8, pp. 3302–3317, Mar. 2013.

[21] O. S. Finikova, A. V. Cheprakov, and S. A. Vinogradov, "Synthesis and luminescence of soluble meso-unsubstituted tetrabenzo- and tetranaphtho[2,3]porphyrins," *J. Org. Chem.*, vol. 70, no. 23, pp. 9562–9572, Nov. 2005.

[22] O. S. Finikova, S. E. Aleshchenkov, R. P. Briñas, A. V. Cheprakov, P. J. Carroll, and S. A. Vinogradov, "Synthesis of Symmetrical Tetraaryltetranaphtho[2,3]porphyrins," *J. Org. Chem.*, vol. 70, no. 12, pp. 4617–4628, May 2005.

[23] O. S. Finikova, A. V. Cheprakov, P. J. Carroll, and S. A. Vinogradov, "Novel route to functionalized tetraaryltetra[2,3]naphthaloporphyrins via oxidative aromatization," *J. Org. Chem.*, vol. 68, no. 19, pp. 7517–7520, Sep. 2003.

[24] H. Yamada *et al.*, "Synthesis and Characterization of Tetraanthroporphyrins," *Org. Lett.*, vol. 10, no. 14, pp. 2947–2950, Jul. 2008.

[25] T. Tanaka and A. Osuka, "Conjugated porphyrin arrays: synthesis, properties and applications for functional materials," *Chem. Soc. Rev.*, vol. 44, no. 4, pp. 943–969, Feb. 2015.

[26] V. V. Diev *et al.*, "Porphyrins Fused with Unactivated Polycyclic Aromatic Hydrocarbons," *J. Org. Chem.*, vol. 77, no. 1, pp. 143–159, Nov. 2011.

[27] J. D. Spence and T. D. Lash, "Porphyrins with Exocyclic Rings. 14.1 Synthesis of Tetraacenaphthoporphyrins, a New Family of Highly Conjugated Porphyrins with Record-Breaking Long-Wavelength Electronic Absorptions," *J. Org. Chem.*, vol. 65, no. 5, pp. 1530–1539, Feb. 2000.

[28] J. P. Lewtak and D. T. Gryko, "Synthesis of π-extended porphyrins via intramolecular oxidative coupling," *Chem. Commun.*, vol. 48, no. 81, pp. 10069–10086, Sep. 2012.

[29] F. Niedermair *et al.*, "Tunable Phosphorescent NIR Oxygen Indicators Based on Mixed Benzo- and Naphthoporphyrin Complexes," *Inorg. Chem.*, vol. 49, no. 20, pp. 9333–9342, Sep. 2010.

[30] B. J. Müller, T. Burger, S. M. Borisov, and I. Klimant, "High performance optical trace oxygen sensors based on NIR-emitting benzoporphyrins covalently coupled to silicone matrixes," *Sens. Actuators B Chem.*, vol. 216, pp. 527–534, Sep. 2015.

[31] S. M. Borisov, G. Nuss, W. Haas, R. Saf, M. Schmuck, and I. Klimant, "New NIR-emitting complexes of platinum(II) and palladium(II) with fluorinated benzoporphyrins," *J. Photochem. Photobiol. -Chem. - J PHOTOCHEM PHOTOBIOL -CHEM*, vol. 201, no. 2, pp. 128–135, 2009.

[32] J. M. Hancock, A. P. Gifford, Y. Zhu, Y. Lou, and S. A. Jenekhe, "n-Type Conjugated Oligoquinoline and Oligoquinoxaline with Triphenylamine Endgroups: Efficient Ambipolar Light Emitters for Device Applications," *Chem. Mater.*, vol. 18, no. 20, pp. 4924–4932, Oct. 2006.

[33] J. A. Hur†, S. Y. Bae, K. H. Kim, T. W. Lee, M. J. Cho, and D. H. Choi, "Semiconducting 2,6,9,10-Tetrakis(phenylethynyl)anthracene Derivatives: Effect of Substitution Positions on Molecular Energies," *Org. Lett.*, vol. 13, no. 8, pp. 1948–1951, Apr. 2011.

[34] G. A. Crosby and J. N. Demas, "Measurement of photoluminescence quantum yields. Review," *J. Phys. Chem.*, vol. 75, no. 8, pp. 991–1024, Apr. 1971.

[35] A. Loudet, R. Bandichhor, L. Wu, and K. Burgess, "Functionalized BF2 Chelated Azadipyrromethene Dyes," *Tetrahedron*, vol. 64, no. 17, pp. 3642–3654, Apr. 2008.

[36] P. W. Zach, S. A. Freunberger, I. Klimant, and S. M. Borisov, "Electron-Deficient Near-Infrared Pt(II) and Pd(II) Benzoporphyrins with Dual Phosphorescence and Unusually Efficient Thermally Activated Delayed Fluorescence: First Demonstration of Simultaneous Oxygen and Temperature Sensing with a Single Emitter," *ACS Appl. Mater. Interfaces*, vol. 9, no. 43, pp. 38008–38023, Nov. 2017.

[37] E. R. Carraway, J. N. Demas, B. A. DeGraff, and J. R. Bacon, "Photophysics and photochemistry of oxygen sensors based on luminescent transition-metal complexes," *Anal. Chem.*, vol. 63, no. 4, pp. 337–342, Feb. 1991.

[38] S. M. Borisov, G. Nuss, and I. Klimant, "Red light-excitable oxygen sensing materials based on platinum(II) and palladium(II) benzoporphyrins," *Anal. Chem.*, vol. 80, no. 24, pp. 9435–9442, Dec. 2008.

[39] R. R. Islangulov, J. Lott, C. Weder, and F. N. Castellano, "Noncoherent low-power upconversion in solid polymer films," *J. Am. Chem. Soc.*, vol. 129, no. 42, pp. 12652–12653, Oct. 2007.

[40] T. N. Singh-Rachford, J. Lott, C. Weder, and F. N. Castellano, "Influence of temperature on low-power upconversion in rubbery polymer blends," *J. Am. Chem. Soc.*, vol. 131, no. 33, pp. 12007–12014, Aug. 2009.

[41] T. N. Singh-Rachford, A. Haefele, R. Ziessel, and F. N. Castellano, "Boron dipyrromethene chromophores: next generation triplet acceptors/annihilators for low power upconversion schemes," *J. Am. Chem. Soc.*, vol. 130, no. 48, pp. 16164–16165, Dec. 2008.

[42] A. Monguzzi *et al.*, "Efficient Broadband Triplet–Triplet Annihilation-Assisted Photon Upconversion at Subsolar

Irradiance in Fully Organic Systems," *Adv. Funct. Mater.*, vol. 25, no. 35, pp. 5617–5624, Sep. 2015.

[43] J.-H. Kim, F. Deng, F. N. Castellano, and J.-H. Kim, "High Efficiency Low-Power Upconverting Soft Materials," *Chem. Mater.*, vol. 24, no. 12, pp. 2250–2252, Jun. 2012.

[44] K. Xu, J. Zhao, X. Cui, and J. Ma, "Photoswitching of triplet-triplet annihilation upconversion showing large emission shifts using a photochromic fluorescent dithienylethene-Bodipy triad as a triplet acceptor/emitter," *Chem Commun*, vol. 51, no. 10, pp. 1803–1806, 2015.

[45] J.-H. Kim, F. Deng, F. N. Castellano, and J.-H. Kim, "Red-to-Blue/Cyan/Green Upconverting Microcapsules for Aqueous- and Dry-Phase Color Tuning and Magnetic Sorting," *ACS Photonics*, vol. 1, no. 4, pp. 382–388, Apr. 2014.

[46] Y. Y. Cheng *et al.*, "On the efficiency limit of triplet–triplet annihilation for photochemical upconversion," *Phys. Chem. Chem. Phys.*, vol. 12, no. 1, pp. 66–71, Dec. 2009.

[47] S. M. Borisov, R. Saf, R. Fischer, and I. Klimant, "Synthesis and properties of new phosphorescent red light-excitable platinum(II) and palladium(II) complexes with Schiff bases for oxygen sensing and triplet-triplet annihilation-based upconversion," *Inorg. Chem.*, vol. 52, no. 3, pp. 1206–1216, Feb. 2013.

[48] W. Wang *et al.*, "Efficient Triplet–Triplet Annihilation-Based Upconversion for Nanoparticle Phototargeting," *Nano Lett.*, vol. 15, no. 10, pp. 6332–6338, Oct. 2015.

[49] M. Seydack, "Nanoparticle labels in immunosensing using optical detection methods," *Biosens. Bioelectron.*, vol. 20, no. 12, pp. 2454–2469, Jun. 2005.

[50] A. Gnach and A. Bednarkiewicz, "Lanthanide-doped up-converting nanoparticles: Merits and challenges," *Nano Today*, vol. 7, no. 6, pp. 532–563, Dec. 2012.

7.5 Supporting Information

7.5.1 Synthesis

Pd-benzoyl-Cl
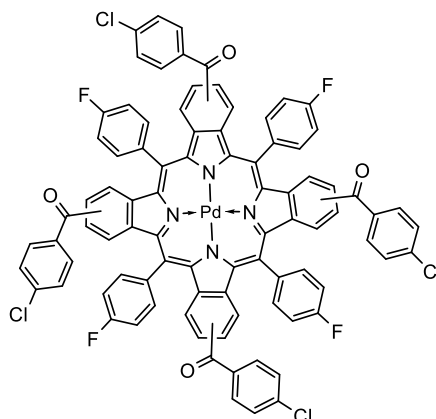
Figure S 7.1 Chemical structure of Pd-benzoyl-Cl

Pd-TPTBPF (10.0 mg, 10.1 µmol, 1.00 eq) was dissolved in 1,2-dichlorobenzene (6 mL) under argon atmosphere. 4-Chlorobenzoyl chloride (0.064 mL, 0.50 mmol, 50.0 eq) and $AlCl_3$ (30.0 mg, 0.23 mmol, 22.3 eq) were added to the solution. The reaction mixture was heated to 130 °C and stirred for 45 min. The reaction progress was monitored via absorption spectroscopy (solvent: $CHCl_3$, 50 µL of ethanol (EtOH)). The reaction progress was monitored via UV-Vis spectroscopy. After complete conversion the reaction mixture was cooled down to RT and treated with $EtOH:H_2O$ (1:1 v/v, 20 mL) and stirred for 10 minutes to neutralize the excess of $AlCl_3$. After addition of DCM, the organic layer was washed with H_2O and dried over Na_2SO_4 and the solvent was removed under reduced pressure. The crude product was purified via column chromatography (silica-gel, cond. toluene, DCM:Tol, 7:1), yielding a dark green solid. Yield: 5 mg, 32%

^{1}H-NMR (300 MHz, CD_2Cl_2) 8.25 (dq, J = 9.6, 4.7 Hz, 2H), 8.18 – 8.07 (m,3H), 7.98 (dt, J = 10.7, 5.4 Hz, 2H), 7.80 (dt, J = 14.0, 7.7 Hz, 4H), 7.72 – 7.61 (m, 2H), 7.60 –7.43 (m, 16H), 7.38 (t, J = 6.8 Hz, 5H), 7.32 – 7.23 (m, 2H), 7.21 – 7.13 (m, 2H), 7.09 (dq, J =8.3, 5.4, 4.5 Hz, 2H)

MALDI-TOF: m/z [M$^+$] $C_{88}H_{44}Cl_4F_4N_4O_4Pd$ calcd: 1544.11, found: 1543.96

7.5.2 Photophysical properties

Table S 7.3 Comparison of photophysical properties of the Pd(II)-benzoyl-Cl complex and Pd-TPTBPF in anoxic toluene at 25 °C.

Complex	λ_{max} abs (ε), nm ($M^{-1}cm^{-1}$)	λ_{max} em, nm	Stokes shift, cm^{-1}	QY, Φ	τ, μs
Pd-TPTBPF	443 (268.000); 579 (12.700); 629 (115.000)	796	3340	0.09	297
Pd-benzoyl-Cl	461 (282.000); 595 (16.000); 645 (107.000)	799	2990	0.12	313
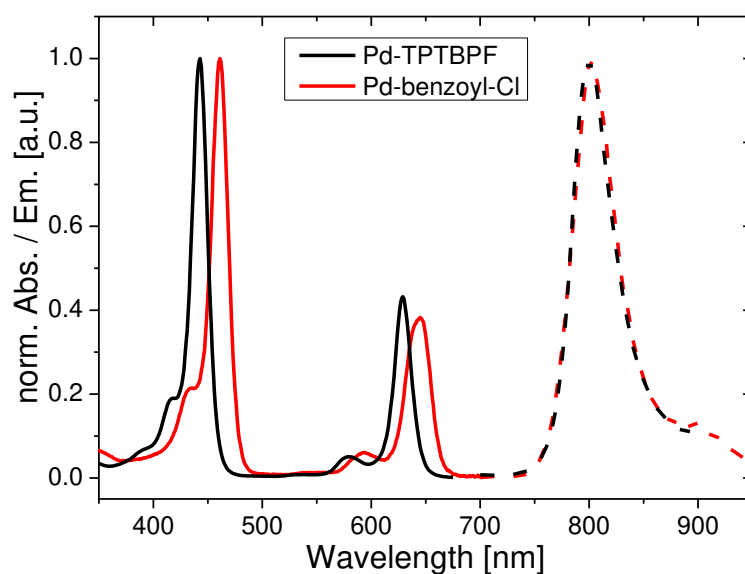
Figure S 7.2 Absorption and emission spectra of new Pd-benzoyl-Cl and precursor Pd-TPTBPF in toluene at 25 °C; anoxic conditions for emission measurements

7.5.3 Optical oxygen sensor

Table S 7.4 Fit parameters for the oxygen sensors based on the new benzoporphyrins embedded in polystyrene

Complex	f	m	τ_0/K_{SV1} at 5 °C, μs/kPa^{-1}	τ_0/K_{SV1} at 25 °C, μs/kPa^{-1}	τ_0/K_{SV1} at 45 °C, μs/kPa^{-1}	dτ/dt, %/K at 25 °C
Pd-TPTBPF	0.85	0	-	356/1.04	-	0.32
Pd-benzoyl-Cl	0.82	0.061	372/0.873	346/0.103	320/0.120	0.38
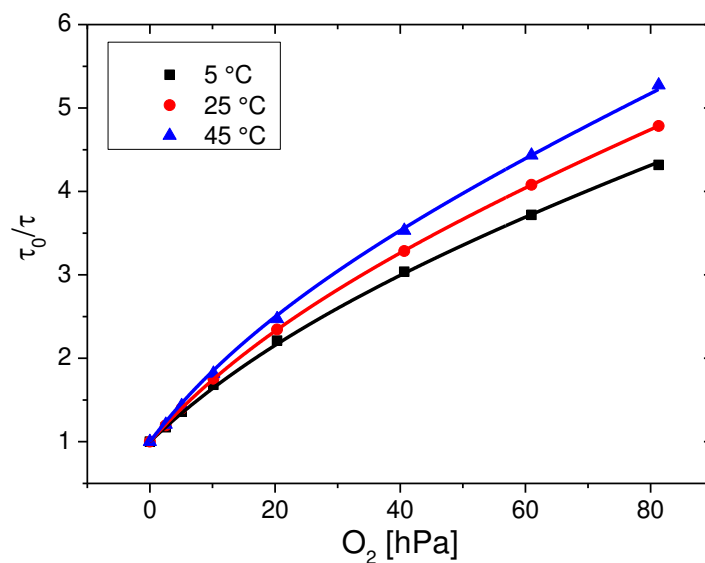
Figure S 7.3 Stern-Volmer plot of Pd-benzoyl-Cl embedded in polystyrene (at 25 °C).

7.5.4 Dyes as sensitizers in TTA-based upconversion systems

$$\mathbf{S}\,(S_0) + h\nu_1 \rightarrow \mathbf{S}\,(S_1)$$

$$\mathbf{S}\,(S_1) \rightarrow \mathbf{S}\,(T_1)$$

$$\mathbf{S}\,(T_1) + \mathbf{A}\,(S_0) \rightarrow \mathbf{S}\,(S_0) + \mathbf{A}\,(T_1)$$

$$\mathbf{A}\,(T_1) + \mathbf{A}\,(T_1) \rightarrow \mathbf{A}\,(S_1) + \mathbf{A}\,(S_0)$$

$$\mathbf{A}\,(S_1) \rightarrow \mathbf{A}\,(S_0) + h\nu_2$$
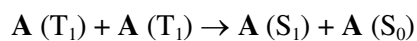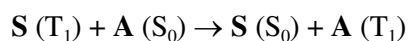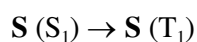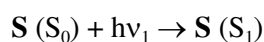
Scheme S 7.1 Mechanism of the triplet-triplet annihilation-based upconversion. S = Sensitizer, A = annihilator
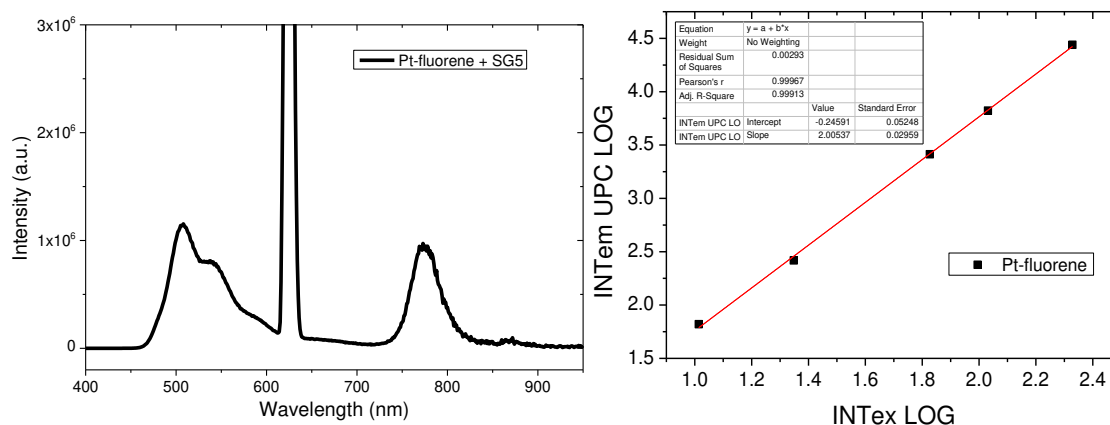
Figure S 7.4 Emission spectra of toluene solution of Pt-fluorene (C = 1*10^{-4} M) with Solvent Green 5 (SG5) as annihilator (C = 5*10^{-4} M) excited with 450 W xenon-lamp at 627 nm (left) and dependence of the upconverted fluorescence intensity on the intensity of the excitation light (right)
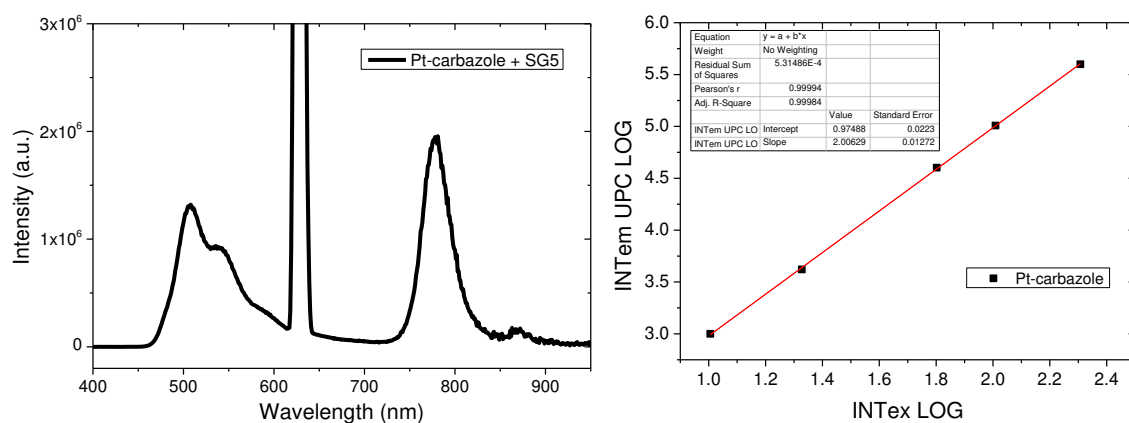
Figure S 7.5 Emission spectra of toluene solution of Pt-carbazole (C = 1*10⁻⁴ M) with Solvent Green 5 (SG5) as annihilator (C = 5*10⁻⁴ M) excited with 450 W xenon-lamp at 630 nm (left) and dependence of the upconverted fluorescence intensity on the intensity of the excitation light (right)
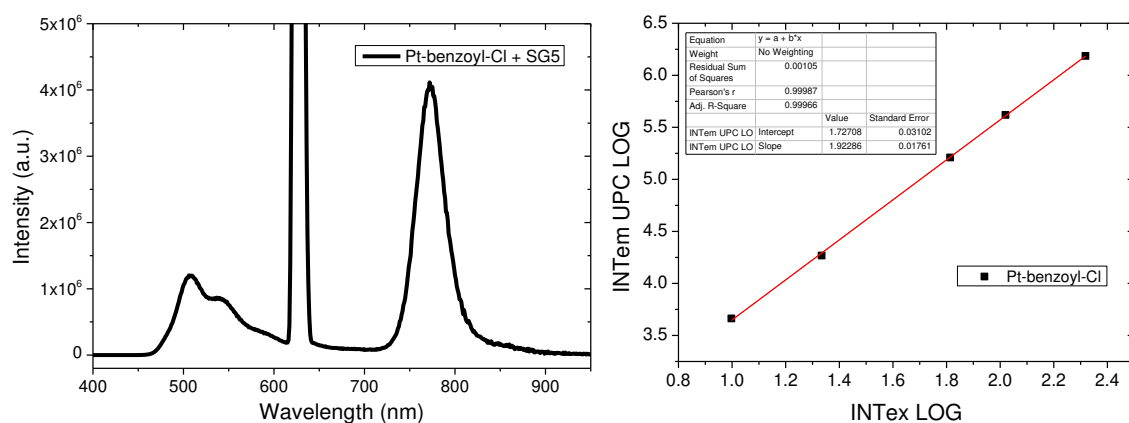
Figure S 7.6 Emission spectra of toluene solution of Pt-benzoyl-Cl (C = 1*10⁻⁴ M) with Solvent Green 5 (SG5) as annihilator (C = 5*10⁻⁴ M) excited with 450 W xenon-lamp at 631 nm (left) and dependence of the upconverted fluorescence intensity on the intensity of the excitation light (right)
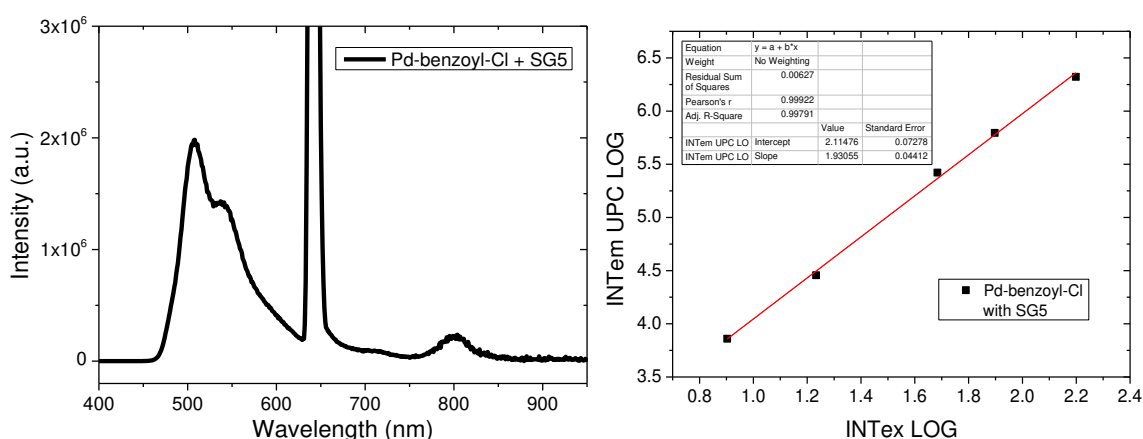
Figure S 7.7 Emission spectra of toluene solution of Pt-acetyl (C = 1*10⁻⁴ M) with Solvent Green 5 (SG5) as annihilator (C = 5*10⁻⁴ M) excited with 450 W xenon-lamp at 629 nm (left) and dependence of the upconverted fluorescence intensity on the intensity of the excitation light (right)
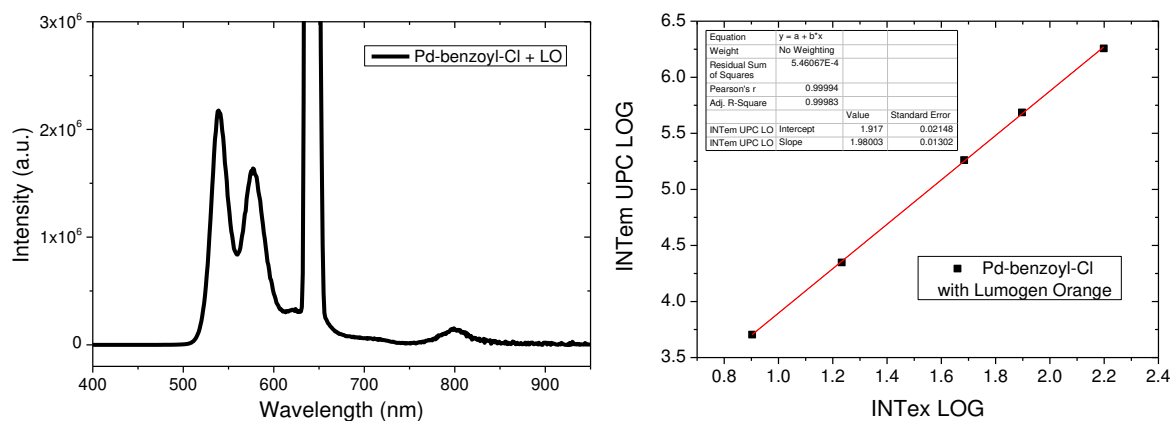
Figure S 7.8 Emission spectra of toluene solution of Pd-benzoyl-Cl (C = $1*10^{-4}$ M) with Solvent Green 5 (SG5) as annihilator (C = $5*10^{-4}$ M) excited with 450 W xenon-lamp at 645 nm (left) and dependence of the upconverted fluorescence intensity on the intensity of the excitation light (right)
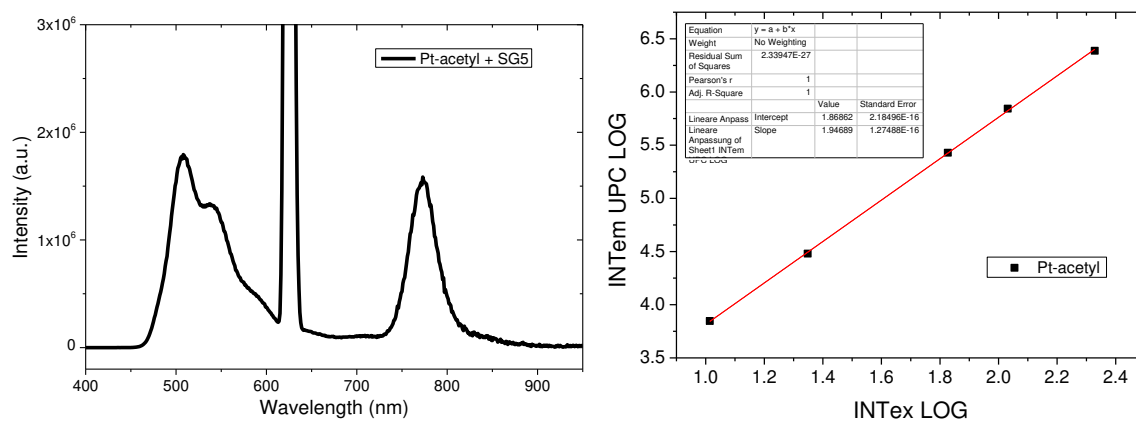
Figure S 7.9 Emission spectra of toluene solution of Pd-benzoyl-Cl (C = $1*10^{-4}$ M) with Lumogen Orange (LO) as annihilator (C = $5*10^{-4}$ M) excited with 450 W xenon-lamp at 645 nm (left) and dependence of the upconverted fluorescence intensity on the intensity of the excitation light (right)
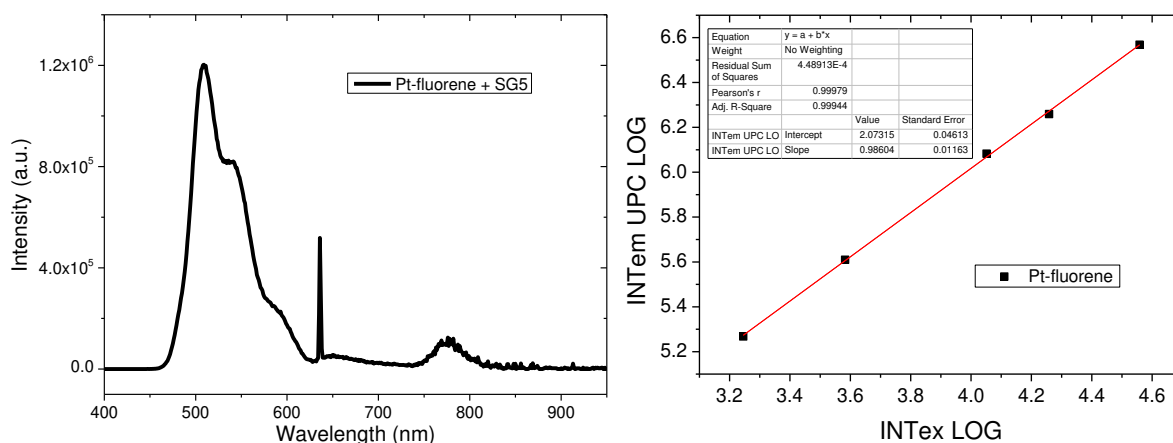
Figure S 7.10 Emission spectra of toluene solution of Pt-fluorene (C = $5*10^{-5}$ M) with Solvent Green 5 (SG5) as annihilator (C = $2.5*10^{-4}$ M) excited with 635 nm laser diode (left) and dependence of the upconverted fluorescence intensity on the intensity of the excitation light (right)
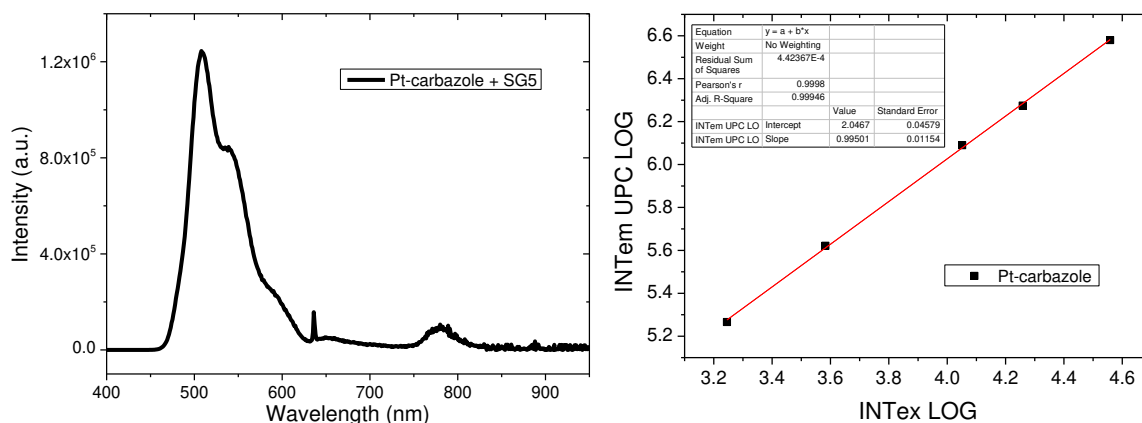
Figure S 7.11 Emission spectra of toluene solution of Pt-carbazole (C = 5*10⁻⁵ M) with Solvent Green 5 (SG5) as annihilator (C = 2.5*10⁻⁴ M) excited with 635 nm laser diode (left) and dependence of the upconverted fluorescence intensity on the intensity of the excitation light (right)
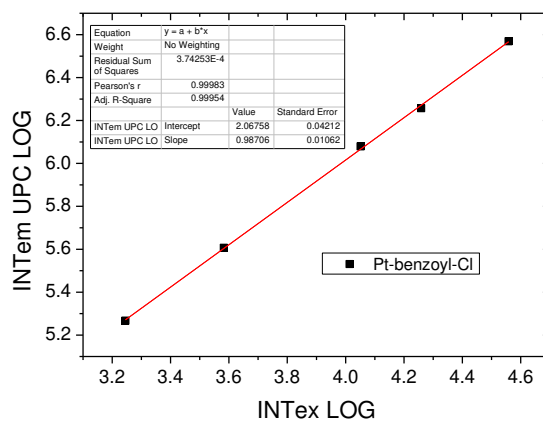
Figure S 7.12 Dependence of the upconverted fluorescence intensity on the intensity of the excitation light for anoxic toluene solution of Pt-benzoyl-Cl (C = 5*10⁻⁵ M) and Solvent Green 5 (SG5) as annihilator (C = 2.5*10⁻⁴ M) excited with 635 nm laser diode.
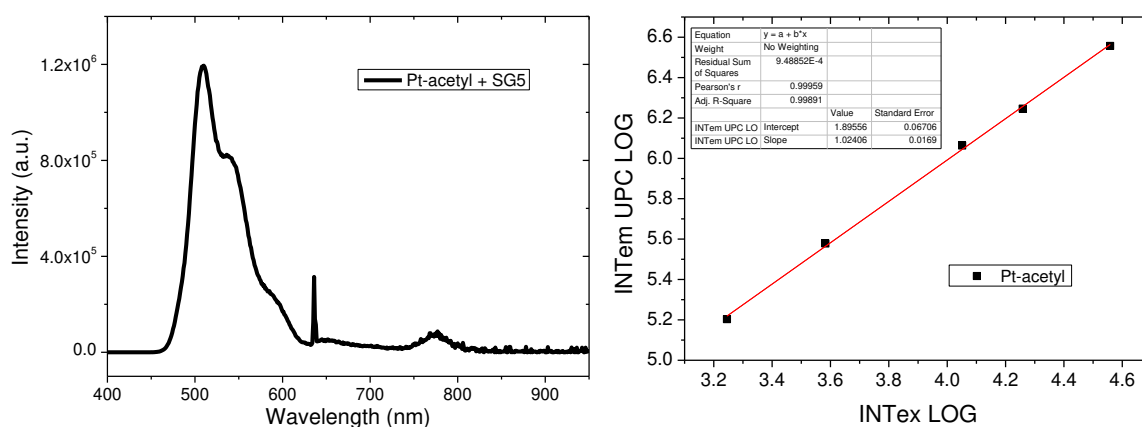
Figure S 7.13 Emission spectra of toluene solution of Pt-acetyl (C = 5*10⁻⁵ M) with Solvent Green 5 (SG5) as annihilator (C = 2.5*10⁻⁴ M) excited with 635 nm laser diode (left) and dependence of the upconverted fluorescence intensity on the intensity of the excitation light (right)
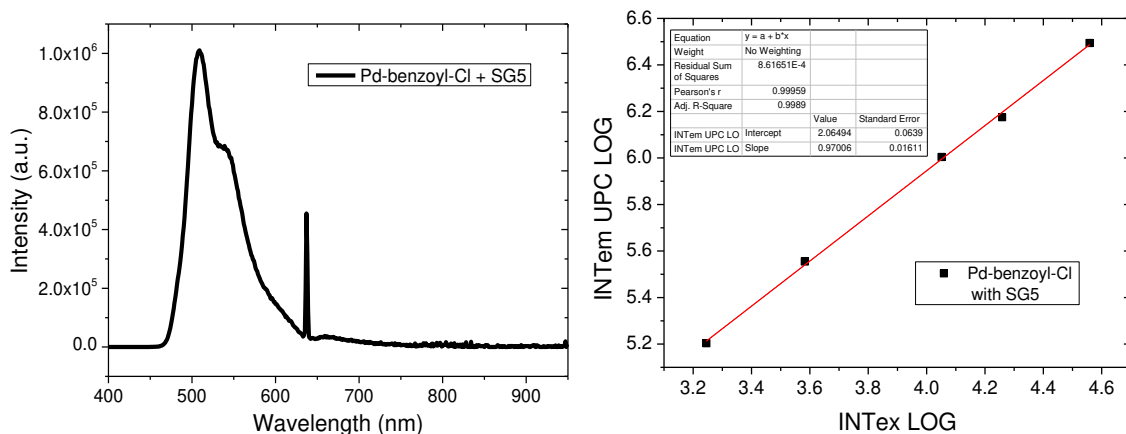
Figure S 7.14 Emission spectra of toluene solution of Pd-benzoyl-Cl (C = 5*10⁻⁵ M) with Solvent Green 5 (SG5) as annihilator (C = 2.5*10⁻⁴ M) excited with 635 nm laser diode (left) and dependence of the upconverted fluorescence intensity on the intensity of the excitation light (right)
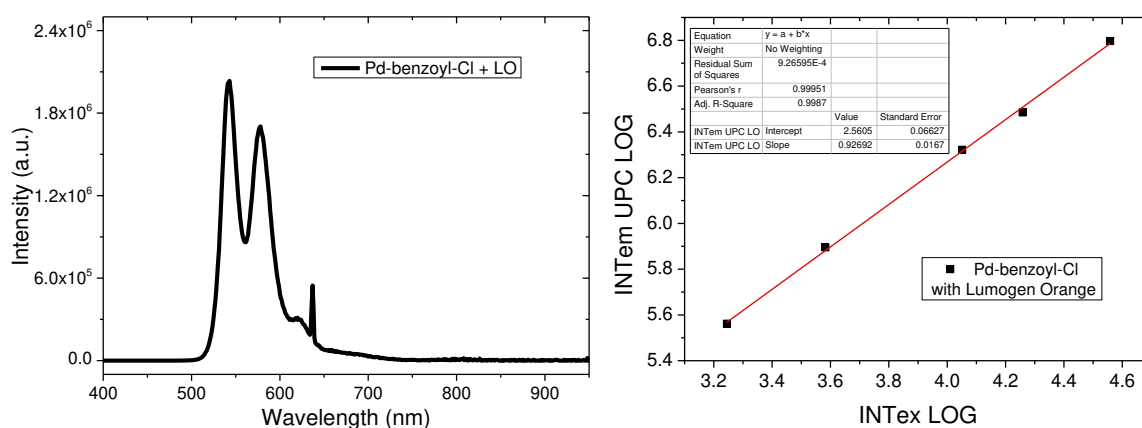
Figure S 7.15 Emission spectra of toluene solution of Pd-benzoyl-Cl (C = 5*10⁻⁵ M) with Lumogen Orange (LO) as annihilator (C = 2.5*10⁻⁴ M) excited with 635 nm laser diode (left) and dependence of the upconverted fluorescence intensity on the intensity of the excitation light (right)
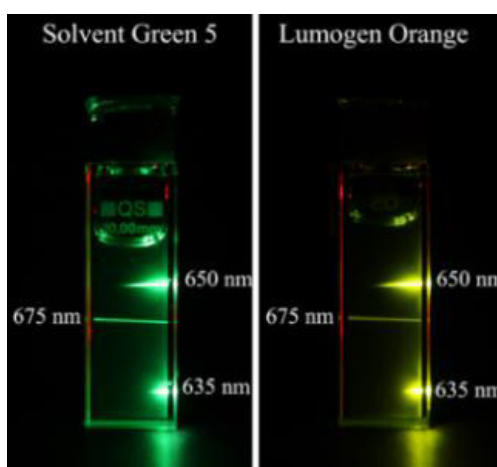
Figure S 7.16 Photographic images of the upconverted fluorescence for systems based on Pd-benzoyl-Cl and Solvent green 5 (left) and Pd-benzoyl-Cl and Lumogen Orange (right) upon excitation with different red laser diodes.

Table S 7.5 Upconversion quantum yields (Φ_{UPC}) of platinum(II) and palladium(II) benzoporphyrin sensitizers with Solvent Green 5 (SG5) or Lumogen Orange (LO) as the annihilator in anoxic toluene solutions excited by a xenon lamp (450 W) and the relative light intensity of the excitation source at different wavelengths.

Sensitizer	Annihilator	λ_{Exc} [nm]	light intensity [μmol/s*m^2]	norm. light intensity (I)	QY UPC lamp [%]	QY UPC norm. to I [%]
Pt-fluorene	SG5	627	213	1.00	2.00	2.00
Pt-carbazole	SG5	630	203	0.95	1.06	1.16
Pt-benzoyl-Cl	SG5	631	208	0.98	0.42	0.44
Pd-benzoyl-Cl	SG5	645	158	0.74	3.01	5.48
Pd-benzoyl-Cl	LO	645	158	0.74	2.17	3.95
Pt-acetyl	SG5	629	213	1.00	1.77	1.77
Pd-TPTBP	SG5	628	213	1.00	1.56	1.56

Note that in case of the xenon lamp (450 W), the intensity of the excitation source reduces in the red part of the spectrum and is not identical for different sensitizers. Therefore, we normalized the φ to the intensity of the xenon lamp at 628 nm assuming the quadratic dependence of the upconverted fluorescence on the intensity of the excitation light.

7.5.5 NMR Spectra

^{1}H NMR (300 MHz, Methylene Chloride-d$_2$) δ 8.29 – 8.01 (m, 16H), 7.97 – 7.71 (m, 7H), 7.66 – 7.40 (m, 28H), 7.39 – 7.27 (m, 13H), 7.26 – 7.00 (m, 12H), 1.65 (t, J = 4.1 Hz, 9H), 1.53 – 1.45 (m, 18H), 1.35 – 1.25 (m, 9H).
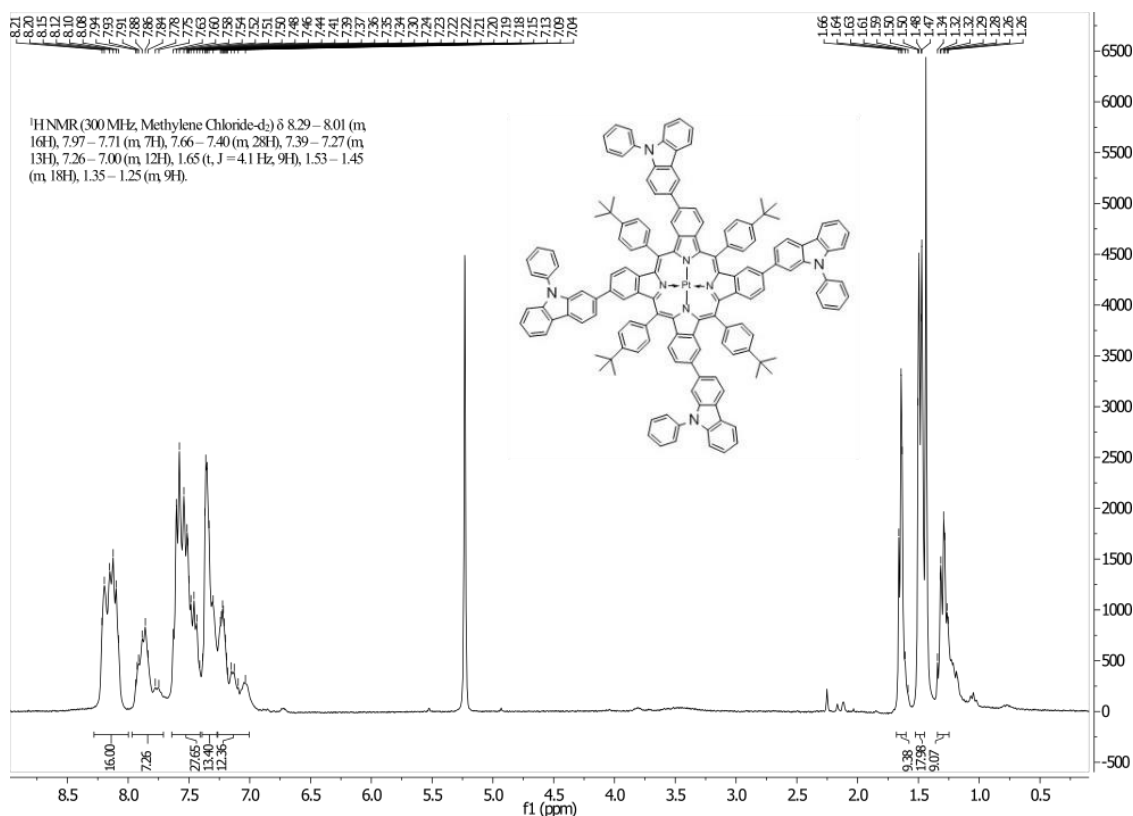
Figure S 7.17 ^{1}H-NMR spectrum of Pt-fluorene
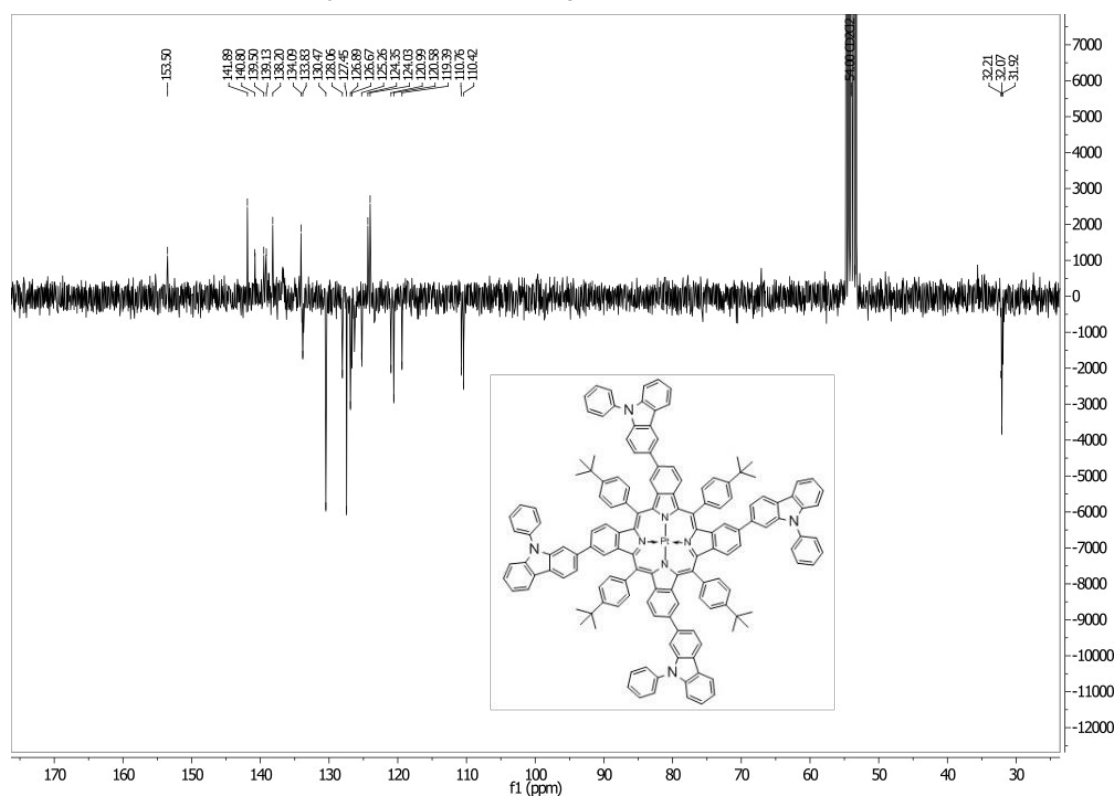
Figure S 7.18 ^{13}C-APT-NMR spectrum of Pt-fluorene

¹H NMR (300 MHz, Methylene Chloride-d₂) δ 8.37 – 8.19 (m, 8H), 8.08 – 7.94 (m, 8H), 7.84 – 7.53 (m, 22H), 7.54 – 7.48 (m, 4H), 7.42 – 7.27 (m, 14H), 7.21 (d, J = 8.9 Hz, 2H), 7.10 (d, J = 8.6 Hz, 2H), 1.77 – 1.62 (m, 36H), 1.50 (s, 28H).
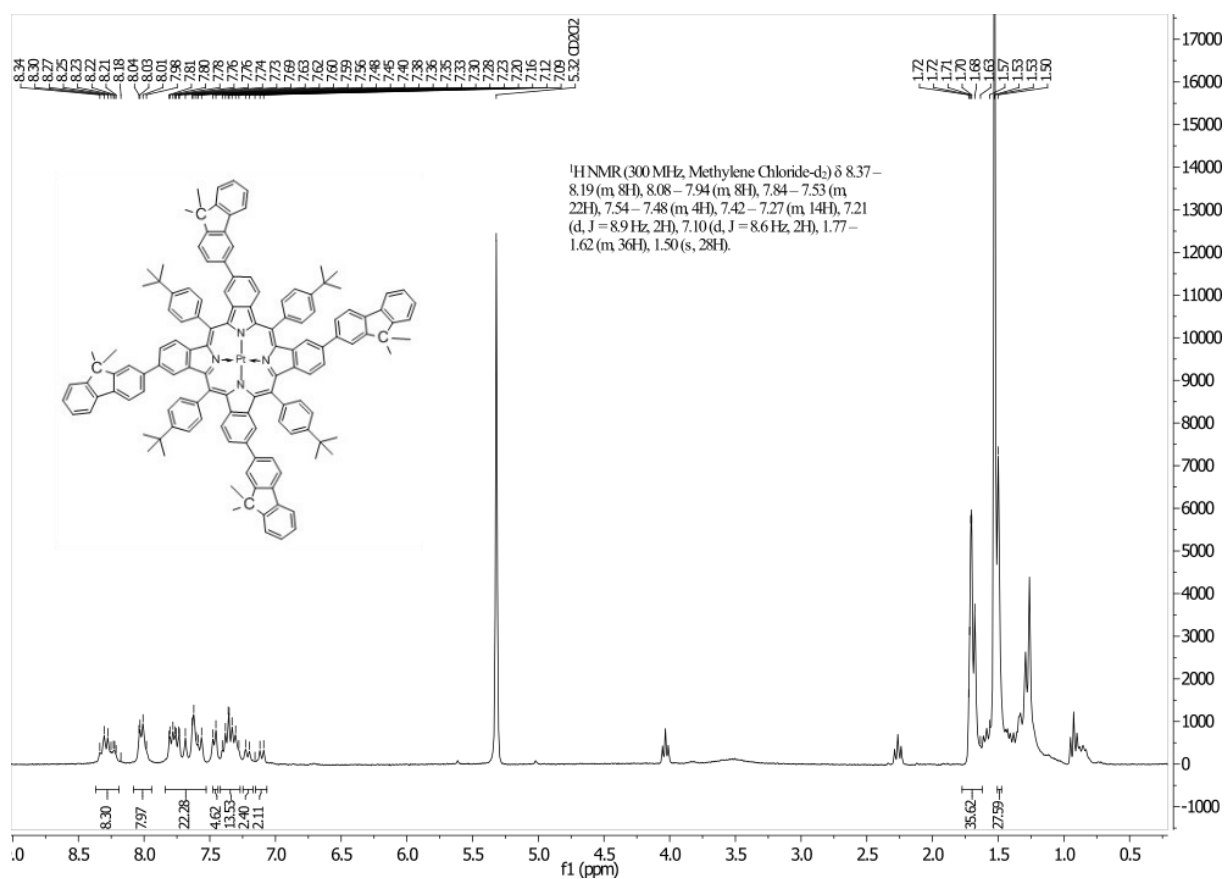
Figure S 7.19 ¹H-NMR spectrum of Pt-carbazole

¹H NMR (300 MHz, Methylene Chloride-d₂) δ 8.33 – 8.18 (m, 2H), 8.18 – 8.07 (m, 3H), 8.06 – 7.92 (m, 2H), 7.80 (dt, J = 13.5, 7.5 Hz, 4H), 7.66 (d, J = 7.4 Hz, 2H), 7.53 (dd, J = 11.8, 5.4 Hz, 16H), 7.44 – 7.32 (m, 5H), 7.31 – 7.19 (m, 2H), 7.19 – 7.02 (m, 4H).
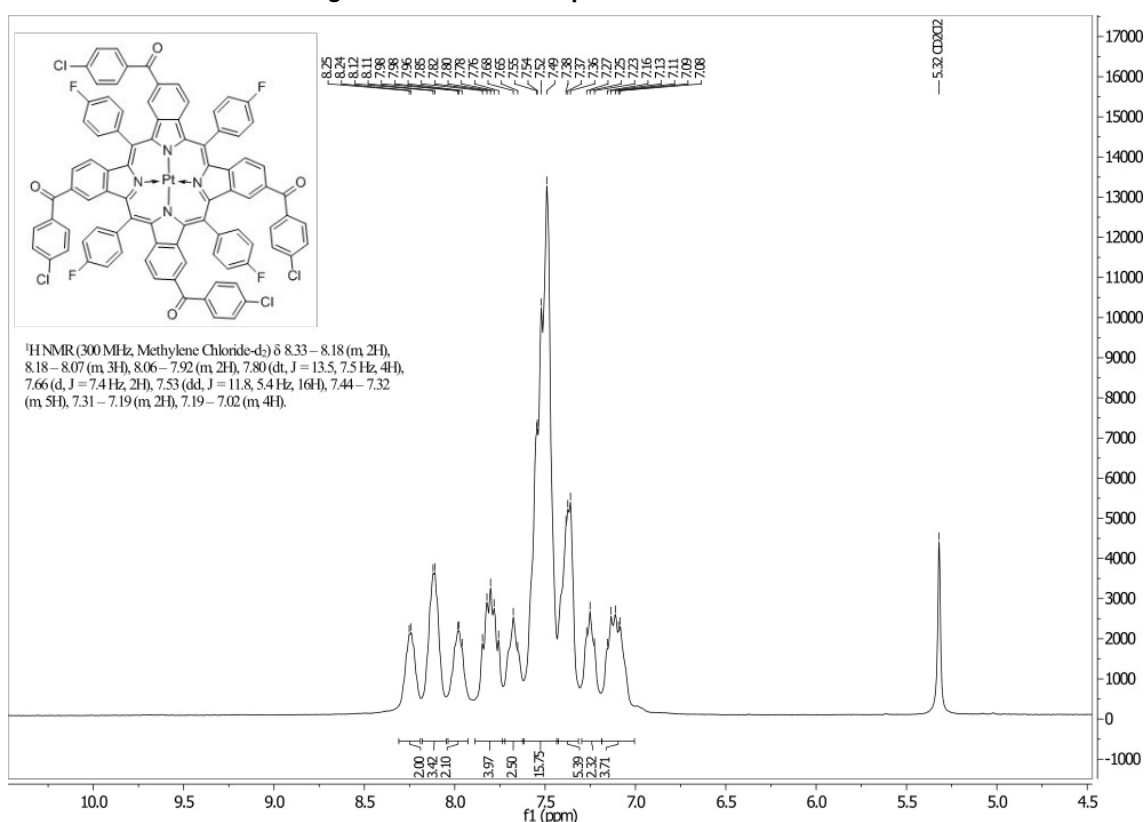
Figure S 7.20 ¹H-NMR spectrum of Pt-benzoyl-Cl

196

Figure S 7.21 ^{13}C-APT-NMR spectrum of Pt-benzoyl-Cl

^{1}H NMR (300 MHz, Methylene Chloride-d$_2$) δ 8.37 – 8.09 (m, 8H), 8.07 – 7.43 (m, 16H), 7.28 – 7.03 (m, 4H), 2.43 – 2.17 (m, 12H).

Figure S 7.22 ^{1}H-NMR spectrum of Pt-acetyl

¹H NMR (500 MHz, Methylene Chloride-d₂) δ 8.16 (m, J = 14.8, 14.4, 9.0 Hz, 8H), 7.98 (td, J = 20.4, 5.7 Hz, 8H), 7.49 (m, J = 4.6 Hz, 5H), 7.37 (m, J = 5.1 Hz, 10H), 7.32 (s, 1H), 7.29 (d, J = 5.4 Hz, 2H), 7.25 (m, J = 14.6, 7.1 Hz, 5H), 7.22 – 7.19 (m, 1H), 7.16 (m, J = 13.1, 7.4 Hz, 7H), 7.10 – 7.03 (m, 2H), 1.68 (d, J = 8.1 Hz, 36H).
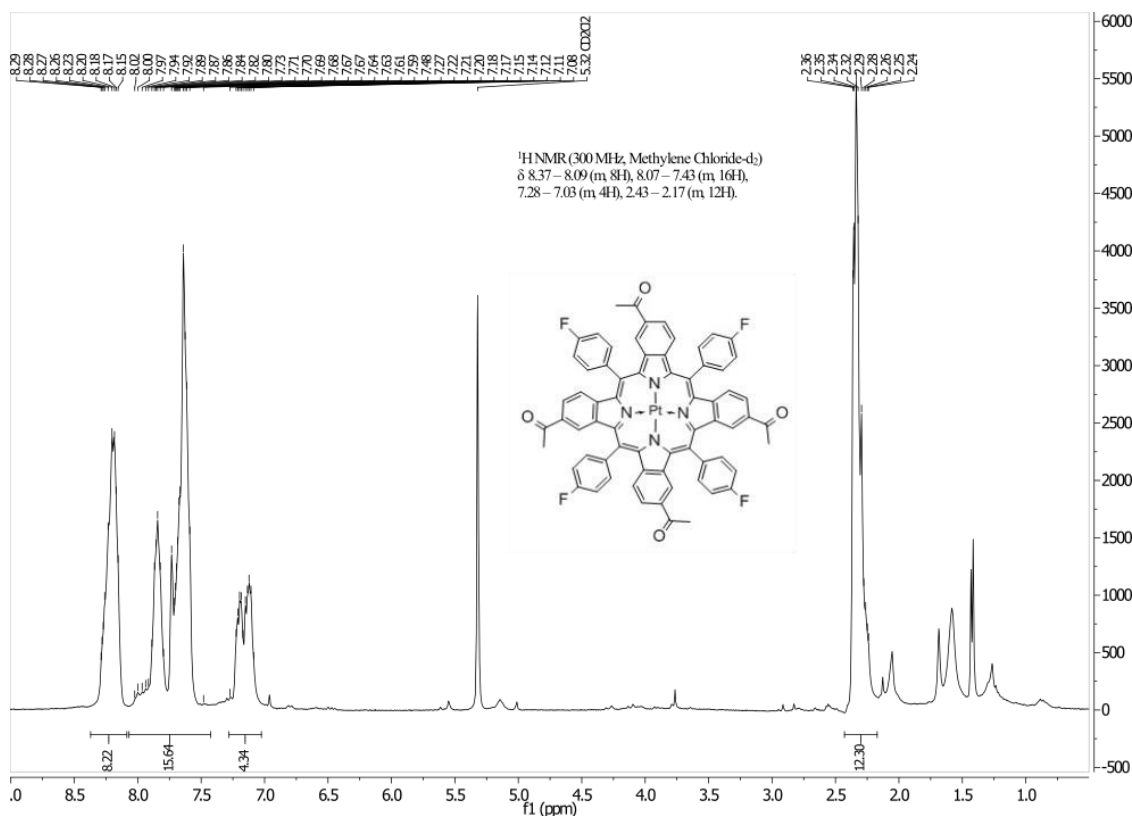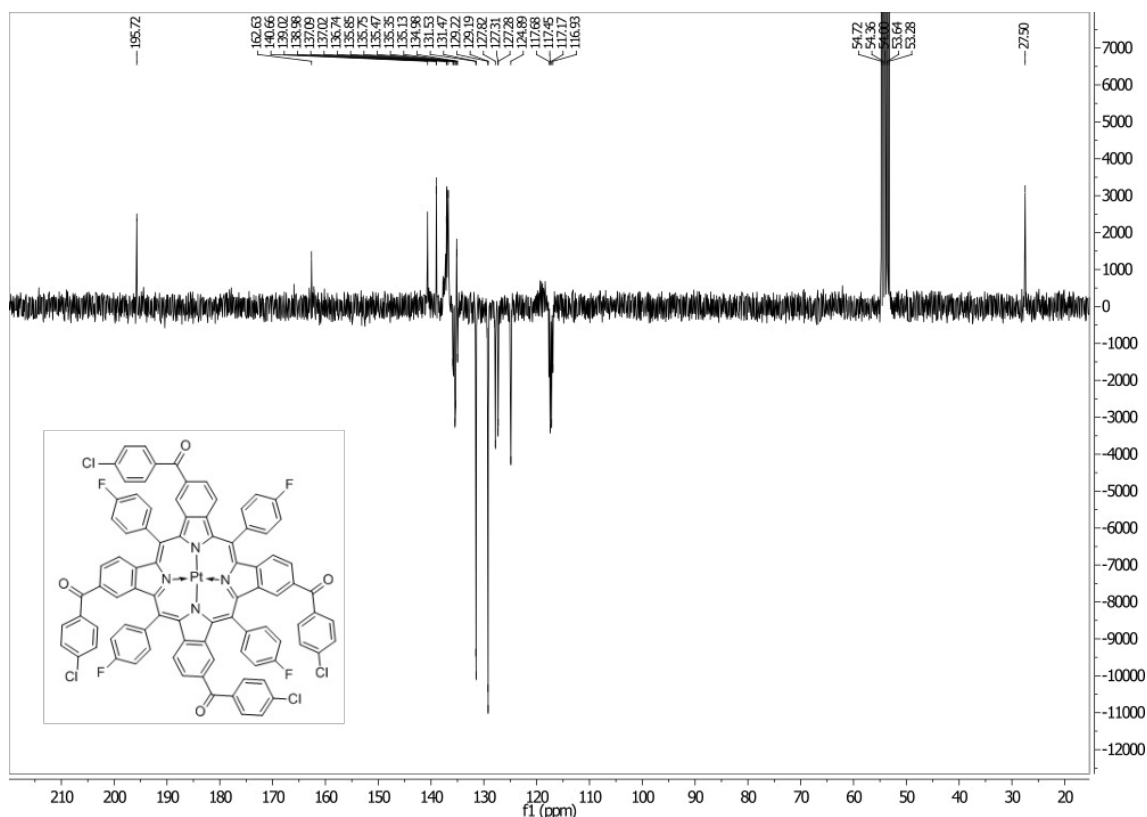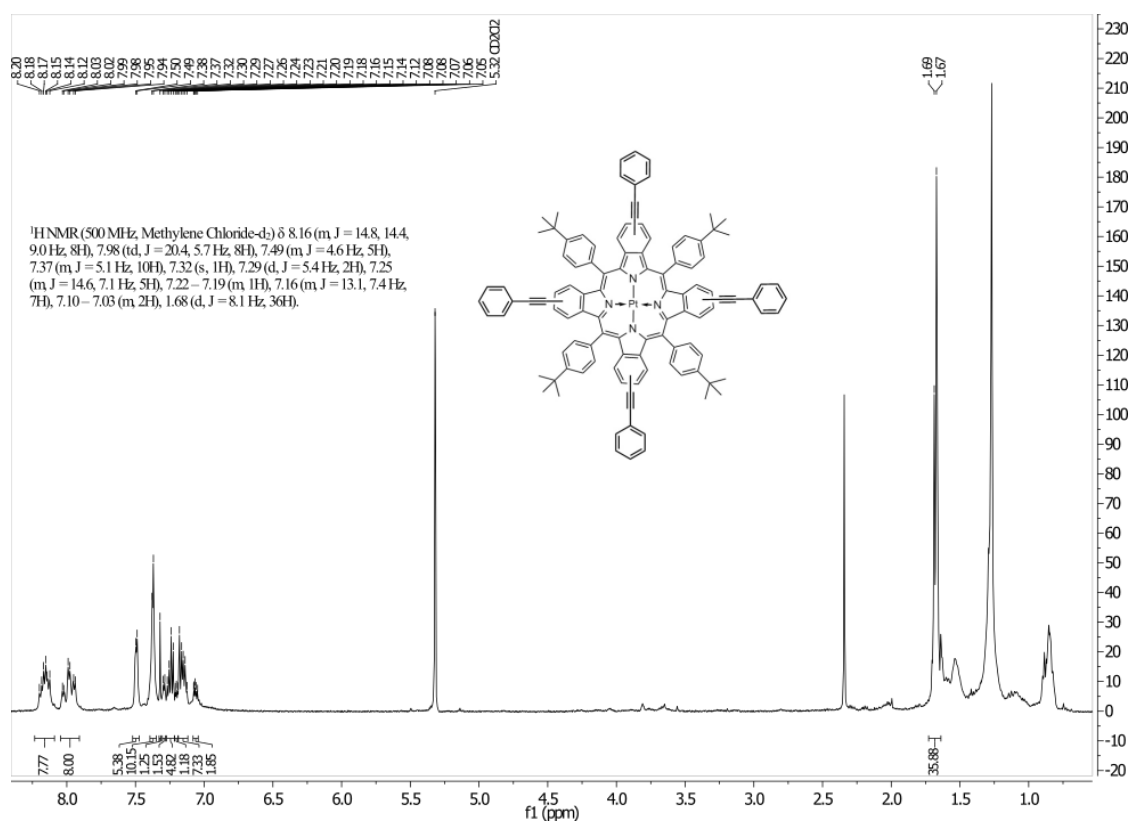
Figure S 7.23 ¹H-NMR spectrum of Pt-Ph-acetylene
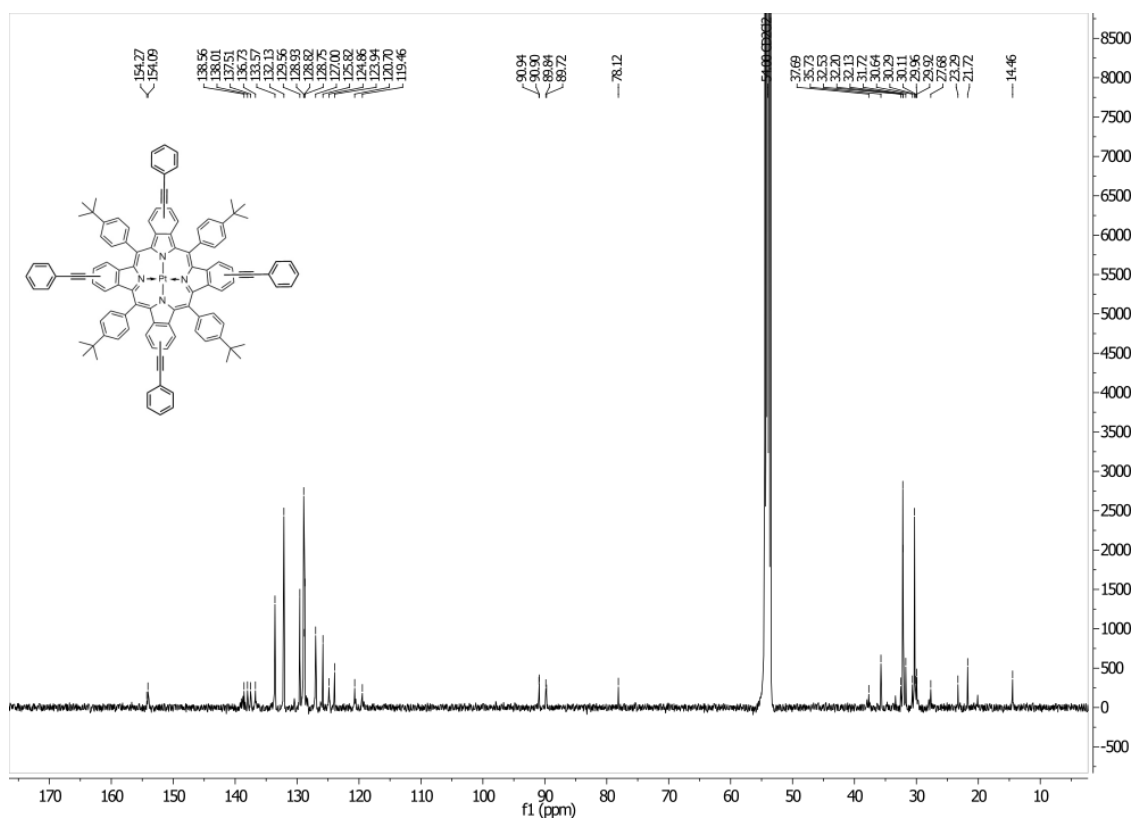
Figure S 7.24 ¹³C-APT-NMR spectrum of Pt-Ph-acetylene

^{1}H NMR (300 MHz, Methylene Chloride-d$_2$) δ 8.25 (dq, J = 9.6, 4.7 Hz, 2H), 8.18 – 8.07 (m, 3H), 7.98 (dt, J = 10.7, 5.4 Hz, 2H), 7.80 (dt, J = 14.0, 7.7 Hz, 4H), 7.72 – 7.61 (m, 2H), 7.60 – 7.43 (m, 16H), 7.38 (t, J = 6.8 Hz, 5H), 7.32 – 7.23 (m, 2H), 7.21 – 7.13 (m, 2H), 7.09 (dq, J = 8.3, 5.4, 4.5 Hz, 2H).
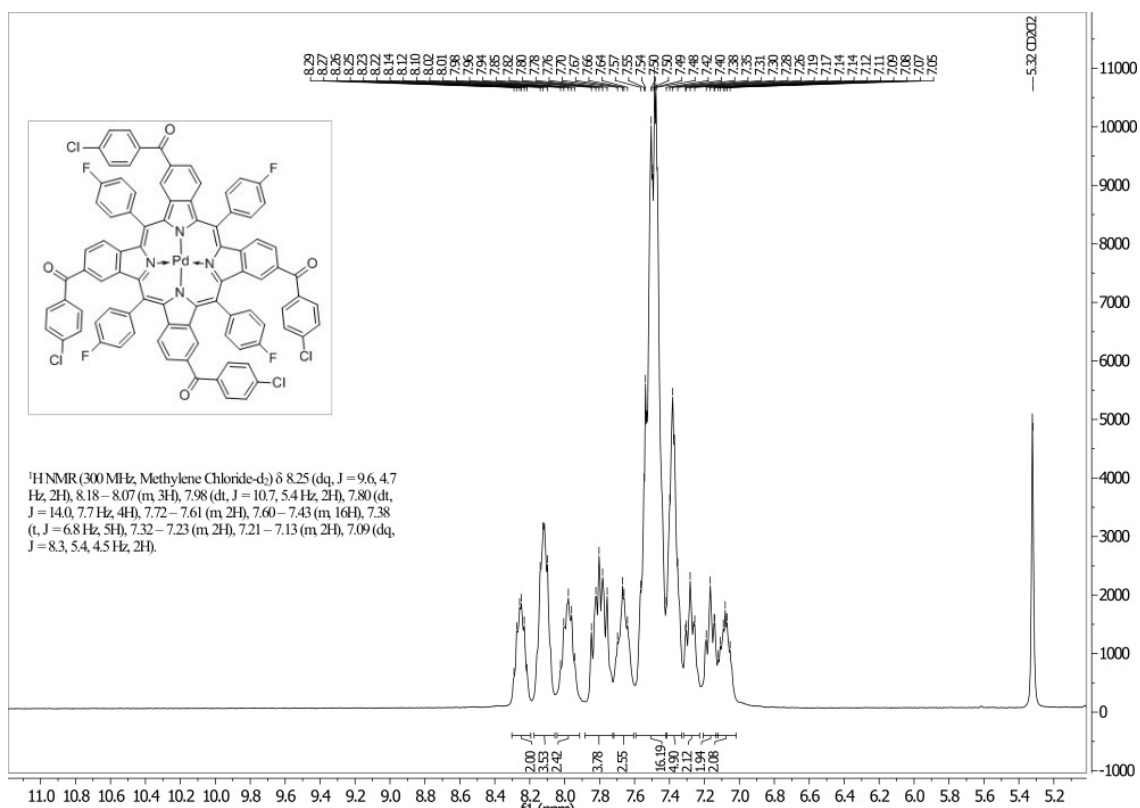
Figure S 7.25 ^{1}H-NMR spectrum of Pd-benzoyl-Cl
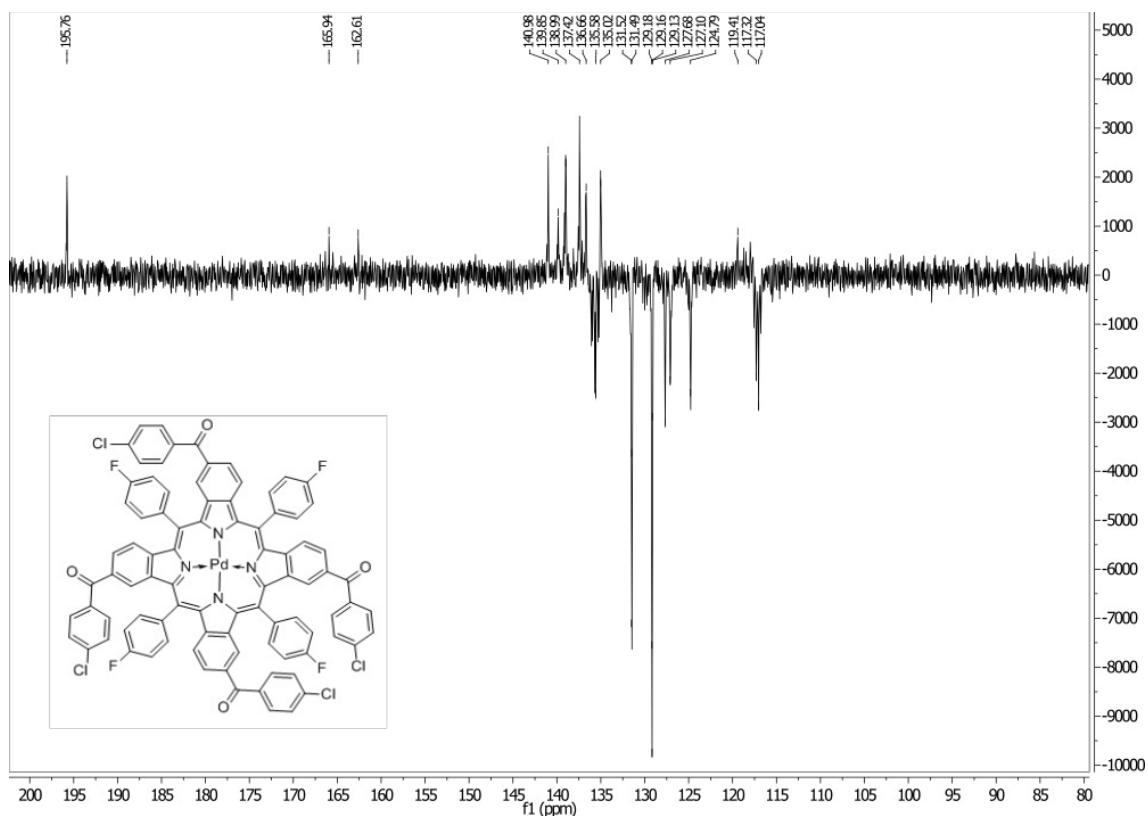
Figure S 7.26 ^{13}C-APT-NMR spectrum of Pt-benzoyl-Cl

7.5.6 MALDI-TOF Spectra

Figure S 7.27 Mass-Spectra of Pt-fluorene

Figure S 7.28 Mass-Spectra of Pt-fluorene 2
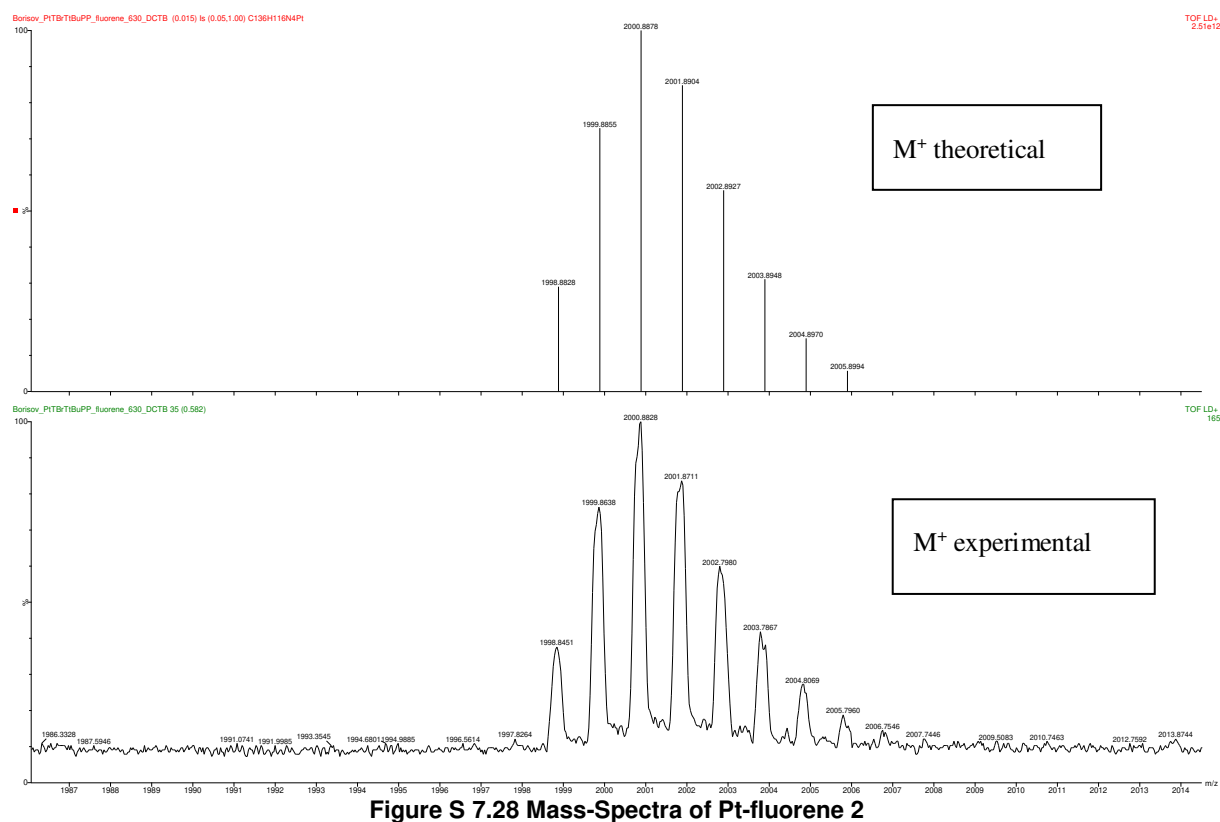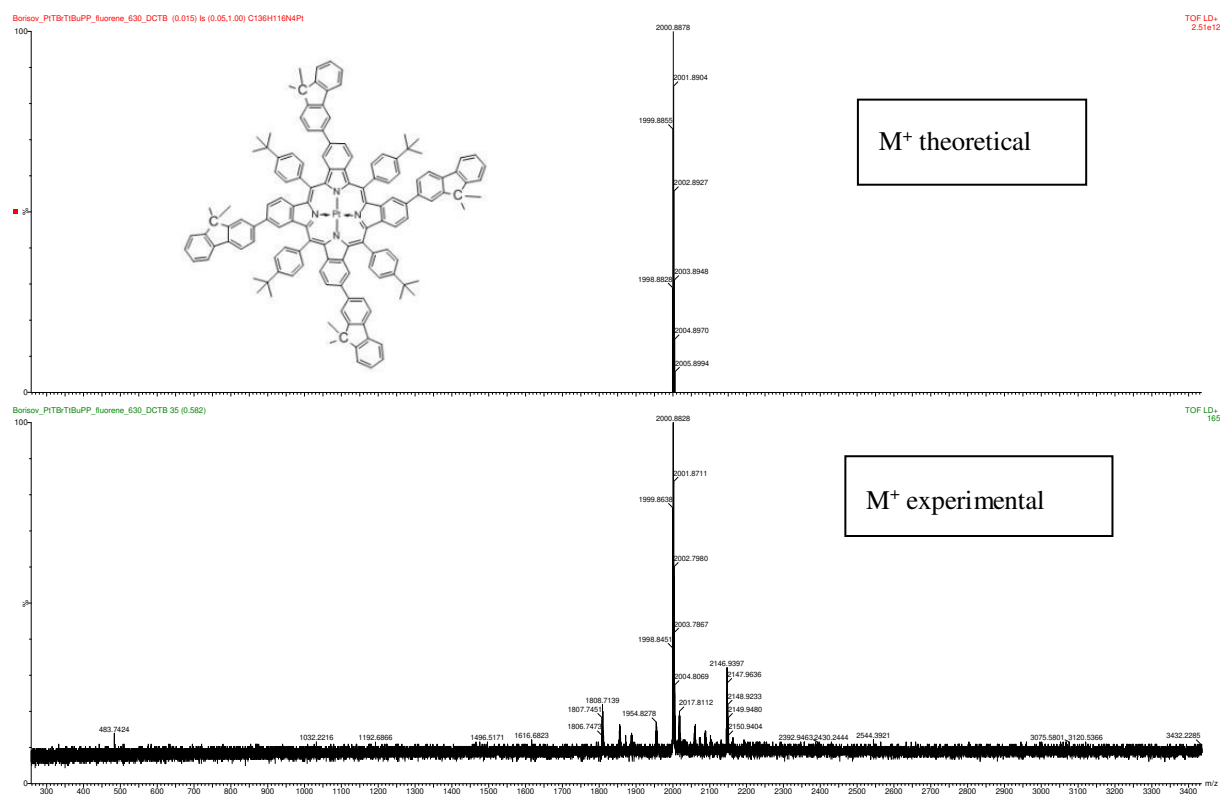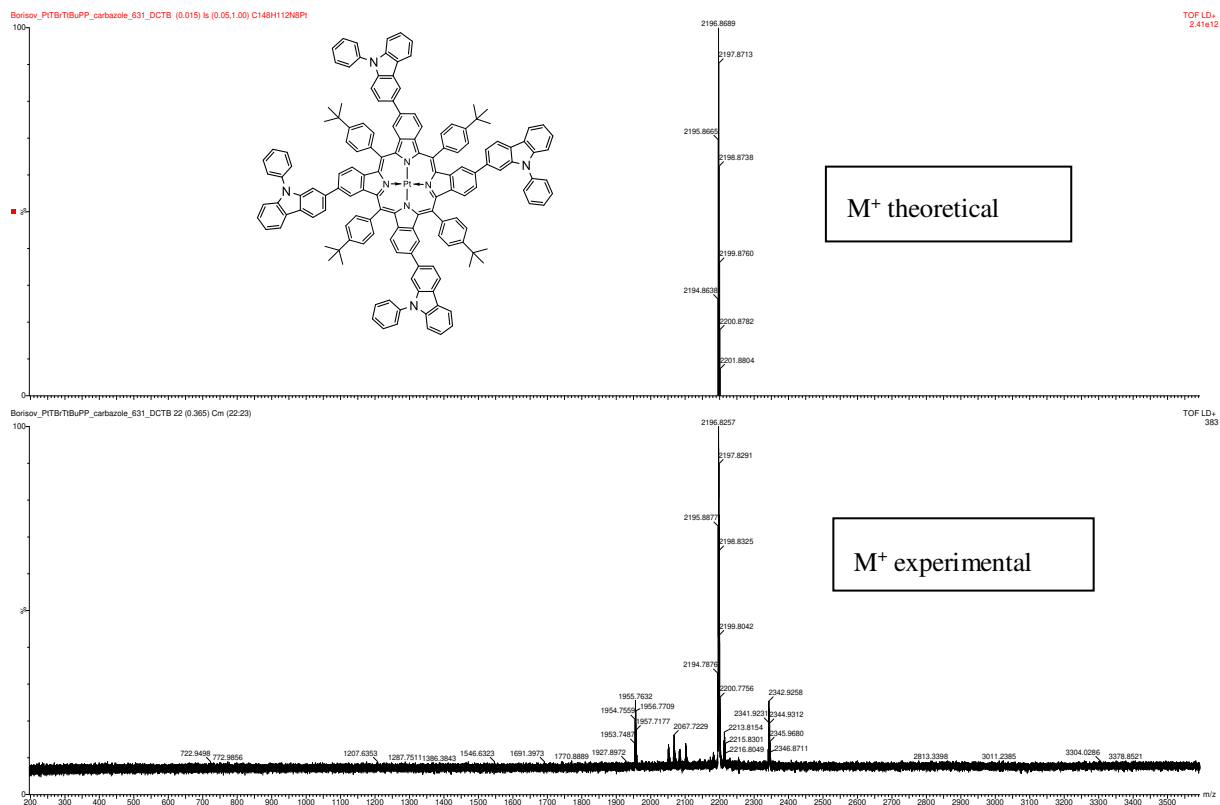
Figure S 7.29 Mass-Spectra of Pt-carbazole
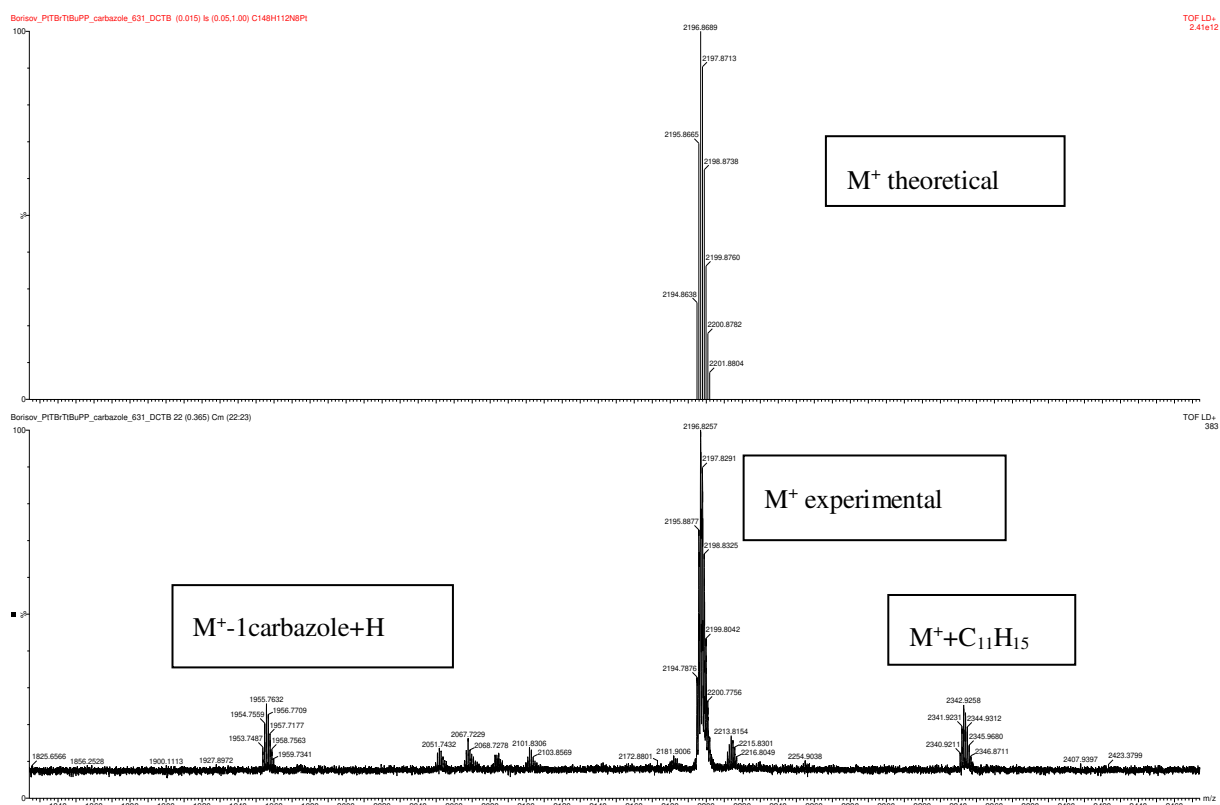
Figure S 7.30 Mass-Spectra of Pt-carbazole (zoomed in).

Figure S 7.31 Theoretical and experimental isotope patterns for Pt-carbazole

Figure S 7.32 Mass-Spectra of Pt-benzoyl-Cl

Figure S 7.33 Theoretical and experimental isotope patterns for Pt-benzoyl-Cl

Figure S 7.34 Mass-Spectra of Pt-acetyl
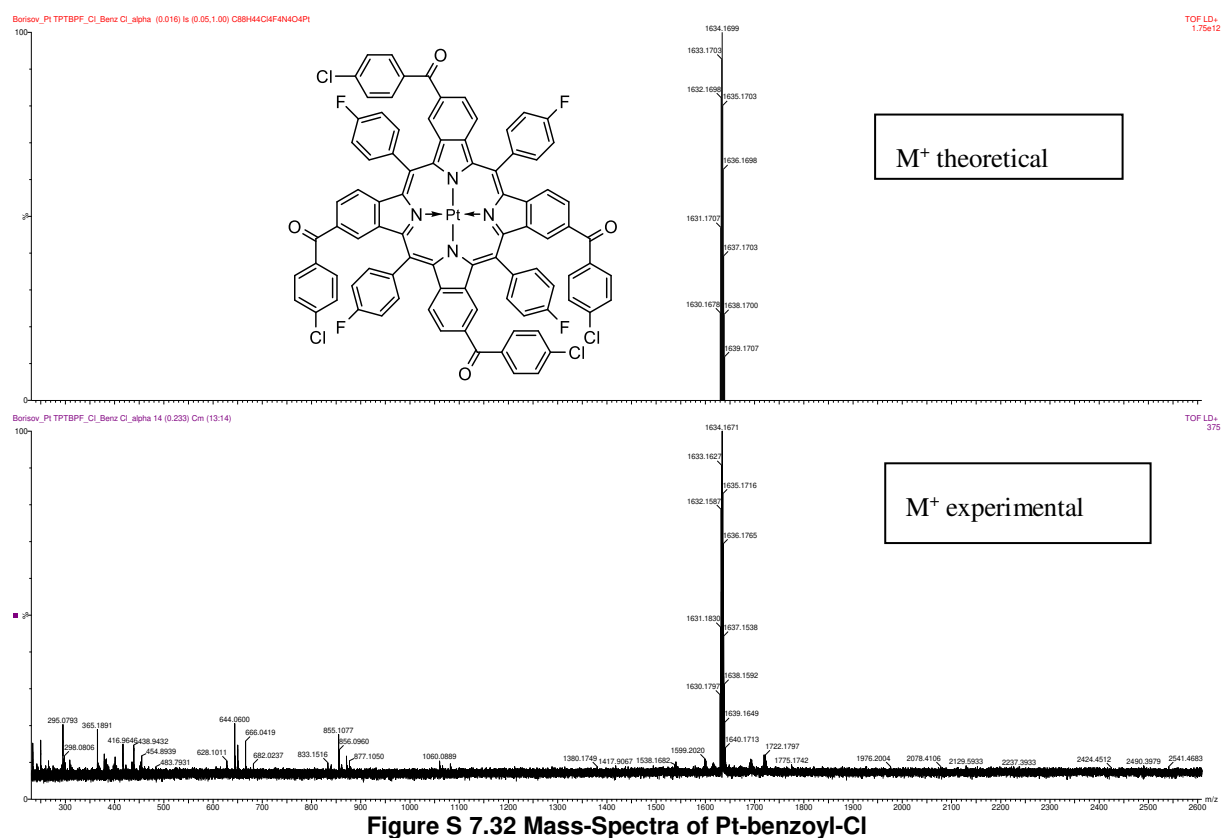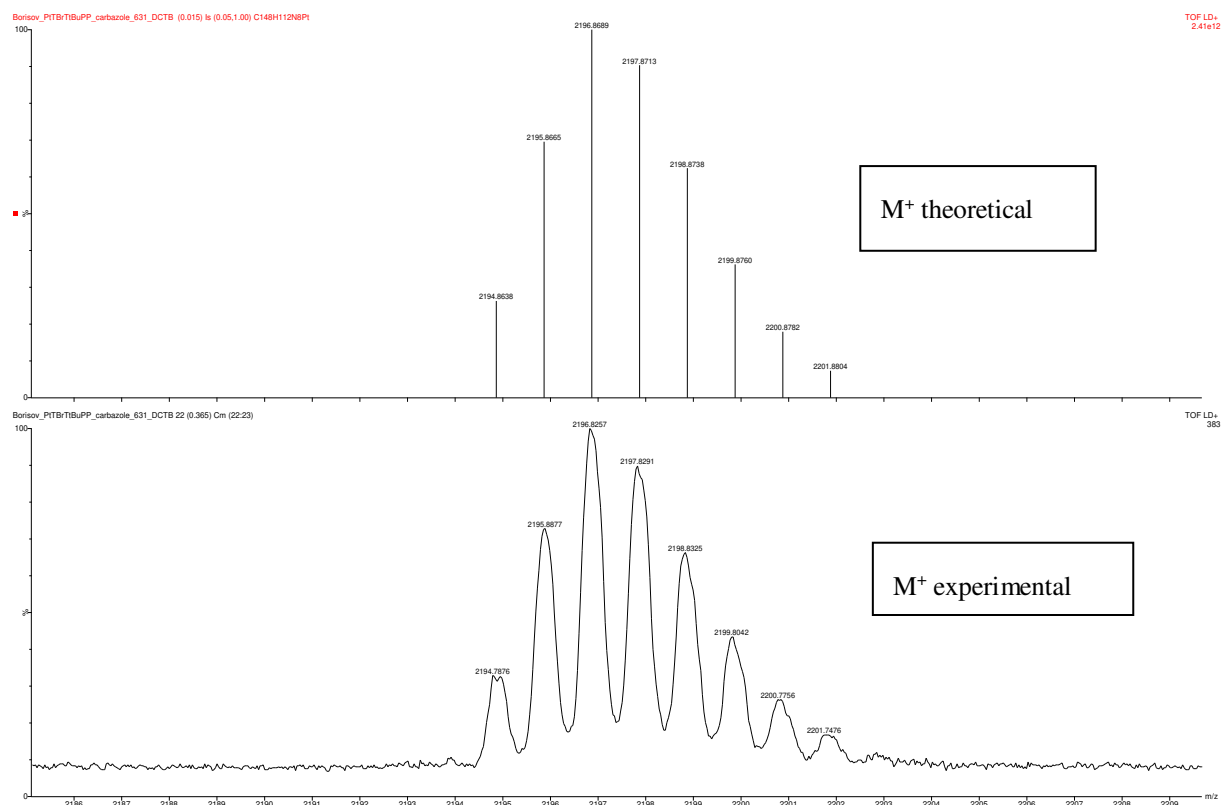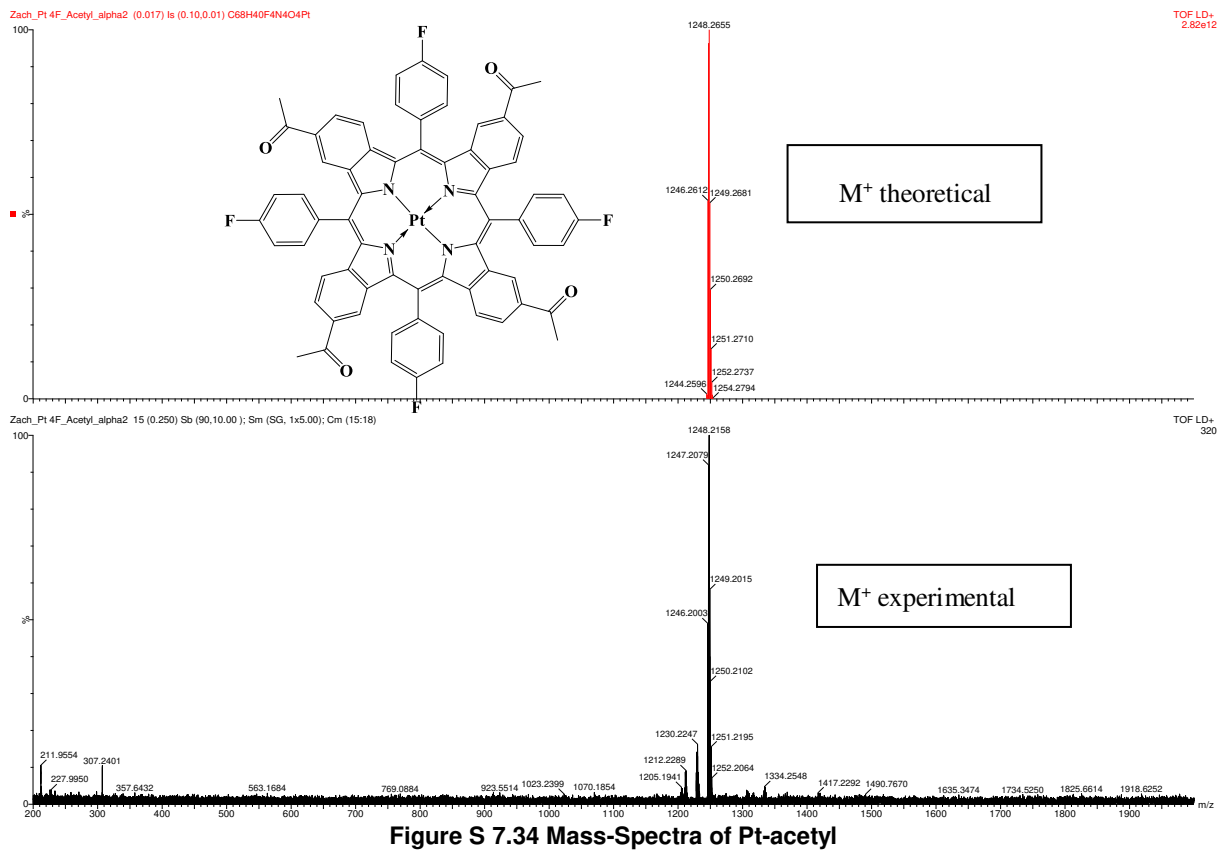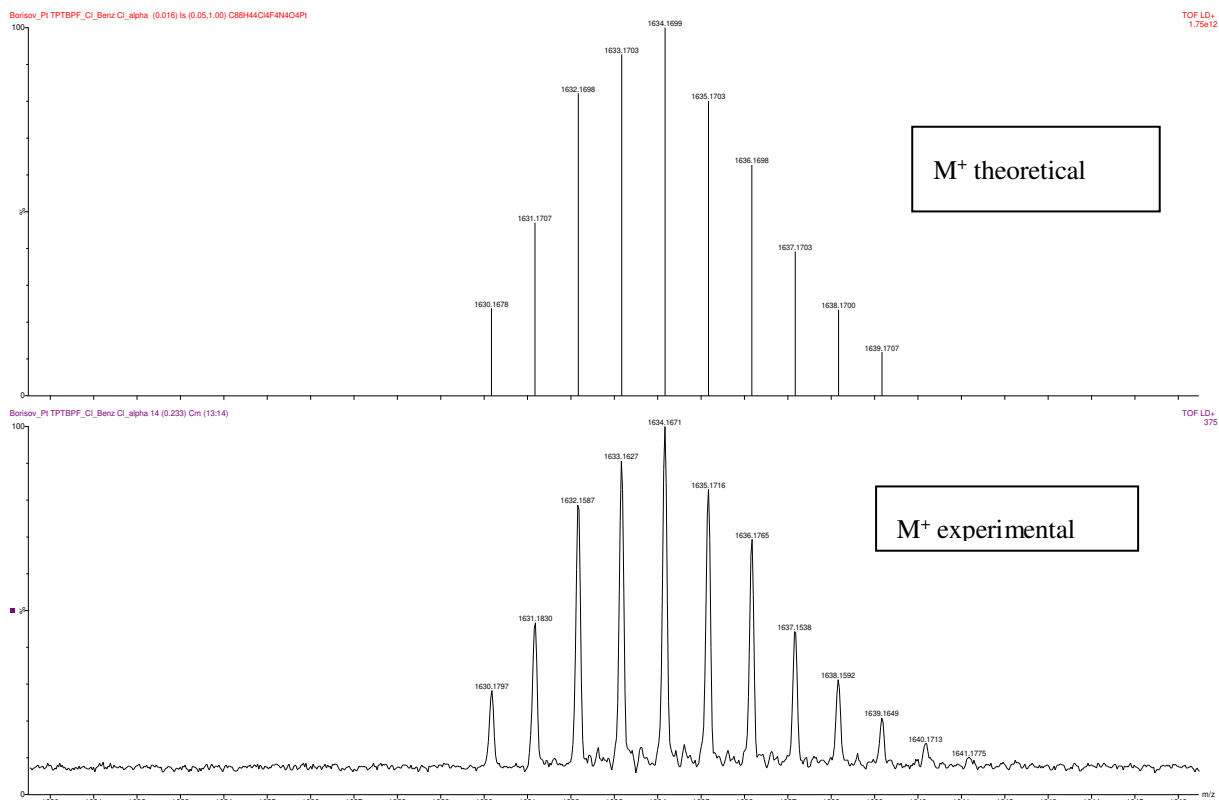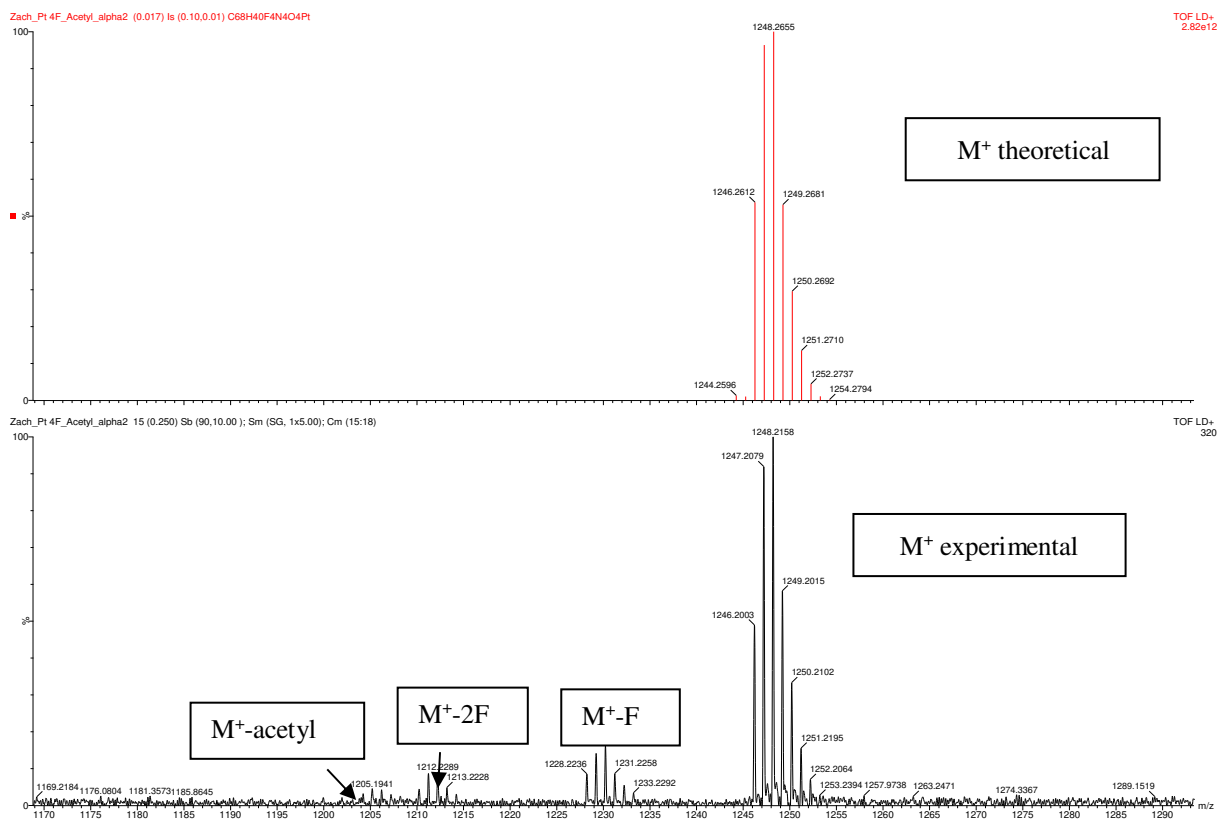
Figure S 7.35 Theoretical and experimental isotope patterns for Pt-acetyl
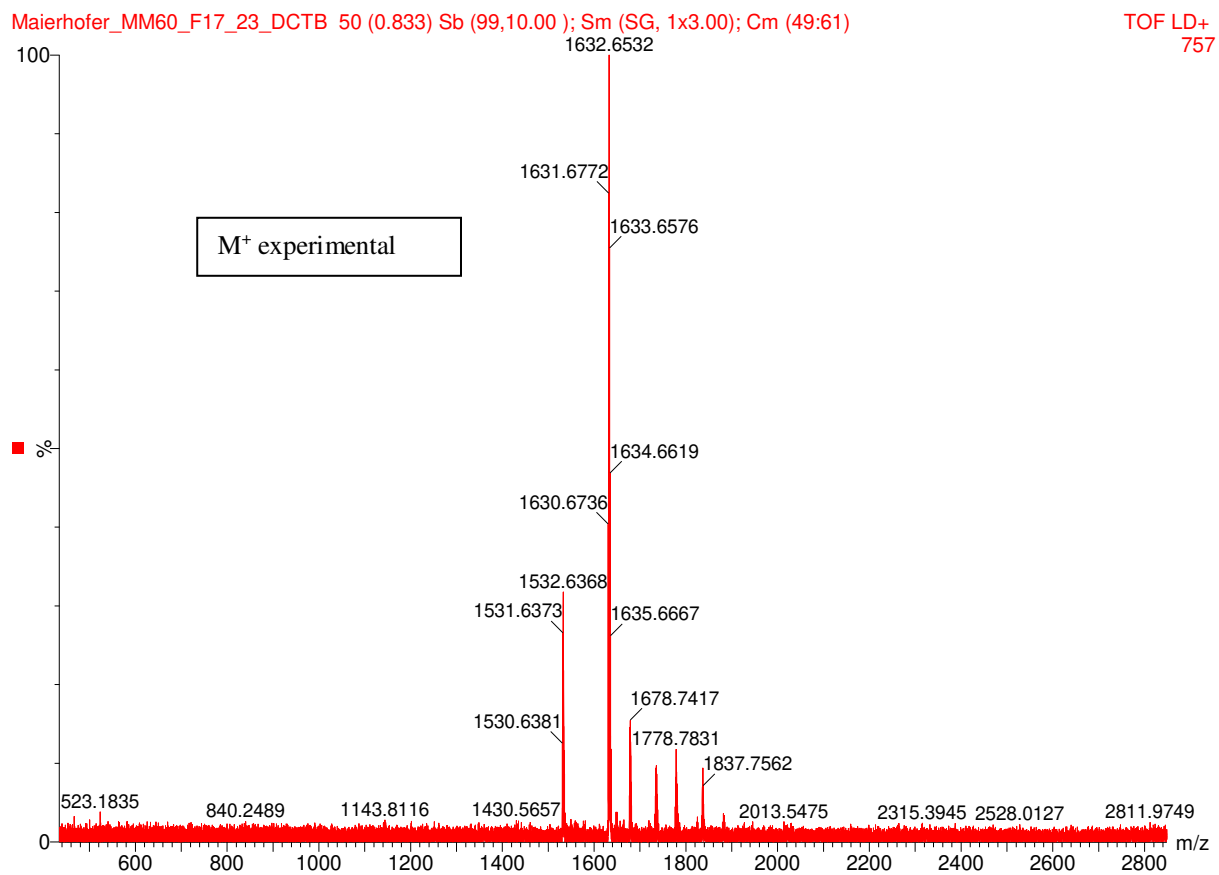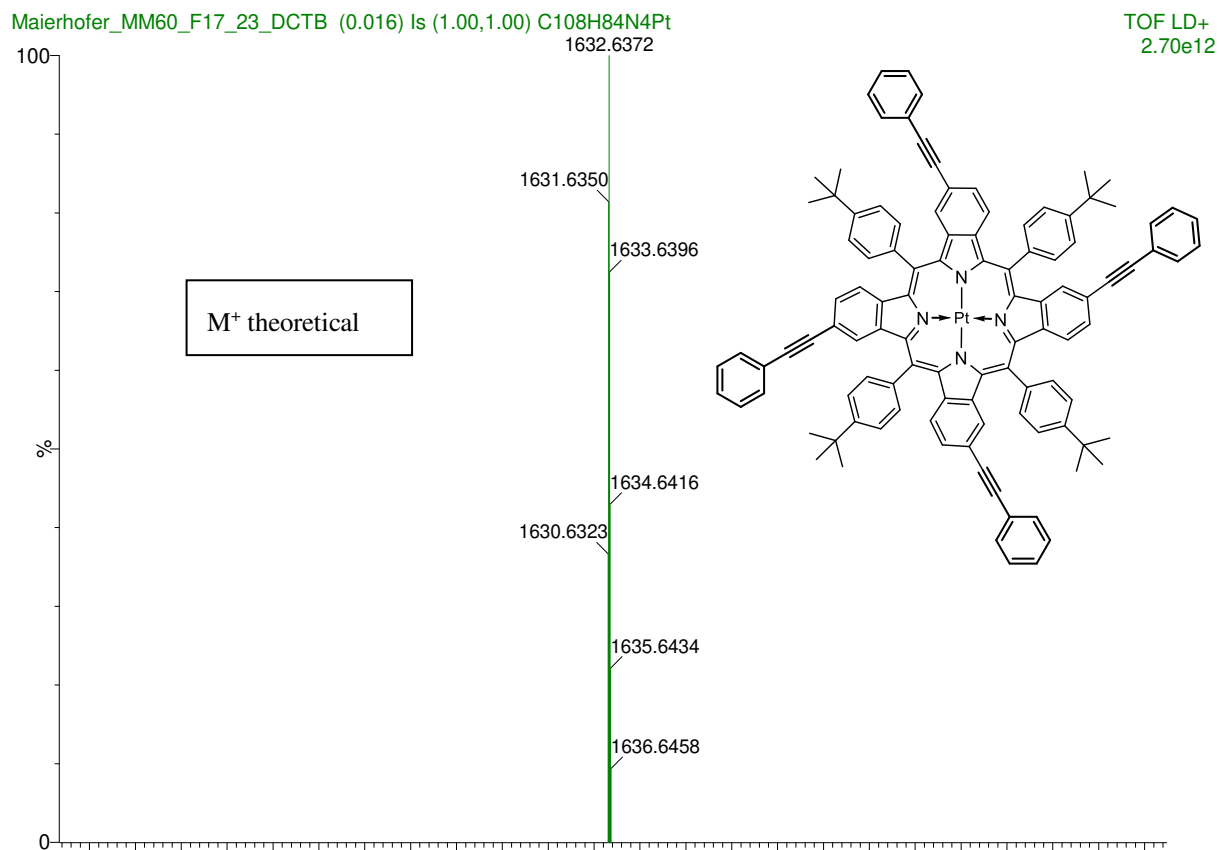
Figure S 7.36 Mass-Spectra of Pt-Ph-acetylene
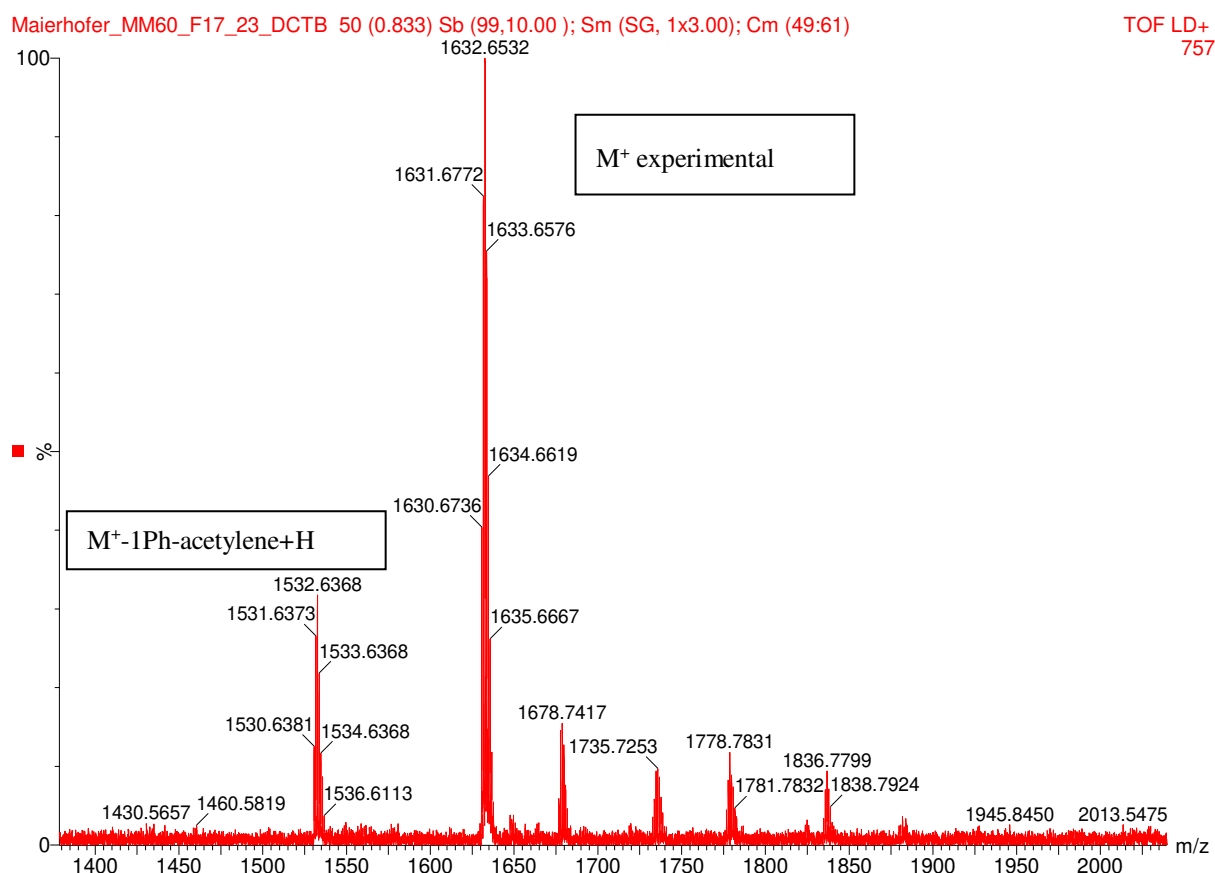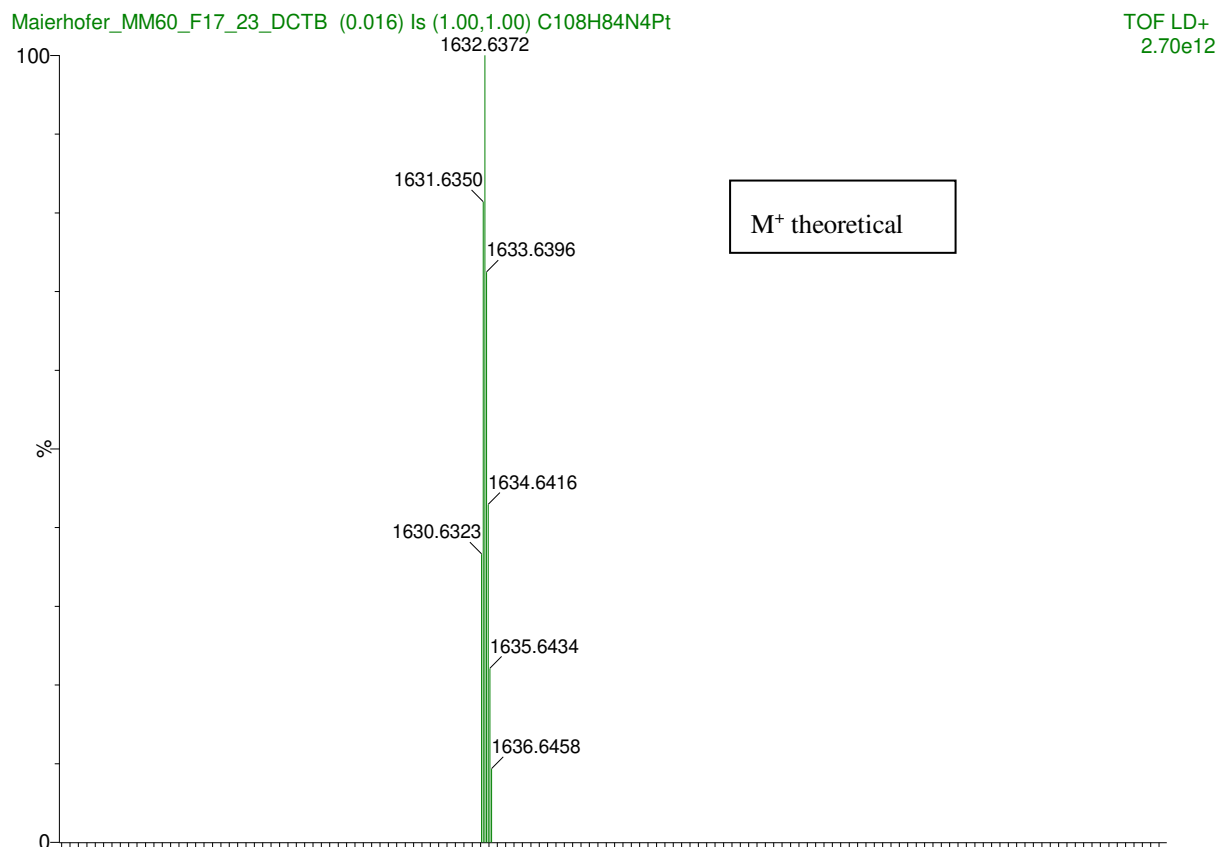
Figure S 7.37 Mass-Spectra of Pt-Ph-acetylene (zoomed in)
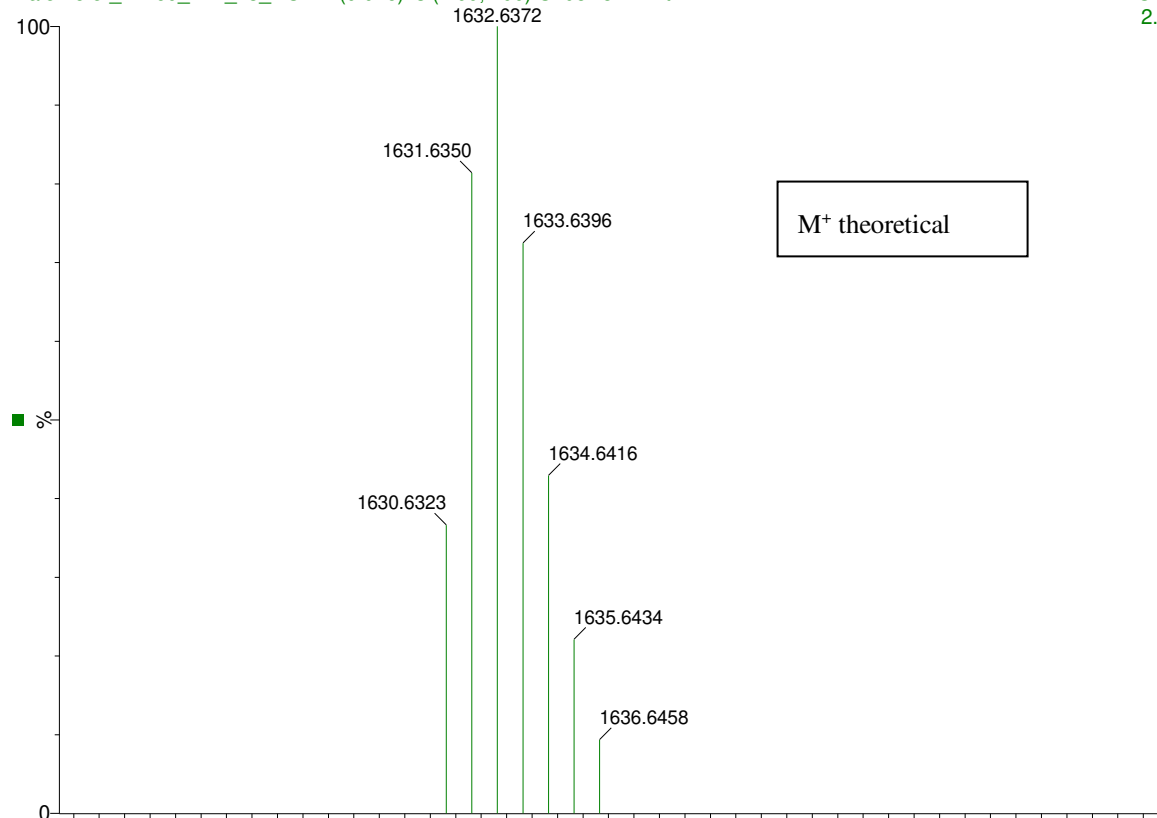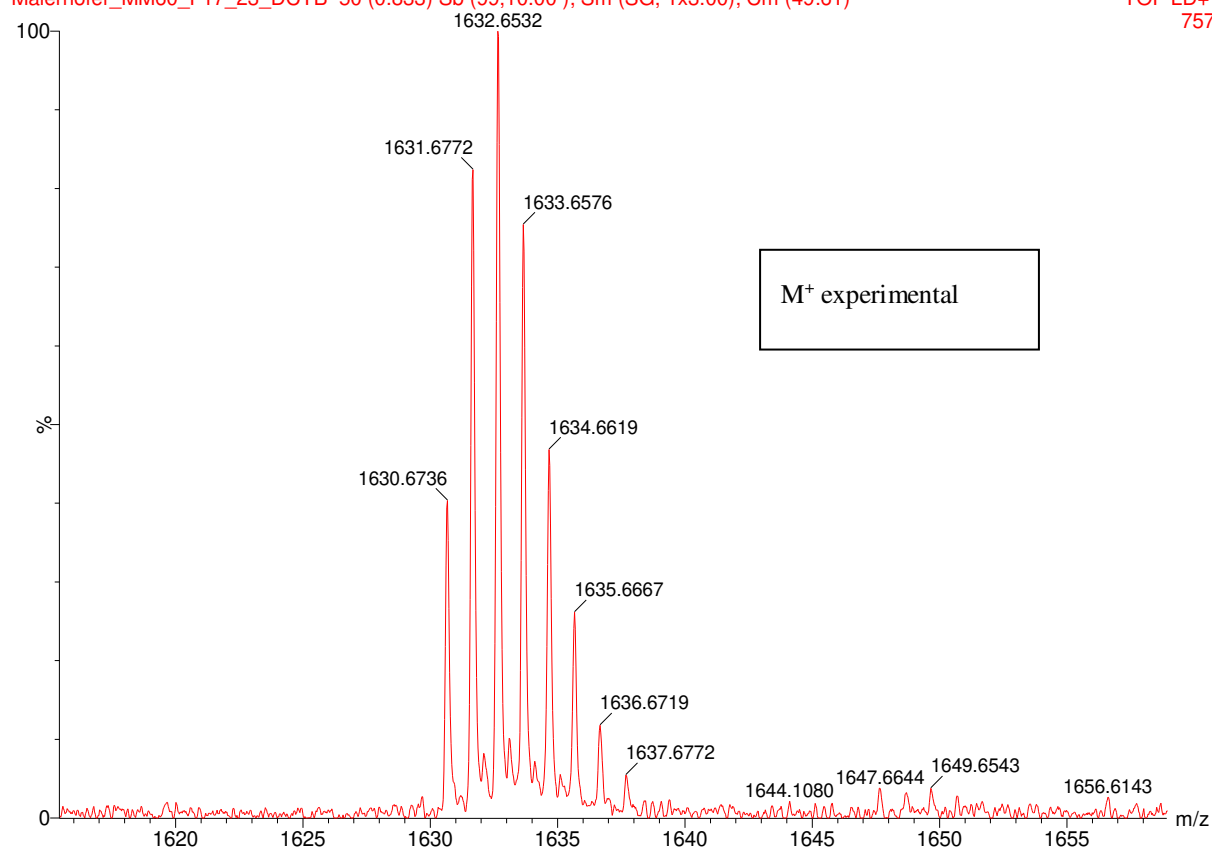
Figure S 7.38 Theoretical and experimental isotope patterns for of Pt-Ph-acetylene
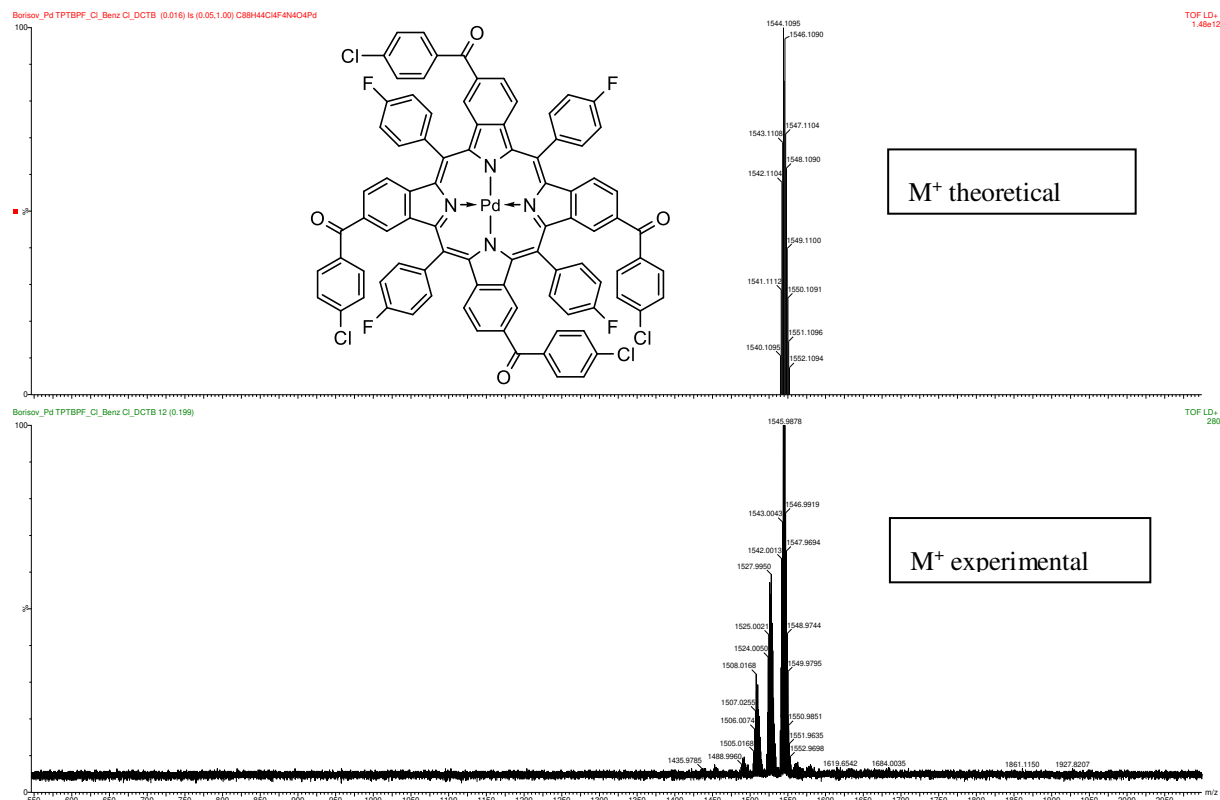
Figure S 7.39 Mass-Spectra of Pd-benzoyl-Cl
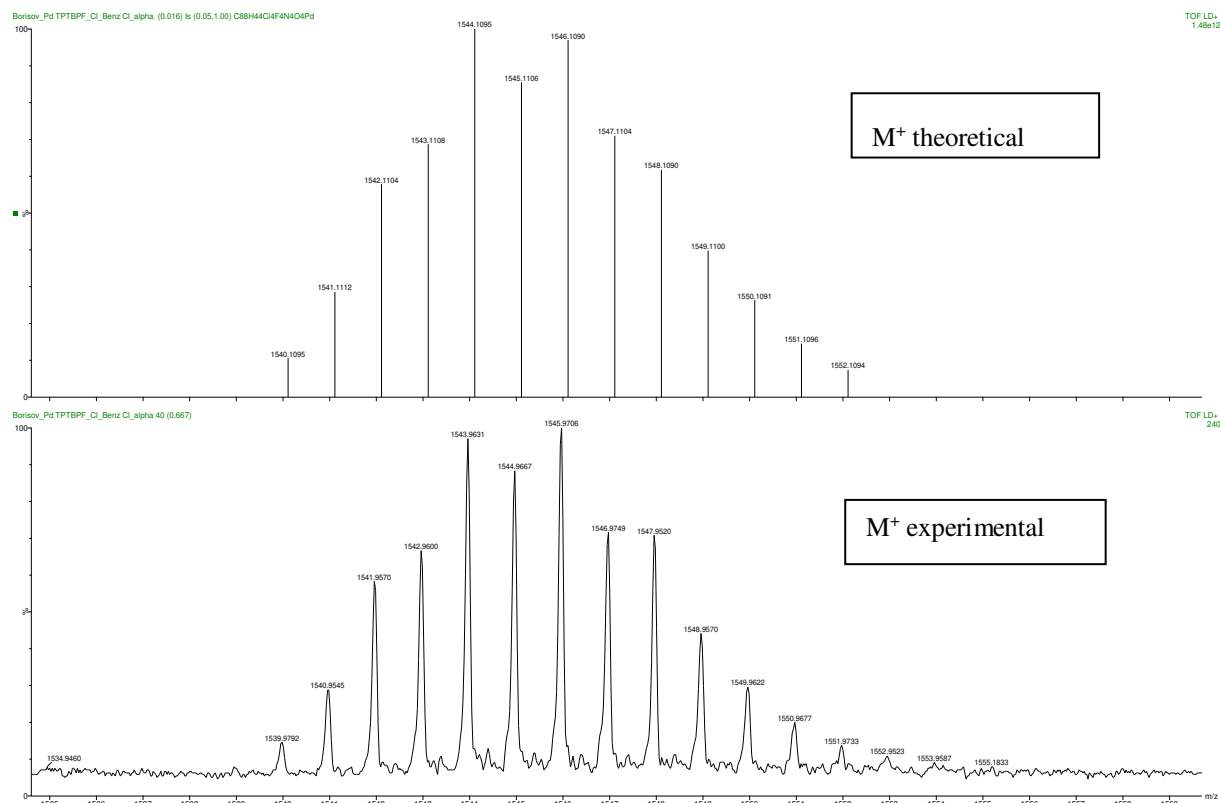
Figure S 7.40 Theoretical and experimental isotope patterns for Pd-benzoyl-Cl
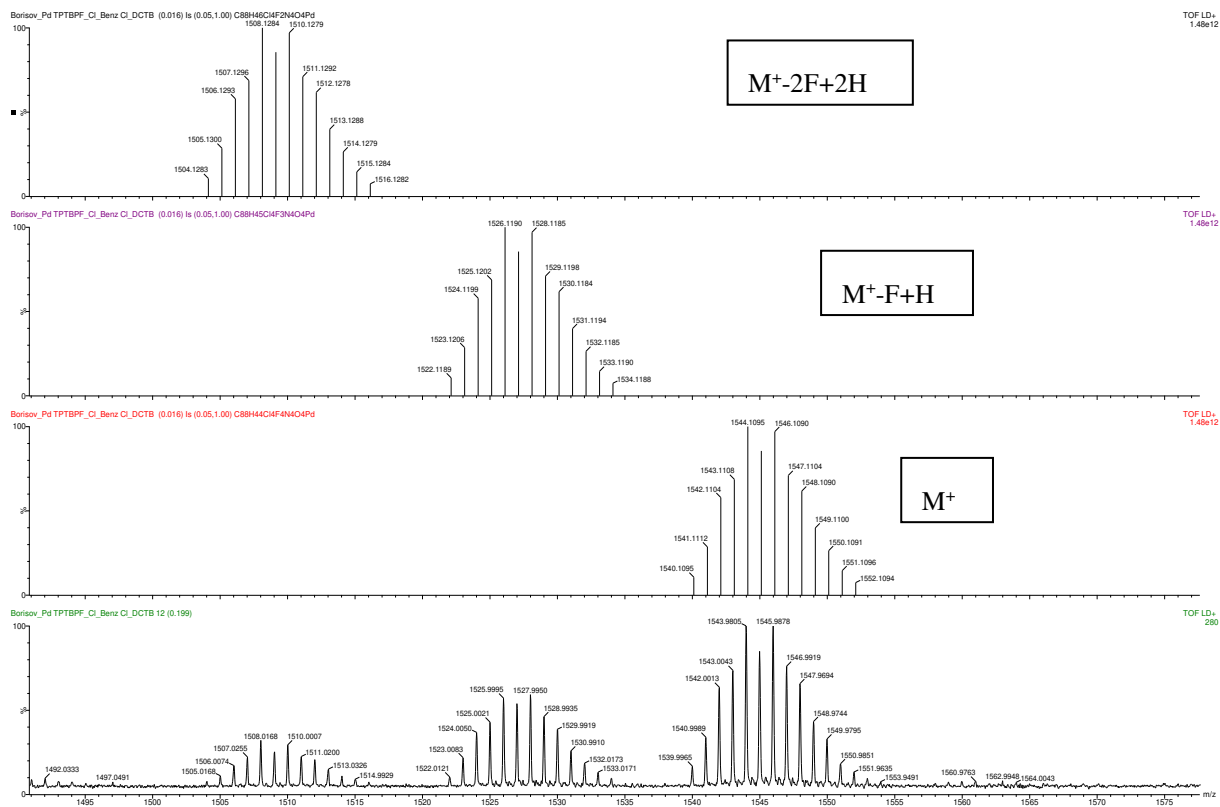
Figure S 7.41 Theoretical and experimental isotope patterns for Pd-benzoyl-Cl

8 Other Work

This chapter covers the additional results obtained during the course of the thesis, which were not (included or) published in peer reviewed journals. Since they still contain relevant information and for the sake of completeness these results are summarized and presented here.

8.1 Addendum to the 2nd publication in chapter 6: Application of bridged benzoporphyrin as sensitizer for TTA upconversion, further attempts using Scholl reaction & an alternative route to bridged porphyrins

This chapter contains the synthesis via template method to platinum(II) meso-tetra-anisole-tetra-benzoporphyrin (Pt-TATBP; substituted with four anisole groups in meso-position of the benzoporphyrins core) and the attempt to bridge this compound using Scholl reaction. Moreover, intramolecular bridging of platinum(II) meso-tetra-phenyl-di(di-methyl)benzoporphyrin (Pt-TPTBPdM2) via Scholl reaction was also investigated as well as an alternative route using a Ni-porphyrin to enable controlled bridging of compounds. These experiments were performed by Maximilian Maierhofer during the project laboratory under my co-supervision.

8.1.1 Application of bridged benzoporphyrin as sensitizer for TTA upconversion

Benzoporphyrins and their molecular hybrids with naphthoporpyhrins proved to be efficient sensitizers for TTA upconversion systems, [1], [2] but the photostability of the latter compounds is poor. [3] Since new bridged benzoporphyrins Pt-B1 and Pt-B2 benefit from much better photostability they are expected to be promising sensitizers for upconversion of red light. In order to achieve maximum efficiency of TTA, the energy of the triplet state of a sensitizer should be higher than that of the annihilator. Therefore, different perylenes (solvent green 5, lumogen orange and lumogen red, Figure 8.1) were tested as annihilators due to their very high fluorescence quantum yields (close to unity), good solubility in organic solvents and outstanding photostability. [4] As can be seen in Figure 8.1, bright upconversion from perylenes ($2.5*10^{-4}$ M) is observed upon excitation of compound Pt-B2 ($5*10^{-5}$ M) with a 675-nm laser diode. Moreover, the upconverted fluorescence demonstrates quadratic dependence of the light intensity (Figure 8.2), resulting in a slope of the logarithmic plot with approximately 2. The most intense upconversion is achieved with lumogen red as annihilator with quantum yield of 2.5 %, when excited with 675-nm laser diode, whereas the energy of the triplet state of other perylene dyes may be too high for efficient triplet-triplet energy transfer. Due to the high concentration of the sensitizer/annihilator solution, it is however important to consider possible aggregation of the molecules as well as inner-filter effect. Considering recent progress in the development of nanoparticles featuring TTA, [5] the combination of the NIR-excitable sensitizers with red-light emitting annihilator may lead to a new generation of imaging

agents for in vivo measurements with much higher brightness than lanthanide nanoparticles. [6]
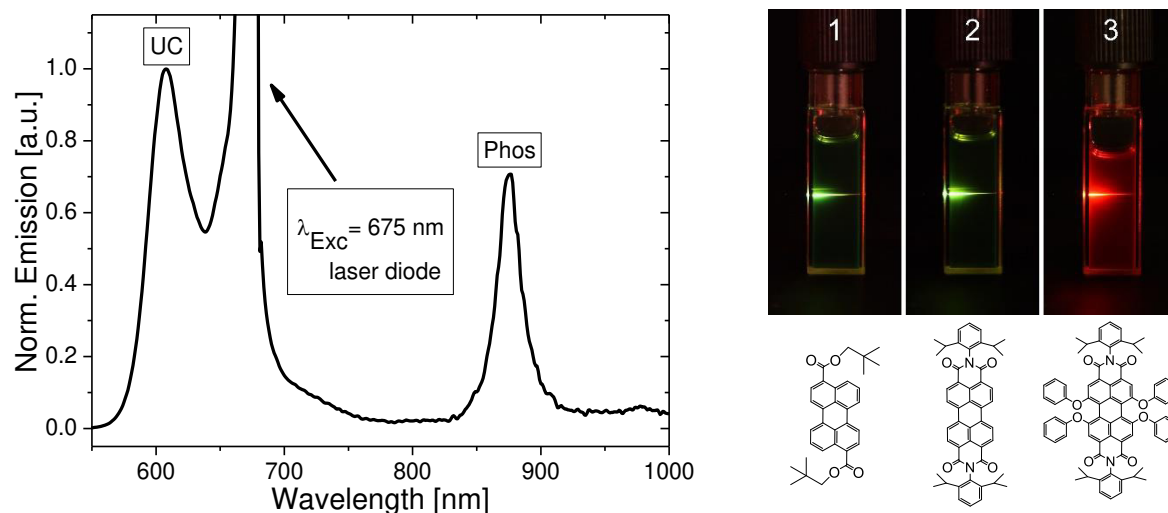
Figure 8.1 Left: Normalized emission spectra for the mixture of sensitizer Pt-B2 (5*10^{-5} M) and annihilator lumogen red (2.5*10^{-4} M) in anoxic toluene solution at r.t. upon excitation with a 675 nm laser diode showing bright red upconverted fluorescence (UC); Right: Photographic images of TTA-based upconversion of Pt-B2 mixed with different perylenes annihilators (1: solvent green 5, 2: lumogen orange and 3: lumogen red) upon excitation with the same laser diode.
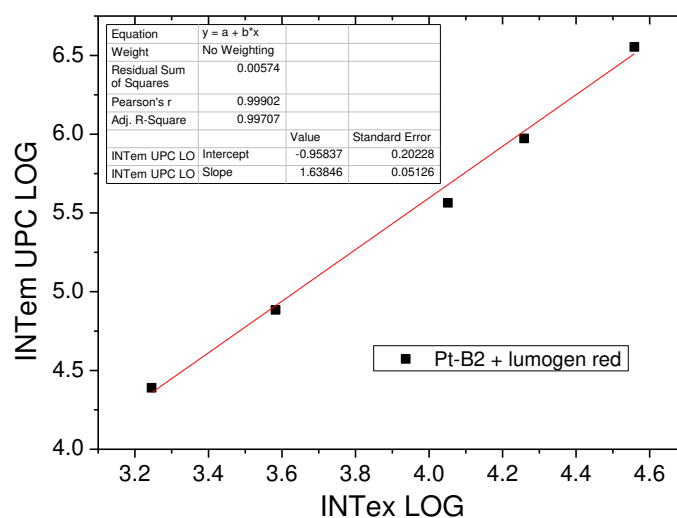
Figure 8.2 Quadratic dependence of the light intensity of Pt-B2 (5*10^{-5} M) and annihilator lumogen red (2.5*10^{-4} M) in anoxic toluene solution at r.t. upon excitation with a 675 nm laser diode

8.1.2 Experimental Part of meso-tetra-anisole-tetra-benzoporphyrin (TATBP)

Zinc (II) meso-tetra-anisole-tetra-benzoporphyrin (Zn-TATBP)
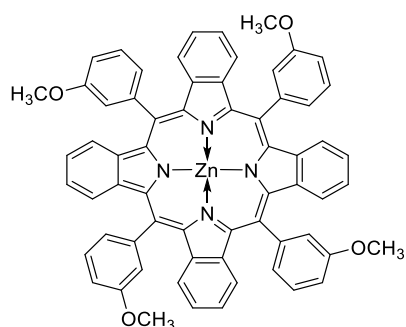
Figure 8.3 Chemical structure of Zn-TATBP

2-(3-methoxyphenyl)acetic acid (3.04 g, 18.29 mmol, 5.00 eq), phthalonitrile (1.88 g, 14.67 mmol, 4.00 eq) and zinc-(di-2-3(methoxyphenyl)acetate) (1.44 g, 3.64 mmol, 1.00 eq) were mixed together and homogenized with a ceramic pestle in a mortar and approximately 700 mg of the reaction mixture were weighed in each 4 mL supelco-vial with a stirring bar on top. After sealing the vials with a metal cap they were placed on a preheated heating block at 250°C under stirring and heated up to 280°C, where the reaction mixture was kept for 40 minutes. Afterwards the vials were cooled down to room temperature. The reaction mixture was dissolved in 200 mL acetone and put on the ultrasonic bath for ten minutes. The solvent was reduced under reduced pressure to 80 mL. The concentrated reaction mixture was added dropwise to a 500 mL solution of ethanol/water (1:1 + 20 mL saturated $NaHCO_3$ + 20 mL brine), producing a dark-green precipitate, which was then filtered off under vacuum. After this the residue was washed with an ethanol/water solution (2:1, 3 x 50 mL) and dried in the vacuum oven at 70°C. The crude product was purified via column chromatography (silica-gel, cond. CH, CH:EE, 10:1) yielding a dark-green solid. The product was washed with cyclohexane and dried in the vacuum oven at 70°C. Yield: 500 mg, 14 %

UV-VIS absorption spectra. λ_{max}/relative intensity (nm) in toluene: 40/ 1.00; 604/ 0.07; 654/ 0.38.

Meso-tetra-anisole-tetra-benzoporphyrin (H$_2$-TATBP)
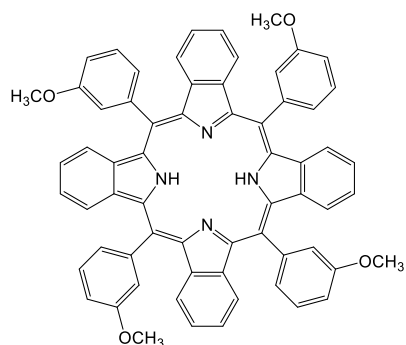
Figure 8.4 Chemical structure of H$_2$-TATBP

Zn-TATBP (500.00 mg, 500 µmol, 1.00 eq) was dissolved in 200 mL dichloromethane; 50 mL of 6 M HCl were slowly added. The resulting protonated ligand could be determined via absorption spectra in acetone (λ_{max} 499 nm). The acid was removed by shaking the organic phase with dest. H_2O (2 x 150

mL) and then with saturated $NaHCO_3$-solution (2 x 100 mL) until only free ligand was observed in the absorption spectra. Finally the organic layer was once more washed with dest. H_2O (30 mL), dried over Na_2SO_4 and the solvent was removed under reduced pressure. Yield: dark green solid, 450 mg, 96%

UV-VIS absorption spectra. λ_{max}/relative intensity (nm) in toluene: 464/ 1.00; 591/ 0.0447; 637/ 0.1230; 698/ 0.0421.

Platinum (II) meso-tetra-anisole-tetra-benzoporphyrin (Pt-TATBP)
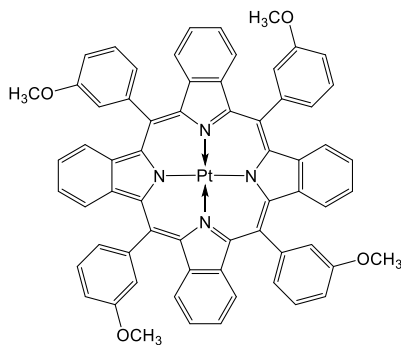
Figure 8.5 Chemical structure of Pt-TATBP

H_2-TATBP (310 mg, 331 µmol, 1.00 eq) was dissolved in 1,2,4-trimethylbenzene (250 mL) in a 2-neck-round bottom flask and heated to 145 °C, while bubbling N_2 through the reaction mixture. Then $Pt(C_6H_5CN)_2Cl_2$ (235 mg, 497 µmol, 1.50 eq) was added slowly in small portions (5 x 0.3 eq pre-dissolved in 1,2,4-trimethylbenzene) from a pre-heated addition funnel (100°C) over 3 hours. The reaction progress was monitored via absorption spectra (solvent: acetone). After complete conversion the reaction mixture was cooled down to room temperature, the metallic platinum removed via centrifugation and the solvent was removed under reduced pressure at 80 °C. The crude product was finally purified via column chromatography (silica-gel, cyclohexane:dichloromethane, 3:1). The product containing fractions were determined via absorption spectra, yielding a dark green solid. Yield: dark green solid, 186 mg, 50%

UV-VIS absorption spectra. λ_{max}/relative intensity (nm) in toluene: 430/ 1.00; 613/ 0.6898.

8.1.3 Results and Discussion of meso-tetra-anisole-tetra-benzoporphyrin (TATBP)

The synthesis of platinum(II) meso-tetra-anisole-tetra-benzoporphyrin (Pt-TATBP) using the template method could be performed successfully. The attempt to bridge this compound via Scholl reaction using either $AlCl_3$ or $FeCl_3$ as Lewis acid, however, was not successful. In the experiment (standard procedure for Scholl reaction described in 2nd publication) using $AlCl_3$, the bridged species (figure 8.6) could be observed for a short time at 110 °C, but disappeared immediately after increasing the temperature. A second attempt to isolate this species at 110 °C failed, similarly as the experiment using $FeCl_3$ under milder conditions (up to 100 °C). Here, formation of the species could not even be observed, therefore it was decided not to pursue further the project concerning this dye.
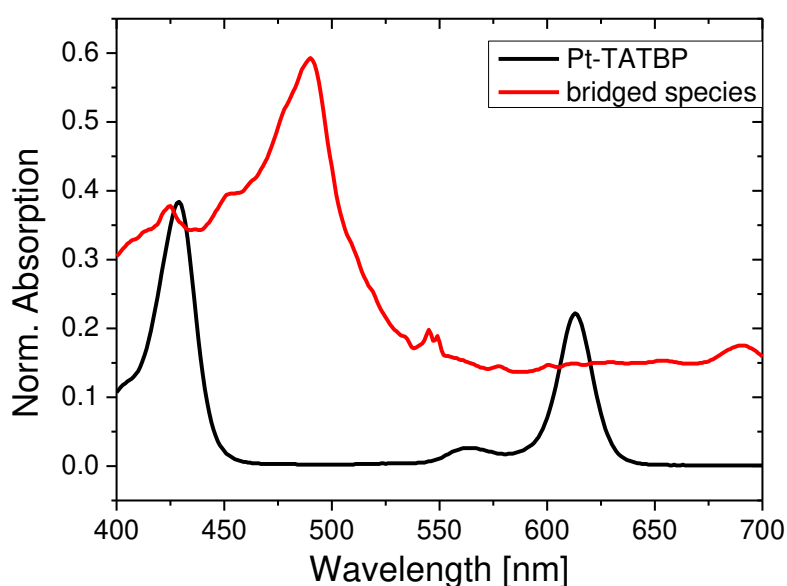
Figure 8.6 Absorption spectrum of Pt-TATBP (purified) and bridged product during Scholl reaction using $AlCl_3$ in dichloromethane

8.1.4 Experimental Part of meso-tetra-phenyl-di(di-methyl)benzoporphyrin (TPTBPdM$_2$)
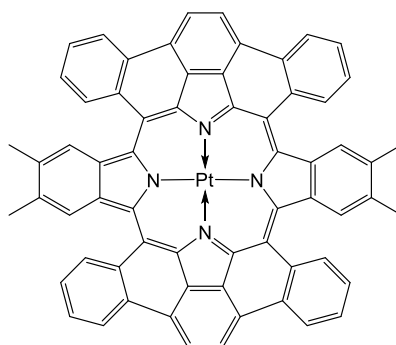
Figure 8.7 Assumed chemical structure of bridged Pt-TPTBPdM$_2$

Bridged platinum(II) meso-tetra-phenyl-di(di-methyl)benzoporphyrin (bridged Pt-TPTBPdM$_2$)

Pt-TPTBPdM$_2$ (25.00 mg, 23.5 µmol, 1.00 eq), as a mixture of isomers, was dissolved in 15 mL dichlorobenzene in a closed 25 mL round bottom flask. Then aluminum trichloride (407 mg, 3.05 mmol, 130 eq) was added and the solution was ultrasonicated for 10 minutes, resulting in a color change from dark-green to a brownish-red. The reaction mixture was quickly heated to 155 °C in an oil bath accompanied by bubbling of oxygen through the solution. The reaction progress was monitored via absorption spectra; the samples (10 µl) were neutralized with 30 µl of TEA and diluted with dichloromethane (DCM). After completion the reaction mixture was allowed to cool to room temperature under continuous O$_2$-bubbling through the solution. The reaction mixture was neutralized with a DCM:TEA solution (40:1 v/v) and the obtained precipitate was removed via centrifugation. The solution was shaken with H$_2$O (3 x 80 mL) to remove the excess of TEA and dried over Na$_2$SO$_4$. The solvent was removed under reduced pressure. The product was purified via column chromatography (silica-gel) and subsequently washed with cyclohexane (3 x 10 mL), yielding a green solid. Yield: 2.3 mg, 9%

UV-VIS absorption spectra. λ_{max}/relative intensity (nm) in toluene: 441/0.44; 454/0.44; 485/1.00; 611/0.08; 624/0.13; 641/0.24; 677/0.58.

8.1.5 Results and Discussion of bridged platinum(II) meso-tetra-phenyl-di(di-methyl)benzoporphyrin (bridged Pt-TPTBPdM$_2$)

The three synthetic steps using the template method, leading finally to the unsymmetrically substituted platinum(II) meso-tetra-phenyl-di(di-methyl)benzoporphyrin (Pt-TPTBPdM$_2$), could be conducted as expected but the separation of the differently substituted products by column chromatography could not be performed. Nevertheless, we decided to investigate intramolecular bridging via Scholl reaction using Pt-TPTBPdM$_2$. As can be seen in figure 8.8 this reaction led to the formation of a bridged species, that could even be isolated. Since the attempt to purify the isolated compound or more precisely the separation of the differently substituted bridged products via column chromatography failed several times, further investigation of this mixture was not conducted.
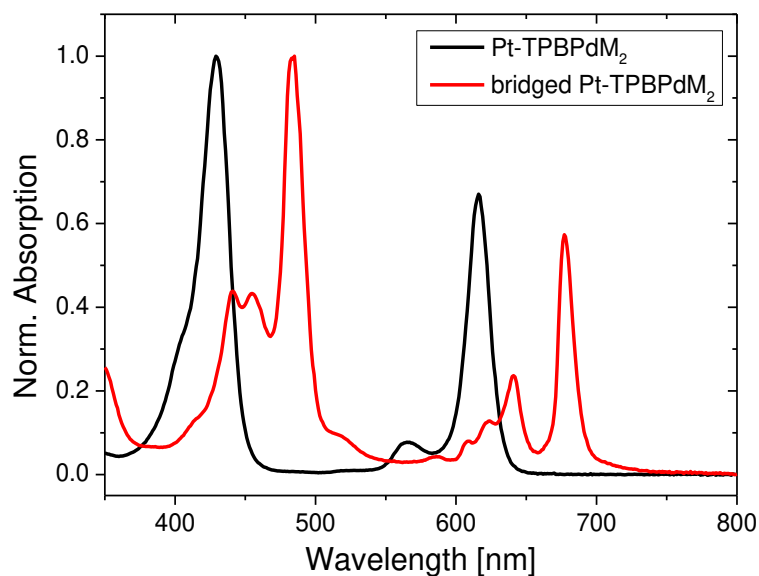
Figure 8.8 Absorption spectrum of purified Pt-TPTBPdM₂ and bridged Pt-TPTBPdM₂ in toluene

8.1.6 Experimental Part of meso-tetra-phenyl-porphyrin (TPP)

Nickel (II) meso-tetra-phenyl-porphyrin (Ni-TPP)
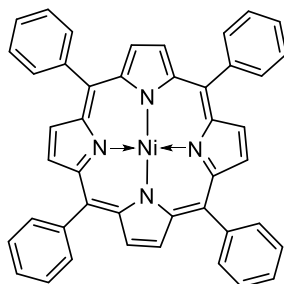
Figure 8.9 Chemical structure of Ni-TPP

The synthesis of this compound were performed according to Yao et al. [7]

TPP-Ligand (297 mg, 483 µmol, 1.00 eq) was dissolved in 150 mL NMP. Afterwards Ni(OAc)$_2$*4H$_2$O (364 mg, 1.46 mmol, 3.03 eq) was added to the dark red solution and heated to 150°C for 45 minutes. The reaction progress was monitored via absorption spectra (solvent: toluene). After complete conversion the reaction mixture was cooled down to room temperature. To the solution 150 mL of dest. H$_2$O was added and stirred for 10 minutes. The precipitate was separated via centrifugation (2 times) and dissolved in dichloromethane. The organic layer was washed with dest. H$_2$O (2 times) and dried over Na$_2$SO$_4$. After filtration and removal of the solvent under reduced pressure a dark red solid was gained. Yield: 284 mg (423 µmol, 88 %).

UV-VIS absorption spectra. λ_{max}/relative intensity (nm) in toluene: 415/1.00; 530/0.09; 618/0.03.

Nickel (II) meso-tetra-phenyl-porphyrin-NO₂ (Ni-TPP-NO₂)
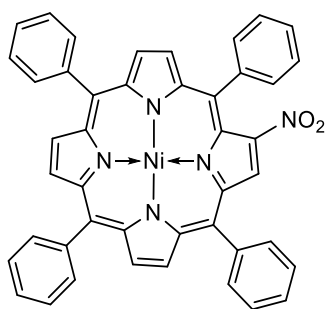
Figure 8.10 Chemical structure of Ni-TPP-NO₂

This and the following synthesis were performed according to Richeter et al. [8]

To a 45°C warm solution of Ni-TPP (50.0 mg, 74 µmol, 1.00 eq) in 30 mL CHCl₃, a solution of lithium nitrate (85.7 mg, 1.24 mmol, 16.7 eq) in 5 mL acetic acid and 4.75 mL acetic anhydride (red solution) was added. The reaction progress was monitored via TLC (CH:EE, 5:1) and absorption spectra (solvent: toluene). After complete conversion (2h reaction time) the reaction mixture was cooled down to room temperature, carefully neutralized with aqueous NaHCO₃ solution and washed three times with dest. H₂O. The organic layer was dried over Na₂SO₄ and the solvent removed under reduced pressure. For further purification column chromatography was used (silica-gel, cond. CH, CH:EE, 8:1), yielding a dark red solid. Yield: 43.0 mg (60.0 µmol, 81 %)

UV-VIS absorption spectra. λ_{max}/relative intensity (nm) in toluene: 429/1.00; 537/0.10; 578/0.07.

Nickel (II) meso-tetra-phenyl-porphyrin-NH (Ni-TPP-NH)
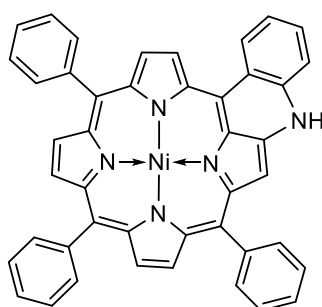
Figure 8.11 Chemical structure of Ni-TPP-NH

A degassed solution of Ni-TPP-NO₂ (40.0 mg, 56 µmol, 1.00 eq) in dichlorobenzene (2mL) and triethyl phosphite (50.5 µL, 294 µmol, 5.27 eq) was heated under argon atmosphere up to 155°C and stirred for 3h (dark red solution). The reaction progress was monitored via TLC (CH:EE, 5:1). After complete conversion (color change to green) the raw product was purified via column chromatography (silica-gel, cond. CH, CH:EE, 101), yielding a green solid. Yield: 19.4 mg (28.3 µmol, 51 %).

UV-VIS absorption spectra. λ_{max}/relative intensity (nm) in toluene: 429/1.00; 554/0.09; 578/0.07; 597/0.11; 628/0.22.

Nickel (II) meso-tetra-phenyl-porphyrin-N-tert-butyl-benzene (Ni-TPP-N-t-butyl-benzene)
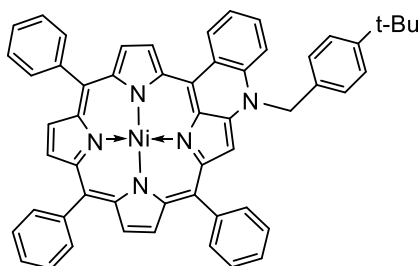
Figure 8.12 Chemical structure of Ni-TPP-N-t-butyl-benzene

The synthesis of this compound were performed according to Chevrier et al. [9]

Ni-TPP-NH (20.0 mg, 29.2 µmol, 1.00 eq) was dissolved in 4 mL THF in a Schlenk flask under argon atmosphere. Afterwards 1-(bromomethyl)-4-(tert-butyl)benzene (5.91 µL, 32.1 µmol, 1.10 eq) and 60% NaH (5.84 mg, 146 µmol, 5.00 eq) were added while N_2 was bubbling through the reaction mixture. The reaction mixture was heated up to 70°C for 17h. The reaction progress was monitored via TLC (CH:EE, 10:1) and absorption spectra (solvent: toluene). For the work-up to the reaction mixture DCM was added and the organic layer was washed three times with dest. H_2O. The organic layer was dried over Na_2SO_4 and the solvent was removed under reduced pressure. For further purification column chromatography was used (silica-gel, cond. CH, CH:EE, 10:1), yielding the product. Yield: 23.0 mg (28.0 µmol, 95 %)

Note: with this column chromatography the product could not be separated from all the impurities.

UV-VIS absorption spectra. λ_{max}/relative intensity (nm) in toluene: 440/1.00; 602/0.10; 645/0.17.

Meso-tetra-phenyl-porphyrin-NH (TPP-NH)
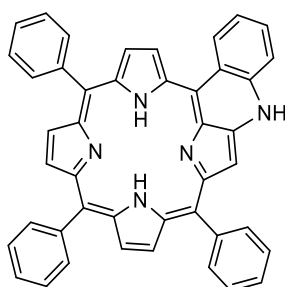
Figure 8.13 Chemical structure of TPP-NH

To Ni-TPP-NH (20.0 mg, 29.3 µmol) 3 mL of methanesulfonic acid were added, heated up to 50°C and stirred for 15 minutes. The reaction progress was monitored via absorption spectra (solvent: dichloromethane). For the work-up 15 mL DCM were added to the reaction mixture as well as 100 mL aqueous $NaHCO_3$ for neutralization. Then the organic layer was washed three times with dest. H_2O, dried over Na_2SO_4 and the solvent removed under reduced pressure. Yield: 18 mg (29.2 µmol, 98 %).

UV-VIS absorption spectra. λ_{max}/relative intensity (nm) in toluene: 412/1.00; 445/0.60; 592/0.14; 610/0.13; 660/0.11.

Zinc (II) meso-tetra-phenyl-porphyrin-NH (Zn-TPP-NH)
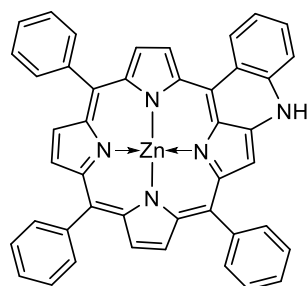
Figure 8.14 Chemical structure of Zn-TPP-NH

TPP-NH (4.30 mg, 6.85 µmol, 1.00 eq) was dissolved in 2.5 mL THF. Zinc acetate dehydrate (2.26 mg, 10.3 µmol, 1.50 eq) was added and the reaction mixture was stirred for 30 minutes at 45°C. The reaction progress was monitored via absorption spectra (solvent: toluene). The reaction mixture was cooled down to room temperature. Afterwards DCM was added to the mixture and the organic layer was washed with dest. H_2O. The organic layer was dried over Na_2SO_4 and the solvent was removed under reduced pressure. For further purification column chromatography was used (silica-gel, cond. CH, CH:EE, 10:1), yielding a green solid. Yield: 1.90 mg (2.75 µmol, 40 %)

UV-VIS absorption spectra. λ_{max}/relative intensity (nm) in toluene: 411/0.30; 458/1.00; 570/0.05; 611/0.08; 643/0.16.

Meso-tetra-phenyl-porphyrin-N-tert-butyl-benzene (TPP-N-t-butyl-benzene)
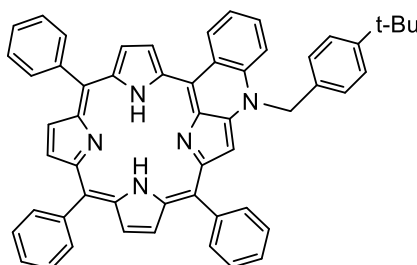
Figure 8.15 Chemical structure TPP-N-t-butyl-benzene

To Ni-TPP-N-t-butyl-benzene (20.0 mg, 24.0 µmol) 3 mL of methanesulfonic acid were added, heated up to 50°C and stirred for 15 minutes. The reaction progress was monitored via absorption spectra (solvent: dichloromethane). For the work-up 15 mL DCM were added to the reaction mixture as well as 100 mL aqueous $NaHCO_3$ for neutralization. Then the organic layer was washed three times with dest. H_2O, dried over Na_2SO_4 and the solvent removed under reduced pressure. Yield: 18 mg (23.2 µmol, 97 %).

UV-VIS absorption spectra. λ_{max}/relative intensity (nm) in toluene: 415/1.00; 448/0.60; 596/0.14; 613/0.13; 663/0.11.

Platinum (II) meso-tetra-phenyl-porphyrin-N-tert-butyl-benzene (Pt-TPP-N-t-butyl-benzene)
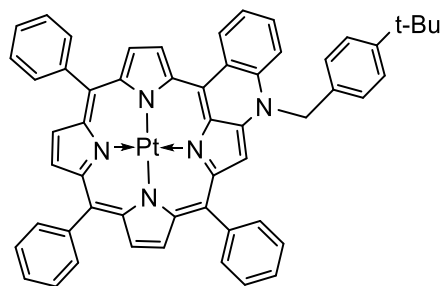
Figure 8.16 Chemical structure of Pt-TPP-N-t-butyl-benzene

TPP-N-t-butyl-benzene (18 mg, 23.2 µmol, 1.00 eq) was dissolved in 1,2,4-trimethylbenzene (15 mL) in a 2-neck-round bottom flask and heated to 145 °C, while bubbling N_2 through the reaction mixture. Then $Pt(C_6H_5CN)_2Cl_2$ (13 mg, 27.9 µmol, 1.20 eq) was added slowly in small portions (4 x 0.3 eq pre-dissolved in 1,2,4-trimethylbenzene) from a pre-heated addition funnel (100°C) over 3 hours. The reaction progress was monitored via absorption spectra (solvent: acetone). After complete conversion the reaction mixture was cooled down to room temperature, the metallic platinum removed via centrifugation and the solvent was removed under reduced pressure at 80 °C. The crude product was finally purified via column chromatography (silica-gel). The product containing fractions were determined via absorption spectra, yielding a dark green solid. Yield: dark green solid, 16 mg, 71%

Note: with this column chromatography the product could not be separated from all the impurities. UV-VIS absorption spectra. λ_{max}/relative intensity (nm) in toluene: 440/ 1.00; 623/ 0.10; 650/ 0.15.

8.1.7 Results and Discussion of Pt-TPP-N-t-butyl-benzene complex

As can be observed from the formation of the Nickel(II)-meso-tetra-phenl-porphyrin towards Nickel(II) complex bridged over a secondary amine and bridged Nickel(II) complex substituted with t-butyl-benzene moiety a significant bathochromic shift of the absorption spectra of 25 nm for the Soret band and 18 nm for the Q band could be obtained. The t-butyl-benzene moiety was introduced to increase the solubility of the compound and to shift the absorption spectrum further bathochromically, due to its electron donating character. Moderate yields and simplicity of the straightforward synthetic strategy make this approach a potential candidate for controlled bridging of porphyrinoids in future. Moreover, demetalation of the Ni(II) complex (7.1.5.5) with subsequent formation of the Zinc(II) complex (7.1.5.6) as well as formation of the t-butyl-benzene substituted platinum(II) complex was also performed. Platination of this complex led to an even further red shift by 5 nm in the Q band, as can be seen in figure 8.17. This complex was then investigated concerning its emission characteristics in anoxic toluene solution at room temperature and 77K (figure 8.18). As can be seen, the dye features red fluorescence and NIR phosphorescence. The phosphorescence at room temperature is very weak, however it is clearly visible at 77 K. It can be concluded that despite the strong bathochromic shift of the absorption and emission the new Pt(II) complexes are not promising as NIR phosphorescent emitters. However, they may be interesting for other applications, e.g. as triplet sensitizers.
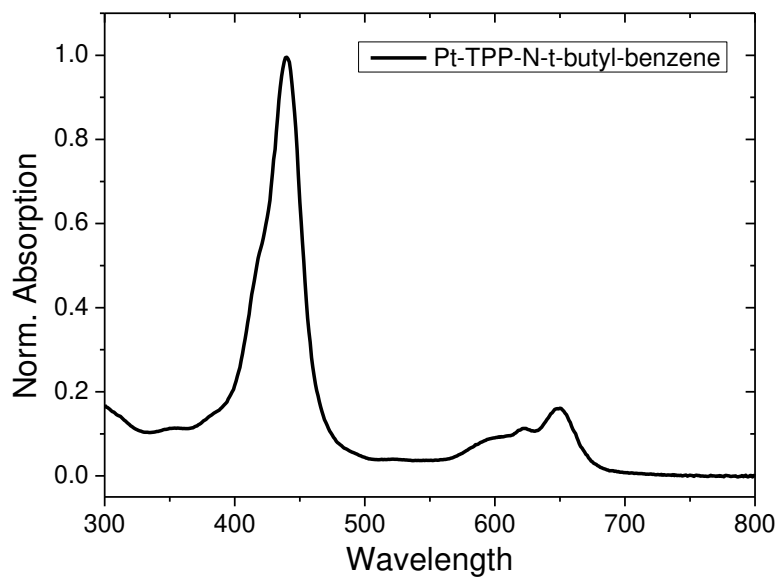
Figure 8.17 Normalized emission spectra of Pt-TPP-N-t-butyl-benzene in toluene at RT
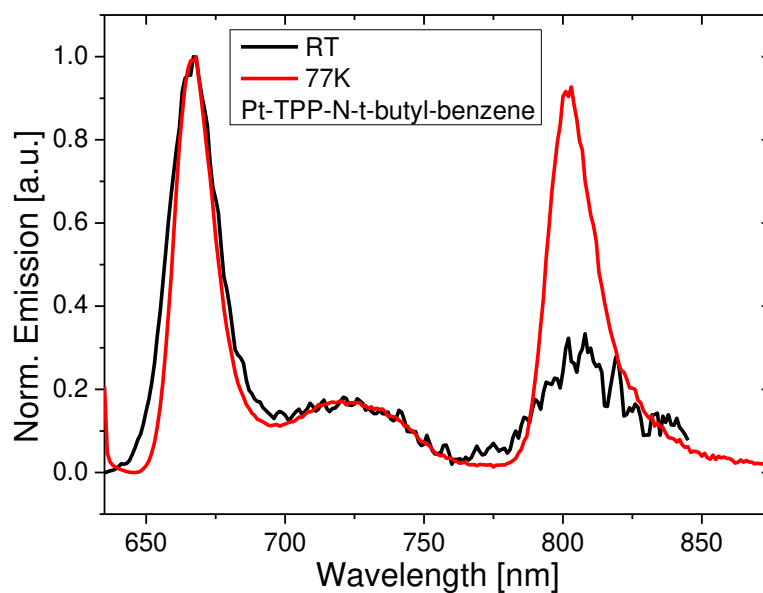
Figure 8.18 Normalized emission spectra of Pt-TPP-N-t-butyl-benzene in anoxic toluene at RT and 77K

8.2 Investigating the Influence of Pressure on Sensing Materials

This side project has its origins in the PhD thesis of Philipp Lehner (with the title: Ultra Trace Oxygen Sensors) in the project "Oxygen" and was further investigated by Laura Martínez Vidal in the course of a bachelor thesis under my co-supervision within the project "SenseOcean". Since all the new obtained data in detail are comprised within this bachelor thesis, only a short summary based on Philipp Lehner's work and an overview of the developments of this topic in the course of the project "SenseOcean" are given here.

8.2.1 Introduction

If a sensor is applied for in-situ measurements in the ocean, it is exposed to a harsh environment as well as big changes in hydrostatic pressure. Such pressure differences can change the properties of the sensor due to mechanical alteration of the matrix and as a consequence the dyes environment e.g. leading to a lower permeability for matrices with large internal volumes or a higher efficiency of interaction for the dye molecules caused by the compression. Since so far the influence of hydrostatic pressure on sensing properties and calibration of various sensing materials (in this case investigated for oxygen sensors) is unknown, following setup was build.

8.2.2 Setup and experiments performed by Philipp Lehner

The setup is built up of a home-made pressure chamber (figure 8.19) composed of a stainless steel tube covered with fittings of the same material, which are connected by hardened metal screws. The bottom fitting is equipped with a connector for a manual hand pump (with electronic pressure gauge), enabling the control of the hydrostatic pressure within the chamber. The top has openings usable for fiberoptic feedthroughs, enabling fixation of the sensors inside the pressure chamber connected with a read-out device (a phase fluorimeter module by Pyro Science), on the outside. The construction of the described pressure chamber allows measurements up to 400 – 500 bar, simulating an ocean depth of 4000 to 5000 meters. With a modified, strengthened bottom and top (without any openings) pressure measurements up to 700 bar are possible.

Figure 8.19 Photographic images (© Laura Martínez Vidal) of the pressure chamber consisting of stainless steel tube equipped with metal screws (left), the top fitting with fiber-optic feedthroughs (middle) and the inside of the pressure chamber with a sac (composed of oxygen impermeable aluminum foil) connected to the tube of the manual hand pump (right)

Since initial measurements showed a high inhomogeneity of the medium inside the pressure chamber as well as oxygen consumption of the brushless motor (1st generation), a submersible, pressure stable stirring mechanism was constructed. Therefore a brushless motor (2nd generation) with a strong magnet fixed inside a closed, silicon oil filled tube with shielded electronic connectors and a magnetic stirring bar on the outside was built. This modification led to a significant decrease of oxygen consumption and fluctuations inside the pressure chamber during measurements. However, in the following experiments another artefact, a peak visible in the intensity signal and lifetime of the oxygen sensors when pressure is applied to the system the first time was observed, which origins could so far be not elucidated that time.

8.2.3 Experiments performed by Laura Martínez Vidal

Unfortunately, during the course of the experiments conducted within the bachelor thesis no reason for the above mentioned artefact could be found. Moreover, the investigations using this setup revealed an extremely low reproducibility of the obtained results, concerning the sensitivity towards pressure on the used oxygen sensing materials in air saturated solution. Therefore a closer examination of the setup was conducted, revealing a leakage of the sac in the pressure chamber. Thus resulting in water exchange between the tube of the manual pump and the water within the chamber, leading to slight but constant change in oxygen concentration over time. The drifting of the obtained oxygen values at constant pressure continued, even after exchanging the sac and modification of its fixation in the chamber. Since the error within this measurement setup (pressure chamber or optical setup) could not be found after several attempts (details contained in the bachelor thesis) as well as the mentioned artifacts could not be explained, it was decided to terminate the investigation of pressure influence on oxygen sensors using this setup. However, the pressure chamber with strengthened bottom and top fitting (without openings), which works perfectly (figure 8.20) was successfully applied in several pressure measurements for different pH and CO_2 sensors.
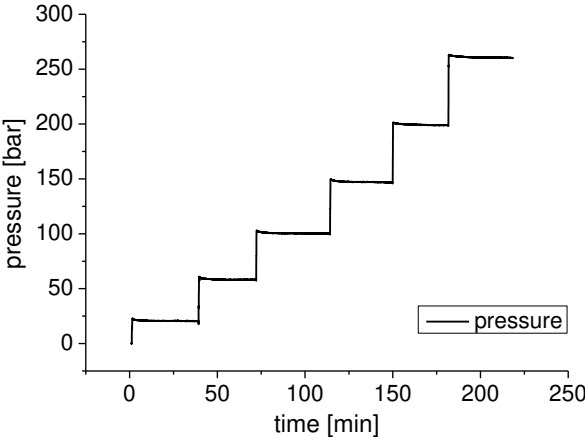
Figure 8.20 Schematic course of a pressure measurement from 0 to 250 bar

9 Summary and Conclusion

After more than 30 years of innovations, the field of (fiber-) optical chemical sensors (FOCS) is still incessantly growing and becoming more and more popular, due to its various advantages over other transduction methods and has therefore found several applications in highly diversified areas of research as well as industries. [10]–[12] One of the first, best investigated and most successfully applied fields of FOCS concerns the sensing of oxygen (gaseous or dissolved). Contingent on their high sensitivity and selectivity as well as their ability to be easily miniaturized and produced at low costs, these sensors are predicted to displace almost 70% of the commercially available amperometric sensors for O_2 (based on the Clark electrode) within the next years. [13] The measurement principle of commonly investigated and all commercial sensors is based on the luminescence quenching of indicator dyes by molecular oxygen. [12]

Here, the most popular and conclusively wide spread class of luminophores are metalloporphyrins, with either platinum(II) or palladium(II) as central atom. Reason therefore, is the high potential of structural modification and substitution, including extension of their π-system (e.g. benzoporphyrins), enabling outstanding tuneability of their optoelectronic as well as photophysical properties. Although decades of intensive research led to a huge number of oxygen indicators based on porphyrins, several parameters still display room for further modification, which was the subject of this work. Moreover, the thesis described the modified dyes, their drastically altered properties and revealed the high potential for different applications, by far exceeding usage as oxygen indicators.

Overall, this thesis described the preparation of two new classes of benzoporphyrin derivatives, accessible with only little synthetic effort compared to known alternatives. First, the introduction of electron withdrawing sulfone moieties combined with long aliphatic chains at the benzoporphyrins core led to the synthesis of compounds with increased solubility and photostability as well as a bathochromic shift of the absorption spectrum. Moreover, these dyes, platinum(II) and palladium(II) complexes, displayed higher brightness (increased molar absorption coefficient and quantum yields), reduced lifetime and most importantly a decreased energy gap between the excited singlet and triplet state, resulting in unexpected thermally-activated delayed fluorescence (TADF) in the red part of the electromagnetic spectrum besides phosphorescence in the NIR region. This unique dually emissive character of the dyes enabled the design of a dual sensor for simultaneous determination of oxygen and temperature, in a self-referenced manner, with one single probe for the first time. Additionally, application of these compounds as efficient sensitizers for triplet-triplet-annihilation (TTA) upconversion could be demonstrated.

Secondly, intramolecular bridging of known Pt-TPTBP via one step Scholl reaction, resulted in a new class of π-extended benzoporphyrin derivatives with outstanding bathochromic shift of absorption and emission spectra, which could further be applied as oxygen sensor within a new

concept for optical glucose sensing. Here, the quantification of glucose is obtained with a single optode, using a new three layer approach, consisting of two oxygen sensitive layers (bottom layer doped with the enzyme GOx) separated by a diffusion barrier responsible for the internal oxygen and glucose gradient. This concept in combination with the bridged species enables not only almost complete separation of excitation and emission signals of the used dyes, but also oxygen referenced determination of glucose for the first time in one single spot.

Finally, one step π-extension of known benzoporphyrin complexes via Friedel-Crafts acylation as well as Suzuki and Sonogashira coupling reaction could be achieved. The resulting compounds displayed bathochromic shifts of the absorption spectra and increased quantum yields in the NIR region as well as similar lifetimes compared to standard benzoporphyrins. Moreover, efficient quenching of phosphorescence by molecular oxygen, makes them promising indicators for in vivo applications. The possibility of excitation by red light combined with high brightness, enables utilization of these dyes as powerful sensitizers for TTA upconversion, applicable in photovoltaics.

In conclusion, this thesis demonstrated that mere modification of existing features doesn't compulsory only lead to the expected improvements, but can even result in completely new, unpredictable phenomena, opening unprecedented possibilities for a brilliant future. Although this work provides only small insights into the huge field of optical (oxygen sensing) technology, it still uncovers its great potential for prospective innovations and further promotes optical sensors to become an even more valuable analytical tool in the future.

10 References

[1] K. Xu, J. Zhao, X. Cui, and J. Ma, "Photoswitching of triplet–triplet annihilation upconversion showing large emission shifts using a photochromic fluorescent dithienylethene-Bodipy triad as a triplet acceptor/emitter," *Chem. Commun.*, vol. 51, no. 10, pp. 1803–1806, Jan. 2015.

[2] A. Monguzzi *et al.*, "Efficient Broadband Triplet–Triplet Annihilation-Assisted Photon Upconversion at Subsolar Irradiance in Fully Organic Systems," *Adv. Funct. Mater.*, vol. 25, no. 35, pp. 5617–5624, Sep. 2015.

[3] F. Niedermair *et al.*, "Tunable Phosphorescent NIR Oxygen Indicators Based on Mixed Benzo- and Naphthoporphyrin Complexes," *Inorg. Chem.*, vol. 49, no. 20, pp. 9333–9342, Sep. 2010.

[4] T. N. Singh-Rachford, J. Lott, C. Weder, and F. N. Castellano, "Influence of temperature on low-power upconversion in rubbery polymer blends," *J. Am. Chem. Soc.*, vol. 131, no. 33, pp. 12007–12014, Aug. 2009.

[5] W. Wang *et al.*, "Efficient Triplet–Triplet Annihilation-Based Upconversion for Nanoparticle Phototargeting," *Nano Lett.*, vol. 15, no. 10, pp. 6332–6338, Oct. 2015.

[6] A. Gnach and A. Bednarkiewicz, "Lanthanide-doped up-converting nanoparticles: Merits and challenges," *Nano Today*, vol. 7, no. 6, pp. 532–563, Dec. 2012.

[7] S. A. Yao, C. B. Hansen, and J. F. Berry, "A convenient, high-yielding, chromatography-free method for the insertion of transition metal acetates into porphyrins," *Polyhedron*, vol. 58, pp. 2–6, Jul. 2013.

[8] S. Richeter, C. Jeandon, J.-P. Gisselbrecht, R. Graff, R. Ruppert, and H. J. Callot, "Synthesis of New Porphyrins with Peripheral Conjugated Chelates and Their Use for the Preparation of Porphyrin Dimers Linked by Metal Ions," *Inorg. Chem.*, vol. 43, no. 1, pp. 251–263, Jan. 2004.

[9] M. Chevrier *et al.*, "Expanding the light absorption of poly(3-hexylthiophene) by end-functionalization with π-extended porphyrins," *Chem. Commun.*, Oct. 2015.

[10] O. S. Wolfbeis, "Fiber-Optic Chemical Sensors and Biosensors," *Anal. Chem.*, vol. 78, no. 12, pp. 3859–3874, Jun. 2006.

[11] C. McDonagh, C. S. Burke, and B. D. MacCraith, "Optical Chemical Sensors," *Chem. Rev.*, vol. 108, no. 2, pp. 400–422, Feb. 2008.

[12] X. Wang and O. S. Wolfbeis, "Fiber-Optic Chemical Sensors and Biosensors (2013–2015)," *Anal. Chem.*, vol. 88, no. 1, pp. 203–227, Jan. 2016.

[13] X. Wang, R. J. Meier, C. Schmittlein, S. Schreml, M. Schäferling, and O. S. Wolfbeis, "A water-sprayable, thermogelating and biocompatible polymer host for use in fluorescent chemical sensing and imaging of oxygen, pH values and temperature," *Sens. Actuators B Chem.*, vol. 221, pp. 37–44, Dec. 2015.

Part III
Appendix

11 List of Figures

234

12 List of Tables

13 Curriculum Vitae

Personal Details:

Last Name:	Zach	Date of Birth:	09.05.1990
First Names:	Peter Wilhelm	Address:	Harrachgasse 16, 8010 Graz
Title:	Dipl.-Ing., B.Sc.	Family Status:	unmarried
Nationality:	Austria	Phone Number:	+43 660 5391866

Education:

12/2014 – 04/2018	Graz University of Technology, PhD program of Technical Chemistry; Institute of Analytical Chemistry and Food Chemistry; Sensor Materials, PhD Thesis: "*New Phosphorescent Benzoporphyrin Complexes with Remarkable Photophysical Properties - From Synthesis to Applications*" within the ERC Project "SenseOcean" (Grant Number 614141); Supervisor: Ass. Prof. kand. Sergey Borisov
10/2012 - 11/2014	Graz University of Technology, Master program of Technical Chemistry; Institute of Analytical Chemistry and Food Chemistry; Sensor Materials, Master Thesis: "*New phosphorescent porphyrins with enhanced solubility & absorption in the NIR region for oxygen sensing materials*"; Supervisors: Prof. Dr. Ingo Klimant & Ass.Prof. kand. Sergey Borisov; *graduation with honors*
10/2009 - 09/2012	Graz University of Technology, Bachelor program of Chemistry; Institute of Analytical Chemistry and Food Chemistry; Sensor Materials, Bachelor Thesis: "*Synthesis of intracellular oxygen probes*"; Supervisor: Prof. Dr. Ingo Klimant
9/2000 - 6/2008	Akademisches Gymnasium Graz (grammar school); *graduation with honors*

Abroad Research Experience:

12/2016	Field-survey (sensor deployment & testing) at National Oceanography Center, Southampton, United Kingdom; monitoring of pH, O_2 and CO_2 in seawater
07/2015	Advanced Study Course on Optical Chemical Sensors and Biosensors (ASCOS); Summer School at the Center of Applied Photonics INESC TEC, Porto, Portugal
08 - 09 2013	Advanced Studies of Polymer Electrolyte Fuel Cells; Summer School at National University Yokohama, Japan

Practical Experience:

07 - 08/2011-2013	Sappi GmbH, Gratkorn, Austria Research & Development Department, manufacturing line
03 - 05/2012	Graz University of Technology, Institute for Chemistry and Technology of Materials; *Modification of TiO_x-Layer for inverse nanocomposite solar cells on flexible substrates*

Teaching Experience:

10/2014 - 01/2018	Mentoring of project laboratories, trainees, Bachelor and Master-students
10/2014 - 02/2017	Analytical Chemistry (Laboratory Course), Graz University of Technology
10/2013 - 06/2014	Technical Chemistry (Laboratory Course), Graz University of Technology
03 - 06/2012	Basic Organic Chemistry (Laboratory Course), Karl-Franzens University Graz

Awards and Scholarships:

05/2017	Best Speaker Award at 13th ASAC JunganalytikerInnen-Forum; Vienna, Austria
2012/2013	Academic Merit Scholarship (Leistungsstipendium)

Training and Qualifications:

Languages:	German (Native), English (Fluent), French (Advanced), Spanish (Basic), Latin
Volunteer Work:	Emergency medical technician at the Austrian Red Cross (since 2013), first aider at Graz University of Technology (2014-2018) and lecturer for first aid (since 2017)
IT Skills:	Microsoft Office, chemical Databases (Scifinder, ChemDraw, MestReNova)

Activities:

Football & Table Tennis (club), Marathon (running & biking), reading, meeting Friends & cooking

14 List of publications

14.1 Articles in peer reviewed journals

Zach, P. W*.; Maierhofer, M*.; Püschmann, S. D.; Klimant, I.; Borisov, S. M. Tuning Photophysical Properties of Phosphorescent Benzoporphyrin Complexes via 1-step-Extension. In submission; * these authors contributed equally

Staudinger, C.; Strobl, M.; Fischer, J. P.; Thar, R.; Mayr, T.; Aigner, D.; Müller, B. J.; Müller, B.; Lehner, P.; Mistlberger, G.; Fritzsche, E.; Ehgartner, J.; **Zach, P. W.**; Clarke, J.S.; Geißler., F.; Mutzberg, A.; Müller, J. D.; Achterberg, E. P.; Borisov, S. M.; Klimant, I. A versatile optode system for oxygen, carbon dioxide, and pH measurements in seawater with integrated battery and logger. In submission

Zach, P. W.; Hofmann, O. T.; Klimant, I.; Borisov, S. M. NIR Phosphorescent Intramolecularly Bridged Benzoporphyrins and Their Application in an Oxygen-Compensated Glucose Optode. In press: *Anal. Chem.* 2018, 90 (4), 2741–2748.

Zach, P. W.; Freunberger, S. A.; Klimant, I.; Borisov, S. M. Electron-Deficient Near-Infrared Pt(II) and Pd(II) Benzoporphyrins with Dual Phosphorescence and Unusually Efficient Thermally Activated Delayed Fluorescence: First Demonstration of Simultaneous Oxygen and Temperature Sensing with a Single Emitter. *ACS Appl. Mater. Interfaces* 2017, *9* (43), 38008–38023.

Stadlbauer, S.; Fischer, R.; Flock, M.; **Zach, P. W.**; Borisov, S. M.; Torvisco, A.; Uhlig, F. Structure and Spectroscopic Properties of Porphyrinato Group 14 Derivatives: Part I – Phenylacetylido Ligands. Z. Für Naturforschung B 2017, 72 (11), 801–811.

Hollauf, M.; **Zach, P. W.**; Borisov, S. M.; Müller, B. J.; Beichel, D.; Tscherner, M.; Köstler, S.; Hartmann, P.; Knall, A.-C.; Trimmel, G. Dye Functionalized-ROMP Based Terpolymers for the Use as a Light up-Converting Material via Triplet–triplet Annihilation. *J. Mater. Chem. C* 2017, *5* (30), 7535–7545.

Chien, H.-T.; **Zach, P. W.**; Friedel, B. Short-Term Environmental Effects and Their Influence on Spatial Homogeneity of Organic Solar Cell Functionality. ACS Appl. Mater. Interfaces 2017, 9 (33), 27754–27764.

Knall, A.-C.; Jones, A. O. F.; Kunert, B.; Resel, R.; Reishofer, D.; **Zach, P. W.**; Kirkus, M.; McCulloch, I.; Rath, T. Synthesis of a Conjugated Pyrrolopyridazinedione–benzodithiophene (PPD–BDT) Copolymer and Its Application in Organic and Hybrid Solar Cells. *Monatshefte Für Chem. - Chem. Mon.* 2017, *148* (5), 855–862.

14.2 Oral presentations

Zach, P. W.; Klimant, I.; Borisov, S. M. New Classes of NIR phosphorescent Benzoporphyrin Dyes for Optical Oxygen Sensing and Application in Photonic Materials. JunganalytikerInnenforum Austrian Society of Analytical Chemistry (ASAC) 2017; Vienna, Austria; 2017. Best Speaker Award

Zach, P. W.; Klimant, I.; Borisov, S. M. New Phosphorescent Benzoporphyrin Complexes for Optical Sensing of Oxygen and Triplet-Triplet-Annihilation based Upconversion; DocDays 2017 NAWI Graz; Graz, Austria; 2017.

Hollauf, M., Beichel, D., **Zach, P. W.**, Borisov, S., Köstler, S., Knall, A-C. & Trimmel, G. First ROMP based Terpolymers for the Use as a Light Up-Converting Material via Triplet-Triplet-Annihilation; XXVI International Materials Research Congress; Cancun, Mexico; 2017.

14.3 Poster Presentations

Hollauf, M.; **Zach, P. W.**; Borisov, S. M.; Beichel, D.; Tscherner, M.; Köstler, S.; Hartmann, P.; Knall, A-C.; Trimmel, G. Light up-converting ROMP based terpolymers via triplet-triplet annihilation; Advanced Materials Day 2017; Graz, Austria, 2017

Zach, P. W.; Klimant, I.; Borisov, S. M. New Classes of NIR phosphorescent Benzoporphyrin Dyes for Optical Oxygen Sensing and Application in Photonic Materials; DocDays 2017 NAWI Graz; Graz, Austria; 2016.

Zach, P. W.; Klimant, I.; Borisov, S. M. New Phosphorescent Benzoporphyrin Complexes for Optical Sensing of Oxygen and Triplet-Triplet-Annihilation based Upconversion; Europtrode XIII - Conference On Optical Chemical Sensors And Biosensors; Graz, Austria; 2016.

Borisov, S. M; Püschmann, S.; **Zach, P. W.**; Maierhofer, M.; Klimant, I. New pi-extended benzoporphyrins as readily available phosphorescent dyes for application in optical oxygen sensors and triplet-triplet-annihilation upconversion systems; Europtrode XIII - Conference On Optical Chemical Sensors And Biosensors; Graz, Austria; 2016.

Zach, P. W.; Klimant, I.; Borisov, S. M. Simple and Versatile Synthesis of new Highly-Soluble and Photostable Phosphorescent Pt(II)- and Pd(II)-Benzoporphyrin Dyes; Conference on Methods and Applications in Fluorescence (MAF-14); Würzburg, Germany, 2015.

Zach, P. W.; Klimant, I.; Borisov, S. M. Convenient and Time-saving Synthesis for Highly Soluble and Photostable Phosphorescent Benzoporphyrin dyes; ANAKON 2015; Graz, Austria; 2015.